ADAPTIVE MODELLING OF DYNAMIC CONJUGATE HEAT TRANSFER AND AIR MOVEMENT USING COMPUTATIONAL FLUID DYNAMICS

Tobias Zitzmann

PhD

This thesis is submitted to De Montfort University, Leicester, UK, in partial fulfilment of the requirements for the degree of Doctor of Philosophy.

The research was conducted in cooperation with the University of Applied Sciences Coburg, Germany.

May 2007

De Montfort University

Institute of Energy and Sustainable Development

The Gateway

LE1 9BH Leicester, England

TO THE MEMORY OF MY GRANDFATHER HANS ZITZMANN

Abstract

Zonal dynamic thermal simulation (DTS) programs are commonly used to analyse dynamic thermal behaviour of buildings. Computational Fluid Dynamics (CFD), although potentially more accurate, is currently mainly restricted to steady-state simulations due to the high computational resources required. An invariable freeze-flow control method for CFD was recently developed which 'freezes' the air flow patterns for fixed time periods. This method has been shown to be capable of modelling dynamic (time-dependent) thermal room behaviour. However, its control strategy did not exploit the full potential of the method.

The main aim of the research reported in this thesis was to develop, automate and verify an enhanced, adaptive freeze-flow control method for CFD. The intention of the new control method is to ensure that unfrozen flow periods are no longer than necessary and frozen flow periods are as long as possible, which should significantly increase the performance of the freeze-flow method. The new controlling parameters developed, which automatically trigger a switch between unfrozen and frozen flow modes, are: MAXLOOPS, which is the maximum number of iterations permitted within the time period EXTENSION after which a switch from unfrozen to frozen flow mode is triggered; MAXTEMP, which is the maximum change in local air temperature permitted during frozen flow periods after which a switch from frozen to unfrozen flow mode is triggered; and an overriding control EVENT (e.g. velocity, temperature or heat flux) which prohibits a switch from unfrozen to frozen flow or forces a switch from frozen to unfrozen flow periods when significant changes are likely to occur due to imminent changes in the user-defined boundary conditions.

Parametrical studies were carried out to verify the models in CFD for accurate modelling of the heat transfer mechanisms which are responsible for the dynamic thermal behaviour of buildings. Three new benchmarks are introduced which are intended to demonstrate the performance of the new control method. The first is a small 2D model with combined solid and fluid domain and purpose-provided openings for natural and mechanical ventilation and is used to verify the performances of the

dynamic CFD methods. Results agreed well when compared with fully dynamic CFD predictions. The second is a 3D room of typical office size enclosed by high thermal building mass and is used to verify the dynamic CFD method for modelling dynamic thermal behaviour of buildings. Results agreed well when compared with predictions of a zonal DTS program. The third comprises a typical office room with purpose-provided openings for night-time ventilation. CFD predictions using the newly developed CFD method agreed well with DTS results.

All benchmarks showed that the new control method provides improved performance over the other modelling methods used for comparison. When compared with a fully transient CFD simulation, the new method showed improvements in CPU performance of 74-89%. Due to the spatial discretisation used in CFD compared with simplified zonal assumptions used in DTS, the predicted room air temperatures showed differences of 0.4-0.7K at the end of the dynamic simulation periods.

Acknowledgements

The PhD programme was an invaluable and unforgettable experience, so thank you to the financial support of the Bundesministerium für Bildung und Forschung (BMBF) and the Institute of Energy and Sustainable Development (IESD) which has made this doctoral research possible.

Many thanks to my first supervisor Dr. Malcolm J. Cook (De Montfort University) and second supervisor Prof. Dr. Peter Pfrommer (University of Applied Sciences Coburg): Malcolm, for his paper and manuscript revisions during many endless nights and guidance throughout my doctorate whenever it was required and Peter, for his enthusiastic help, encouragement and guidance throughout my doctorate. Thank you to Dr. Simon Rees and second supervisor Dr. Ljiljana Marjanovic (De Montfort University) for sharing their professional ideas and knowledge.

I would also like to thank all of the staff at the Institute of Energy and Sustainable Development and the University of Applied Sciences Coburg for their moral support and assistance with IT matters.

I would like to thank my precious family, Gunter, Ingrid, Christoph, Norbert and Wilhelm for providing their endless love, encouragement and support, and my partner in life Kathrin for her patience, tolerance and loving support through all the ups and downs.

Table of Contents

List of Figures

List of Tables

Nomenclature

a	thermal diffusivity	$[m^2/s]$
A_{net}	net floor area	$[m^2]$
B	incident radiation	$[W/m^2]$
c	specific heat capacity	$[J/(kg \cdot K)]$
C_{eff}	effective heat capacity	$[W \cdot h/K]$
E	radiative heat emission	$[W/m^2]$
g	gravity, scalar	$[m/s^2]$
$\vec{g}$	gravity vector	$[m/s^2]$
h_c	convective heat transfer coefficient	$[W/(m^2 \cdot K)]$
h	specific static enthalpy	$[m^2/s^2]$
I_b	blackbody radiance	$[W/(m^2 \cdot sr)]$
I_v	spectral radiance	$[W/(m^3 \cdot sr)]$
k	kinetic energy per unit mass	$[m^2/s^2]$
K_{av}	spectral absorption coefficient	[1/m]
K_{sv}	spectral scattering coefficient	[1/m]
L	length along a device surface	[m]
l	macroscopic length scale of turbulence	[m]
$\dot{m}$	mass flow rate	$[m^3/s]$

n	air change rate	[ach^{-1}]
n_j	scalar of the outward normal vector of surface j	[m]
p	modified pressure	[$kg/(m \cdot s^2$]
P	absolute pressure	[$kg/(m \cdot s^2$]
P_{kb}	buoyancy production source term	[$kg/(m \cdot s^3$]
$\dot{q}$	heat flux	[W/m^2]
$\vec{r}$	position vector	[m]
r_ϕ	residual of a transport variable	(varies)
R_e	external heat resistance	[$(m^2 \cdot K)/W$]
R_i	internal heat resistance	[$(m^2 \cdot K)/W$]
s	thickness, path length	[m]
$\vec{s}$	direction vector of path	[m]
S_E	energy source term	[$kg/(m \cdot s^3)$]
S_k	turbulence production source term	[$kg/(m^2 \cdot s^2)$]
S_M	momentum source term	[$kg/(m^2 \cdot s^2)$]
S_ν	spectral source term	[$W/(m^4 \cdot sr)$]
T	temperature	[K]
T_i	initial wall temperature	[K]
T_{in}	inlet temperature	[K]
T_{out}	outlet temperature	[K]

t	time	[s]
u	horizontal component of velocity	[m/s]
$\vec{u}$	velocity fluctuation	[m/s]
U	thermal transmittance	[W/(m^2·K)]
$\vec{U}$	velocity vector	[m/s]
v	vertical component of velocity	[m/s]
x, y, z	Cartesian coordinates	[m]
X, Y, Z	model dimensions in a Cartesian system	[m]

Greek Symbols

β	thermal expansivity	[1/K]
δ	hydraulic wall boundary layer thickness	[m]
δ_T	thermal wall boundary layer thickness	[m]
ε	turbulence dissipation rate	[m^2/s^3]
λ	thermal conductivity	[W/(m·K)]
μ	molecular (dynamic) viscosity	[kg/(m·s)]
μ_t	turbulent viscosity	[kg/(m·s)]
ν	kinematic viscosity	[m^2/s]
ν	frequency specific to radiative wave length	[1/s]
ρ	density	[kg/m^3]
τ_w	wall shear stress	[kg/(m·s^2)]

Φ	arbitrary variable	(varies)
ω	frequency	[1/s]
Ω	solid angle	[sr]

Dimensionless quantities

A_P	central coefficient of momentum equation	
$C_{1,2,3}$	constant	
erf(z)	error function of z	
f	velocity	$f(\eta) = \frac{v_y \cdot y}{\nu} \cdot \frac{1}{2 \cdot \sqrt{Gr_y}}$
Gr	Grashof number	$Gr = \frac{g \cdot L^3 \cdot \beta \cdot \Delta T}{\nu^2}$
Nu	Nusselt number	$Nu_y = 0.386 \cdot Ra_Y^{0.25} \cdot \left(\frac{y}{Y}\right)^{-0.25}$ (laminar)
Pr	Prandtl number	$\mathrm{Pr} = \frac{\nu}{a}$
Ra	Rayleigh number	$\mathrm{Ra} = \mathrm{Gr} \cdot \mathrm{Pr}$
Re_t	turbulence Reynolds number	$\mathrm{Re}_t = \frac{v_a \cdot l}{\nu}$
T_{eff}	effective temperature	$T_{eff} = \frac{T_{out} - T_{in}}{T_{room,ave} - T_{in}}$
y+	distance from the wall	$y+ = \frac{\sqrt{\tau_w / \rho}}{\nu} \cdot \Delta y$

z	distance from the wall	$z = \frac{x_1}{2 \cdot \sqrt{a \cdot t}}$
α	radiation absorption coefficient	
α_p	control volume coefficient	
β_b	blending factor	
ε	radiation emission coefficient	
η	distance from the wall	$\eta = \frac{x}{y} \cdot (\frac{Gr_y}{4})^{0.25}$
Θ	temperature	$\Theta(x,t) = \frac{T - T_S}{T_w - T_S}$ and $\Theta(\eta) = \frac{T - T_a}{T_S - T_a}$
τ	radiative transmission coefficient	
φ	view factor	
Φ	in-scattering phase function	

Subscript

a	air
ave	average
diff	diffusive
glob	global
i, j, k	surface indices
in	flow into a volume space
int	internal

ip	integration point
m	mean
max	maximum
norm	normalized
out	flow out of a volume space
rad	radiative
ref	reference
room	room
S	surface
t	turbulent
up	upwind
W	wall
y	value in y-direction

Superscript

T	transponed
’	solution field of the old time level
’’	solution field before the old time level

Constants

e	base of the natural logarithm ≈2.718281828[-]

σ	Stefan-Boltzmann constant ≈5.67·10-8	$[W/(m^2 \cdot K^4)]$
π	Archimedes constant ≈3.14159	

Mathematical symbols

δ_{KDF}	Identity Matrix (Kronecker Delta Function)	$=\begin{bmatrix} 1 & 0 & 0 \\ 0 & 1 & 0 \\ 0 & 0 & 1 \end{bmatrix}$
∂	differential operator	
∇	vector differential operator	$\nabla = \frac{\partial}{\partial x} u_i + \frac{\partial}{\partial y} u_j + \frac{\partial}{\partial z} u_k$
Δ	Lapace operator	$\Delta = \frac{\partial^2}{\partial x^2} u_i + \frac{\partial^2}{\partial y^2} u_j + \frac{\partial^2}{\partial z^2} u_k$

Abbrevations

ach^{-1}	air changes per hour
AIVC	Air Infiltration and Ventilation Centre
ASHRAE	American Soc. of Heating, Refrigerating and Air-Conditioning Engineers
ASME	American Society of Mechanical Engineers
BC	boundary condition
BSRIA	Building Services Research and Information Association
CFD	Computational Fluid Dynamics
CEL	CFX Expression Language

CHT	conjugate heat transfer
CIBSE	Chartered Institution of Building Services Engineers
CPU	Computer Power Unit
DIN	Deutsche Norm
DLL	Dynamic Link Library
DT	Discrete Transfer
DTS	Dynamic Thermal Simulation
EnEV	Energieeinsparverordnung
EN	European norm
FVM	Finite Volume Method
GUI	Graphical User Interface
HVAC	Heating, Ventilation and Air-Conditioning
IEA	International Energy Agency
LES	Large Eddy Simulation
LRR-IP	Launder-Reece-Rodi Isotropic Production
MC	Monte Carlo
MP	monitor point
NISTIR	National Institute of Standards and Technology
RANS	Reynolds Averaged Navier Stokes
RMS	root mean square

SMC	Second Moment Closure
SST	Shear Stress Transport
UNFCCC	United Nations Framework Convention on Climate Change
VDI	Verein Deutscher Ingenieure

CHAPTER 1

INTRODUCTION

1 Introduction

1.1 Background

"Climate change is a global problem
that requires local action"

(Bill Clinton, Former president of the United States of America,
president of the Clinton Climate Initiative at a press conference)
(Clinton Foundation 2007))

Buildings account for nearly 40% of global greenhouse gas emissions (Clinton Foundation 2007). Energy consumption in commercial and residential buildings throughout Europe also represents approximately 40% of Europe's energy budget (Santamouris et al. 1994). Modern office buildings are sealed, have facades with a high proportion of glazing and increasing quantities of electrical equipment. This leads to a significant increase of the room heat gains and to high summer cooling loads. Heating, Ventilation and Air Conditioning (HVAC) systems are often used in office buildings to maintain the required levels of thermal comfort. However, they consume large amounts of energy. The European consumption by room air conditioners was 2GWh in 1990, 11GWh in 1996 and is estimated to reach 44GWh in 2010 (Lopes et al. 2001). A European Union Energy Performance of Buildings Directive was published in 2003 to "promote the improvement of energy performance of buildings within the Community taking into account outdoor climatic and local conditions, as well as indoor climate requirements and cost-effectiveness" (European Union 2003). Each EU member state is required to transpose the Directive into law by the beginning of 2006 with a further three years being allowed for full implementation of specific articles. As one objective

of the directive, an energy certificate should come into force at the end of this period which shows the energy-efficiency of all new buildings, buildings and flats of the building stock that are subject to major renovation or are rented or proposed for sale. The German Energieeinsparverordnung EnEV (2006) intends to transfer the Directive into German building regulations. Another, international Community convention for energy reduction is the Kyoto protocol (UNFCCC 2005), which has the aim of reducing the CO_2 emissions to the value of 1990 by 2010.

Consequently, passive cooling strategies are increasingly being used for commercial buildings which exploit existing constructional building (e.g. window orientation, building fabric properties, shape and orientation) or landscape properties (e.g. using evaporation from trees surrounding a building leading to convenient microclimates) to reduce the building energy consumption, as described by Santamouris and Asimakopolous (1996). Brown (1990), for example, described energy savings of up to 20% for a numerically investigated two-storey office building for which the thermal mass of the building structure was increased. However, the reduction could be much less today due to high insulation and air-tightness of the buildings. One strategy which is increasingly used in moderate climates (especially to supplement natural ventilation) is night-time cooling which exploits the effect of the heat absorption capacity of the thermal mass of a building (Kolokotroni et al. 1998). Consequently, depending on the site, type and usage of the building, no air-conditioning might be needed for such a strategy in moderate climates (e.g. BINE 2003).

The key factors influencing passive cooling are: internal and external temperature, internal and solar heat gains, air flow rates due to natural ventilation during night-time and daytime and the heat capacity of the building mass. These are interrelated in a non-linear complex way (Yam et al. 2003). Voss et al. (2005) pointed out that these complex interactions can lead to the risk of an inefficient passive cooling concept. Simple tools were developed from empirical investigations which can help to increase the cooling efficiency of the building structure (e.g. Shaviv et al. 2000). However, it is difficult to determine whether air-conditioning for a specific building is required or not. New combination of different passive cooling components in a concept and other weather conditions etc. might lead to a different thermal room behaviour compared with similar

concepts. Thus, simulation programs are required which predict the dynamic internal room temperatures accurately to make such recommendations possible. Building guidelines advocate the use of simulation programs. The DIN 4108-2 (2003), for example, points to such engineering methods to calculate the internal air temperatures of buildings during the summer periods and to take into account the heat protection requirements for buildings during this time. CIBSE Guide A-5 (2006), for example, provides numerical calculation procedures to determine peak summer-time temperatures and space cooling loads in buildings.

Zonal dynamic thermal simulation (DTS) programs are commonly used for the investigation of dynamic thermal room behaviour due to their relative simplicity. They calculate thermal average values for zones and surface temperatures, and only one-dimensional heat conduction is considered in the building fabric. However, since they only predict average zone conditions, these assumptions can give significant prediction errors, for example where temperature stratification exists in high atria (Heiselberg et al. 1998). Another type of simulation program is Computational Fluid Dynamics (CFD) which has historically been developed and used in the aerospace and automotive industries to investigate for example the aerodynamics of wings and processes in engine and turbines. Most CFD programs are based on the Finite Volume Method (Versteeg and Malalasekera 1995) which means that each zone and building component is discretised in a fine mesh of finite volume elements which enables spatial predictions of flow and energy. Thus, CFD is potentially more accurate than DTS. However, the use of CFD for dynamic thermal building simulations is currently impractical since they require large amounts of computational resources. Hence, investigations using CFD are often restricted to steady-state simulations. New methods are therefore required for which CFD can be applied to investigate dynamic thermal behaviour of buildings. This research intends to addresses this issue.

The main aims of the research conducted are listed in section 1.2 and the research methodology and contents of the thesis are described in section 1.3. The original contribution of the work to the body of knowledge is discussed in section 1.4.

1.2 Aims of Research

The aims of the research are as follows:

1. to develop CFD methods for effectively modelling the dynamic thermal performance of buildings with and without ventilation to predict internal temperature distributions;

2. to verify these methods by comparison with fully transient CFD methods and DTS programs;

3. to develop guidelines for modelling dynamic thermal performance of buildings using these CFD methods;

4. to demonstrate the use of CFD for modelling dynamic night-time ventilation of an office room using the new methods.

Three fully documented benchmarks are produced (see section 1.3.1) and used to offer guidance on how to use CFD methods for modelling dynamic thermal behaviour of buildings and night-time ventilation. This work comprises a detailed description of how key model parameter settings affect the accuracy of the result. The influence of single-sided and cross ventilation design are also documented. It is intended that these new methods and the guidelines will help engineers who wish to undertake research involving dynamic CFD simulations as well as those who wish to investigate and develop night-time cooling strategies.

1.3 Research Methodology and Thesis Contents

1.3.1 Research Methodology

Parametrical studies (e.g. for discretisation techniques, turbulence and radiation models etc.) are carried out at the beginning of the research to verify CFD models to accurately predict the heat transfer mechanisms relevant in buildings. Three benchmarks are then defined to investigate dynamic thermal room behaviour. The first benchmark is a 2D

small scale room with combined solid domain of high thermal mass and air flow domain with purpose-provided openings for natural ventilation and mechanical ventilation or pure free convection. The second benchmark is a large scale 3D room of typical office size enclosed by high thermal mass building structure. Using these models CFD methods are verified for modelling dynamic thermal behaviour of buildings. The performances of the CFD methods are verified by inter-model comparison with the fully transient CFD using the first benchmark. Dynamic thermal simulation results for CFD are then verified and established by comparison with a DTS program using the second benchmark based on verification procedures of building simulation guidelines. The third benchmark is based on a typical office room with a medium thermal mass building fabric and with purpose-provided openings. Time-varying internal conditions and external weather conditions, which are based on verification procedures from building simulation guidelines, are used to influence the dynamic thermal behaviour of the office. Using this benchmark, simulations are carried out to investigate the performance of night-time cooling. The research aims are achieved through the following objectives:

1. a literature review is carried out covering the fundamental principle of night-time ventilation including key parameters for an efficient cooling performance, and covering the various dynamic thermal building simulation methods available, in particular CFD-based methods;

2. CFD modelling skills are developed using the CFD program CFX. This comprises verification of modelling heat transfer mechanisms relevant in buildings by comparison with analytical and experimental data;

3. benchmark 1 (2D room of conjugate heat transfer with purpose-provided openings for ventilation) is defined and used for developing CFD methods for modelling dynamic thermal room behaviour influenced by different flow driving mechanisms (e.g. natural ventilation, mechanical ventilation and free convection) which can often occur in buildings. This includes inter-model comparison of existing and newly developed CFD methods and parametrical studies for method specific settings;

4. benchmark 2 (3D room of high thermal mass) is defined and used to verify the new CFD methods for predicting dynamic thermal room behaviour. This includes parametrical studies and comparisons with DTS. Compared with benchmark 1, which contained only one building wall element, the room in benchmark 2 contains a more realistic room enclosure of multi-layer components;

5. benchmark 3 (3D office room of medium thermal mass and purpose-provided openings for ventilation) to use it to verify the plausibility of the new CFD method for investigating the influence of night-time cooling on dynamic thermal room behaviour. This includes parametrical studies and comparisons with DTS.

1.3.2 Thesis contents

The thesis is divided into 8 chapters:

Chapter 2 describes the background to dynamic thermal modelling of night-time ventilation. The principle of night-time ventilation and factors influencing its efficiency are presented. Common methods used for simulating the dynamic thermal performance of buildings and air flow patterns in buildings and the associated advantages and drawbacks are discussed. A literature review summarises previous work undertaken to simulate dynamic thermal building behaviour and night-time ventilation.

Chapter 3 presents relevant heat transfer processes which lead to the characteristic thermal behaviour of buildings. A theoretical background and results of verification of CFD models for these heat transfer mechanisms are presented.

Chapter 4 introduces a new CFD method for dynamic thermal simulations. The development of this method, the intended function and advantages over former dynamic thermal CFD methods are described. The procedures of implementation and automation of the methods in the CFD program are explained.

Chapter 5 contains the results of the verification of the performances of the dynamic CFD methods described in chapter 4 using inter-model comparison for benchmark 1.

The methods are tested for typical flow mechanisms which can occur in buildings. Advantages and possible problems are discussed which could evolve due to the dynamic CFD methods.

Chapter 6 presents the verification of dynamic CFD results for modelling dynamic thermal behaviour of a room with a size typical for offices using benchmark 2. Results are compared with predictions of a DTS program to show the plausibility of results and the influence of modelling techniques and parameter settings on the accuracy of results.

Chapter 7 shows the dynamic results for the application of CFD to night-time ventilation for a more realistic office room using benchmark 3. Two night-time ventilation concepts with different opening positions are investigated to compare influences on the dynamic thermal behaviour of the room and on the night-time ventilation efficiency. Comparison of CFD results with a DTS program verifies the plausibility of predictions and shows the influence of modelling techniques and model parameter settings on the accuracy of results.

Chapter 8 contains the conclusions of the research and suggestions for further work.

1.4 Original Contribution to the Body of Knowledge

The areas of originality in the work are summarised as follows:

- Due to the historical development of CFD for the automotive and aerospace industry (e.g. optimizing engines and wings) models were mainly applied to forced flow phenomena. However, in buildings pure forced flow exists only close to the inlets or outlets in mechanical systems, and free convection prevails in most parts of the room. Since free convection has a strong influence on the heat exchange between the space and the building structure and therefore on the dynamic thermal behaviour of buildings, a CFD program must be capable of modelling this mechanism accurately. However, practical information about model parameter settings for free convection and the other heat transfer processes (i.e. conduction and radiation) relevant for modelling the dynamic

thermal behaviour of buildings is sparse for the commercial CFD program used in this research. Therefore the modelling of these heat transfer mechanisms are verified in this research by conducting parametrical studies and comparing predictions with analytical and experimental data.

- Modelling the dynamic thermal behaviour of buildings using CFD alone is relatively new. A promising method to overcome the incompatibility of the time constants of solids and the air was shown by Onishi et al. (1998) and Somarathne et al. (2002). In this so-called freeze-flow method, the flow equations are intermittently frozen for certain time periods. However, the developed control method needs further refinement and automation is required to increase the efficiency of the freeze-flow method. This research intends to address this issue and presents the stages of development, verification, automation and application of a new enhanced control method. Former research used inter-model comparison of the new dynamic CFD methods with the same basic CFD code to verify their performances. However, this methodology does not show the plausibility of predictions compared to real building behaviour. Therefore, results are compared in this research with a fundamentally different DTS code based on dynamic thermal simulation verification procedures of building simulation guides.

- Night-time ventilation has often been investigated by conducting time intensive field measurements or simulations with zonal DTS programs. However, simulations using the potentially more accurate CFD have not been carried out due to the significant computational resources required. This research intends to address this issue: night-time ventilation in a typical office room is numerically investigated using the newly developed dynamic CFD method and results are compared with prediction of a DTS program often used for dynamic thermal simulation of buildings.

The main research results carried out during the PhD program have been published (or are in press) in peer reviewed journals and peer reviewed academic international conferences. Details of these are shown in chapter Bibliography and chapter F.

CHAPTER 2

BACKGROUND OF THE NIGHT-TIME COOLING STRATEGY AND DYNAMIC THERMAL MODELLING

2 Background of the Night-Time Cooling strategy and Dynamic Thermal Modelling

2.1 Preamble

Chapter 1 has shown the demand for energy-efficient cooling strategies in office buildings, particularly for the summer season when the room heat gains are significantly higher due to higher ambient temperatures and solar radiation. A passive cooling strategy which is increasingly used in moderate climates is night-time cooling.

Various parameters can influence the performance of night-time cooling in terms of energy efficient operation. The main parameters are discussed in this chapter. Simulation programs are often used to investigate the thermal behaviour of buildings and are also used to optimise strategies for heating and cooling. The chapter contains a discussion of advantages and drawbacks of the common simulation program types and a literature review of previous work relating to modelling of night-time cooling in buildings. The review focuses particularly on the attempts to verify the accuracy of predictions to model night-time cooling.

Section 2.2 comprises a description of the principle of night-time cooling and the parameters influencing the energy efficient operation. Section 2.3 discusses the advantages and drawbacks of actual simulation programs. Section 2.4 presents a literature review covering the modelling of night-time cooling and the verification of predictions. Section 2.5 gives a summary of the simulation programs used in this research. Section 2.6 gives a summary of the operation of the night-time cooling strategy and possible methods for modelling the strategy.

2.2 Principle of night-time cooling

Passive cooling strategies (which use no fossil fuel as part of their operation) exploit the advantages of the natural environment, including natural driving forces for ventilation, the building shape, form and fabric etc. Santamouris and Asimakopolous (1996) describe several passive cooling design methods and their energy saving potential. One strategy which is increasingly being used in moderate climates is the night-time cooling in offices, also known as night-time ventilation.

The principle of night-time cooling exploits the capacity of the building structure to store and release heat. During the daytime, the building fabric absorbs heat (by conduction, convection and radiation) generated by internal heat gains. During the following night, cool air from outside enters the room through purpose-provided openings or inlets due to natural ventilation or mechanical ventilation respectively, absorbs heat by contact with the building fabric and then flows out of the building driven by buoyancy that the air gains as a result of cooling the fabric. This replenishes the thermal mass, enabling it to once again absorb heat. Peak indoor air temperatures can be reduced by 1-3K (Santamouris and Asimakopolous 1996).

Generally two principles can be used to ventilate building spaces:

- Mechanical ventilation which forces mass flow in a room due to momentum pressure from fans.

- Natural ventilation which is based on natural pressure differences across the openings due to wind or temperature differences.

Natural ventilation is the preferred ventilation method for night-time cooling in terms of energy-efficiency since no electrical energy is required for operation. If properly designed, in moderate climates, night-time ventilation can help to provide comfortable room conditions during the occupancy hours without any additional requirement of mechanical air-conditioning systems. However, natural forces are sometimes small which then leads to insufficient ventilation rates. Mechanical ventilation might then assist natural ventilation as suggested by Martin and Fletcher (1996). However, they

point out that "the additional energy fan operation should be weighted against the potential benefit which can be obtained by night cooling in order that the net energy costs are not greater than that for a system with no night-cooling".

The efficiency of night-time cooling depends mainly on the following parameters: the properties of the building fabric; the surface heat transfer; the air flow distribution and the weather conditions. These are described in detail in the following sub-sections. Kolokotroni and Aronis (1999) also describe other parameters (e.g. building orientation, air infiltration, glazing area and shading devices) which only marginally (up to 6%) influence the potential cooling efficiency. Since many parameters influence the operation efficiency of a night-time cooling strategy, simulation programs are necessary to assess and optimise the strategy.

2.2.1 Building fabric properties

Using the DIN 4108-2 (2003) building fabric can be categorized as follows:

Light-weight: $(C_{eff}/A_{net}) < 50$ W·h/(m²·K)

Medium-weight: 50 W·h/(m²·K) $< (C_{eff}/A_{net}) <$ 130 W·h/(m²·K)

Heavy-weight: $(C_{eff}/A_{net}) > 130$ W·h/(m²·K)

where A_{net} = net floor area [m^2] and C_{eff} = effective heat capacity of the room [W·h/K]. The effective heat capacity, C_{eff}, is the thermal capacity [W·h/K] of the room envelope which thermally interacts with the room interior and therefore has an influence on the thermal room conditions. C_{eff} is calculated in the DIN 4108-6 (2003) as follows:

$$C_{eff} = \Sigma(\rho \cdot c \cdot s \cdot A) \qquad \text{Eq. (2.1)}$$

where ρ = density [kg/m^3], c = heat capacity [J/(kg·K)], s = thickness [m] and A = surface area [m^2] of each building component. Typically, the first 10cm (approx.) of the building fabric adjacent to the room interior, the so-called effective heat storage thickness, takes part in the thermal room heat transfer processes (DIN 4108-6 (2003)). Thus, for the calculation of Eq. (2.1) only building fabric layers with a thermal

conductivity of $\lambda<0.1$W/(m·K) and up to a total thickness of 10cm from the interior room surfaces should be considered. If there is an insulation layer in the construction (i.e. defined as materials with $\lambda\geq0.1$W/(m·K) and a thermal transmittance $U<0.04$W/(m^2·K)) then only the thickness up to the insulation layer should be used. Materials of high density and a high specific heat capacity can store significant amounts of heat and are therefore referred to as materials with high thermal mass. Commonly used building components with high thermal mass are common concrete, bricks and tiles. Materials such as the gypsum plaster board contain lower thermal mass.

However, even in a building with high thermal mass, only a fraction of the heat gained at the surfaces can be transferred in the building fabric within a certain time interval due to the fabric's thermal resistivity. The reciprocal value is referred to as the thermal conductivity, λ [W/(m·K)]. Another important thermal parameter is the thermal inertia represented by the product of the density, ρ [kg/m^3], and heat capacity, c [J/(kg·K)], and is the resistance of a material to temperature changes being responsible for the amount of heat storage possible in the building fabric. Thermal conductivity and thermal inertia are correlated by the transient heat conduction equation:

$$\frac{\partial T}{\partial t} = a \cdot \frac{\partial^2 T}{\partial x^2} \qquad \text{Eq. (2.2)}$$

$$\text{where } a = \frac{\lambda}{\rho \cdot c} \qquad \text{Eq. (2.3)}$$

with t = time [s], x = distance from the surface [m], T = temperature at x [K] and a = thermal diffusivity [m^2/s]. The thermal diffusivity determines the speed of temperature wave propagation in a material.

High thermal mass building elements lead to smaller diurnal temperature swings and to a time lag in peak room temperatures relative to the ambient conditions and room heat gains. However, Santamouris and Asimakopolous (1996) pointed out that "the very properties that make a wall perform well as an interior thermal storage element, will make it perform poorly as an exterior envelope insulating element". Thus, an interior thermal storage element should consist of a high thermal mass with a high thermal

conductivity whereas an insulating exterior wall should contain a low thermal conductivity.

2.2.2 Surface heat transfer

The efficiency of the building structure to absorb and release heat depends significantly on the surface heat transfer, i.e. the heat which is exchanged between the building fabric and its environment. The dominating mechanisms of surface heat transfer are radiation and convection (for details about the physical principles see sections 3.3.1 and 3.4.1).

The principle of radiation, a mass-less heat transfer between the surfaces which enclose the space, is quite well understood and many analytical and numerical solutions exist for calculation of radiative heat transfer (see section 3.4). Therefore it is not further described in this section.

Convection is the mechanism of mass transport which is also the dominating parameter responsible for energy transport within the air space. Therefore convection has a high influence on the surface heat transfer between the building fabric and the air.
Convection is divided in two groups:

Forced convection, which is mass and energy transport due to momentum forces (e.g. instigated by fans). This type of flow contains typically high turbulences (i.e. fluctuations in the momentum) since the velocity is relatively high. The non-dimensional turbulence Reynolds number, Re_t, is often used to determine the amount of turbulence of flow (see for example Wyrwa 2003):

$$Re_t = \frac{v_a \cdot l}{\nu} \qquad \text{Eq. (2.4)}$$

with v_a = variance of velocity due to turbulences in the air flow [m/s], l = macroscopic length scale the turbulence [m] and ν = kinematic viscosity [m^2/s].

However, in buildings forced flow normally exist only close to the inlets of mechanical systems and is therefore normally not relevant (an exception is, for example, the Coanda-effect) for the near wall region and therefore not relevant for the most of the

convective surface heat transfer. Hence forced convection is not further described in more detail here.

The other type of convection, which is dominating in buildings, is free convection. It is mass transport due to unsteady natural density gradients (i.e. wind and temperature differences). Since warm air has a lower density than cool air, the air rises driven by buoyancy. Thus, if the temperature of the surface is different to that of the adjacent air, heat transfer occurs there leading to a change of the air temperature close to the wall. Consequently the air moves (rises or falls) due to buoyancy which leads to the so-called convective surface heat transfer. Since the air speed from free convection is typically significantly smaller than for forced flow, the Re_t is also smaller and is called low-Reynolds flow. However, the fluctuations are still quite high and lead to unstable flow patterns which are difficult to determine experimentally and numerically. If free and forced convection coexist, then it is called mixed convection.

The amount of convective heat transported from the surface depends significantly on the air flow patterns in the near wall region. Therefore the flow in the near wall region is briefly described in the following for cool air of initially zero speed (i.e. free convection case) adjacent to a hot vertical surface (see Figure 2.1). The near wall region in which the air flow and temperature distribution is influenced by the wall is called the hydraulic wall boundary layer and the thermal wall boundary layer respectively (Wagner 1998). For air, the thermal wall boundary layer thickness, δ_T [m], is slightly larger compared with the hydraulic wall boundary layer thickness, δ [m].

The boundary layer thickness is zero at the leading edge of the plate. Further away, the warm surface (T_s) warms the adjacent air (T_a) which leads to a rise of the flow due to buoyancy. A laminar boundary layer develops which increases gradually as the flow passes along the plate. Molecular viscosity is the dominant heat transport mechanism and hence diffusion and heat conduction are dominating the heat transfer process within this layer. At some point transition to turbulence occurs. Transition exists when diffusion (i.e. molecular viscosity) and convection (i.e. turbulent viscosity) likewise affect the flow (see more information in section 3.3.1). This occurs at $Re_{critical} \approx 3 \cdot 10^5$ (Wagner 1998). At the transition point the flow is unstable and the flow regime is

continuously altering between laminar and turbulent flow. Afterwards, further apart from the leading edge the flow regime is fully turbulent and the total boundary layer thickness rapidly increases (see Figure 2.1). The boundary layer is then separated in a turbulent outer layer where turbulent viscosity effects are dominating, a laminar sub-layer at the wall where molecular viscosity is prevailing and a small buffer layer in-between these layers where both forces are coherent.

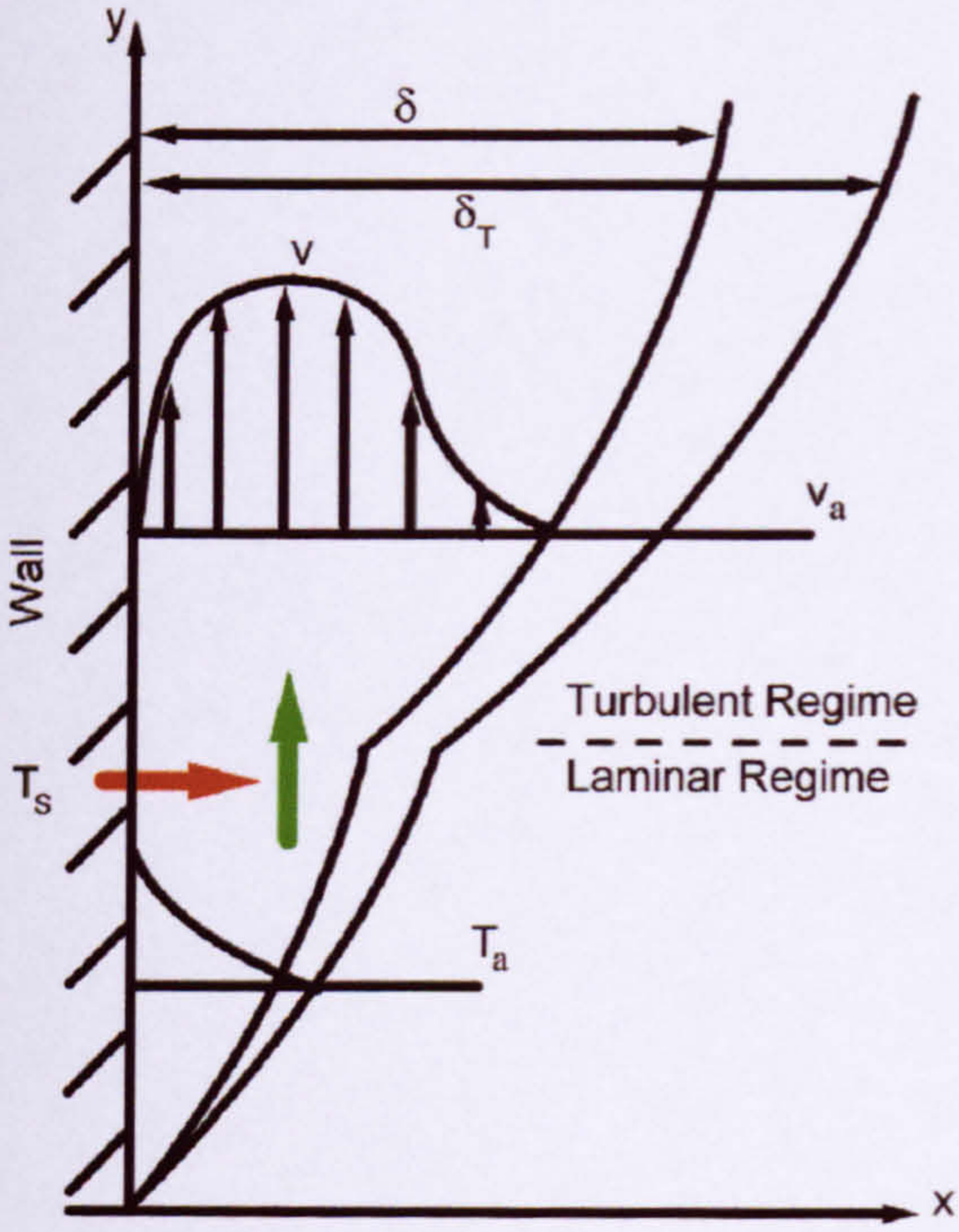

Figure 2.1: Sketch of the wall boundary layer for low-Reynolds numbers. Due to heat transfer from the wall to the adjacent air (red arrow) the air rises because of the reduced density (green arrow).

Figure 2.1 shows the velocity profile which typically develops within the turbulent flow regime. The speed, v_a [m/s], approaches zero near the wall surface due to shear stresses caused by the viscosity of the air. The velocity gradient normal to the surface causes resistance which significantly reduces the convective surface heat transfer. After a velocity peak the speed falls again in the outer layer region until it approaches the velocity of flow outside the hydraulic wall boundary layer, since the density differences are reduced due to turbulent mixing with the air in the outer layer which leads to

reduced buoyancy forces. The temperature profile falls exponentially between the wall and the air temperature outside the thermal wall boundary layer. The numerical methods for predicting the wall boundary layer for free convection are described in section 2.3.4. The significance of the local wall boundary layer profiles on the spatial convective heat transfer is for example shown in section 3.3.2.

The wall boundary layer for forced flow is different to that of free convection and can be reasonably approximated by logarithmic laws as described in section 2.3.4. It is not described here for the reasons described above for forced flow in buildings.

2.2.3 Air flow distribution

For effective night-time ventilation design it is important to achieve a high convective surface heat transfer by optimizing the contact of the cool ambient air with high thermal mass building components (Saeidi and Khodadadi 2006). Consequently the ventilation system (whether naturally or mechanically driven) should be designed such that air is encouraged to flow across surfaces. However, this is not always possible. For example, single-sided ventilation through a window might lead to short-circuiting leaving rear parts of the room with insufficient ventilation for effective night cooling. A cross-ventilation strategy can potentially lead to improved distribution of fresh air and greater contact of fresh air with the thermal mass. Gratia et al. (2004) investigated numerically the influence of several combinations of opening positions for single-sided and cross ventilation strategies on the overall night-time cooling efficiency. They found that a single-sided ventilation strategy was more effective than cross-ventilation using the same ventilation rate, however, larger opening areas were necessary for the single-sided case to achieve the same ventilation rate. Suspended ceilings (comprising for example polystyrene tiles) are sometimes used in offices which can potentially lead to a reduction of the contact of the room air with the concrete ceiling. However, specific ventilation strategies are possible to reactivate the thermal mass of the concrete in these cases (Barnard 2002).

2.2.4 Weather conditions

The air speed in occupation zones during occupancy periods is limited for thermal comfort reasons (DIN EN 13779 (2005)) which often restricts the air flow rate at the inlets and outlets for mechanical or at the openings for natural ventilation systems. Outside these periods, this restriction is lifted and higher ventilation rates are theoretically possible compared with occupancy periods which consequently lead to an increased efficiency of night-time ventilation. However, weather conditions (e.g. wind speed and temperature) can restrict natural ventilation rates. Furthermore, ambient temperatures should not fall below the dew point without preconditioning to avoid condensation inside the building. Additionally, if the external temperatures are very low, care is needed to avoid over-cooling the building at night to avoid unnecessary pre-heating before occupancy.

2.3 Building simulation

2.3.1 Building simulation program types

Two main types of simulation programs have been established for building thermal and air flow analysis: Zonal dynamic thermal simulation (DTS) programs and computational fluid dynamics (CFD) models. Each type is suited to specific types of application.

DTS programs

Using zonal DTS programs such as TAS (2006), IES (2006), TRNSYS (2006), DOE-2 (1995) and ESP-r (Pfafferott and Henkel 2003) parametric and design studies can be examined relatively quickly to predict the thermal and energy performance of a building for several months or years. This is possible by accepting that only spatially averaged temperatures (i.e. assuming that the room air is perfectly mixed) and one-dimensional heat fluxes are calculated. Typically only one 'node' is used to represent a thermal zone in which the energy heat transfer is calculated. Thus the effect of air flow patterns and temperature distribution throughout a space cannot be investigated. However, results can vary from real building behaviour if detailed airflow is neglected (Zhai et al. 2001).

For example, in high spaces such as atria where temperature stratification often occurs this can lead to large prediction errors of surface heat transfer. For DTS programs the convective surface heat transfer is approximated by specifying mean convective surface heat transfer coefficients which are either based on empirical data for certain configurations or on assumptions made by the user (see also section 2.3.4). Furthermore, transient storage effects in the building structure are calculated using one-dimensional transfer functions such as implemented in TRNSYS (2005). Common differences of simulation capabilities of several dynamic thermal simulation programs are summarized by Crawley et al. (2005).

By combining DTS with network air flow models such as COMIS (Feustel and Raynor-Hoosen 1990) and CONTAM (Walton 1997), the effect of air flow from one zone to another can be approximated. Here the mean air change and infiltration rates between zones and between the interior and exterior are considered by taking into account pressure differences generated by wind and buoyancy. However, the limitation of failing to predict local spatial variations in environmental conditions still remains.

CFD programs

CFD programs such as CFX (2006), FLUENT (2006), PHOENICS (2006) and FLOVENT (2006) are based on the Finite Volume Method (FVM) whereby each domain fluid and solid domain is discretised using small volume elements (Versteeg and Malalasekera 1995). Thus, CFD is potentially capable of predicting complex spatial flow and energy distributions in a domain. The assembly of all the finite volumes is called the 'mesh' (see also section A.6). The properties are assumed to be homogenous within each cell which is similar to DTS but at a much finer resolution. However, in contrast to DTS where only energy and mass equations are calculated, CFD also solves the momentum conservation equations for each spatial direction. These five equations are called the Navier Stokes equations (see section A.1). Several mathematical models are provided in the CFD programs to solve these equations including the effects of turbulence. Radiative heat transfer is calculated by the radiative heat transport equation for which various radiation models are provided in CFD. Further details of the relevant CFD models used within this research are provided in chapter A.

The very first CFD codes developed, calculated the air flow patterns and temperature distributions in fluid domains only. Modern CFD programs such as CFX (2006) can calculate the temperature fields in solid and fluid domains simultaneously by a coupled calculation approach for the energy transport equations within these domains. Energy equations which are used for fluid and solid domains are Eq. (A.3) and (A.4) respectively. This is called conjugate heat transfer (CHT) (see section A.1). This approach is required for a CFD program to simulate dynamic thermal behaviour of buildings.

The more volume elements that are used the higher normally the prediction accuracy since high spatial gradients of pressure, velocity and temperature can be represented more accurately. However, an increase of the elements leads to an increase in complexity of the solution matrix for all equations in the model and consequently often leads to higher convergence problems and to a significant increase of computational resources required. In practical terms it is therefore necessary to find a trade-off between accuracy and computational effort. Due to the small time scale over which air flow patterns can change for weak and unstable air flow, a small time discretisation (i.e. time step) is required for dynamic simulations to represent the turbulent nature of fluid flow accurately. In this context, simulations carried out using time steps in the order of minutes for the air flow are therefore questionable as stated by Haupt (2001). Hensen (1999), Jones and Kippenberg (2000) and Haupt (2001) pointed out that transient CFD procedures are currently impractical for dynamic thermal building simulations due to the small time-scales required for these programs. This is also reflected by the literature review in which many publications were found for the application of CFD to steady-state cases but very few were found using pure CFD for the investigation of the dynamic thermal behaviour of buildings.

2.3.2 Program coupling methods

To overcome the limitations of each technique, CFD and DTS programs are sometimes coupled. The air flow patterns typically change relatively slowly for free convection in buildings, since the thermal conditions in the building fabric change only slowly due to the high thermal inertia. During the period of small changes in thermal conditions a

DTS program can be used. If thermal conditions have changed significantly, CFD is then used to update the air flow patterns and hence to adjust the convective surface heat transfer to the actual thermal conditions, which is important for accurate predictions of dynamic thermal behaviour of buildings using DTS. The same principle can be used for flow driven by mechanical ventilation systems by updating the flow patterns using CFD if the speed at the inlets has changed notably. Examples of coupling procedures are described in Setrakian and McLean (1991), Kendrick (1993), Negrao (1995), Hensen (1999), Beausoleil-M. et al. (2001) and Zhengen (2002). Typical coupling approaches are the 'ping-pong' principle (i.e. sequential) or 'onion' principle where data is dynamically exchanged between both programs (Zhai et al. 2001 and Hensen 1999). However, there are drawbacks to these coupling techniques. For example, results can become inaccurate because information is lost during the data transfer due to different levels of detail between the two program types (Holmes and Davies 2003). For example, when Zhai and Chen (2005) and Beausoleil-M. (2000) predicted the natural convection in a room containing a radiator, the coupled building simulation predicted the response of the room air to the changes of heat gain from the radiator faster than experimental tests. Also, the position of the radiator can not be determined by the zonal program which leads to erroneous predictions of heat distribution during the simulation periods. However, the predicted thermal response of the room is at least improved using the coupled approach compared with the prediction of a pure DTS program (Negrao 1998). Another problem which can occur if a steady-state solution scheme is used for CFD simulations to update air flow patterns and thermal fields is that transient effects due to thermal inertia are neglected (see section 2.3.3).

An improvement in accuracy was demonstrated by Chen and Van der Kooi (1988) for air flow and temperature distributions using a coupled cooling load and air flow program despite the use of a coarse grid. However, this model still required the data input from a coupled external CFD program for updating the environmental patterns after certain time intervals which leads to additional simulation effort. Moreover, the heat transfer within the solid was still one-dimensional and the predicted convective heat transfer coefficients were based on traditional wall functions for forced flow. This

can potentially lead to simulation errors in room airflows dominated by natural convection.

Three main incompatibilities between CFD and DTS programs were summarized by Zhai et al. (2001) which prevent 'simple' coupling between DTS and CFD programs: the time-scale discontinuity (DTS has a characteristic time-scale of hours for building performance, while CFD only a few seconds for air), the modelling discontinuity (the indoor environmental conditions in DTS are space averaged, while CFD predicts field distributions of the variables; DTS requires heat transfer coefficients at the wall surface, while CFD requires temperature boundary conditions) and computational discontinuity (the execution time for DTS is of the order of seconds per zone per year, CFD calculations can be of the order of hours for a zone for the modelling of a single point in time).

Nevertheless, the principal idea of updating the air flow patterns only at certain time intervals as described above, i.e. only when thermal conditions or the speed at inlets of mechanical ventilation systems have changed significantly, was shown to be valuable in terms of balancing computational efficiency and accuracy for dynamic building energy calculations, since the significant additional computational effort required for calculating the air flow patterns fully dynamically (i.e. within each time-step) was significantly reduced.

2.3.3 CFD methods for modelling the dynamic thermal behaviour of buildings

Since it is easier to use only one program and CFD is potentially more accurate than DTS, research is beginning to focus on finding solution methods for dynamic thermal simulation using CFD alone.

To reduce the computational effort for dynamic CFD simulations, one-dimensional finite difference schemes are sometimes applied to calculate the heat conduction in the building fabric (Marenne et al. 1998 and Takeya et al. 1998). However, this procedure might produce errors when spatial effects are important. Moreover, the time scale for

calculating the turbulences in the air flow is small which still means high computational resources are required for the simulation.

Some researchers have successfully started to use 'freeze-flow' methods (e.g. Onishi et al. 1998 and Somarathne et al. 2002) for dealing with the incompatibility of time constants (i.e. time-scale discontinuity) between convection and solid heat transfer. These methods use intermittent periods of frozen and unfrozen flow, i.e. simulation periods when only the energy equation is solved (frozen flow) and periods when all equations are solved (unfrozen flow). This approach is similar to the methods described above for the code coupling procedure between CFD and DTS programs. However, since the whole simulation runs on a CFD platform only, three dimensional effects are considered within the fluid and the solid domains. For free convection modelling in a small-scale enclosure, the CPU time required for the dynamic simulation was only 64% of the time required by a fully transient simulation in which all equations were calculated every time step (Somarathne et al. 2002). Although small cumulative errors are inevitably present with the freeze-flow procedure the errors were small (Somarathne et al. 2003). The predicted temperatures at the end of each unfrozen flow period agreed well with the fully transient CFD simulation. The method used by Somarathne was based on a transient-transient solution method using a transient solution scheme for unfrozen and frozen flow periods. Although another freeze-flow method was developed (i.e. transient-steady method, Somarathne et al. 2002) which further reduced the CPU time required, this method neglected the thermal lag of air because the unfrozen flow period was calculated using a steady-state calculation scheme. Significant simulation errors were, for example, produced using the steady-state scheme for an office room after mechanical ventilation was switched off and free convection became the only driving force (Somarathne et al. 2005).

Despite generally good performance of the freeze-flow method, the procedure contained some drawbacks. The frozen and unfrozen flow periods had to be instigated by manually stopping and restarting each period which makes the handling of the method cumbersome and time consuming for the user. Two main factors must be considered when determining the maximum lengths of the frozen flow periods to achieve high accuracy:

- thermal inertia of the building fabric: light-weight rooms require smaller periods of frozen flow.

- frequency and magnitude of boundary condition changes: rapidly changing weather conditions of high magnitude require shorter frozen flow periods.

Somarathne et al. (2002) used a simple control method which switched between frozen and unfrozen flow periods using fixed time intervals. To avoid large prediction errors the length of the frozen flow periods must be set with consideration for the period of the fastest thermal condition and air flow pattern changes expected in the room during the simulation. However, the length of the frozen flow period could be larger in other periods where the environmental conditions change only slowly, which would increase the performance of the freeze-flow method. An enhanced control method is therefore required which adapts the lengths of the frozen flow periods to the thermal room conditions. As a conclusion Somarathne et al. (2003) suggested the use of 'triggers' at the internal wall surfaces and around internal sources, which restrict the lengths of the frozen flow periods to maximum thermal condition changes of about 0.5K within these periods.

Onishi et al. (1998) developed a similar freeze-flow method for CFD for dynamically modelling mechanically conditioned rooms in which the transient flow fields were periodically stored over a certain time period. The same flow field was then used in sequence for the following simulation period. Although the temperature swing of the room temperature was close to that for a fully dynamic simulation, a phase lag was observed which was thought to be a result of the control method of the mechanical system.

From the literature review it was concluded that the most promising technique for predicting the dynamic thermal behaviour of buildings using pure CFD was that of Somarathne et al. (2002). However, the control of the freeze-flow method needs further refinement.

2.3.4 Modelling methods for convective surface heat transfer

One of the most challenging tasks in building simulation is the accurate modelling of the convective surface heat transfer (Setrakian and McLean 1991). This is also one of the main causes of differences in energy predictions between programs, resulting in deviations of up to 40% (Beausoleil-M. 1999). Modelling convective surface heat transfer for natural convection is difficult due to the nature of turbulence within low Reynolds number flows and the related treatment of flow in near-wall regions (Beausoeil-M. 1999 and Tian and Karayiannis 2000). Details are shown later in this section.

The convective surface heat transfer depends on the air flow patterns in the wall boundary layer (see section 2.2.2). Since the gradients of pressure, velocity and temperature in the wall boundary layer cannot be numerically resolved by zonal programs, simplified functions are used instead. As a consequence the convective surface heat flux, $\dot{q}_c$ [W/m^2] is calculated using Eq. (2.5):

$$\dot{q} = h_c \cdot \Delta T \qquad \text{Eq. (2.5)}$$

with h_c = convective surface heat transfer coefficient [W/m^2·K], and ΔT = temperature difference [K] between the surface and some reference which is often the average room temperature. Simplified semi-empirical correlations exist for h_c for forced, free and mixed convection (see Yuan et al. 1994, Santamouris and Asimakopolous 1996, Carrilho da Graca and Linden 2002, Awbi 1998, Beausoleil-M. 1999 and Bartak et al. 2002). However, each correlation is only valid for specific applications (i.e. geometry and air flow pattern). An approach on a per time-step basis where the appropriate function is automatically chosen was an issue for future investigation (Beausoleil-M. and Strachan 1999).

CFD programs can numerically resolve the wall boundary layer. Two general methods have been established for this: one is the use of wall-functions valid for high Reynolds numbers (i.e. for forced convection) and one is the use of the low-Reynolds method (i.e. for free convection).

For high Reynolds numbers the wall boundary layer comprises linear and (predominantly) logarithmic profiles (Awbi 1998). Since high velocity and temperature gradients exist close to the wall, a high number of mesh nodes would be necessary to numerically resolve this region. Assuming that the logarithmic profile reasonably approximates the velocity distribution near the wall, the fluid shear stress can be numerically computed as a function of the velocity at a certain distance from the wall (see Heiselberg 1998). This function is called the wall-function. Since the velocity shape in the wall boundary layer is almost mesh-size independent for high Reynolds numbers, a relatively coarse near wall mesh resolution can be applied using the wall-function, which saves computational resources. For a good representation of the flow patterns the distance of the first air node apart from the wall must lie within a non-dimensional distance, $y+$, of the wall (CFX 2006):

$$y+ = \sqrt{\frac{\tau_w}{\rho \cdot \nu^2}} \cdot \Delta y \qquad \text{Eq. (2.6)}$$

with τ_w = wall shear stress [kg/(m·s^2)] , ρ = density [kg/m^3], ν = kinematic viscosity [m^2/s] and Δy = distance of the first node from the wall [m]. A range of $20 \leq y+ \leq 100$ is required for the wall function (CFX 2006). Since pure forced air flow does typically not exist in the entire room near the surfaces, the wall-function approach might be not a suitable method to calculate the velocity profile there and is therefore not described further.

In contrast to high Reynolds number flows, no grid-independent solution exists for the wall boundary layer for low Reynolds number flows. Awbi (1998) describes this as the reason why the near wall region must be resolved numerically in this case. Furthermore, the wall-function method neglects the influence of the viscous sub-layer which is an important factor in the convective surface heat transfer for low Reynolds flows (Vieser et al. 2004 and Awbi 1998). The low-Reynolds method resolves the wall boundary layer numerically. The first air node from the wall must lie within the viscous sub-layer. Since the thickness of the sub-layer is very thin, the distance of the first node from the wall must also be very small and should lie at $y+ < 2$ (CFX 2006). To predict an accurate convective surface heat transfer in an enclosure using CFD, a distance of 0.1mm was

used by Awbi (1998) for the first node from the surfaces. This distance value is comparable with a non-dimensional range of $0.02<y+<4$ depending on the local speed at the specific room model location. Principally the low-Reynolds method can also be applied to high Reynolds number flows. However, it requires significant computational resources, and thus the wall-function approach is more practical for high Reynolds number flows.

Although the wall-function method is valid for high Reynolds numbers only, it is often used for free convection flows due to its simplicity and low computation costs and thus predict the surface heat transfer incorrectly (Mueller and Renz 1998 and Vogl 1996). Standard wall-functions should only be used for low Reynolds flows if the convective surface heat transfer is negligible (e.g. in cases where the room enclosing surfaces are adiabatic). More information about the air flow characteristics in the wall boundary layer and the derivation of mathematical models (i.e. wall function and the low-Reynolds method) can be found in Awbi (1998). Since the room dimensions are typically large relative to the strength of the buoyant driving forces, low Reynolds number flows commonly exist in many regions of the rooms. Since the thermal interaction between the building fabric and the air has a significant influence on the thermal behaviour of high thermal mass rooms, the low-Reynolds method was therefore used for CFD simulations in this research.

2.4 Modelling of night-time cooling

Meldem and Winkelmann (1995) carried out simulations of night-time cooling using DOE-2 (1995) and compared data with measurements from test houses. Temperature deviations of over 1K were observed between predictions and measurements. They suggested improving the calculation code using solid heat transfer models which consider the spatial distribution rather than using one-dimensional approximations. They also pointed out that more details of the building and the site (e.g. building material, material surface properties and ground surface temperature) are required for a precise boundary condition definition, since these directly affect the heat transfer. Similar comparisons with DOE-2 were carried out by Ren and Dalenbeck (1995) who

explained observed deviations of up to 2K as a consequence of the irregular occupancy times and user behaviour of manually controlled ventilation systems which deviated from those of the simulation model input.

Blondeau et al. (1997) verified predictions using TRNSYS (2006) with field measurements for mechanical night-time ventilation and showed small over-predictions in temperature. Although research from other authors was cited which state that the convective heat transfer coefficients must be different for high and low speeds, only coefficients for still air were used during night-time ventilation.

Marenne et al. (1998) started to investigate transient predictions of night-time ventilation in a building using a non-commercial 3D CFD code. However, the simulation lasted only for a period of 1min due to the high computational resources needed.

Flourentzou et al. (1998) noted the importance of wind effects. Although measurements were conducted by night at low wind speed, the precision of experiments was of the order of 25%. Wind fluctuations significantly influenced the air flow at the openings which had a significant effect on the investigated discharge coefficient. Alloca et al. (2003) investigated pure buoyant and wind driven assisted single-sided natural ventilation using steady-state CFD. The ventilation rate driven by pure buoyant flows could be reasonably well predicted. However, for the wind assisted ventilation the CFD significantly underestimated empirical results by 25%. They cited other authors which observed the same prediction problem for wind driven flows.

Geros et al. (1999) has demonstrated the advantage of high thermal mass for night-time ventilation using TRNSYS (2006). The peak indoor air temperature was 3K lower for high thermal mass and only 0.2K lower for light-weight buildings using night-time ventilation compared with the case in which no night-time ventilation was used. A comparison of the predictions with field measurements from Givoni (1998) showed occasional deviations of more than 1K for environmental conditions.

Geros et al. (2005) have measured microclimatic weather data in street canyons. A parametrical study was carried out using TRNSYS to investigate the differences of

night-time ventilation due to different microclimates. It was shown that the numerical result is very sensitive to the external boundary conditions used. Care is needed when the weather data from weather stations of the region is used for investigation instead of real microclimate conditions which exist around the building object.

Farvarolo and Manz (2005) used a steady-state CFD scheme to optimize the ventilation strategy for night-time ventilation. They pointed out that "the night-time cooling is an inherently transient thermal process, but current CFD techniques might not be capable of simulating the transient behaviour of real rooms in the near future due to the lack of computing power in design practises".

Although numerical predictions shown above compared favourably with the measurements for night-time ventilation, it was impossible to obtain perfect agreement (differences of about 1K were mainly displayed). This common observation might often be the consequence of the model approximations, such as one-dimensional heat conduction assumptions, unrealistic convective surface heat transfer coefficients or simplified homogeneous environmental conditions. However, the review has also shown that it is difficult to obtain accurate data from field measurement for program validation due to uncertainties in, for example, weather data and building construction properties. Although reliable measurement data might exist for light-weight rooms shown by Jensen (1995) and Lomas et al. (1997), night-time ventilation is only efficient for rooms which contain sufficient thermal mass. However, reliable experimental data for a high thermal mass test chamber which contains precise boundary conditions was not found during a refined literature review. Only one high thermal mass environmental test chamber was found for which transient measurement data exists. Kusuda and Bean (1981) investigated the night-time cooling using this test chamber. However, during the experiments they experienced a significant moisture release from the newly built building structure to the air during the daytime which had a significant influence on the thermal room conditions caused by enthalpy changes due to condensation and evaporation. This also led to deviations in temperature and cooling load predictions using TRNSYS (2006) which did not take into account these effects. Hence this data cannot be used for validation of simulations without using computationally intensive

multi-phase and phase-change modelling and without exactly knowing the initial conditions of the moisture distribution in the environmental chamber.

The literature review has also shown that investigations of night-time cooling strategies using CFD alone have been based on steady-state cases only (except Marenne et al. 1998) due to the high computational resources required. The use of CFD for modelling of coupled building energy and air flow is still very much in its infancy, as stated by Hensen (1999). Thus, a comparison of DTS predictions for night-time cooling with data from the potentially more accurate CFD is currently impossible. Building guides such as the VDI 6020-1 (2001) or CIBSE AM11 (1998) provide verification procedures for DTS programs using inter-model comparison with other DTS programs for transient simulation cases. However, verification procedures specific for night-time ventilation were not found.

It was felt that the freeze-flow method described in section 2.3.3 might be a viable option for using CFD to model dynamic thermal behaviour and to apply it to investigate night-time ventilation.

2.5 Software selection and computer power

The criteria for the selection of a CFD platform used for investigations in this research were:

- commercial CFD software in common use
- opportunity to add user-defined routines to the code
- ability to model all heat transfer mechanisms (i.e. conduction, conjugate heat transfer, convection, radiation)
- near wall treatment for low Reynolds numbers
- three-dimensional energy, mass and momentum calculation.

The state-of-the-art CFD platform CFX version 10 (2006) fulfils these requirements and has already been applied to building simulations (for example Cook et al. 2003). Thus, this CFD platform was used in this research. Although it is theoretically possible to run CFX in parallel, only one license was available for research.

The zonal program used for comparison with the CFD program was the state-of the-art program TRNSYS Version 16 (2006). This program has been well established for dynamic thermal building simulations. Results of TRNSYS have also been used as a reference in the VDI 6020-1 (2001) for verifications of other zonal building models.

Since TRNSYS contains only one-dimensional heat transfer functions for heat conduction the two-dimensional thermal bridging program HEAT2D (Blomberg 2000) was used for comparison of CFD predictions for conductive heat transfer in chapter 3.2.

Simulations in chapter 3 were conducted using a Pentium 3, 2.0GHz CPU, 1GB RAM. Simulations shown in later chapters were carried out on a Pentium 4, 3.6GHz CPU, 2GB RAM workstation. Investigations were restricted to the capability of the computer and the software.

2.6 Summary

Night-time ventilation is a passive cooling strategy which exploits the capacity of the thermal mass of a building to store internal heat during the daytime and to release it during the night to the cool ambient air which is ventilated across the building. This strategy can avoid energy consumption for mechanical systems in offices in moderate climates for certain types and use of buildings and properly designed. The main factors of influence for a high cooling efficiency have been discussed (i.e. fabric material properties, surface heat transfer, flow distribution and weather conditions).

Simulation programs are required to optimise the complex interaction between the influencing parameters to optimise the efficiency of such a system. One of the main challenging problems is the modelling of free convection, which is typically driving the flow in buildings. Zonal dynamic thermal simulation programs which have emerged for

modelling dynamic thermal behaviour of buildings are simple (i.e. assumption of one-dimensional heat transfer in the building structure and mixed flow conditions for each thermal zone) which can lead to significant prediction errors. Computational Fluid Dynamics (CFD) programs are potentially more accurate since the thermal zone is discretised in many small cells and thus spatial air flow and temperature distribution can be calculated. Since significant computational resources are required for the simulations, CFD is restricted to steady-state building simulations. Coupling methods linking DTS and CFD to overcome the drawbacks of each program, however, must overcome the natural incompatibilities between both programs which are the different time-scale, the different modelling of a problem and the differences in computational effort. A so-called 'freeze-flow' method was found in the literature review, which showed promising results for predicting the dynamic thermal behaviour of buildings using CFD alone. The air flow patterns are frozen for certain time periods in which the thermal conditions are assumed to change only marginally. The reduction of equations calculated and the larger time steps used during frozen flow periods potentially leads to significant savings of computational resources. However, the control of the freeze-flow method needs further refinement. Automation is required and 'triggers' could be for example used which control the lengths of frozen and unfrozen flow periods to improve the performance of the freeze-flow method.

Field measurements and DTS programs have often been used to investigate night-time ventilation. However, there are always differences between the measured and predicted internal room air temperatures which is not only a result of uncertainties in the numerical modelling, but also of uncertainties in the field measurements. The literature review did not show any reliable experimental data from a test chamber which contains high thermal mass to validate numerical data for the prediction of night-time cooling in buildings. Comparison of DTS predictions with data from the potentially more accurate CFD is currently impossible due to the high computational resources required for the latter. DTS verification procedures from building simulation guidelines (e.g. VDI 6020-1 (2001) and CIBSE AM11 (1998)) are therefore often used. However, verification procedures specific for night-time ventilation were not found. It was felt that the freeze-

flow method found in the literature review might be a viable option for using CFD to model dynamic thermal behaviour and to apply it to investigate night-time ventilation.

CHAPTER 3

HEAT TRANSFER MODELS IN CFX

3 Heat Transfer Models in CFX

3.1 Preamble

The dynamic thermal behaviour of buildings depends on the thermal distribution in the rooms and on the portions of heat which are stored in and released from the building structure (see chapter 2.2). Thus, for an accurate prediction of the thermal behaviour of a building, a CFD program must accurately model the three mechanisms of thermal heat transfer relevant in buildings: (i) conduction, (ii) convection and (iii) radiation.

As described in section 2.3, high computational resources are required for CFD simulations due to the spatial discretisation of the thermal zone in many finite elements. It has therefore been mainly used for investigation of steady-state cases only. The first paragraphs in sections 3.2-3.4 comprise a literature review about the verification of models in CFX Version 5 and later to predict the heat transfer mechanisms relevant in buildings accurately. The review has shown that verification of modelling conduction, free convection and radiation is still required. The purpose of this chapter is to verify these heat transfer mechanisms, investigating each mechanism separately. Analytical solutions and experimental data were used to verify heat transfer models in CFX.

Each heat transfer mechanism is discussed separately in sections 3.2, 3.3 and 3.4. Each section contains a theoretical background, analytical solutions to calculate the heat transfer in or between materials and results and discussion of air flow and heat transfer model predictions which are compared with analytical solutions or experiments to verify the models. Section 3.5 comprises a summary of the verification of CFX for all heat transfer mechanisms. Various studies are carried out to investigate parameter settings for the different models in CFX to achieve accurate solutions of heat transfer and results are provided in chapter B.

3.2 Conduction

3.2.1 Theoretical background and analytical solutions

A detailed literature review did not show any verification of CFX Versions 5 and later for modelling the dynamic thermal behaviour of the building structure due to heat conduction or information about parameter settings for mathematical models in CFX. A CFX-5 study of Indinger and Shevchuk (2004) was found for the natural cooling of a thin plastic disc showing temperature deviations of up to 10% compared with an analytical solution. Descriptions of detailed model parameter settings were not described. A verification of CFX-5 for dynamic heat conduction was therefore considered necessary. A background of dynamic heat conduction and analytical solutions are described in the following.

Heat transport, $\dot{q}$ [W/m^2], by conduction occurs due to temperature differences and is described by the law of Fourier in the general form (Wagner 1998):

$$\dot{q} = -\lambda \cdot \frac{\partial T}{\partial s} \qquad \text{Eq. (3.1)}$$

with λ = thermal conductivity [W/(m^2·K)] and T = temperature at distance, s [m], from a reference point (e.g. wall surface).

For steady-state conditions in a material of constant λ, a simple linear correlation exists between the heat flux and the temperature gradient between two locations (see Wagner 1998). However, due to the thermal capacity of the building mass the time scale to reach steady-state conditions can be large. The temperature gradient is non-linear until steady-state conditions are reached and the term $\partial T/\partial s$ must be calculated based on the correlation of Eq. (2.2) shown in section 2.2.1 in which the temperature change depends on the time, the position and the thermal diffusivity (see Eq. (2.3)). However, a general analytical solution of Eq. (2.2) is not possible since the equation is non-linear. Only for certain cases of transient heat conduction do some analytical formulations exist, for example the one-dimensional gradual cooling of an initial thermally homogeneous solid wall of finite thickness for which the surfaces at both sides of the wall are fixed at a

lower temperature at time zero (Wagner 1998) (see Figure 3.1). The analytical solution for this example is described in the following.

A non-dimensional temperature, Θ, is introduced here:

$$\Theta(x,t) = \frac{T - T_S}{T_w - T_S} \qquad \text{Eq. (3.2)}$$

with T_w = initial wall temperature [K], T_S = surface temperature [K] and T = analytically calculated temperature within the solid [K]. Depending on the time elapsed after time zero, Θ is determined using two different approximations.

For a small time scale:

$$\Theta = \text{erf}(z) \qquad \text{Eq. (3.3)}$$

$$z = \frac{x_1}{2 \cdot \sqrt{a \cdot t}} \qquad \text{Eq. (3.4)}$$

where erf (z) = error function of Gauß, x_1 = distance between the wall surface and the location of temperature calculation [m], t = time elapsed after time zero [s], z = auxiliary non-dimensional variable linking x_1 and t [-] and a = thermal diffusivity [m^2/s]. Solutions for the error function can for example be obtained from diagrams in relevant literature for different z values (e.g. Wagner 1998).

For a large time scale:

$$\Theta = \frac{4}{\pi} \cdot \cos\left(\frac{\pi}{2} \cdot \frac{x_2}{X}\right) \cdot e^{-\frac{\pi^2}{4} \frac{a \cdot t}{X^2}} \qquad \text{Eq. (3.5)}$$

where x_2 = distance between the wall symmetry plane and the location of temperature calculation [m], X = half distance of the total wall thickness [m].

By inserting Eq. (3.3) or (3.5) in Eq. (3.2), the temperature at any time at any location in the solid can be calculated analytically. The surface heat flux, $\dot{q}$ [$W/(m^2 \cdot K)$], at a specific time, t [s], is then calculated as follows (Wagner 1998):

$$\dot{q} = \sqrt{\frac{\lambda \cdot \rho \cdot c}{\pi \cdot t}}(T_w - T_S) \qquad \text{for small time scales} \qquad \text{Eq. (3.6)}$$

$$\dot{q} = \frac{2 \cdot \lambda}{X} \cdot e^{-\frac{\pi^2 \cdot a \cdot t}{4 \cdot X^2}} \cdot (T_w - T_S) \qquad \text{for large time scales} \qquad \text{Eq. (3.7)}$$

3.2.2 Verification of modelling heat conduction using CFX

Model description

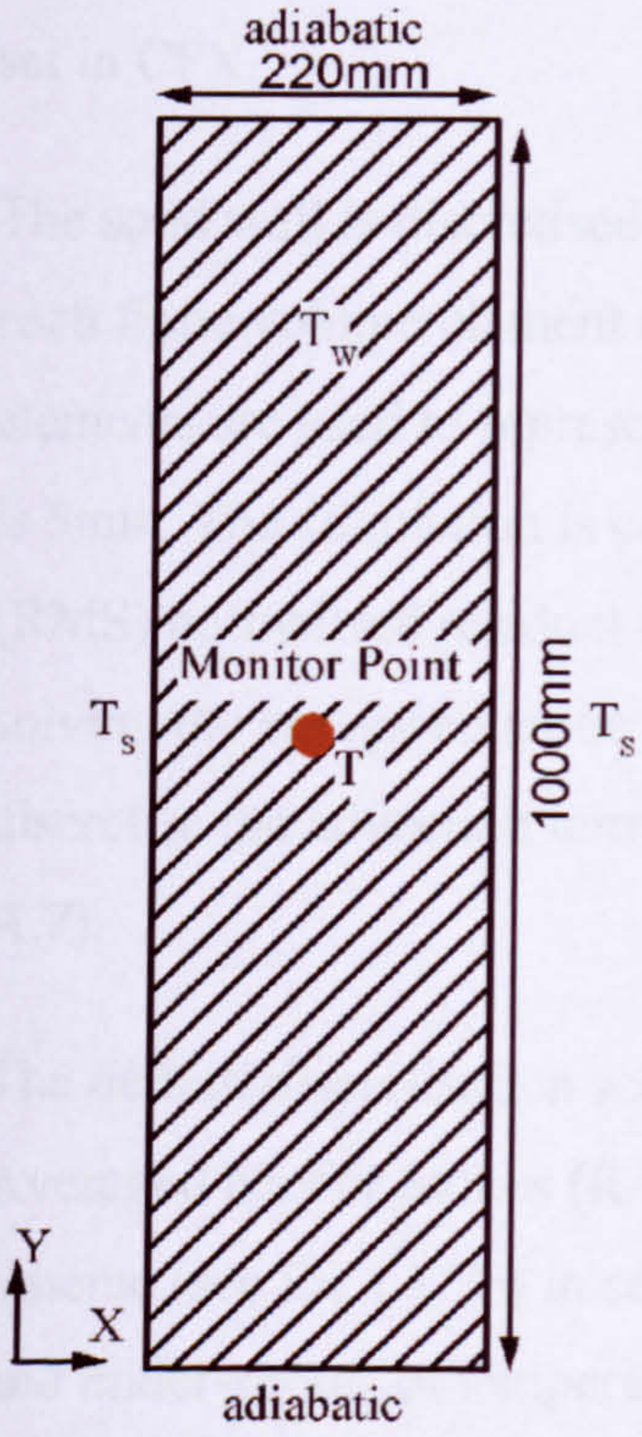

Figure 3.1: Sketch of the brick wall model for verification of modelling heat conduction with CFX.

The 2D model contains a solid brick wall (λ=0.72W/(m·K), ρ=1920Kg/m^3 and c=835J/(Kg·K)) with dimensions of Y=1.00m and X=0.22m (see Figure 3.1). The wall has an initial temperature of T_w=27°C; the surface temperatures are fixed at T_s=23.75°C at both sides of the wall. Horizontal boundaries are adiabatic. The monitor point at x/Y=0.5 and y/Y=0.5 displayed in Figure 3.1 is used for evaluation of the transient

temperature change in the solid due to the cooler surface temperatures compared to the initial internal wall temperature.

Model implementation in CFX

Based on the boundary conditions the temperature changes in the solid are one-dimensional in x-direction. Generally, a 2D geometry cannot be calculated in CFX since it is based on the Finite Volume Method. A quasi-2D geometry is therefore used, i.e. a model depth of one finite volume element, and the z-planes form symmetry boundaries. Section A.5 shows how symmetry, adiabatic and temperature boundary conditions are set in CFX.

The solid wall is discretised using a fine mesh with an edge length scale of 10mm for each finite volume element to obtain high accuracy. A total number of 34,600 volume elements are used to represent the geometry. The time discretisation (i.e. time step size) is 5min. The simulation is considered to have converged if the Root Mean Square (RMS) normalised residual (see section A.8 and Eq. (A.28)) of 10^{-5} is achieved for solving the energy equation (Eq. (A.15)). A high resolution advection scheme is used to discretise the advection term in transport equations by using Eq. (A.26) (see section A.7).

The default discretisation scheme for solving the transient term in the Reynolds Averaged Navier Stokes (RANS) equations in CFX is the 2nd order backward Euler scheme (see Eq. (A.25) in section A.7). A preliminary study has shown numerical over- and under-shoots of temperatures in the solid at different monitoring points during the simulation (see section B.1). These over- and under-shoots are a typical drawback of the 2nd order-backward Euler scheme (Eq. (A.25)) as described in the CFX user manual (CFX 2006). The 1st order backward Euler scheme (Eq. (A.24)) is therefore used in the following study.

Results and Discussion

The temperature predictions for CFX at the monitor point shown in Figure 3.1 are compared with the analytical solution described in section 3.2.1 using Eqs. (3.2)-(3.5)

and a numerical solution for the thermal bridging program HEAT2D. The simulation has achieved the convergence criterion of RMS normalised residual of 10^{-5}.

The temperature results over a simulation period of 20h are presented in Figure 3.2. The temperature decreases exponentially due to a cooling of the solid wall from the cooler surface temperatures and reaches a steady-state solution at the end of the simulation period (i.e. solid temperature at the MP equals the surface temperature). The curve shapes of the analytical solutions for small and large time scales (i.e. for Eqs. (3.3) and (3.5)) intersect at about 1h of simulation time showing that the different analytical solutions are only valid for certain time ranges. The predictions for CFX and HEAT2D compare well with each other and compare favourably with the analytical solution for small and for large time scales (except at about 1h after the simulation start). A small deviation of less than 0.1K is shown for CFX during the simulation compared with the analytical solution.

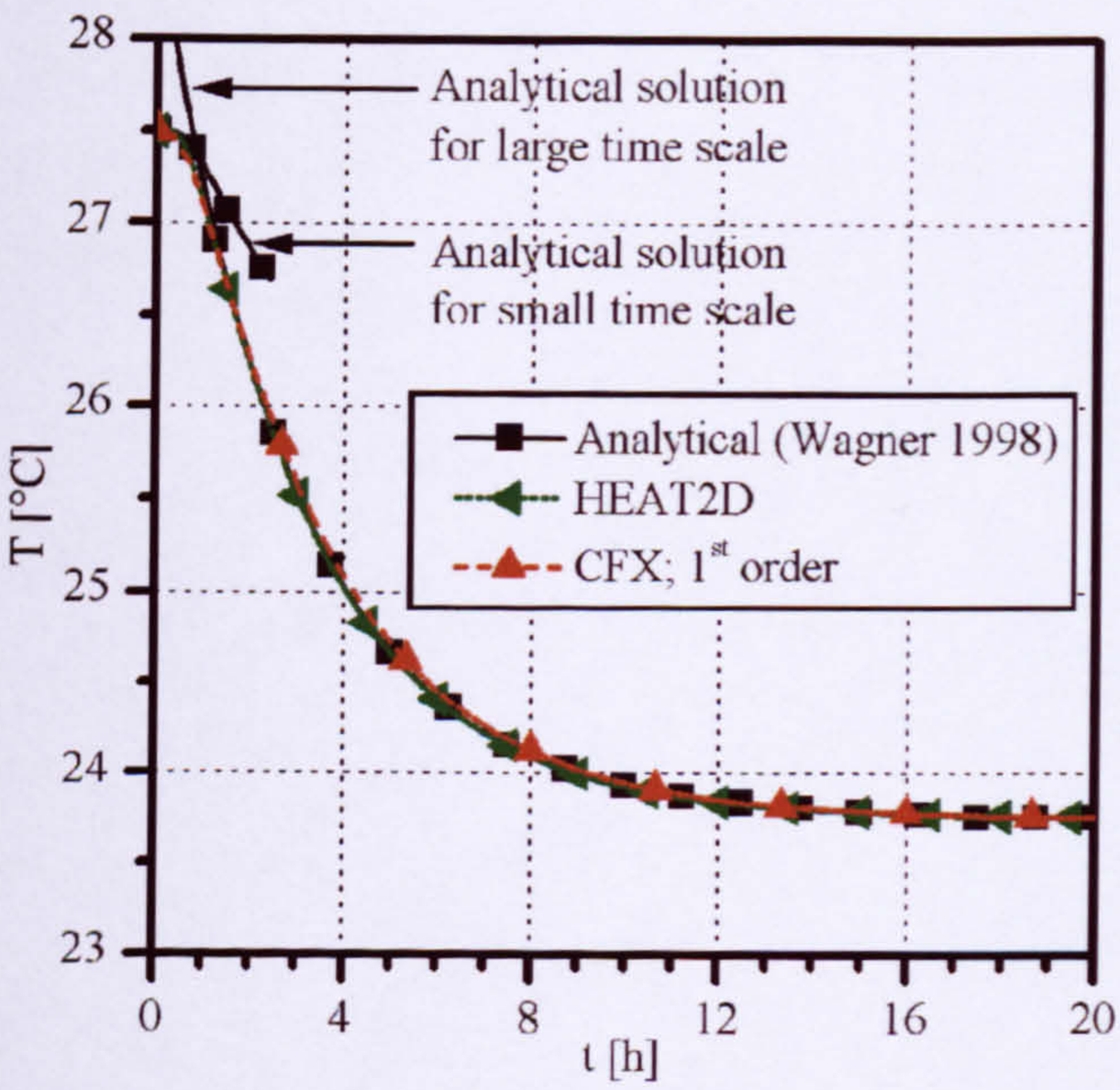

Figure 3.2: Comparison of temperature predictions for CFX using the 1st order backward Euler scheme in comparison with analytical solutions and numerical data from HEAT2D.

Calculating the surface wall heat flux after a simulation period of 4h using Eq. (3.7), the analytical solution shows a value of 13.1W/m^2. In comparison, CFX predicts a heat flux of 13.7W/m^2 (5% error).

3.3 Convection

3.3.1 Theory and analytical solutions

CFD was historically developed by the aerospace and automotive industry for predicting forced convection flow (Zhengen 2002). CFX-5 has therefore been thoroughly validated for this type of flow (e.g. Vieser et al. 2004) and recommendations for appropriate model parameter settings exist (e.g. CFX 2006). However, free convection is the main type of flow in most regions of a room and forced flow exits typically only near the inlets and outlets of a ventilation system. As described in section 2.2.2, free convection flow at the wall boundary layer has a high influence on the surface heat transfer between the building fabric and the air, and therefore highly influences the dynamic thermal behaviour of a building. Thus it is important to model free convection at the surfaces accurately. Since the air flow in the wall boundary layer depends on the air flow and thermal patterns outside the boundary layer, it is also necessary to predict the air flow patterns in the other parts accurately.

However, information about appropriate mesh and model parameter settings for CFX Versions 5 and later for free convection in buildings are rare. Garli (2003) tested CFX-5 for modelling laminar free convection flow in an enclosure. Small prism elements were used near the surfaces to resolve the steep gradients of flow in this region. However, no information about the mesh size and mathematical models and settings for CFX was given and numerical errors of up to 26% compared with benchmark solutions were displayed. Zhai and Chen (2003) showed analytically that the size of the first volume element adjacent to the surfaces is crucial for the correct prediction of convective surface heat transfer for forced convection flow. However, turbulent free convection was not investigated. The CFX user manual recommends using a low-Reynolds method for near wall treatment and a discretisation of the wall boundary layer using at least 15

volume elements and a non-dimensional distance of y+<2 (CFX 2006). Thus a direct numerical simulation of turbulent flow would require a highly refined mesh to resolve all eddies in the turbulent flow regime. Various numerical turbulence models exist in CFD to achieve a trade-off between accuracy and computational effort (see section A.3). Investigations of turbulent free convection in enclosures using CFD platforms based on structured (i.e. hexahedral finite volume element) meshes showed significant errors of surface heat transfer using the standard k-ε turbulence model (e.g. Thompson et al. 1987, Henkes and Hoogendoorn 1995, Peng and Davidson 1999). Improved accuracy was obtained using the k-ω and the SST model (Peng and Davidson 1999 and Stamou and Katsiris 2006). However, CFX-5 uses an unstructured (i.e. tetrahedral element) mesh which has the advantage that local numerical diffusion is reduced and is therefore suitable for complex flows which, for example, contain flow reversal regions (see section A.6). Verification and recommendations of model parameter settings for turbulent free convection for CFX-5 and later and settings based on unstructured meshes are still required.

Verification of CFX-5 for free convection was considered necessary from the literature review shown above. This section therefore focuses on modelling of free convection flow with respect to an accurate prediction of the convective surface heat transfer. A theoretical background of free convection and analytical solutions for the calculation of the laminar near wall boundary layer and the calculation of the related convective surface heat transfer are described in the following. For verification of heat transfer due to turbulent flow, reliable experiments were used for comparison since general analytical solutions do not exist for resolving the complex character of turbulences.

Convection can occur due to density or pressure differences in fluids (see section 2.2). The motion in convective flow can be laminar or turbulent. Laminar flow exists when a fluid flows in parallel layers without disruption between the layers due to shear stress. It is characterized by domination of diffusion and the mathematical formulation for the heat transfer is identical to that of heat conduction. In contrast, turbulence appears due to shear stresses between air layers of different speeds. The viscosity (i.e. inertia of mass) of the fluid influences the strength of the shear stress. As the speed increases, transition from laminar to turbulent flow occurs. Vortices, also called eddies, with

different length scales appear and dissipate interacting with each other and leading to fluctuations in the flow. During the dissipation the kinetic energy of the vortices are transformed into heat. In turbulent flows the convective heat transfer is high relative to diffusive heat transfer.

The characteristic motion in free convection flows can be expressed by non-dimensional numbers (Wagner 1998):

Grashof number (Gr): calculated as the ratio of buoyant to viscous forces and is an indicator for the strength of buoyancy.

$$Gr = \frac{g \cdot L^3 \cdot \beta \cdot (T_1 - T_2)}{\nu^2} \qquad \text{Eq. (3.8)}$$

with $\beta = \frac{1}{T_m}$

with L = length of the device at which the fluid is flowing along [m], g = gravity [m/s^2], ν = kinematic viscosity of the fluid [m^2/s], T_1, T_2 = temperatures at the boundary conditions [K], β = thermal expansivity [1/K] (see Eq. (A.8)) and T_m = mean temperature of T_1 and T_2 [K].

Prandtl number (Pr): the ratio between heat generation due to kinematic viscosity and heat dissipation due to thermal diffusivity ($Pr_{air} \approx 0.72$).

$$\mathrm{Pr} = \frac{\nu}{a} \qquad \text{Eq. (3.9)}$$

where a = thermal diffusivity [m^2/s]

Rayleigh number (Ra): a Rayleigh number of $Ra < 10^8$ indicates a domination of molecular heat transfer (i.e. heat conduction) and therefore a laminar flow regime; $Ra > 10^{10}$ indicates a fully turbulent flow and heat transfer occurs primarily due to viscous forces.

$$\mathrm{Ra} = \mathrm{Gr} \cdot \mathrm{Pr} \qquad \text{Eq. (3.10)}$$

Nusselt Number (Nu): measures the enhancement of heat transfer from a surface that occurs due to convection compared to the heat transferred if just conduction occurred. It is equivalent to the heat flux $\dot{q}$ since Nu and $\dot{q}$ are linearly correlated for constant λ.

$$Nu_y = \frac{\dot{q} \cdot y}{\lambda \cdot (T_1 - T_2)} \qquad \text{Eq. (3.11)}$$

where $\dot{q}$ = convective wall heat flux [W/m^2] at the local device height, y [m], λ = thermal conductivity of the air [W/(m·K)] and T_1, T_2 = the surface and air temperature respectively [K].

The theoretical local Nusselt number for *laminar* flow at a heated vertical plate can be calculated using the following analytical correlation (Philips et al. 2001):

$$Nu_y = 0.386 \cdot Ra_Y^{0.25} \cdot \left(\frac{y}{Y}\right)^{-0.25} \qquad \text{Eq. (3.12)}$$

with the Rayleigh number, Ra_Y [-], for device of length, Y [m]. As described in section 2.3.4, the CFD program must predict the air flow and thermal patterns in the wall boundary layer accurately to calculate the convective wall heat flux correctly. Analytical solutions exist to calculate the velocity, v_y [m/s], and temperature, T [K], at every point in the wall boundary layer of a heated vertical wall for laminar flow which can be used to verify CFD predictions for the wall boundary layer (Baehr and Stephan 1996 and Ostrach 1953):

$$\eta = \frac{x}{y} \cdot \left(\frac{Gr_y}{4}\right)^{0.25} \qquad \text{Eq. (3.13)}$$

$$\Theta(\eta) = \frac{T - T_a}{T_S - T_a} \qquad \text{Eq. (3.14)}$$

$$f(\eta) = \frac{v_y \cdot y}{\nu} \cdot \frac{1}{2 \cdot \sqrt{Gr_y}} \qquad \text{Eq. (3.15)}$$

where

y	local height [m]
v	kinematic viscosity [m^2/s]
v_y	local vertical velocity component [m/s]
T_a	temperature of the air outside the wall boundary layer [K]
T_S	temperature of the wall surface [K]
η	non-dimensional distance from the leading edge and the wall [-]
Θ	non-dimensional temperature [-]
$f(\eta)$	non-dimensional velocity [-]

The non-dimensional temperature and velocity in Eqs. (3.14) and (3.15) are a function of η in Eq (3.13) and can be obtained from diagrams or tables (e.g. Baehr and Stephan 1996 and Ostrach 1953). The analytical solutions of Ostrach compare well with experiments of Schmidt and Beckmann (1930). Eqs. (3.14) and (3.15) must then be resolved for v_y and T. The analytically calculated velocities and temperatures can then be used for comparison with CFD predictions. The resulting numerically predicted $\dot{q}$ can be inserted in equation Eq. (3.11) and compared with the analytical solution of Eq. (3.12).

For *turbulent* flow regimes Eq. (3.12) is not valid. Thus, experiments are for example required here which measure the velocities, temperatures and the resulting wall heat flux in the wall boundary layer. The experimental and predicted $\dot{q}$ can then be inserted in Eq. (3.11) for comparison.

3.3.2 Verification of CFX for free convection

Model Description

The 2D model is based on the experimental enclosure of Tian and Karayiannis (2000) and has dimensions of X=0.75m and Y=0.75m (Figure 3.3). Constant temperatures of

T_1=50°C and T_2=10°C are used at the isothermal vertical walls (see details about general boundary condition settings in section A.5. The Rayleigh number calculated from Eq. (3.10) for this model is $Ra=1.56 \cdot 10^9$. Hence the flow regime lies at the lower bound of the turbulent flow regime. A two-dimensional mean velocity field has been measured by Tian and Karayiannis (2000).

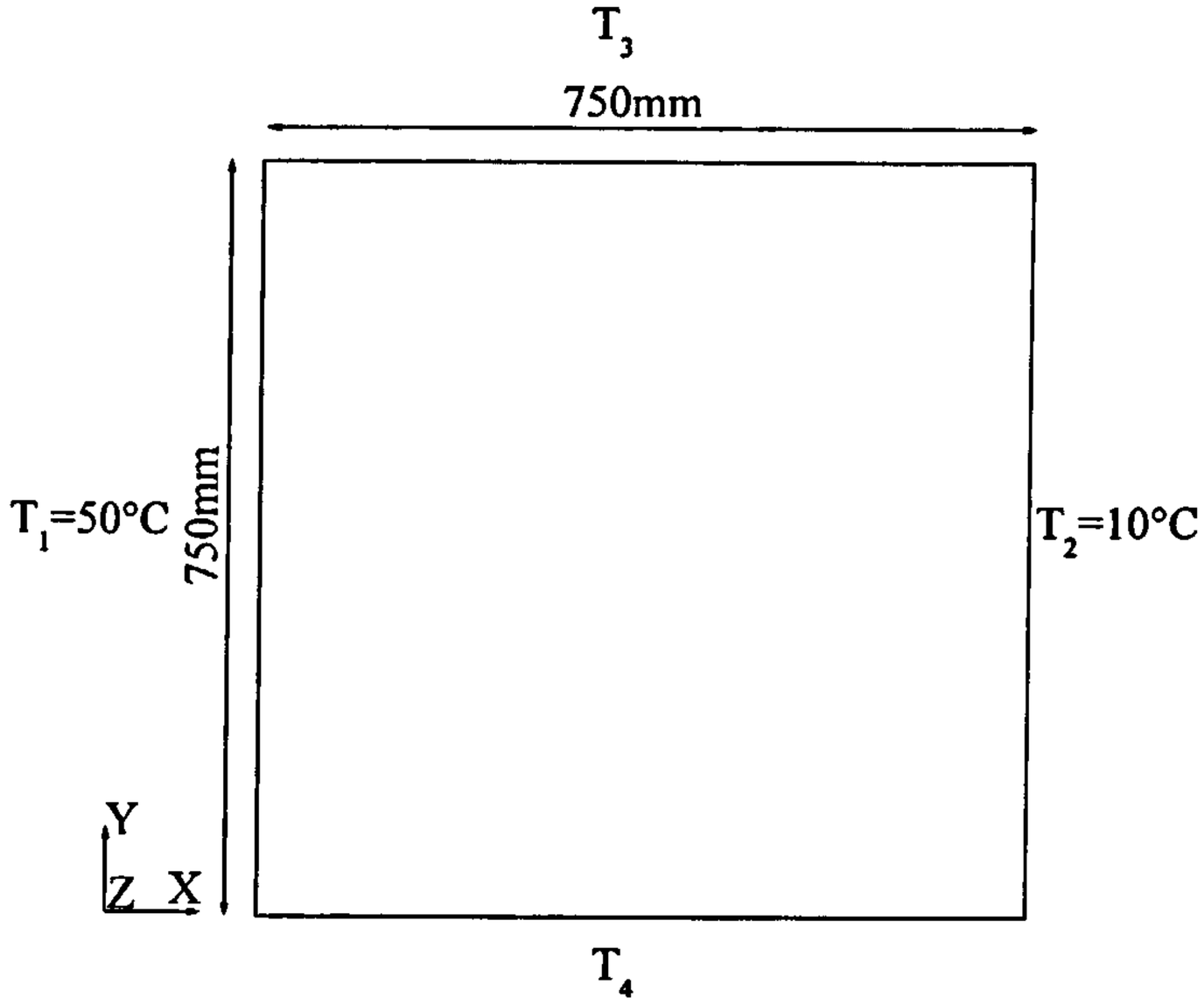

Figure 3.3: Sketch of the model for verification of modelling turbulent free convection in CFX.

The horizontal enclosure boundaries in the experiments contain insulation material and thin metal layers at the inner surfaces. For an accurate comparison of experimental with numerical results, the boundary conditions must agree exactly. However, perfect adiabatic conditions are difficult to achieve in experiments. Therefore, Tian and Karayiannis (2000) measured the temperature profiles T_3 and T_4 along the horizontal surfaces for use in numerical simulations. These profiles are adopted for the room model (see Figure 3.4).

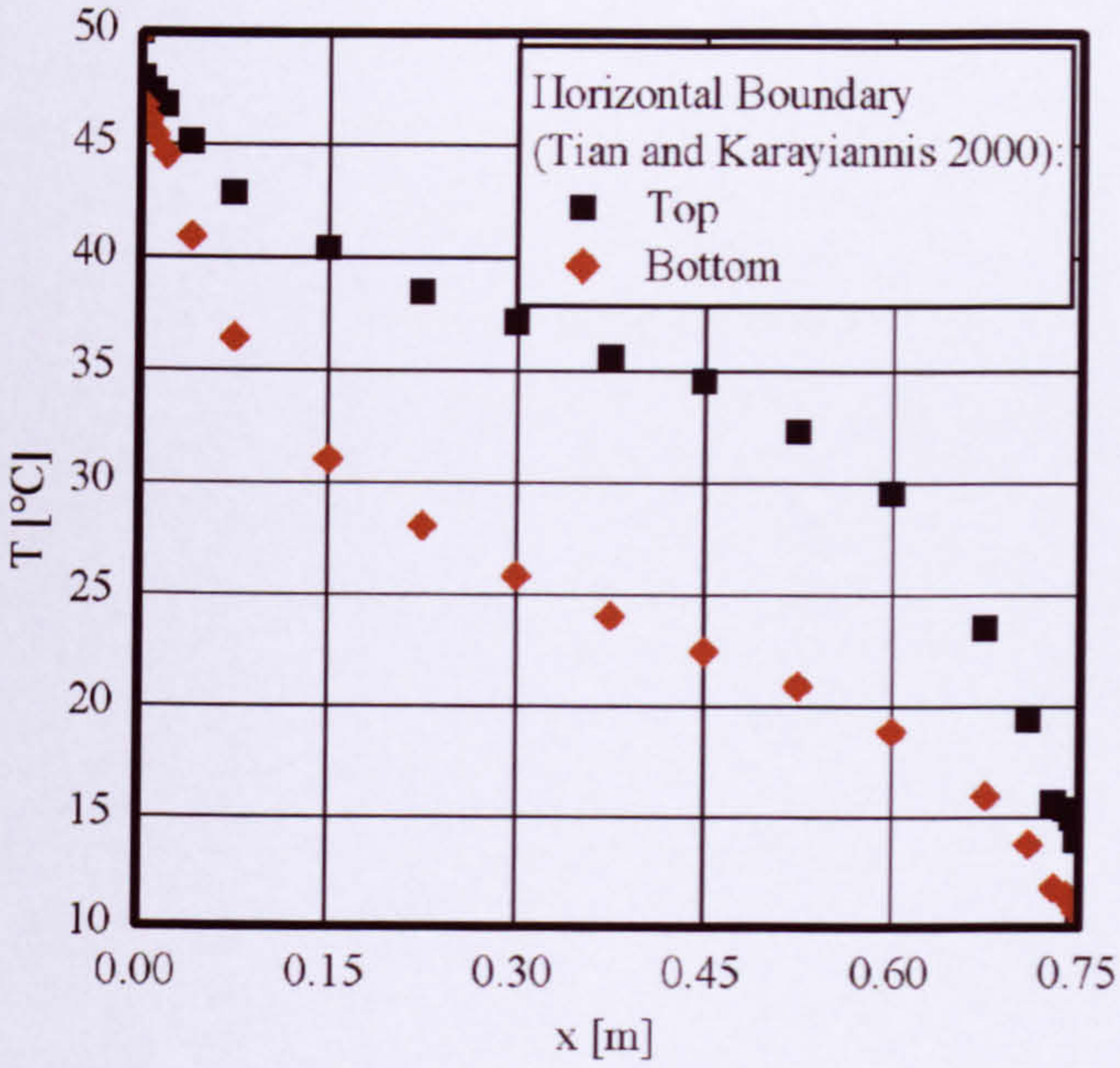

Figure 3.4: Temperature profiles measured at the horizontal top and bottom surfaces.

Model implementation in CFX

Specific parameter settings (i.e. so-called expert parameters and time scale discretisation) are adopted from section B.2.1 which are necessary to carry out steady-state simulations for free convection efficiently and accurately.

A preliminary study was carried out to investigate the influence of the mesh resolution in the wall boundary layer on the surface heat transfer comparing numerical results with analytical data for steady-state laminar flow (see section B.2.2 and a also a summary in Zitzmann et al. 2005). To reduce the computational effort required for refining the near wall boundary layer, prism elements were used in this region (see section B.2.2 for further details). The numerical solution compared favourably with analytical solution. However, it was necessary to sufficiently refine the mesh in the wall boundary layer to accurately predict the velocity and temperatures and the surface heat transfer. The surface heat transfer is particularly sensitive to the size of the first volume element away from the wall.

The mesh for the model for the investigation of turbulent free convection is based on the outcomes of the sensitivity analyses reported in section B.2.2 and suggestions in the

CFX user manual (i.e. using at least 15 prism elements and y+<2). Prisms with edge length scales of 0.1mm and 0.4mm for the first two prism layers and additional 13 prism layers with inflation factor 1.1 starting at 1mm from the walls are used. CFX calculates y+≤0.3 for Eq. (2.6) depending on the location in the room model. At the surface and the core of the room, tetrahedral elements with maximum edge length scales of 10mm and 20mm are used respectively. The mesh is refined (i.e. surface elements of 3mm edge length scale) where the vertical and horizontal walls approach each other to obtain a high numerical resolution. The model contains a total number of 53,800 volume elements. Since a 2D room model cannot be implemented in CFX a quasi-2D model is used using a model thickness of Z=10mm (c.f. section 3.2.2).

Radiative heat transfer can be neglected since all surfaces of the room enclosure are highly reflective due to the metal sheets, the boundary conditions are fixed and the absorption of air for radiation is negligible. Radiation is therefore not modelled.

To resolve the turbulences in the flow, various turbulence models exist in CFX (see for example section A.3). To resolve the wall boundary layer for low Reynolds numbers numerically, a turbulence model must be based on the ω-equation (i.e. turbulence frequency equation) because only those turbulence models in CFX use the low-Reynolds approach which has been described in section 2.3.4. Models based on the ε-equation (i.e. turbulence eddy dissipation equation) would use the wall function approach which is only valid for forced flow patterns. Several turbulence models were compared in a preliminary study which showed that the best performance was achieved using the k-ω and the Shear Stress Transport (SST) turbulence model (see section B.2.3 and a summary in Zitzmann et al. 2005). However, since a marginally better performance was shown for the k-ω model and fewer equations need to be solved compared with the SST model, the k-ω model is used here.

All RANS equations (i.e. mass, momentum and energy) and the additional equations for the k-ω turbulence model are solved (i.e. Eqs. (A.13)-(A.15) and Eqs. (A.19) and (A.20)). Simulations are considered to have converged if a RMS normalized residual of 10^{-5} is achieved for these equations. To reduce the number of iterations required for convergence, a false-time stepping method (i.e. steady-state solution scheme, see

section A.7) is imposed which uses the physical time step of the transient term as a factor to accelerate the convergence rate to achieve steady-state conditions. For high convergence rates and robust solutions the time-scale for the false-time stepping is calculated automatically in CFX (see section B.2.1).

Buoyancy is modelled using the Boussinesq approximation in which the forces are modelled as source terms in the momentum equations (see section A.2, Eq. (A.7)). The reference temperature used for this approximation is 10°C.

A high resolution advection scheme is used for the RANS equations and an upwind advection scheme is used for the k-equation and ω-equation as used by default (see details in section A.7).

The numerical room model contains an initially homogeneous temperature of 30°C for which a zero velocity field is calculated.

Results and Discussion

The spatial predictions of the air flow patterns, temperatures and surface heat transfer for CFX are compared with experimental data from Tian and Karayiannis (2000) and numerical results of Beghein et al. (1993). The convergence criterion of RMS normalised residual of 10^{-5} was achieved. Evaluation is carried out at the model mid-depth plane, z/Z=0.5.

Figure 3.5 shows the predicted and the measured velocity (vertical component) and temperature curve shapes in the wall boundary layer at y/Y=0.5. The velocity and temperature profiles compare qualitatively favourably with the measurements. The speed predicted in the region between the surface and the velocity peak are slightly higher than for the measurements (Δv=0.014m/s for the peak values, which means 6% deviation). For the outer region of the wall boundary layer, further away from the velocity peak, the prediction and measurement compare quantitatively well. The predicted temperature difference is gradually smaller with increasing distance from the wall compared with the measurement ($\Delta T_{max} \approx 1.5K$).

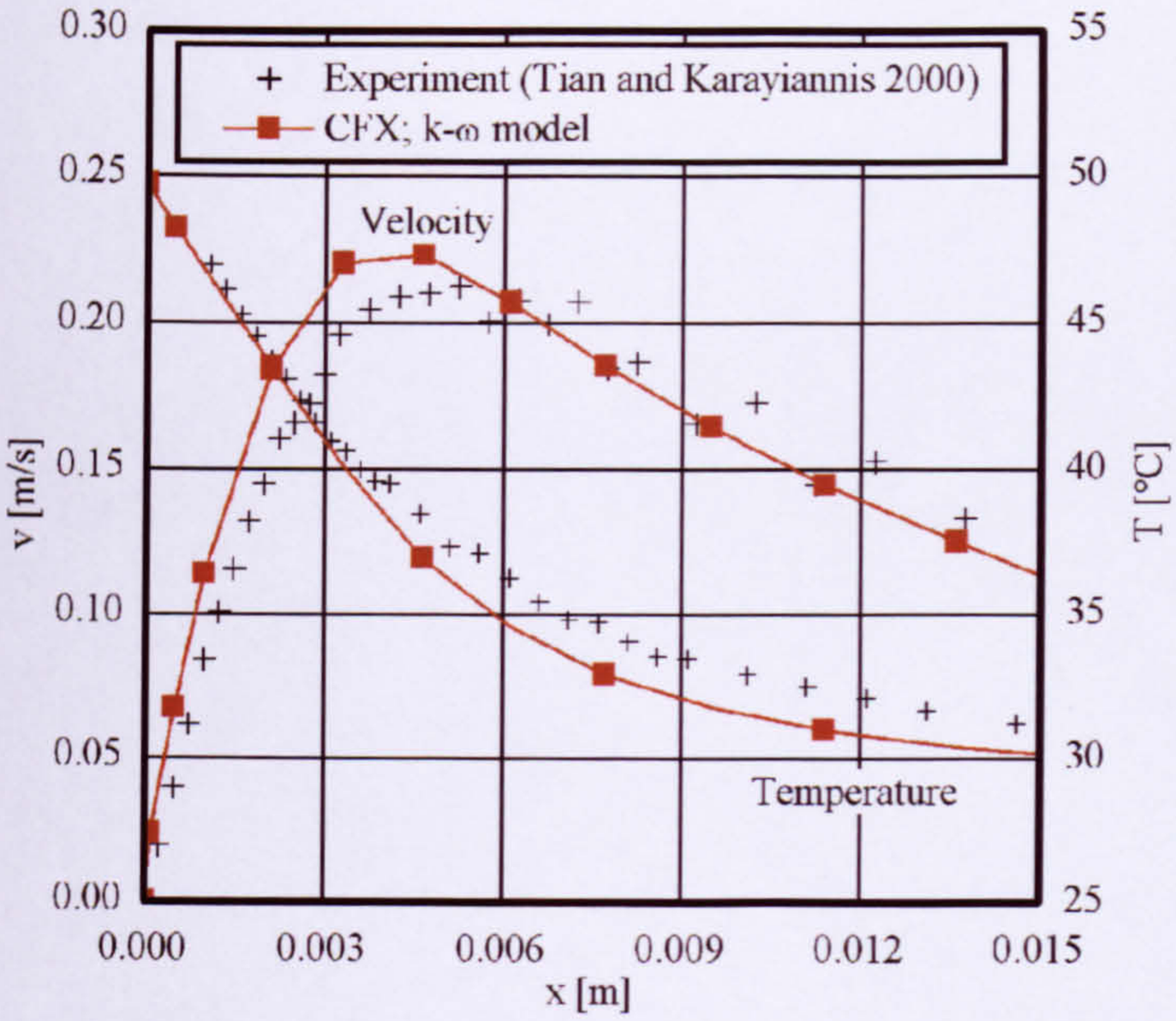

Figure 3.5: Predicted and measured velocities (vertical component) and temperatures in the wall boundary layer at the hot vertical wall at mid height for CFX using the k-ω model compared with experimental reference data.

The predicted surface heat transfer (indicated by the local Nusselt number, Nu_Y, Eq. (3.11)) along the hot vertical wall is compared with the experimental data and numerical solutions of Beghein et al. (1993) for two ideal horizontal surface boundary conditions and is presented in Figure 3.6. The heat flux gradually decreases with the cavity height which is expected since the air adjacent to the wall gradually warms while it rises along the surface leading to a decrease of the temperature difference between the surface and the air. The calculated Nusselt number from experiments at the isothermal vertical walls lies somewhere between the model of adiabatic and perfectly conducting boundary conditions for the horizontal surfaces investigated by Beghein et al. (1993), which demonstrates that a perfect adiabatic condition could not be achieved in the experiments. The prediction for CFX compares well with the prediction of Beghein et al. (1993) for the perfectly conducting boundary condition model and from the mid height to the top also favourably with the experiments ($\Delta Nu_{y,max} \approx 2$). The disagreement with the measurements at the bottom end of the vertical wall is a result of the different boundary condition. Compared with the experiment where adiabatic conditions were

used for the horizontal boundary, the numerical model uses perfectly conducting conditions. The air is warmed (i.e. 'pre-conditioned') at the horizontal surface for the numerical model which leads to a smaller temperature difference between the vertical wall bottom and the adjacent air and consequently to a smaller convective surface heat transfer compared with the experiments (see Figure 3.6).

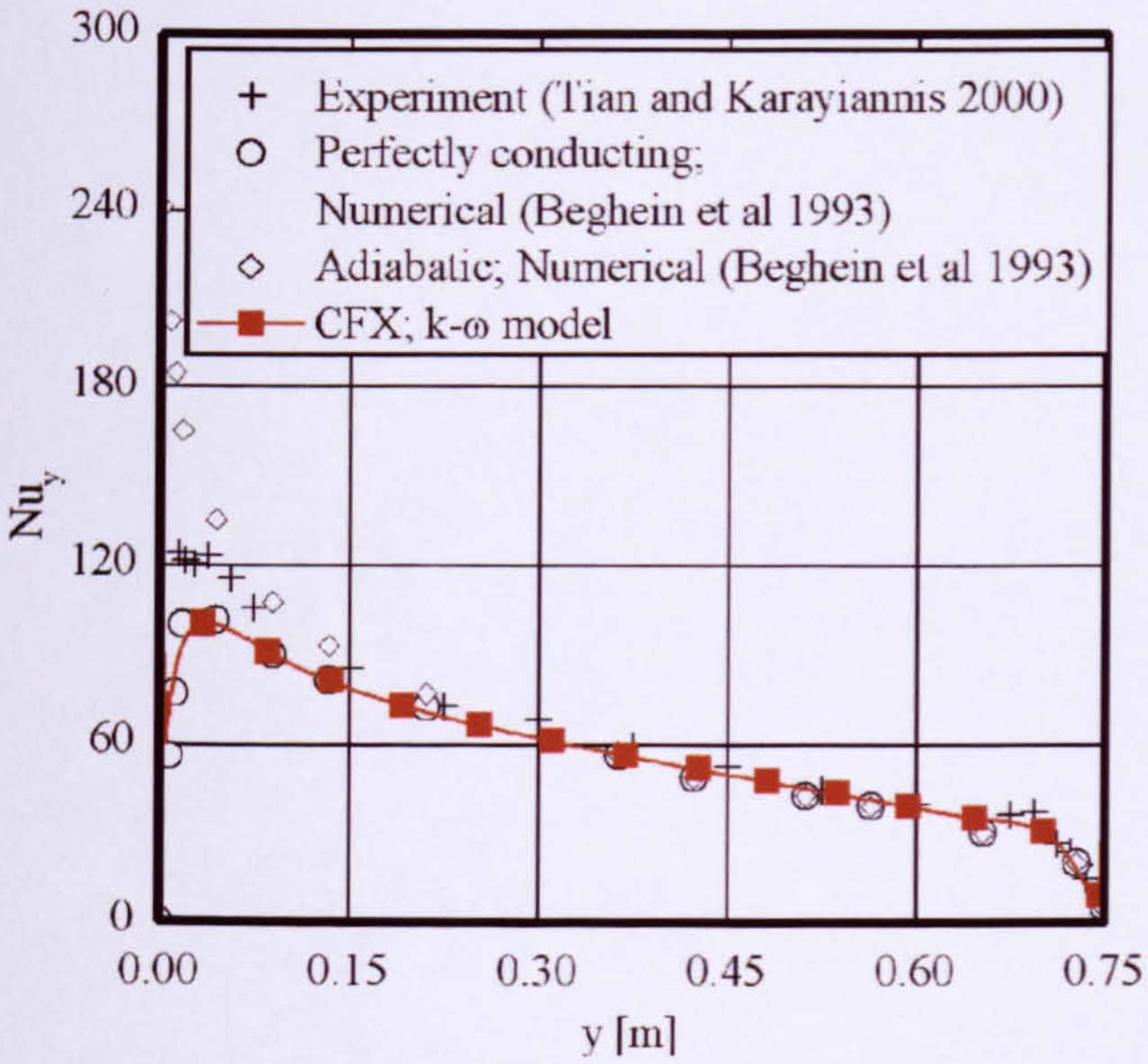

Figure 3.6: Predicted local Nusselt numbers at the vertical hot wall for different heights for CFX using the k-ω model compared with experimental and numerical reference data.

The predicted temperatures at cavity mid width for different heights for CFX compared with the experimental reference data are shown in Figure 3.7. A temperature stratification of about 20°C is displayed from the bottom to the top due to buoyancy and heat conduction. The measured temperatures are not perfectly asymmetric since the difference between the peak temperature at the low end and the temperature at mid height is smaller than for the high end of the cavity. The temperature at the mid height of the cavity should theoretically contain the mean temperature of the warm and cool vertical wall because the geometry is symmetric. The mean temperature of 30°C at the cavity mid height is well predicted for CFX. The higher temperatures in the enclosure at

mid height (1K deviation) for the experiments explain the higher temperatures at the wall boundary layer in Figure 3.4 compared with the numerical calculation.

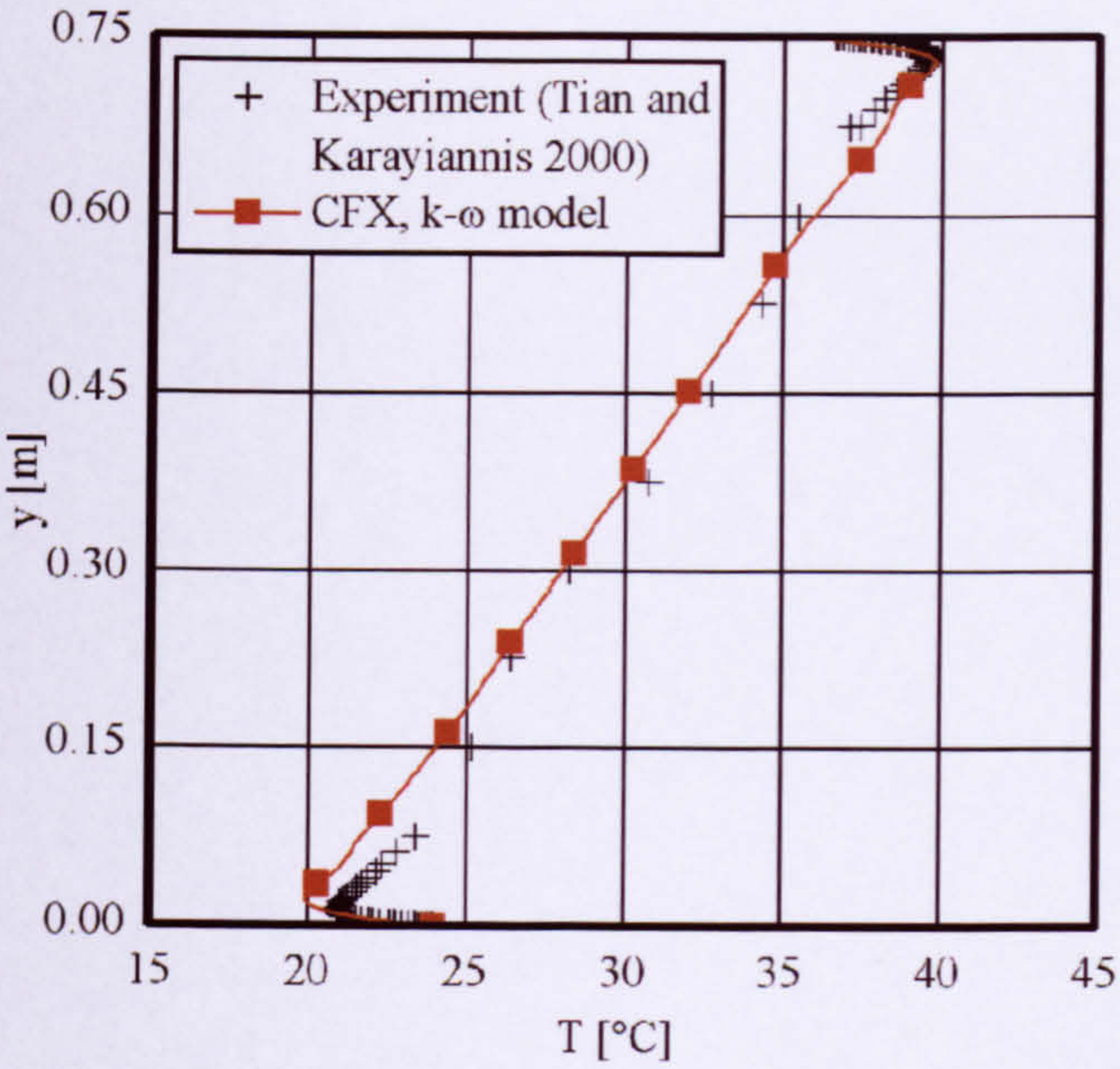

Figure 3.7: Predicted temperatures for different heights at cavity mid width for CFX using the k-ω model compared with the analytical reference data.

The u-velocity at the cavity mid width for different heights compared between numerical results for CFX and measurements are shown in Figure 3.8. The experiment shows high velocity peaks near the horizontal surfaces in clockwise direction and small peaks in the opposite direction which indicates regions of flow reversal. In comparison, the numerical solution slightly under-predicted the main flow peak values (Δu=0.01m/s which means 12.5% deviation). A reason could be the mesh resolution. However, another reason is thought to affect mainly the strength of the air speed at cavity mid width: two flow disturbances at the bottom-right and top-left corners, which were not displayed in the experiments, are shown in a velocity vector plot for the cavity mid plane (z/Z=0.5) in Figure 3.9. These disturbances lead to a distribution of the flow streams of away from the horizontal surfaces which leads to a decrease of the speed in the near wall region at the horizontal boundary.

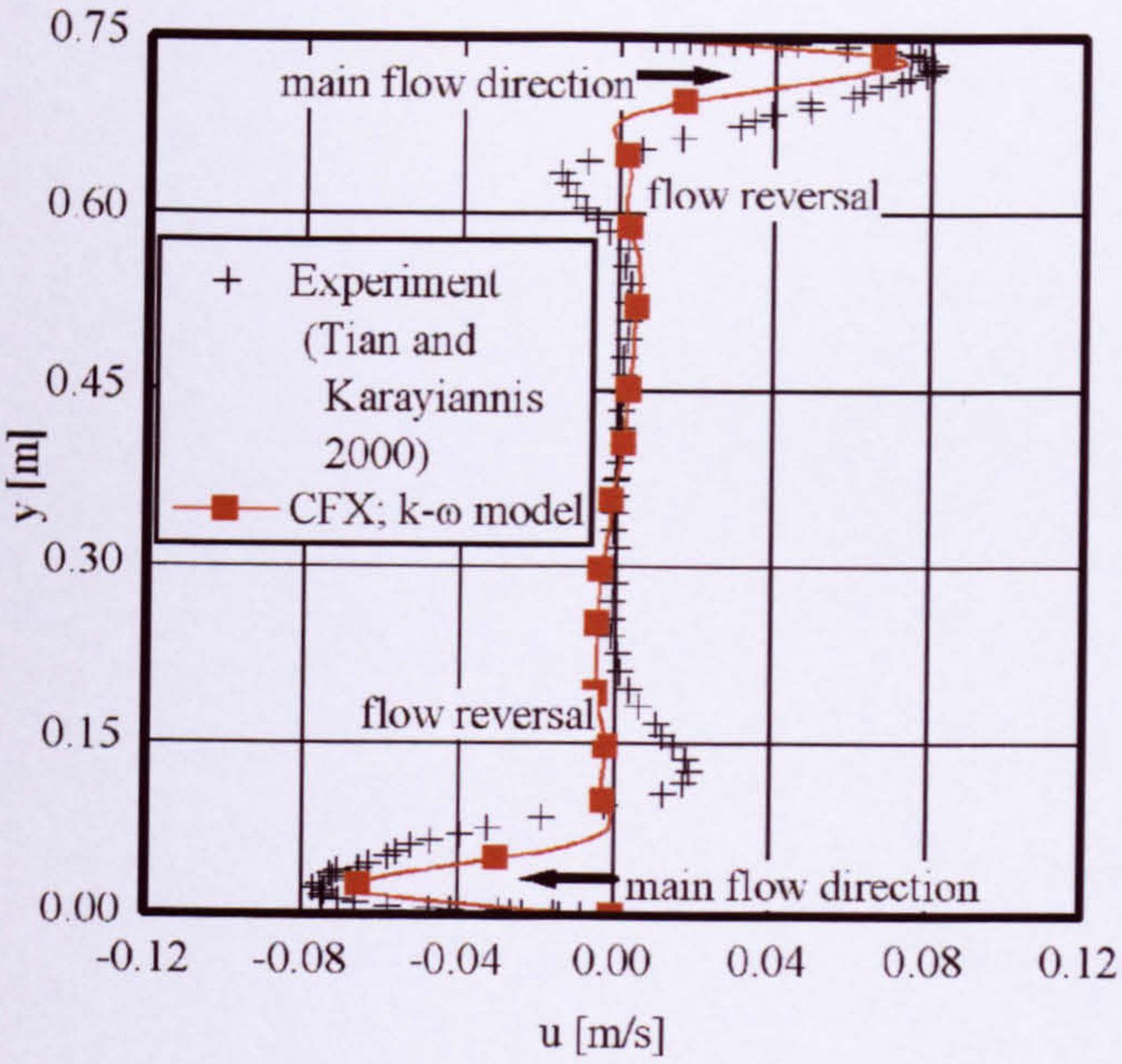

Figure 3.8: Horizontal velocity components at mid width at different heights comparing predictions for CFX using the k-ω model with experimental reference data; the flow directions are labelled by black arrows.

The disturbances could have emerged due to the small distance between the high and low end z-planes of the quasi-2D model which prohibit 3D dissipation of turbulence. For a test with a 3D geometry no flow disturbances were observed (see Figure B.25 and a summary in Zitzmann et al. 2005). Also the Large Eddy Simulation carried out by Peng and Davidson (2001) did not show any disturbances in the corners. In contrast, flow disturbances were also displayed in investigations of Barhaghi (2004) for the k-ω model. However, no information was given if a quasi-2D or a 3D geometry model was used. Wu et al. (2006) investigated experimentally the effect of boundary condition of the enclosing horizontal surfaces on the air flow in the relevant corners. They found that no flow disturbance exists when using adiabatic horizontal walls as shown by Tian and Karayiannis (2000). However, when the top horizontal boundary contains isothermal conditions (i.e. heated plate), comparable to the horizontal boundary conditions in the numerical study of the thesis, characteristic vortices develop in the corners as shown in Figure 3.9. Furthermore, when the surface temperature of the top horizontal boundary was increased in the experiments, the disturbances were more prominent and evolved

closer to the corner (Wu et al. 2006). Thus, the comparison with other publications has shown that the flow disturbances in the corner displayed for the quasi-2D geometry are not necessarily a numerical error. A detailed further investigation of this phenomenon was not possible within this project due to the high computational resources required for simulations. However, comparing the numerical results with measurements for Figures (3.4)-(3.7), it was demonstrated that the local flow disturbances in the quasi-2D model do only marginally influence the over-all convection prediction in the enclosure. Moreover, deviations in the local air flow patterns between the experiments and predictions did not influence the convective surface heat transfer (shown by the local Nusselt number in Figure 3.6). A negligible effect on the convective surface heat transfer was also shown for coarser mesh sizes used for the tetrahedral elements at the surfaces and the core of the cavity as long as the wall boundary was sufficiently resolved (see section B.2.5). In terms of a balance between accuracy and computational effort it is therefore considered sufficient to use the quasi-2D model for modelling turbulent free convection if the mean flow patterns are two-dimensional.

The measurement claims a stationary flow field of zero velocity in the core region of the enclosure (see Figure 3.9). Small fluctuations which occurred in the core region during the measurements were thought to be caused by noise. However, Peng and Davidson (2001) also predicted fluctuations when they investigated the air flow in the enclosure using a LES model. They pointed out that this was caused by the unsteady flow behaviour. Small oscillation behaviour was also displayed for the monitored RMS normalised residuals for the RANS equations and for monitored velocities and temperatures throughout the iteration process for the SMC-ω model in section B.2.3 and for the 3D room model in section B.2.4 indicating transient flow behaviour. Although numerical results agree favourably with the experiments for turbulent free convection in a quasi-2D geometry using the steady-state solution scheme the results from the 3D geometry suggest to use of a transient solution scheme to consider the spatial fluctuations in the turbulent air flow.

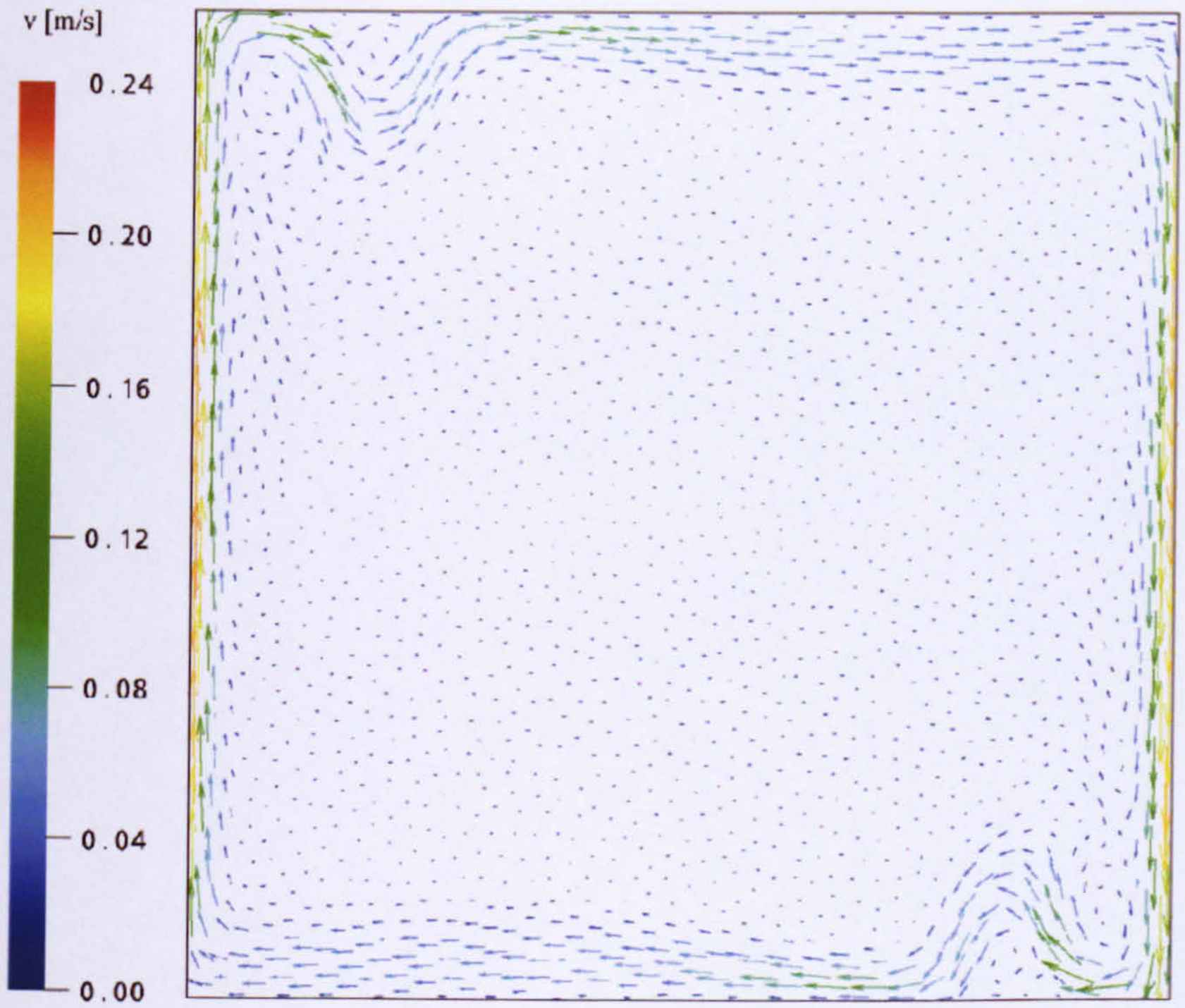

Figure 3.9: Velocity vector plot for the CFX simulation using the k-ω model.

3.4 Radiation

3.4.1 Theoretical background and analytical solutions

In many CFD simulations, radiation heat transfer is neglected (e.g. in Thompson et al. 1987, Henkes and Hoogendoorm 1995, Peng and Davidson 1999). This assumption might be valid if all enclosing boundaries have fixed conditions and contain highly reflective surfaces as for example in the experimental benchmark model setup of Tian and Karayiannis (2000). However, radiation heat transfer is often important in buildings. Thus, the radiative surface heat transfer can significantly influence the thermal room behaviour, particularly for buoyancy dominated air flow (Müller and Renz 1998 and Potter and Underwood 2004). Thus radiative heat transfer cannot be neglected in buildings and should be modelled. However, guidance on how to model radiation accurately using CFX is sparse. The CFX user manual provides two radiation

models for optically thin (i.e. transparent to radiation) media such as air: the Monte Carlo and the Discrete Transfer model (see section A.4). However, no information is provided about the radiation model parameter settings necessary to achieve high prediction accuracy. Investigations were carried out by Cumber (1995), Song et al. (2002), Feldheim and Lybaert (2004) and Haarhoff and Mathews (2006) using these radiation methods. Predictions showed good agreement compared with analytical solutions. Some model parameter settings are given for the Discrete Transfer model which can be used as a starting point for radiation simulations using CFX.

Verification of CFX-5 for radiation was considered necessary from the literature review shown above. The background of radiative heat transfer and analytical solutions are described in the following.

The radiation incident on a surface must fulfil the following requirement to satisfy the law of energy conservation:

$$\alpha + \tau + \gamma = 1 \qquad \text{Eq. (3.16)}$$

where α, τ and γ are the absorption, transmission and reflection coefficients respectively. They determine the percentage of the incident radiation which is absorbed or reflected at the surface or transmitted through the material. The reflection of radiation can occur in two different ways, reflection by the same angle as the incident radiation (i.e. specular reflection) or by diffuse reflection. Typical building materials are 'grey' (i.e. independent of the wave length) and reflect radiation diffusively; metals which contain glossy surfaces reflect specularly. The transmission is zero for opaque materials. Furthermore, the law of Kirchhoff states (Wagner 1998):

$$\varepsilon = \alpha \qquad \text{Eq. (3.17)}$$

where ε = emission coefficient (or emissivity) [-]. The radiative heat flux, E [W/m^2], emitted from a grey body is derived from the law of Stefan-Boltzmann and is calculated as follows:

$$E = \varepsilon \cdot \sigma \cdot T^4 \qquad \text{Eq. (3.18)}$$

where σ = Stefan-Boltzmann constant [W/(m^2·K^4)] and T = surface temperature of the body [K].

The radiative heat exchange between surfaces can be analytically derived for certain simple cases (see Wagner 1998). Two analytical cases are described here and are based on the assumption that the surfaces are grey and diffuse reflective.

Parallel plates (Infinite surfaces)

For two parallel infinite large surfaces, with rays reflected multiple times between the surfaces before the reflected radiation intensity approaches zero, Eq. (3.19) is used for calculating the radiative heat exchange (Wagner 1998):

$$\dot{q}_{ik} = \frac{\sigma}{\frac{1}{\varepsilon_i} + \frac{1}{\varepsilon_k}} \cdot (T_i^4 - T_k^4) \qquad \text{Eq. (3.19)}$$

where $\dot{q}_{ik}$ = radiative heat transfer between surface i and k [W/m^2], ε_i, ε_k = emission coefficients at surfaces i and k respectively [-], T_i, T_k = temperatures at surfaces i and k respectively [K].

Enclosure (Finite surfaces)

For the case of finite surfaces in a room, the total incident radiation at a surface is the sum of the emitted and reflected radiation from n participating surfaces (Sharma et al. 2007):

$$B_i = \sum_n (\varphi_{ki} \cdot \sigma \cdot \varepsilon_k \cdot T_k^4 + \varphi_{ki} \cdot (1 - \varepsilon_k) \cdot B_k) \qquad \text{Eq. (3.20)}$$

where B_i, B_k = radiation incident on surface i and k respectively [W/m^2] ,φ_{ki} = view factor between surface elements i and k [-], ε_k = emission coefficient at surface k [-], T_k = temperature at surface k [K]. The surface may be divided into sub-elements using different view factors for each finite surface element to increase accuracy.

For simple geometries, typical view factors are known, which consider the spatial distribution of the geometrical conditions (see for example Wagner 1998). Eq. (3.20) leads to an equation-system which couples all surfaces. An implicit solution of the system in a matrix becomes difficult due to the non-linearity of the temperature terms. If the surface temperatures are known, the system becomes linear and can be solved with standard matrix solution techniques giving the total incident radiation, B_i, at each surface. The radiative heat absorbed at each surface is given by the difference between the incident and emitted radiation:

$$\dot{q}_i = \varepsilon_i \cdot B_i - \varepsilon_i \cdot \sigma \cdot T_i^4 \qquad \text{Eq. (3.21)}$$

No heat can be stored at adiabatic wall conditions so Eq. (3.21) can be set to zero. The equation simplifies to:

$$\sigma \cdot T_i^4 = B_i \qquad \text{Eq. (3.22)}$$

Inserting Eq. (3.22) into Eq. (3.20) the emissivities and temperatures disappear in the equations for the adiabatic surfaces which simplifies the solution of the matrix. The resulting surface temperatures for the adiabatic walls are then determined by inserting the calculated relevant B_i in Eq. (3.22).

3.4.2 Verification of modelling radiation using CFX

Model description

The model contains a square cavity of X=1000mm and Y=1000mm which interacts thermally with an adjacent internal wall (c=880 J/(kg·K), ρ=2300kg/m^3, λ=1.4W/(m·K)) of X=220mm thickness (see Figure 3.10). The surfaces are opaque to radiation and the outer solid wall boundaries and the horizontal surfaces of the cavity are adiabatic. A constant temperature T_3=20°C is imposed on surface 3 while the temperature T_1 at surface 1 adjusts to the heat balance at the interface between the solid and fluid domain. The solid has an initial temperature of 27.5°C and the air has an initial temperature of 20°C throughout the domain. The horizontal and vertical surfaces of the cavity contain an emissivity of ε=0.01 and ε=0.9, respectively.

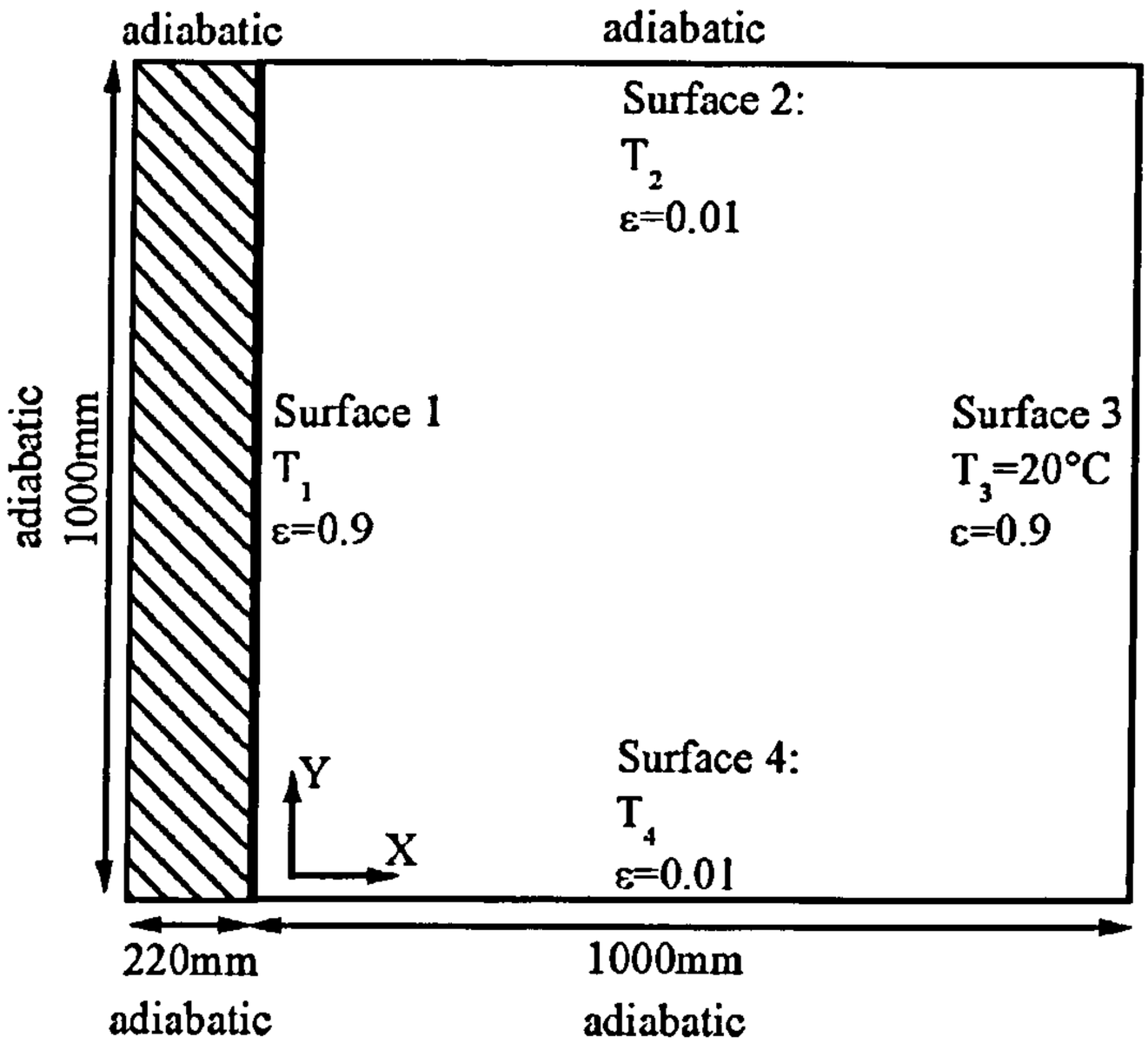

Figure 3.10: Sketch of the room model with conjugate heat transfer for verification of radiation modelling in CFX.

Model implementation in CFX

Although verification could have been carried out using a steady-state solution scheme, the transient scheme is used in order to investigate the suitability of the radiation models in later parts of this research where transient problems are investigated. To consider the conjugate heat transfer between the solid wall and the air, heat conduction is calculated together with the radiation equation (i.e. Eq. (A.15) and Eq. (A.22)). Convective heat transfer is neglected, i.e. mass, momentum and turbulence equations are not solved.

The convergence for the radiation equation does not further improve during the iteration procedure because (i) additional inner iterations are carried out by the solver within each outer iteration to calculate the radiation solution and (ii) radiation becomes rapidly quasi steady-state compared with the energy equation. The reasons for the latter are that the wall surface temperatures change significantly slower than in the air domain due to the larger thermal time constant, and radiation is correlated to temperature by the 4^{th} power. Further iterations do not improve the accuracy of the solution but they only

increase the computational effort. Thus, radiation is calculated only at the first iteration for each time step here.

It can normally be assumed that the spatial gradient for radiation is relatively small at the surfaces of a building, and thus a less refined mesh is possible to calculate radiative heat transfer compared with the calculation of the RANS equations. Therefore, CFX uses a virtual mesh for the calculation of the radiation equation which is significantly coarser than the mesh used for the calculation of the RANS equations (see also section A.4). The solver tries to achieve a mesh element number coarsening factor of 64 by default which is also adopted in this research.

A high resolution advection and a 1^{st} order backward Euler transient scheme is used (see section A.7). The simulation is considered to have converged if a RMS normalized residual of 10^{-5} has been achieved for all calculated equations.

The radiation and energy equations are calculated every time step in CFX using a time step size of 60s. The room model depth used in CFX is Z=0.5m and the high and low end z-planes form symmetry boundaries. The mesh surface and core elements contain maximum edge length scales of 50mm and 100mm, respectively. Close to the surfaces the mesh is refined using prism inflation (first prism layer height 0.1 mm, total number of prisms 4). The total number of 33,200 volume elements is used for the discretisation of the model.

The CFX user manual suggests two radiation models, for calculating radiation in optically thin media such as air: the Discrete Transfer and the Monte Carlo model (see section A.4). A preliminary study was carried out for the radiative heat transfer between two parallel walls of infinite size (see section B.3.1 and a summary in Zitzmann et al. 2007d). The predicted total radiative heat transfer between the walls agreed for both radiation models well with the analytical solution (error less than 0.4%). However, in contrast to the Discrete Transfer model an unrealistic spatial distribution of radiative heat transfer was displayed for the Monte Carlo model, which is thought to be caused by an insufficient long tracking of radiation particles. Moreover, the Discrete Transfer model required only a small fraction of the simulation time required for the Monte Carlo model. For these reasons the following investigation is carried out using the Discrete

Transfer model. The Discrete Transfer model assumes an isotropic radiation emission from each surface. To solve the radiation equation, the hemisphere above each surface element is discretised into 30 elements leading to radiation emission along 30 isotropic rays.

Symmetry, adiabatic and temperature wall boundary conditions are set for CFX as described in section A.5.

Results and Discussion

The radiative surface heat transfer at surfaces 1 and 3 is evaluated for the thermal conditions after a simulation period of 2h (see also Zitzmann et al. 2007d for results).

Figure 3.11 shows the distribution of the radiative heat flux at the surfaces 1 and 3. Smaller wall radiative heat fluxes are observed near the top and bottom where the surfaces approach the horizontal adiabatic surfaces. Such distribution was expected since the elements close to the boundary of the surface 'see' the opposite wall with a smaller view factor than the elements in the centre of the surface. Due to the higher radiative heat transfer at the centre regions, the solid wall (surface 2) cools down faster than in the regions close to the horizontal adiabatic surfaces. Temperature differences of about 0.1K are observed along surface 2. Average absolute values predicted for surfaces 1 and 3 are 20.7W/m^2 and 21.2 W/m^2 respectively. The small differences between the values for surfaces 1 and 3 could be the consequence of (i) numerical inaccuracies due to mesh discretisation and equation imbalances or (ii) heat conduction considered within the transient simulation. The latter case means that the adiabatic surfaces adopt the temperatures of the adjacent air which can lead to a change of the radiative surface heat transfer at the adiabatic surfaces and therefore to a change of the radiative heat transfer at the surfaces 1 and 3 compared with the case in which no thermal conduction is included.

The predicted average surface temperature obtained at surface 1 after 2h simulation is 26.16°C. Using Eqs. (3.20) and (3.22) and inserting them in Eq. (3.21) a wall radiative heat flux of 22.3W/m^2 is calculated analytically (see section B.3.2). For the analytical model, the surfaces are not discretised. However, the average view factors used from

Wagner (1998) for the model geometry consider implicitly the spatial distribution of the local view factors.

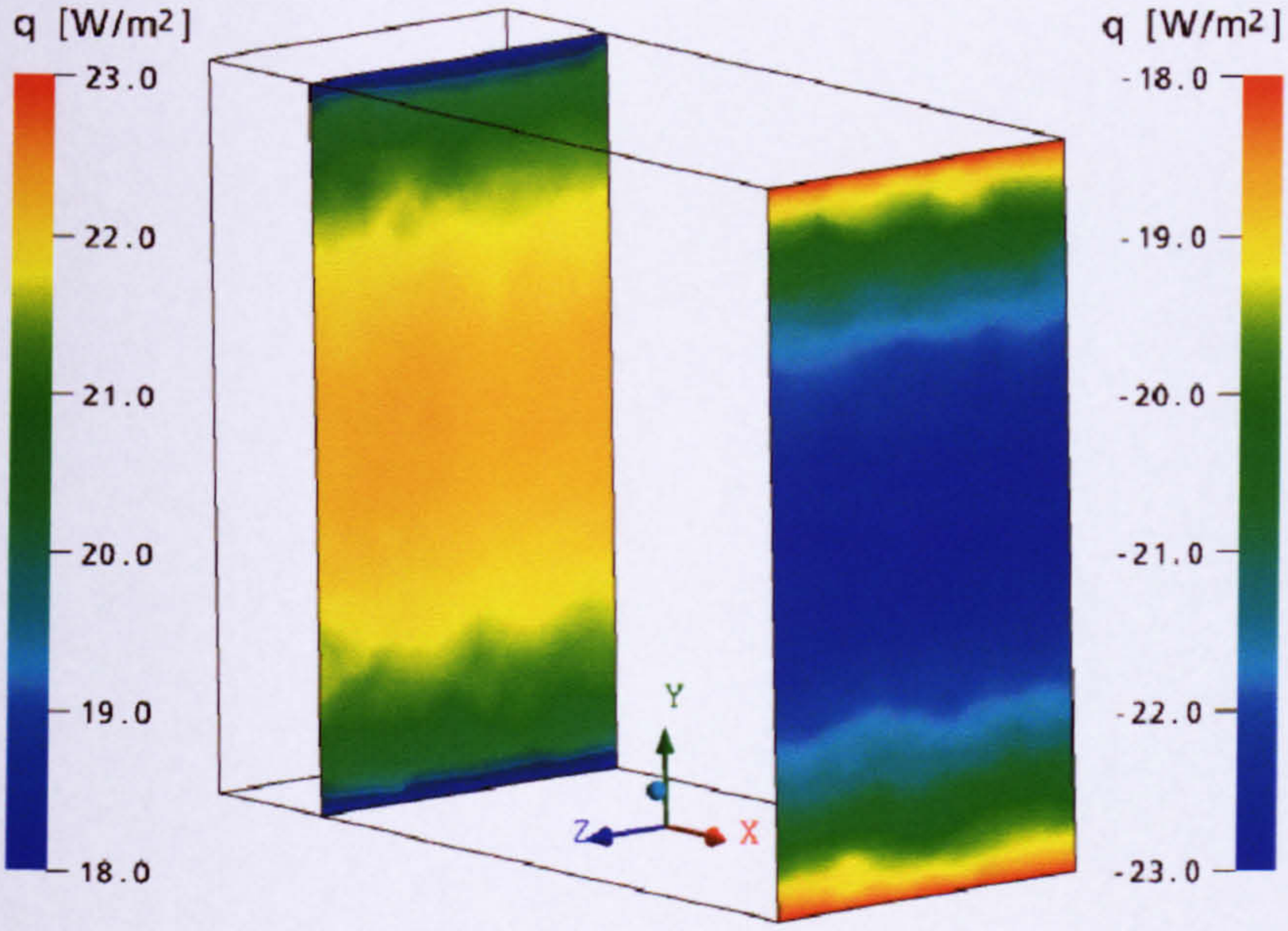

Figure 3.11: Predicted wall radiative heat flux for surfaces 1 and 3 using the Discrete Transfer model with 30 rays.

The average radiative heat transfer predicted between surfaces 1 and 3 was 20.95W/m^2 which compares favourably with the analytical solution (6% difference). The small differences between the analytical solution and the numerical predictions may be due to any of the following:

- Inaccuracies of view factor values used for the analytical solution obtained from view-factor diagrams from the literature.

- The simplified use of average surface temperatures for the analytical solution. A change of the temperature difference of 0.15K at the investigated temperature level for example leads to a change of 0.7W/m^2 of the radiative wall heat exchange for the analytical calculation (3% deviation from the analytical solution obtained above). The numerical solution contains temperature differences of up to 0.1K along surface 1.

An increase of the number of rays for radiation emission did not generate an improvement of accuracy but led to a significant increase of computational effort as shown in section B.3.2. An additional simulation using an emissivity of ε=0.9 instead of ε=0.01 for the adiabatic horizontal surfaces of the enclosure led only to marginal changes in the numerical predictions (deviation of average heat flux at surface 1 was less than 1%). This corresponds with the theory of section 3.4.1 that the emission coefficient at the adiabatic boundaries is irrelevant.

Simulations for the enclosure model were carried out using the Monte Carlo model (see section B.3.2). The unrealistic spatial distribution observed for the model of two parallel infinite walls was also displayed for the enclosure model, although a similar total average heat flux was calculated as for the Discrete Transfer model. The reason is thought to be an insufficient tracking of the radiation photons through the domain. The CPU time required was 65,205s for the simulation with the highest possible accuracy investigated (2,000,000 histories). In contrast, a CPU time of only 1169s was required using the Discrete Transfer model which is a reduction of 98% compared with the Monte Carlo model.

3.5 Summary

Experimental data and analytical solutions have been used in this research to verify heat transfer models in CFX. The average error for modelling each heat transfer mechanism (i.e. conduction, convection and radiation) was about 5% only for the verification models investigated, which has demonstrated that CFX is potentially capable to model the heat transfer mechanisms relevant in buildings accurately. The main outcomes of the verification are summarized in the following.

The modelling of dynamic heat conduction has been verified by comparing predictions with analytical solutions (Wagner 1998) and numerical data from the thermal bridging program HEAT2D. It was shown that CFX can accurately model dynamic heat conduction in a typical building material of high thermal mass. However, the 1st order backward Euler transient scheme is required for the discretisation of the transient terms

since the use of the default 2nd order scheme potentially leads to over- and under-shoots due to numerical dispersion effects typical for even-order schemes.

Free convection is the dominating driving force of flow in buildings. For verification of CFX models to predict free convection, analytical solutions (Ostrach 1953) and experimental data (Tian and Karayiannis 2001) were used. The velocities and temperatures in the wall boundary layer influence the convective surface heat transfer significantly. The wall-function approach in CFX is only valid for forced flow regimes. Thus, the numerical mesh in the wall boundary layer must be refined to resolve the high gradients of velocity and temperature. The ω-equation based turbulence models support the numerical resolution in the wall boundary layer by using the so-called low-Reynolds approach. However, the high mesh resolution leads to a significant requirement of computational effort. The research has shown that especially the sizes of the first mesh elements in the air domain adjacent to the wall do highly influence the convective surface heat transfer and must be sufficiently small. To decrease the computational effort without a loss in accuracy, prism elements were used with inflation (i.e. a gradual increase of the mesh size to the outside of the wall boundary layer) to resolve the wall boundary layer. A first prism size of maximum 0.2mm edge length scale adjacent to the wall and prism inflation with a factor 1.2 using a total of 16 prism elements was found to give accurate results for free convection in the enclosure model investigated (0.4% error of convective surface heat transfer compared with the analytical solution).

The best agreement of predictions of turbulent free convection with experiments was achieved for the k-ω turbulence model. Although some deviations in the air flow patterns were locally displayed for free convection in a quasi-2D compared with a 3D room enclosure, for which further investigations are recommended to find the possible reasons, these deviations caused only a negligible effect on the convective surface heat transfer. In terms of a balance between accuracy and computation effort the use of a quasi-2D model was considered sufficient for modelling turbulent free convection in the enclosure accurately. It was further shown that the surface mesh and the mesh in the domain centre could be significantly increased with only marginal effects on the accuracy of convective surface heat transfer as long the wall boundary layer was sufficiently numerically resolved. Small fluctuations were displayed within the air flow

field for the 3D model indicating transient flow behaviour. This leads to the suggestion to use a transient solution scheme rather than a steady-state solution scheme to model turbulent free convection in 3D spaces using CFX.

The CFX models for predicting radiative heat transfer were verified by comparison with analytical solutions. Two radiation models are suggested in CFX: the Monte Carlo and the Discrete Transfer model. Spatial discretisation errors were displayed for the Monte Carlo model compared with the analytical solution for radiative surface heat exchange. An insufficient long tracking of the radiation particles in the air domain was thought to cause these errors. Although, the error might be potentially reduced for a longer tracking, the calculation effort was restricted due to the limitation of computational resources available in this research. The Monte Carlo model is unlikely to be suitably for dynamic thermal building simulations due to the high computational resources required to predict radiative heat transfer accurately. In contrast, results for radiation heat transfer for the Discrete Transfer model compared favourably with the analytical solution (6% error) and only a fraction of the time (2%) of that for the Monte Carlo model with the highest possible accuracy investigated was required. This suggests that the Discrete Transfer radiation model might be suitable for dynamic thermal building simulations.

The investigations in this chapter have provided confidence in the ability of CFX to accurately predict the heat transfer mechanisms relevant in buildings.

CHAPTER 4

DYNAMIC THERMAL MODELLING METHODS USING CFD

4 Dynamic Thermal Modelling methods using CFD

4.1 Preamble

Building simulation programs vary in their capabilities and limitations (see section 2.3.1). CFD programs are potentially more accurate than zonal simulation programs since they use a fine computational grid. However, they are currently impractical for dynamic thermal building simulations due to the high computational resources required. The main problem is the different time scales over which the solution in the air and the building structure domains evolve. To overcome this, research is beginning to use a so-called freeze-flow method for dealing with the incompatibility of the thermal time constants (Onishi 1998 and Somarathne 2003; see also section 2.3.3). The air flow field is intermittently frozen for certain time periods assuming that the thermal conditions change only slowly within this time. The flow field is then 'unfrozen' to adjust the air flow patterns to the actual environmental thermal conditions.

The freeze-flow method was shown to be capable to conduct dynamic thermal building simulations using purely CFD since the computational effort was significantly reduced (Somarathne 2003). However, the method developed by Somarathne has still some drawbacks as described in detail in section 2.3.3. The periods of unfrozen and frozen flow were fixed. It is therefore suggested to use new controls which trigger a switch between frozen and unfrozen flow mode depending on the environmental thermal conditions. This should improve the performance of the freeze-flow method by reducing the computational resources required whilst maintaining accuracy. Another drawback of the control method was that simulations had to be instigated manually by stopping and restarting simulations of unfrozen and frozen flow periods making the method cumbersome for the user. Automation of the procedure is required.

This chapter addresses the drawbacks indicated for the freeze-flow control method developed by Somarathne (2003). The control method based on fixed unfrozen and frozen flow periods, hereafter referred to as the ***'invariable control method'***, is

implemented in the CFD platform CFX in this research. A new control method, hereafter referred to as the ***'adaptive control method'***, is developed which adapts the unfrozen and frozen flow periods to the environmental room conditions. The control methods are automated in an attempt to avoid stopping and restarting of the simulation when switching between unfrozen and frozen flow modes.

Details of the invariable and the adaptive control method are given in section 4.2 and 4.3. The methods of automation and implementation of the freeze-flow control methods in CFX are shown in section 4.4. A summary of the function and automation of the freeze-flow control methods is given in section 4.5.

4.2 Invariable control method

The invariable control method is based on the transient-transient scheme developed by Somarathne et al. (2002) for fixed periods of frozen and unfrozen flow (see chapter 2.3.3). Small time steps of the order of 1 second are required to calculate the transient, turbulent behaviour of the air accurately which leads to a requirement for high computational resources. Larger time steps often lead to convergence problems (see section 2.3.1). The values of the solution at the end of the unfrozen flow period are used during the frozen flow period for the momentum and turbulence equations. For keeping the simulation errors small when using the freeze-flow method, the changes in the thermal room conditions must be small during frozen flow periods (which restricts the possible lengths of frozen flow periods). Due to the small changes in the solution fields, the time step can be significantly larger. Figure 4.1 illustrates the basic principle of the invariable control method. Due to the larger time steps used and due to the reduction of equations solved during the frozen flow periods compared to a fully transient CFD simulation (i.e. all RANS and turbulence equations are continuously updated at each time step), the computational resources required can be significantly reduced as demonstrated by Somarathne et al. (2002) (see section 2.3.3). Furthermore, the convergence behaviour is potentially more stable and the speed is increased during periods of frozen flow.

During an unfrozen time period, Eqs. (A.13)–(A.15) (i.e. the RANS equations) and Eqs. (A.19)-(A.20) (i.e. turbulence equations, if the k-ω turbulence model is used) are solved at each time step. During a frozen flow period Eqs. (A.13), (A.14), (A.4.19) and (A.20) are not updated, i.e. the equations are not solved and the values at the last time step of the previous unfrozen period are used. Eq. (A.15) is solved throughout the simulation process. If radiation modelling is considered, then Eq. (A.22) is additionally solved throughout the simulation process. A description of the developed method is also summarised in Zitzmann et al. (2006a).

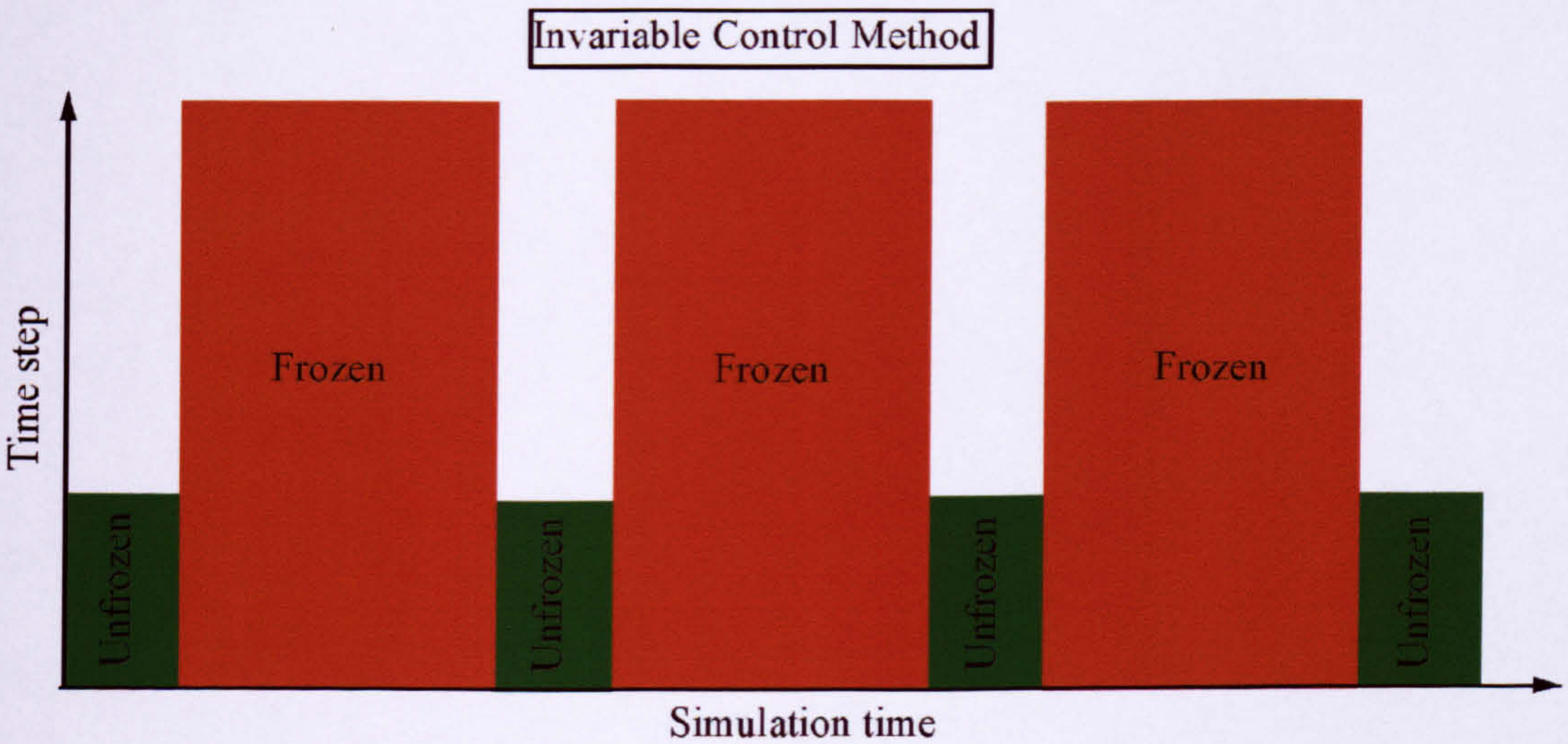

Figure 4.1: Sketch of the invariable freeze-flow control method showing time step vs. simulation time elapsed for unfrozen (green solid rectangles) and frozen flow periods (red solid rectangles).

The invariable control method exhibits some drawbacks. The response of the control method to significant changes at the boundary conditions can only be predicted accurately if these occur within unfrozen flow periods when the flow can respond to the change. The length of the frozen flow period is therefore restricted to the boundary condition change with the smallest time scale. Since the length is fixed for all frozen and unfrozen flow periods throughout the simulation for the invariable control method, the frozen flow period is shorter than necessary at times when the boundary conditions change only slowly. Similarly, the unfrozen flow period is longer than necessary when

the air flow patterns and the thermal field adjust rapidly to the new room conditions for stable flow fields, for example for forced convection flow. This reduces the potential performance of the freeze-flow method by increasing the computational resources needed. Furthermore, the user needs to know exactly in advance when significant boundary condition or room condition changes occur in order to set the required lengths of unfrozen and frozen time periods. The worst case scenario exists if periods of very strong boundary condition changes exist, since this reduces significantly the length of frozen flow periods.

However, an advantage of the invariable control method is its simplicity since the time step sizes and the lengths of frozen and unfrozen flow periods are specified by the user once before the simulation is started and requires only a relative small programming effort compared to more complex control strategies. For simple simulation cases the invariable control method might therefore sometimes be favourable compared with more complex control strategies and is therefore also investigated in the thesis.

4.3 Adaptive control method

The newly developed adaptive control method intends to overcome the drawbacks for the invariable control method described in section 4.2. The principle of the adaptive freeze-flow control method is shown in Figure 4.2. A comparison with the sketch in Figure 4.1 demonstrates similarities and differences of both control methods. Fixed time step sizes for the unfrozen and frozen flow periods are adopted from the invariable control method. The same equations are solved or frozen during unfrozen and frozen periods for the adaptive control method as for the invariable control method shown in section 4.2. However, the lengths of the unfrozen and frozen periods adapt based on prevailing room and imminent boundary conditions. The description of the developed method has also been summarised in Zitzmann et al. (2006b), Zitzmann et al. (2007a) and Zitzmann et al. (2007b).

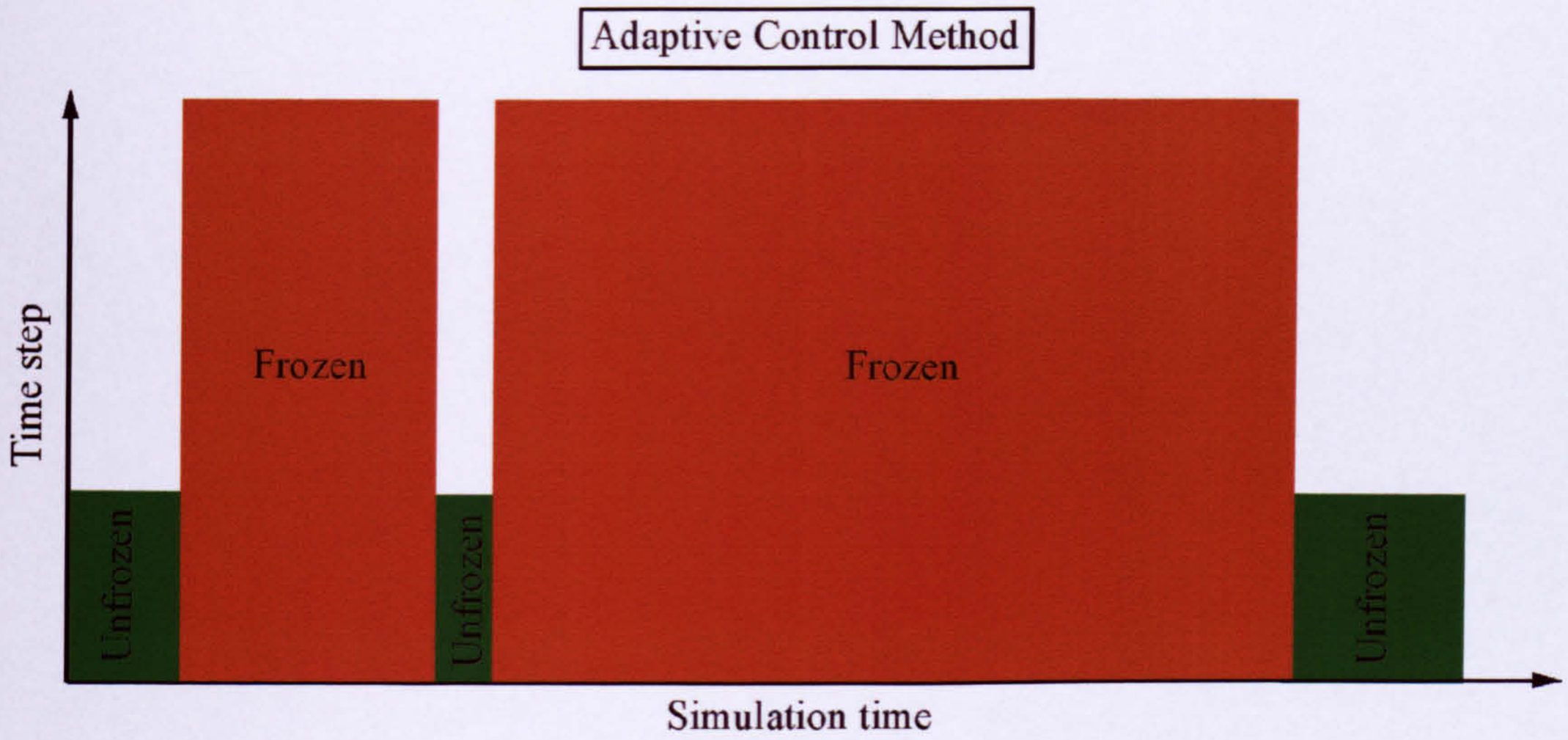

Figure 4.2: Sketch of the adaptive freeze-flow control method showing the time step vs. the simulation time elapsed for unfrozen (green solid rectangles) and frozen flow periods (red solid rectangles).

For future work, Somarathne et al. (2003) suggested restricting the length of the frozen periods by using triggers at the internal surfaces of the room enclosure and around heat sources which respond to maximum permitted thermal changes at these locations and automatically instigate a switch from frozen to unfrozen flow periods. However, the reaction of the air adjacent to the internal wall surface condition changes depends on the strength of the convective surface heat transfer. Thus it is possible that thermal conditions in the air domain change marginally despite more significant thermal changes at the surfaces. To keep the length of frozen flow periods as long as possible, it is therefore better to use triggers only in the air domain rather than at the surfaces since only the air nodes contain the equations of mass and momentum. Moreover, for unstable flow fields the environmental conditions may significantly change in areas some distance away from heat sources. However, the location where the thermal conditions will change most is generally not always predictable in advance which makes an efficient positioning of triggers difficult. Therefore a method is needed which monitors any changes in the entire thermal solution field of the air domain in order to switch from frozen to unfrozen flow mode in time to keep calculation errors small. Furthermore, a

trigger is required which restricts the lengths of the unfrozen flow periods to the time-scale over which the thermal field and air flow patterns evolve.

Generally, the unfrozen flow periods should be no longer than necessary and the frozen flow periods should be as long as possible to increase the performance of the freeze-flow method. The following paragraphs describe the function and control criteria of the newly developed adaptive control method. A flow chart illustrating the adaptive control method is shown in Figure 4.3 to aid the understanding of the underlying control procedure.

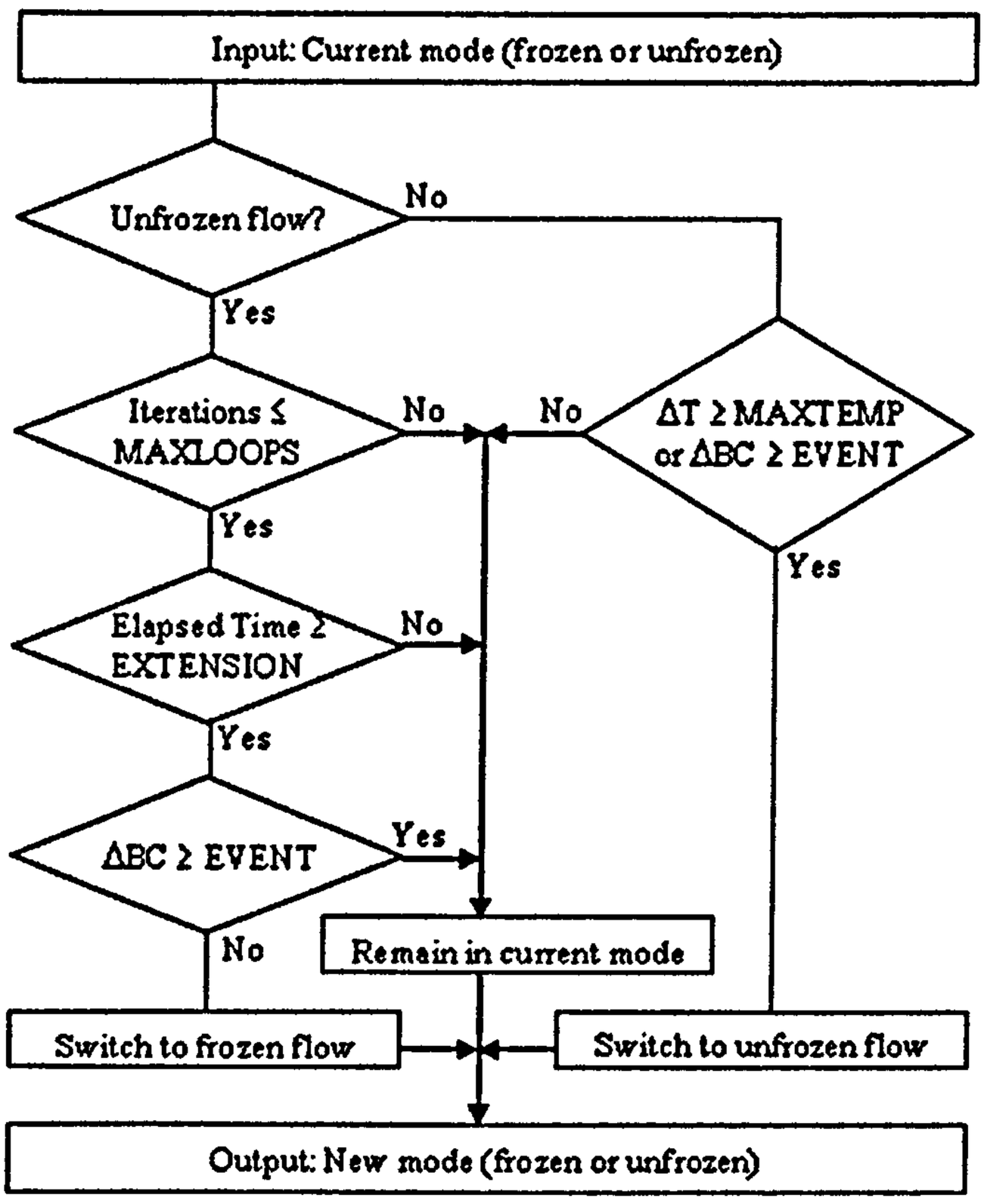

Figure 4.3: Flow chart for the adaptive freeze-flow control method (MAXLOOPS is a maximum number of iterations required for a switch, EXTENSION is the minimum time extension of the unfrozen time period, ΔT is a change in the local temperature, MAXTEMP is the maximum allowed temperature difference, ΔBC is a change in the boundary conditions and EVENT is the maximum change permitted in a boundary condition).

4.3.1 Control criteria for switching from unfrozen to frozen flow mode

The transient solution scheme in CFX uses coefficient iteration loops to achieve convergence for each time step. Convergence is achieved when a specified RMS normalised residual of the momentum, mass and energy equations is reached, which is usually of the order of 10^{-4}-10^{-5}. The solver then proceeds to the next time step.

Discrepancies between the flow field and the temperature field can be large at the start of a simulation (if the initial values for environmental variables are poor) or at the end of a frozen flow period. If so, then the number of iterations per time step required for convergence during the early stages of the subsequent unfrozen flow period will be large. As the unfrozen flow period progresses, then the number of iterations required gradually reduces as the agreement between the temperature and airflow fields improves. The possible minimum number of iterations depends on the case being investigated and thus on the physical characteristics of the air flow and the quality of the mesh.

To achieve the maximum benefit from the unfrozen flow period, a switch to a frozen flow period should occur after a quasi-stationary solution (i.e. unchanging flow and temperature patterns between the former and the next time step) has been reached. The solution is considered to be quasi-stationary if the minimum number of iterations has been achieved and remains constant in time. To ensure this state has been achieved, the minimum iteration number achieved should hold over some time period which is specified by the parameter, EXTENSION. Each time the number of iterations required exceeds the minimum iteration number during the EXTENSION period, the unfrozen flow period is increased again by a further period, EXTENSION.

Due to the turbulent nature of the flow, the required number of iterations can sometimes increase, although the quasi-steady state still remains. This would reduce the performance of the freeze-flow control method due to an unnecessarily extended unfrozen flow period. In practice it was found that by adopting a strategy in which the period EXTENSION was increased and a less restrictive user defined value, MAXLOOPS, was used as a switching criterion rather than the minimum number of iterations, acceptable calculation times and accuracy could be achieved. MAXLOOPS is

the maximum number of iterations permitted within the time period EXTENSION after which the solver will switch from the unfrozen to a frozen flow period (see Figure 4.3).

4.3.2 Control criteria for switching from frozen to unfrozen flow mode

During periods of frozen flow, when all hydrodynamic and turbulence equations are frozen, only values for enthalpy and temperature can change. Since moisture is not considered in this simulation model, the numerical problem can therefore be reduced to the task of predicting the local temperature values in each finite volume. Since the frozen air flow distribution represents a certain thermal situation, each change in the temperature field leads to increasing calculation errors in the frozen air flow field and in the heat transfer at room surfaces.

To minimize these errors, the changes in thermal conditions of the air should be less than a certain value, 'MAXTEMP'. Therefore, the new criterion for switching from frozen to unfrozen flow is defined as the point at which the maximum local temperature difference in the air domain between the last time step of the previous unfrozen flow period and the current time step in the frozen flow period reaches or exceeds 'MAXTEMP' (see Figure 4.3).

4.3.3 Control criterion for responding to imminent changes in boundary conditions

When significant changes are likely to occur due to imminent changes in the user-defined boundary conditions, an additional, and overriding control is required which prohibits a switch from unfrozen to frozen flow or forces a switch from frozen to unfrozen flow periods, despite all other criteria being met. For example, if computers are turned on in a simulated office at 8am and turned off at 6pm, the solver needs to force an unfrozen flow mode at that time in order to respond accurately to these changes.

A controlling subroutine automatically checks for changes in the boundary conditions within the subsequent period (equivalent to the duration of a frozen time step). This information is typically stored in a model definition setup file (often in the form of time

dependent functions). If a change in boundary condition reaches or exceeds the value of a specified criterion 'EVENT', the controlling subroutine responds as described above (see Figure 4.3). A different value for 'EVENT' can be set for each variable.

4.3.4 Parameter settings for MAXLOOPS, EXTENSION, MAXTEMP and EVENT

The parameters 'MAXLOOPS', 'EXTENSION', 'MAXTEMP' and 'EVENT' can be specified by the user before the simulation starts, and depend mainly on the physical characteristics of the flow. If the flow field is continuously unstable and weak in most parts of the air domain, 'EXTENSION' needs to be large and all other values small to minimise errors in the air flow and temperature fields. If the flow field is predominantly stable, 'EXTENSION' can be smaller and other parameters larger, which increases the performance of the freeze-flow method by reducing computation time. Depending on the values for the controlling criteria specified, the user can restrict the simulation to the accuracy requested specific to the application. However, an increase of accuracy leads to a significant increase of computational resources for dynamic thermal predictions which leads to the requirement of careful use of parameter values. A parametrical study is for example shown in section C.2.2 for a naturally ventilated space.

The worst case scenario exists for the adaptive freeze-flow control method if the unfrozen flow periods are long and the frozen flow periods are small or if the solver never switches to frozen flow mode. This can for example happen if the boundary conditions change rapidly or if highly unstable flow fields exist. In the latter the invariable control method might give a better performance than the adaptive control in terms of computational time reduction since it forces frozen flow periods for certain time intervals. However, the freezing of a highly unstable flow field over long periods can lead to significant prediction errors due to the fixing of momentum vectors of arbitrary directions, since the time-scale for flow direction changes would normally be small.

4.4 Automation and implementation in CFX

A general drawback of the freeze-flow procedure developed by Somarathne et al. (2002) was that frozen and unfrozen flow periods had to be instigated manually by stopping and restarting each period by hand, which makes the method cumbersome. This has been overcome in this work.

The freeze-flow control method should automatically determine at the end of each time step whether the next time step should belong to the frozen or unfrozen flow period. Two procedures are discussed for the implementation and automation of the freeze-flow method in CFX: (i) linking an external program to CFX or (ii) implementing an internal routine in CFX.

In case (i) a windows (linux) based batch-file (shell-script) executes successively a list of commands. Two strategies are possible. For the first strategy, the batch-file automatically starts a new simulation using the solution of the previous simulation as the initial condition. However, the solver is stopped and restarted similar to the procedure shown by Somarathne (2003) requiring additional time for writing out output files and for loading the solution of the previous file as an initial condition.

The second strategy overwrites the model definition file (CFX Command Language - CCL format) during runtime. However, in preliminary tests the CFX solver did sometimes not respond to the commands from the batch file sufficiently quickly and did so some time steps later which led to an inaccurate communication between the batch-file and CFX. The delay was larger when the physical computer storage required was high and the CPU usage rate had reached its limit.

A further problem related to both batch-file strategies is thought to be the implementation of the control criteria to instigate a switch between frozen and unfrozen flow modes. This is more complex for the adaptive control method relative to the invariable method since permanent access to the entire solution field of the fluid temperature is required. An external file has to be written storing the thermal solution field which can be called by the batch-file in order to calculate the thermal changes which occur during the frozen periods. This significantly increases the output file size

and the computational effort. A strategy is required for which no external data storage file is created and for which the CFX solver continues only with the calculation of the solution of the next time step after the freeze-flow control method has decided whether it belongs to the unfrozen or frozen flow mode. This is possible by using the internal routine method described in the following.

In case (ii) the freeze-flow control method is implemented in CFX as a dynamic link library (DLL). A so-called User Junction Box is provided by the CFX pre-processor for inclusion of this DLL in a shared library giving the user access to the CFX code structure, the calculated solution fields stored in a Management Memory System and the CCL definition file (see CFX 2006). The DLL can include compiled FORTRAN 77/90 language based or CFX specific commands and sub-routines. The DLL can be called at various stages during runtime (e.g. at the start or end of a simulation, iteration or time step) and the CFX solver continues only after the sub-routine in the DLL has been executed. An intermediate stopping and restarting of the solver is avoided since the DLL modifies the CFX code during runtime. Since case (ii) fulfils all requirements for the implementation and automation of both freeze-flow control methods, this method was used in the thesis.

One DLL routine was programmed for the invariable and one for the adaptive freeze-flow control method. The routines were included in CFX using the User Junction Box option. The DLL is called at the end of each time-step to determine whether the next time step belongs to the frozen or unfrozen flow mode. The parameter input for the freeze-flow control parameters (i.e. time step sizes for and lengths of the unfrozen and frozen flow periods, MAXLOOPS, EXTENSION, MAXTEMP and EVENT) was outsourced to the User Control section of the CFX pre-processor. Thus these input parameters can be changed easily using the GUI without changing the DLL code and recompilation of the routines.

The Command Expression Language (CEL) used in CFX to set the time varying model boundary conditions (e.g. air flow rates at the inlets or outlets, internal and external heat sources, etc.) in the model definition file requires a different format for the definition of the input and output variables than FORTRAN. Therefore the DLL cannot

automatically access the functions from CEL but the functions have to be included in the freeze-flow routine separately. However, except for the specification of the parameter values required for the switching criteria of the freeze-flow control methods and the inclusion of the boundary condition functions in the pre-processor , the freeze-flow control routine works automatically during the simulation using the DLL option.

4.5 Summary

Two automated freeze-flow control methods were developed in this research and implemented in CFX. The first control method is based on the fixed periods of unfrozen and frozen flow used by Somarathne (2003) and is referred to as the *invariable control method.* To overcome the drawbacks of the invariable control method (i.e. fixed periods of unfrozen and frozen flow) a second method was developed in the thesis which adapts the lengths of the unfrozen and frozen flow periods to the room conditions by using triggers for a switch between unfrozen and frozen flow modes and is referred to as the *adaptive control method.* The intention of the adaptive control method was to remain in the frozen flow mode for as long as possible and to keep the unfrozen flow period no longer than necessary in order to improve the performance of the freeze-flow method. Within this method the criterion MAXLOOPS defines the maximum number of iterations permitted during the specified period EXTENSION after which a switch from unfrozen to frozen flow mode is triggered. The criterion MAXTEMP defines the maximum local temperature difference allowed in the air domain between the last time step of the previous unfrozen flow period and the current time step in the frozen flow period, above which a switch from frozen to unfrozen flow mode is triggered. When significant changes are likely to occur due to imminent changes in the user-defined boundary conditions, a switch from unfrozen to frozen flow is prohibited or a switch from frozen to unfrozen flow is forced. This is realized using the criterion EVENT which determines the maximum allowed change in imminent boundary conditions (within the period of a frozen time step) for which the solver can operate in frozen flow mode. The optimal size of parameters for the adaptive control criteria depend on the

physical phenomena which drive the flow in the room (e.g. unstable or prominent flow patterns).

A linking of CFD with an external program such as a batch-file to implement the freeze-flow method is difficult, since access to the internal code structure and storage system of the CFD program is necessary. A better solution was found by implementing the freeze-flow control methods in the shared library of CFX as an internal DLL-file. The advantage of this method is that the DLL has full access to the CFD code structure and the predicted solution fields stored. The parameter values for the criteria MAXLOOPS, EXTENSION, MAXTEMP and EVENT and values for the time step sizes for unfrozen and frozen periods can be simply set by the user using the pre-processor GUI of the CFD program.

Using the DLL option, the freeze-flow method was successfully implemented and automated whereby the lengths of the frozen and unfrozen flow periods are automatically adapted to the room conditions by the solver without stopping and restarting of the simulation. Only the functions for the time-varying boundary conditions set in the definition file had to be inserted in the DLL-file separately which was a result of format differences between the program language used by CFX and that used for writing the DLL subroutine.

CHAPTER 5

DYNAMIC 2D MODELLING OF CONJUGATE HEAT TRANSFER (BENCHMARK 1)

5 Dynamic 2D Modelling of Conjugate Heat Transfer (Benchmark 1)

5.1 Preamble

Two methods have been described for the freeze-flow method in chapter 4 which control the lengths of unfrozen and frozen flow periods, referred to as the 'invariable control method' which uses fixed periods of unfrozen and frozen flow and the newly developed 'adaptive control method' which adapts the period lengths to the environmental conditions. The application of the invariable freeze-flow control method developed by Somarathne et al. (2002) to free convection in a simple room enclosure has shown good performance in reducing the simulation time for dynamic thermal CFD simulations. However, the method has still not been automated and verification does not exist for other typical air flow mechanisms which can occur in buildings (e.g. natural ventilation and mechanical ventilation).

The main aim of this chapter is to test and discuss the new adaptive freeze-flow control method. To do this, four tasks are undertaken: (i) implementation of the new adaptive control method, (ii) testing the automation of the freeze-flow method, (iii) comparison of the performances between the invariable and the adaptive control method and (iv) verification of the methods for various air flow mechanisms.

To address these issues the freeze-flow methods are applied to a simple room model of conjugate heat transfer, referred to as benchmark 1. The methods are applied to three air flow mechanisms (natural ventilation, mechanical ventilation and pure free convection in an enclosure) and compared with fully dynamic CFD simulations in which all equations are calculated without interruption (base case). In the case of natural ventilation wind effects are not considered since the realistic modelling of fluctuations of wind is difficult as described in section 2.4. Since the modelling of radiation requires

additional and significant computational resources, radiation is considered only in the final test.

The details of benchmark 1 are provided in section 5.2. Specific model settings in CFX are given in section 5.3 and results for both freeze-flow methods and the base case are presented and discussed in section 5.4. Section 5.5 gives a summary of the results and the relative performance of the different simulation methods.

5.2 Definition of Benchmark 1

Benchmark 1 is based on a simple 2D small-scale room model to verify the freeze-flow control methods since the use of a large-scale or a 3D model would lead to a significant increase of simulation time for CFX simulations which is unnecessary for the first stage of these parametric studies. The room consists of a solid domain (i.e. 220mm thick massive internal brick wall with c=835J/(kg·K), ρ=1920kg/m^3, λ=0.72W/(m·K)) and an adjacent air domain which forms a square cavity of 1000mm x 1000mm (Figure 5.1). Openings measuring 10mm in the top and bottom of the cavity are located 100mm from the internal and external wall, respectively.

The following cases were investigated using benchmark 1:

- Natural ventilation (Case 1)
- Mechanical ventilation (Case 2)
- Free convection flow for constant ambient temperature conditions (Case 3)
- Free convection flow for varying ambient temperature conditions (Case 4)

In all cases (cases 1-4) the boundary conditions BCs 1-5 are adiabatic. The temperature condition at the interface between the solid and the fluid domain (BC 6) adjusts to the heat balance between the solid and the adjacent air. In cases 1 and 2 the boundary condition BC 7 is also adiabatic. In case 1, air moves freely into or out of the space at a rate dependent upon the temperature difference across the low and high level openings

(BCs 8 and 9). In case 2, a fan at the low level (BC 8) forces air into the room at a constant velocity of 1m/s. The air subsequently leaves the room at high level (BC 9). In cases 1 and 2 the ambient temperature for BCs 8 and 9 is 20°C.

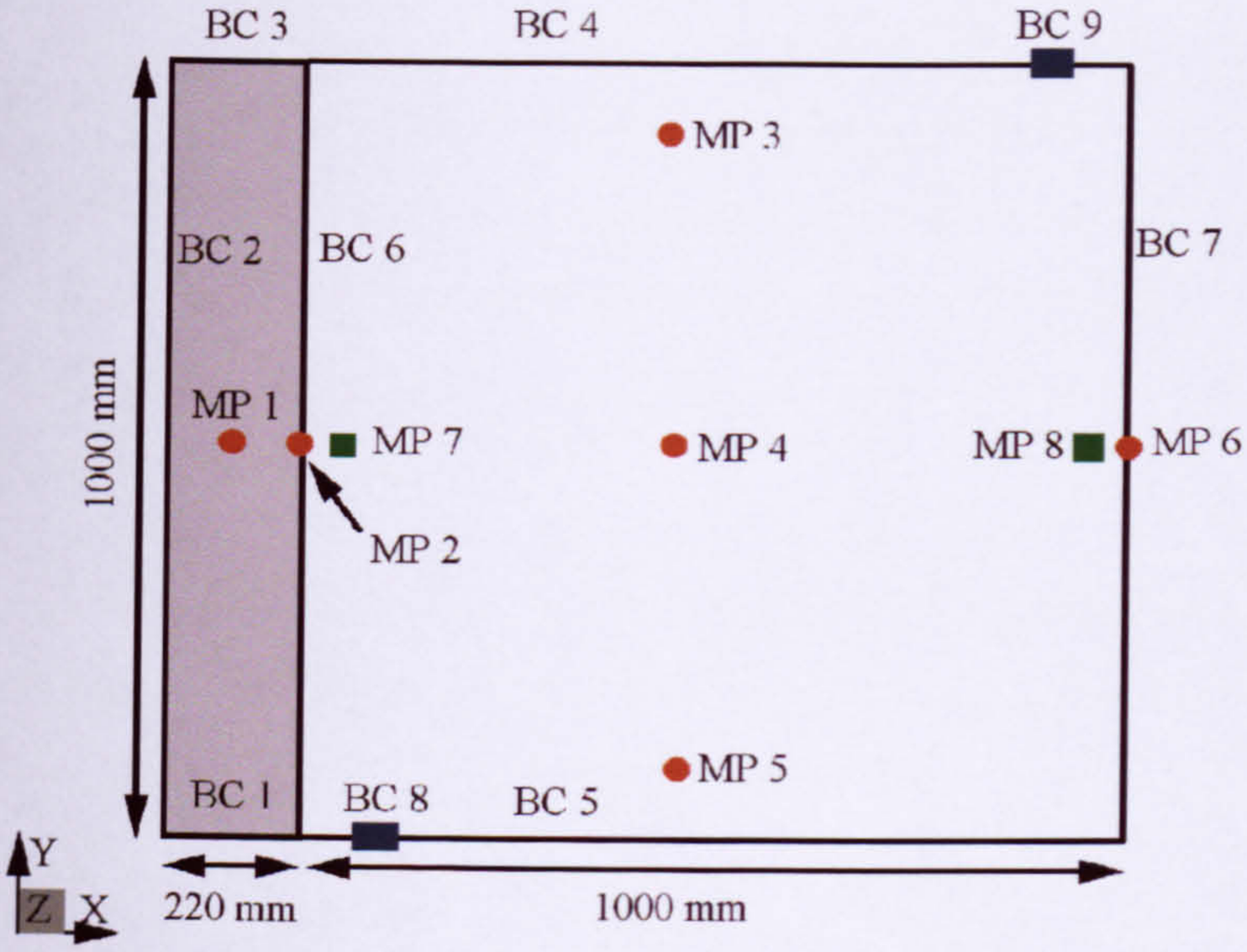

Figure 5.1: Benchmark 1 contains a massive internal wall (shaded) and a square air cavity with optional opening (filled rectangles). Monitor points (MPs) are positioned at various locations in the solid and fluid domain to measure temperatures (filled circles) and velocities (filled squares). The boundary conditions (BCs) are varied for each test case.

For cases 3 and 4, the boundary conditions BCs 8-9 are adiabatic and a constant temperature is imposed on BC 7, which is 20°C for case 3 and varies sinusoidal in time for case 4 as follows:

$$T = 7.5 \cdot \sin(2 \cdot \pi \cdot \frac{t}{86400}) + 20 \qquad \text{Eq. (5.1)}$$

where t = simulation time [s]. In cases 1-3, the solid and air domain initially contain homogeneous temperatures of 27.5°C and 23.75°C at time zero, respectively. In case 4 the entire computational domain comprises an initial temperature of 20°C which leads to air flow patterns of zero velocity at the beginning of the simulation.

Radiation is neglected in cases 1-4 (natural ventilation, mechanical ventilation and free convection) since the modelling of radiation requires significant additional computational resources. Radiative heat transfer is then included later for free convection (case 3) to discuss the influence of radiative heat transfer on the thermal room behaviour and on the performance of the freeze-flow method. The free convection case was selected for this investigation, since in this case the air flow patterns near the surfaces depend directly on the convective surface heat transfer which strongly depends on the surface temperatures which are influenced by radiation. All enclosing surfaces of the fluid domain contain a radiative emissivity of ε=0.9 which is a typical value used for building simulations.

Monitor points (MPs) are placed throughout the solid and fluid domain for the assessment of the temperature field and air flow patterns (see Figure 5.1 and Table 5.1, MPs 7 and 8 are placed within the wall boundary layer; zero point of the coordinate system is the bottom left corner of the room model).

Table 5.1: Locations and units of monitor points in benchmark 1.

Monitor Point	x-Coordinate [m]	y-Coordinate [m]	Units
MP 1	0.11	0.5	°C
MP 2	0.22	0.5	°C
MP 3	0.72	0.9	°C
MP 4	0.72	0.5	°C
MP 5	0.72	0.1	°C
MP 6	1.22	0.5	°C
MP 7	0.226	0.5	m/s
MP 8	1.214	0.5	m/s

5.3 CFX model settings for Benchmark 1

A 2D model cannot be numerically calculated using CFX since it is based on the FVM-method. A quasi-2D model was therefore used as described in chapter 3.3. The model contains only one mesh element in the z-direction which determines the model depth.

The xy-planes at the low- and high-z faces contain symmetry conditions. In section B.2.5 it was found that tetrahedral surface and volume elements with an edge length scale of up to 50mm were possible without influencing the surface heat transfer predictions provided the mesh in the wall boundary layer was sufficiently refined. The mesh used for benchmark 1 is based on the results of these investigations and a maximum tetrahedral edge length scale of 50mm is used. The prism resolution in the wall boundary layer is adopted from section 3.3 (same prism inflation into the fluid and into the solid domain). The model contains a total number of 18,300 mesh elements.

Opening boundary conditions are used at BCs 8 and 9 for case 1, whereas mass flow (inlet) and pressure (outlet) boundary condition are used at low and high level for case 2, respectively (see section A.5). The air is considered as an incompressible fluid with constant properties for 25°C.

Buoyancy is modelled using the Boussinesq approximation (see section A.2). Since the best overall result was obtained with the k-ω turbulence and the Discrete Transfer radiation model in previous simulations (see sections 3.3 and 3.4), these models are also used here. For the energy equation the 1st order transient scheme is used instead of the default 2nd order scheme as a result of the verification of modelling conduction in section 3.2.

Parameter settings used for the invariable and adaptive control method are given in section 5.4.1. The simulations were considered to have converged if a RMS normalize residual of 10^{-5} for all calculated equations (i.e. all RANS equations for unfrozen and only the energy equation for frozen flow periods) was achieved. Simulation results are stored every 5min for both control methods. For the adaptive control method the simulation results are additionally stored at the last time step before the program switches between frozen to unfrozen flow periods to obtain a similar output frequency as for the invariable control method for comparison, since the periods of unfrozen and unfrozen flow are not constant during the simulation compared with the invariable control method.

5.4 Results and Discussion

5.4.1 Preliminary studies

The transient-transient and the transient-steady freeze-flow method of Somarathne (2002) described in chapter 2 were implemented in CFX and the performances were investigated (see section C.1). Both methods have demonstrated a similar performance when unfrozen and frozen periods were switched manually by stopping and restarting simulations. The results were independent of the time step size for frozen flow periods. However, the transient-transient method was slightly more accurate. The reason was thought to be the thermal lag of air which is neglected for the steady-state based simulations. Automation of the transient-steady method was not possible due to the different calculation scheme used for transient and steady-state simulations. An automation (i.e. no stopping and restarting of the simulation) of the transient-transient method additionally increased the accuracy since the simulation errors which were observed for the manual method at the beginning of each simulation restart were not displayed. Hence, only the automated transient-transient freeze-flow method, i.e. the invariable control method, was used from here onwards in the following chapters.

A second preliminary parametrical study investigated the impact of the key parameter settings (i.e. 'MAXLOOPS', 'EXTENSION' and 'MAXTEMP' and frozen and unfrozen period lengths) for the invariable and the adaptive freeze-flow control method on accuracy and computational effort (see section C.2). During periods of unfrozen flow a time step size of 1s was used. A time step size of 5min was used during frozen flow periods for the invariable control method. In an attempt to react more precisely and quicker to changes in the thermal conditions and thus to ensure a switch to an unfrozen flow period at the appropriate time, a time step size of 1min was used for the adaptive control method. The investigation was restricted to case 1 of benchmark 1 since the most difficulties were expected here due to driving force at the solid-fluid interface being free convection only, continuous condition changes at the openings and unstable flow patterns in the core of the domain. Based on the outcomes of these investigations, the control parameter settings presented in Tables 5.2 and 5.3 are used for the four cases investigated in this chapter. An additional improvement of the performance of the

freeze-flow method for the other test cases might be achieved for other less restricted key parameter settings. However, separate parametrical studies would be required for each test case requiring significant additional computational time which is thought to be unnecessary for the early stage of testing the developed freeze-flow control methods.

A fully transient preconditioning time of 1500s was applied at the beginning of the simulation to ensure a fully developed air flow and temperature field before a switch to the first frozen period was permitted. This preconditioning time is assumed to be generally unnecessary for the adaptive control method as this method determines a switch automatically when it is possible. However, for comparison with the invariable control method the same preconditioning time was used in cases 1-3. The simulation period for case 4 is double of that of cases 1-3 and requires significant computational resources. In an attempt to reduce the simulation time, no preconditioning time was used in case 4 for the adaptive control method by testing this automatic approach.

Table 5.2: Parameter settings for the invariable control method for benchmark 1.

Case	Time step unfrozen period [s]	Time step frozen period [s]	Unfrozen period length [s]	Frozen period length [s]
1-4	1	300	300	1800

Table 5.3: Parameter settings for the adaptive control method for benchmark 1.

Case	Time step unfrozen period [s]	Time step frozen period [s]	MAX-LOOPS [-]	EXTEN-SION [s]	MAX-TEMP [K]	EVENT [K]
1-3	1	60	2	300	0.2	0.2
4	1	60	3	180	0.5	0.5

5.4.2 Natural ventilation (Case 1)

In the base case, air enters the room through the low level opening driven by the pressure difference across the opening. The cool air is warmed by the wall, rises along the wall and leaves the air domain through the high level opening (see Figure 5.2). The flow field elsewhere is weak and temperature stratification occurs (see Figures 5.3 and

5.4, showing different temperature values at MPs 3 – 5 and different velocity magnitudes at MPs 7 and 8). Since the temperature difference between the wall and the adjacent air is greater at low level, a higher heat transfer occurs relative to high level which subsequently leads to more rapid cooling of the solid at low level (see Figure 5.2). The descending curves for MPs 1 and 2 indicate a gradual cooling of the solid wall.

The invariable and the adaptive control methods produce similar results (Figures 5.3 and 5.4) and agree well with the base case at the end of the unfrozen flow period. The main difference between the methods is the gradual increase of frozen flow period length for the adaptive control displayed at MP 7 in Figure 5.4 by the step change of velocity. Periods of up to 2h 10mins towards the end of the 12h simulation occur for the adaptive control, while it is constant at 30min for the invariable control. Furthermore, no step is visible in the temperature graph for MP3 at the beginning of the simulation for the adaptive control compared to the invariable control since the frozen flow period was sufficiently short.

For the invariable control method, the CPU time required 75% less than that required by the base case. The size of the output file (required for post-processing) was 63% less than that generated by the base case despite the data being stored at the same frequency (every 5min) in both cases. In comparison, by using the adaptive control method, the CPU time and output data were reduced by 88% and 70% relative to the base case, respectively. Results are also presented in Zitzmann et al. (2007b) which has been accepted for publication.

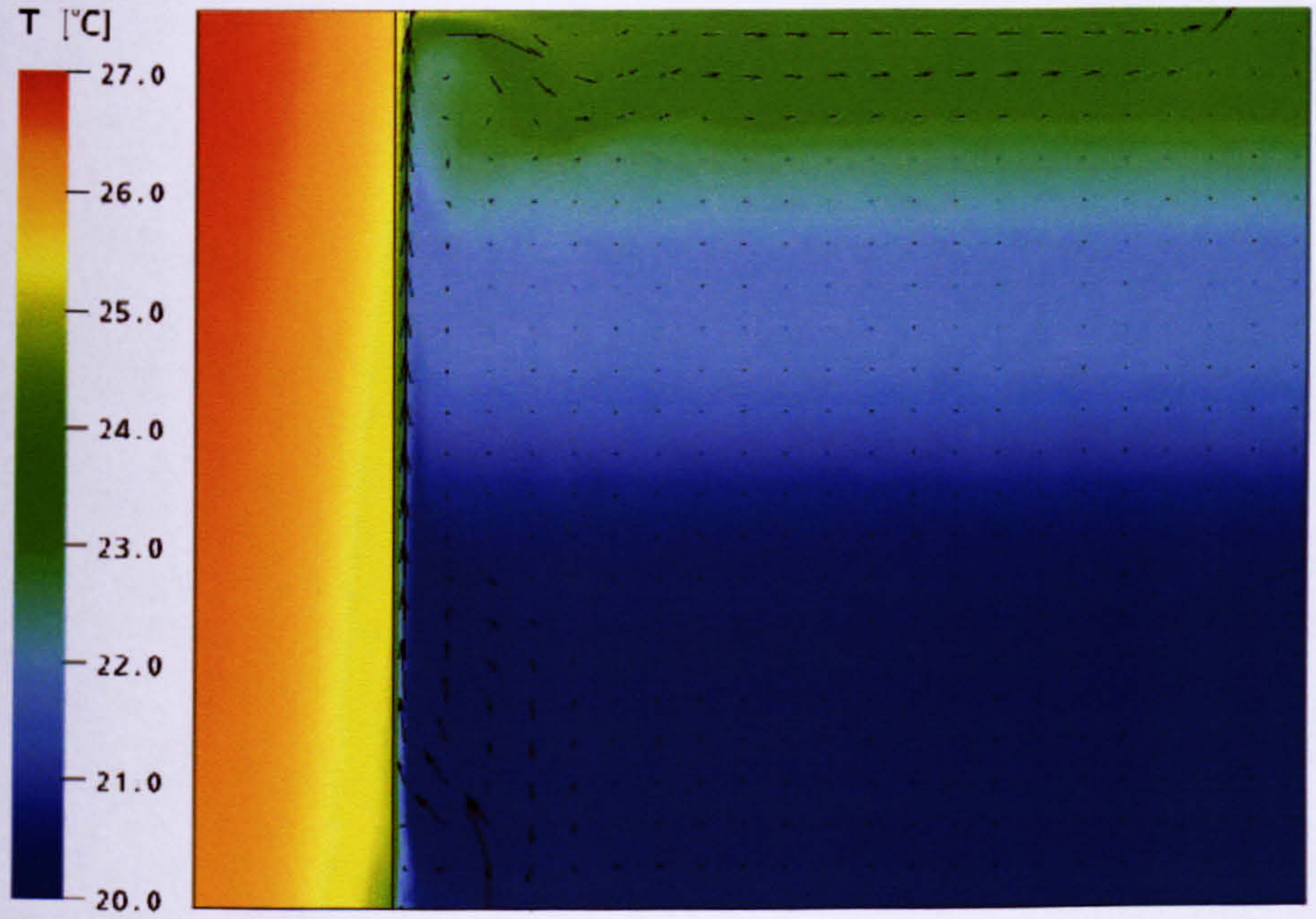

Figure 5.2: Temperature and velocity field for the base case after a simulation time of 12h (Benchmark 1, Case 1).

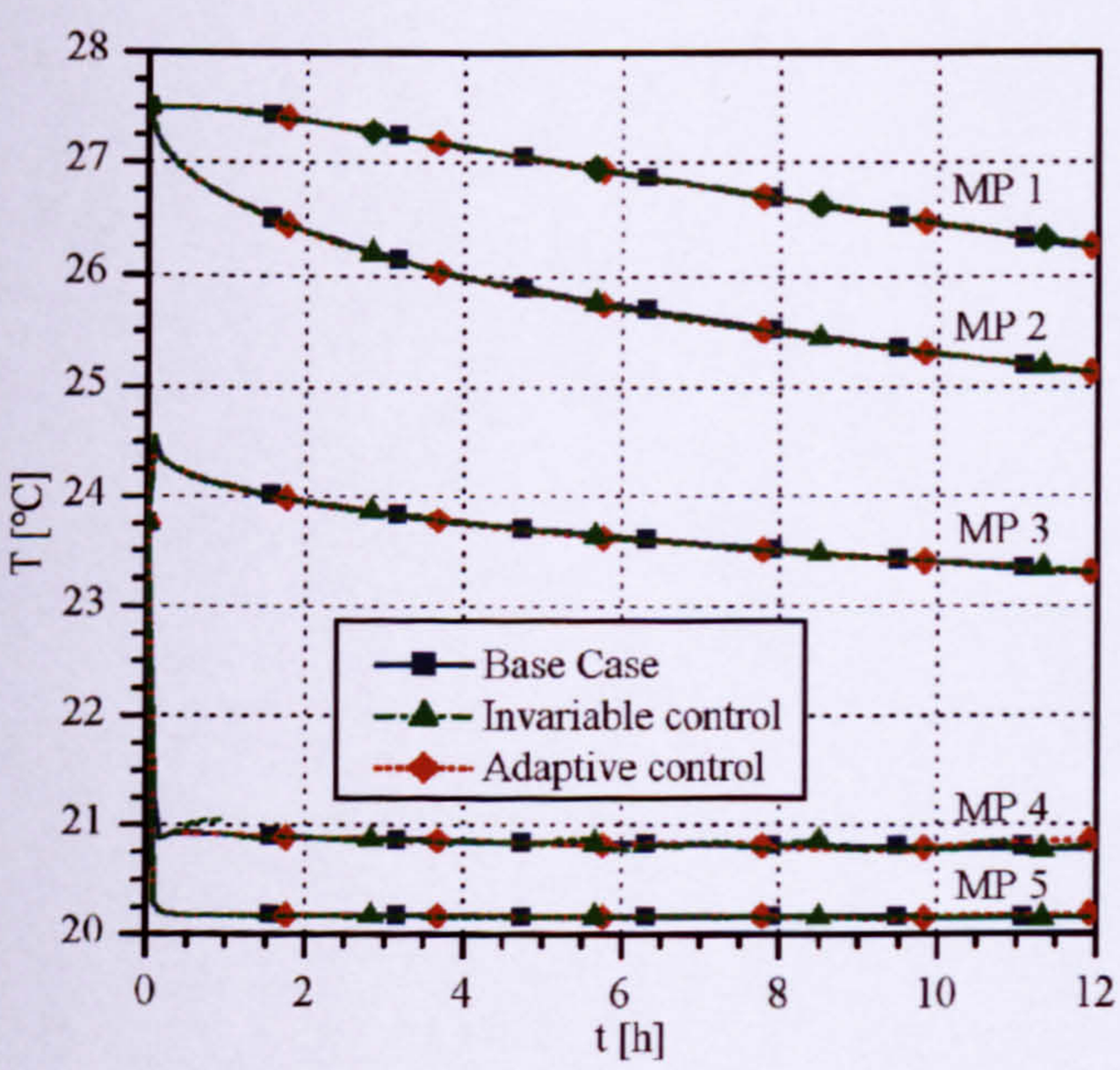

Figure 5.3: Temperature predictions at the monitor points (Benchmark 1, Case 1).

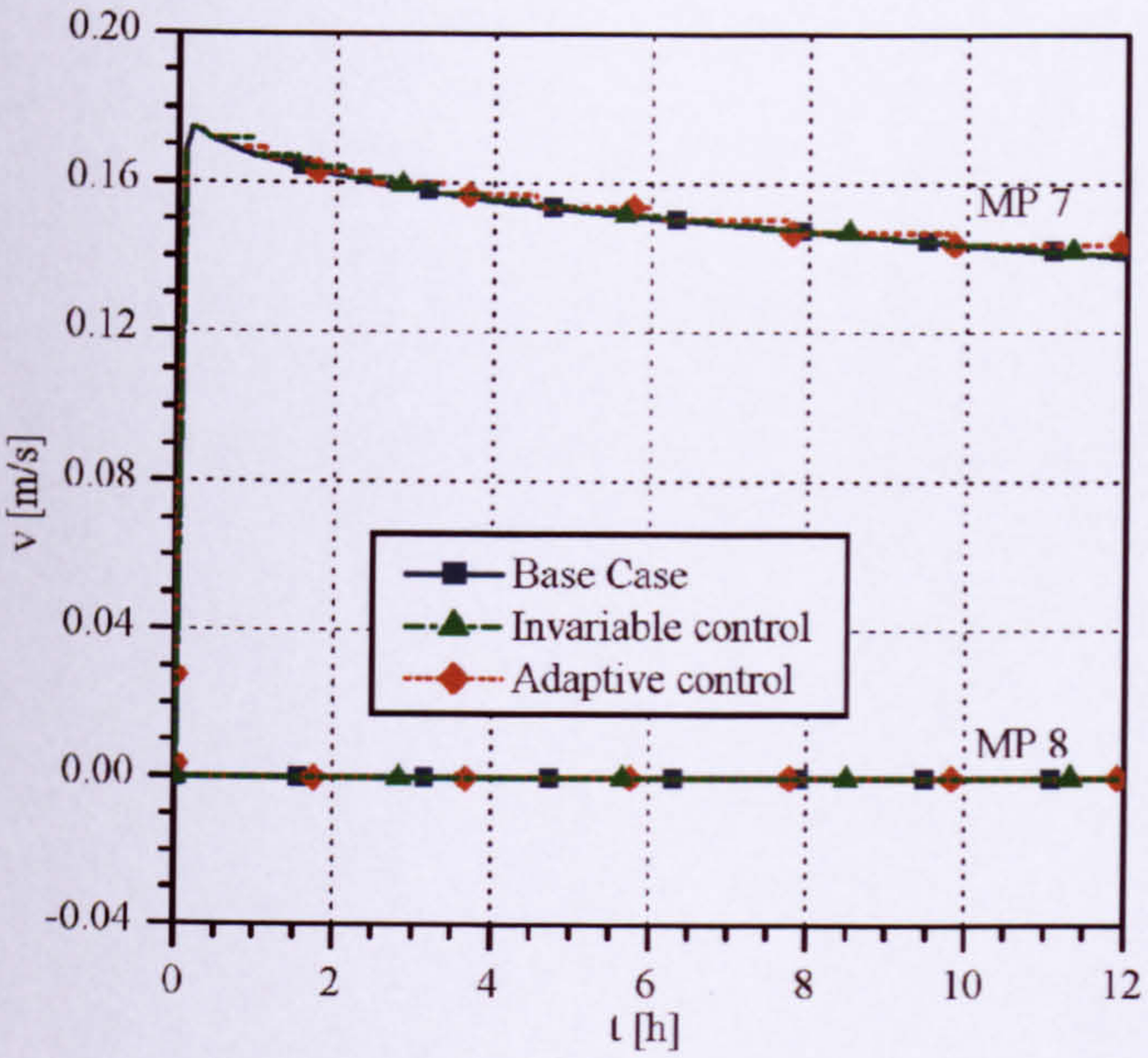

Figure 5.4: Velocity predictions at the monitor points (Benchmark 1, Case 1).

5.4.3 Mechanical ventilation (Case 2)

In the base case, air enters the room at low level through the inlet and warms as it rises along the hot surface (see Figure 5.5). The warm air leaves the room at high level through the outlet as observed in case 1. Elsewhere in the room a circulating air flow develops creating a homogeneous air temperature as illustrated in Figure 5.5 and indicated by equal values for MPs 3 - 5 in Figure 5.6. In the case of mechanical ventilation the cooling of the solid material is faster compared with the natural ventilation case since the air entering the room has a higher flow-rate and leads to a higher heat transfer at the wall surfaces (compare Figures 5.3 and 5.6).

The curve shapes in Figures 5.6 and 5.7 show similar results for the invariable and adaptive freeze-flow control methods and the base case. However, the freeze flow methods predict a greater cooling rate for the solid wall than the base case (see MPs 1-2) leading to a temperature difference of about 0.2K at the end of the 12h simulation. This is thought to be due to an over-predicted surface heat transfer due to the frozen flow periods which contain velocity values from the last unfrozen flow period. Although this behaviour was not shown for case 1 for the monitoring points, the faster

cooling might have occurred at other regions in the computational model which were not monitored.

In comparison with the base case, simulations with the invariable control method required only 79% and 62% of CPU time and output data, respectively. Better performance was achieved using the adaptive control method (84% and 66% respectively). The reason for this improvement is the gradual increase of frozen flow periods for the adaptive control, resulting in a frozen time period of up to 1h 31mins compared to the fixed periods of 30min in the invariable control simulation. Results are also presented in Zitzmann et al. (2007b) which has been accepted for publication.

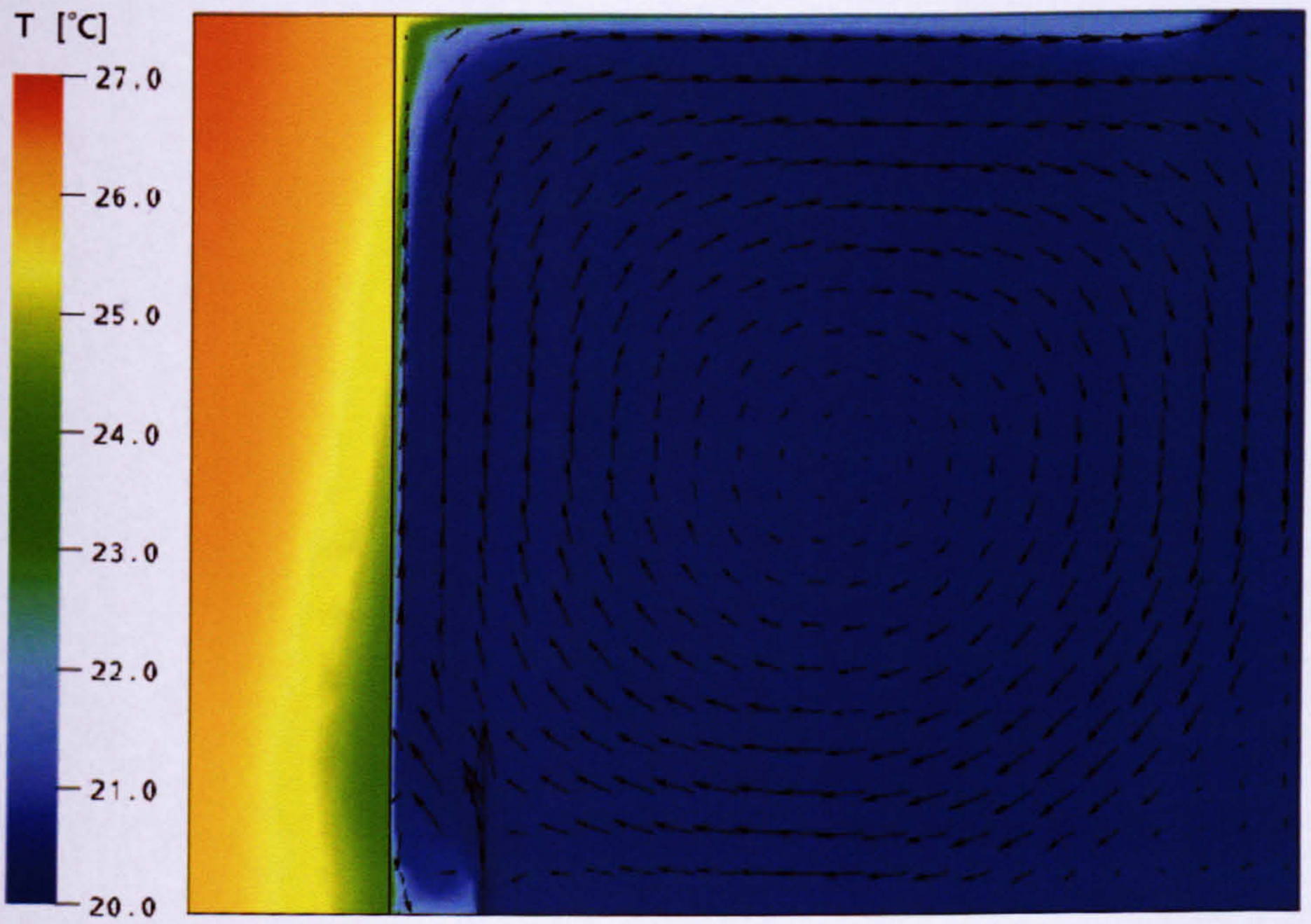

Figure 5.5: Temperature and velocity field for the base case after a simulation time of 12h (Benchmark 1, Case 2).

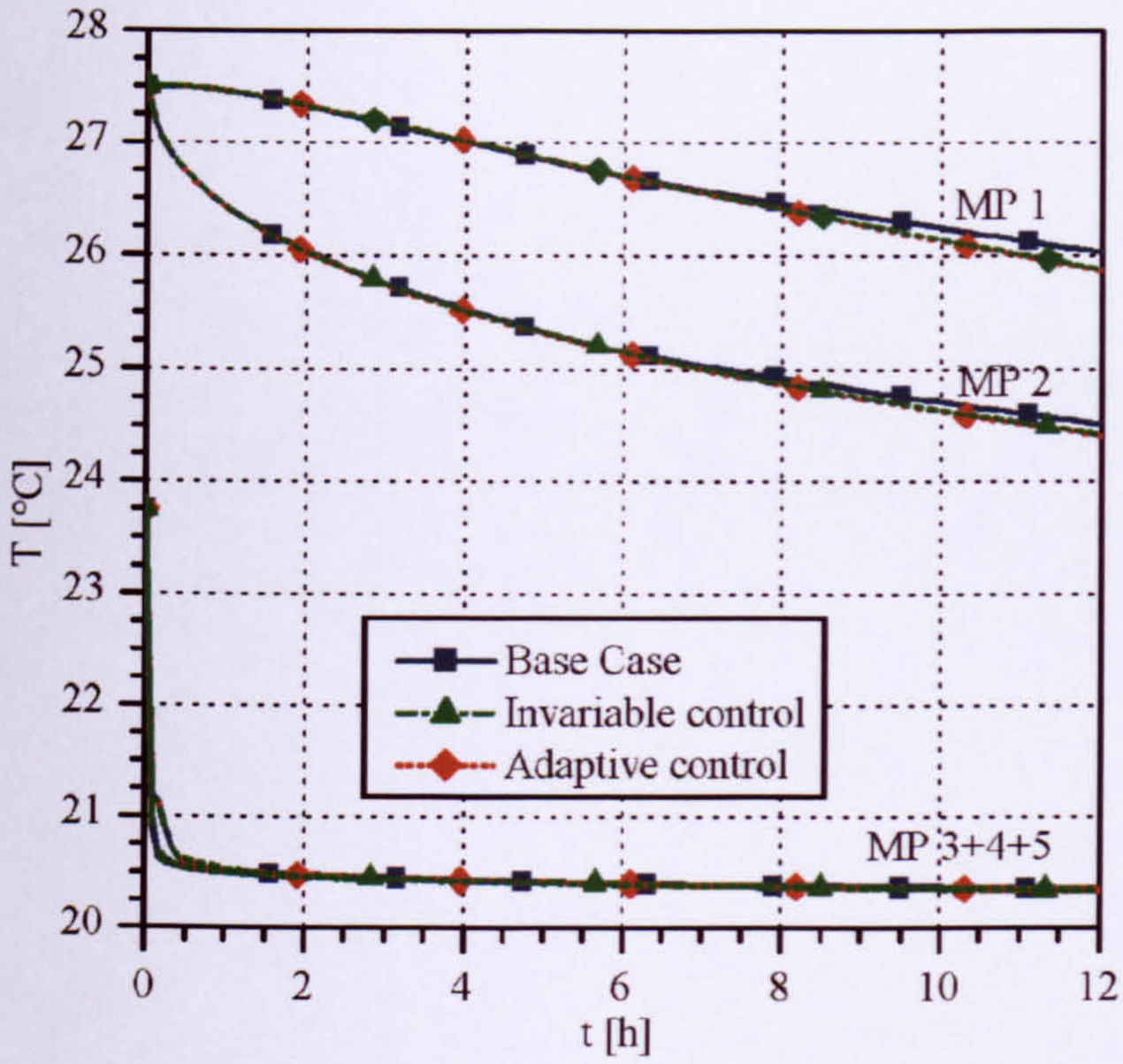

Figure 5.6: Temperature predictions at the monitor points (Benchmark 1, Case 2).

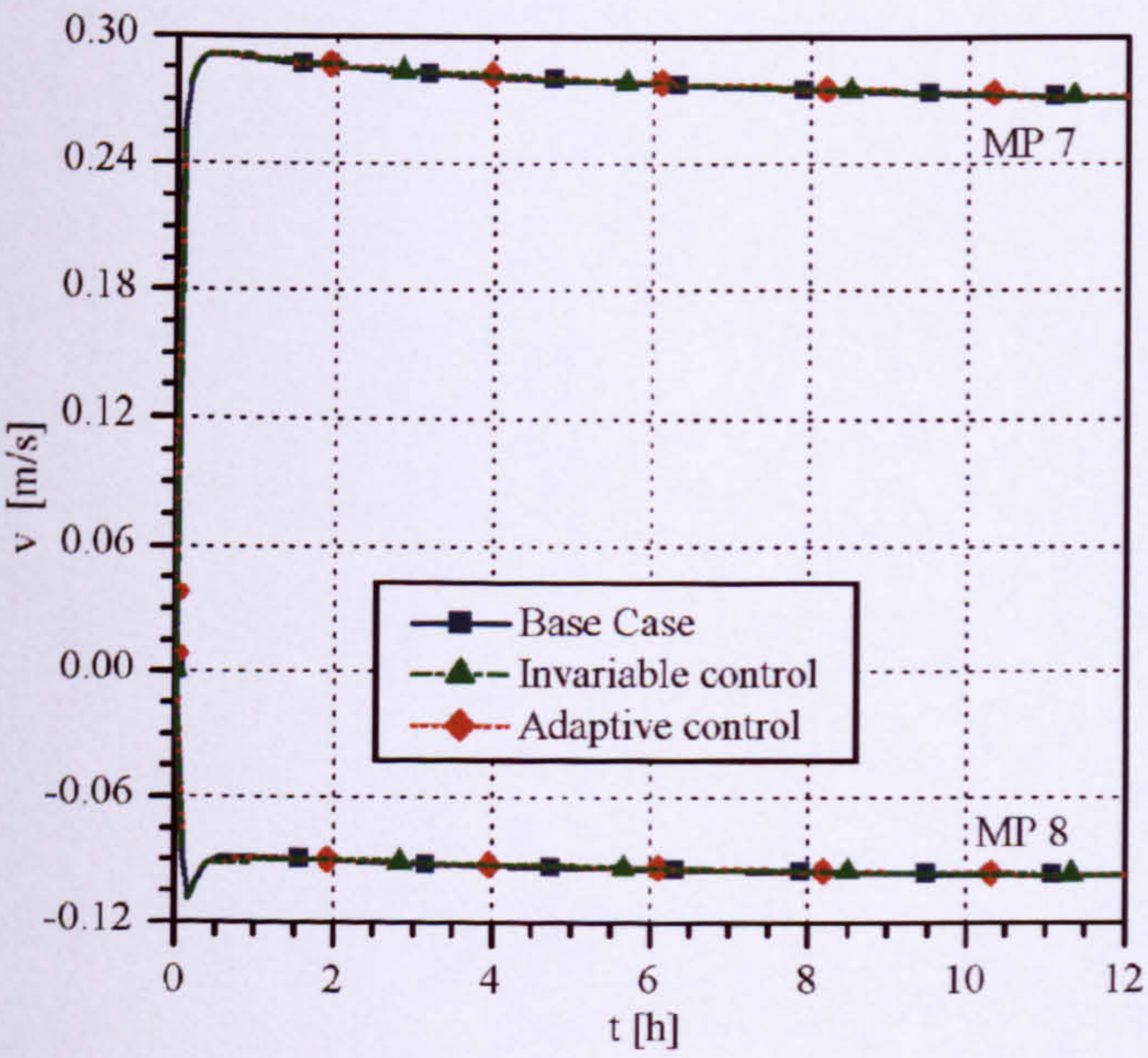

Figure 5.7: Velocity predictions at the monitor points (Benchmark 1, Case 2).

5.4.4 Free convection for constant ambient temperature conditions (Case 3)

In this case all openings are closed. The air flow is driven purely by free convection which occurs at the hot solid wall surface (BC 6) and at the cold opposite wall surface (BC 7). This causes a flow circulation in a clockwise direction (Figure 5.8). Temperatures of different magnitude at MPs 3-5 (Figure 5.9) indicate the development of temperature stratification in the room.

Figures 5.9 and 5.10 display the same temperatures and velocities for the invariable and adaptive control method and the curves align well with results for the base case. Only at MP 3 do the temperatures cool down marginally quicker using the freeze-flow methods due to a higher convective heat transfer caused by using velocities from the last unfrozen flow period. However, the maximum deviation is only 0.15K.

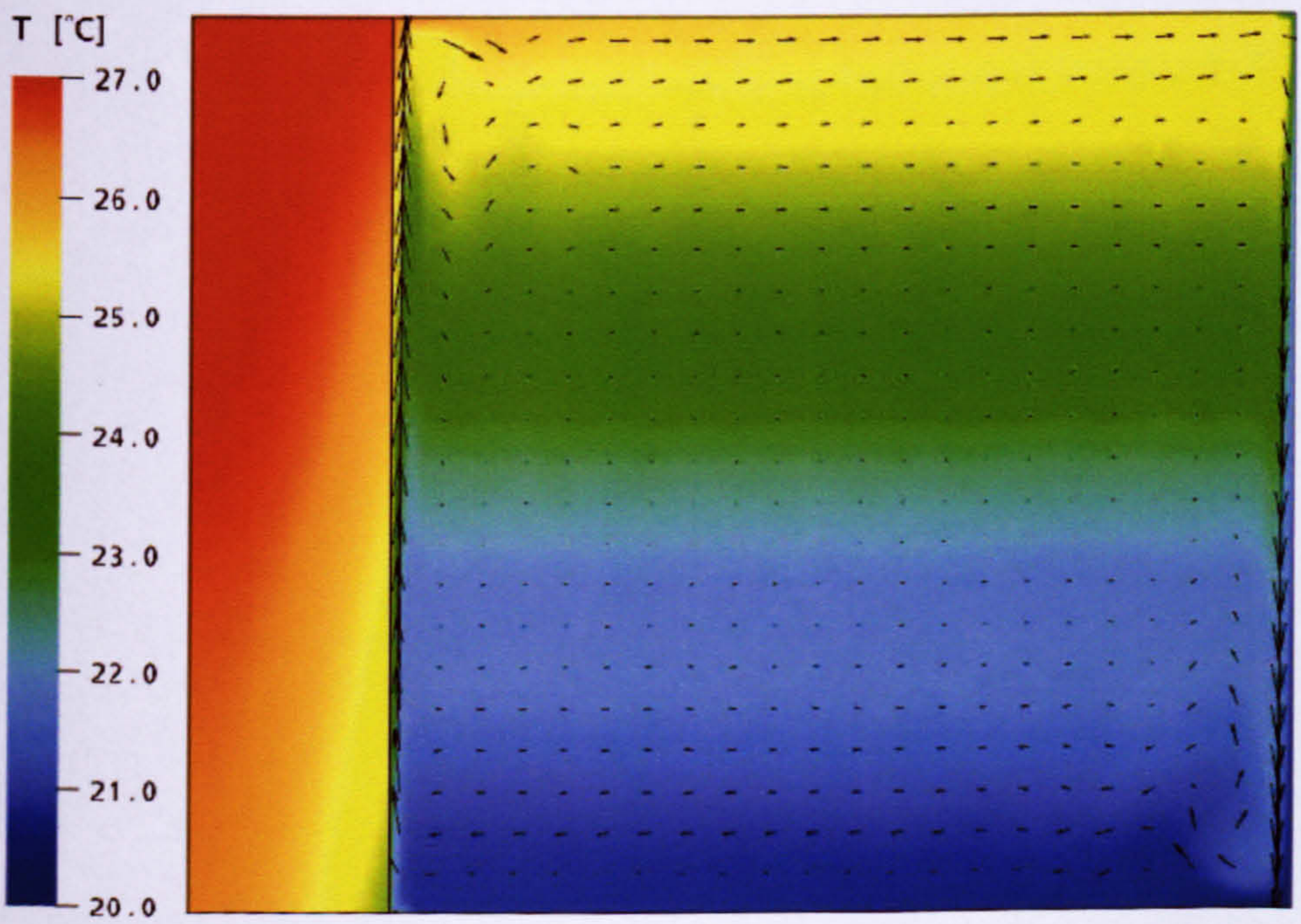

Figure 5.8: Temperature and velocity field for the base case after a simulation time of 12h (Benchmark 1, Case 3).

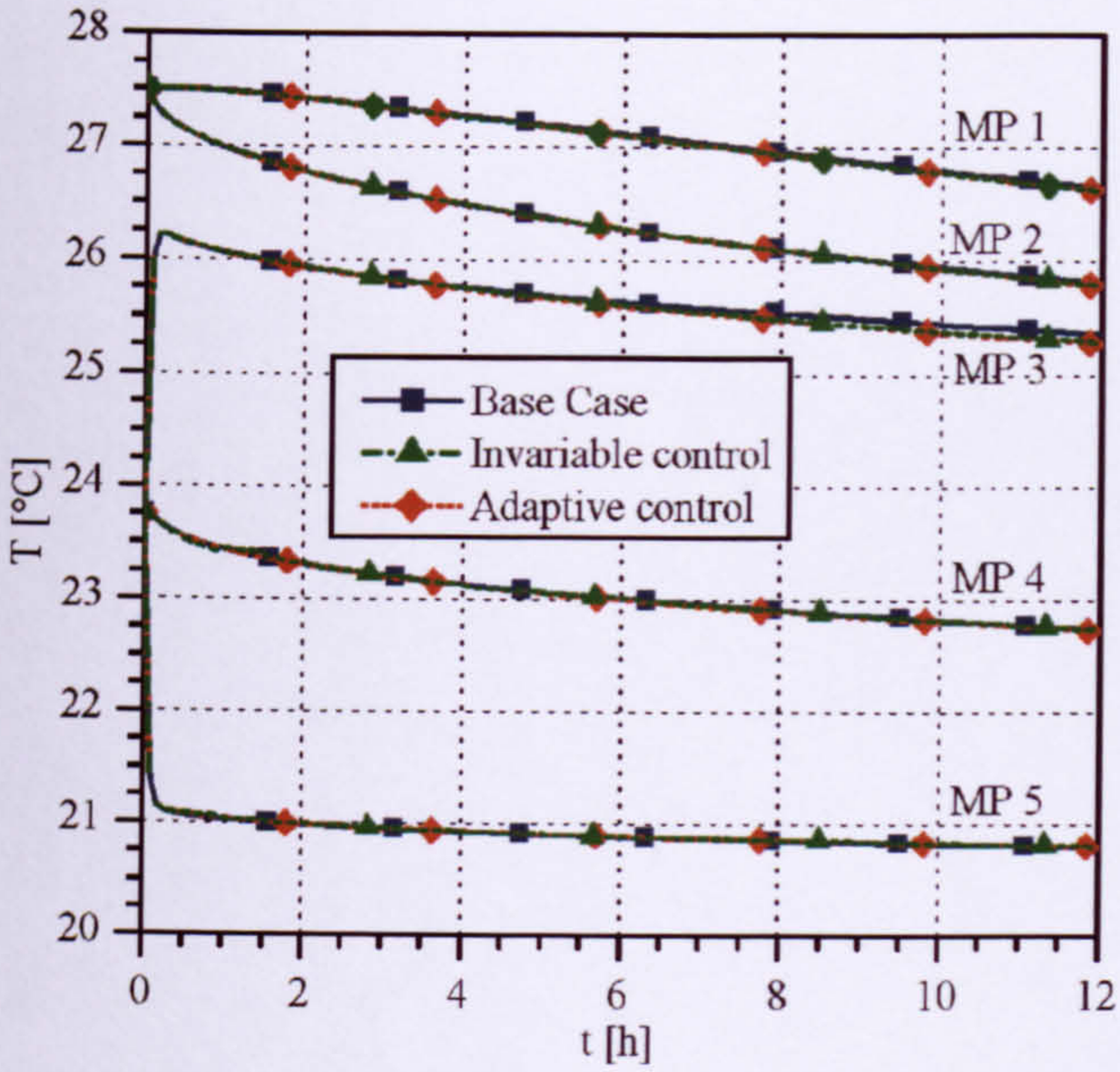

Figure 5.9: Temperature predictions at the monitor points (Benchmark 1, Case 3).

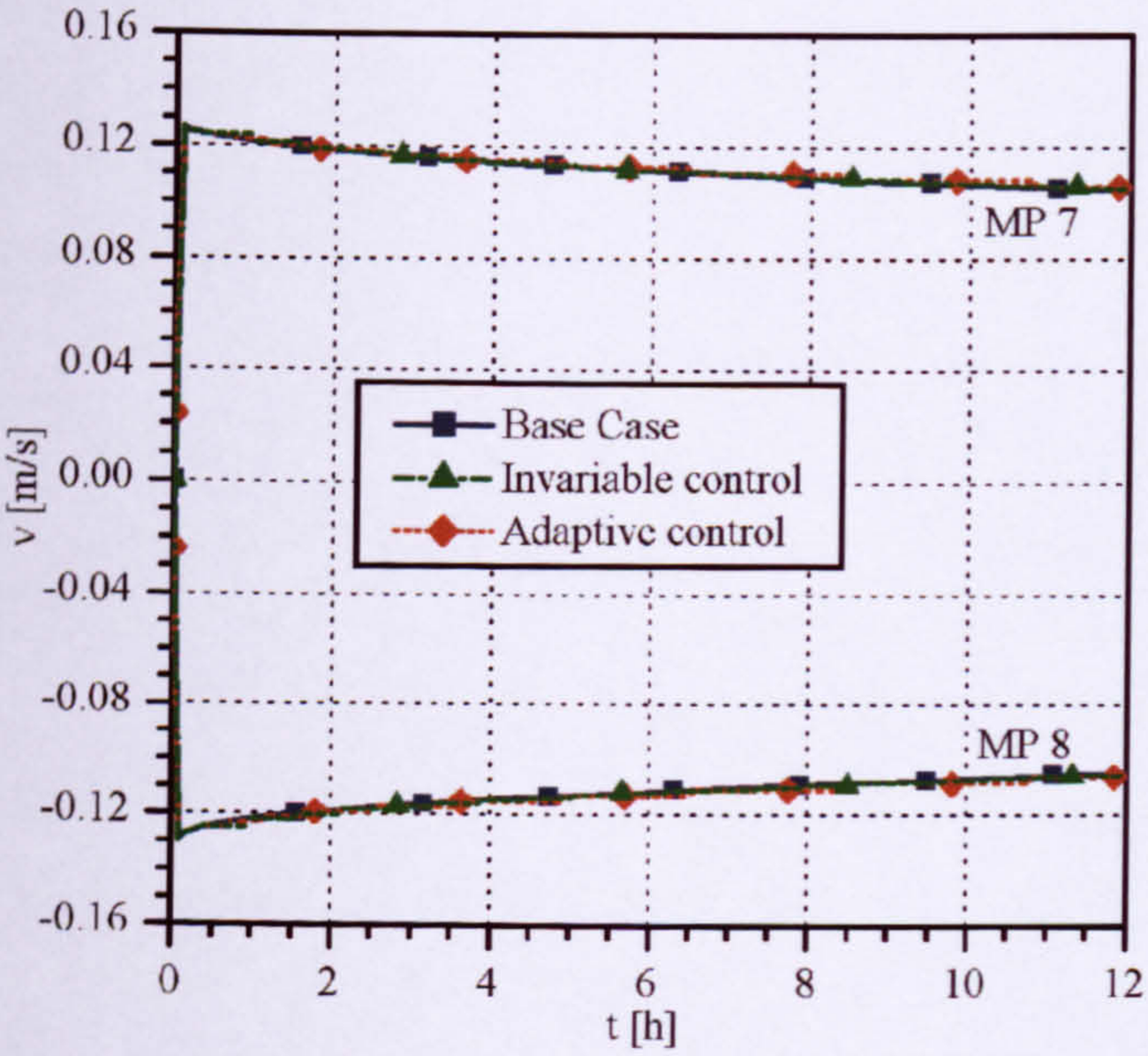

Figure 5.10: Velocity predictions at the monitor points (Benchmark 1, Case 3).

Compared with the base case, the simulation required 78% and 66% less CPU time and data output size using the invariable control method, respectively. Better performance was again achieved using the adaptive control method (89% and 74% respectively).

Frozen flow periods gradually increased up to 2h 12mins at the end of the 12h simulation. Results have also been summarised in Zitzmann et al. (2006a), Zitzmann et al. (2006b) and Zitzmann et al. (2007a).

5.4.5 Comparison of results for cases 1-3

When comparing the real time required for base cases 1-3 using a desktop PC (Intel Pentium 4, 3.6GHz, 2GB RAM) to achieve a converged simulation of 12h, the free convection case displays the highest computational cost (44h 3mins 34s) followed by the natural ventilation case (39h 40mins 50s) and then the mechanical ventilation with the lowest cost (28h 5mins 4s). The lower costs correspond to the cases in which there is ambient air entering the domain which possibly stabilises the primary air flow and generates faster convergence. Looked at another way, pure buoyancy driven flows often yield slower convergence rates due to the weak coupling between the momentum and energy equation.

The figures in sections 5.4.2, 5.4.3 and 5.4.4 have shown that the flow field with the lowest velocities and thus with the lowest cooling rate is the free convection case followed by the natural ventilation case and mechanical ventilation case. Due to the slower changes in the temperature field for the free convection case, the periods of frozen flow are longer and in most cases result in a better CPU time and output data reduction performance compared to case 1 and case 2 (see Table 5.4). The simulation time was reduced by a further 50% for most cases using the adaptive control method when compared with the invariable control method. Although, longer time periods of unfrozen flow for the invariable control method might reduce the computational effort, this potentially leads to an increase of simulation errors in periods when the thermal conditions in the room change faster.

Table 5.4: Summary of reductions for CPU time and output file data size using the invariable and adaptive control methods for cases 1-3 compared to the base case (Benchmark 1).

Case	Invariable control		Adaptive control	
	CPU time reduction [%]	Output data reduction [%]	CPU time reduction [%]	Output data reduction [%]
1	75	63	88	70
2	79	62	84	66
3	78	66	89	74

5.4.6 Free convection in an enclosure for varying ambient temperature conditions (Case 4)

An additional monitor point, MP 6, located at the wall surface of BC 7 is used to track the time varying temperature condition through the simulation; this provides a check that the boundary condition is behaving as intended. At the beginning of the simulation, the temperature increase at BC 7 gradually warms the air domain primarily due to free convection (see Figure 5.11). The solid wall (BC 6) partially absorbs the room heat load. When the external temperature (MP 6) falls below the internal wall surface temperature (MP 2) the process switches and the internal wall emits heat back to the room. After this time period (lasting about 11h 40mins), the primary air flow direction also switches. This is illustrated by MP 7 and MP 8 (Figure 5.12) where the signs of the velocity change. Figure 5.13 illustrates the flow field and the temperature gradients a few minutes before the velocity field inverts for the base case. A gradient of 1.2K is observed between the bottom and the top of the solid wall surface. This is a perfect example of the type of feature that can be modelled using dynamic CFD but cannot be predicted using zonal programs of dynamic thermal simulations.

Both freeze-flow methods reflect the results of the base case well. In the solid wall (MP 1 and MP 2) only small temperature over-predictions exist towards the end of the simulation period which shows a small accumulation effect of simulation error due to

the freeze-flow method. However, a more detailed analysis at different wall heights confirmed no deviation exceeding 0.2K.

Figure 5.12 shows that the deviations of the velocities for the invariable freeze-flow control method compared with the base case are largest when the temperature gradient in time (Figure 5.11) is at largest, while the maximum deviations in velocities remain almost constant for the adaptive control method. The largest errors in the predicted temperature field in the air domain compared with the base case are displayed at about 12h where the highest temperature gradient exists. The temperatures displayed at this time period at MPs 3-5 are shown in Figure 5.14 and the related maximum errors at the monitor points for the invariable and the adaptive control method are listed in Table 5.5. The table shows significantly smaller errors for the adaptive control compared with the invariable control method. This demonstrates the advantage of the adaptive control method: the error is minimized due to a shorter frozen flow period when the temperature is undergoing its greatest change. Moreover, the simulation has shown that the adaptive control method performs well without a user defined preconditioning period.

Comparing the CPU time and data output size with the base case, both control methods gave similar results, 75% and 77% for the invariable control respectively, 74% and 78% for the adaptive control method, respectively. However, the errors are smaller for the adaptive control method than for the invariable control as observed before in case 1. Results are also summarised in Zitzmann et al. (2006a), Zitzmann et al. (2006b) and Zitzmann et al. (2007a).

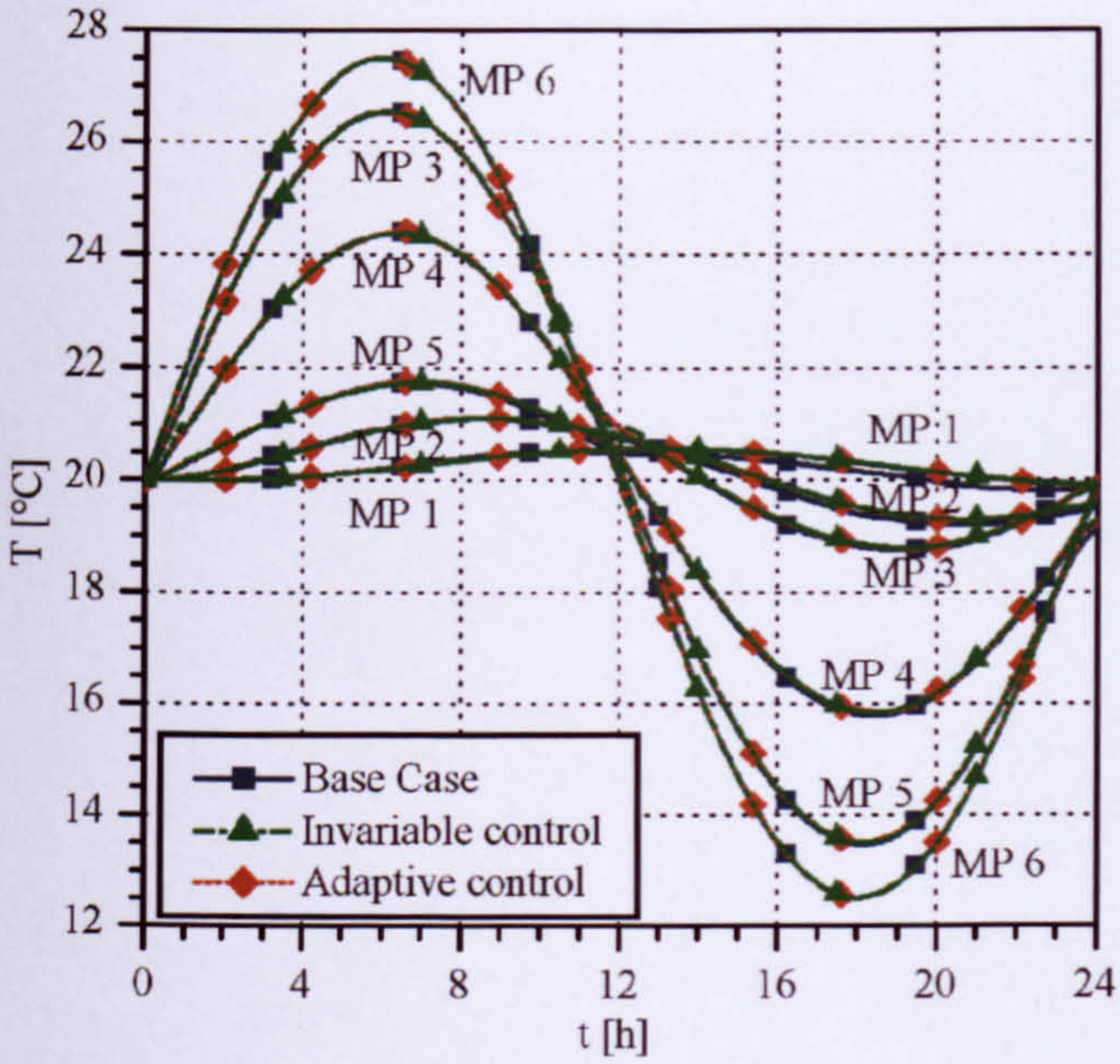

Figure 5.11: Temperature predictions at the monitor points (Benchmark 1, Case 4).

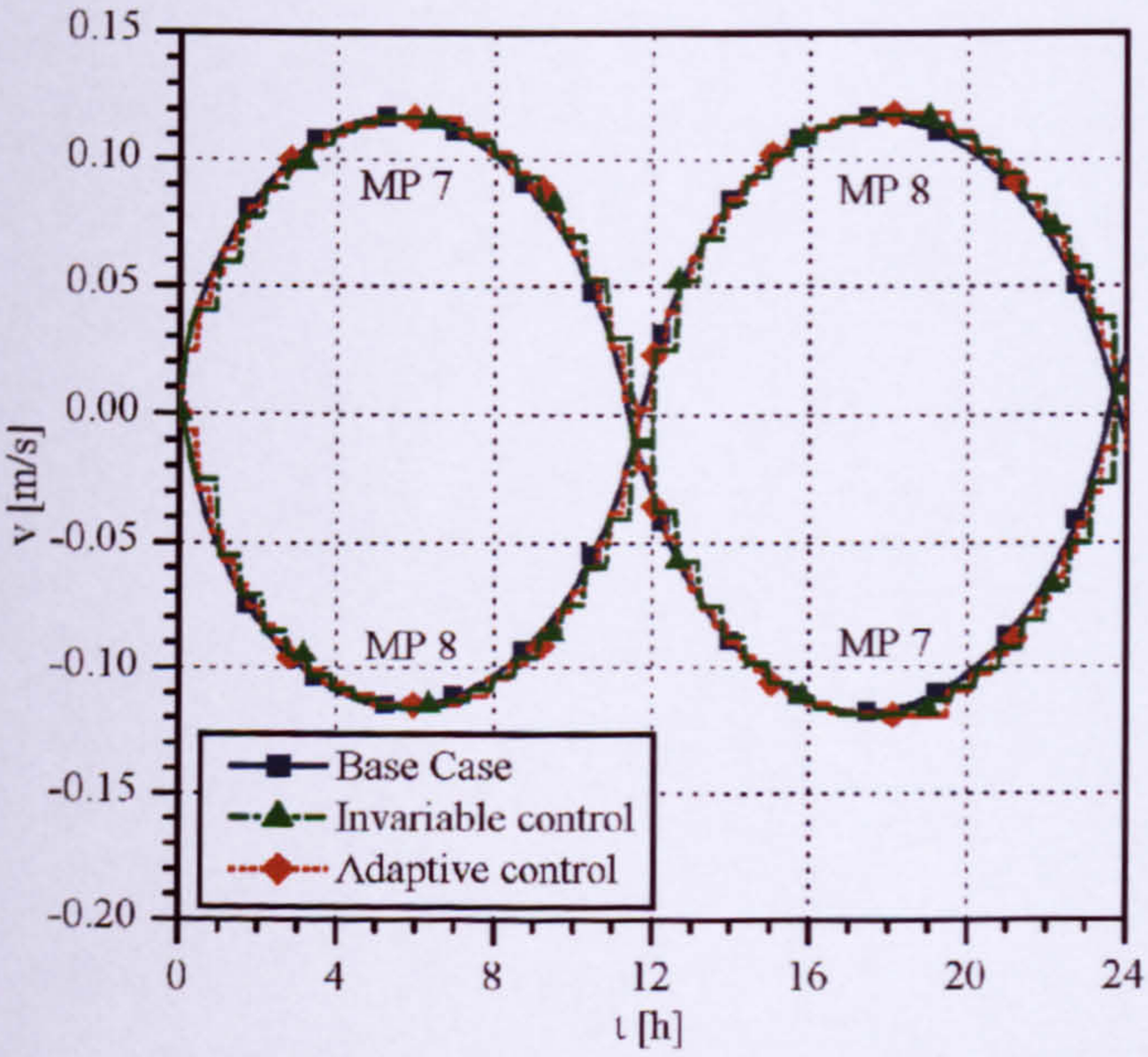

Figure 5.12: Velocity predictions at the monitor points (Benchmark 1, Case 4).

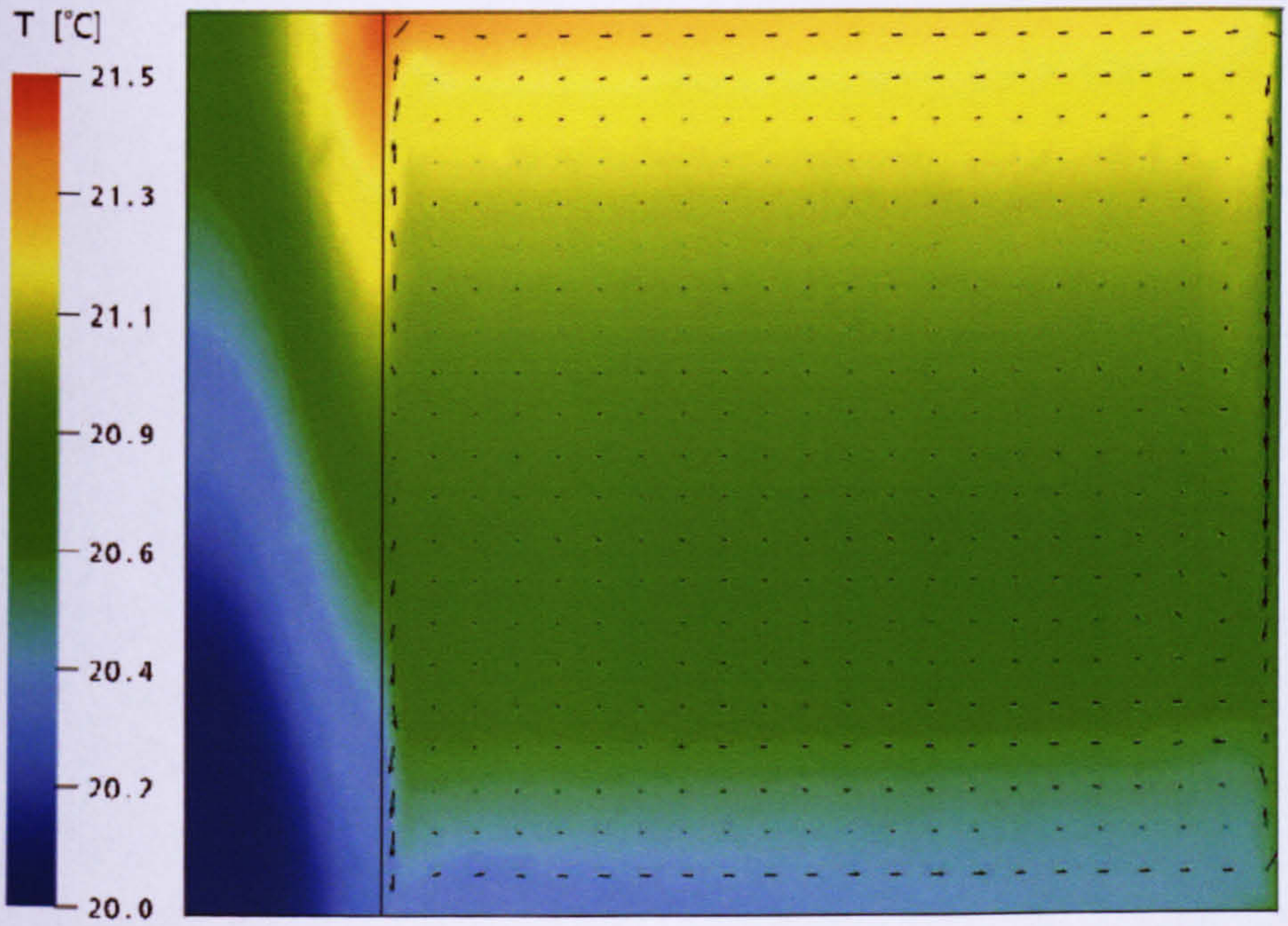

Figure 5.13: Temperature and velocity field for the base case after a simulation time of 11h 40min (Benchmark 1, Case 4).

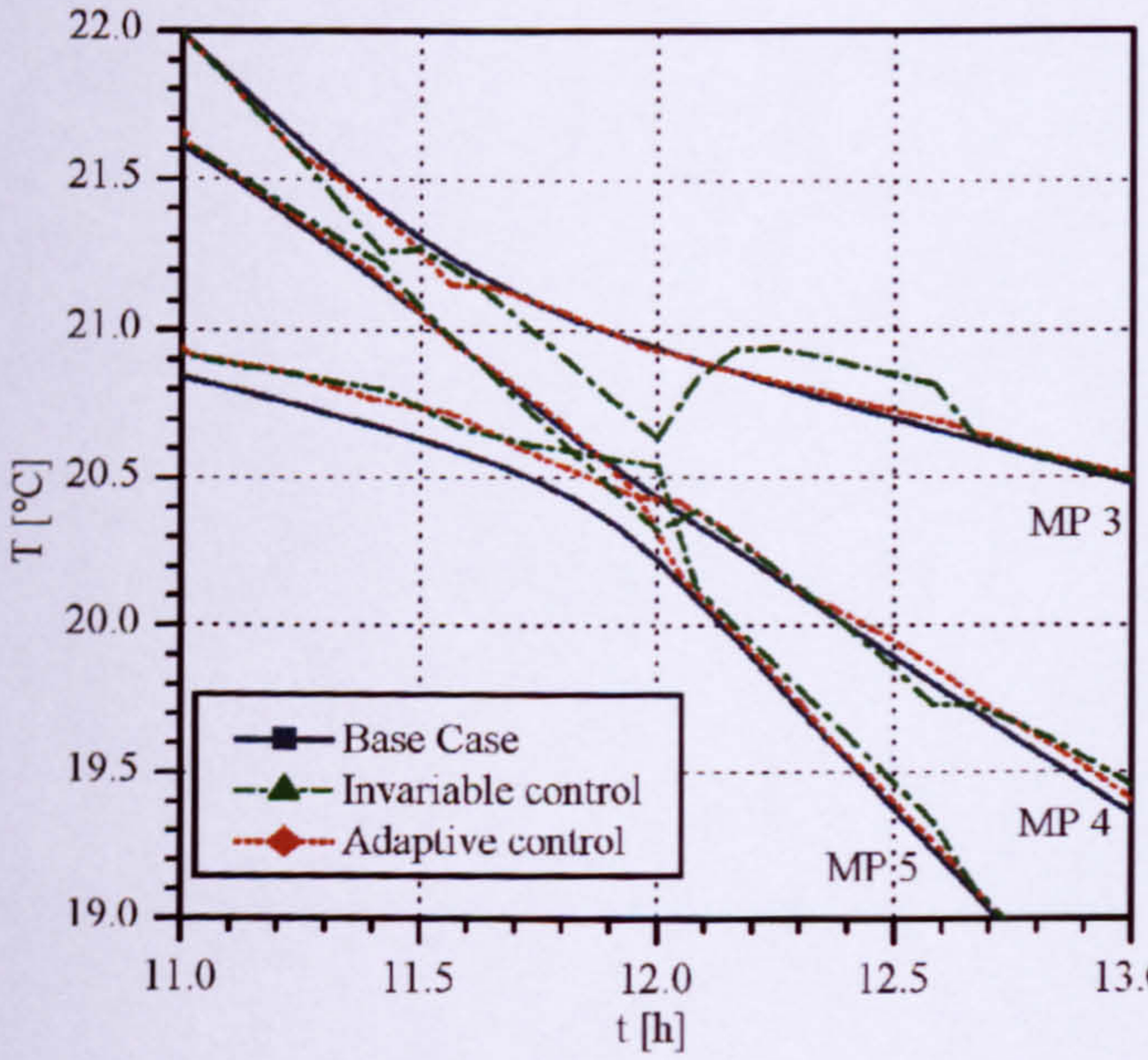

Figure 5.14: Temperatures at MPs 3-5 at a simulation time between 11 hours to 13 hours (Benchmark 1, Case 4).

Table 5.5: Maximum errors at MPs 3-5 for the invariable and the adaptive control method in comparison with the base case (Benchmark 4, Case 4).

Monitor Point	Invariable control method		Adaptive control method	
	at time [h]	Error [K]	at time [h]	Error [K]
3	12.0	0.30	11.6	0.10
4	12.0	0.10	12.1	0.05
5	12.0	0.35	11.9	0.15

5.4.7 Inclusion of radiation heat transfer in benchmark 1

The objective of the investigation in this section was to verify the adaptive freeze-flow method when radiation heat transfer is included for case 3 (free convection). The investigation focused on the adaptive control method since it has shown a better performance in the previous sections in comparison with the invariable freeze-flow control method.

Temperature predictions at each monitor point using the adaptive freeze-flow method were compared with those of the base case for a simulation of 12h (Figure 5.15). Radiation was calculated every time step. The temperatures predicted using the adaptive freeze-flow control method, agree well with those of the base case. Temperature under-predictions are less than 0.03K (see MP 1 at the end of a simulation period of 12h). In comparison with the case in which no radiation is calculated, the errors have decreased. Since the wall potentially cools down faster during frozen flow periods compared to the base case, radiation heat transfer is consequently smaller at the same time which compensates for the faster cooling due to convection. Compared with the base case, a CPU time reduction of 84% was achieved using the freeze-flow method. Results are also summarised in Zitzmann et al. (2007d) which is submitted for publication.

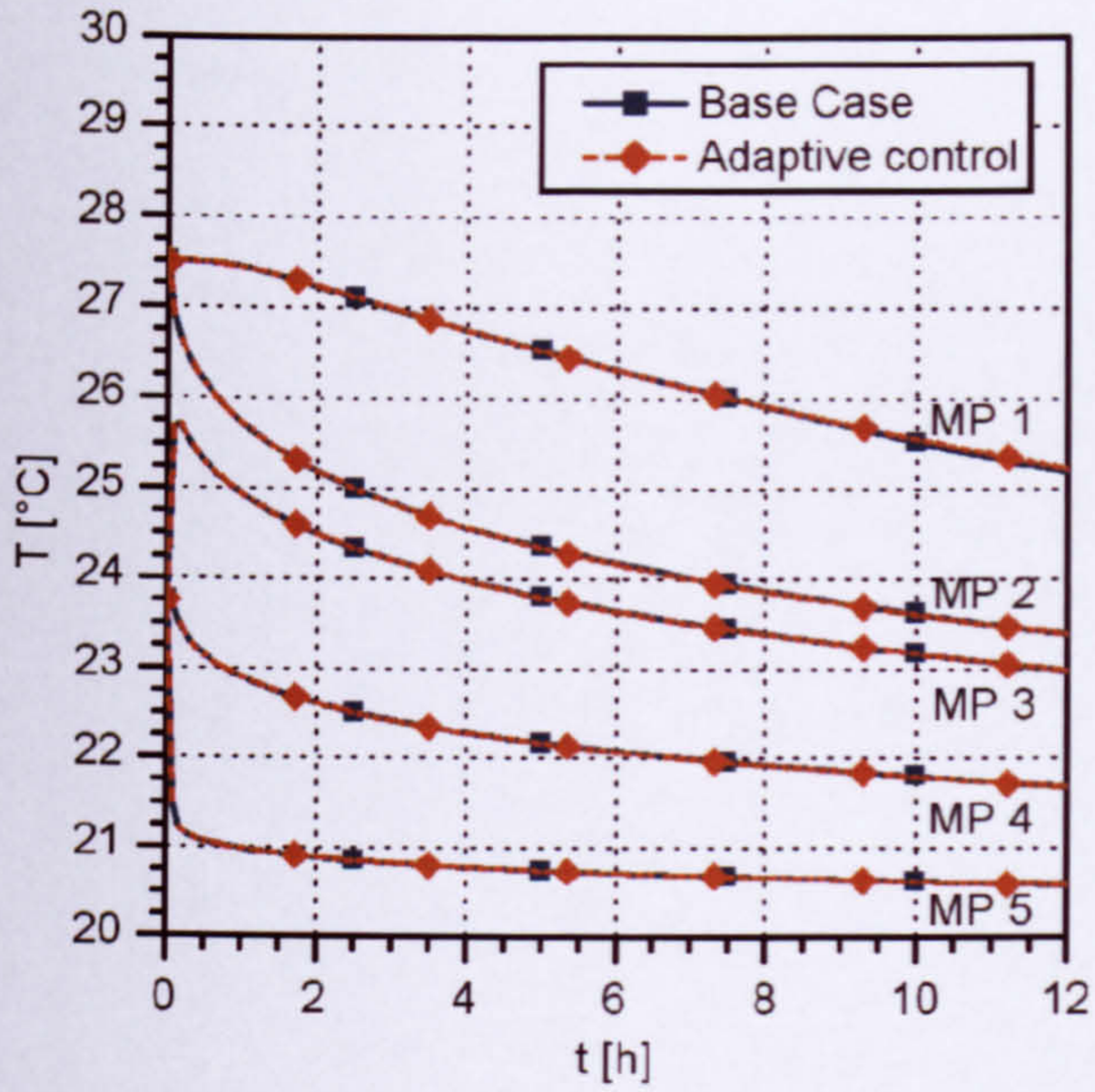

Figure 5.15: Temperature predictions for test case 3 of benchmark 1 including radiation heat transfer – application of the adaptive freeze-flow control method.

5.5 Summary

A small scale room model of conjugate heat transfer between a solid of high thermal mass and a fluid domain with purpose-provided openings for ventilation (benchmark 1) was introduced in this chapter to verify the automated invariable and the adaptive freeze-flow control method for various air flow mechanisms (i.e. case1: natural ventilation, case 2: mechanical ventilation and case 3 and 4: free convection). CFD results were compared with those of full dynamic CFD simulations in which all equations were continuously solved without interruption (base case).

The intention of the new adaptive control method was that frozen flow periods are as long as possible and unfrozen flow periods are no longer than necessary (see chapter 4). This chapter has demonstrated the advantage of this feature compare with the invariable control method: frozen flow periods increased when the thermal conditions changed only slowly and decreased when the thermal conditions changed rapidly or when the flow field was unstable.

Small prediction errors (i.e. up to 0.3K) were seen for the automated invariable freeze-flow control method when the boundary conditions changed rapidly. The errors were reduced for the automated adaptive control method since the frozen flow periods were shorter at this time in the latter. Furthermore, the invariable control method required a user-defined pre-conditioning time to allow for a full development of the air flow patterns before the first frozen flow period was permitted to start. It was demonstrated for case 4 (free convection with sinusoidal time varying boundary conditions) that this was not necessary for the adaptive control method since the adaptive control automatically switches from unfrozen to unfrozen periods when the air flow patterns have fully developed (i.e. this is when only a small number of iterations is required). This approach is a further advantage of the adaptive control method, since the preconditioning time in the unfrozen flow mode is only as long as necessary.

Results for both control methods compared favourably with the base cases for each test. However, the investigation has also shown a general potential drawback of the freeze-flow method. That is, during long periods of cooling/heating from a source, a room can cool faster/warm slower due to the over/under-prediction of the surface heat transfer, if radiation heat transfer is neglected. However, the errors predicted were small (not more than 0.3K within the solid for benchmark 1 for a simulation period of 12h).

The CPU time and output data size was significantly reduced using both freeze-flow control methods. For the gradual cooling of a massive wall, the CPU time and output data size was only about 21% and 34% respectively for the invariable control method compared with the base case. The adaptive control method demonstrated that only about 11% and 26% in CPU time and output data size was required, respectively. Thus, it was possible to reduce the required simulation time again by a further 50% for some test cases using the adaptive control method rather than the invariable control method. For the test case with time varying ambient conditions the methods showed similar performances for the reduction of computational resources.

When radiative heat transfer was included, the adaptive freeze-flow method demonstrated an improved performance compared with the case of free convection where radiation was excluded, and the results agreed well with those of the base case

(0.03K instead of 0.2K of error compared with the base case for the exemplary investigated case 3).

The investigation in this chapter has shown that the overall performance of the freeze-flow method can be significantly improved using the newly developed adaptive control method. This control method has demonstrated a good trade-off between accuracy of predictions and computation effort for dynamic thermal simulations for various flow mechanisms.

CHAPTER 6

DYNAMIC 3D MODELLING OF A HIGH THERMAL MASS ENCLOSURE (BENCHMARK 2)

6 Dynamic 3D Modelling of a High Thermal Mass Enclosure (Benchmark 2)

6.1 Preamble

In the previous chapter it was demonstrated that the freeze-flow method can be successfully automated and transferred to the CFD platform CFX. The invariable and the adaptive control methods showed a good trade off between simulation accuracy and computational effort for various flow phenomena. Further investigations in this chapter focus on the adaptive control method since this has shown a general improvement in performance over the invariable control method.

Former investigations were based on inter-model comparison using the same CFD code in order to verify the performance of the freeze-flow method (e.g. Somarathne et al. 2002). However, this procedure gives no evidence of the trueness of results for long thermal building simulations using CFD because prediction errors can also evolve due to other code specific approximations (e.g. discretisation techniques, radiation and turbulence models, equation linearization procedures, etc.). Validation of CFX results for long dynamic thermal simulations does not exist due to the restriction of computational resources and thus validation with experimental data is still required. Especially rooms which contain high thermal mass are interesting for modelling since the difference between the time constants of the air and the building fabric are particularly high.

Experimental data of the long-term thermal behaviour from test chambers with high thermal mass is rare. Most measurements are from field studies in real buildings which are exposed to real weather conditions and thus measurements potentially contain considerable uncertainties (see chapter 2.4). It is therefore more practical to define a benchmark room which can be handled by the CFD program and for which all boundary conditions are known. CFD results can then be compared with those of other

fundamentally different types of programs such as DTS programs to evaluate the plausibility of results.

This procedure of inter-model comparison between different codes is used in this chapter. The room model, referred to as benchmark 2, is based on the dynamic thermal simulation verification procedures of the VDI 6020-1 (2001). Thermal room predictions of CFX are compared with those of the zonal program TRNSYS, a reference model in the VDI 6020-1 (2001).

The details of benchmark 2 are given in section 6.2. Section 6.3 describes the implementation procedures of benchmark 2 in CFX and TRNSYS. The numerical results for CFX are compared with those of TRNSYS in Section 6.4. A summary of results is given in section 6.5.

6.2 Definition of Benchmark 2

6.2.1 The room model

The room model of benchmark 2 is based on the VDI 6020-1 (2001) and contains an air domain of 5m x 3.5m x 3m (L x W x H) which is a typical size for an office room. The room is enclosed by composite building fabric of high thermal mass (see Figures 6.1, 6.2 and 6.3). The following description of the benchmark contains some modifications of the geometry of the VDI model (for more details about the modifications see section 6.2.2). Details of the building component properties are shown in Table 6.1. Using Eq. (2.1), the ratio between the effective heat capacity and the net ground area for benchmark 2 is C_{eff}/A_{net}=199W·h/(m^2·K), which assigns the room to the 'heavy-weight' building category (see section 2.2.1) and thus the room contains a high thermal mass.

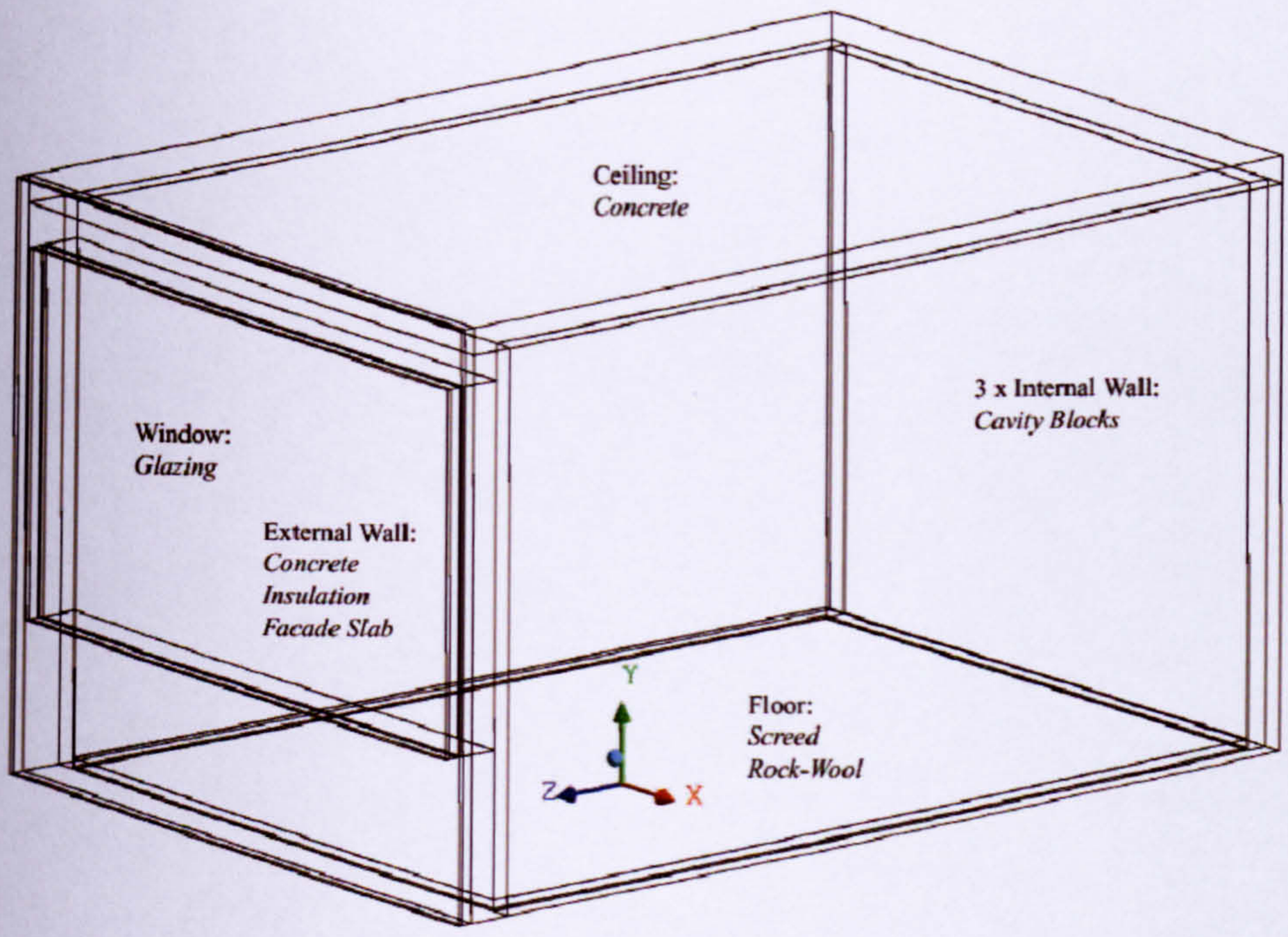

Figure 6.1: Benchmark 2 represents a large scale room enclosed by composite building fabric of high thermal mass (list order of components from room inside to outside).

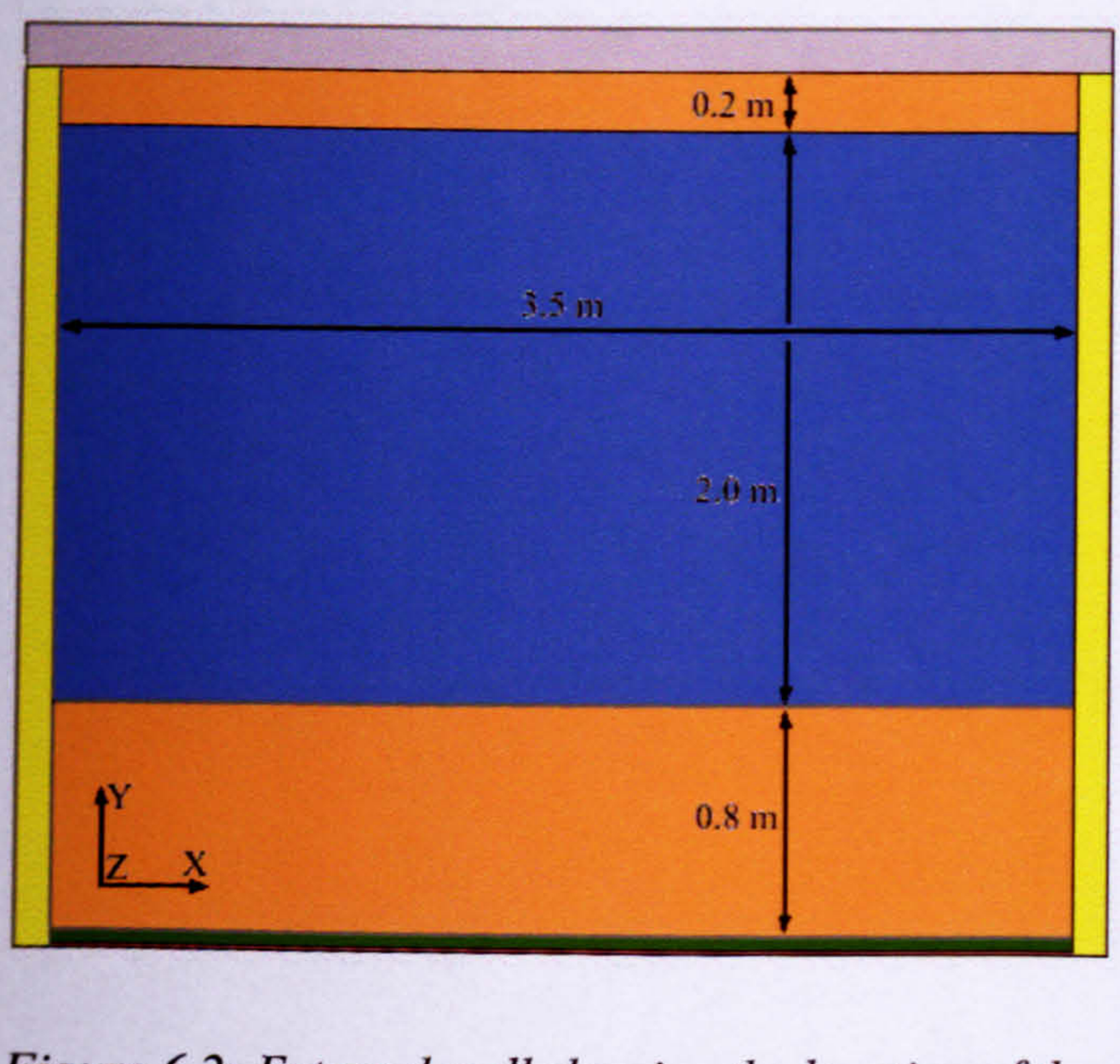

Figure 6.2: External wall showing the location of the window (Benchmark 2); concrete ceiling (grey shaded), external concrete wall (orange shaded), screed (green shaded), rock wool (pink shaded), cavity blocks (yellow shaded) and window (blue shaded).

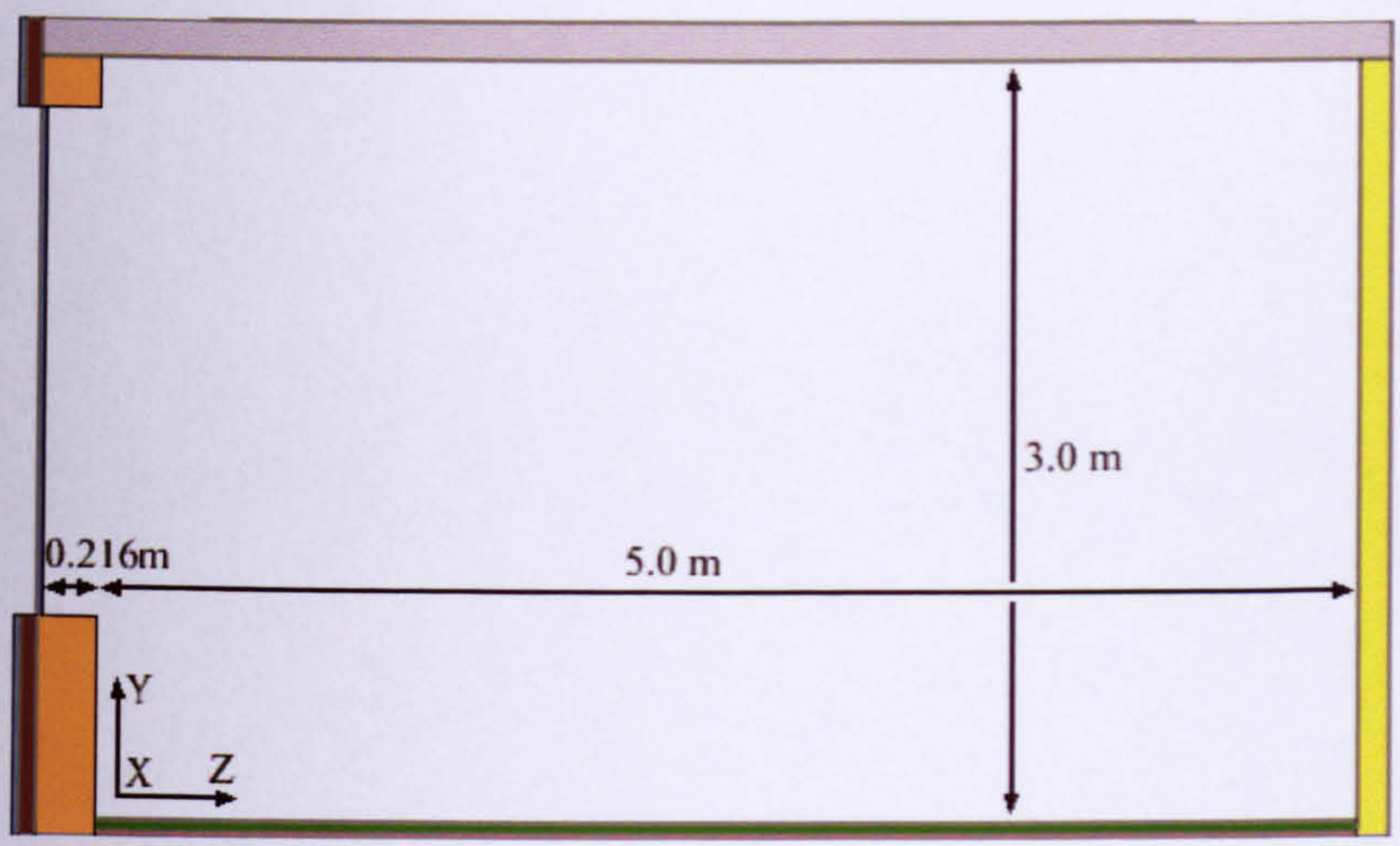

Figure 6.3: Side view of the model showing the window location (Benchmark 2); concrete ceiling (grey shaded), external concrete wall (orange shaded), screed (green shaded), rock wool (pink shaded), cavity blocks (yellow shaded), facade insulation (purple shaded), façade slab (cyan shaded) and window (blue shaded).

Examples 1 and 2 in the VDI 6020-1 (2001) represent an unventilated room with different internal heat sources. Investigations in this chapter are based on these examples and are hereafter referred to as benchmarks 2.1 and 2.2.

Benchmark 2.1 contains a radiative heat source of 1000W. To prevent CFD programs from convergence problems caused by highly unstable flow patterns due to spatially similar boundary condition assumptions as described in the VDI 6020-1 (2001), the heat sources are unevenly distributed imitating more realistic room conditions. 70% of the radiative heat source was evenly distributed on the floor and the back wall and 30% on the other room surfaces (i.e. ceiling, window, external and the two internal walls on the x-plane) to imitate an incident solar radiation through the window considering the differences in direct and diffuse radiation (see Figure 6.4).

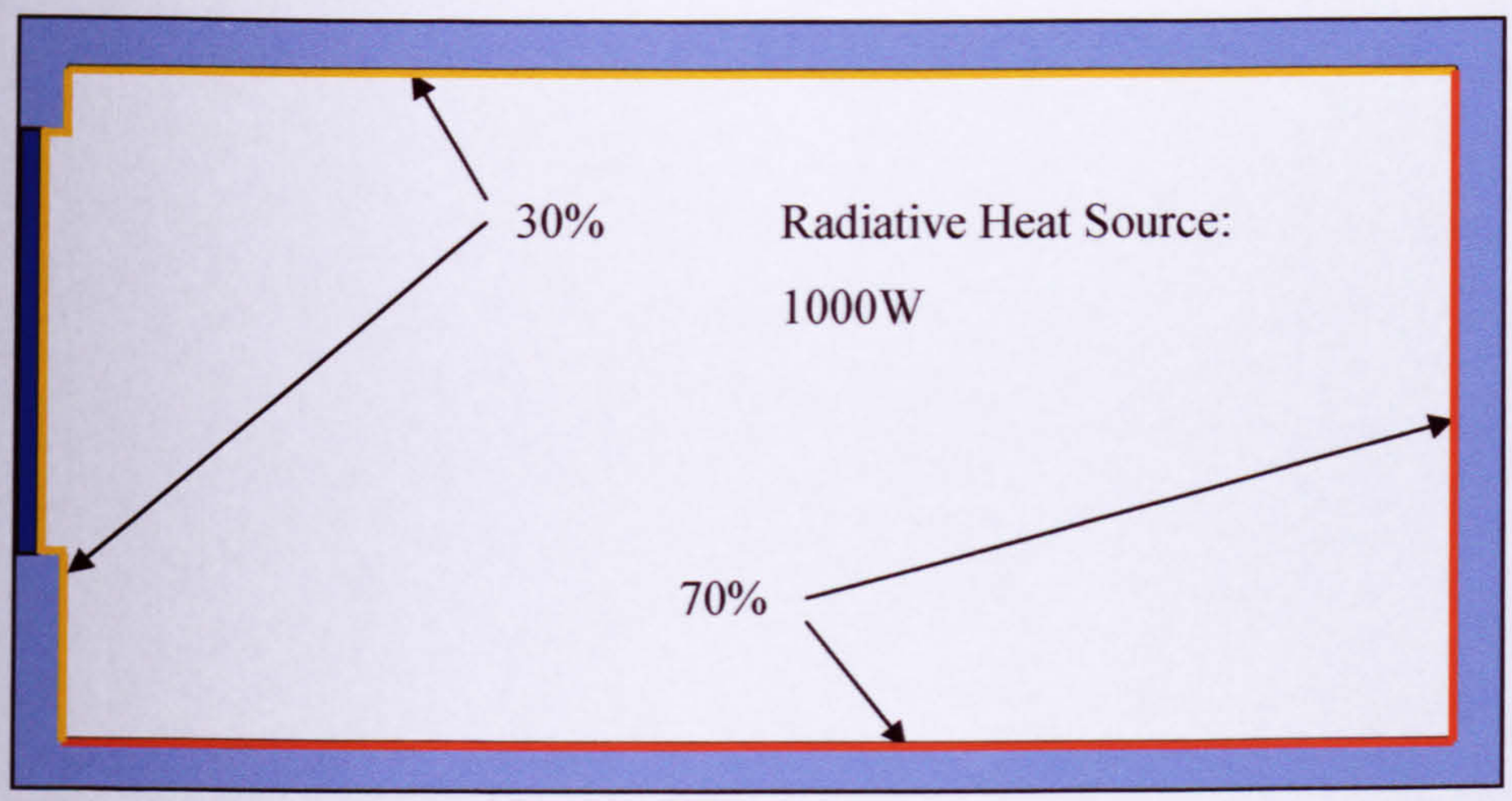

Figure 6.4: Sketch of the room model of benchmark 2.1 which contains an unevenly distributed radiative heat source imitating incident solar radiation.

Benchmark 2.2 contains a convective heat source of 1000W which is located below the window (see Figure 6.5). The heat source (i.e. a 'virtual convector' of X x Y x Z = 5.0m x 0.5m x 0.1m) is located 0.1m from the external wall and 0.25m from the floor and spans the entire x-direction between the internal wall surfaces. In contrast to a 'real' convector which typically contains hot solid surfaces and thus a radiation part, the heat source is pure convective in benchmark 2.2.

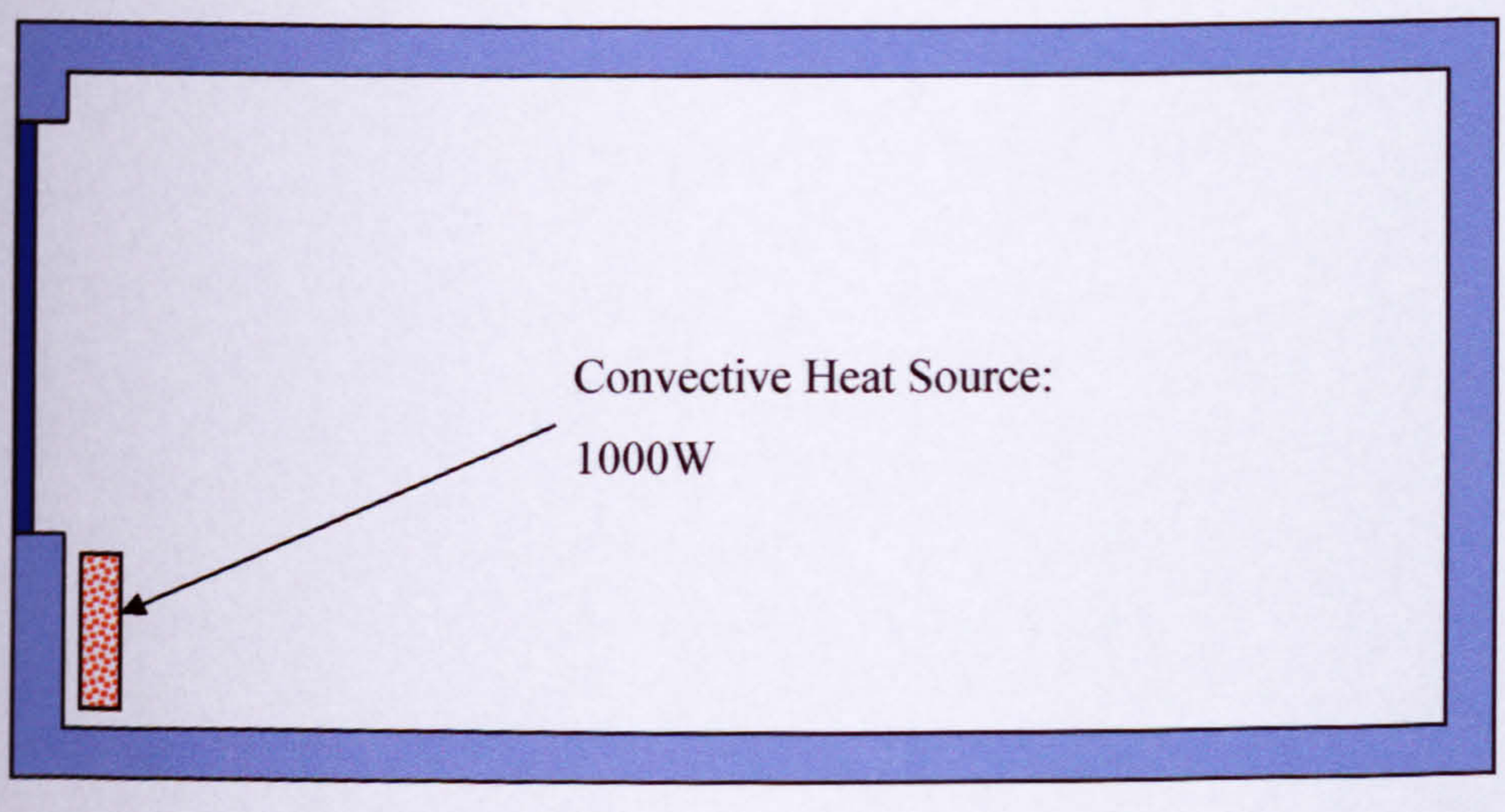

Figure 6.5: Sketch of the room model of benchmark 2.2 which contains a convector as an internal convective heat source.

The heat sources are operational from 0600-1800 for benchmarks 2.1 and 2.2. Neighbouring rooms contain the same conditions as the investigated room. The window is an opaque material without thermal mass. The outer surfaces of the room model (i.e. surfaces adjacent to the neighbour rooms) contain adiabatic boundary conditions (except the external wall). The outer surfaces of the external wall contains a convective heat transfer coefficient of $20 W/m^2 \cdot K$ as stated in the VDI 6020-1 (2001). Where the convective heat transfer at the inner surfaces is not automatically calculated by the simulation program, the convective heat transfer coefficients from the VDI 6020-1 (2001) are adopted (see Table 6.2). A radiation emissivity of $\varepsilon=0.9$ is assumed at the room surfaces. The air, solid and surface temperatures in the entire room model are initially 22°C which leads to air flow patterns of zero velocity at the beginning of the simulation.

Table 6.1: Properties of the building components for the room model (Benchmark 2).

Type	Construction	s [m]	λ [W/(m·K)]	ρ [kg/m³]	c [J/(kg·K)]
Floor	Screed	0.047	1.4	2200	1050
	Rock wool	0.012	0.06	50	840
Ceiling	Concrete	0.15	2.035	2400	1050
Internal Walls	Cavity blocks	0.12	0.56	1300	1050
External wall	Concrete	0.24	2.035	2100	920
	Insulation	0.062	0.047	75	840
	Façade slab	0.025	0.045	1300	1050
Window	Glazing	0.024	0.078	-	-

Table 6.2: Convective heat transfer coefficients based on the VDI 6020-1 (2001).

Type	$h_{c,int}$ [W/(m²·K)]
External wall	2.7
Internal wall	2.7
Floor	1.67
Ceiling	1.67
Window	2.7

6.2.2 Modification of the VDI model for benchmark 2

The VDI model (2001) was specified for the use in zonal simulation programs, therefore some modification of the original model was necessary for use in the CFD simulation. Benchmark 2 in section 6.2.1 already contains these modifications. They are summarised as follows:

- Heat conduction in the building structure is treated as one-dimensional in zonal simulation programs. Thermal mass at the joints of building components present in real rooms is therefore neglected. No information exists about the room construction at the joints in the VDI model and hence the construction in these regions was considered as for typical modern office buildings in benchmark 2. Additionally, no specific information is provided about the location of the window and the size of the door. Details of the window location are given in Figures 6.2 and 6.3. The wooden door was ignored because no construction details were stated in the VDI model (2001).

- The original model contains a 6/12/6 double glazed window. The numerical discretisation of the thin layers and the simulation of free convection in the air gap would require a fine numerical mesh which would exceed the computational capacity for dynamic CFD simulations of rooms. Therefore, the double glazed window was replaced by single glazing of the same thickness. The properties were modified to obtain an equivalent thermal transmittance (see section D.1).

- Heat sources are evenly distributed in the original model since zonal simulation programs assume homogeneous (i.e. well mixed) conditions in the air space. However, this distribution would lead to weak and unstable flow patterns and therefore to possible convergence problems in CFD calculations. Thus, heat sources were unevenly distributed in the room as explained in section 6.2.1.

- A discretisation of the thin PVC layer on the floor requires a fine numerical mesh which requires high computational resources and leads to poor quality mesh elements with large aspect ratio. The PVC layer was therefore not modelled.

- Conditions of the neighbouring rooms are the same as for the benchmark room investigated (VDI 6020-1 (2001)). Thus, the heat transfer within the (single layer) internal walls is symmetric and the heat transfer at the middle plane section can be assumed to be zero. Subsequently only half of the internal wall thickness of the VDI room model was considered in benchmark 2 using adiabatic wall conditions at the boundary. The layers of the building elements above the concrete ceiling and below the floating screed at the floor for the VDI room are almost fully thermally decoupled from the room investigated as shown by Engert et al. (2007) which leads to a heat flux approaching zero at the interface between the rock-wool and concrete layer. Thus, adiabatic boundary conditions were considered there.

6.3 CFX and TRNSYS model settings for Benchmark 2

6.3.1 CFX model settings

For benchmark 2.1, the radiative heat sources were imposed on the room surface boundaries as described in section 6.2.1. The time scheduled heat sources were implemented using Fortran routines.

Two possible modelling techniques were investigated for representing a pure convective heat source below the window in benchmark 2.2 (i) an air sub-domain which contains an evenly distributed volume heat source or (ii) a sample of heat point sources. Option (i) would require a modification of the model geometry. This is not necessary in (ii) where an additional heat source S_e is implemented in the energy equation of the mesh node next to the location of each point source (see section A.15). The same basic room model and mesh can be used for test benchmarks 2.1 and 2.2. Thus the point heat source option was used to model the 'virtual' convector. Since the heat sources are not imprinted on any surface, radiation effects are eliminated as desired in section 6.2.1. A number of 39 point heat sources were placed below the window and evenly distributed on three rows (0.25m distance between each point source and the floor and 0.15m

distance from the external wall). A total convective heat source of 1000W means a heat source of 25.64W per heat point source.

An interface boundary condition (see section A.5) was used between each solid or fluid domain which allows for a conservative heat transfer. The thermal mass of the window was neglected by setting the density and thermal capacity properties close to zero. Turbulence, radiation and buoyancy were modelled using the same methods described in chapter 5. A first order backward Euler scheme (Eq. (A.24)) and a high resolution advection scheme (see Eq. (A.26)) were applied to the equations and the reference temperature for the Boussinesq approximation was 22°C. Air was considered to be incompressible with typical properties for 25°C. A simulation was considered to have converged if the solution was below a RMS normalized residual of 10^{-4} for all calculated RANS equations.

The mesh was based on that of test 4 of the mesh consistency study shown in section D.2. The mesh was deemed to be sufficiently consistent for the first 2 hours of simulation (ΔT_{max}=0.2K). Investigation for longer periods was not possible due to the restriction of computational resources. The total number of 159,000 volume elements was used for room discretisation.

The key parameters for the adaptive freeze flow method were 'MAXLOOPS'=5 (benchmarks 2.1 and 2.2), 'EXTENSION'=300s (benchmarks 2.1 and 2.2), 'MAXTEMP'=0.8 (benchmark 2.1) and 'MAXTEMP'=0.5 (benchmark 2.2). Slightly higher values were used compared with test case 4 in chapter 5 since the flow is potentially more unstable due to the smaller surface temperature differences and hence smaller driving forces. More restricted parameter values might decrease the lengths of frozen flow periods which would lead to a reduction of the performance of the adaptive-freeze flow method. The same time step sizes for the unfrozen and frozen flow period used in chapter 5 (1s and 60s, respectively) were used here.

6.3.2 TRNSYS model settings

Since benchmark 2 is a modification of the VDI model, the reference data from TRNSYS from the VDI 6020-1 (2001) could not be used for comparison. Thus, new calculations were carried out for benchmark 2 using TRNSYS.

Radiation was unevenly distributed at the room surfaces as stated in benchmark 2.1. For benchmark 2.2, an uneven distribution of a convective heat source in the air space cannot be specified in TRNSYS due to the assumption of well mixed air conditions. The source was therefore equally distributed in the air space instead. Since the internal convective heat transfer cannot be calculated in TRNSYS based on the local air flow patterns, the convective heat transfer coefficients from Table 6.2 were adopted. Eq. (2.5) is used to calculate the convective heat flux at the surfaces. Since the ceiling is restricted to the concrete slab and the floor is restricted to the screed and rock-wool layer, adiabatic conditions were specified at their outer boundaries by using infinitely thick insulation layers with high thermal resistance. The 'identical boundary' option was used for the internal wall boundaries (i.e. the zone temperature of the neighbouring room is equal to that of the investigated room and the location of zero heat flux in the building structure is automatically determined by TRNSYS).

Since the heat transfer in the building fabric is only calculated in a one-dimensional manner in TRNSYS, the thermal mass is neglected at the joints of the building fabric components. Two simulations were therefore considered for each benchmark model. The first used the model's inner dimensions of the building structure, typical for zonal program simulations. The second used the model's outer dimensions to consider the additional thermal mass. Since the air volume and the surface area are not directly linked in TRNSYS, it is possible to set an arbitrary volume independent of the enclosing area. The air volume of the room is therefore the same for both benchmark models. It was expected that the CFX prediction of the thermal behaviour of the room of benchmark 2 lies between the results of both extreme conditions.

6.4 Results and Discussion

Dynamic CFD predictions were obtained for benchmarks 2.1 and 2.2 by using the adaptive freeze-flow method. Predictions were compared with those of TRNSYS. The average room air temperature was used as the only verification parameter in examples 1 and 2 of the VDI 6020-1 (2001). The average air temperature was therefore also used here for verification. For TRNSYS, the data output interval was 1h and for CFX it was 5min (and additionally at the last time step before switching between the unfrozen and frozen flow modes as in chapter 5). Since the heat sources are switched on at 0600 in benchmark 2, the room is assumed to be in thermal equilibrium before this time. This would lead to convergence problems for CFX if the simulation was started earlier because dominating momentum forces are missing which would lead to a stable air flow field. CFX simulations were therefore started at 0600. All CFX simulations have achieved the convergence criterion.

6.4.1 Radiative heat source (Benchmark 2.1)

The predicted average room air temperatures for CFX and TRNSYS are shown in the Figure 6.6 for a simulation period of 24h. A radiative heat source is imposed on the surfaces of the building fabric from 0600. A significant portion of the heat is transferred into the building structure while the remainder is released to the air by free convection. Thus, the average room air temperature increases gradually (see Figure 6.6). After 1800 when the heat source is switched off, the temperature begins to fall. However, the temperature remains higher than at the beginning of the simulation since the building fabric has been warmed during the day and the thermal air conditions are mainly determined by the temperature of the enclosing surfaces after the heat source is switched off at 1800.

The TRNSYS simulation using the outer solid dimensions contains a higher thermal mass than that for the inner solid dimensions. Thus, more radiative heat gain can be stored in the building fabric and the air temperature increases slower (Figure 6.6). However, the use of the outer solid dimensions leads to a larger enclosing surface area which leads to an increased heat release to the air and subsequently to a reduction of the

thermal mass effect. An air temperature difference of 0.7K between both TRNSYS simulations is observed at 1800.

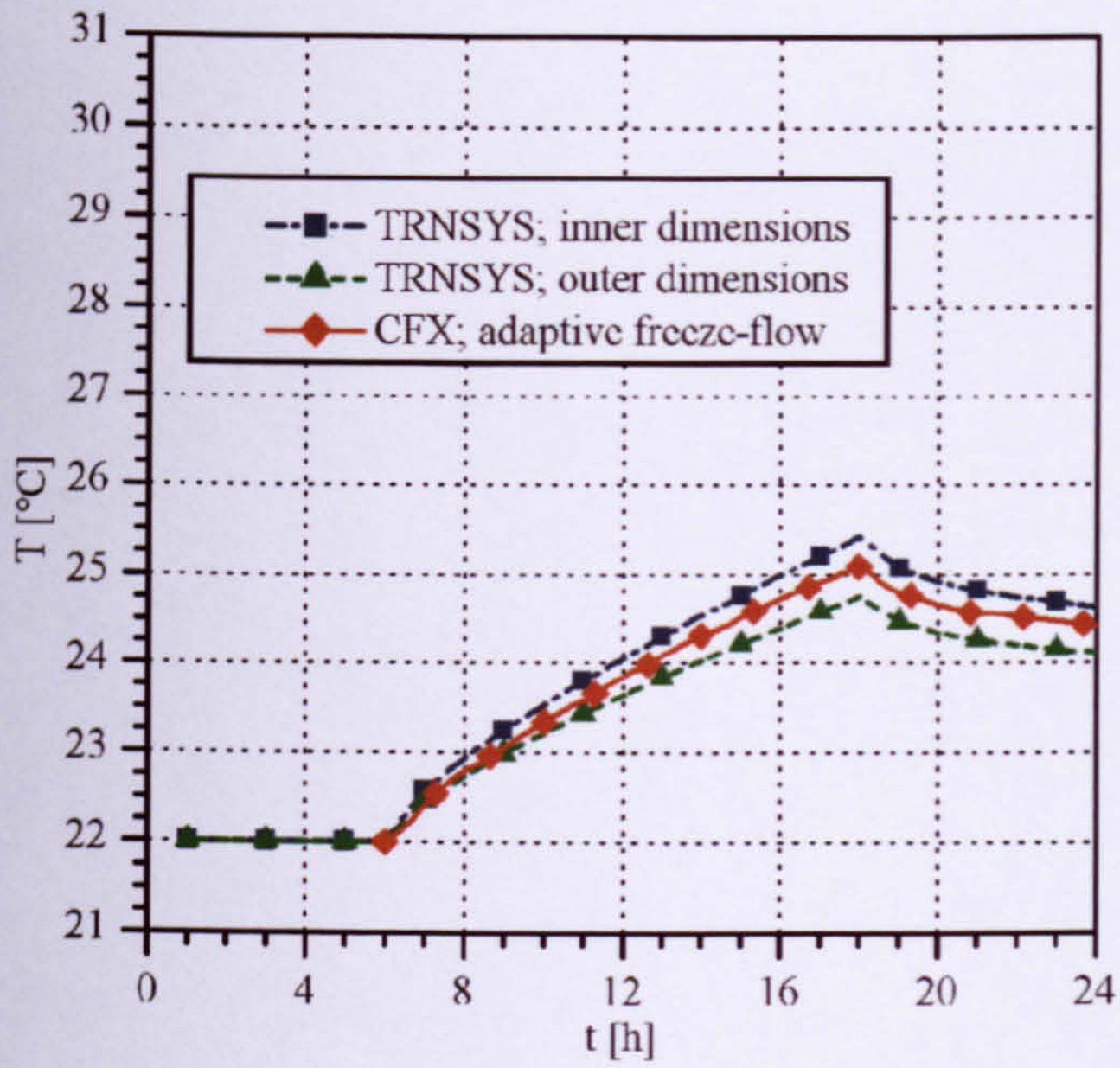

Figure 6.6: Average room air temperature predictions for CFX and TRNSYS for a radiative heat source which is on from 0600-1800 (Benchmark 2.1).

The CFX room model contains more thermal mass at the joints of the building structure and a larger surface area at the opening due to the location of the window than the TRNSYS simulation with inner solid dimensions. In comparison with the TRNSYS model with outer dimensions, the CFX model contains less thermal mass and a smaller surface area. This is reflected in Figure 6.6 since the curve of CFX lies between those of TRNSYS for the predicted average air temperature throughout the simulation.

Considering the differences in thermal mass and surface area size, the predictions of CFX and TRNSYS compare well.

6.4.2 Convective heat source (Benchmark 2.2)

Figure 6.7 shows the predicted average room air temperatures for TRNSYS and CFX for a simulation period of 24h. After the convective heat source is switched on at 0600,

the average air temperature rapidly increases from 0600-0700 due to the low thermal capacity of the air. From 0700-1800 the warming of the air temperature is reduced since parts of the heat gain are absorbed by the building fabric. After 1800 the air temperature falls rapidly again when the heat source is switched off. The air temperature remains higher than at the beginning of the simulation as observed in benchmark 2.1. However, the temperature reaches a higher temperature during the day than in benchmark 2.1, since the heat gain is implemented as a source in the air domain and not on the surfaces. The thermal resistance between the air and the surfaces and the radiative heat exchange explicitly control the heat transfer to the building fabric.

The air temperature increases slower for the TRNSYS simulation for the model outer solid dimensions than for the inner solid dimensions as observed in benchmark 2.1. However, the temperature difference is significantly greater during the day (ΔT=1.7K at 1800) than for the simulation using the inner solid dimensions, since the larger surface area assists the effect of the higher thermal mass and both lead to a better absorption of the heat in the building fabric. The building fabric follows a smaller temperature swing than the air due its higher heat capacity and density (i.e. thermal mass). Since the thermal air conditions adjust to the conditions of the enclosure when the heat source is switched off and both TRNSYS curves approach each other after 1800.

The air temperature prediction for CFX compares favourably with that of TRNSYS for the inner solid dimensions. However, the air temperature increases slightly slower in the CFX simulations and the temperature difference between the CFX and the TRNSYS predictions is similar to that of benchmark 2.1 (ΔT=0.4K at the end of the day). The difference is a result of the higher thermal mass and the larger surface area for the CFX model as described above and the temperature increase from 0700-1800 for CFX lies between those of both TRNSYS simulations (ΔT=2.1K and 2.6K for TRNSYS using inner and outer solid dimensions, respectively, and ΔT=2.3K for CFX). Since the temperature level of CFX is close to that of TRNSYS with inner solid dimensions, this indicates a dominating influence of the surface heat transfer rather than the thermal mass. The steeper gradients from 0600-0700 and 1800-1900 predicted by the CFX simulation compared with the TRNSYS simulation are a result of the different data output intervals between CFX and TRNSYS.

Despite the differences in the thermal mass, the predictions of CFX and TRNSYS (for inner dimensions) compared well.

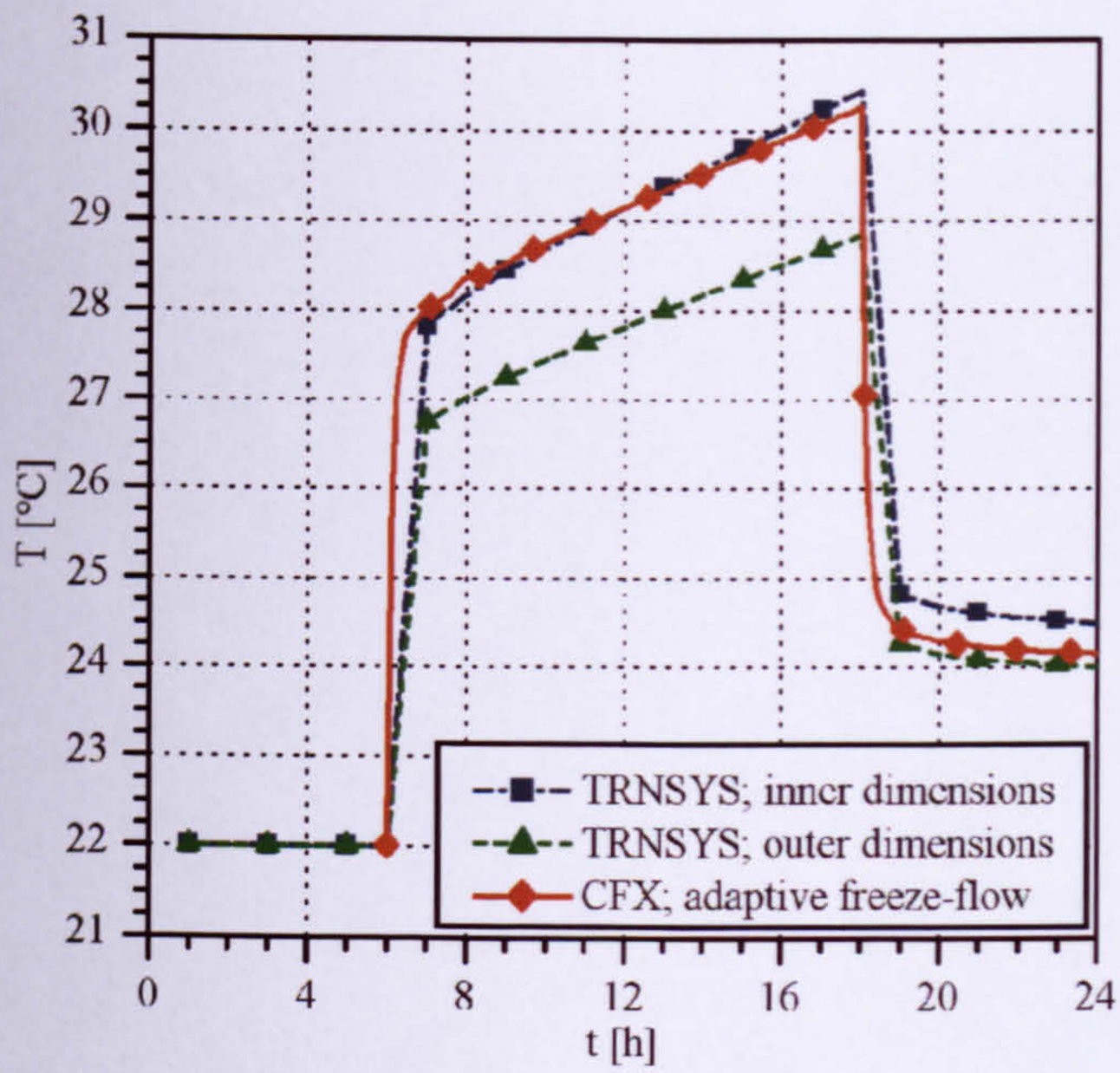

Figure 6.7: Average room air temperature predictions for CFX and TRNSYS for a convective heat source which is on from 0600-1800 (Benchmark 2.2).

6.4.3 Discussion of further possible modelling influences on the predictions

The differences of the thermal mass and the surface area size were indicated as probable reasons for the differences between CFX and TRNSYS results in sections 6.4.1 and 6.4.2. Other possible reasons are briefly discussed here.

The freeze-flow method can lead to prediction errors of convective surface heat transfer (see section 5.4.4). However, the radiative heat transfer counteracts and almost compensates for any such potential errors as shown in section 5.4.7.

Although a sufficient mesh consistency was demonstrated for CFX for a simulation period of 2h (see section D.2), it might be necessary to conduct further investigations for longer simulation periods in order to account for the high thermal mass of the

building fabric. However, due to the restriction of the computational capacity this was not possible in this work.

Figure 6.8 shows the vertical temperature gradient in the centre of the room for CFX at different simulation hours for benchmark 2.1. No temperature gradient is visible in the core of the air space which would compare well with the 'well mixed' assumption of TRNSYS. However, at thin layers close to the top and bottom surfaces the temperature is different. The figure also shows that the floor releases heat to the air throughout the simulation while the ceiling absorbs the heat. The TRNSYS model uses constant h_c values from Table 6.2 (a value of 1.67W/(m^2·K) is used for the ceiling and the floor). This assumption deviates from the current state of knowledge that the convective surface heat transfer depends on the direction of heat flow which is also reflected by the standard values stated in the DIN EN ISO 6946 Table 1 (1996) (i.e. suggested values are 5.0W/(m^2·K) for upward heat flow and 0.7W/(m^2·K) for downward heat flow). Thus, the assumption of same h_c values for upward and downward flow leads to an under-prediction of convective surface heat transfer from the floor to the air and from the air to the ceiling for benchmark 2.1. It is thought that the increased decoupling of the air from the building fabric leads to reduced air temperatures. Figure 6.9 shows vertical temperature gradients in the room centre for CFX at different simulation hours for benchmark 2.2. Heat is transferred from the warmer air to the cooler surrounding building fabric and a gradient of about 3.5K over the height of the room exists during the day for which TRNSYS assumes a well mixed condition. The deviation of the heat transfer coefficients from standard values and the well mixed assumption led to an under-prediction of the heat transfer at the ceiling and an over-prediction at the floor. However, more detailed studies would be necessary to quantify this simulation error which was not possible here due to the high computational resources required for the simulations.

In practice, the convective and radiative surface heat exchange is smaller at the room edges and corners than at the surface centres due to flow stagnation and the restriction of view factors for radiation, respectively. This leads to a reduction of the total effective surface heat transfer and the effective dynamic thermal mass. CFX predictions reflect this behaviour due to the fine numerical discretisation as shown in Schulz et al. (2007).

TRNSYS considers homogeneous conditions at the surfaces and thus potentially leads to an over-prediction of surface heat transfer. This would lead to an under-prediction of the air temperature for benchmark 2.2. For benchmark 2.1, a more detailed study would be necessary to describe the tendency of an over- or under-prediction. Furthermore, the assumption of constant h_c values throughout the simulation might be inappropriate since the air flow distribution in buildings typically changes over time.

A convective heat source is placed locally below the window in benchmark 2.2 and leads to a spatial variation of surface heat transfer (i.e. higher convective surface heat transfer at the room surfaces close to the convector and lower convective surface heat transfer elsewhere). In the TRNSYS model, the convective heat source is evenly distributed in the air domain which leads to deviations of convective surface heat transfer compared with the benchmark room model.

It is also noted from examples 1 and 2 in the VDI 6020-1 (2001), that temperature differences of up to 0.4K are displayed in the comparison of results for the zonal reference models for the first day of simulation. Differences between CFX and TRNSYS results lie within this range.

However, although simulations were carried out with fundamentally different computer codes, and different possible reasons discussed above might have led to prediction errors, the results for CFX and TRNSYS compared well.

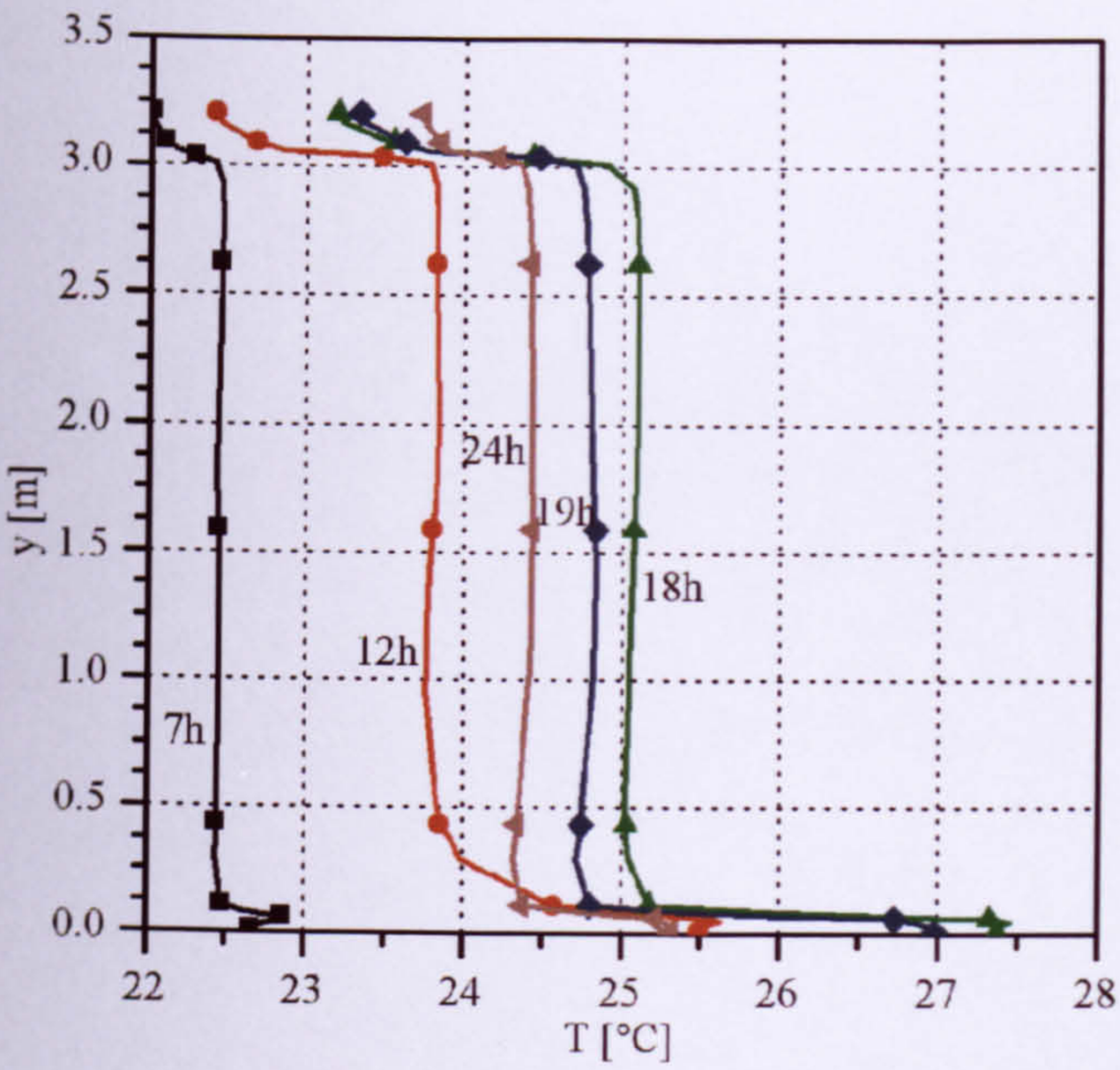

Figure 6.8: Temperature predictions along the model height in the room centre at 0700, 1200, 1800, 1900 and 2400 (Benchmark 2.1). Temperatures in the floor and the ceiling are displayed between heights of 0-0.059m and 3.059-3.209m, respectively.

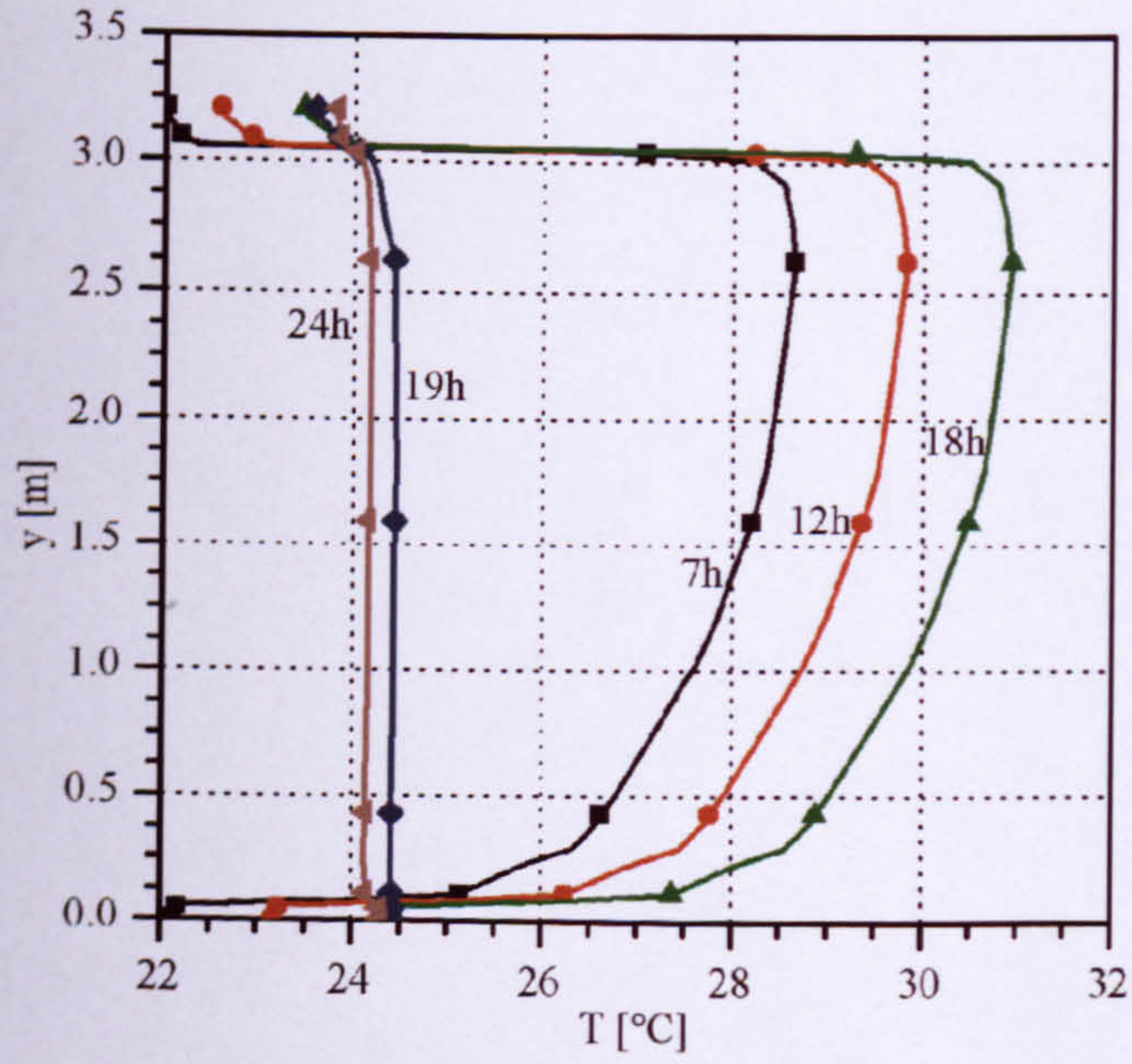

Figure 6.9: Temperature predictions along the model height in the room centre at 0700, 1200, 1800, 1900 and 2400 (Benchmark 2.2). Temperatures in the floor and the ceiling are displayed between heights of 0-0.059m and 3.059-3.209m, respectively.

6.5 Summary

Previous investigations contained simulation comparison with the same basic calculation code to evaluate the performance of the freeze-flow method. However, verification of simulation results was still required to provide evidence of trueness for the predicted dynamic thermal room behaviour. This chapter addressed this verification for an unventilated large scale 3D room model of high thermal mass, referred to as benchmark 2, which contained convective and radiative internal heat sources based on the VDI 6020-1 (2001). Dynamic results of CFX were compared with those of the zonal program TRNSYS.

TRNSYS simulations, which typically use the model's inner dimensions of the building fabric, predicted a slightly more rapid increase in average air temperatures throughout the simulations compared with CFX. The maximum air temperature differences were 0.4K throughout the simulations. This was thought to be mainly caused by the neglect of thermal mass at the joints of the building fabric components and by the smaller surface area at the opening in the TRNSYS model. This was proved by conducting TRNSYS simulations which used the benchmark model's outer dimensions. Other possible reasons for the small differences between the CFX and TRNSYS predictions were discussed. More detailed investigations would be required to quantify the error for each influence separately. However, this was restricted here due to the limitation of computational resources.

The differences between CFX and TRNSYS were within the prediction differences between zonal reference models of the inter-model comparison shown in the VDI 6020-1 (2001). Although both programs are based on different calculation codes, the results of CFX and TRNSYS compared favourably for benchmark 2.

CHAPTER 7

DYNAMIC 3D MODELLING OF NIGHT-TIME COOLING (BENCHMARK 3)

7 Dynamic 3D Modelling of Night-Time Cooling (Benchmark 3)

7.1 Preamble

The night-time ventilation in office buildings has been numerically investigated in the past using zonal programs. Subsequent possible problems due to the program assumptions of well mixed room conditions and one-dimensional heat conduction in the building fabric have been discussed in chapter 2. The adaptive freeze-flow method was applied to a large 3D room enclosure of high thermal mass in the previous chapter. Dynamic CFD results of predicted space averaged internal room temperatures compared favourably with those of a DTS program for a convective and a radiative internal heat source. The successful verification of this method for the simplified room has led to the suggestion that the newly developed dynamic CFD method might be a suitable tool for modelling the dynamic thermal behaviour in more complex rooms also.

The investigations in this chapter focus on the dynamic thermal simulation for night-time ventilation in a room which has the size and (medium) thermal mass of a typical office room using dynamic CFD to investigate the influence of different night-time ventilation strategies on the dynamic thermal room behaviour. Another aim is to gain further trust in the results of the dynamic CFD predictions. Reliable experimental data for verification of the numerical results for night-time cooling in high and medium thermal mass buildings is rare since most data is based on field measurements from existing buildings or chambers exposed to real weather conditions which potentially contain many uncertainties (see chapter 2). This makes an accurate comparison of measurements with CFD predictions cumbersome. Since inter-model comparisons are often used to verify the plausibility of zonal simulation programs, as for example shown in chapters 6, the same method is used here to gain information about the dynamic CFD procedure. The room, defined as benchmark 3, is based on the model geometry described in the VDI 2078 (1996) and boundary conditions from a dynamic thermal

simulation verification procedure of the VDI 6020-1 (2001) which refers to the VDI 2078 (1996). Predictions of CFX are compared with those of the zonal program TRNSYS.

Details about benchmark 3 are given in section 7.2. Section 7.3 describes the implementation procedures of benchmark 3 in CFX and TRNSYS. The results and discussion of the investigation of night-time ventilation using CFD and the comparison with predictions of TRNSYS are presented in section 7.4. A summary of results is given in section 7.5.

7.2 Definition of Benchmark 3

The room of benchmark 3 contains inner dimensions of 5m x 3.5m x 3m (L x W x H) and is similar to that of benchmark 2 in chapter 6 (i.e. room space size, floor, ceiling and external wall building structure material and window location) (see Figure 7.1). However, the heavy-weight room of benchmark 2 is modified to represent a more realistic modern office room which often contains internal walls of light-weight material. The geometry is based on the VDI 2078 (1996) (i.e. reference guide for room models in the VDI 6020-1 (2001)).

Conditions of the neighbouring rooms are the same. The internal walls in the VDI 2078 (1996) are light-weight structured and hence have only a marginal effect on the thermal room conditions as demonstrated in Engert et al. (2007). Thus, the internal wall structure is not modelled in benchmark 3 and adiabatic conditions are considered instead at the room surfaces. The layers of the building elements above the concrete ceiling and below the floating screed at the floor are almost fully thermally decoupled from the room investigated as shown by Engert et al. (2007) which leads to a heat flux approaching zero at the interface between the concrete and the insulation layer in both the ceiling and the floor. Thus, only the thermal mass components which lie adjacent to the room space are modelled (neglecting the insulation layer) to save computational resources. An adiabatic boundary condition is applied at their outer boundaries. The window position and properties are similar to benchmark 2. Details of the properties of the building components are listed in Table 1. The calculated ratio between the effective

heat capacity and the net ground area for the room is C_{eff}/A_{net}=111W·h/(m^2·K), which assigns it to the 'medium-weight' building category containing medium thermal mass (see chapter 2).

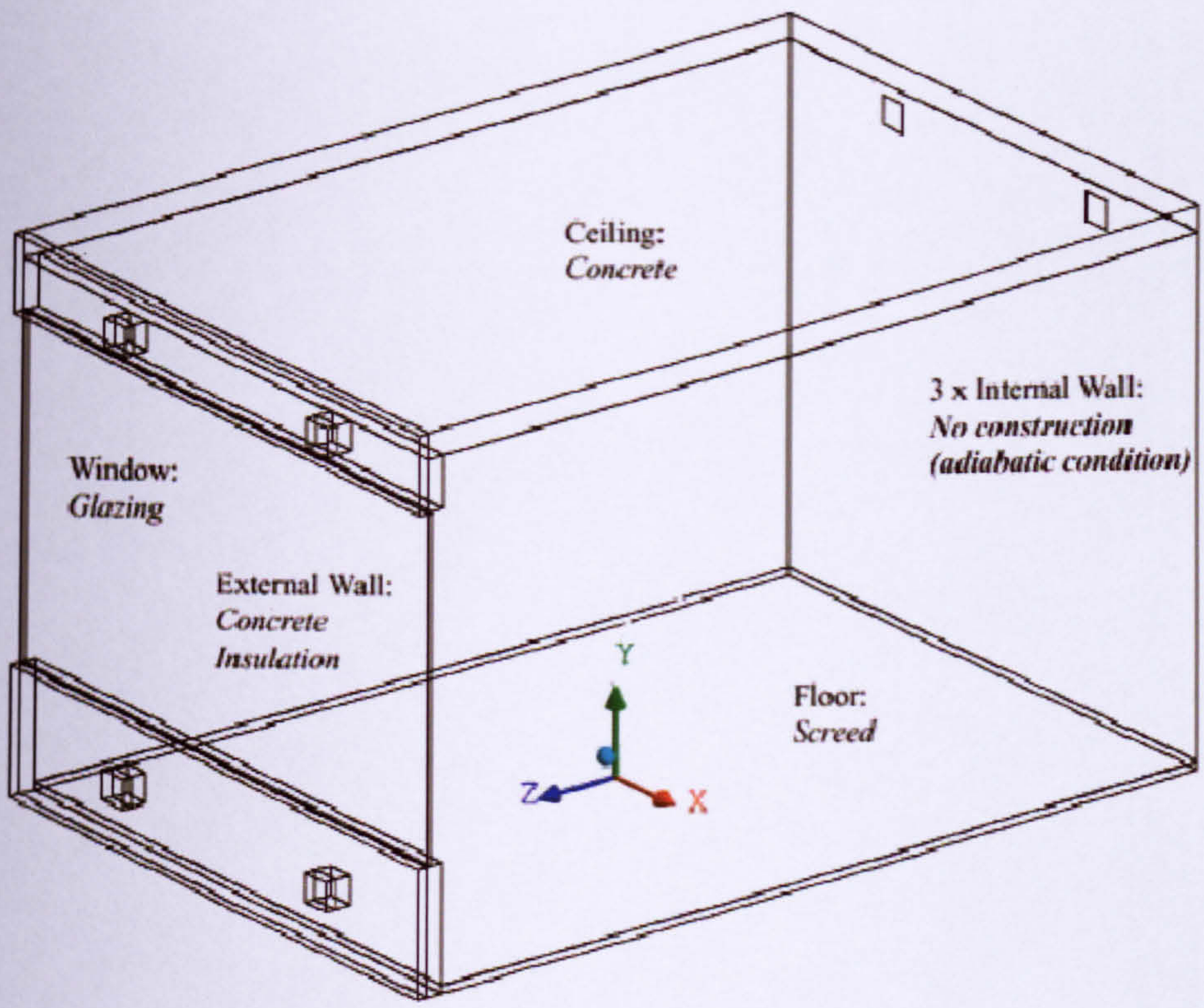

Figure 7.1: Benchmark 3 room model which contains medium thermal mass and openings for ventilation at the external and rear wall.

The model boundary conditions are based on the verification procedure of example 5 described in the VDI 6020-1 (2001). Various realistic boundary conditions are applied to the benchmark model using a shading device and hourly values of external temperature, solar radiation and internal heat gains (see Tables 7.2 and 7.3). The simulation time scheme considers a preconditioning period of 3 days without internal heat gains and without solar radiation (e.g. comparable to a long weekend of cloudy days and shading devices fully closed). This period is then followed by a period of 3 days in which all conditions of Table 7.2 apply (i.e. where additional heat gains existed due to equipment, occupancy and solar radiation). In benchmark 3, the diffusive solar

radiation is distributed evenly on all internal room surfaces and the direct solar radiation is distributed evenly on the floor area. Internal convective and radiative heat gains from equipment and persons are distributed evenly in the air space and on all room surfaces, respectively. No interpolation is used between the hourly data (i.e. step functions are assumed as typically used in the DTS program TRNSYS). The heat transfer coefficient at the surfaces of the external wall is assumed to be 20W/(m^2·K) based on the VDI 6020-1 (2001). Where the convective heat transfer at the inner surfaces is not automatically calculated by the simulation program, the convective heat transfer coefficients are adopted from the VDI 6020-1 (2001), i.e. 2.7W/(m^2·K) for the horizontal heat flow and 1.67W/(m^2·K) for the vertical heat flow. A radiation emissivity of ε=0.9 is assumed at the room surfaces. The external temperature is constantly 22°C throughout the simulation and the air, solid and surface temperatures in the entire room model are initially 22°C which leads to air flow patterns of zero velocity at the beginning of the simulation.

Table 7.1: Building fabric properties for the room model of benchmark 3.

Component	Material	d [m]	λ [W/(m·K)]	ρ [kg/m^3]	c [J/(kg·K)]
Floor	Screed	0.047	1.4	2200	1050
Ceiling	Concrete	0.15	2.035	2400	1050
External wall	Concrete Insulation	0.10 0.062	2.035 0.047	2100 75	920 840
Window	Glazing	0.024	0.078	-	-

Table 7.2: Boundary conditions for benchmark 3 adopted from the VDI 6020-1 (2001).

Boundary conditions	Value
External temperature	see Table 7.3
Solar radiation	see Table 7.3
Maximum global radiation limit for closing the shading device	100W/m^2
Shading factor[1]	0.15
Equipment, convective	200W
Equipment operation time	0800-1700
Persons, convective	80W
Persons, radiative	80W
Occupation time	0800-1700

[1] global solar radiation through the window is reduced by 85% due an external shading device.

Table 7.3: External temperature and solar radiation measured behind the window, VDI 6020-1 (2001).

t [h]	T [°C]	$\dot{q}_{rad,glob}$ [W/m^2]	$\dot{q}_{rad,diff}$ [W/m^2]
1	17.3	0	0
2	16.9	0	0
3	16.1	0	0
4	16.1	0	0
5	16.8	17	17
6	18.7	38	38
7	21.8	59	59
8	23.8	98	80
9	25.8	186	99
10	27.5	287	115
11	28.6	359	125
12	29.4	385	129
13	30.0	359	125
14	30.7	287	115
15	31.6	186	99
16	31.0	98	80
17	30.5	59	59
18	29.6	38	38
19	28.1	17	17
20	25.9	0	0
21	23.5	0	0
22	22.3	0	0
23	21.4	0	0
24	20.3	0	0

To simulate room ventilation, two square openings are considered in benchmark 3 at low level of the external wall (in comparison, the room in the VDI 6020-1 (2001) is not ventilated). Another two openings of the same size are placed at high level of the external wall for the investigation of single-sided ventilation and two openings are placed in the back wall at high-level for the investigation of cross-ventilation (see Figures 7.1 and 7.2). For the single-sided ventilation strategy, the openings at high level at the rear wall are closed and treated as adiabatic walls; for cross ventilation, the openings at high level at the exterior wall are closed and treated as adiabatic walls.

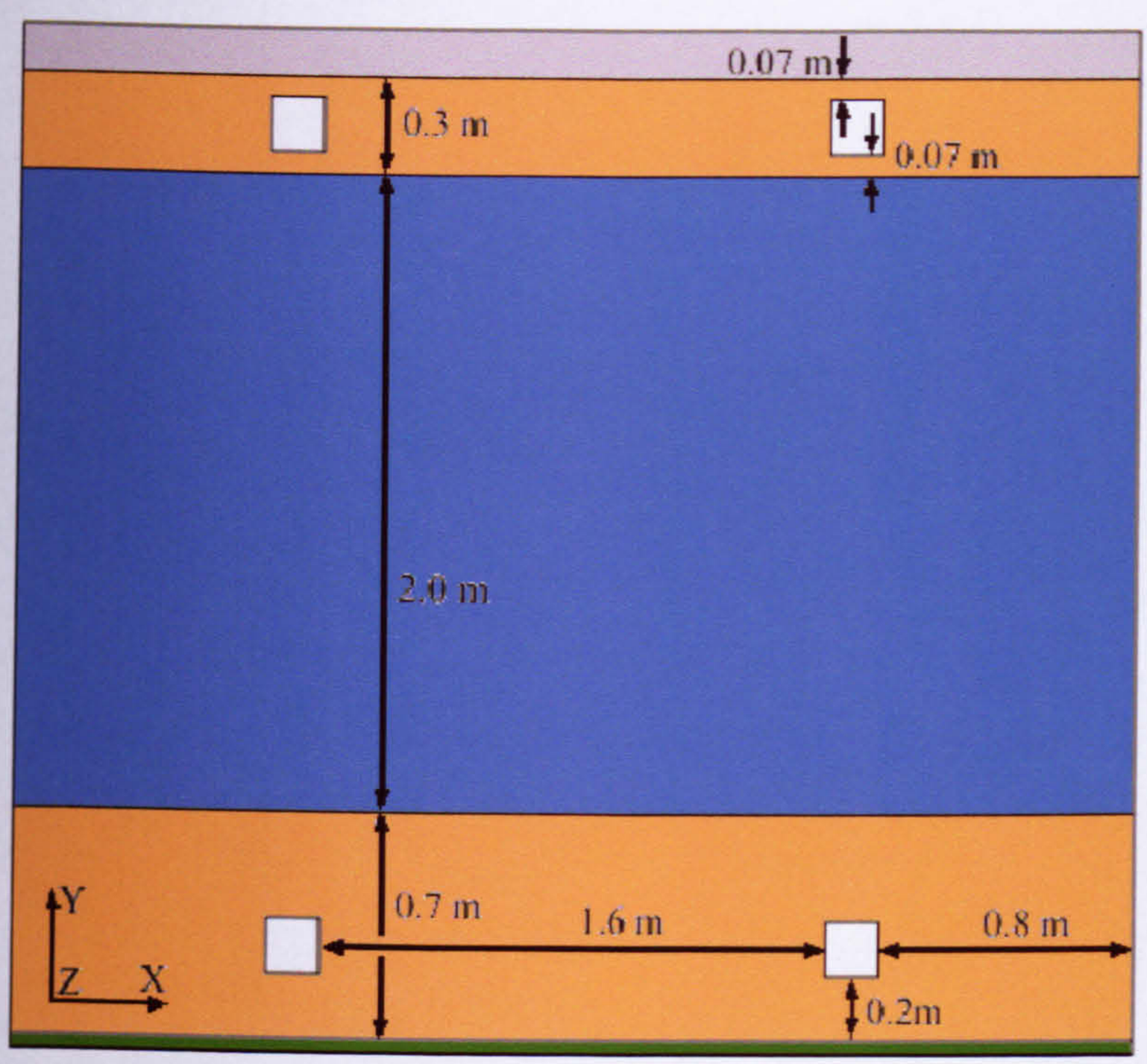

Figure 7.2: Positions of the openings (white shaded) for benchmark 3; concrete ceiling (grey shaded), external concrete wall (orange shaded), screed (green shaded) and window (blue shaded).

Since the calculation of the air flow rate for natural ventilation might lead to discrepancies between the simulation codes and hence lead to different boundary conditions, a specified air flow rate is therefore considered for the benchmark model assuming fans at the high level openings to exhaust the contaminated room air. Subsequently the air which enters the room through the low level openings is at ambient temperature. A typical air change rate of $n=0.7ach^{-1}$ as stated in the DIN 4108-6 (2003) and DIN EN 13779 (2005) is considered during the daytime. Each opening has an area size of 17cm x 17cm resulting in an inlet air speed of about 0.18m/s. Hence thermal discomfort during occupancy times due to a draft risk from high air speeds is avoided (see DIN EN 13779 (2005)). For night-time ventilation, a rate of $n=0.7ach^{-1}$ is used during the preconditioning period and a higher ventilation rate of $n=3ach^{-1}$ operational from 2000-0600 is considered for the following 3 days of high global radiation and internal heat gains. Additional room heat gains from increased ventilation rates are

avoided since the external temperature remains below the internal temperature from 2000-0600 as stated by Engert et al. (2007). For the preconditioning period, only the single-sided ventilation is considered since the ventilation rates are low and thus the ventilation strategy is thought to influence the internal room condition only marginally. Results for the internal room temperatures for the cross ventilation strategy are then compared with the single-sided ventilation strategy for the last 3 days at which the internal heat gains are high during the day and at which the ventilation rates are higher during the night.

7.3 CFX and TRNSYS model settings for Benchmark 3

7.3.1 CFX model settings

The same methods as for benchmark 2 are used to define the model boundary conditions (i.e. using interface and wall boundary conditions at the surfaces, boundary energy flux source option, Fortran routines etc.). For the openings at high level an 'outlet' boundary condition is used to extract the room air to the outside. The air speed normal to the boundary and in direction to the outside contains a value of 0.18m/s for the preconditioning period and the same during the day and 0.76m/s during the night for the last 3 days. For the inlets at low level, an opening boundary condition is used which assumes a flow direction normal to the boundary and a medium turbulence intensity of 5% (see section A.5). The relative pressure is 0Pa and the inlet and blackbody temperature are equal the external air temperature. Models used for simulating the benchmark were the k-ω turbulence model, the Discrete Transfer radiation model and the buoyancy Boussinesq approximation using settings adopted from chapter 6. The reference temperature for the Boussinesq approximation is 16.1°C. A 1st order backward Euler scheme is applied to the transient term of the calculated equations (see section A.7).

Preliminary studies were carried out for benchmark 3 finding parameter values for the adaptive freeze-flow control method to achieve a trade off between accuracy and computational effort (see details in Schulz et al. 2007). The final parameter values are

shown in Table 7.4. The switch from frozen to unfrozen flow due to the external boundary condition changes at the beginning of each hour was skipped at 6 times of the day. By doing this, a CPU time reduction of 7% was possible with negligible loss of accuracy ($\Delta T \leq 0.1K$) compared with a simulation in which the solver switched to unfrozen flow mode at the beginning of every new hour. A time step size of 2s during the unfrozen flow periods was possible without leading to convergence problems. The simulation was considered to have converged if the solution reached a RMS normalized residual of 10^{-3} for the RANS equations. A study for a similar room model indicated only marginal deviations between the indoor air temperatures compared with a simulation where a residual of 10^{-4} was obtained. These settings investigated by Schulz et al. (2007) described above are used for investigations in chapter 7.

Table 7.4: Key parameters for the adaptive freeze-flow control method (Benchmark 3).

Parameter	Specification	Value	Unit
MAXTEMP	-	1.0	[K]
MAXLOOPS	-	5	[-]
EXTENSION	-	300	[s]
EVENT	External Temperature	1.0	[K]
	External diffuse radiation	0.31	[W/m^2]
	External direct radiation	1.33	[W/m^2]
	Internal Convective heat source	0.01	[W/m^2]
	Internal radiative heat source	0.01	[W/m^2]
	Air speed at the fan	0.01	[m/s]
Time step	Unfrozen flow period	2	[s]
	Frozen flow period	60	[s]

A total of 59,000 volume elements is used to discretise the room model using CFX (see details for mesh 1 in chapter E). Prism elements are used near the wall to represent the existing high pressure, velocity and temperature gradients in this region sufficiently accurate. Further from the walls tetra-elements are used. The mesh resolution near the wall showed only a small effect on the predicted convective heat transfer and negligible effect on the surface temperatures compared with a finer near wall resolution for which, however, convergence problems were observed (see chapter E).

7.3.2 TRNSYS model settings

The TRNSYS simulations for benchmark 3 were conducted by Engert et al. (2007). Details about program specific model settings can be found there. In TRNSYS, a time step size of 60 mins was used. The TRNSYS program does not calculate the convective heat transfer directly. Therefore, the internal h_c values stated in the VDI 6020-1 (2001) were used.

7.4 Results and Discussion

All CFX simulations achieved the convergence criterion of 10^{-3} for all residuals. The data output interval for TRNSYS was 60 mins, for CFX it was every 5 mins and additionally immediately before the solver switches between unfrozen and frozen flow modes. The smaller time interval for CFX compared with TRNSYS was possible due to the significantly smaller time resolution for solving the equations which hence provides more information about the changes in room condition changes.

7.4.1 CFX predictions for the single-sided and cross ventilation strategy

The average air temperature and the average surface temperatures of the ceiling and the floor for the preconditioning period and the following period of high global solar radiation and internal heat gains predicted for CFX are shown in Figure 7.3. The external wall was not evaluated since its geometry and spatial thermal conditions are more complex and difficult to compare with TRNSYS. The general results of the dynamic thermal room behaviour predicted by CFX are described first, followed by the comparison between single-sided and cross ventilation strategy.

During the preconditioning period (0-72 hours in Figure 7.3) the room air temperature follows the external temperature changes. However, a thermal lag of 2h and a damping of the amplitudes (amplitudes of 1.0K) are observed mainly due to thermal mass effects of the building fabric and the restriction of the ventilation rate. A further thermal lag of about 3h and a smaller temperature swing occurs for the ceiling (amplitudes of 0.3K) and the floor (amplitudes of 0.6K). The peak daytime room temperature increases only

slightly by 0.6K during the preconditioning period. Thus, the thermal mass of the building fabric absorbs sufficient heat during the daytime to maintain the room air temperature below 24°C.

During the first night of the following 3 day period (72-80 hours in Figure 7.3) the room temperature drops below the temperatures of the preconditioning period due to the increased ventilation rate. However, during the daytime the room temperature increases significantly despite the increased night-time ventilation and the use of a shading device (T_{max}=30°C at 88h). This is because the heat gains are higher than the dynamic absorbance potential in the thermal mass of the building fabric. In particular, after the shading device is removed from the window in the afternoon, the room temperature increases significantly. Figure 7.3 also shows that the ceiling cools only slightly during the night which indicates that only a limited amount of heat is released back to the room which subsequently reduces its effective heat absorption capacity during the following day. During the second day the room air temperature exceeds the external temperature. A maximum temperature of 33 °C is observed at the last day.

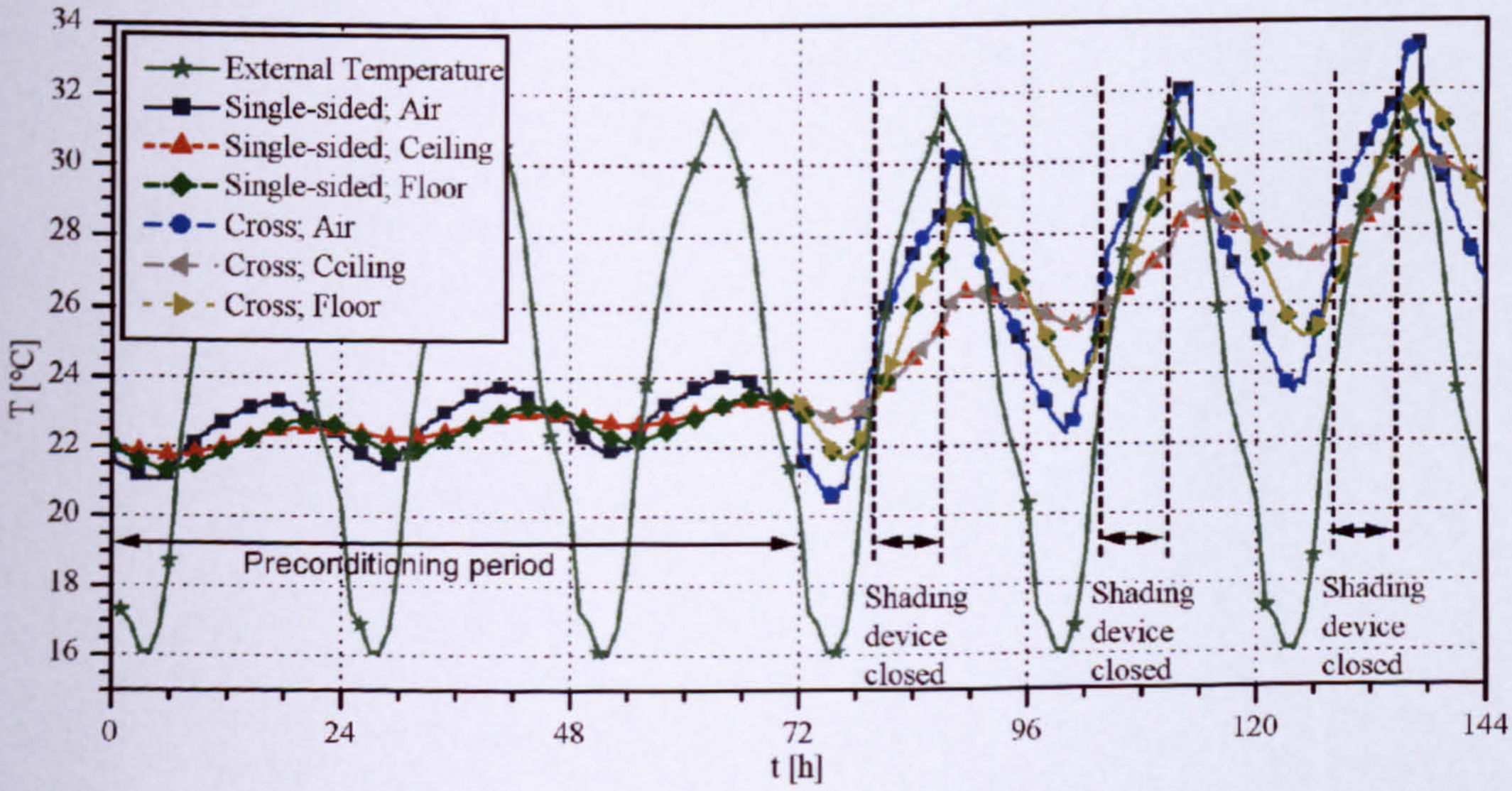

Figure 7.3: Predictions of average air and surface temperatures of the ceiling and the floor for CFX comparing a single-sided and a cross ventilation strategy (Benchmark 3).

Figure 7.4 shows the heat flux at the surfaces of the ceiling and the floor. During the preconditioning period the diurnal swing is almost constant and maximum heat transfer rates of 5W/m^2 are shown. The heat loss during the nights is slightly higher for the floor than for the ceiling and the heat gain during the daytimes is slightly lower for the floor than for the ceiling. During the following 3 day period the amplitudes are greater. This is a consequence of the higher room heat gains during the daytimes and higher ventilation rates during the nights as also indicated by the higher temperature swings in Figure 7.3. The ceiling reaches maximum heat losses of up to 15W/m^2 at night and heat gains of up to 30W/m^2 during the daytimes; the floor reaches maximum heat losses of up to 20W/m^2 at night and heat gains of up to 10W/m^2 during the daytimes. In particular, after the shading device is removed from the window in the afternoon, the heat transfer increases significantly. This also explains the rapid surface temperature decrease observed in Figure 7.3.

The total heat gain or loss during a certain time at a surface is calculated by integrating the surface heat flux values over this period which is visualized by the area between the curves and the zero line in Figure 7.4. For example, the total absorption of heat at day 5 (i.e. 117-127 hours) calculated for the ceiling is 159W·h/m^2 for CFX while the total heat release calculated for the following night (127-140 hours) is 89W·h/m^2. This shows that more heat is absorbed during the day than is released during the night. This indicates a gradual increase of the room temperature throughout the simulation which is reflected by the gradual increase of the room temperature curves in Figure 7.3. Furthermore, a gradual shift of the curves in Figure 7.4 towards smaller heat gains and higher heat losses towards the end of the simulation period is displayed. This demonstrates that a net heat gain occurs to the building fabric during the last 3 days of the simulation period.

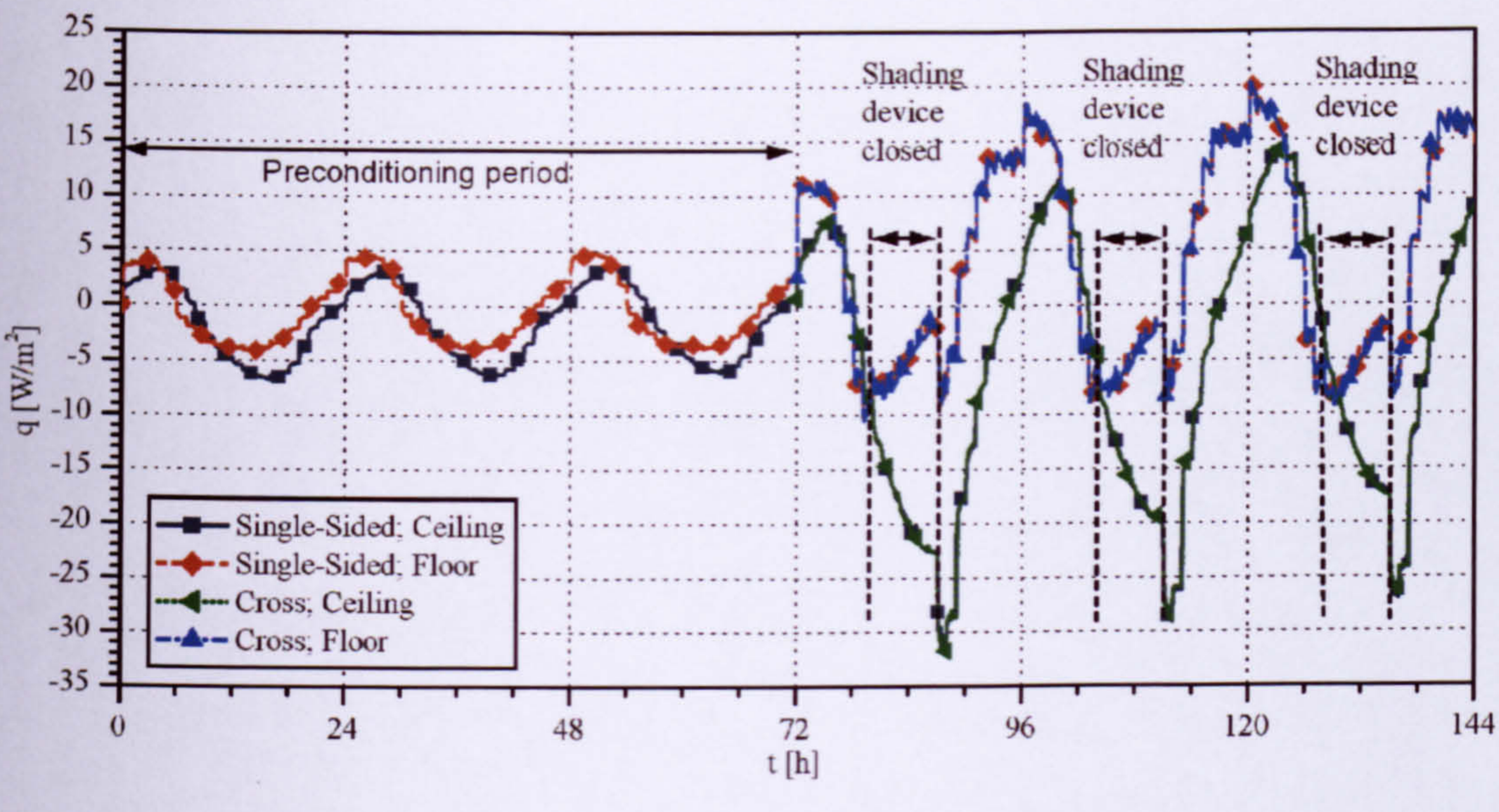

Figure 7.4: Predictions of the surface heat flux at the ceiling and the floor for CFX comparing a single-sided and a cross ventilation strategy (Benchmark 3).

A decrease of the heat gain at the floor is observed in Figure 7.4 for both ventilation strategies when the shading device is placed at the window. This falls together with the time the floor temperature exceeds the ceiling temperature in Figure 7.3. The gradual decrease indicates that the heat transfer might be dominated by radiation between the ceiling and the floor. Figure 7.5 shows the heat flux at the ceiling and the floor separated in proportions of convection and radiation (for clarity, only the results for the single-sided ventilation are shown). The figure clearly shows the domination of radiation heat transfer at the floor at that time (radiative heat flux is $7W/m^2$ while convective heat flux is $2W/m^2$ at 80h). Furthermore, the figure shows that the heat transfer at the ceiling occurs (almost) entirely by radiation (maximum radiative heat flux is $13W/m^2$ while maximum convective heat flux is $3W/m^2$) while the floor is cooled down primarily by convection during the nights (maximum radiative heat flux is $7W/m^2$ while maximum convective heat flux is $15W/m^2$). During most of the daytime periods the convective heat transfer at the floor is small relative to radiation. Comparing Figure 7.3, where the air temperature is cooler during the night (for example at 118h) and warmer during the daytime (for example at 135h) than the surface temperatures, with

Figure 7.4 at the same time, it is noticed that the upward convective heat flow is small relative to the downward heat flow. Radiative heat transfer is generally significant.

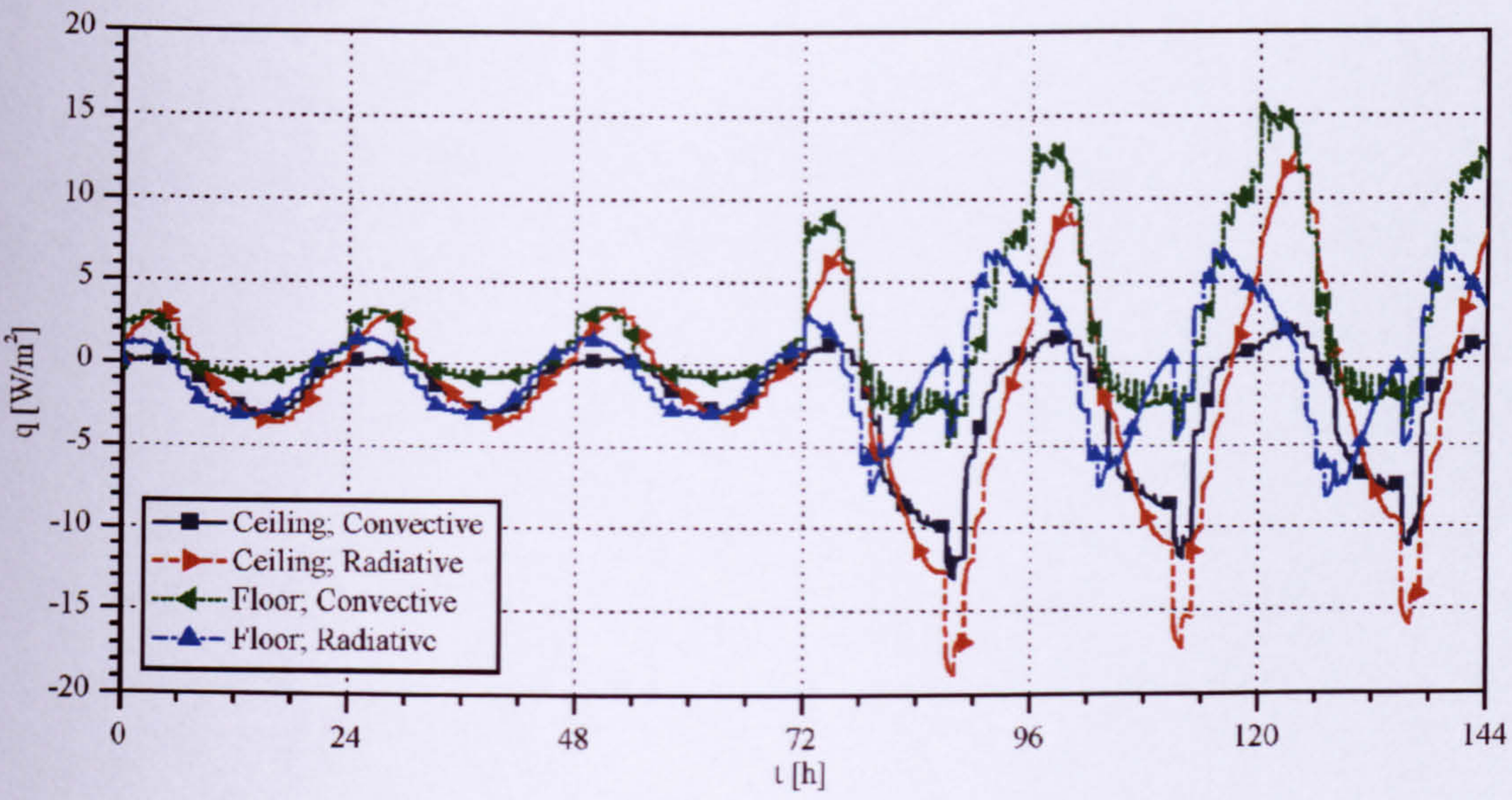

Figure 7.5: Heat flux predictions at the ceiling and the floor for CFX for single-sided ventilation separated in convective and radiative proportions (Benchmark 3).

The vertical temperature profiles in the centre of the room for the single-sided ventilation strategy are shown for the last day at 0400 and 1600 for the thermal distribution in the room as predicted by CFX (Figure 7.6). These times are intended to be representative of the developing vertical temperature stratification in the room during the night and day. A temperature difference of about 5K is exhibited between bottom and top of the air domain during the night. During the day the air temperature is smaller close to the surfaces than in the room centre since the air is cooled by the cooler building fabric. Particularly for the night, the distribution reflects the observation of a larger upward convective heat flow relative to the downward heat flow, since the temperature difference between the ceiling and the air is smaller than between the floor and the air. Furthermore, the development of a cool air layer at low level shown in Figure 7.6 demonstrates that the air entering at the inlets does not mix with the adjacent air layer above which leads to higher air speeds than if full mixing occurred and hence to higher convective heat transfer rates.

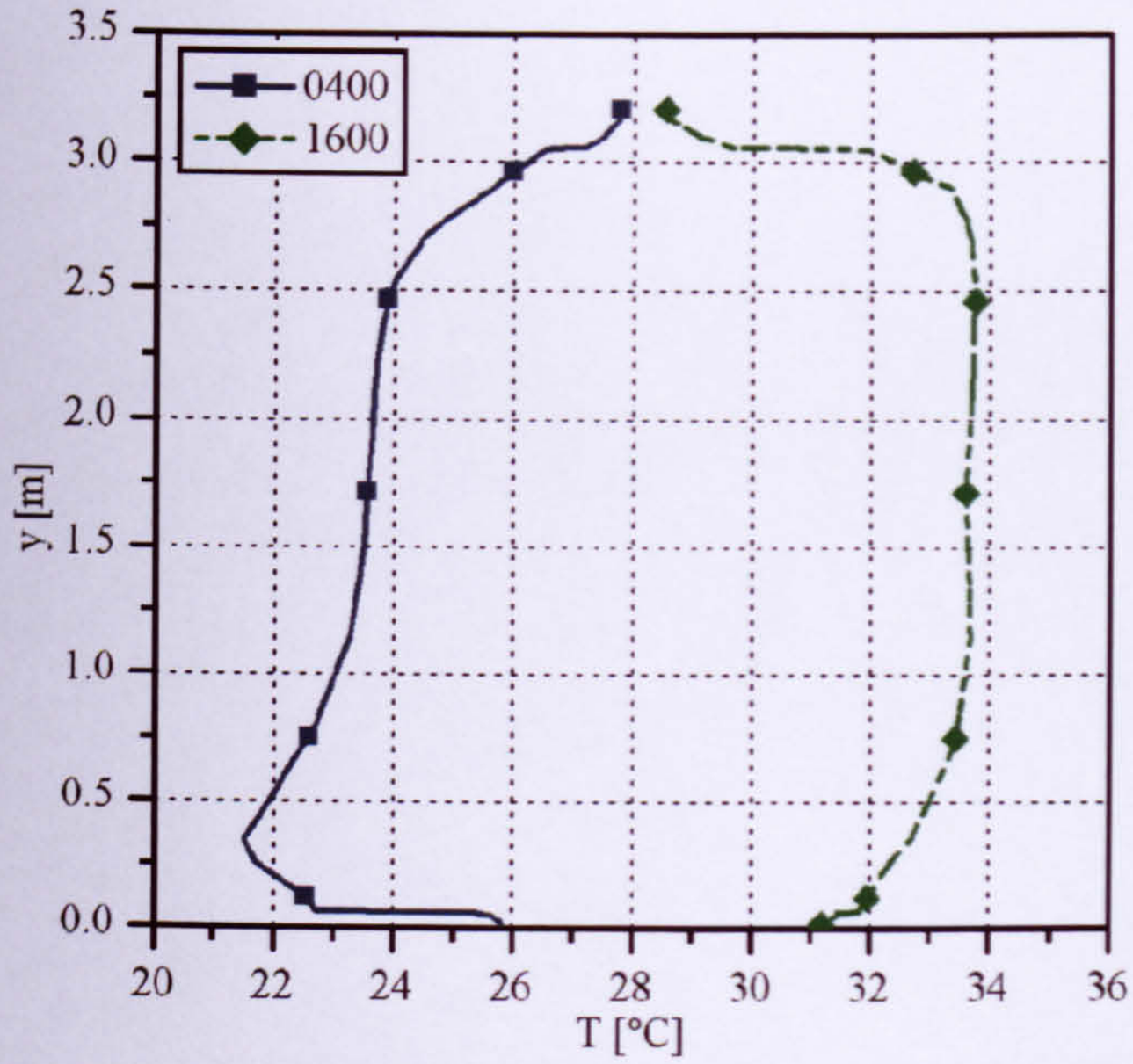

Figure 7.6: Predictions of the vertical temperature distribution in the core of the room for single-sided ventilation at 0400 and 1600 for the last day (Benchmark 3).The temperatures within the building fabric are shown between 0m-0.059m and between 3.059m-3.209m.

A comparison of CFX results for the single-sided and cross ventilation strategy for the period of high global solar radiation and internal heat gains exhibits only marginal differences in the thermal room conditions (see Figure 7.3) and negligible differences for wall heat fluxes at the ceiling and the floor (see Figure 7.4). The single-sided ventilation strategy shows only occasional higher peak air temperatures of less than 0.1K during the daytime and marginal lower temperatures during the night ($\Delta T \leq 0.01K$). The good agreement of results for both ventilation strategies indicate that the distance between the inlet and outlet might be sufficiently large to avoid short circuiting (i.e. a flow directly from the inlet to the outlet) and that the air flow distribution is similar in both cases.

The temperature efficiency, T_{eff}, defined by Hagström et al. (2000) can be used for assessing the efficiency of the night time ventilation strategies and is given by:

$$T_{eff} = \frac{T_{out} - T_{in}}{T_{room,ave} - T_{in}} \qquad \text{Eq. (7.1)}$$

where T_{out} is the temperature at the outlets, T_{in} is the temperature at the inlets and $T_{room,ave}$ is the average room temperature. The temperature efficiency is an indicator of the efficiency of a ventilation system to exhaust the contaminated warm air to the outside as for example demonstrated by Chen et al. (1988). If a short-circuit effect exists, the outlet temperature is close to the inlet temperature and the efficiency approaches zero. In the case of perfectly mixed conditions in the room, the outlet temperature is close to the room temperature and the temperature efficiency approaches one. For ventilation strategies similar to displacement ventilation, the outlet temperature is higher than the average room and inlet temperature and the temperature efficiency is higher than one.

Figure 7.7 shows the temperature efficiencies for the single-sided and cross ventilation night-time cooling strategy for the last day of the simulation using Eq. (7.1). The temperature efficiency increases from 1 to 1.3 when the external temperature falls below the room temperature and the ventilation rate is increased (c.f. Figure 7.3). During the daytime using a reduced air-change rate of $0.7ach^{-1}$, the temperature efficiency remains above 1 for the cross ventilation strategy while it falls below 1 for the single sided ventilation strategy which indicates a small short-circuit effect. However, this short-circuit effect is negligible and only marginally influences the thermal conditions in the room as demonstrated in Figure 7.3. The temperature efficiency greater than 1, predicted during the night by CFX, demonstrates a high night-time ventilation efficiency relative to displacement ventilation, which is also confirmed by the vertical temperature gradient at night shown in Figure 7.6. Such an assessment for different ventilation strategies would not be possible for a zonal simulation program which assumes a perfectly mixed room air condition and hence always predicts a temperature efficiency of 1. This would lead to a slight under-prediction of the night-time ventilation efficiency using a zonal program.

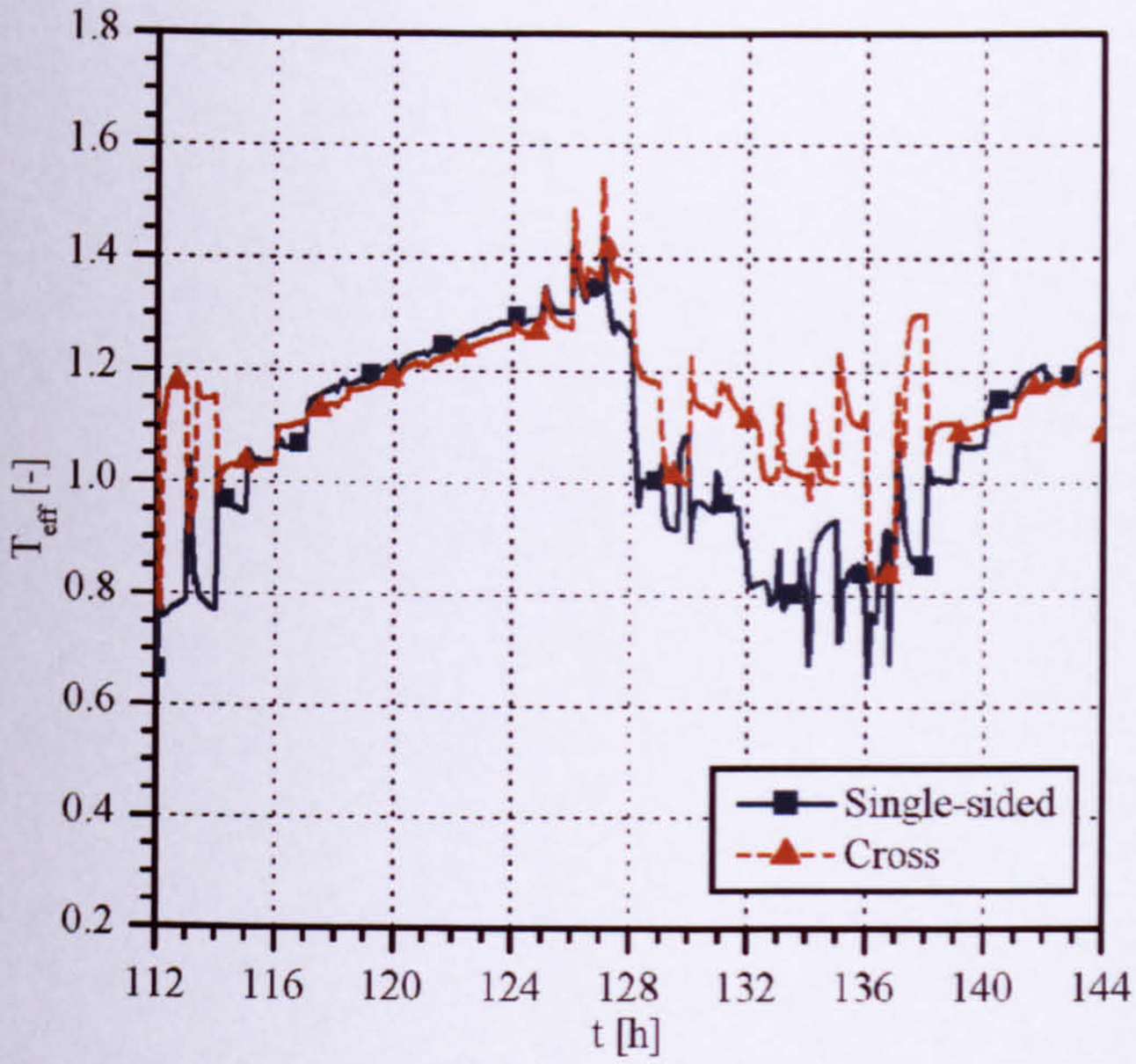

Figure 7.7: Temperature efficiencies for the single-sided and cross ventilation strategy calculated from CFX simulations (Benchmark 3).

The investigation of the night-time ventilation with dynamic CFD has demonstrated that a similar performance can be obtained for a single-sided ventilation strategy as for a cross-ventilation strategy if the inlets are sufficiently apart from the outlet to prevent from short-circuiting. Although the temperature efficiency and therefore the ventilation efficiency was high during the night, the gradual increase of the daily room air temperatures, which exceed the outdoor air temperature within the simulated period (see Figure 7.3), demonstrated that the use of the night-ventilation strategy alone was insufficient in maintaining the daily room air temperatures at a constant level of thermal comfort. However, the investigation was based on a period of extreme high global solar radiation and external daytime temperatures. It is possible that the night-time ventilation might work well for moderate climate periods, or for more thermal mass, or longer operating periods of more efficient solar shading devices.

7.4.2 Comparison of predictions for CFX and TRNSYS

The previous section has shown that there are only marginal differences between single-sided and cross ventilation. Thus, for comparison of CFX predictions with the

predictions of the zonal simulation program TRNSYS, only one strategy was used. Since data existed for the entire simulation period for the single-sided ventilation strategy the results for this strategy were used.

CFX predictions for the single-sided night-time ventilation strategy were compared with those of TRNSYS for a period of 6 days (thus including the preconditioning time). The average temperatures for the air and the surfaces of the ceiling and the floor are shown in Figure 7.8; the average surface heat flux at the ceiling and the floor are presented in Figure 7.9. The curve shapes for CFX and TRNSYS compare favourably. The maximum differences between CFX and TRNSYS predictions are summarized in Table 7.5. The differences are greater during the following 3 day period of high global solar radiation and internal heat sources compared with the preconditioning period whereby the differences gradually increase throughout the simulation period. The reason for these differences is thought come due to differences in the predicted surface heat transfer which is discussed below.

Table 7.5: Maximum differences of average internal temperatures and wall heat fluxes between CFX and TRNSYS predictions (Benchmark 3).

Time	ΔT [K]			$\Delta \dot{q}$ [W/m^2]	
	Air	Ceiling	Floor	Ceiling	Floor
Preconditioning period	0.2 at 65h	0.1 at 70h	0.25 at 54h	1.0 at 52h	0.5 at 50h
Period of high global solar radiation and internal heat gains	0.7 at 136h	1.1 at 137h	0.7 at 137h	4.0 at 135h	7.0 at 121h

No thermal lag is observed between the predictions of TRNSYS and CFX. The amplitudes of the surface temperatures tend to be slightly smaller for TRNSYS than for CFX (Figure 7.8). Less cooling of the floor during the nights and a generally slower warming of the ceiling during the 3 day period of high global solar radiation and internal heat gains is evident in the TRNSYS predictions relative to the CFX predictions, particularly when the shading device is removed from the window. This indicates that the predicted surface heat transfer is different for the simulation programs. This is reflected by the differences in the surface wall heat flux between the TRNSYS

and CFX predictions shown in Figure 7.9. Particularly at night, the heat flux at the floor is smaller for TRNSYS in comparison with CFX. During daytime, particularly when the shading device is removed, the heat flux at the floor and the ceiling is smaller for TRNSYS than for CFX. The smaller heat gain at the ceiling at that time for TRNSYS leads to a gradual deviation from CFX predictions since the ceiling cools only marginally during the nights for the room model, which subsequently leads to a smaller heat accumulation throughout the simulation. For the floor the deviations do not increase which is thought to be due to an efficient cooling during the night. The main reasons thought for the differences in the surface heat transfer at the ceiling and floor for CFX and TRSNYS are discussed below.

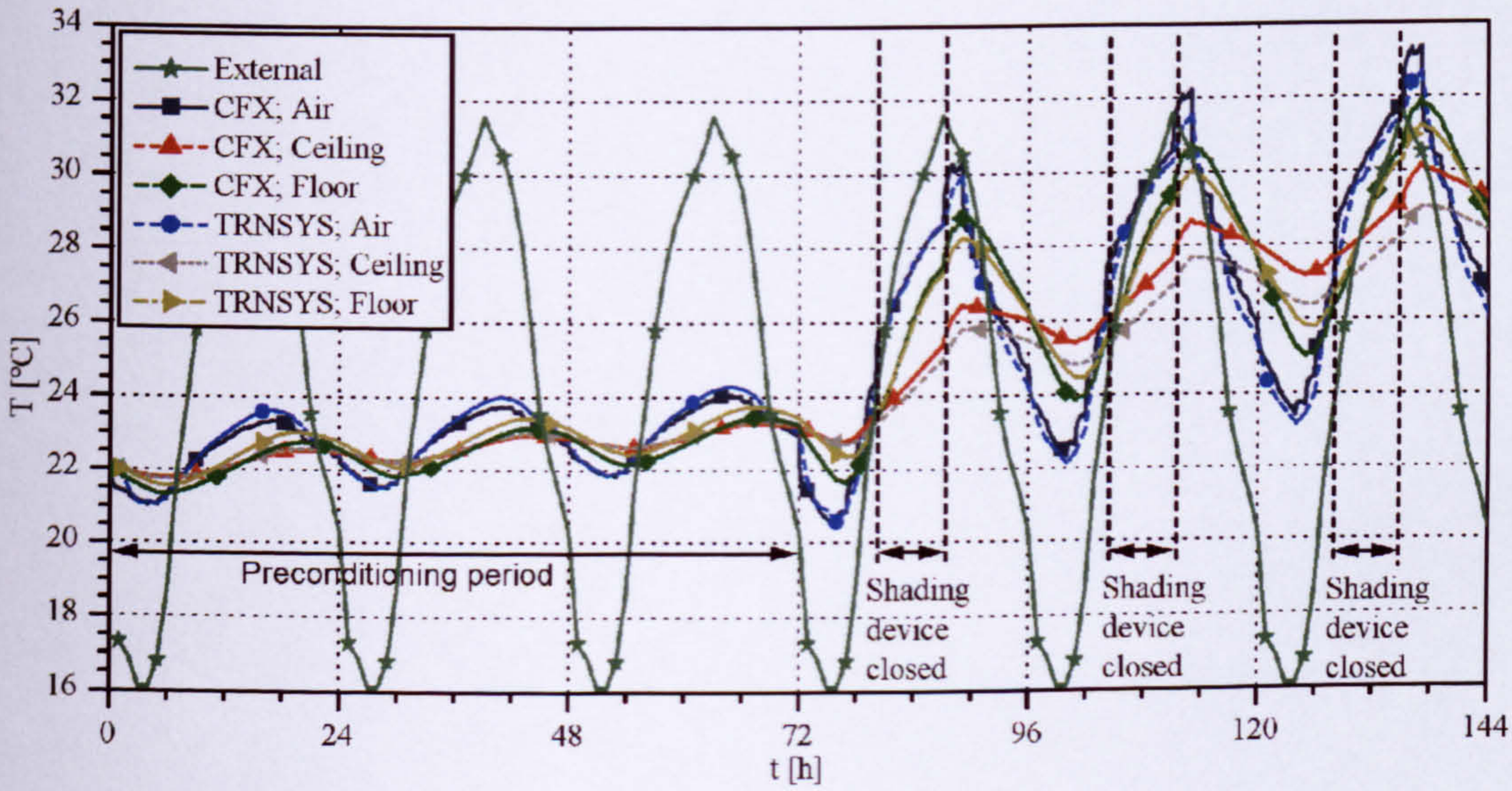

Figure 7.8: Average air and surface temperatures of the ceiling and the floor comparing CFX and TRNSYS predictions (Benchmark 3).

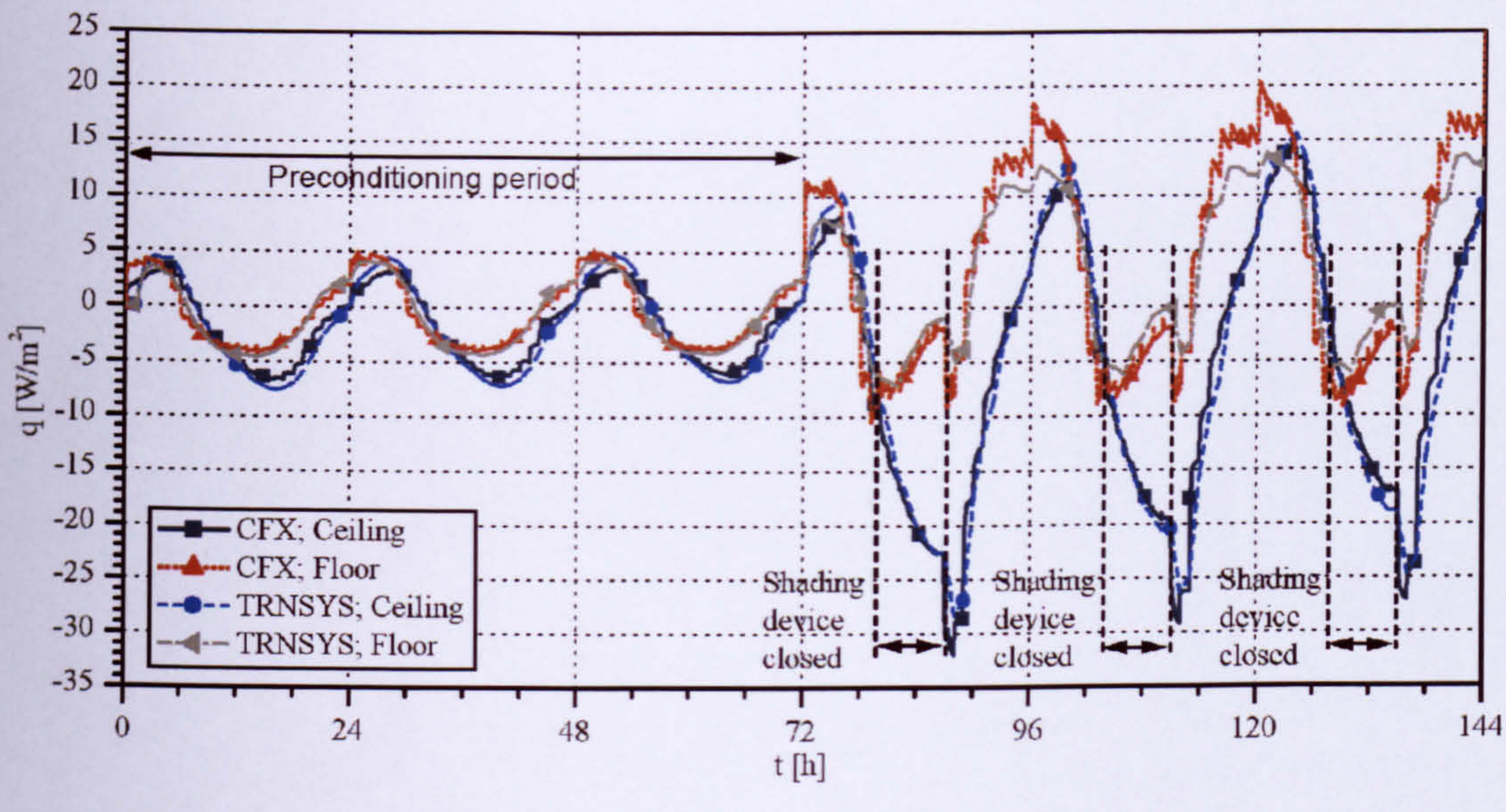

Figure 7.9: Average surface heat flux at the ceiling and the floor comparing CFX and TRNSYS predictions (Benchmark 3).

Although, the agreement between the CFX and TRNSYS results is good in Figures 7.8 and 7.9, there are small differences in the surface heat transfer which can be explained as follows.

TRNSYS uses fixed h_c values for the floor and ceiling as stated in the VDI 6020-1 (2001), whereas CFX calculates the convective heat transfer due to the time-varying flow and thermal conditions in the room. For example, a vertical temperature gradient develops in the air space for CFX during the night which can not be predicted by TRNSYS (see Figure 7.6). Moreover, differences of convective surface heat transfer exist for upward and downward flow as observed for CFX (see Figure 7.5). The expected higher convective heat transfer coefficients for upward heat flow than for the downward heat flow is also reflected in DIN EN ISO 6946 (1996) in which 5.0W/(m^2·K) is suggested for upward and 0.7W/(m^2·K) for downward heat flow. It is therefore expected that the use of direction dependent h_c values would lead to a significant decrease of deviations between TRNSYS and CFX predictions for the internal thermal room conditions and surface heat transfer. A quick test using TRNSYS with higher h_c values for upward flow and lower h_c values for downward flow for the

ceiling confirmed this assumption. However, more studies are required to find h_c values which are more realistic for the specific room conditions.

The convective surface heat transfer does not only depend on the direction of heat flow, but also on the instantaneous temperature difference between the solid and the air. Many investigations have shown that the correlation between the temperature difference and the convective surface heat transfer is non-linear and depends strongly on the spatial flow patterns, for example see a summary of correlations in Santamouris et al. (1996). This might also explain the smaller cooling rates at night at the floor when the air change rate is increased after the preconditioning period using TRNSYS in comparison with CFX. Furthermore, spatial effects exist in CFD which is indicated by a heat flux gradient along the building element surfaces calculated by CFX, which cannot be reflected by the one-dimensional heat transfer calculation using TRNSYS (Figure 7.10).

The representation of the room geometry is different between the models of TRNSYS and CFX. This leads to a simplified one-dimensional approximation of heat transfer in the building fabric using TRNSYS, which means the thermal mass at the joints of two building fabric components is neglected. This thermal mass can significantly influence the dynamic thermal behaviour of a room as shown in a preliminary study for a high thermal mass room in chapter 6. However, the additional effective thermal mass is relatively small in benchmark 3, since no internal solid walls are modelled. Additional thermal mass exists only at the room edge of benchmark 3 where the screed and the external wall approach each other and at the room edge where the external wall and the concrete ceiling approach each other. Therefore it is thought that this effect is relatively small.

Although prediction errors could occur due to the use of a freeze-flow method these are deemed to be small as demonstrated in section 5.4.7.

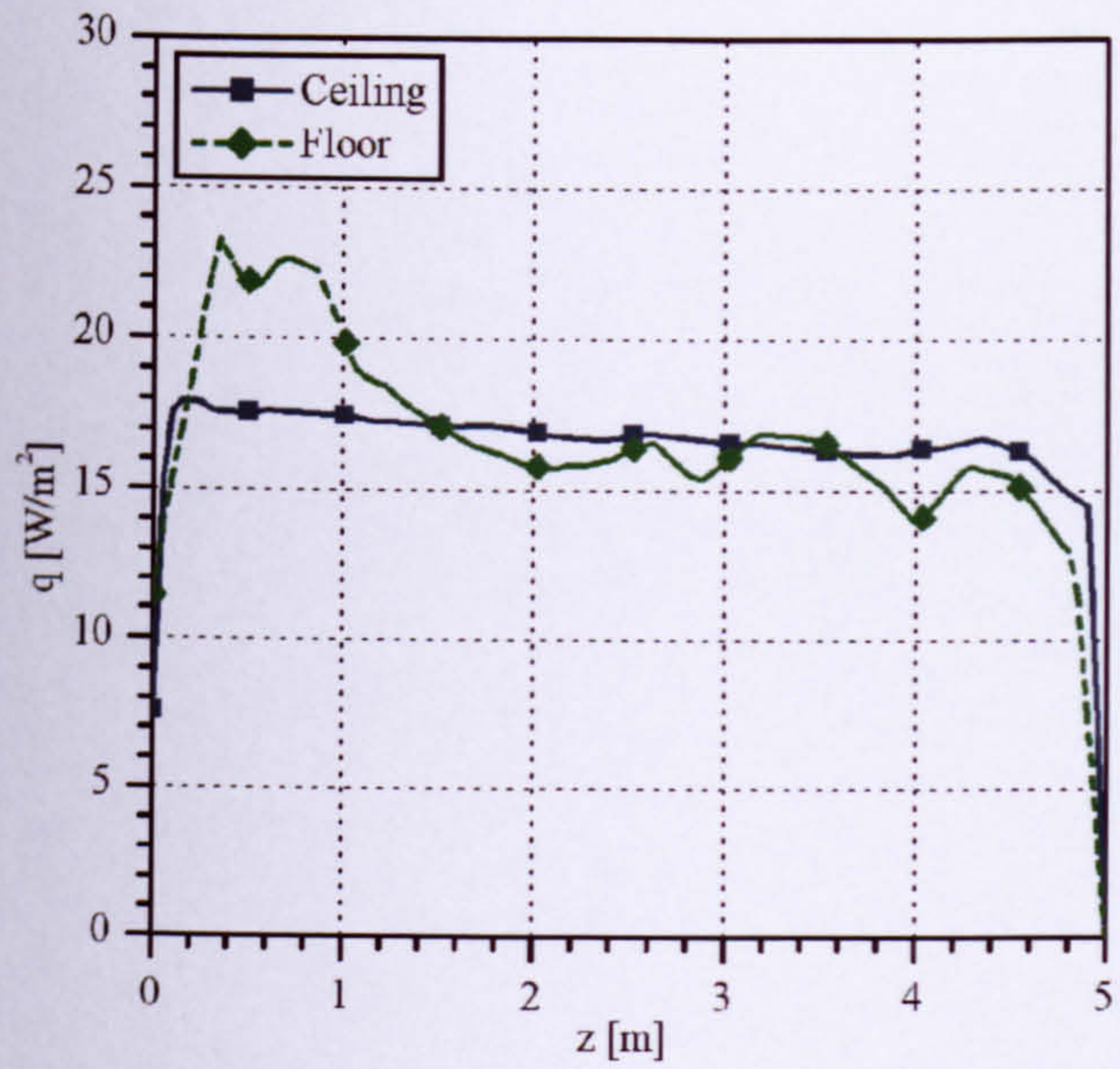

Figure 7.10: Predictions of the surface heat flux distribution along the ceiling and the floor for single sided-ventilation using CFX (Benchmark 3). Values are shown in z-direction at the height of the right opening at the last simulation day at 1600.

The close agreement between CFX and TRNSYS shown above might only be valid for very simple room geometries without obstructions such as furniture, and with those parameter settings for mechanical ventilation and opening positions (which prevent short-circuiting of the air flow) etc. used during this research. It is likely that DTS will give significant errors for other cases in which the spatial air flow distribution is more complex (e.g. for obstructions, other ventilation strategies and different heat source distribution). CFD should then give significantly better results as it is potentially more accurate due to the discretisation of the thermal zone in many small finite volume elements.

For example, the dry resultant temperature in the occupied zone for benchmark 3 was predicted in Schulz et al. (2007) for CFD using the correlations of CIBSE Guide A-1 (2006). A conclusion of the research was that only simplified formulations could be used for the calculation for the DTS program since information about local air flow patterns required for the calculation did not exist due to the assumption of well mixed flow conditions in the thermal zone.

7.5 Summary

Exemplary for the verification of dynamic CFD for more realistic room conditions compared to chapter 6, simulations were carried out for a room which has the geometry of a typical office room of medium thermal mass and typical internal time varying heat sources (from equipment and occupancy), referred to as benchmark 3. Time varying weather conditions and internal heat gains etc. were based on a dynamic thermal simulation verification procedure of the VDI 6020-1 (2001). Dynamic CFD simulation predictions carried out using the adaptive freeze-flow control method were compared with results of DTS.

The investigation using dynamic CFD has shown that a cool air layer develops at low level during the night due to high ventilation rates which brings cool air at low level into the room. This creates spatially different flow patterns and temperature distributions in the room. The temperature stratification displayed in the room led to a larger temperature difference between the floor and the air than between the ceiling and the air. Consequently larger convective upward heat flow relative to the downward heat flow was observed. This was, for example, reflected for the heat flux at the ceiling which was cooled (almost) entirely by radiation during the night (for the ventilation strategies investigated the maximum radiative heat flux was 13W/m^2 while maximum convective heat flux was 3W/m^2). This led to the conclusion that the amount of convective surface heat transfer at least depends on the direction of heat flow. This should be considered when values for the heat transfer coefficients in DTS are given.

The comparison between a single-sided and a cross ventilation strategy has shown that a similar performance (in terms of night-time ventilation efficiency and internal room temperatures) can be achieved for both strategies, similar to that for displacement ventilation. However, the distance between the inlet and outlet must be sufficient to prevent short-circuiting of air. Although, a small short-circuit effect was exhibited during the daytime for the single-sided ventilation strategy this had a negligible effect on the general thermal behaviour of the room. Such an assessment would not be possible if a zonal simulation program is used as it generally assumes a perfectly mixed room air condition.

Despite the high ventilation efficiency during the night periods, the gradual increase of the daily room air temperatures throughout the simulation period indicated that the use of the night-ventilation strategy alone was insufficient in maintaining the daily room air temperatures at a constant level. However, the investigation was based on a period of extreme weather conditions. It is likely that the night-time ventilation strategy might work well for moderate climate periods, or if more thermal mass or solar shading at the windows is provided.

Predictions of CFX and TRNSYS agreed well for the average internal room temperatures. Maximum deviations of 0.7K were displayed for a simulation period of 6 days. However, higher deviations were displayed for the ceiling (ΔT_{max}=1.1K) which resulted from the different heat flux values predicted by CFD and TRNSYS ($\Delta \dot{q}_{max}$ =4W/m^2), which therefore influenced the internal room temperature. The differences were thought to be mainly the consequence of the fixed, heat flow direction independent convective surface heat transfer coefficients used for the zonal DTS program during the simulation. An adaptation of the convective surface heat transfer coefficients to different flow patterns and heat flow directions (for example as suggested by the DIN standard EN ISO 6946 (1996)) are thought to lead to a reduction in the differences between CFD and zonal simulation program predictions. Thus, convective surface heat transfer coefficients should be selected carefully for DTS simulations as noticed above.

Model predictions between CFX and TRNSYS agreed favourably for benchmark 3. This room did not contain obstructions such as furniture; specific opening positions were used to avoid short-circuiting of the air flow; and mechanical ventilation was applied. However, for other cases in which the spatial air flow distribution is more complex, DTS model predictions might lead to significant errors. The CFD program potentially produces higher accurate results for these cases since the thermal zone is discretised in many finite elements.

The investigation has shown for an office room model that it is possible to predict the dynamic thermal room behaviour for night-time ventilation using dynamic CFD by applying the adaptive-freeze flow method. From the outcomes of the verification of the

adaptive freeze-flow control method by using benchmarks 1- 3 it is thought that this method might be a useful and efficient tool to give accurate results for other complex dynamic thermal room problems when dynamic CFD simulations are intended for use.

CHAPTER 8

CONCLUSIONS AND SUGGESTIONS FOR FURTHER WORK

8 Conclusions and suggestions for further work

8.1 Summary of Research Undertaken

Modern Computational Fluid Dynamics (CFD) programs contain an approach to calculate the coupled temperature fields in the air space and in the surrounding building fabric simultaneously (i.e. conjugate heat transfer). However, the time constant of the building fabric to respond to thermal changes is significantly larger than that for air which leads to significantly higher computational resources required for full dynamic CFD, restricting simulations largely to steady-state cases. A previously developed 'freeze-flow' method (Somarathne et al. 2002) has demonstrated good performance for overcoming the incompatibility of the different time constants, by freezing the air flow patterns over constant time periods using an ***invariable control method***. The number of equations necessary for the calculation of the thermal field can be reduced and large time steps can be used during these periods which leads to a significant decrease of computational resources required for CFD to conduct dynamic thermal simulations. This method has been shown to be capable of modelling dynamic thermal room behaviour using CFD. However, further refinement of the invariable control method and automation was required to further increase the performance and therefore extend the applicability of the freeze-flow method.

Field measurements and zonal dynamic thermal simulation (DTS) programs have often been used to investigate night-time cooling in offices and numerical investigations using potentially more accurate CFD programs are not available. To address this, use of the freeze-flow method in CFD provided a valuable approach for investigating dynamic night-time cooling, but also for other dynamic phenomena such as free convection and natural ventilation etc. In this research, a new, so-called ***adaptive freeze-flow control method*** was developed. This method was automated and implemented in the commercial CFD program CFX.

The new adaptive control method was tested using three benchmarks. In all cases, results compared favourably with predictions for full transient CFD simulations (for benchmark 1) and (a fundamentally different) zonal DTS program (benchmarks 2 and 3). Substantial reductions in CPU performance were achieved compared with the fully transient CFD simulations and a significant increase of performance in accuracy and computational time reduction was obtained compared with the invariable control method. The CFD results of modelling heat transfer mechanisms relevant in buildings compared favourably with analytical solutions and experimental results.

In this research dynamic thermal behaviour of building zones with and without night-time ventilation were modelled successfully using the newly developed CFD method.

8.2 The Benchmarks

The work has produced three clearly defined benchmarks which have been used to develop and verify new CFD methods to predict dynamic thermal room behaviour and to investigate night-time ventilation. The benchmarks are simple and easy to implement in CFD and DTS, thereby enabling new models and algorithms within CFD programs to be tested.

Benchmark 1 – Dynamic 2D Modelling of Conjugate Heat Transfer

The first benchmark considered a simple two-dimensional rectangular space (1.0m wide x 1.0m high) with upper and lower purpose-provided openings for natural and mechanical ventilation and the option to investigate pure free convection when the openings are closed. The space is thermally coupled to a high thermal mass material (solid brick), thereby facilitating conjugate heat transfer.

Benchmark 2 – Dynamic 3D Modelling of a High Thermal Mass Enclosure

The second benchmark is a typical office space size (3.5m wide x 3.0m high x 5.0m deep) which is enclosed by composite building fabric of high thermal mass. It is based on the model described in the building simulation guideline VDI 6020-1 (2001) and contains a convective heat source which is located below the window and a radiative

heat source which is unevenly distributed on the room surfaces to represent solar heat gain. Both sources are individually operated over specific time intervals.

Benchmark 3 – Dynamic 3D Modelling of Night-Time Cooling

The third benchmark contains a ventilated space (3.5m wide x 3.0m high x 3.5m deep) of medium thermal mass (i.e. massive external wall, floor and ceiling and adiabatic internal walls) and time varying internal heat sources typical for an office room. It is based on the model described in the building simulation guideline VDI 2078 (1996) and time varying boundary conditions of the building simulation guideline VDI 6020-1 (2001). Inlets and outlets at the external wall top and bottom respectively are used for a single-sided night-time cooling strategy. Outlets in the back wall at high level are used for a cross-ventilation night-time cooling strategy.

8.3 Development of an Adaptive CFD Freeze-Flow Control Method

Using the so-called freeze-flow method, the air flow field is 'frozen' over certain time periods which significantly reduces the number of equations to be solved and increases the possible time step for dynamic simulations. This method was shown to significantly reduce the computational resources required for modelling dynamic thermal room behaviour using CFD (Somarathne et al. 2002). Based on this freeze-flow method, Somarathne et al. (2002) developed an ***invariable control method***. The method gave generally good performance for predicting dynamic thermal behaviour in a small enclosure due to free convection; however, Somarathne et al. (2002 and 2003) identified some limitations. In order to address these, a new, ***adaptive control method*** has been developed in this research.

The ***adaptive control method*** uses 'triggers' which adapt the lengths of frozen and unfrozen flow periods to the environmental conditions. One of the aims of this method is to ensure that periods for frozen flow are as long as possible and periods of unfrozen flow are no longer than necessary. Therefore the following criteria were used to trigger a switch between unfrozen and frozen flow:

- Switch from *unfrozen to frozen* flow: the number of iterations per time step decreases gradually when the air flow patterns approach quasi steady-state conditions. At this stage the environmental air flow and thermal patterns have fully adapted to the room boundary conditions which suggests switching to frozen flow. The criterion MAXLOOPS is the maximum number of iterations permitted within the time period EXTENSION after which the solver should switch from the unfrozen to a frozen flow period;

- Switch from *frozen to unfrozen* flow: since the frozen air flow patterns represent a certain thermal situation, each change in the temperature field leads to increasing calculation errors in the frozen air flow field and in the heat transfer at room surfaces. To minimize these errors, the changes in thermal conditions of the air during frozen flow periods should be small. The criterion for switching from frozen to unfrozen flow is defined as the point at which the maximum local temperature difference in the air domain between the last time step of the previous unfrozen flow period and the current time step in the frozen flow period reaches or exceeds 'MAXTEMP'.

- When significant changes are likely to occur due to imminent changes in the user-defined boundary conditions, an additional, and overriding control is required which prohibits a switch from unfrozen to frozen flow or forces a switch from frozen to unfrozen flow periods, despite all other criteria being met. Thus, a controlling subroutine automatically checks for changes in the boundary conditions within the subsequent period (equivalent to the duration of a frozen time step). If a change in boundary condition reaches or exceeds the value of a specified criterion 'EVENT', the controlling subroutine responds as described above. 'EVENT' values are assigned to all likely time varying variables at boundaries (i.e. temperature, velocity, pressure and heat flux).

Optimal parameter values for 'MAXLOOPS', 'EXTENSION', 'MAXTEMP' and 'EVENT' depend mainly on the physical characteristics of the flow and need to be set by the user before the simulation begins. If the flow field is continuously unstable and weak in most parts of the air domain, 'EXTENSION' might need to be large and all

other values small to reduce errors in the air flow and temperature fields. If the flow field is more stable, 'EXTENSION' might be smaller and other parameters larger, which increases the performance of the freeze-flow method by reducing computation time.

Consequently, depending on the accuracy required (note: high accuracy is strongly coupled with the computational resources required) the user can set different values for these criterion parameters to reduce the simulation time required. This can, for example, facilitate faster turnaround of modelling predictions in the early stages of the building design process as detailed solutions are often not necessarily required at this stage.

For the adaptive freeze-flow control method the worst case scenario exists if the unfrozen flow periods are long and the frozen flow periods are small or if the solver never switches to the frozen flow mode. This may occur if the boundary conditions change rapidly or if highly unstable flow fields exist.

In order to automate the procedures, a sub-routine was written (based on Fortran and CFD specific commands) and converted into DLL-format to automate the invariable and the adaptive control methods. Consequently the solver is instructed to switch between unfrozen and frozen flow modes without stopping and restarting the simulation. This DLL-file can be simply implemented in the shared library of the CFD program. This has the advantage that full access to the internal code structure of the CFD program and the calculated solution fields stored, is given, which is required for the implementation of the new method.

The criteria for 'MAXLOOPS', 'EXTENSION', 'MAXTEMP' and 'EVENT' can be simply set by the GUI of the CFD program. Only the transfer of the boundary condition functions from the model definition file of the CFD program into the DLL file for the EVENT-sub-routine could not be automated, since the format was different to that used for the definition file (i.e. CFX Expression Language). Thus, the functions had to be included in the DLL file separately.

8.4 Verification of the new Adaptive Freeze-Flow Control Method

8.4.1 *Dynamic 2D Modelling of Conjugate Heat Transfer* (Benchmark 1)

For the cooling of the massive solid wall of benchmark 1 over a period of 12h due to natural ventilation, mechanical ventilation and free convection, the results of the adaptive and invariable freeze-flow control method agreed favourably with the solution for a fully dynamic CFD simulation in which all equations were solved without interruption (base case).

Small errors of about 0.2K were observed in all cases in the thermal field due to a slight over-prediction of convective surface heat transfer due to the frozen flow periods. For the invariable control method, only about 22% and 34% of the CPU time and output data file size used by the base case were required. For the automated adaptive control method these figures were further reduced to about 11% and 28% respectively (a further 50% reduction in the CPU requirements).

These results were based on freeze-flow parameter settings found to be optimal for the natural ventilation case investigated which were also used for the other cases. For the invariable control method, these settings were: time steps of 1s and 300s and period lengths of 300s and 1800s for unfrozen and frozen flow periods. For the adaptive control method the parameter settings were: 'MAXLOOPS'=2, 'EXTENSION'=300s, 'MAXTEMP'=0.2K and 'EVENT'=0.2K and 1s and 60s of time step lengths for unfrozen and frozen flow periods.

In a further test case of free convection in which a sinusoidal time varying external temperature condition was applied, a similar performance of time reduction was shown for both control methods (about 25% of the CPU time required by the base case). However, during periods of rapid thermal boundary condition changes, errors in temperature of up to 0.35K were displayed for the invariable control method compared with the base case while only 0.15K of error was displayed for the adaptive control method. This clearly demonstrated the advantage of the adaptive over the invariable

control method for which the length of frozen flow periods was much smaller during the rapid boundary condition changes. For this test the following parameter settings were used for the adaptive control method: 'EXTENSION'=180s, 'MAXTEMP'=0.5K and 'EVENT'=0.5K. Time step sizes were used as for the former cases investigated. Parameters for the invariable control method were the same as for the previous case.

For simulations described above, radiation was not modelled, since this would require significant additional computational resources. However, in a further test for the cooling of the wall due to free convection where radiation modelling was included, the small errors which occurred due to the freeze-flow method were significantly reduced. The inclusion of radiation modelling significantly influenced the dynamic thermal room behaviour since the cooling of the solid wall was influenced by radiative surface heat transfer. Thus, radiation modelling should be included in modelling the dynamic thermal behaviour of buildings.

The over-/under-prediction of convective surface heat transfer which would normally lead to a faster/slower cooling or warming of the building fabric is almost eliminated due to a simultaneous compensation by reduction/increase of radiative heat transfer (0.2K error if radiation was excluded, 0.03K error if radiation was included compared to the base). When all heat transfer mechanisms were considered for the cooling of the wall, the simulation required only 16% of the time required by the base case by using the adaptive freeze-flow control method.

For benchmark 1 it was shown that the adaptive freeze-flow method performs significantly better than other CFD methods (i.e. fully dynamic CFD and invariable control methods) in terms of a trade-off between accuracy and computational effort.

8.4.2 Dynamic 3D Modelling of a High Thermal Mass Enclosure (Benchmark 2)

Predictions using the adaptive freeze-flow control method were compared with results from a zonal DTS program (TRNSYS). The predictions of dynamic internal mean room

temperature compared favourably between both programs. Maximum deviations of 0.4K were observed at the end of a 24h simulation.

The main reason for this difference is thought to be the one-dimensional treatment of heat conduction of the DTS program which neglects the thermal mass in the building structure where two building components meet each other. Typically the inner dimensions of a room are used in DTS to calculate the heat conduction in the solid. It was found that CFD results lay between these results and those for DTS in which the room outer dimensions were used. This clearly demonstrates the plausibility of the dynamic thermal predictions for both programs for benchmark 2.

For this benchmark, the following parameters were used for the adaptive freeze-flow control: 'MAXLOOPS'=5, 'EXTENSION'=300s, 'MAXTEMP'=0.8K, 'EVENT'=0.8, time steps of 1s and 60s for the unfrozen and frozen flow periods were used.

The results for the relatively simple model of benchmark 2 have demonstrated the potential of dynamic CFD when using the adaptive freeze-flow control method.

8.4.3 Dynamic 3D Modelling of Night-Time Cooling (Benchmark 3)

The influence of night-time cooling on the dynamic thermal behaviour of an office room was investigated using the adaptive freeze-flow control method.

Comparison of dynamic CFD predictions agreed favourably with the predictions of the zonal DTS program, TRNSYS, for space-averaged evaluation of internal temperatures and surface heat transfer. This demonstrated the plausibility of results for both programs to predict the dynamic thermal behaviour of this room.

Maximum differences of 0.7K of internal room air temperature were observed at the last day of a 6 day simulation period with time varying internal heat sources and weather conditions. Only at the ceiling, were slightly higher temperatures predicted by CFD compared with DTS (ΔT_{max}=1.1K).

The main reason for the deviations between the programs is thought to be the simplified convective heat transfer coefficient values used for the DTS program which did not

consider the direction of heat flow. It is thought that the deviations between DTS and CFD will decrease if this is taken into consideration.

Using the CFD program the dynamic thermal room behaviour was compared for a single-sided and a cross-ventilation night-time cooling strategy. For both strategies similar night-ventilation efficiencies were obtained which were similar to that of displacement ventilation. This shows that the positions of the inlets and outlets are sufficiently far apart to prevent short-circuiting effects. Such an evaluation would not be possible using a zonal DTS program since it always assumes perfectly mixed conditions for the thermal zone.

For the adaptive control method the following parameter values were found to give good results: 'MAXLOOPS'=5, 'EXTENSION'=300s, 'MAXTEMP'=1K (values for 'EVENT' were different for each internal heat source and weather condition), time steps of 2s and 60s for unfrozen and frozen flow periods were used respectively.

The results for this night-time ventilation case in a more realistic room have demonstrated the potential of dynamic CFD to model the complex dynamic thermal room behaviour by using the adaptive freeze-flow control method.

8.5 General Conclusions

In order to model dynamic thermal behaviour of buildings accurately, all the heat transfer mechanisms relevant in buildings (i.e. heat conduction, convection and radiation) must be modelled accurately.

Parametrical studies were carried out and compared with analytical solutions and experiments for the heat transfer models in CFX to evaluate optimal parameter settings and gain confidence in the models. The main conclusions obtained from these studies are as follows.

8.5.1 Heat Conduction

In order to model the dynamic heat conduction in the building material it was found that a first order accurate Backward Euler scheme to solve the transient term in the energy equation gave accurate predictions. For example, the simulation of dynamic heat conduction in a massive solid wall showed an error of only 5% of surface heat flux after a simulation period of 4 hours compared with the analytical solution of Wagner (1998). In contrast, over- and under-shoots were displayed for a second order accurate transient scheme. These effects are thought to be caused by numerical dispersion which is a typical drawback of even-order schemes (Oertel and Laurien 1995). Consequently, the second order scheme is likely to be unsuitable for modelling dynamic thermal behaviour of buildings.

8.5.2 Free Convection

Turbulence model

To model turbulent flow which is typical for free convection flow in buildings, a turbulence model is required. Favourable results were achieved for the k-ω model when pure free convection was modelled in an enclosure and results were compared with experiments from Tian and Karayiannis (2001) (e.g. 6% deviation of the maximum vertical velocity in the wall boundary layer compared with the experiments). To predict the fluctuations in the turbulences for free convection flow (which usually have small time-scales) and hence to achieve convergence, small time steps are required which should be in the order of a few seconds (i.e. 1-2s). For times when air flow is not calculated (e.g. 'frozen'), then significantly larger time steps can be used.

Parameter settings for the steady-state solution scheme

The research has shown that some parameter modifications in the CFD program are required to achieve good convergence rates and solutions when steady-state free convection is modelled by using the steady-state solution scheme. These were:

- mass relaxation (which relaxes the mass terms in the equations solved) had to be increased from default 0.75 to 1 to accelerate the mass flow to reach steady-state;

- an automatic calculation of the physical time step should be used to accelerate the convergence rate for the slow air flow motion in the enclosure due to the small buoyancy forces;

- the 'timescale update frequency' (which determines the iteration interval at which the time step size is updated) had to be reduced to 1 (i.e. every iteration), since the change of the size of the time step during the first few iterations is often likely to be significant due to large driving forces when starting simulation from an initial condition of zero flow which would then lead to a solution divergence;

- the additional source terms in the momentum equation due to buoyancy (production and dissipation) should be included.

<u>Mesh Type and Mesh resolution</u>

An unstructured volume mesh of tetrahedral elements is recommended for complex flows (e.g. flow reversal regions) and room geometries since structured meshes are likely to lead to notable local numerical diffusion effects (i.e. gradients 'smear out').

Since the velocities and temperatures in wall boundary layers significantly influence the convective surface heat transfer (shown in a comparison of experimental results of Tian and Karayiannis (2000) with numerical predictions), these must be predicted accurately by the simulation program. Semi-empirical wall-functions, which are often used to resolve the wall-boundary layer efficiently for forced flow regimes, are not valid here, since the velocity patterns in the wall boundary are different for free convection. Thus, ε-equation based turbulence models in CFX are likely to be unsuitable since these are based on the semi-empirical wall functions. A numerical resolution is required by using mesh refinement in this region (at least 15 elements are suggested in the CFX user

manual to resolve the wall boundary layer). Turbulence models based on the ω-equation (e.g. k-ω model) support this option in CFX using a low-Reynolds approach.

The research has shown that the size of the first volume element adjacent to the wall has a significant influence on the heat transfer in the wall boundary layer compared with the elements further away. This is due to the requirement to resolve the laminar sub-layer accurately. For example, for a parametrical study for free convection at a vertical hot wall accurate predictions of convective heat transfer, a high degree of accuracy could be achieved with a size of no larger than 0.2mm for the first element adjacent to the wall (deviation of 0.2% compared to analytical solutions of Ostrach 1953).

However, since the high mesh refinement potentially leads to a significant increase of the computational effort, methods are required to reduce the effort. By using prism elements for the wall boundary layer and prism inflation (i.e. gradual increase of the prism element size from the surface to the outer layer of the boundary), the computational effort can be increased with a marginal loss in accuracy. For example, using a size of 0.2mm for the first mesh element adjacent to the wall and prism inflation of factor 1.2 after the second prism element (i.e. 0.5mm) from the wall, the error was only 0.4% compared with the analytical solution.

It is possible to increase the surface and volume mesh in the room without influencing the convective surface heat transfer. An increase of the volume element size, for example, from 10mm (surface) and 20mm (core volume) to entirely a maximum of 50mm, a loss of accuracy of less than 1% was observed for the convective surface heat transfer compared with the finer mesh as long the wall boundary layer region was sufficiently refined.

However, the larger elements lead to larger ratios of prism element sizes normal and parallel to the surface. This potentially leads to convergence problems. In some cases where large volume elements are required (e.g. for long dynamic thermal simulation processes in large buildings), the required mesh resolution in the wall boundary layer cannot always be guaranteed and some small errors in accuracy have to be accepted. A decrease of the number of prism elements from 8 to 4 for the numerical resolution of the wall boundary layer, for example, led to errors of about 0.2-0.4K in this research.

8.5.3 Thermal Radiation

Two models exist in CFX for modelling radiation in optically thin media (i.e. air and windows): the Monte Carlo and the Discrete Transfer models. However, using the Monte Carlo model, significantly high computational resources were required and an unphysical spatial distribution of radiative heat transfer was observed. The unphysical solution is thought to be the insufficient period of tracking radiation particles through the domain which is limited by the computational resources available. Consequently it is likely that the Monte Carlo model might be unsuitable for modelling radiation in dynamic thermal simulations.

In contrast, the Discrete Transfer Model predictions agreed well with the analytical solution of Wagner (1998). The model assumes isotropic emission of the radiation from the surface elements along rays. However, the use of a sufficient number of rays is required for accurate predictions. A number of 30 rays for the spatial discretisation of the surface elements, for example, resulted in a deviation of 6% compared with the analytical solution.

8.6 Suggestions for Further Work

8.6.1 Adaptive Freeze-Flow Control Method

An adaptive control method was developed in this research using triggers to adjust the length of unfrozen and frozen flow periods to the environmental thermal conditions, which led to a significant improvement of the freeze-flow method. However, further investigations are suggested to find, for example, general parameter values for the controlling switching criteria which might be applicable to a wide range of applications (e.g. natural ventilation, mechanical ventilation, pure free convection, different ventilation strategies, stable and unstable flow fields, low and high thermal mass rooms). The current freeze-flow method uses fixed time steps throughout frozen and unfrozen flow periods. However, the efficiency of the freeze-flow method could be further increased, if the time step sizes could be increased. The time steps could be larger, for example, when the air flow patterns are stable and are adjusted to smaller

values if they are unstable. A so-called optional 'adaptive time-step method' has been implemented in the new CFD program release which adjusts the current time step size depending on the number of iterations which were necessary during the old time level by using a hysteresis approach. The criterion of maximum number of iterations (i.e. MAXLOOPS) used in the current adaptive freeze-flow control method might be replaced by a maximum time step size (i.e. MAXTSTEP) to instigate a switch from unfrozen to frozen flow mode. However, an additional trigger would be required which reduces the time step size in advance to avoid convergence problems if significant boundary condition changes are imminent.

8.6.2 Automation of the Adaptive Control Method

The time varying boundary condition functions had to be implemented during definition file setup in the DLL file for the adaptive freeze-flow control method. Further research is required to implement a sub-routine which automatically uses the data from functions or weather data files stored in the model definition file to further automate the approach.

Reliable experimental data from test chambers which contain high thermal mass was not found during the literature review. Accurate data would be valuable for further verification of numerical predictions and new algorithms.

8.6.3 Design of Night-Time Ventilation

Two night-time cooling strategies were successfully investigated for a typical office room using the adaptive freeze-flow control method. However, the office room did not contain any obstructions which could reduce the efficiency of the thermal mass of the building fabric. A topic for future work is the investigation of different obstructions (e.g. suspended ceiling and acoustic panels) to investigate the influence of such modifications on the cooling potential of the thermal mass of the building fabric.

8.6.4 Mesh Consistency and Near Wall Treatment

It was difficult to achieve full mesh consistency for the dynamic thermal simulation models investigated since significant errors might only be displayed after long time

intervals due to the high thermal mass of the building fabric. However, the parametrical mesh studies were restricted to relative short time periods of some hours due to the limitation of the computer capacity. It would therefore be valuable to conduct further mesh consistency studies, to determine whether further mesh refinement is required or if the mesh can be further coarsened locally, for example, in the near wall boundary layer. Furthermore, the high numerical resolution of the wall boundary layer required for the low-Reynolds method used to model the convective surface heat transfer for free convection accurately, led to convergence problems. It would therefore be valuable to develop wall-functions for CFD which can be applied to free and forced convection flow to reduce the numerical discretisation effort. Some research was planned in Beausoleil-M. and Strachan (1999).

8.6.5 Modelling Radiation in CFX

The Monte Carlo radiation model is the only model provided in CFX for which radiation can be calculated through optically transparent solid materials (e.g. window). However, the computational effort is currently too high to obtain sufficiently accurate results for dynamic thermal building simulations. A recent release of the CFD software used provides improved modelling techniques for radiation models such as the Monte Carlo method which should be investigated. Another possibility to improve the performance might be the development of a freeze-radiation method in which the equations for radiation are frozen for certain time periods.

REFERENCES AND BIBLIOGRAPHY

References

Alloca C., Chen Q. and Glicksman L., 2003: *Design analysis of single-sided natural ventilation*, Energy and Buildings 35, pp. 785-795.

Awbi H., 1998: *Calculation of convective heat transfer coefficients of room surfaces for natural convection*, Energy and Buildings 28, pp. 219-227.

Baehr H., Stephan K., 1996: *Wärme- und Stoffübertragung*, 2nd Ed., Springer Verlag.

Barhaghi D., 2004: *DNS and LES of turbulent natural convection boundary layer*, PhD thesis, University of Goeteborg, Sweden.

Barnard N., 2002: *Thermal mass and night ventilation – utilizing 'hidden' thermal mass*, International Journal of Ventilation 1 (2), pp. 81-90.

Bartak M., Beausoleil-Morrison I., Clarke J., et al., 2002: *Integrating CFD and building simulation*, Building and Environment 37 (8-9), pp. 865-871.

Barth T. and Jesperson D., 1989: *The Design and Application of Upwind Schemes on Unstructured Meshes*, AIAA 89-0366.

Beausoleil-Morrison I., 1999: *Modelling mixed convection heat transfer at internal building surfaces*, Proceedings: Building Simulation 1999, Kyoto, Japan, 8 pages.

Beausoleil-Morrison I. and Strachan P., 1999: *On the significance of modelling internal surface convection in dynamic whole-building simulation programs*, ASHRAE Transactions 105 (2), pp. 929-940.

Beausoleil-Morrison I., 2000: *The adaptive coupling of heat and air flow modeling within dynamic whole-building simulation*, PhD thesis, University of Strathclyde, UK.

Beausoleil-Morisson I., Clarke J. and Denev J., 2001: *Further developments in the conflation of CFD and building simulation*, Proceedings: Building Simulation 2001, Rio de Janeiro, Brazil, pp. 1267-1273.

Beghein C., Penot F., Mergui S. and Allard F., 1993: *Numerical and experimental evaluation of turbulent models for natural convection simulation in a thermally driven square cavity*, Proceedings: ASME Conference, pp. 1-12.

BINE, 2003: *Passive Kuehlung mit Nachtlueftung*, Themeninfo I/03, Fachinformationszentrum Karlsruhe, Germany.

Blomberg T., 2000: *HEAT 2D User Manual*, Version 5.01, Building Technology Group, Lund University, Cambridge, UK.

Blondeau P., Sperandio M. and Allard F., 1997: *Night ventilation for building cooling in summer*, Solar Energy 61 (5), pp. 327-335.

Brown M., 1990: *The thermal mass of buildings in reducing energy consumption*, Journal of Solar Energy Engineering 112, p. 273-279.

Carrilho da Graca G. and Linden P., 2002: *Defining a global room surface heat transfer coefficient*, Proceedings: Roomvent 2002, Copenhagen, Denmark, 4 pages.

CFX, 2006: *CFX User Solver and Theory manual*, Version 10.0, ANSYS Ltd.

Chen Q. and Van der Kooi J., 1988: *ACCURACY – a computer program for combined problems of energy analysis, indoor airflow and quality*, ASHRAE Transactions 94 (2), pp 196-214.

Chen Q., Kooi J. and Meyers A., 1988: *Measurements and computations of ventilation efficiency and temperature efficiency in a ventilated room*, Energy and Buildings 12 (2), pp. 85-99.

CIBSE AM11, 1998: *Building energy and environmental modelling - Applications manual*, CIBSE, UK.

CIBSE Guide A-1, 2006: *Environmental design. Chapter 1- Environmental criteria for design*, London, England

CIBSE Guide A-5, 2006: *Environmental design. Chapter 5 – Thermal response and plant sizing*, Chartered Institution of Building Services Engineers, UK.

Clinton Foundation, 2007: *President Clinton announces landmark program to reduce energy use in buildings worldwide*, Press article from 16.05.07, http://www.clintonfoundation.org, last viewed at 17.05.2007.

Cook M., Ji Y and Hunt G., 2003: *CFD modelling of natural ventilation: combined wind and buoyancy forces*, International Journal of Ventilation 1 (3), pp. 169-179.

Crawley D., Hand J., Kummert M. and Griffith B., 2005: *Contrasting the capabilities of building energy performance simulation programs*, Proceedings: Building Simulation 2005, Montreal, Canada, pp. 231-238.

Cumber P., 1995: *Improvements to the Discrete Transfer method of calculating radiative heat transfer*, International Journal of Heat and Mass Transfer 38 (12), pp. 2251-2258.

DIN 1946-6, 1998: *Ventilation and Air conditioning – Ventilation for residential buildings. Requirements, performance, acceptance*, Beuth Verlag, Germany.

DIN 4108-2, 2003: *Thermal protection and energy economy in buildings - Part 2: Minimum requirements to thermal insulation*, Beuth Verlag, Germany.

DIN 4108-6, 2003: *Thermal protection and energy economy in Buildings- Part 6: calculation of annual heat and annual energy use*, Beuth Verlag, Germany.

DIN EN 13779, 2005: *Ventilation for non-residential buildings – performance requirements for ventilation and room-conditioning systems*, Beuth Verlag. Germany.

DIN EN ISO 6946, 1996: *Building components and building elements – thermal resistance and thermal transmittance – Calculation method*, Beuth Verlag, Germany.

DOE-2, 1995: *Reference manual*, Report LBL-8706, Lawrence Berkley Laboratory, USA.

EnEV, 2006: *Verordnung über energiesparenden Waermeschutz und und Energiesparende Anlagentechnik bei Gebäuden*, Bundesministerium fuer Wirtschaft und Technologie, Germany.

Engert G., Pfrommer P., Zitzmann T. and Casties M., 2007: *Dynamische Simulation des sommerlichen Waermeschutzes gemaeß DIN 4108-2 und der Nachtkuehlung mit TRNSYS*, diploma thesis, University of Applied Sciences Coburg, Germany.

European Union, 2003: *DIRECTIVE 2002/91/EC - Energy-Performance of Buildings*, Official Journal of the European Communities, pp. L1/65-L1/71.

Farvarolo P. and Manz H., 2005: *Temperature-driven single-sided ventilation through large rectangular opening*, Building and Environment 40, pp. 689-699.

Feldheim V. and Lybaert P., 2004: *Solution of radiative heat transfer problems with the discrete transfer method applied to triangular meshes*, Journal of Computational and Applied Mathematics 168, pp. 179-190.

Feustel H. and Raynor-Hoosen A., 1990: *Fundamentals of the multizone airflow model – COMIS,* Technical Note TN29, AIVC, Coventry, UK.

Flourentzou F., Van der Mass J., Roulet C., 1998: *Natural ventilation of passive cooling: measurement of discharge coefficients*, Energy and Buildings 27, pp. 283-292.

FLOVENT, 2006: *CFD software*, Flomerics Group PLC, http://www.flowvent.com accessed 19.03.07.

FLUENT, 2006: *FLUENT User Guide*, Version 6.2, ANSYS Ltd.

Garli I., 2003: *The application of computational fluid dynamics techniques to the analysis of building fires*, 1st Conference of the Graduate School, University of Central Lancashire, Preston.

Geros V., Santamouris M., et al., 1999: *Experimental evaluation of night ventilation phenomena*, Energy and Buildings 29, pp. 141-154.

Geros V., Santamouris M., et al., 2005: *On the cooling potential of night ventilation techniques in the urban environment*, Energy and Buildings 27, pp. 243-257.

Givoni B., 1998: *Effectiveness of mass and night ventilation in lowering the indoor daytime temperatures. Part 1: 1993 experimental periods*, Energy and Buildings 28, pp. 25-32.

Gratia I., Bruyere I. and De Herde A., 2004: *How to use natural ventilation to cool narrow office buildings*, Building and Environment 39, pp. 1157-1170.

Haarhoff J. and Mathews E., 2006: *A Monte Carlo method for thermal building simulation*, Energy and Buildings 38 (12), pp. 1395-1399.

Haupt W., 2001: *Zur Simulation von auftriebsinduzierten Innenraumstroemungen*, Doctoral thesis, University Kassel.

Heiselberg J., Murakami S. and Roulet C.-A., 1998: *Ventilation of large spaces in buildings – Analysis and prediction techniques*, IEA Annex 26, Aalborg University, Denmark.

Henkes R. and Hoogendoorn C., 1995: *Comparison exercise for computations of turbulent natural convection in enclosures*, Numerical Heat Transfer 28 (2), pp. 59-78.

Hensen J., 1999: *A comparison of coupled and de-coupled solutions for temperature and air flow in a building*, ASHRAE Transactions 105 (2), pp. 962-969.

Holmes M. and Davies G., 2003: *Data exchange for thermal modelling and ventilation simulation*, International Journal of Ventilation 2 (1), pp. 55-63.

IES, 2006: *IES User Manual*, Version 5.6.1, IES Ltd., UK.

Indinger T. and Shevchuk I., 2004: *Transient laminar conjugate heat transfer of a rotating disc: theory and numerical solutions*, International Journal of Heat and Mass Transfer 47, pp. 3577-3581.

Jensen S., 1995: *Validation of building energy simulation programs: a methodology*, Energy and Buildings 22, pp. 133-144.

Jones P. and Kippenberg K., 2000: *Effect of thermal mass on the airflow and ventilation in passive building design*, Proceedings: Roomvent 2000, Reading, UK, pp. 273-279.

Kendrick J. 1993: *An overview of combined modelling of heat transport and air movement*, AIVC Technical Note 40, Coventry, UK.

Kolokotroni M., Webb B. and Hayes S., 1998: *Summer cooling with night ventilation for office buildings in moderate climates*, Energy and Buildings 27, pp. 231-237.

Kolokotroni M. and Aronis A., 1999: *Cooling-energy reduction in air conditioned offices by using night ventilation*, Applied Energy 63 (4), pp. 241-253.

Kusuda T. and Bean J., 1981: *Comparison of calculated hourly cooling load and indoor temperature with measured data for a high mass building tested in an environmental chamber*, ASHRAE Transactions 87 (1), pp. 1232-1240.

Launder B., Reece G. and Rodi W., 1975: *Progress in the development of a Reynolds-stress turbulence closure*, Journal of Fluid Mechanics 68 (3), pp. 537-566.

Lomas K., Eppel H., Martin C. and Bloomfield D., 1997: *Empirical validation of building energy simulation programs*, Energy and Buildings 26, pp. 253-275.

Lopes C., Adnot J., et al., 2001: *Managing the growth of the demand for cooling in urban areas and mitigating the urban heat island effect*, Proceedings: ECEEE Congress (2), Mandelieu, France, pp. 130-143.

Marenne C., Groleau D. and Raymond F., 1998: *Simulation of the cooling effect of the night time natural ventilation: a 3D numerical application to the "Maison*

Ronde" of Mario Botta, Environmentally Friendly Cities, Procedings: PLEA '98, Lisbon, Portugal, pp. 495-498.

Martin J. and Fletcher A., 1996: *Night cooling control strategies*, BSRIA, Final Report 11621/4.

Meldem R. and Winkelmann F. 1995: *Comparison of DOE-2 with measurements in the Pala Test houses*, Final Report, California Institue for Energy Efficiency, 40 pages.

Menter F., 1994: *Two-equation eddy viscosity turbulence models for engineering applications,* AIAA Journal, Vol 32 (8), pp. 1598-1605.

Mueller D. and Renz U., 1998: *Measurements and predictions of room airflow patterns using different turbulence models*, Proceedings: Roomvent '98 (1), Stockholm, Sweden, pp. 109-116.

Negrao C., 1995: *Conflation of computational fluid dynamics and building thermal simulation*, Dissertation, University of Strathclyde, Glasgow, UK.

Negrao C., 1998: *Integration of computational fluid dynamics with building thermal and mass flow simulation*, Energy and Buildings 27, pp. 155-165.

Oertel H. and Laurien E., 1995: *Numerische Strömungsmechanik*, Springer Verlag, Germany.

Onishi J., Koga S., Mizuno M., et al., 1998: *Computer effort saving methods in unsteady calculations of room airflows and thermal environments*, Proceedings: Roomvent 98, Stockholm, Sweden, pp. 117-123.

Ostrach S., 1953: *An analysis of laminar free-convection flow and heat transfer about a flat plate parallel to the direction of the generating body force*, NACA, Report 1111, Madison, USA.

Peng S. and Davidson L., 1999: *Computation of turbulent buoyant flows in enclosures with low-Reynolds-number k-ω models*, International Journal of Heat and Fluid Flow 20, pp. 172-184.

Peng S.-H. and Davidson L., 2001: *Large Eddy Simulation for turbulent buoyant flow in a confined cavity*, International Journal of Heat and Fluid Flow 22 (2001), pp. 323-331.

Pfafferott J. and Henkel S., 2003: *Evaluation of a parametric model and building simulation for design of passive cooling by night ventilation*, Proceedings: Building Simulation 2003 (3), Eindhoven, Denmark, pp. 1033-1040.

Phillips J., Naylor D., et al., 1999: *Free convection from a window glazing with a Venetian blind: Numerical model development*, Transactions of CSME 23 (1b), pp. 159-172.

Phillipson S., 2004: *Comparison of accuracy for various element types: laminar flow*, ANSYS CFX-Validation Report (CFX-VAL11/0404), ANSYS Europe Ltd, Pansilvania, pp. 1-26.

PHOENICS, 2006: *PHOENICS Lectures*, Version 3.6.2, CHAM Ltd, UK.

Potter S. and Underwood C., 2004: *A modelling method for conjugate heat transfer and fluid flow in building spaces*, Building Services Engineering Research and Technology 25 (2), pp. 111-125.

Ren J. and Dalenbaeck J., 1995: *Night ventilation for cooling purposes Part 1 – reference building and simulation model*, Proceedings: Building Simulation '95, Madison, Wisconsin, pp. 158-165.

Rhie C. and Chow W., 1982: *A Numerical Study of the Turbulent*, AIAA Paper 82-0998.

Saeidi S. and Khodadadi J., 2005: *Forced convection in a square cavity with inlet and outlet ports*, International Journal of Heat and Mass Transfer 49, pp. 1896-1906

Santamouris M., Argiriou A., et al., 1994: *Energy characteristics and savings potential in office buildings*, Solar Energy 52, pp. 59-66.

Santamouris M. and Asimakopolous D., 1996: *Passive Cooling of buildings*, Earthscan, UK.

Schmidt E. and Beckmann W., 1930: *Das Temperatur- und Geschwindigkeitsfeld vor einer Waerme abgebenden senkrechter Platte bei natuerlicher Konvektion*, Technische Mechanik und Thermodynamik 1 (10 and 11), pp. 341-349 and 391-406.

Schulz M., Pfrommer P., Zitzmann T. and Casties M., 2007: *Dynamische Simulation der Nachtkühlung mit CFD*, diploma thesis, University of Applied Sciences Coburg, Germany.

Setrakian A. and McLean D., 1991: *Building simulations using thermal and CFD models*, Proceedings: Building Simulation '91, Nice, France, pp. 235-240.

Sharma A., Velusamy K. et al., 2007: *Conjugate turbulent natural convection with surface radiation in air filled rectangular enclosures*, International Journal of Heat and Mass Transfer 50, pp. 625-639.

Shaviv E., Capeluto I. and Yezioro A., 2000: *A simple design tool for determining the effectiveness of thermal mass and night ventilation as passive cooling design strategy*, Proceedings: Roomvent 2000, Reading, UK, pp. 887-892.

Somarathne S., Seymour M. and Kolokotroni M., 2002: *Transient solution methods for dynamic thermal modelling within CFD*, International Journal of Ventilation 1 (2), pp. 141-156.

Somarathne S, Seymour M. and Kolokotroni M., 2003: *Efficient dynamic thermal modelling using CFD*, Proceedings: Healthy Buildings, Singapore, 6 pages.

Somarathne S., 2003: *Dynamic Thermal Modelling using CFD*, PhD thesis, Brunel University, UK.

Somarathne S., Seymour M. and Koloktroni M., 2005: *Dynamic thermal CFD simulation of a typical office by efficient transient solution methods*, Building and Environment 40, pp. 887-896.

Song D., Kato S., Murakami S. and Kim T., 2002: *Study on hybrid cooling system coupled with radiation panel cooling and natural cross ventilation - Part 1*, Transactions of the Society of Heating, Air-Conditioning and Sanitary Engineers of Japan 87, pp. 61-68.

Stamou A. and Katsiris I., 2006: *Verification of a CFD model for indoor airflow and heat transfer*, Building and environment, Building and Environment 41, pp. 1171-1181.

Takeya N., Kitagawa K. and Onishi J., 1998: *An application study of a 3D CFD code 'TASC' for predicting transient thermal problems of indoor environments*, Proceedings: Roomvent '98, Stockholm, Sweden, pp. 459-466.

TAS, 2006: *Building Designer*, Version 8.3, EDSL Ltd., Milton Keynes, UK.

Thompson C., Wilkes N. and Jones I., 1987: *Numerical studies of buoyancy-driven turbulent flows in a rectangular cavity*, International Journal of Numerical Methods Engineering 24, pp. 89-99.

Tian Y. and Karayiannis T., 2000: *Low turbulence natural convection in an air filled square cavity Part 1: the thermal and fluid flow fields*, International Journal of Heat and Mass Transfer 43, pp. 849-866.

TRNSYS, 2006: *TRNSYS Documentation*, Version 16, Transsolar Energietechnik GmbH, Germany.

UNFCCC, 2005: *Kyoto protocol*, http://unfccc.int/kyoto_protocol/items/2830.php, last viewed at 10.05.2007.

VDI 2078, 1996: *Cooling load calculation of air-conditioned rooms*, Beuth Verlag, Germany.

VDI 6020-1, 2001: *Requirements on methods of calculation to thermal and energy simulation of buildings and plants*, Springer-VDI-Verlag, Germany.

Versteeg H. and Malalasekera W., 1995: *An introduction to Computational Fluid Dynamics. The Finite Volume Method,* Pearson Education Limited, UK.

Vieser W., Esch T. and Menter F., 2004: *Heat transfer predictions using advanced two-equation turbulence models*, CFX Validation Report 10/0404, Ansys Ltd., pp. 1-66.

Vogl N., 1996: *Numerische Simulation von auftriebsbeeinflussten Raumstroemungen,* Dissertation, RWTH, Aachen, Germany.

Voss K., Herkel S., et al., 2007: *Energy efficient office buildings with passive cooling – results and experiences from a research and demonstration program*, Solar Energy 81 (3), pp. 424-434.

Wagner W., 1998: *Waermeuebertragung*, Würzburg, Vogel Verlag, Germany.

Walton G., 1997: *CONTAM 96 User manual*, NISTIR 6065, USA.

Wilcox D., 1998: *Turbulence modeling for CFD,* 2nd Edn., DCW Industries Inc., Canada.

Wu W., Ewing D. and Ching C., 2006: *The effect of the top and bottom wall temperatures on the laminar natural convection in an air-filled square cavity,* International Journal of Heat and mass Transfer 49, pp. 1999-2008.

Wyrwa J., 2003: *Turbulenzmodellierung für stabil dichtegeschichtete Stroemungen bei der Simulation des Transports von kohaesiven Sedimenten in Aestuaren,* Dissertation, Technical University Berlin, Germany.

Yam J., Li Y. and Theng Z., 2003: *Nonlinear coupling between thermal mass and natural ventilation in buildings*, International Journal of Heat and Mass Transfer 46, pp. 1251-1264.

Yuan X., Moser A. and Suter P., 1994: *Wall functions for numerical simulation of turbulent natural convection*, Proceedings: International Heat Transfer Conference, Brighton, UK, pp. 191-196.

Zhai Z., Chen Q., Haves P. and Klem J., 2001: *Strategies for coupling energy simulation and Computational Fluid Dynamics programs*, Proceedings: Building Simulation 2001, Rio, Brazil, pp. 59-66.

Zhai Z. and Chen Q., 2003: *Impact of determination of convective heat transfer on the coupled energy and CFD simulation for buildings*, Proceedings: Building Simulation 2003, Eindhoven, Netherlands, pp.1467-1474.

Zhai Z. and Chen Q., 2005: *Performance of coupled building energy and CFD simulations*, Energy and Buildings 37, pp. 333-344.

Zhengen R., 2002: *Enhanced modelling indoor airflows, temperatures, pollutant emission and dispersion by nesting sub-zones within a multizone model*, PhD thesis, Queen's University of Belfast, North Ireland.

Bibliography

Refereed Journals

Zitzmann T., Cook M. and Pfrommer P., 2006a: *Simulation dynamisch thermischen Langzeitverhaltens in Gebäuden mittels CFD*, Bauphysik 28 (1), pp 96-102.

Zitzmann T., Pfrommer P. and Cook M., 2007a: *Dynamisch thermisches CFD-Verfahren mit angepasster Regelungsmethode*, Bauphysik 29 (1), pp 12-16.

Zitzmann T., Cook M. and Pfrommer P., 2007b: *Dynamic CFD modelling of thermal mass and air movement*, International Journal of Ventilation, in press (state 30.05.2007).

Refereed Conferences

Zitzmann T., Cook M., Pfrommer P., Rees S. and Marjanovic L., 2005: *Simulation of steady-state natural convection by using CFD*, Proceedings: Building Simulation 2005, Montreal, Canada, pp 1448-1456.

Zitzmann T., Pfrommer P. and Cook M., 2006b: *Dynamisch thermisches CFD-Verfahren*, Proceedings: BauSIM 2006, Munich, Germany, pp 217-219.

Zitzmann T., Pfrommer P. and Cook M., 2007c: *Modelling Thermal Mass and Night-Time Ventilation using Dynamic CFD*, Proceedings: Roomvent 2007, Helsinki, in press (state 30.05.2007).

Zitzmann T., Pfrommer P. and Cook M., 2007d: *Dynamic Thermal Building analysis with CFD – Modelling Radiation*, Proceedings: Building Simulation 2007, Peking, China, accepted for publication (state 30.05.2007).

Miscellaneous

Leonhardt H., Mayer E., Schwab R., Sinnesbichler H., Zitzmann T., 2003: *Untersuchungen an einem hybriden Lueftungssystem mit innovativen Systemkomponenten*, Annex 35 - IBP Report RK-07, Fraunhofer Institut fuer Bauphysik, Holzkirchen, Germany.

Engert G., Pfrommer P., Zitzmann T. and Casties M., 2007: *Dynamische Simulation des sommerlichen Waermeschutzes gemaeß DIN 4108-2 und der Nachtkuehlung mit TRNSYS*, diploma thesis, University of Applied Sciences Coburg, Germany.

Schulz M., Pfrommer P., Zitzmann T. and Casties M., 2007: *Dynamische Simulation der Nachtkühlung mit CFD*, diploma thesis, University of Applied Sciences Coburg, Germany.

APPENDICES

APPENDIX A

MATHEMATICAL MODELS OF CFX

A Mathematical Models of CFX

In this section the mathematical models used in CFX to calculate air flow and energy fluxes are described. Information is also given about mesh types and possible modelling errors which can occur due to model assumptions.

A.1 Governing equations

The CFD platform CFX (CFX 2006) is based on the Finite Volume Method (FVM). Thus, each zone in a building model is discretised in small finite volume elements in which the conditions are assumed to be homogeneous. One set of equations relevant to the prevailing physical mechanisms is solved within each computational cell. The standard equations which are solved in CFD are the unsteady Navier Stokes equations which contribute to mass, momentum and energy (CFX 2006) (further information in section A.3):

Continuity equation

$$\frac{\partial \rho}{\partial t} + \nabla \bullet (\rho \cdot \vec{U}) = 0 \qquad \text{Eq. (A.1)}$$

Conservation of momentum equation

$$\frac{\partial (\rho \cdot \vec{U})}{\partial t} + \nabla \bullet (\rho \cdot \vec{U} \otimes \vec{U}) = \nabla \bullet (\mu \cdot (\nabla \vec{U} + (\nabla \vec{U})^T) - p \cdot \delta_{KDF}) + S_M \qquad \text{Eq. (A.2)}$$

Conservation of thermal energy equation

$$\frac{\partial (\rho \cdot h)}{\partial t} - \frac{\partial p}{\partial t} + \nabla \bullet (\rho \cdot \vec{U} \cdot h) = \nabla \bullet (\lambda \cdot \nabla T) + S_E \qquad \text{Eq. (A.3)}$$

with h = enthalpy [m^2/s^2], p = modified pressure [$kg/(m \cdot s^2)$], t = time [s], T = temperature [K], $\vec{U}$ = velocity vector [m/s], δ_{KDF} = Identity Matrix (Kronecker Delta

Function), λ = thermal conductivity [W/(m·K)], ρ = density [kg/m^3] and μ = dynamic viscosity [kg/(m·s)].

S_M and S_E are additional momentum and energy sources which can apply in certain situations.

For solid domains, the thermal energy equation simplifies to:

$$\frac{\partial \rho \cdot c \cdot T}{\partial t} = \nabla \bullet (\lambda \cdot \nabla T) + S_E \qquad \text{Eq. (A.4)}$$

where c = heat capacity [J/(kg·K)]. The simultaneous calculation of heat transfer in solid and fluid domains is called conjugate heat transfer (CHT).

A.2 Modelling buoyancy

Free convection is an important driving force of air flow in buildings and hence buoyancy must be taken into account in the calculations. This is realized in CFX by using the 'full buoyancy' or the 'Boussinesq approximation' model.

The pressure calculated by the solver in the momentum equations in section A.1 is a 'modified pressure' which excludes the hydrostatic pressure gradient due to the buoyancy reference density, ρ_{ref}. This modified pressure, p [kg/(m·s^2)], is often called motion pressure because it is responsible for driving the flow. The reference density is in the order of the approximate average value of the room domain and the modified pressure is related to the true pressure, P [kg/(m·s^2)], by Eq. (A.5):

$$P = p + p_{ref} + \rho_{ref} \cdot \vec{g}(\vec{r} - \vec{r}_{ref}) \qquad \text{Eq. (A.5)}$$

with $\vec{r}$ = position vector [m], $\vec{r}_{ref}$ = reference position vector [m], $\vec{\rho}_{ref}$ = reference density [kg/m^3] and $\vec{g}$ = gravity vector [m]. The pressure reference location is automatically determined by the solver if not user defined and is usually located at an opening (inlet, outlet or opening condition).

Full Buoyancy Model

This model is used when the fluid density is a function of temperature or pressure (which includes all ideal gases and real fluids) and when density variations are significant (e.g. for $\Delta T \geq 20K$). The buoyancy source term, Eq. (A.6), is then included in the momentum Eq. (A.2):

$$S_M = (\rho - \rho_{ref}) \cdot \vec{g} \qquad \text{Eq. (A.6)}$$

Boussinesq approximation model

Density differences are usually small for buoyancy driven flow in buildings. Thus the use of the full buoyancy model might lead to round off errors in the calculation of the source term. The Boussinesq approximation treats the density of the fluid as a constant property and applies a local gravitational body force throughout the fluid. The force is a linear function of fluid thermal expansivity, β [1/K], and the local temperature difference. In all terms of the RANS equations the density is replaced by the reference density, ρ_{ref}. The buoyancy source term in Eq. (A.6) is approximated as:

$$(\rho - \rho_{ref}) = \rho_{ref} \cdot \beta \cdot (T - T_{ref}) \qquad \text{Eq. (A.7)}$$

with:

$$\beta = -\frac{\partial \rho}{\rho \cdot \partial T}\bigg|_{\rho} \approx \frac{1}{T_m} \qquad \text{Eq. (A.8)}$$

The thermal expansivity can be approximated as the reciprocal value of the mean temperature for small density gradients, see Eq. (A.8). T_{ref} [K] is the buoyancy reference temperature and is a user specified value, approximately the average value in the fluid domain.

When the full buoyancy model option is used, a turbulence production and dissipation source term is added to Eq. (A.21):

$$P_{kb} = -\frac{\mu_t}{\rho \cdot C_1} \cdot \vec{g} \bullet \nabla \rho \qquad \text{Eq. (A.9)}$$

where μ_t = turbulence viscosity [kg/(m·s)], ρ = density [kg/m^3]. If the Boussinesq model is applied, the following equation is used instead:

$$P_{kb} = -\frac{\mu_t}{C_2} \cdot \beta \cdot \vec{g} \bullet \nabla \rho \qquad \text{Eq. (A.10)}$$

C_1=1 and C_2=0.9 for the full buoyancy model and for the Boussinesq approximation model in CFX, respectively.

A.3 Turbulence modelling

CFX solves the unsteady Navier Stokes equations by separating the transport equations in average and fluctuating components. For example a velocity, $\vec{U}$ [m/s], is divided into an average component, $\overline{\vec{U}}$, and a fluctuating component, $\vec{u}$:

$$\vec{U} = \overline{\vec{U}} + \vec{u} \qquad \text{Eq. (A.11)}$$

The averaged component is calculated by:

$$\overline{\vec{U}} = \frac{1}{\Delta t} \cdot \int_{t}^{t+\Delta t} \vec{U} dt \qquad \text{Eq. (A.12)}$$

where Δt = time scale [s], which is large relative to the turbulent fluctuations and small relative to the time scale to which the equations are solved. The transport equations of section A.1 are modified by this averaging procedure and are referred to as the Reynolds Averaged Navier Stokes (RANS) equations (CFX 2006). In the following RANS equations, the bar is dropped for time-averaged quantities, except for products of fluctuating quantities:

Continuity

$$\frac{\partial \rho}{\partial t} + \nabla \bullet (\rho \cdot \vec{U}) = 0 \qquad \text{Eq. (A.13)}$$

Conservation of momentum

$$\frac{\partial(\rho\cdot\vec{U})}{\partial t}+\nabla\bullet(\rho\cdot\vec{U}\otimes\vec{U})=\nabla\bullet(\mu\cdot(\nabla\vec{U}+(\nabla\vec{U})^{T})-p\cdot\delta_{KDF}-\rho\cdot\overline{\vec{u}\otimes\vec{u}})+S_{M}$$

Eq. (A.14)

Conservation of thermal energy

$$\frac{\partial(\rho\cdot h)}{\partial t}-\frac{\partial p}{\partial t}+\nabla\bullet(\rho\cdot\vec{U}\cdot h)=\nabla\bullet(\lambda\cdot\nabla T-\rho\cdot\overline{\vec{u}\cdot h})+S_{E}$$ Eq. (A.15)

The additional turbulent flux terms $\rho\cdot\overline{\vec{u}\otimes\vec{u}}$ and $\rho\cdot\overline{\vec{u}\cdot h}$ arise from the averaging of the non-linear convective term in the un-averaged equations (see CFX 2006). Different turbulence models exist for solving these convective flux terms. A common class of turbulence model are Eddy Viscosity models. These are based on the hypothesis that turbulence consists of small eddies which are continuously forming and dissipating, and in which the Reynolds stresses are assumed to be related to mean velocity gradients. The convective terms are calculated as follows:

$$-\rho\cdot\overline{\vec{u}\otimes\vec{u}}=-\frac{2}{3}\rho\cdot k\cdot\delta_{KDF}-\frac{2}{3}\mu_{t}\cdot\nabla\bullet\overline{\vec{U}}\cdot\delta_{KDF}+\mu_{t}(\nabla\overline{\vec{U}}+(\nabla\overline{\vec{U}})^{T})$$ Eq. (A.16)

$$-\rho\cdot\overline{\vec{u}\cdot h}=\frac{\mu_{t}}{\mathrm{Pr}_{t}}$$ Eq. (A.17)

with k = turbulent kinetic energy per unit mass [m^2/s^2] and μ_t = eddy (turbulent) viscosity [kg/(m·s)].

The turbulent kinetic energy and turbulent viscosity are two additional unknowns in the RANS equations for turbulent flow. Various turbulence models exist which are commonly used to calculate these additional unknown, for example the k-ε (CFX 2006), the k-ω (Wilcox 1998) and the Shear Stress Transport (SST) k-ω based (Menter 1994) turbulence models. The way of how the additional variables are determined differs from model to model. The application of each model depends on the character of air flow. For laminar flow, the energy transfer in the fluid is accomplished only by diffusion, and

thus no turbulence model is required to close the set of equations (i.e. a sufficient equations exists to calculate all unknowns). This is called the laminar model in CFX.

The turbulence model which was mainly used in the thesis for investigation was the k-ω model and is explained in the following. Information about the mathematical formulation of the other turbulence models investigated in section B.2.3 can, for example, be found in the CFX manual (CFX 2006).

k-ω turbulence model

The turbulence viscosity, μ_t [kg/(m·s)], is assumed to be proportional to the turbulent kinetic energy per unit mass, k [m^2/s^2], and the turbulent frequency, ω [1/s]:

$$\mu_t = \frac{\rho \cdot k}{\varpi} \qquad \text{Eq. (A.18)}$$

Two additional equations are added to the RANS equations, referred to as the kinetic energy Eq. (A.19) and the turbulent frequency Eq. (A.20):

k-equation

$$\frac{\partial(\rho \cdot k)}{\partial t} + \nabla \bullet (\rho \cdot \vec{U} \cdot k) = \nabla\left[(\mu + \frac{\mu_t}{C_3}) \cdot \nabla k\right] + S_k - C_4 \cdot \rho \cdot k \cdot \varpi \qquad \text{Eq. (A.19)}$$

ω-equation

$$\frac{\partial(\rho \cdot \varpi)}{\partial t} + \nabla(\rho \cdot \vec{U} \cdot \varpi) = \nabla \bullet \left[(\mu + \frac{\mu_t}{C_5}) \cdot \nabla \varpi\right] + C_6 \cdot S_k \cdot \frac{\varpi}{k} - C_7 \cdot \rho \cdot \varpi^2 \qquad \text{Eq. (A.20)}$$

C_3,, C_4, C_5 C_6, and C_7 are empirical constants. Values used in CFX are: C_3=2, C_4=0.09, C_5=2, C_6=5/9 and C_7=0.075.

The source term, S_k [kg/(m^2·s^2)], in Eqs. (A.19) and (A.20) is the turbulence production due to viscous and buoyancy forces and is calculated by:

$$S_k = \mu_t \cdot \nabla\vec{U} \bullet (\nabla\vec{U} + \nabla\vec{U}^T) - \frac{2}{3}\nabla \bullet \vec{U}(3 \cdot \mu_t \cdot \nabla \bullet \vec{U} + \rho \cdot k) + P_{kb} \qquad \text{Eq. (A.21)}$$

See Eqs. (A.9) and (A.10) for the buoyancy source, P_{kb}. The k-ω model in CFX implies a formulation for the near wall treatment which provides an automatic switch from a wall-function to a low-Reynolds number formulation based on the near-wall grid spacing. This makes it potentially more accurate and more robust than ε-equation based turbulence models in CFX which always use the wall-function approach.

A.4 Radiation modelling

In CFX, radiation is represented by particles which are tracked through the air domain using a ray-tracing method. According to CFX documentation the spectral radiative transfer equation can be written as (CFX 2006):

$$\frac{dI_\nu(\vec{r},\vec{s}_1)}{ds} = -(K_{a\nu}+K_{s\nu})\cdot I_\nu(\vec{r},\vec{s}_1) + K_a \cdot I_b(\nu,T) + \\ + \frac{K_{s\nu}}{4\pi}\int_{4\pi}\left(I_\nu(\vec{r},\vec{s}_2)\cdot\Phi\cdot(\vec{s}_1\bullet\vec{s}_2)\cdot d\Omega\right) + S_\nu \qquad \text{Eq. (A.22)}$$

where

I_b	blackbody radiance [W/(m²·sr)]
I_ν	spectral radiance [W/(m²·sr)]
$\vec{r}$	position vector [m]
$\vec{s}$	direction vector [m]
s	path length [m]
K_{av}, K_{sv}	spectral absorption and scattering coefficients [1/m]
ν	frequency [1/s]
T	local temperature [K]
Φ	in-scattering phase function

Ω solid angle [sr]

S_ν spectral source term [W/(m^4·sr)]

The formal solution of the radiative transfer equation is very time consuming and achieved in CFX by using approximate models for the directional and spectral dependencies.

The spectral approximation used in the thesis assumes that the medium which takes part in radiation heat transfer is non-scattering and grey (i.e. independent of the wavelength). Opening, inlet and outlet boundary conditions (see section A.5) are considered as fully transparent to radiation. Opaque walls and solid-fluid interfaces are treated as diffusely emitting and diffusely reflecting opaque boundaries whereas symmetry planes are treated as diffusely emitting and specularly reflecting boundaries in CFX.

Two directional radiation models are reported for optically thin media (i.e. transparent to radiation at wavelengths in which the majority of the heat transfer occurs) in CFX (CFX 2006): one is the Monte Carlo and the other is the Discrete Transfer radiation model. Non-linearities in the systems due to scattering, diffuse reflection, or temperature dependency of radiation quantities are overcome by an iterative solution technique.

Monte Carlo model

The Monte Carlo model treats the radiation field as a photon gas. A photon is selected from a photon source and stochastically tracked through the system until its weight falls below some minimum at which point it 'dies'. Each time the photon experiences an event, for example a surface intersection, scattering or absorption, the physical quantity of the radiation intensity is updated along the ray. Using this method, a complete 'history' of that photon in the system is generated. Many photon histories need to be generated to achieve good estimates of the physical quantity. This value can be specified by the user. The main computational overhead for CFX in generating a history is in tracking the photons across the domain.

Discrete Transfer model

The Discrete Transfer model assumes that the spatial radiation gradients are relatively small and the radiation is emitted isotropically from the surfaces. The user-defined parameter 'number of rays' in CFX determines the degree of spatial discretisation of the hemisphere above each finite surface element for radiation emission. Higher values mean a better representation of the reality and a higher accuracy, but at the same time will result in a significant increase in computational effort. The paths of rays are calculated only once, at the beginning of the simulation, and are then stored and re-used which leads to significant savings of computer resources.

Due to the high computational resources required for the calculation of the radiation field for the Monte Carlo and Discrete Transfer model, it is essential to find a trade-off between accuracy and computational effort. This is, for example, obtained using a coarser mesh for the radiation field than for the flow field assuming that the radiation field changes at a slower rate than any other transport variables. CFX aims to achieve a coarsening rate of 64 by default.

A.5 Mathematical description of boundaries

The boundary conditions available in CFX are wall, symmetry, inlet, outlet, opening and interface boundaries (CFX 2006). For any parameter variable which needs specification by the user, a user function can be included using the CFX Expression Language (CEL) (CFX 2006).

Wall

This boundary can be used for solid and fluid domains. For fluid domains, by using the 'Free Slip' boundary option the velocity component parallel to the wall has a computed finite value while the component normal to the wall and the shear stress are zero at the wall. When the 'No Slip' option is used (as used in this research for the building enclosure surfaces), the velocity of the fluid at the wall boundary is zero which consequently leads to the so-called wall boundary layer. The heat transfer at the wall boundary can be set to adiabatic (no heat transfer across the wall boundary), a specified

temperature, heat flux or heat transfer coefficient (for which the heat flux is calculated from the temperature difference between the ambient and the air node adjacent to the wall). An emissivity coefficient is required if radiation heat transfer is modelled.

Symmetry

The symmetry plane condition imposes constrains which 'mirror' the flow on either both side of it. The velocity component and scalar variable gradients normal to the symmetry plane are zero and any radiation is reflected specularly.

Inlet

An inlet is a boundary condition at which mass enters into a fluid domain. The direction and magnitude of momentum at the inlet can be specified by using the following options:

Speed: U_{in}

Mass Flow Rate: $\dot{m} = \rho \cdot U \cdot \int_S dA$

Total or Relative Pressure: P or p

with the flow in direction of the boundary normal (as used in this research) or in direction of user specified Cartesian coordinates.

The turbulence intensity must be specified for the inlet giving values for the additional variable equations of the turbulence model used or using approximations of low (1%), medium (5%) or high turbulence intensity (10%). A medium intensity value is often used as an approximation for building simulations.

The static temperature of the fluid, which enters the fluid domain at the inlet, and the radiation temperature (i.e. option of local temperature (used in this research) at the inlet or ambient blackbody temperature) must be specified.

Outlet

The fluid is leaving the fluid domain at the outlet. The outlet boundary condition requires mass and momentum specification which is handled a similar way as for the inlet. Options are Normal Speed, Cartesian or Cylindrical Velocity Components, Mass Flow Rate, Static or Average Static pressure. Furthermore, the radiation temperature at the outlet must be specified.

Opening

An opening condition allows the fluid to cross the boundary in either direction. The mass and momentum must be specified applying one of the following options: Cartesian or Cylindrical Velocity Components, Pressure and Direction, Pressure (Entrain). Moreover, the turbulence intensity, the static temperature and the radiation temperature must be specified at the opening on the same way as for the outlet boundary condition.

Interface

The interface boundary condition connects two solid domains, two fluid domains or a solid and a fluid domain at their interface and allows for conservative heat transfer between the domains. Mass can also be transferred if two fluid domains are inter-connected. Solid domains (an exception are windows) are usually opaque to radiation so that radiation is not transferred across the interface, and a solid-fluid interface boundary treats fluid flow and radiation in the same way as a wall boundary condition. To form a well defined physical connection of the mesh at the interface of two domains, CFX provides the Direct (1:1) option if the mesh elements match exactly, and it provides the General Grid Interface (GGI) option if different mesh elements lie on either side or intersect.

A.6 Numerical mesh characteristics

A numerical mesh is an assembly of finite volume elements which are connected among each other. Homogeneous conditions are considered in each volume element. One node is assigned within the centre of each volume cell at which the physical properties and

conditions are calculated. To complete the discretisation of the Navier Stokes equations, additional integration points are located at the centres of the volume surfaces to calculate the fluxes across the surface (see section A.7). An assembly of connected nodes is called numerical grid.

Various types of volume elements exist to obtain numerical meshes. These are grouped in structured and unstructured uniform and non-uniform meshes. The version of the meshing program used for this research creates un-uniform unstructured meshes. The differences and advantages of the types are discussed in the following.

Structured vs. unstructured mesh

A structured mesh basically contains hexahedral and an unstructured mesh contains tetrahedral volume elements. Structured meshes are suitable for simple flows along the coordinate system axis (e.g. straight flow in a duct), whereas unstructured meshes show better performance for complex flows (e.g. air flow circulation) which reduces significant local numerical diffusion problems (see section A.7). Although the effort for meshing complex geometries is smaller using unstructured meshes, more volume elements are required to obtain the same degree of accuracy as for hexahedral elements with the same element edge length sale (Phillipson 2004). Current research is increasingly using a pure unstructured mesh type or a hybrid mesh containing structured and unstructured mesh elements to exploit the advantages of both mesh types.

Uniform vs. non-uniform mesh

The mesh is uniform if all volume elements contain the same edge size (i.e. edge length scale), and the mesh is non-uniform if elements are locally finer or coarser in some regions. The advantage of a non-uniform over a uniform mesh is that the mesh can be refined in regions where high spatial gradients of the transport properties exist and coarse where they are low. This potentially leads to an increase of accuracy and convergence of the solution without increasing the computational effort.

To obtain an accurate representation of the flow patterns in the near wall boundary layer for low Reynolds number flows, the mesh must be refined in this region. To reduce the computational effort for unstructured meshes, prism elements can be used in the near

wall region where the flow is predominantly uni-directional and spatial gradients are high perpendicular to the surface normal as suggested by Phillipson (2004). The mesh in the near wall region looks like illustrated in Figure B.5.

A.7 Discretisation solution methods

Coupled Pressure-Velocity Multigrid solver

Segregated solvers calculate the momentum equations and the mass equation in sequence and correct them in an iterative process. This requires a large number of iterations and a judicious selection of the relaxation parameters of the variables. In contrast the CFX code is based on a coupled solver for solving the differential equations using the fully implicit discretisation method and treating the hydrodynamic equations as one single system. The pressure-velocity coupling used in CFX is an extended, improved form of the Rhie-Chow scheme (1982) and is expressed by (in index notation):

$$\left(\frac{\partial \vec{U}}{\partial x}\right)_i + \frac{\Delta x^3 \cdot A_P}{4 \cdot \rho \cdot \vec{U}_j \cdot \Delta n_j} \cdot \left(\frac{\partial^4 p}{\partial x^4}\right)_i = 0 \qquad \text{Eq. (A.23)}$$

with Δx = mesh length scale [m], ρ = density [kg/m^3], p = pressure [kg/(m·s^2)], A_P = approximation to central coefficient of momentum equation and $_{\Delta nj}$ = outward surface vector [m]. The advantages are robustness, efficiency, generality and simplicity. However, a principal drawback is the requirement of high computer storage for calculating all coefficients. The performance decreases for increasing number of nodes and large element aspect ratios. A multigrid technique implemented in CFX greatly improves the performance. The multigrid process carries out early iterations on a fine mesh and later iterations on progressively coarser virtual meshes, transferring results back to the original fine mesh at the end.

To solve the Navier Stokes equations described in section A.1 they are replaced by algebraic equations. Using the Gauss divergence theorem, the transient terms are converted in volume integrals and the derivates of position are converted in surface

integrals (see CFX 2006). In the following, only the techniques for those terms are described which require a user specific input for solving the integrals. Information about the solution of the other terms (i.e. diffusive and pressure gradient term) can be found in the CFX user manual (2006).

Linear solution of the transient term

Two different schemes exist in CFX for solving the differential transient terms in the RANS equations, the second and first order backward Euler scheme. Both schemes are robust, implicit and conservative in time. The type of scheme can be set separately for each type of RANS equation. The approximation has only an effect on transient predictions but not on steady-state simulations.

The 1st order backward Euler scheme is bounded. Since it is only first order accurate in time, it can induce numerical diffusion in time which is similar to the 1st order discretisation of the advection scheme (see later). The following approximation is used:

$$\frac{\partial}{\partial t}\int_V \rho\cdot\phi\cdot dv = \frac{\rho\cdot V}{\Delta t}\cdot(\phi-\phi') \qquad \text{Eq. (A.24)}$$

with ϕ'= solution field of the previous time step of the field ϕ, V = volume of integration [m^3] and Δt = time period [s].

The 2nd order backward Euler transient scheme is not bounded in time and hence may cause some non-physical over- and under-shoots in the solution. The following approximation is used:

$$\frac{\partial}{\partial t}\int_V \rho\cdot\phi\cdot dv = \frac{\rho\cdot V}{\Delta t}\cdot\left(\frac{3}{2}\cdot\phi-2\cdot\phi'+\frac{1}{2}\cdot\phi''\right) \qquad \text{Eq. (A.25)}$$

where ϕ'' represents the solution field of the time step before the old time level.

For steady-state simulations the same equations as for transient simulations are used. The time-step in the time dependent terms behaves like an acceleration parameter. This false-time stepping method guides the approximate solutions in a physically based

manner to a steady-state solution and reduces the number of iterations required for convergence.

Advection term

The flux of a transport variable, ϕ, across a surface segment is integrated over the surface and assigned to an integration point, ip, which is located at the centre of the segment. To calculate the total flux of the transport variable into and out of a volume element, the fluxes at all integration points which surround the volume element need to be summed together. The value of each integration point is related to the nodal transport variable in the centre of the volume in the following form:

$$\phi_{ip} = \phi_{up} + \beta_b \cdot \nabla\phi \cdot \Delta\vec{r} \qquad \text{Eq. (A.26)}$$

with ϕ_{up} = transport variable at the upwind node, β_b, = blending factor [-] and $\vec{r}$ = vector from the upwind node to the integration point [m]. Various advection schemes exist in CFX which assign different values β_b between $0<\beta_b<1$:

The 1st order *Upwind Differencing Scheme* uses a value of $\beta_b=0$. It leads to a numerically stable solution and does not lead to numerical over- and under-shoots. However, it is susceptible to numerical diffusion (see later).

The *Numerical Advection Correction Scheme* option allows the user to specify a value for β_b. The second term in Eq. (A.26) is used as an anti-diffusive flux added to the upwind scheme. The equation is 2nd order accurate for $\beta_b=1$. The consequence is a reduction of robustness and an increase of non-physical over- and under-shoots in the solution.

The *High Resolution Scheme* computes β_b locally to be as close to 1 as possible without violating boundedness principles, based on the scheme of Barth and Jesperson (1989). The scheme is therefore both accurate and bounded, reducing the solution to 1st order near discontinuities and in the free stream where the solution varies only marginally.

The Central Differencing Scheme uses tri-linear shape functions. However, it is not suitable for solving the RANS equations but only for Large Eddy Simulations.

The numerical solution of the advection term can lead to numerical diffusion and dispersion errors as mentioned above. Both effects are described in detail in the following.

Discretisation effects

Numerical diffusion usually exists where the advection term is approximated using an odd-order scheme, for example, using a 1st order Upwind Differencing Scheme. Considering a flow in a 2D Cartesian coordinate system for a mesh of rectangular and of triangular elements (see Figure A.1): if the flow direction is parallel to the rectangular element surface normal (Figure A.1a), the flow from one element to the next can be accurately represented. However, if the flow is not normal to the surface, such as for regions of flow re-circulation, the flow can marginally pass other cells on its way and some portion of flow moves into the adjacent elements as shown in Figure A.1b. Consequently, the features of the flow are 'smeared out' which is called *numerical diffusion* (CFX 2006).

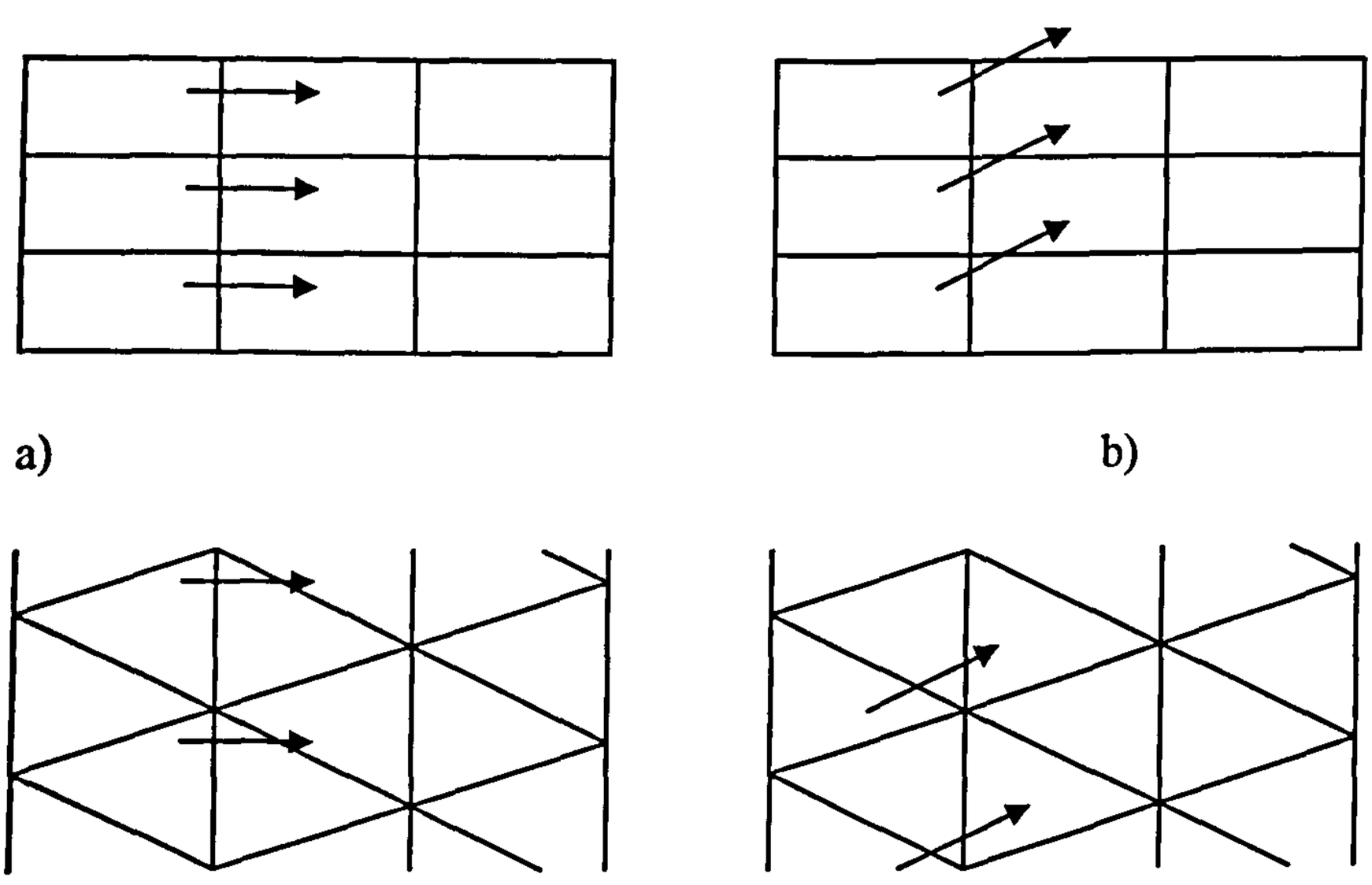

Figure A.1: Numerical diffusion effect for rectangular elements for flow (a) in direction and (b) different to the direction of the surface normal; comparison with numerical diffusion effects for triangular elements ((c) and (d)).

Considering a mesh with triangular elements (Figures A.1c) and A.1d)), there is no flow direction which is more prone to numerical diffusion. The numerical diffusion errors for a tetra-mesh are consistent and of the same order throughout the entire flow domain.

The numerical diffusion effect is illustrated in Figure A.2 for a step function of velocity to define an inlet profile which is not in alignment with the mesh.

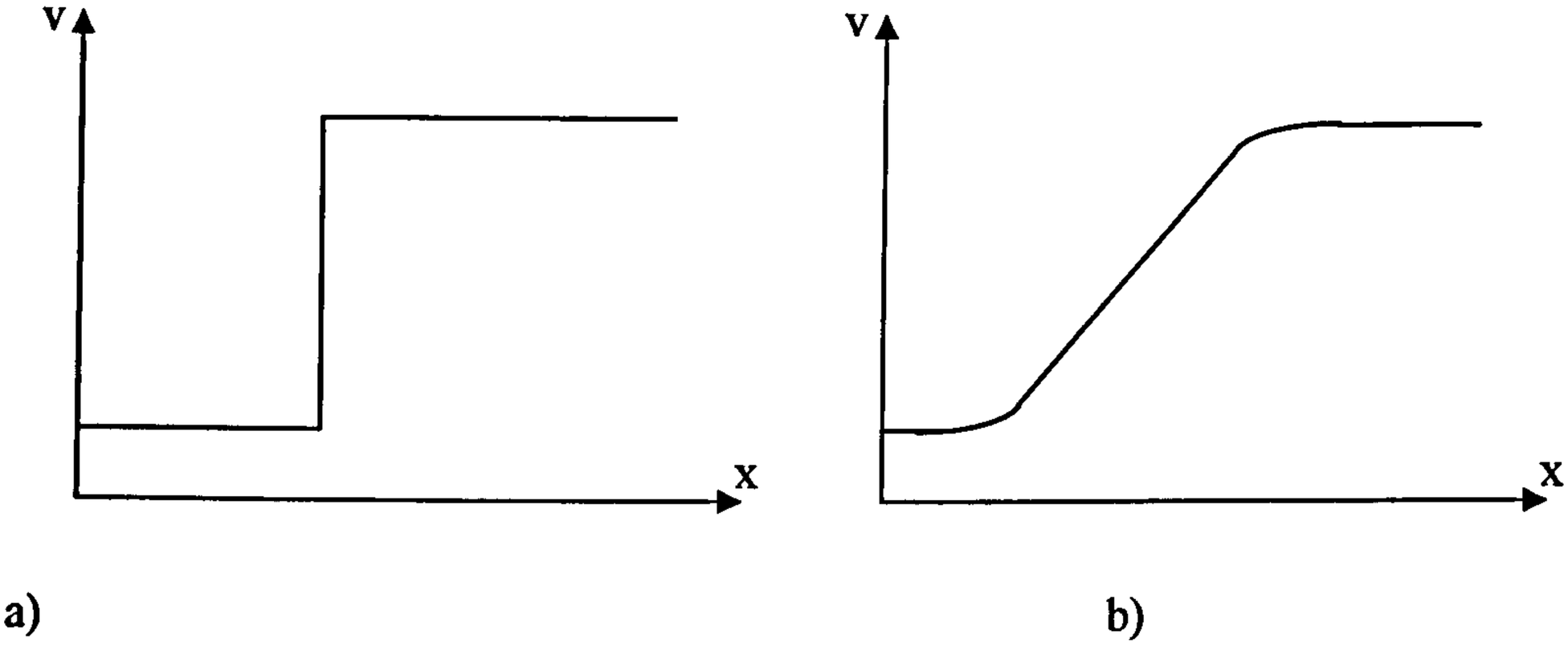

Figure A.2: Numerical diffusion effect illustrated for a step function of the velocity vs. the position; (a) without numerical diffusion and (b) with numerical diffusion effects.

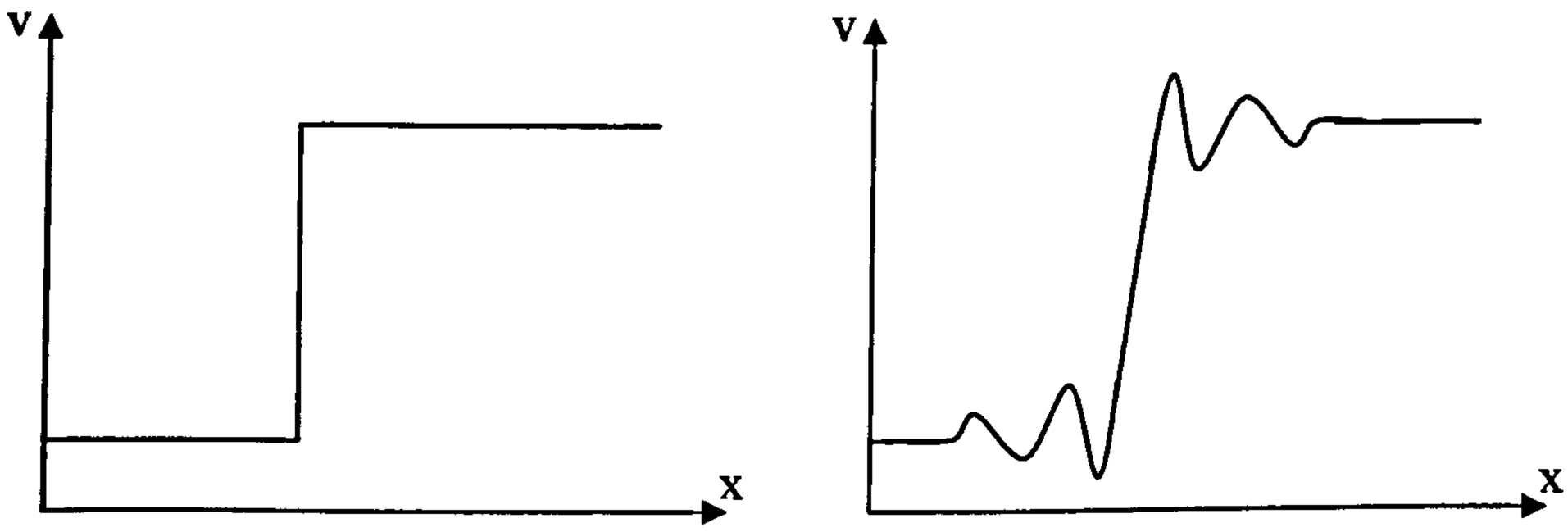

Figure A.3: Numerical dispersion effect illustrated for a step function of the velocity vs. the position; (a) no numerical dispersion and (b) numerical dispersion effect.

Numerical dispersion is usually exhibited for even-order approximations for the advection term. For example, when β=1.0 is used in the advection term in Eq. (A.26) the scheme is second-order accurate. Dispersion leads to oscillation in the solution, particularly at steep flow gradients. The dispersion effect is illustrated in Figure A.3 for the velocity step function.

As stated by Oertel and Laurien (1995) a solution scheme should only be first-order accurate for regions of sudden changes in speed, otherwise numerical oscillation can occur.

A.8 Convergence criteria

Non-linearities are solved by iteration in CFX. During iteration process the solver tries to achieve convergence which means that the solution of the left hand side equals the right hand side of the equations. The residual, r_ϕ, is a measure of the local imbalance of a transport variable, ϕ, between the inflow and outflow for a finite volume element.

$$r_\phi = \phi_{in} - \phi_{out} \qquad \text{Eq. (A.27)}$$

For many engineering applications, sufficient accuracy is often achieved despite small residuals existing in the solution of the equations. The solver stops with iteration and continues with the solution of the next time step if a specified maximum number of iterations or a specified maximum residual is achieved first. Allowing for a less restricted residual often means a reduction of iterations required to achieve convergence which saves simulation time. However, this usually leads to a reduction of accuracy of the solution.

The CFX solver uses a normalised form, $r_{\phi,norm}$, of the raw residual for judging if convergence is achieved and is calculated as follows (CFX 2006):

$$r_{\phi,norm} = \frac{r_\phi}{\alpha_p \cdot \Delta\phi} \qquad \text{Eq. (A.28)}$$

with a_p = representative of the control volume coefficient [-] and $\Delta\phi$ = representative range of the transport variable in the domain, both internally calculated by the solver in a complex process. A normalised residual of 10^{-6}–10^{-7} usually means an error which is in the order the round off error of the computer. The user can decide between two options in CFX for using the normalised residual as the convergence criterion for the solution of the transport equations. An additional more restricted option is also discussed.

MAX-Residual

The solver stops the iteration process before the specified maximum number of iterations has been reached if the user specified normalised residual of each finite volume element has been achieved for the RANS equations.

RMS Residual

The solver stops the iteration process before the specified maximum number of iterations has been reached if the user specified root mean square of the normalised residuals for all finite volume elements has been achieved for the RANS equations. This option has the advantage over the MAX-Residual option that it qualifies small local regions of bad convergence which might not influence the global solution. This option usually reduces convergence problems.

Conservation target

In steady-state simulations, the conservation criteria may be achieved during iteration although the global balances at the domain borders have not been achieved. The imbalance of a transport property for a domain is calculated by:

$$Imbalance = \frac{\phi_{out} - \phi_{in}}{\phi_{in}}$$

A conservation target (cvt) can be specified by the user which continues with iteration until the target domain imbalance between transport property inflow and outflow is achieved. However, the timescale of the building structure is significantly larger than for air leading to a long timescale until the global imbalance is achieved in the solid

domains. In transient simulations the global imbalance means heat storage in the building structure due to the high heat capacity. The conservation target is therefore not suitable for transient building simulations.

APPENDIX B

PARAMETRICAL STUDIES FOR HEAT TRANSFER MODELS IN CFX

B Parametrical studies for heat transfer models in CFX

This section comprises preliminary studies for the verification of heat transfer models for conduction, convection and radiation in CFX.

B.1 Modelling transient heat conduction using the 2nd order backward Euler transient scheme

Model Description

The geometry and boundary conditions of section 3.2.2 are adopted for the solid wall.

Model Implementation in CFX

The boundary condition setup, mesh and times scale discretisation, convergence criterion and advection scheme of section 3.2.2 are adopted. A 2nd order backward Euler scheme is used for discretising the transient term in the energy equation (see section A.7).

Results and Discussion

The temperature in the wall is evaluated at a monitor point at x/X=0.5 and y/Y=0.5 for a simulation period of 20h. Temperature predictions for CFX are compared with analytical data obtained from section 3.2.1 using Eqs. (3.2)-(3.5). Due to the limitation of each analytical solution (i.e. for small and large steps) the solutions at a simulation time around the value of 1h is not displayed.

The results presented in Figure B.1 for an initial wall temperature of T_W=27.5°C and fixed surface temperatures of T_S=23.75°C show an exponential temperature decrease for the analytical solution. Temperature oscillation around the analytical solution is displayed for the CFX predictions. The occurrence of over- and under-shoots is a typical

drawback of the 2nd order scheme as described in the CFX user manual (CFX 2006). A variation of the mesh size and time step did not indicate any trend of improvement.

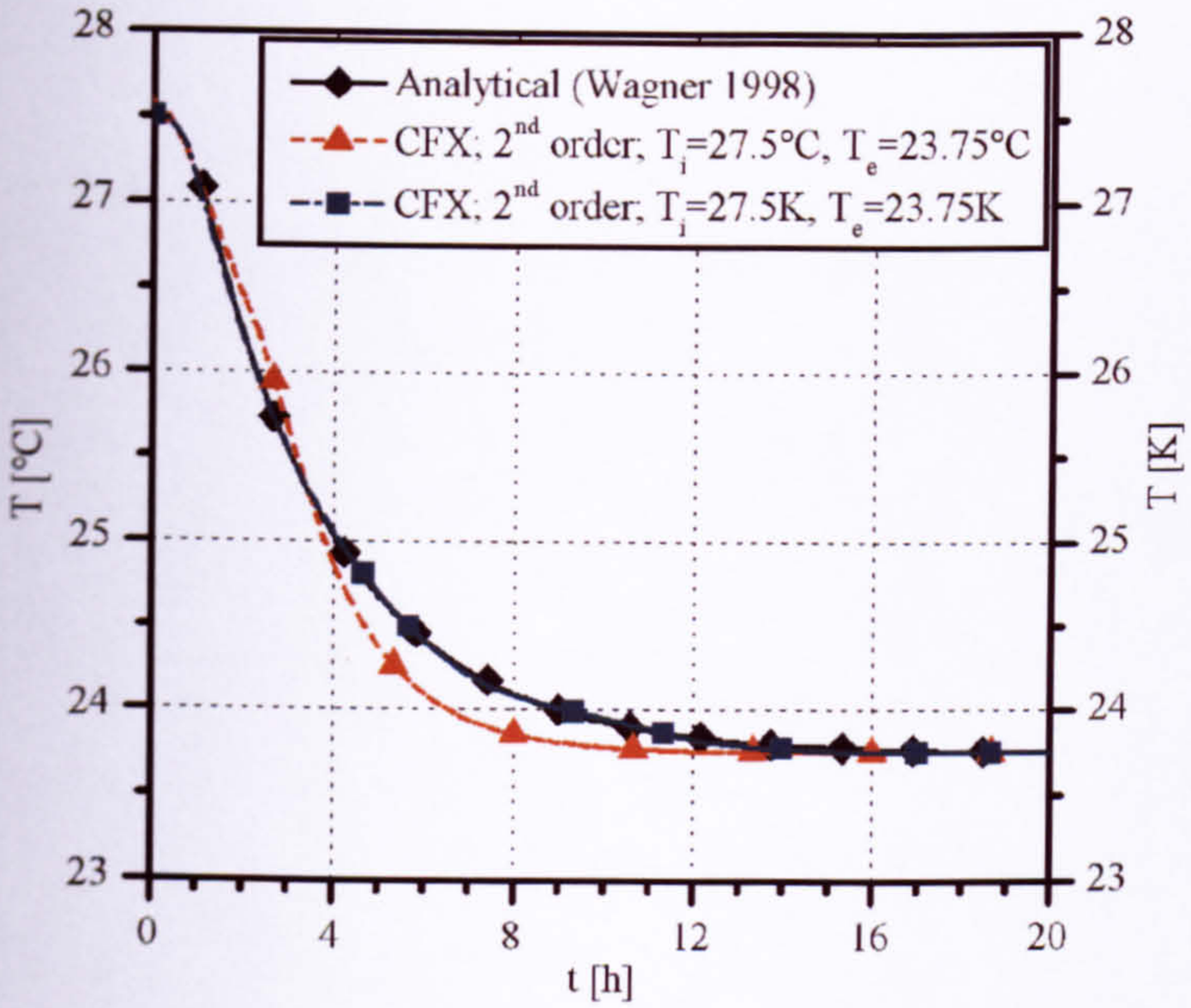

Figure B.1: Temperature predictions in a solid wall at x/X=0.5, y/Y=0.5 for CFX using the 2nd order backward Euler scheme in comparison with an analytical solution.

To test if the problem of over- and under-shoots is only a local effect, the temperature distribution through the solid in x-direction at y/Y=0.5 is evaluated for different points in time comparing CFX results with the analytical solution. However, the errors are displayed throughout the domain and show an increase towards the middle plane section of the wall (Figure B.2).

New boundary conditions are used to investigate these over- and under-shoots further, by keeping the absolute temperature difference between the solid wall and the surface temperatures and changing the temperature level which is T_W=27.5K and T_S=23.75K instead of T_W=27.5°C and T_S=23.75°C. The prediction of CFX compares favourably ($\Delta T \leq 0.03$K) with the analytical solution (Figure B.1). Thus, it seems that accurate predictions could be also possible for higher temperature levels.

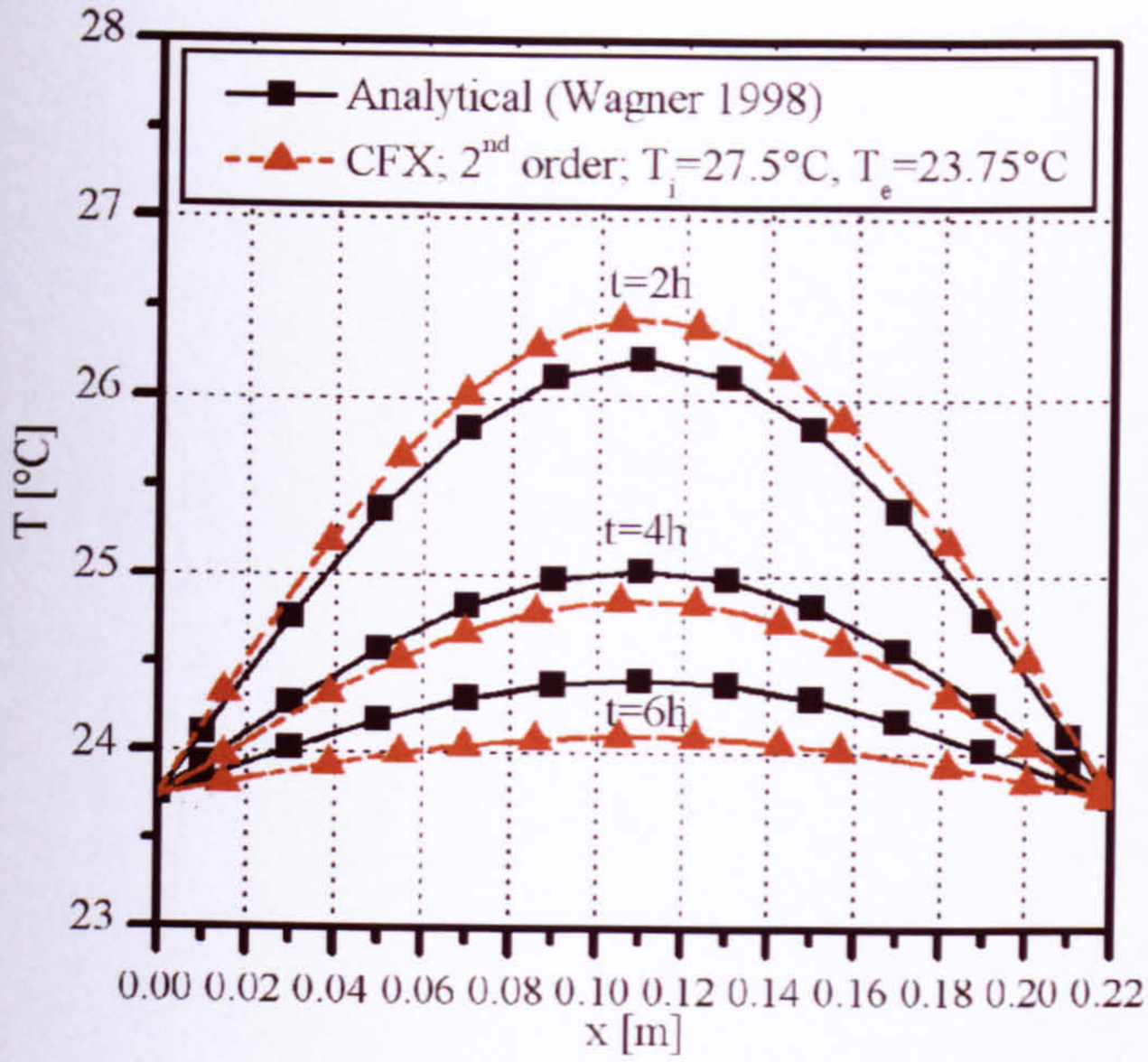

Figure B.2: Temperature predictions throughout the solid in x-direction after 2h, 4h and 6h of simulation for CFX using the 2nd order backward Euler scheme in comparison with an analytical solution.

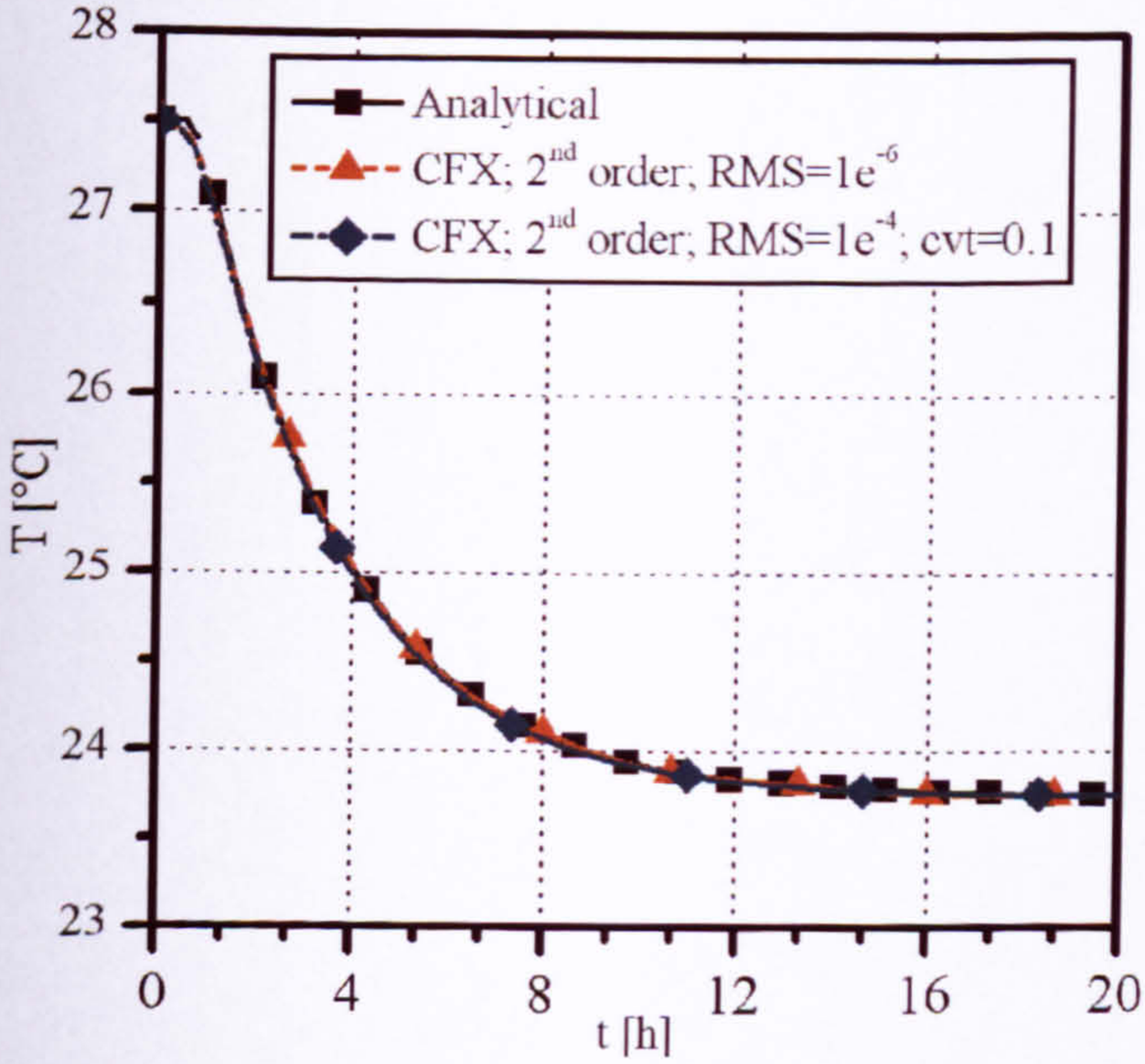

Figure B.3: Temperature predictions at x/X=0.5, y/Y=0.5 for CFX using different convergence criteria in comparison with an analytical solution.

In a further test the convergence criterion is refined. The predictions for a refined RMS residual of 10^{-6} and for a conservation target (cvt, see section A.8) of 0.1 are shown in Figure B.3. The accuracy of numerical results for CFX is significantly improved. However, convergence was not achieved for cvt=0.1 throughout the simulation. Furthermore, a refinement of the convergence criteria leads to a significant increase of computational resources required. The 2nd order transient scheme is unlikely to be suitably for dynamic thermal building simulations due to the high computational resources required to predict transient heat conduction problems in solid domains accurately.

B.2 Parametrical studies for modelling free convection

B.2.1 General modelling parameters for steady-state free convection

To model free convection, additional source terms must be included in the momentum and turbulence model equations to consider buoyancy (see section A.2). In CFX Version 5.7 and later, these terms can be simply included using the GUI option 'production and dissipation'. However, for older CFX versions, for example used for investigations in chapter 3.3, the additional buoyancy terms can not be included by using the common GUI. Depending on the turbulence model used, the buoyancy source terms must be incorporated using the Boolean parameters 'buoyancy tke source' (i.e. for turbulence kinetic energy), 'buoyancy tef source' (i.e. for turbulence eddy frequency) and 'buoyancy ted source' (i.e. for turbulence eddy dissipation rate) which are listed as expert parameters in an expert parameter section provided by CFX for advanced users. Setting these Booleans as 'true' this will include the buoyancy source terms.

For modelling buoyant flow in an enclosure using the steady-state solution scheme (see section A.7) convergence was not achieved in a test using default GUI settings. Specific information about modelling steady-state free convection does not exist in the CFX manual. A parameter study was therefore carried out testing various expert parameters. An influence on the convergence was achieved using the expert parameter 'relax mass' which is an under-relaxation factor in the mass term of the RANS equations. It is 0.75

by default and should not be changed for transient solution schemes (CFX 2006). In the case of a steady-state solution scheme 'relax mass'=1 led to the best convergence rates without leading to accuracy problems.

To reduce the risk of numerical oscillation, the physical time step (i.e. a 'false time step' which is used as the under-relaxation factor in steady-state algorithms) must be in the order of the time scale of the buoyancy forces and must be therefore small (i.e. in the order of seconds). However, since thermal changes are slow for purely naturally driven flow due to the small inertia of mass, a fully converged numerical steady-state solution would require many iterations and would therefore require high computational resources. The GUI provides an automatic calculation option for the time step which can accelerate the solution process. This automatic treatment leads to large time steps at the beginning of the simulation when the initial guess of the solution fields are far from the end solution and leads to small time steps at the end of the simulation. Particularly the difference between the first and second calculated time step is large. By default the solver updates the time step to the new room conditions every 5 iteration numbers which leads to divergence in the calculation procedure. A parameter in the expert parameter section can control the update frequency and is referred to as the 'timescale update frequency'. Using 'timescale update frequency'=1 this led to a relatively fast converged solutions. A good performance was particularly achieved using turbulence models which are based on the ω-equation.

B.2.2 Modelling of the wall boundary layer for laminar air flow

Model description

The model comprises an isothermal heated vertical plate of height Y=0.381m and a fixed surface temperature of T_S=33°C. Based on the suggestion of Phillips et al. (1999) an adjacent ambient flow domain of X=0.076m width, a part of the ambient region at the low end of the isothermal heated wall and an additional adiabatic wall are imposed to allow sufficient space to avoid the surrounding boundaries influencing the results (see Figure B.4). The conditions at the top, the bottom and the right vertical boundary allow air to flow in both directions depending on the pressure field. An ambient temperature

of T_a=21°C and a zero velocity vector field are imposed for initial domain conditions and the boundary inflow. For this model a Rayleigh number of $Ra=6.4 \cdot 10^7$ is calculated using Eqs. (3.8)-(3.10) which indicates a pure laminar flow regarding section 3.3.1. Therefore the model can be two-dimensional since no 3D-effects due to turbulence occur.

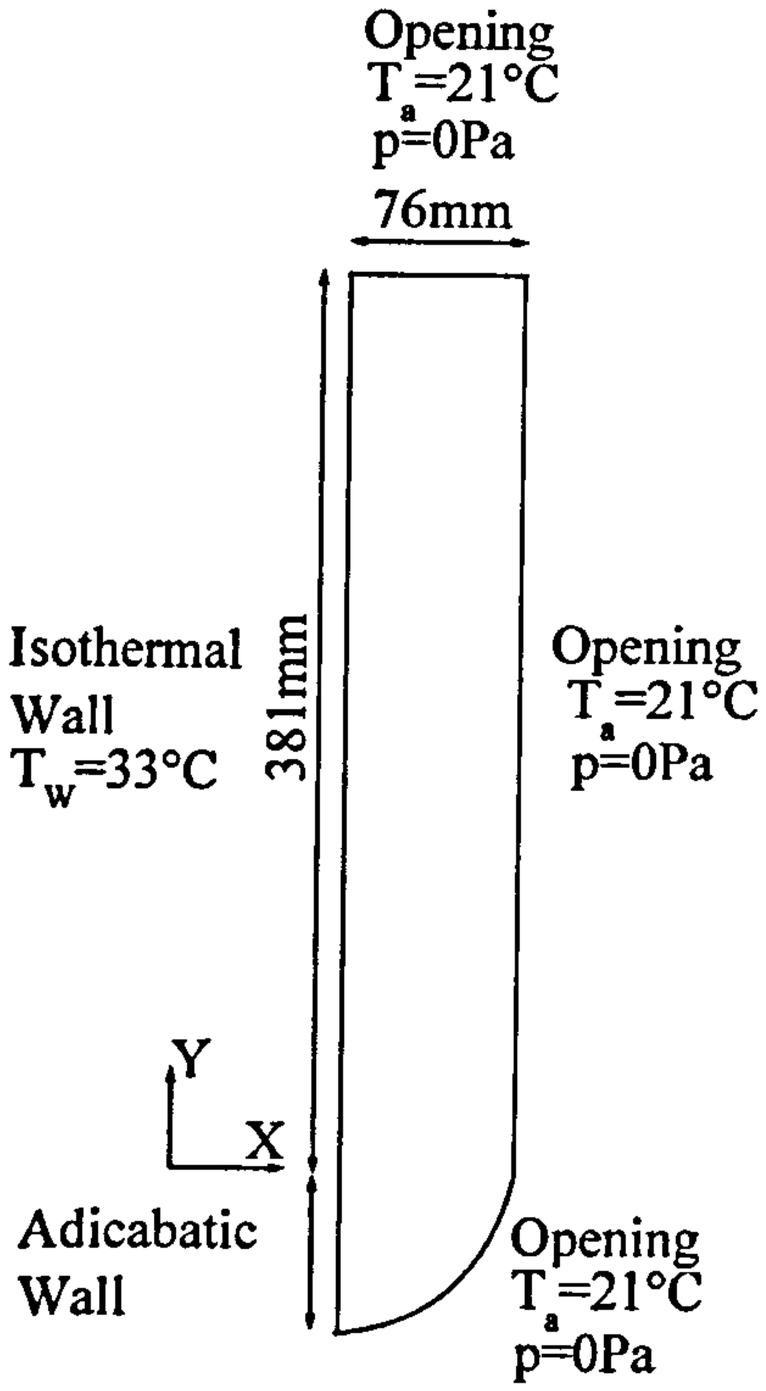

Figure B.4: Numerical model for laminar flow along a heated vertical plate.

Model implementation in CFX

Since the model and the flow are two-dimensional, a quasi-2D model is used for CFX using a model thickness of one volume element (i.e. Z=0.01m) and symmetry boundary conditions at the high and low end z-planes. The mesh at the boundaries and in the core of the fluid domain consists of small triangular and tetrahedral finite elements of 10mm maximum element edge length scale respectively to achieve high resolution. The mesh is refined at the region where the isothermal and adiabatic wall surfaces approach each

other (maximum edge length scale of 2mm) to increase the numerical resolution where the wall boundary layer begins to develop.

The outer edge of the wall boundary layer is reached when the non-dimensional temperature and velocity in Eqs. (3.14) and (3.15) approach zero. Using a diagram of Baehr and Stephan (1996), which shows the correlation between Eqs. (3.13)-(3.15), a zero non-dimensional temperature and velocity value is reached at $\eta \approx 6$. Calculating the Grashof number using Eq. (3.8) ($Gr = 8.98 \cdot 10^7$) and solving Eq. (3.13) for x, a maximum wall boundary layer thickness of about 33mm is calculated at the top of the model (i.e. at y=0.381). The CFX user manual suggests using at least 15 volume elements to calculate the wall boundary layer for free convection flow accurately (CFX 2006). A sufficient nodal resolution in the wall boundary layer region requires the use of prism elements to keep the computational effort within practical limits. The size of the prism element layers in direction of the surface normal can be determined using three key parameters: first prism size, core prism size and prism inflation factor. These are illustrated in Figure B.5.

First Prism Size: It determines the prism edge length in direction of the surface normal for the first prism element layer adjacent to the wall.

Core Prism Size: It determines the prism edge length in direction of the surface normal for the prism elements between the first prism adjacent to the wall and the outer edge of the wall boundary layer.

Prism Inflation Factor: The prism layer size can be gradually increased with distance from the surfaces using a prism inflation factor. Prism inflation can for example be used such that the last prism layer size has a similar scale to the edges of the neighbouring tetrahedral elements outside the wall boundary layer which increases the mesh quality. Using an inflation factor = 1, all prism layers have constant size as for example used for the following investigation of various core prism sizes.

A parametrical study for different mesh resolutions within the wall boundary layer is shown in section 'Results and Discussion".

Section A.5 provides information about how symmetry, opening boundary and adiabatic and isothermal wall boundary conditions are realized in CFX. Further, a high resolution advection scheme is used for the advection term of the RANS equations (see section A.7) and a laminar model is used (i.e. no additional equation is calculated beside the RANS equations). The Boussinesq approximation is applied to calculate the additional buoyancy source terms (section A.2). Radiation is not modelled since air is almost transparent to radiation and has therefore no effect on the patterns in the wall boundary layer for the case investigated. The solution is considered to have converged if a RMS residual of 10^{-5} for all RANS equations has been achieved.

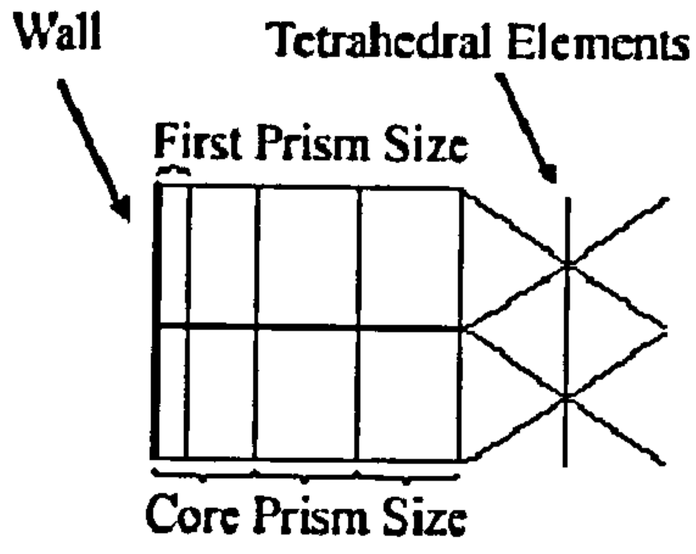

Figure B.5: Sketch of element types and sizing parameters used for the wall boundary layer.

Results and Discussion

In the following, the predictions for temperatures, velocities and surface heat transfer in the wall boundary layer are compared with analytical solutions described in section 3.3.1. All simulations have achieved the RMS residual of 10^{-5} demonstrating converged solutions.

Prism elements are used to numerically resolve the wall boundary layer. The prism layer resolution is varied for the first prism size (0.1mm, 0.2mm, 0.4mm, 1.0mm and 2.0mm), the core prism size (1.33mm, 2mm, 3mm and 4mm) and the prism inflation factor (1.2, 1.5, 2.0 and 2.5). To keep the core prism layers constantly at the same positions for varying first prism sizes, the different first prism sizes are realized dividing the first prism layer with 'core prism size' in two layers of different size ratio.

For the investigation of different core prism sizes a prism inflation factor of 1 and a first prism size of 0.1mm is used. In Figure B.6, the predicted velocity and temperature profiles in the wall boundary layer at y=0.380m are compared with the analytical solution. The velocity profile agrees well with the analytical solution for small core prism sizes and is slightly over-predicted for a core prism size of 4.0mm between the velocity peak and the outer edge of the wall-boundary layer (Δv_{max}=0.015m/s). The temperature profile is not influenced by changing the core prism size.

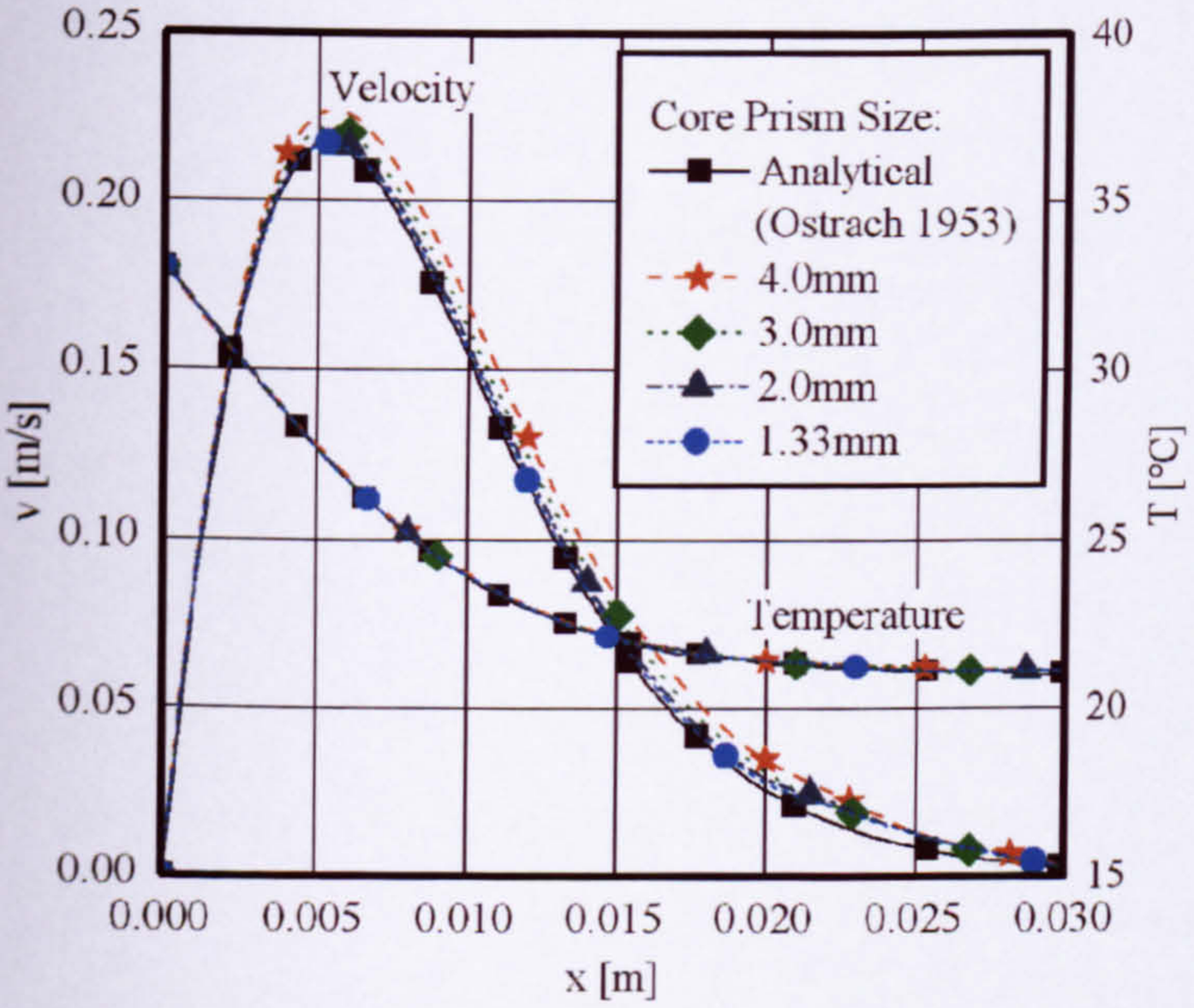

Figure B.6: Predicted vertical velocity components and temperatures in the wall boundary layer at y=0.38m for different core prism sizes compared with the analytical solution.

The non-dimensional local Nusselt number is used to show the surface heat flux along the isothermal plate (Figure B.7). The analytical local Nusselt numbers are calculated using Eq. (3.12); the local Nusselt numbers for the numerical solution is calculated using Eq. (3.11). The numerically result compares well with the analytical solution. At the top end of the heated vertical plate small deviations are displayed for a core prism size of 4.0mm (ΔNu_y=1).

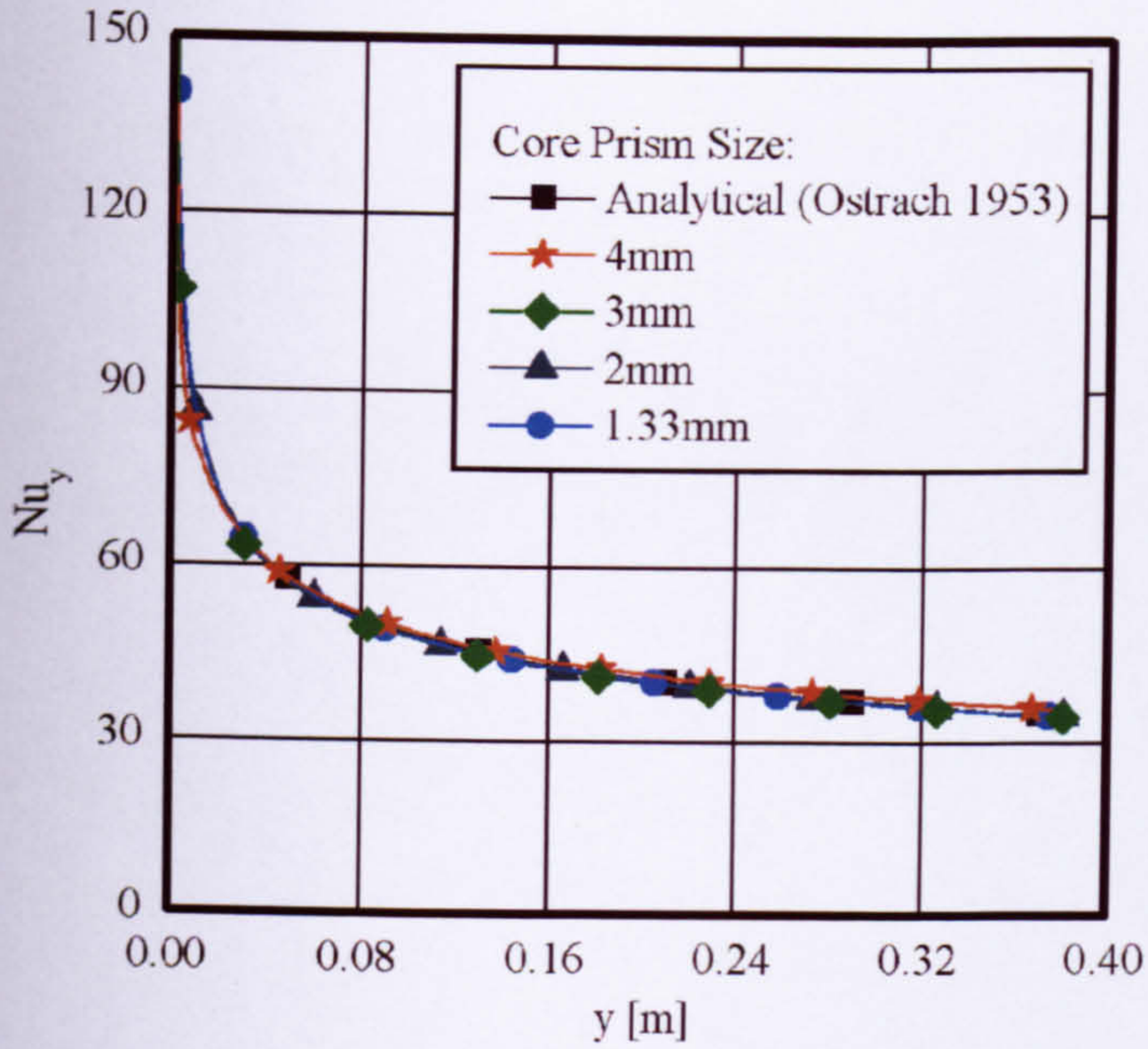

Figure B.7: Comparison of predicted local Nusselt numbers for the isothermal vertical plate for different core prism sizes with the analytical solution.

The Nusselt numbers for the entire heated vertical plate are calculated by integrating the local Nusselt numbers along the plate. The Nusselt numbers are shown in Table B.1. A slight under-estimation is shown for increased core prism size values. However, even for a mesh with a core prism size of 4.0mm only a deviation of less then Nu=1 is shown compared with the analytical result. The smallest deviation exits for a core prism size of 2.0mm. The slightly higher error of the average Nusselt number for the potentially most accurate simulation (prism size of 1.33mm) compared with the Nusselt number for a core mesh size of 2.0mm is thought to be caused by numerical discretisation at the low end of the isothermal wall since the surface heat transfer number undergoes its highest values at the beginning of the wall boundary layer. However, the use of a smaller mesh which approaches a finite size at the leading edge of the plate would lead to a significant increase of computational effort.

The best trade-off between accuracy and computational effort was achieved for a core prism size of 2.0mm. Thus, this mesh scale is used for the prism layers in the core region to investigate the influence of the size of the first prism adjacent to the wall on the patterns in the wall boundary layer.

Table B.1: Comparison of the calculated analytical solution with the numerically calculated total Nusselt numbers over the hot plate for different core prism sizes.

	Analytical solution	Core Prism Size [mm]			
		4.0	3.0	2.0	1.33
Nu [-]	46.18	45.25	45.80	46.12	46.29
Absolute Error [-]	-	0.93	0.38	0.06	0.11
Relative Error [%]	-	2.1	0.8	1.3	0.2

Figure B.8 shows the predicted temperature and velocity (vertical component) profiles in the wall boundary layer at y=0.380m in comparison with the analytical solution. The velocity profiles agree well with the analytical solution for small core prism sizes and deviate slightly between the wall and the location of the velocity peak as the prism size is increased. Only for a numerical mesh with a first prism size of 2.0mm a significant deviation from the analytical solution is shown (Δv=0.08m/s). The temperature profile is not sensitive to the variation of the first prism size.

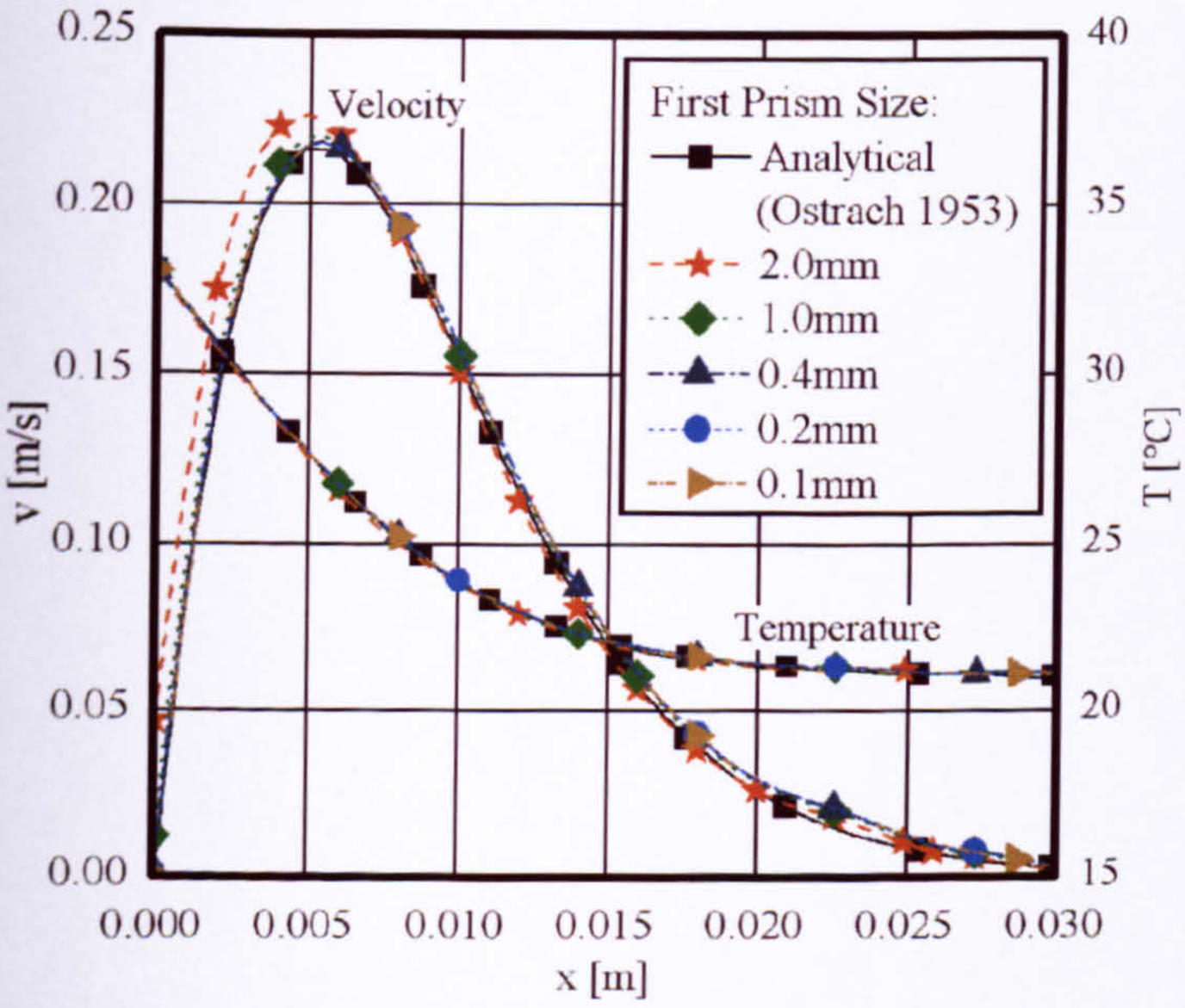

Figure B.8: Predicted vertical velocity components and temperatures in the wall boundary layer at y=0.38m for different first prism sizes compared with the analytical solution.

The local Nusselt numbers at the isothermal vertical wall are presented in Figure B.9. The numerical values agree favourably with the analytical case for first prism sizes of up to 1.0mm. The Nusselt numbers integrated over the entire heated plate are shown in Table B.2. An over-estimation is displayed as the first prism size is increased. For first prism sizes of up to 0.2mm almost no deviation exists compared to the analytical solution. Comparing average Nusselt numbers for variation of core and first prism sizes the values are more sensitive to the first prism size, indicated by stronger deviations.

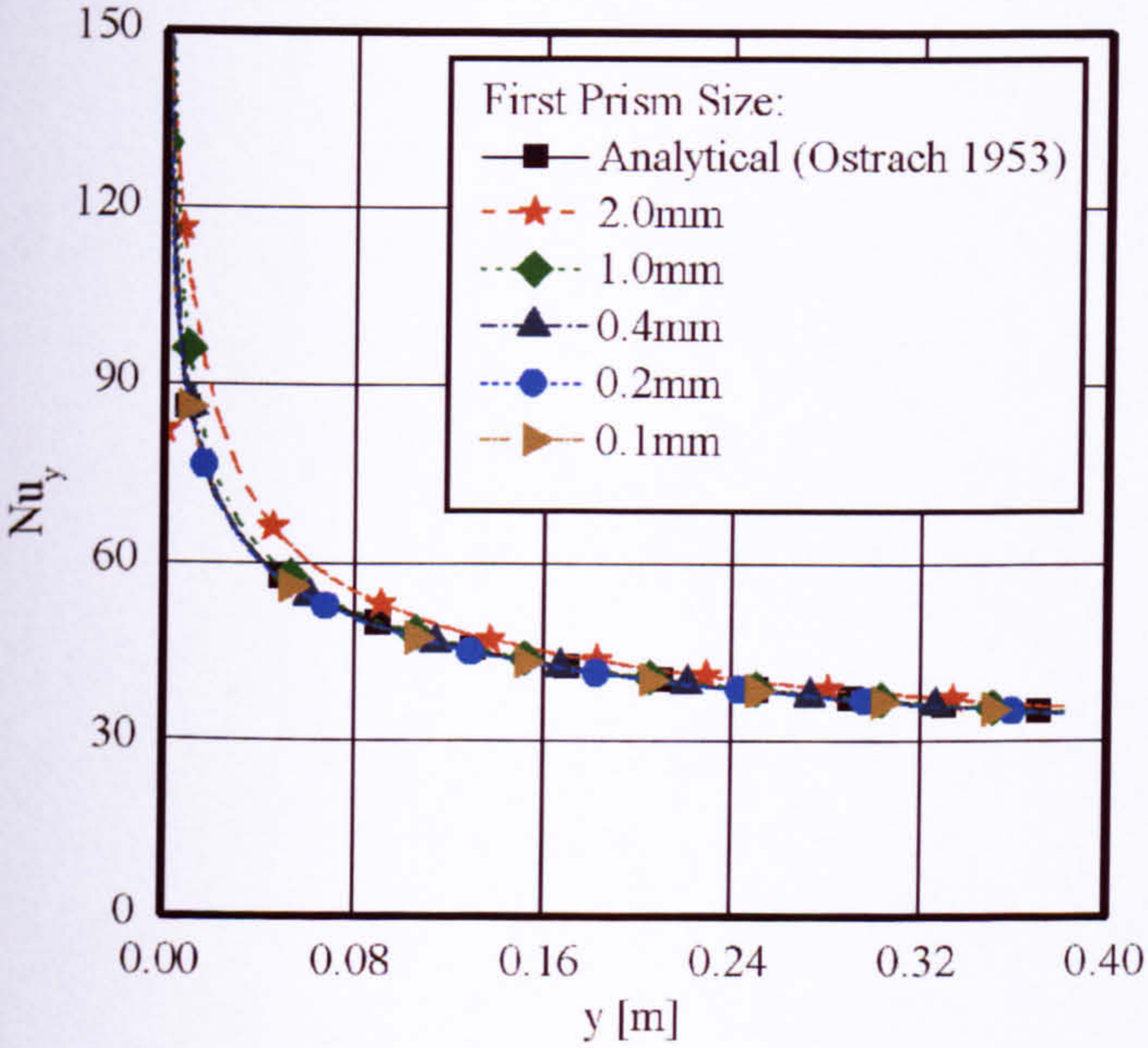

Figure B.9: Predicted local Nusselt numbers at the surface for different first prism sizes compared with the analytical solution.

Table B.2: Comparison of the calculated analytical solution with the numerically calculated total Nusselt numbers over the heated plate for different first prism sizes.

	Analytical solution	First Prism Size [mm]				
		2.0	1.0	0.4	0.2	0.1
Nu [-]	46.18	49.72	47.35	46.48	46.27	46.12
Absolute Error [-]	-	3.54	1.17	0.3	0.09	0.06
Relative Error [%]	-	7.7	2.5	0.6	0.2	0.1

The profiles for velocity and temperature shown above display high gradients close to the wall and smaller gradients towards the outer edge of the wall boundary layer. A high mesh resolution is only necessary at high gradients of pressure, velocity and temperature. Thus the mesh can be coarser in the other regions. The prism inflation factor can be used to gradually increase the prism layer size from the wall towards the outer edge of the wall boundary layer. Furthermore, using this method the prism sizes can be gradually adjusted to the sizes of the tetrahedral elements outside the wall boundary layer which increases the quality of the mesh and therefore convergence. For the sensitivity study of different prism inflation factors, prism inflation starts always from the second prism 0.5mm from the surface. A first prism size of 0.1mm and a second prism size of 0.4mm are therefore used. Prism inflation occurs only as long the prism sizes are smaller than the size of the tetrahedral elements.

In Figure B.10 the temperature and velocity (vertical component) wall boundary layer profiles at y=380mm are shown. The velocity profile for an inflation factor of 1.2 agrees favourably with the analytical solution. The numerical solution deviates from the analytical result towards the outer edge of the wall boundary layer with increased inflation factors showing deviations of 0.005m/s for the smallest and 0.05m/s for the largest inflation factor investigated. A slight deviation in the middle of the thermal wall boundary layer is displayed for the large inflation factors investigated.

The local Nusselt numbers at the isothermal wall are presented in Figure B.11 for different prism inflation factors. The local Nusselt number deviates marginally from the analytical results as the core prism size is increased. The total Nusselt numbers for the entire isothermal plate are shown in Table B.3. The error increases slightly for higher inflation factors. The numerical solution for an inflation factor of 1.2 shows a good trade-off between accuracy and computational effort (i.e. mesh resolution).

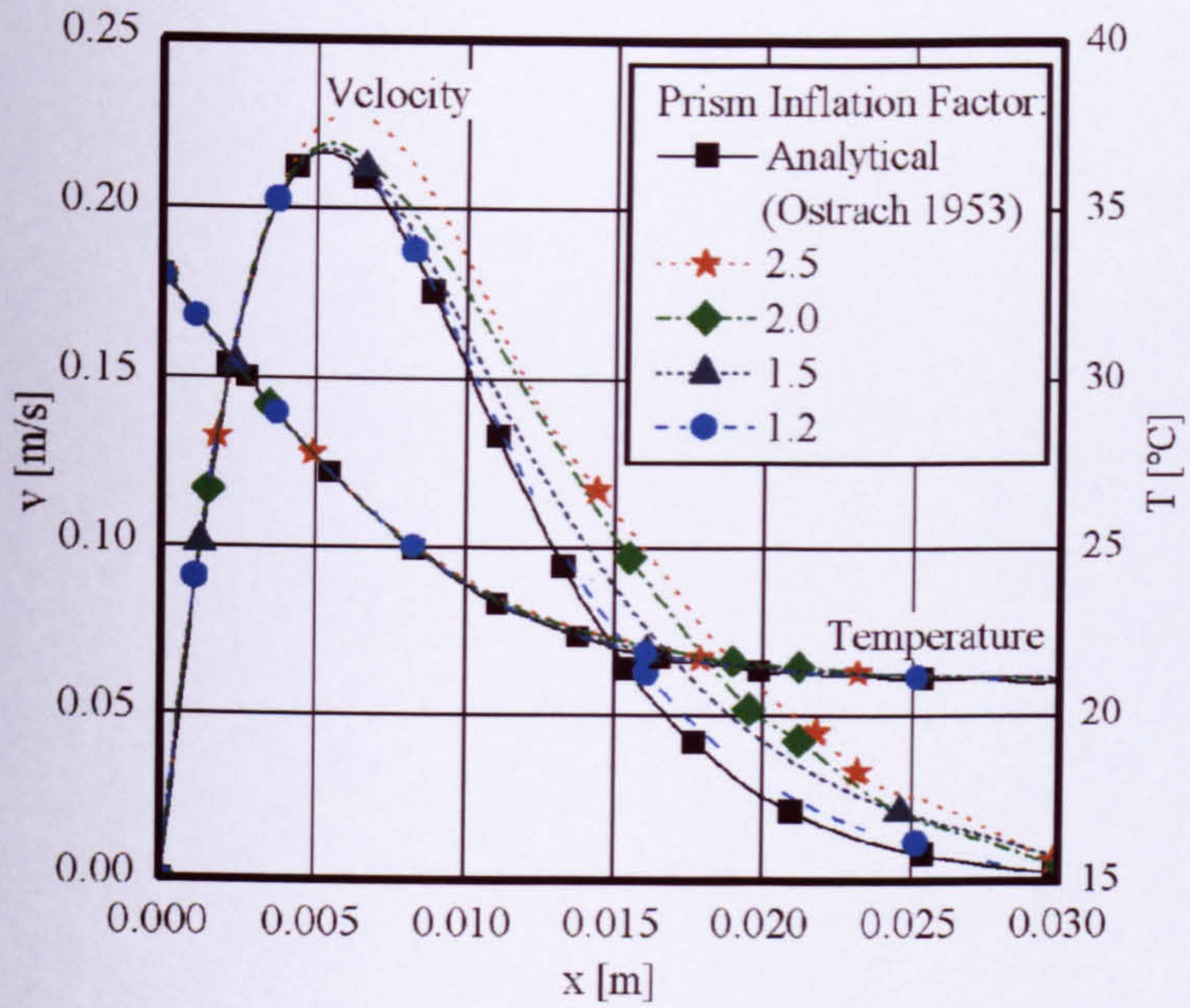

Figure B.10: Predicted vertical velocity components and temperatures in the wall boundary layer at y=0.38m for different inflation factors compared with the analytical solution.

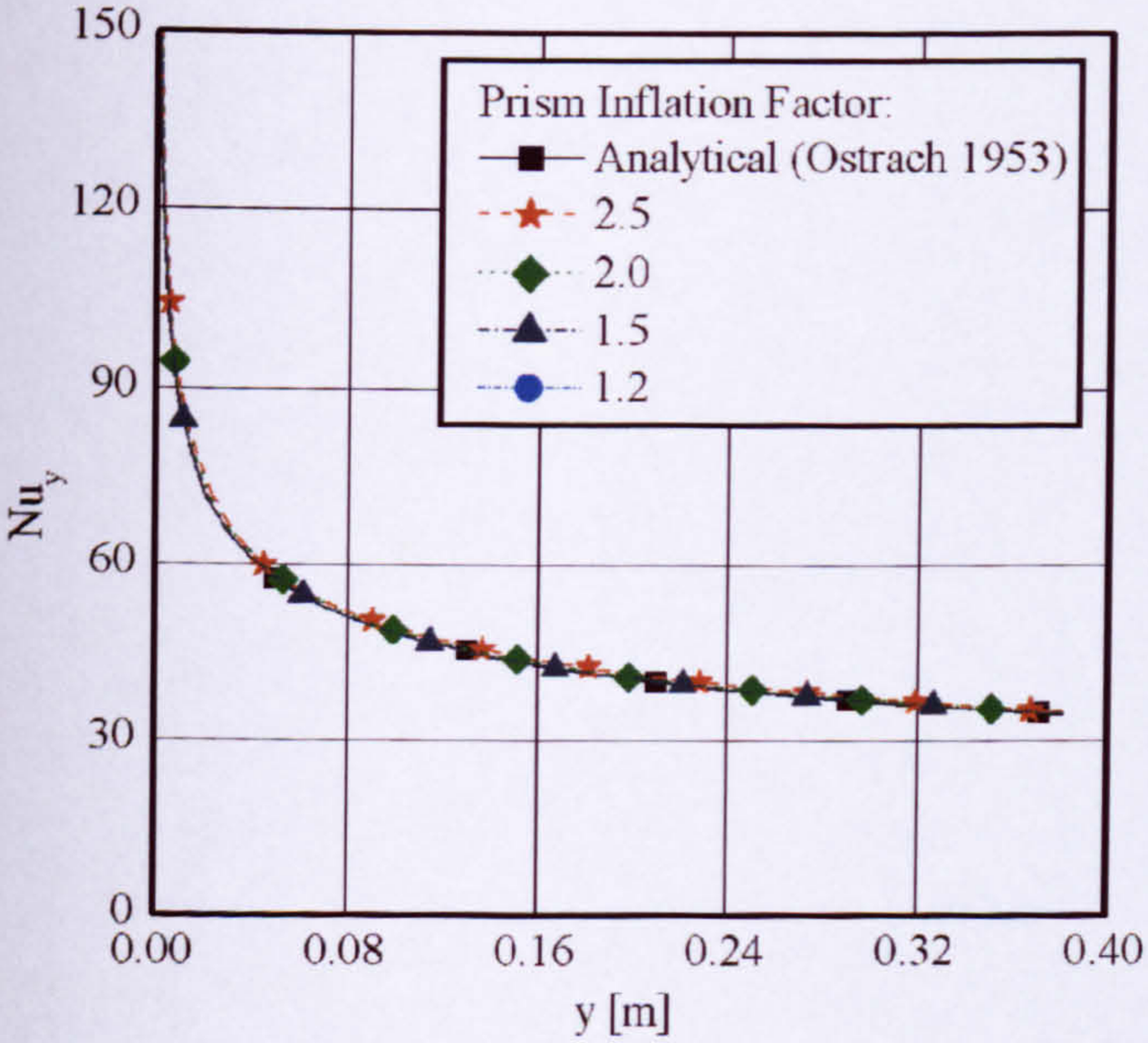

Figure B.11: Predicted local Nusselt numbers at the surface at different heights for different inflation factors compared with the analytical solution.

Table B.3: Comparison of the calculated analytical solution with the numerically calculated total Nusselt numbers over the heated plate for different prism inflation factors.

	Analytical solution	Prism Inflation Factor [-]			
		2.5	2.0	1.5	1.2
Nu [-]	46.18	47.45	46.92	46.55	46.00
Absolute Error [-]	-	1.27	0.74	0.37	0.18
Numerical Error [%]	-	2.7	1.6	0.8	0.4

The parametrical investigation of different mesh resolutions for the near wall boundary layer has shown that heat transfer and air flow patterns in the wall boundary layer are sensitive to the mesh resolution. Prism elements were used for the wall boundary layer to keep the computational effort in a practical limit. Particularly the size of the first prism adjacent to the wall significantly influences the heat transfer in the wall boundary layer. Since a high mesh resolution is only required for the regions with high velocity, temperature and pressure gradients, prism inflation can be used to reduce the number of prism elements in the wall boundary layer. Optimal values were found for a first prism size of up to 0.2mm and prism inflation of 1.2 from the second prism starting 0.5mm from the surface.

B.2.3 Modelling turbulent free convection in a quasi two-dimensional room model

Model Description

The geometry (2D room model) and boundary conditions are adopted from section 3.3.2.

Implementation in CFX

The general settings from section 3.3.2 and section B.2.1 are adopted (i.e. boundary conditions, steady steady-scheme and advection scheme, physical time scale, convergence criterion for solving the RANS and turbulence equations). Different

turbulence models are tested for steady-steady turbulent free convection: k-ω, LRR-IP, SST and SMC-ω model (see model details in section A.3). The turbulence models are based on the ω-equation and use the low-Reynolds method for near wall treatment, except the LRR-IP model which is based on the ε-equation and uses the wall-function approach described in section 2.3.4. This is to investigate how the wall-function method performs for fine numerical meshes in the near wall region for free convection.

Results and Discussion

A quasi-2D room model is used to compare numerical CFX predictions for different turbulence models with experimental data of Tian and Karayiannis (2000) and numerical data of Beghein et al. (1993). All data is plotted on the mid-depth line, $z/Z=0.5$. In this section only a qualitative comparison is carried out to find the turbulence model which shows the best agreement with the experimental and numerical reference data. A quantitative analysis for the over-all favourable model is carried out in section 3.3.2.

Solutions achieved the RMS residual of 10^{-5} and monitored velocities remained constantly during the solution process at the monitoring points (except for the SMC-ω model where it slightly oscillated at RMS=10^{-4}).

The temperature and velocity profiles of the wall boundary layer at mid height of the hot vertical surface for CFX are compared with experimental data in Figure B.12. The k-ω model shows the best agreement with experimental results. Simulations using the SST and SMC-ω model display curve shapes similar to those for the k-ω model, although the over-prediction of the velocity peak value and the under-prediction of the temperatures towards the outer edge of the wall boundary layer are slightly larger than for the k-ω model. Using the LRR-RSM model the thermal and air flow patterns are strongly under-predicted.

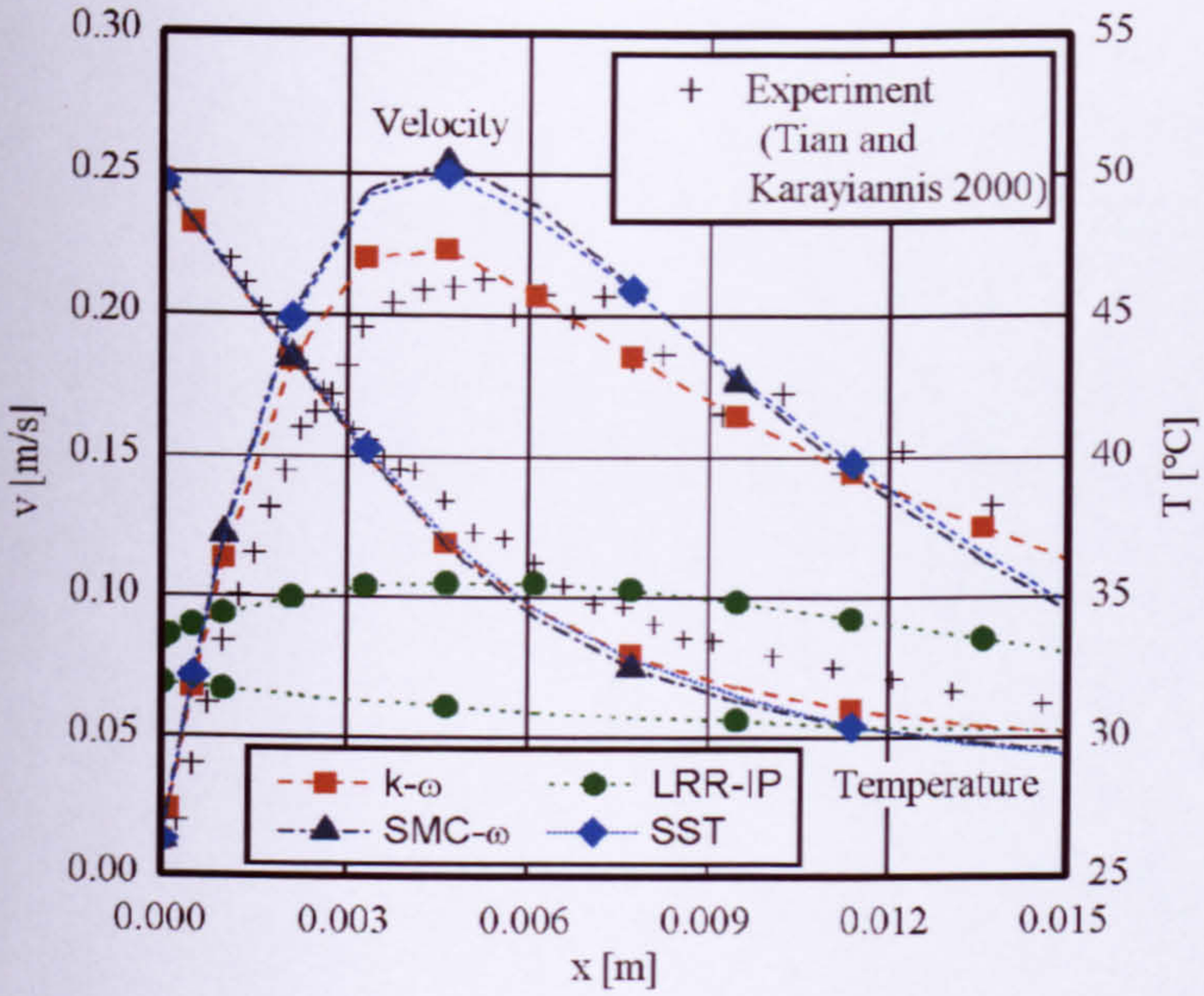

Figure B.12: Predicted vertical velocity components and temperatures at the isothermal hot wall at mid height for different turbulence models compared with experimental data.

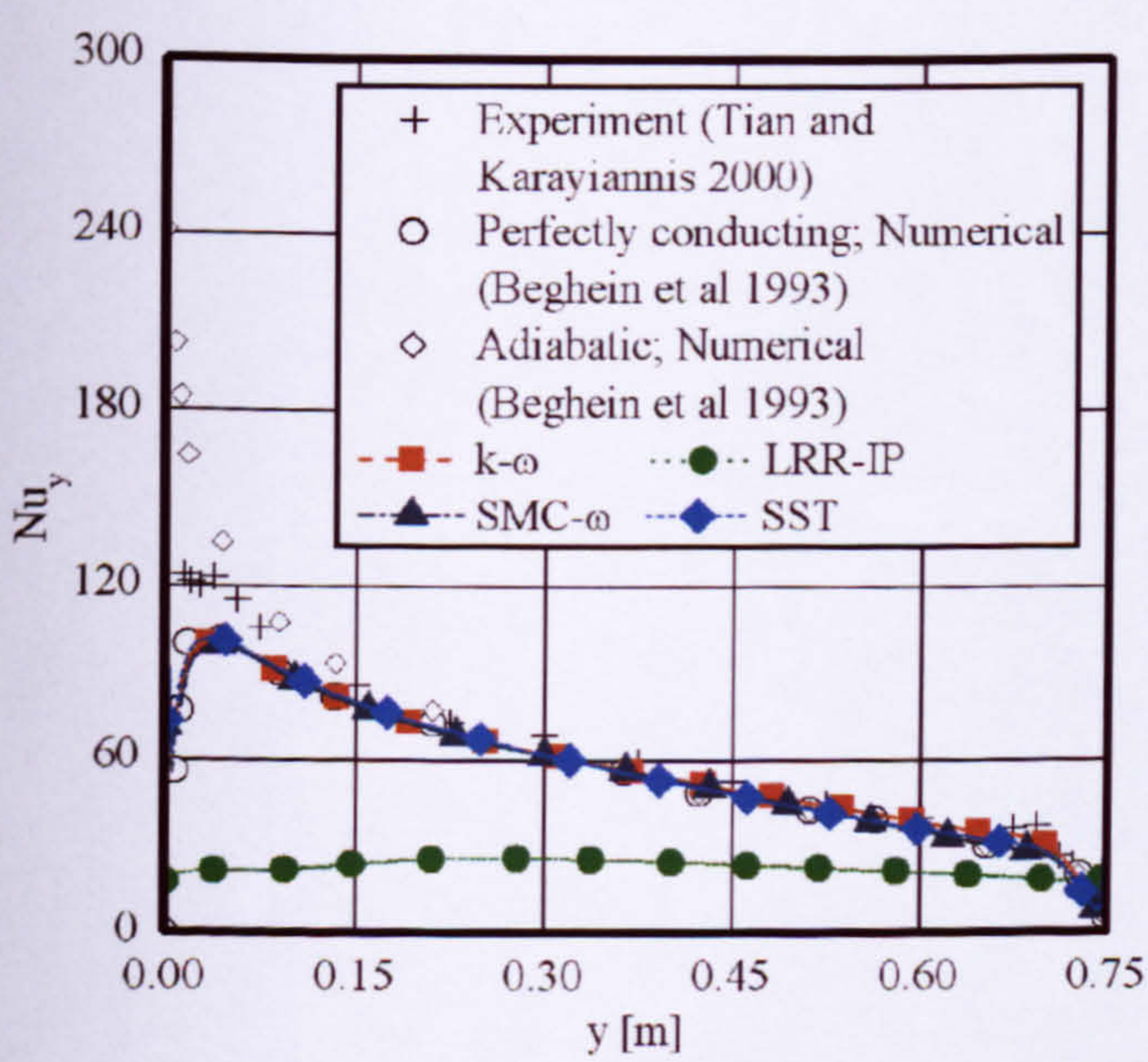

Figure B.13: Predicted local Nusselt numbers at the isothermal hot wall surface for different heights for different turbulence models compared with experimental data.

Figure B.13 shows the local surface heat transfer (i.e. the Nusselt number) along the hot vertical wall comparing numerical and experimental data. Except for the LRR-RSM model, the other investigated turbulence models follow the perfectly conducting curve shape of the numerical solutions of Beghein (1993) well. The strong under-prediction of the wall boundary layer velocity profile and the Nusselt numbers for the LRR-IP model (compare Figures B.12 and B.13) demonstrate the strong influence of the air flow conditions in the wall boundary layer on the surface heat transfer. The higher values measured by Tian and Karayiannis (2000) at the low end of the hot vertical wall compared with the numerical solutions are a result of the boundary condition treatment for the horizontal walls which are neither perfectly adiabatic nor perfectly conducting.

Numerical temperature results at cavity mid width are compared with experiments and are presented in Figure B.14. The simulation for the k-ω model shows the best agreement with the experiments, followed by the SST and SMC- ω model for which higher temperature gradients are displayed. The under-prediction of the surface heat transfer for the LRR-IP model leads to a strong under-prediction of the vertical temperature gradient compared with the other turbulence models.

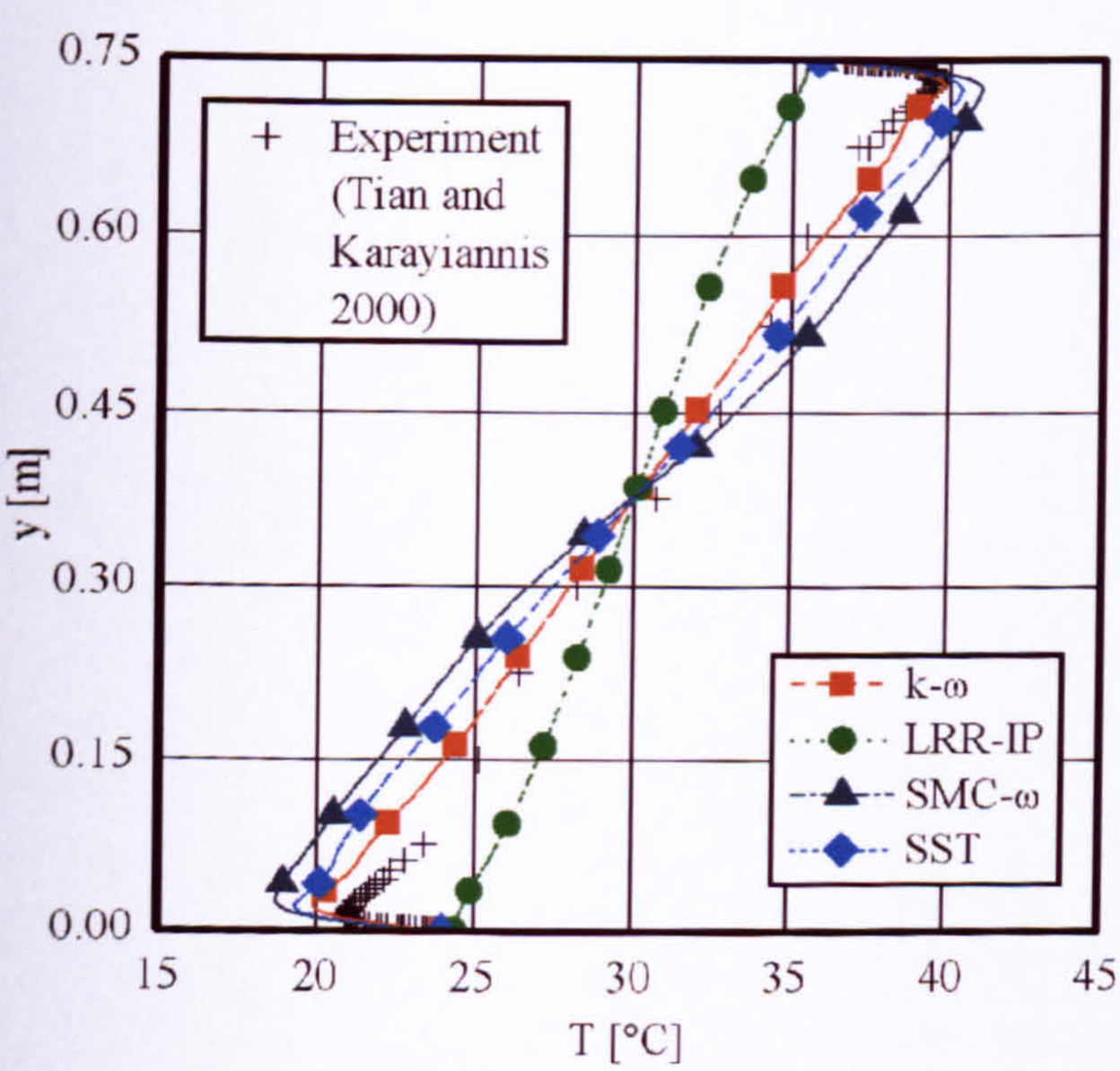

Figure B.14: Predicted temperatures for different heights at mid width for different turbulence model compared with the experimental reference data.

In Figure B.15, predicted and measured velocities (horizontal components) are shown for different heights at the cavity mid width. The results are qualitatively similar for all turbulence models. However, only the simulations using the SST and the SMC-ω model predict flow reversal regions at cavity mid width as measured by Tian and Karayiannis (2000), although the strength of the flow reversal is also under-predicted for these turbulence models. The simulation shows the best agreement with experimental results for the main flow direction (indicated by the large velocity peaks) using the k-ω model, followed by the SST model. The LRR-model gives largest discrepancies.

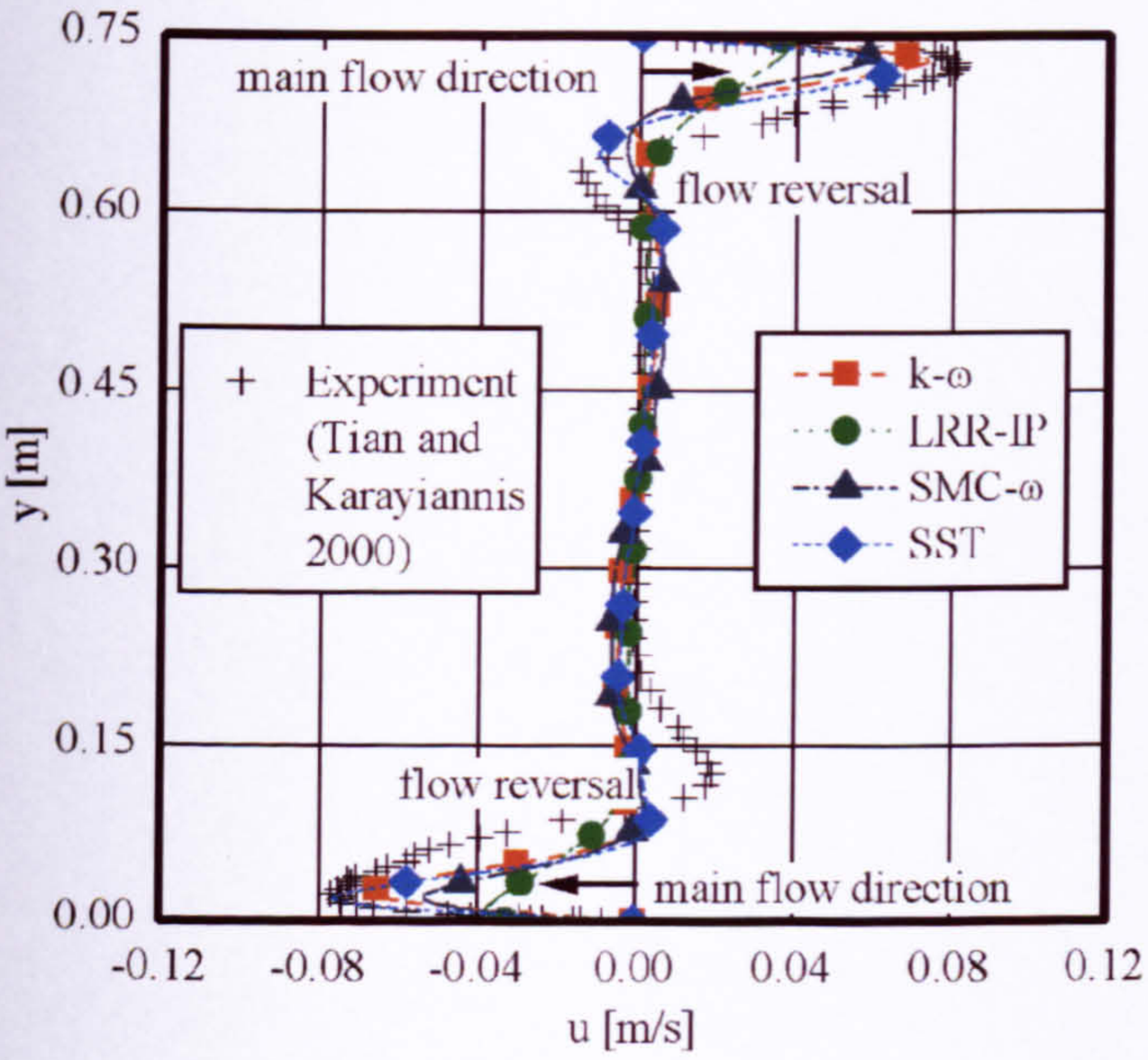

Figure B.15: Predicted horizontal velocity components for different heights at mid width for different turbulence models compared with experimental data; the flow directions are labelled by black arrows.

One more equation is calculated for the SST model compared with the k-ω model since the distance of the first node from the wall must be calculated (CFX 2006). Comparing temperatures, velocities and wall heat fluxes in Figures B.12-B.15 the best over-all performance compared with the experiments is obtained using the k-ω followed by the SST turbulence model. Since the k-ω is simpler than the SST model it is suggested as the favourable model for modelling free convection.

B.2.4 Modelling turbulent free convection in a three-dimensional room model

Flow disturbances were displayed near the high end of the vertical hot wall and the low end of the vertical cold in section 3.3.2 for the modelling of turbulent free convection flow in a quasi-2D cavity. The reason could be distance of the high and low end z-symmetry planes in the quasi-2D model which prohibit turbulences to dissipate in all directions. To investigate the spatial flow effects, the turbulent flow is investigated in this section using a 3D model.

Model Description

The model boundary conditions are based on the 2D cavity of section 3.3.2. However, to investigate spatial (three-dimensional) effects of turbulences, a 3D geometry is considered using a model depth of Z=0.375m.

Model implementation in CFX

The general settings from section 3.3.2 and section B.2.1 are adopted (i.e. boundary conditions, steady steady-scheme and advection scheme, physical time scale, convergence criterion for solving the RANS and turbulence equations). The turbulence models which showed the best performance in section B.2.3 for a quasi-2D model were the k-ω and the SST model. These are applied for the 3D model.

The mesh of the quasi-2D model is modified extending the model from Z=0.01m to Z=0.375m. In the wall boundary layer, prism layers with a first prism size of 0.1mm followed by 15 prisms starting 0.5mm from the wall with an inflation factor of 1.2 are used which is similar to the wall boundary layer resolution of the quasi-2D model. The discretisation of the wall boundary layer using at least 15 layers suggested in the CFX manual (CFX 2006) is achieved. The surface mesh density in the corners is not refined to keep the total number of elements below a practical limit for computing power. The mesh size at the surfaces and in the core region of the cavity are adopted from the quasi-2D model. Consequently a high total number of 1,016,000 volume elements are used for discretisation of the 3D model.

Results and Discussion

The convergence criterion of RMS residual of 10^{-5} has not been achieved during the simulations and values oscillated slightly at RMS=10^{-4}. A screenshot of monitored values over a period of 1000 iterations for the simulation using the k-ω model is shown in Figure B.16. This oscillation was also observed for the SMC-ω model for the quasi-2D geometry in section B.2.3. The oscillation behaviour at RMS=10^{-4} indicates a transient air flow for which a transient calculation scheme is provided in the CFX code. Fluctuations were also measured by Tian and Karayiannis (2000) which were numerically investigated by Peng and Davidson (2001) using a LES model. However, as shown in Figures B.17 - B.20 for monitored velocities and temperatures the transient effects are relatively small ($\Delta T_{max} \approx \pm 1K$, $\Delta u_{max} \approx \pm 0.02m/s$, $\Delta v_{max} \approx \pm 0.02m/s$) and in the order of measured fluctuations. Thus the mean thermal and air flow patterns are constant. Somarathne et al. (2002) have used a steady-steady scheme in one of their freeze-flow methods to adjust the air flow to fixed boundary conditions. In order to find out if this method can be used in the thesis, the results obtained for the steady-state scheme are evaluated in the following, despite the convergence criterion was not achieved. The results can also be found in Zitzmann et al. (2005).

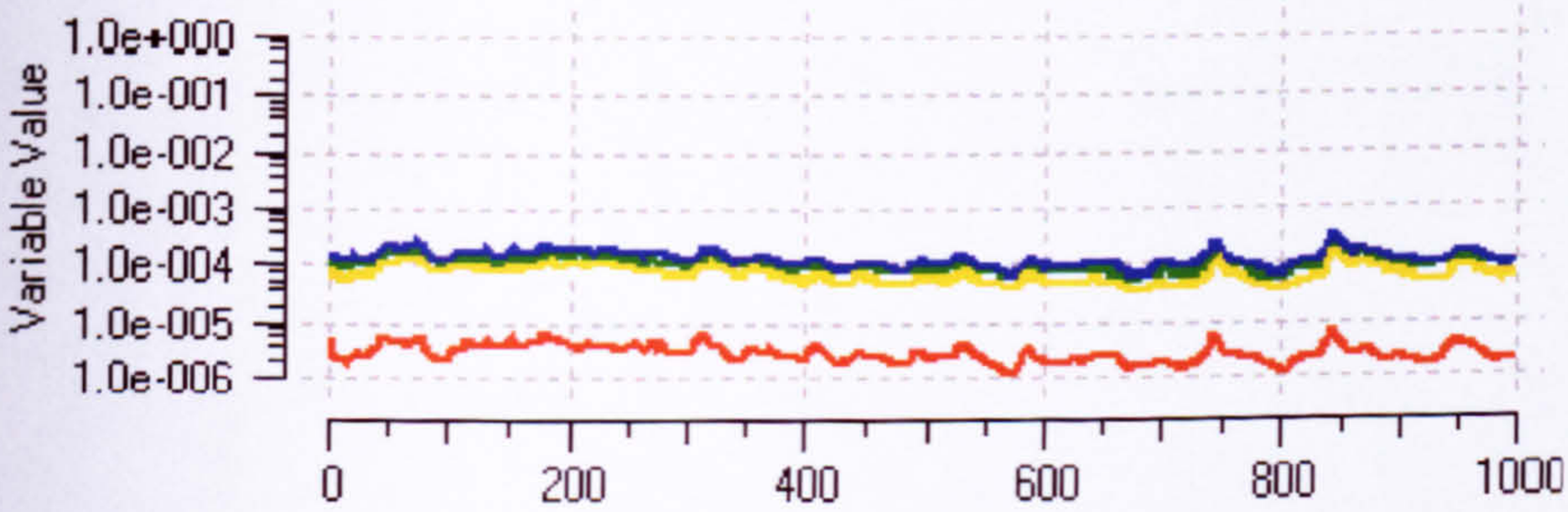

Figure B.16: Monitored RMS residual for the hydrodynamic equations for the 3D room model using the k-ω turbulence model; u-momentum (green) v-momentum (blue), w-momentum (orange) and mass (red).

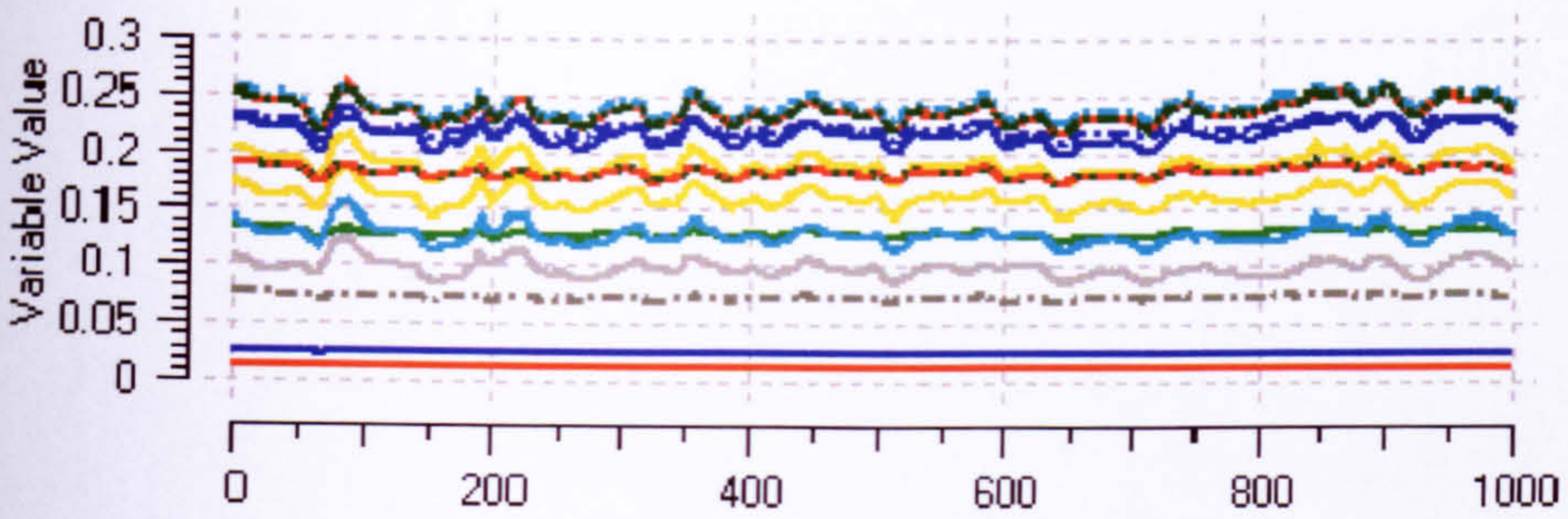

Figure B.17: Monitored vertical velocity components in the wall boundary layer at the hot wall at y/Y=0.5 over a period of 1000 iterations for the 3D room model using the k-ω turbulence model.

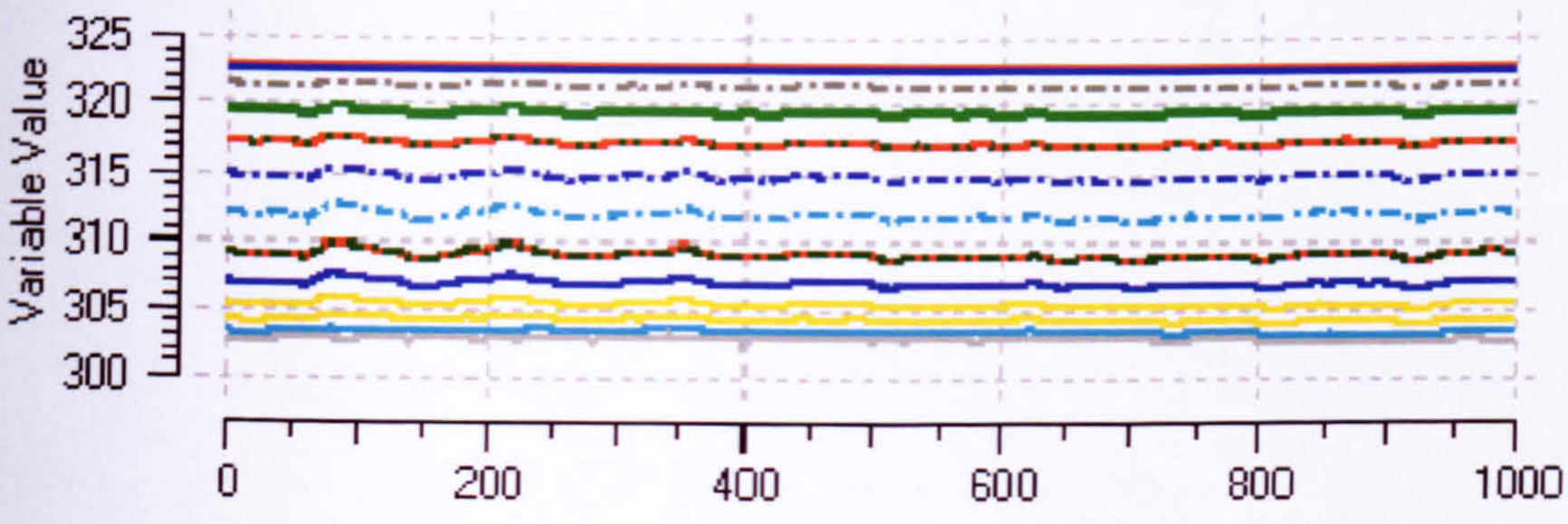

Figure B.18: Monitored temperatures in the wall boundary layer at the hot wall at y/Y=0.5 over a period of 1000 iterations for the 3D room model using the k- ω turbulence model.

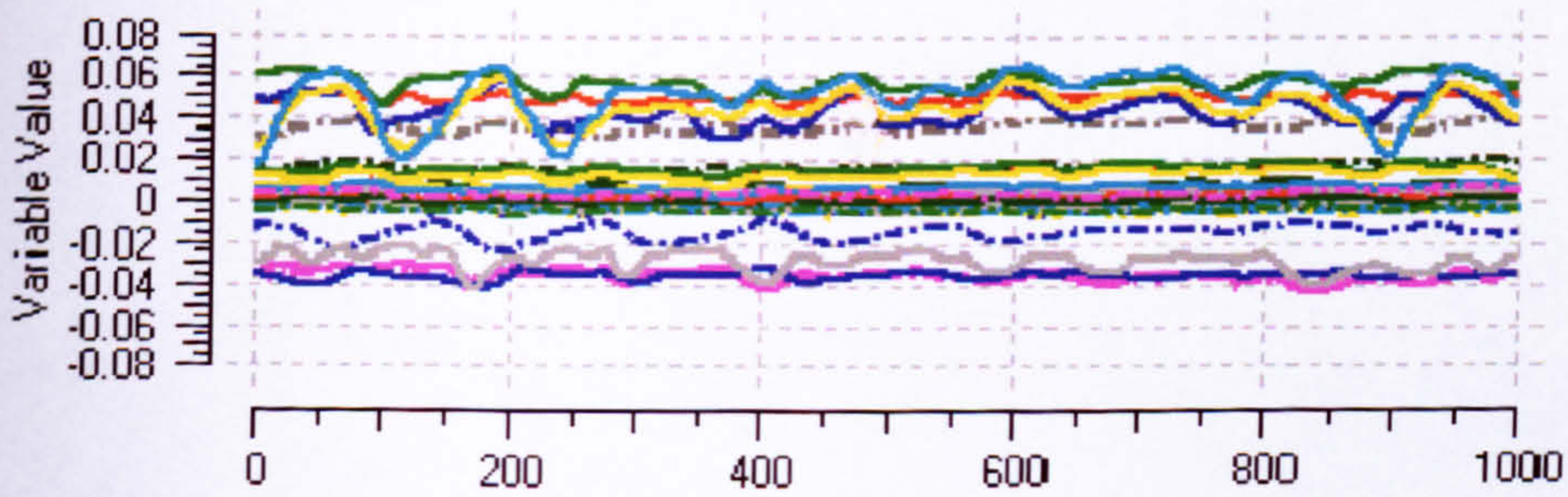

Figure B.19: Monitored horizontal velocity components at different heights at x/X=0.5 over a period of 1000 iterations for the 3D room model using the k- ω turbulence model.

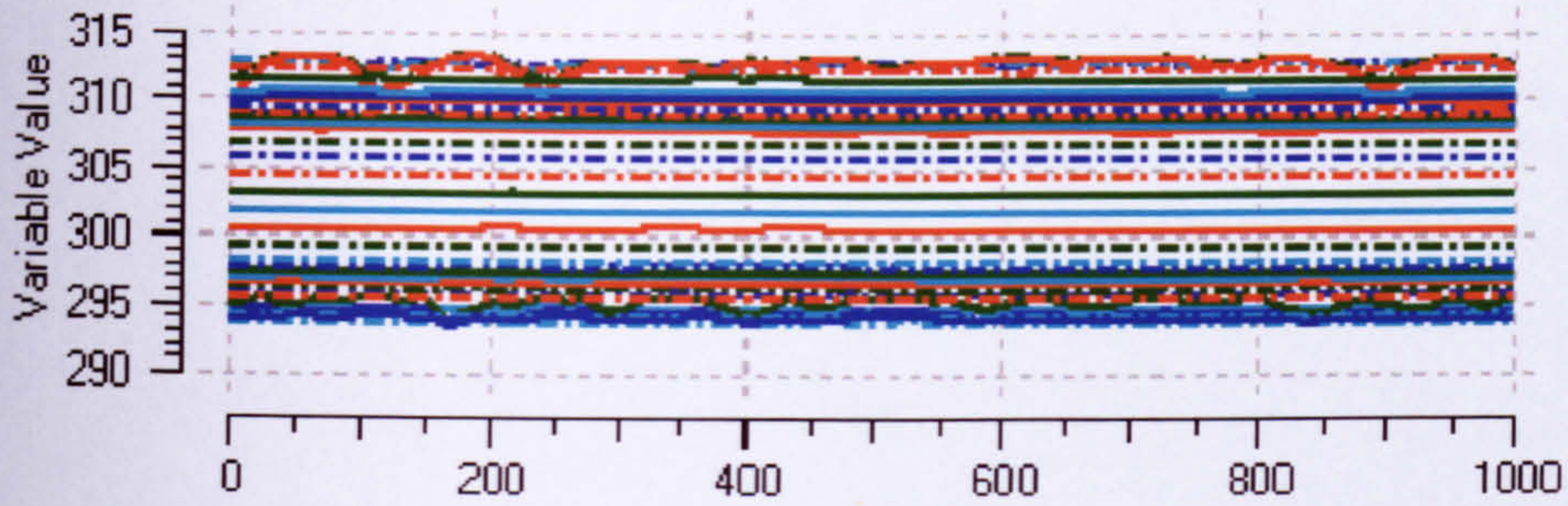

Figure B.20: Monitored temperatures at different heights at x/X=0.5 over a period of 1000 iterations for the 3D room model using the k-ω turbulence model.

For comparison of numerical predictions with experimental time-averaged values the simulation results shown in Figures B.17 – B.20 are averaged over the period of 1000 iterations. This procedure is not possible for evaluation of the Nusselt number since the surface heat transfer cannot be monitored during the simulation. For this case, the heat transfer is statistically analysed (i.e. using the simulation data at the end of five simulations whereby each simulation runs over a period of 200 iterations). Although small errors might occur using this procedure, it might show the general plausibility of results.

Figure B.21 shows the predicted temperatures and velocities (vertical component) at cavity mid height in the near wall boundary layer at the hot vertical wall in comparison with experimental data. The velocity curve for the 3D model are close to those of the quasi-2D model using the k-ω model (compare with Figure 3.4) and shows a maximum difference of 0.03m/s at the velocity peak compared with the experiment. The trend for an over-prediction of velocity peak values shown for the SST model for the quasi-2D are also shown for the 3D model (Δv_{max}=0.08m/s compared with the experiments). Both turbulence models display smaller temperature values towards the outer edge of the wall boundary layer compared with the experiments ($\Delta T \approx 2K$).

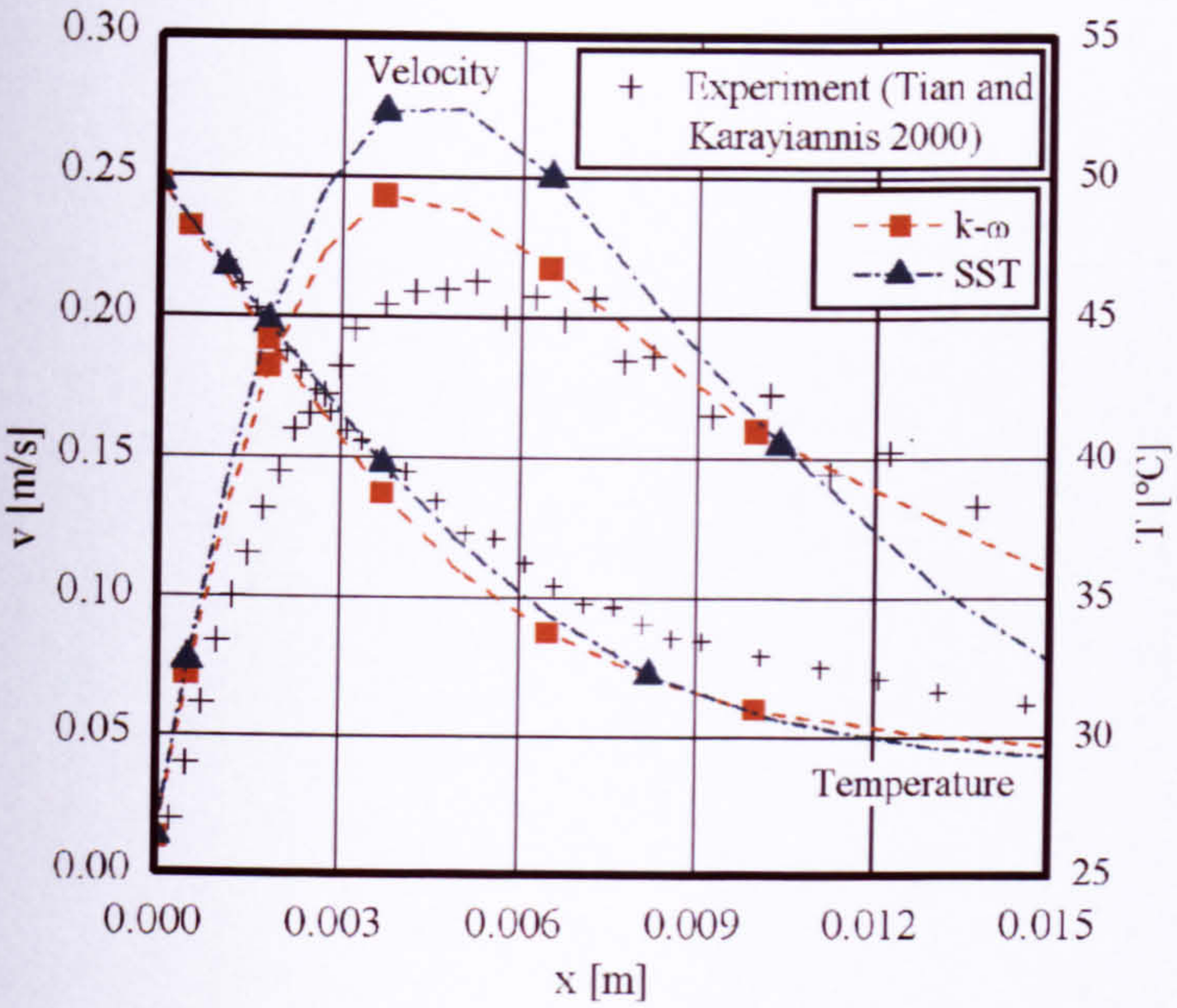

Figure B.21: Predicted vertical velocity components and temperatures in the wall boundary layer for the 3D model at the hot vertical wall at mid height using the k-ω and SST model compared with experimental data.

The local Nusselt numbers from simulations and measurements along the hot vertical wall are shown in Figure B.22. Simulation results for the k-ω and SST model are in good agreement with the numerical and experimental reference data from the top end towards the mid height of the cavity. The simulation under-predicts the heat transfer at cavity mid width using the SST model (ΔNu_{max}=15) whereas the simulation under-predicts the heat transfer at the low end of the vertical wall using the k-ω model (ΔNu_{max}=23). The differences between the simulation results for both turbulence models are mainly thought to be mainly caused by the statistical averaging of Nusselt numbers since both models use the same wall boundary treatment. The Nusselt number peaks at the high and low end of the vertical hot wall are the consequence of the size of the discrete surface mesh elements. However, the Figure B.22 shows that this has almost no influence on the surface heat transfer as the air flow rises.

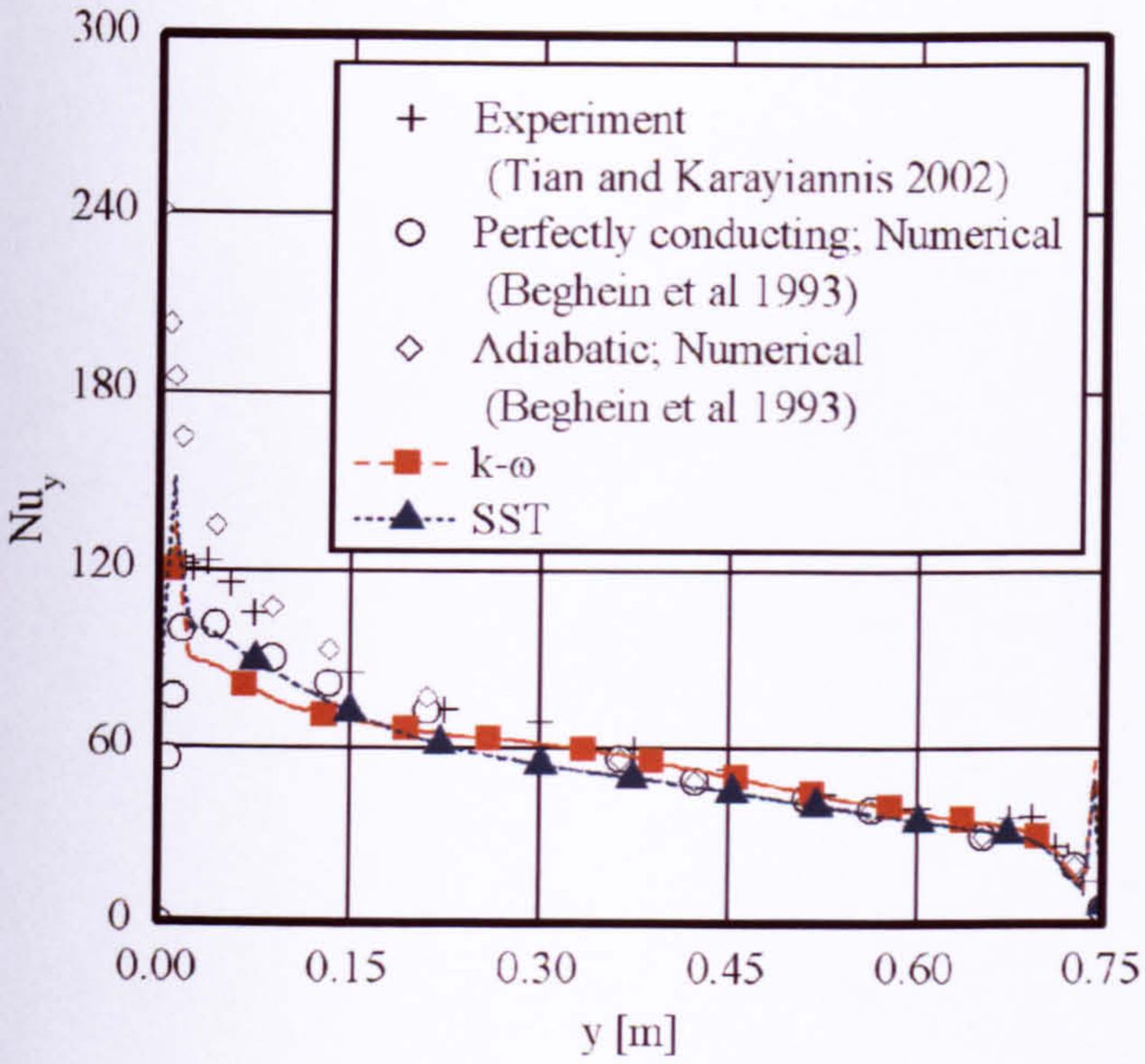

Figure B.22: Predicted local Nusselt numbers at the hot vertical wall for the 3D model using the k-ω and SST model compared with the experimental reference data.

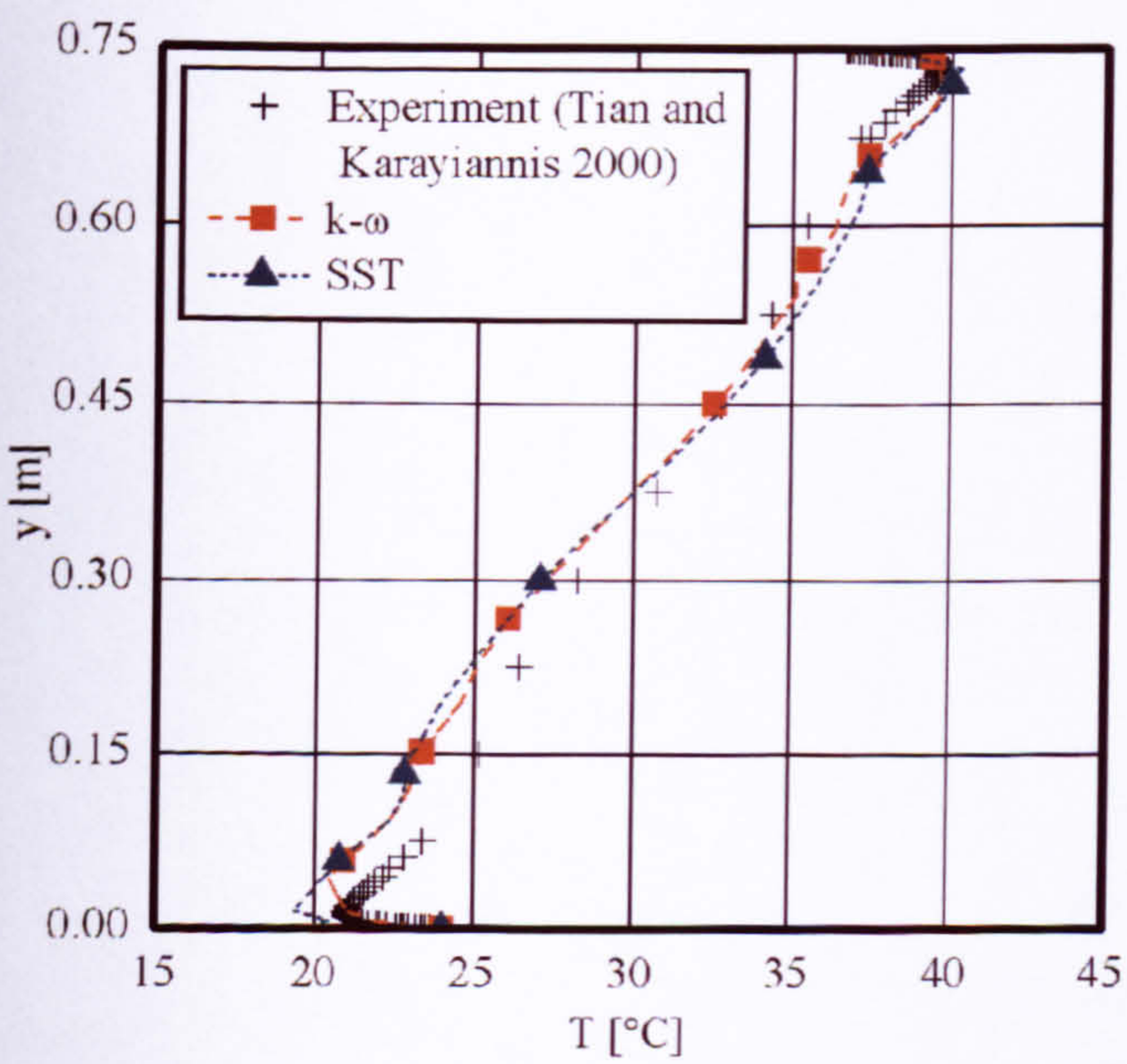

Figure B.23: Predicted temperatures at different heights for the 3D model at mid width using the k-ω and SST model compared with experimental data.

The numerically calculated temperatures at different heights at cavity mid width compared with the experimental reference data are shown in Figure B.23. The results of both simulations agree well with each other. A slightly higher temperature gradient from the bottom to the top of the cavity is displayed away from the horizontal surfaces compared with the experiment.

Figure B.24 shows the velocities (horizontal component) at different heights at mid width of the cavity for the numerical solution in comparison with the experiment. The measured velocity peaks for the main flow direction (clockwise direction) are well represented for the SST model and are under-predicted for the k-ω model (Δu_{max}=0.04m/s). The flow reversal is predicted for both turbulence models although it is slightly under-predicted for both models at the top of the cavity and for the SST model at the bottom of the cavity (Δu_{max}=0.015m/s). The flow reversal at the bottom of the cavity is well predicted using the k-ω model.

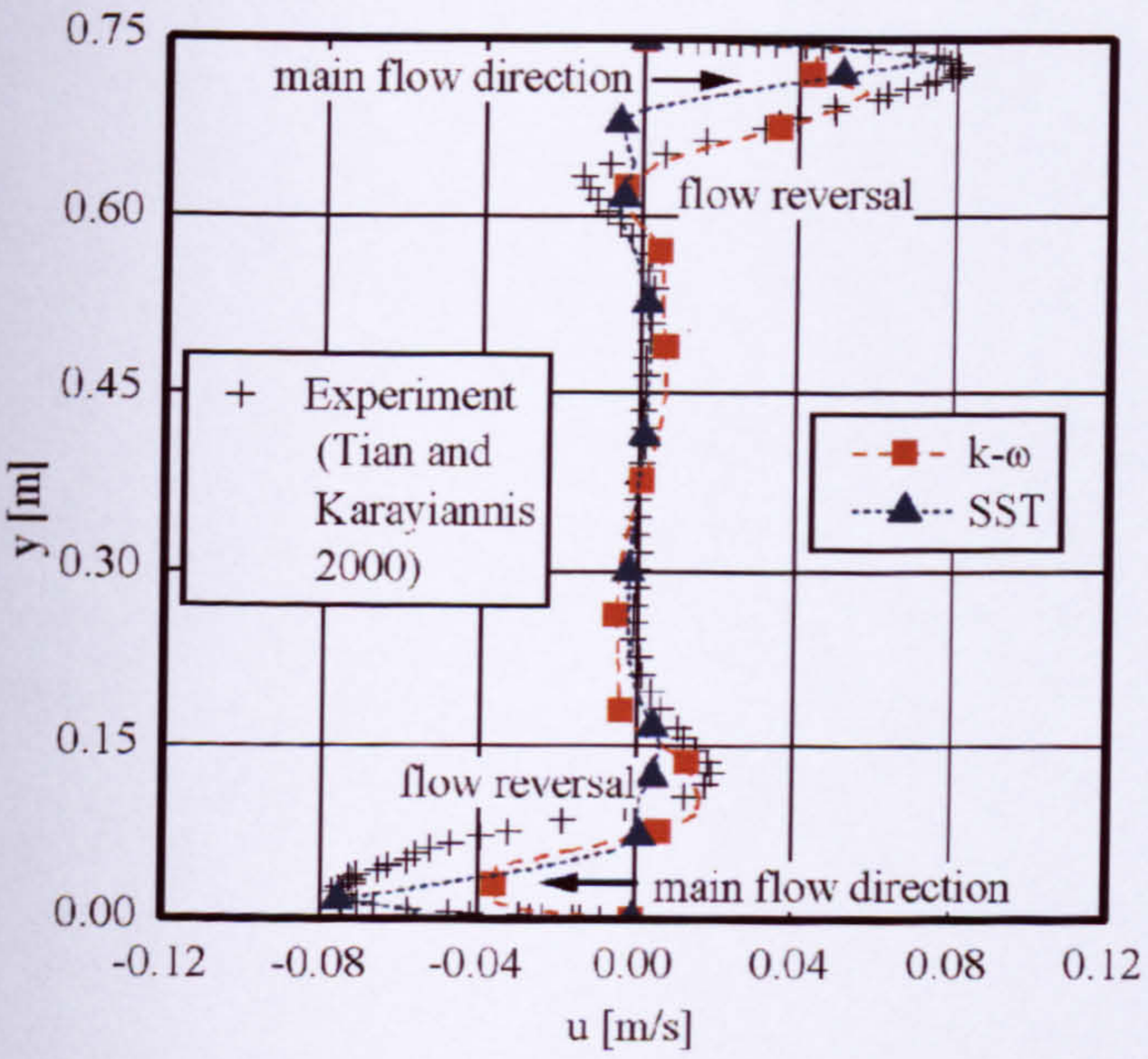

Figure B.24: Horizontal velocity components at different heights at mid width for the 3D model, the flow directions are labelled by black arrows

Flow reversal was not displayed for the k-ω model at cavity mid width when the quasi-2D model was used (see section 3.3.2). A vector plot for the k-ω model at cavity mid

section (z/Z=0.5) of the 3D geometry at the end of the simulation is shown in Figure B.25. In comparison with the quasi-2D model no flow disturbances are displayed in the corners for the 3D model. This would indicate that the flow disturbances for the quasi-2D enclosure were a consequence of the close distance between the high and low end z-planes for which the turbulences could not dissipate in z-direction. Furthermore, comparing Figures B.23 and B.24 with Figures 3.7 and 3.8 demonstrates that the flow disturbances influenced the prediction of the flow reversal in the simulation for the quasi-2D geometry using the k-ω model. The air at the bottom rises due to buoyancy forces at the bottom left corner before it reaches the hot vertical wall in Figure B.25. This is not displayed in Figure 3.8 for the quasi-2D model. As mentioned at the beginning of this section, the flow characteristics are transient. It is therefore thought that the phenomenon shown in Figure B.25 is a transient effect.

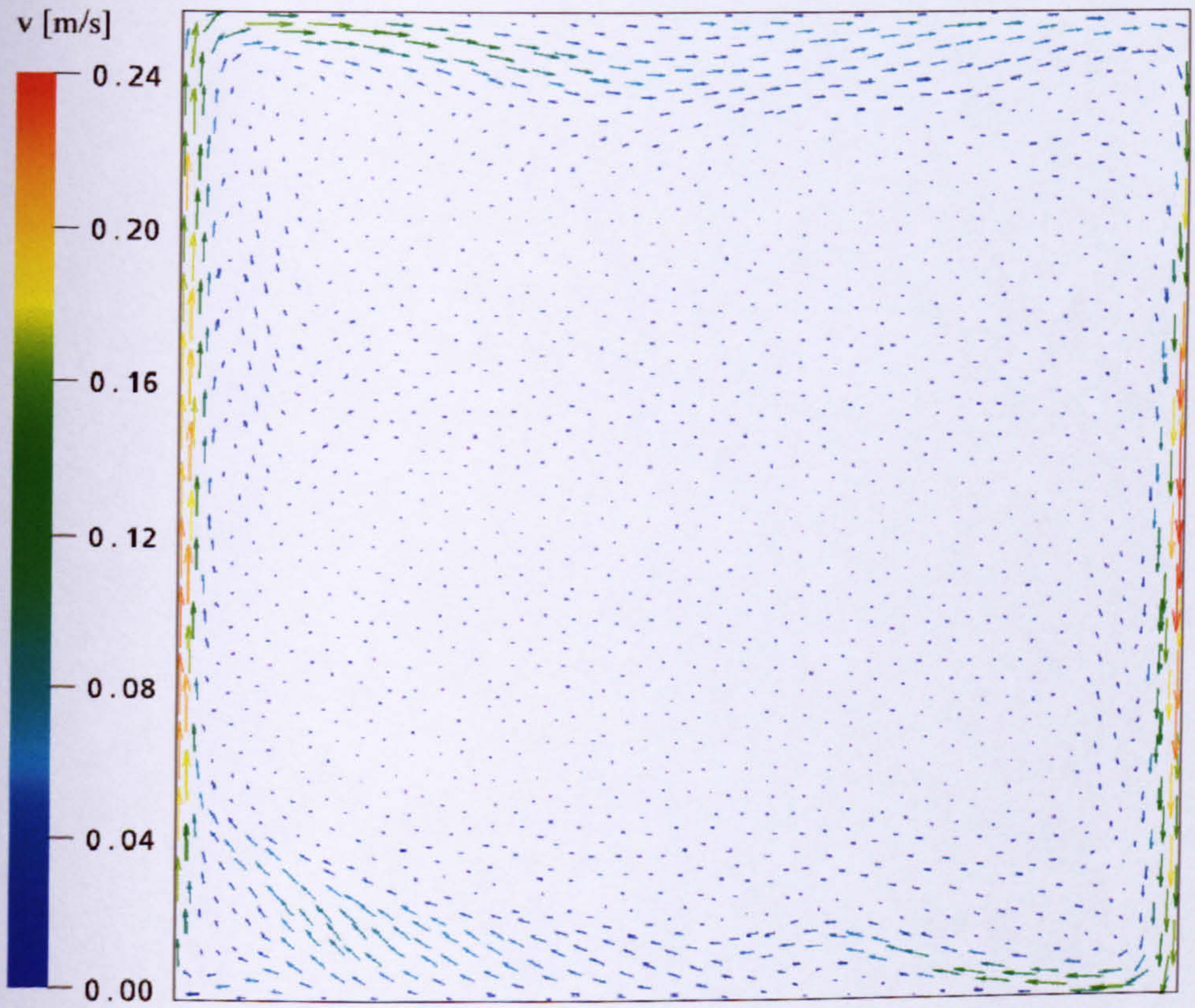

Figure B.25: 3D air flow patterns for the 3D model using the k-ω model.

B.2.5 Investigation of the mesh resolution on the convective surface heat transfer

The over-all aim of research is the dynamic simulation of the thermal room behaviour using CFD. Thus, an accurate prediction of the surface heat transfer is important. However, a fine mesh resolution requires high computational resources. The influence of the surface and core mesh size of the cavity from section B.2.4 is investigated in this section to find a trade-off between accuracy and computational effort.

Model Description

The model geometry and boundary conditions of section B.2.4 are adopted.

Model implementation in CFX

The model settings (i.e. advection and transient scheme, discretisation of time, buoyancy etc.) of section B.2.4 are adopted. The k-ω turbulence model is applied. A fine mesh was used in sections B.2.3 and B.2.4 for which a good agreement was obtained with experiments. The size of the mesh in the wall boundary layer is adopted from section B.2.4. Different surface and core mesh resolutions are used (10mm, 15mm, 20mm, 40mm and 50mm) to investigate the influence of the mesh resolution on the over-all surface heat transfer.

Results and Discussion

The predicted convective surface heat transfer from the hot to the cold vertical wall is compared for different mesh resolutions for the surface and core region. The model with the smallest surface mesh investigated (i.e. 10mm) is thought to give the most accurate solution and is used as the base case. Table B.4 shows the mean heat transfer values obtained for different mesh resolutions. It is shown that the prediction error of the surface heat transfer increases as the mesh resolution is decreased. The reason is thought to be the mesh discretisation at the edges where the vertical and horizontal surfaces approach each other. A refinement of the surface mesh in this region shows that a mesh size with a maximum edge length scale of 50mm is possible without influencing the

surface heat transfer as long the wall boundary layer is sufficiently refined (see Table B.4).

For the quasi-2D geometry in section 3.3.2 an average heat transfer of 2.02W/m^2 is obtained between the vertical hot and cold wall. In comparison with the simulation of the finest surface mesh investigated using the 3D geometry (base case), the difference is only 1%.

Table B.4: Predictions of average heat transfer between the hot and cold vertical wall comparing different surface and core region mesh resolutions.

Maximum mesh edge length scale [mm]	Refinement in the corners [mm]	$\dot{q}_m$ [W/m^2]	Error [%]
10(surface) 20 (core)	-	22.954	0
15	-	23.623	3
20	-	24.138	5
30	-	27.079	18
40	-	27.202	19
40	10mm	24.211	6
40	5mm	23.153	<1
50	5mm	22.987	<1

B.3 Verification of modelling thermal radiation using CFX

B.3.1 Two parallel infinite surfaces of different temperature

Model description

The boundary conditions of the model in section 3.4.2 (Figure 3.10) are modified replacing the adiabatic boundary conditions of the horizontal enclosure surfaces by symmetry boundary conditions.

Model implementation in CFX

Settings for boundary and initial conditions, mesh discretisation, transient and advection scheme are adopted from section 3.4.2. The Monte Carlo and the Discrete Transfer model are investigated for modelling radiation.

Results and Discussion

Simulations are carried out using the Monte Carlo model using 1,000,000 and 200,000 histories, and simulations are carried out using the Discrete Transfer model using 8 rays (default value in CFX). Predictions for the radiative heat flux at surfaces 1 and 3 (see Figure 3.10) are compared with analytical solutions of section 3.4.1 (results are also presented in Zitzmann et al. 2007d).

The predicted maximum, minimum and average wall radiative heat fluxes for the Monte Carlo and Discrete Transfer model after a simulation period of 2h are summarized in Table B.5. For the Discrete Transfer model an average radiative heat flux of 27.7W/m^2 is predicted. No spatial differences are displayed. Similar values are predicted for the Monte Carlo model (27.8W/m^2 for 1,000,000 and 27.6W/m^2 for 200,000 histories, respectively). However, the surface radiative heat transfer ranges spatially considerably for the Monte Carlo model shown by the minima and maxima in Table B.5. This unrealistic behaviour is thought to be caused due to an insufficient long tracking of radiation particles. Figures B.26 and B.27 show the distribution of radiative heat flux for the Monte Carlo and the Discrete Transfer model which reflect the observations shown for Table B.5.

Table B.5: Predicted radiative surface heat transfer for surfaces 1 and 3 using CFX (Parallel infinite plate model); MC=Monte Carlo, DT=Discrete Transfer.

Radiation model	Number of histories/rays	$\dot{q}_1$ [W/m^2]			$\dot{q}_3$ [W/m^2]			CPU time [s]
		Min	Max	Ave	Min	Max	Ave	
MC	1,000,000	20.3	38.4	27.8	-40.6	-19.9	-27.8	33926
MC	200,000	-100.1	60.3	27.5	-58.9	24.5	-27.7	7171
DT	8	27.4	27.8	27.7	-27.7	-27.7	-27.7	280

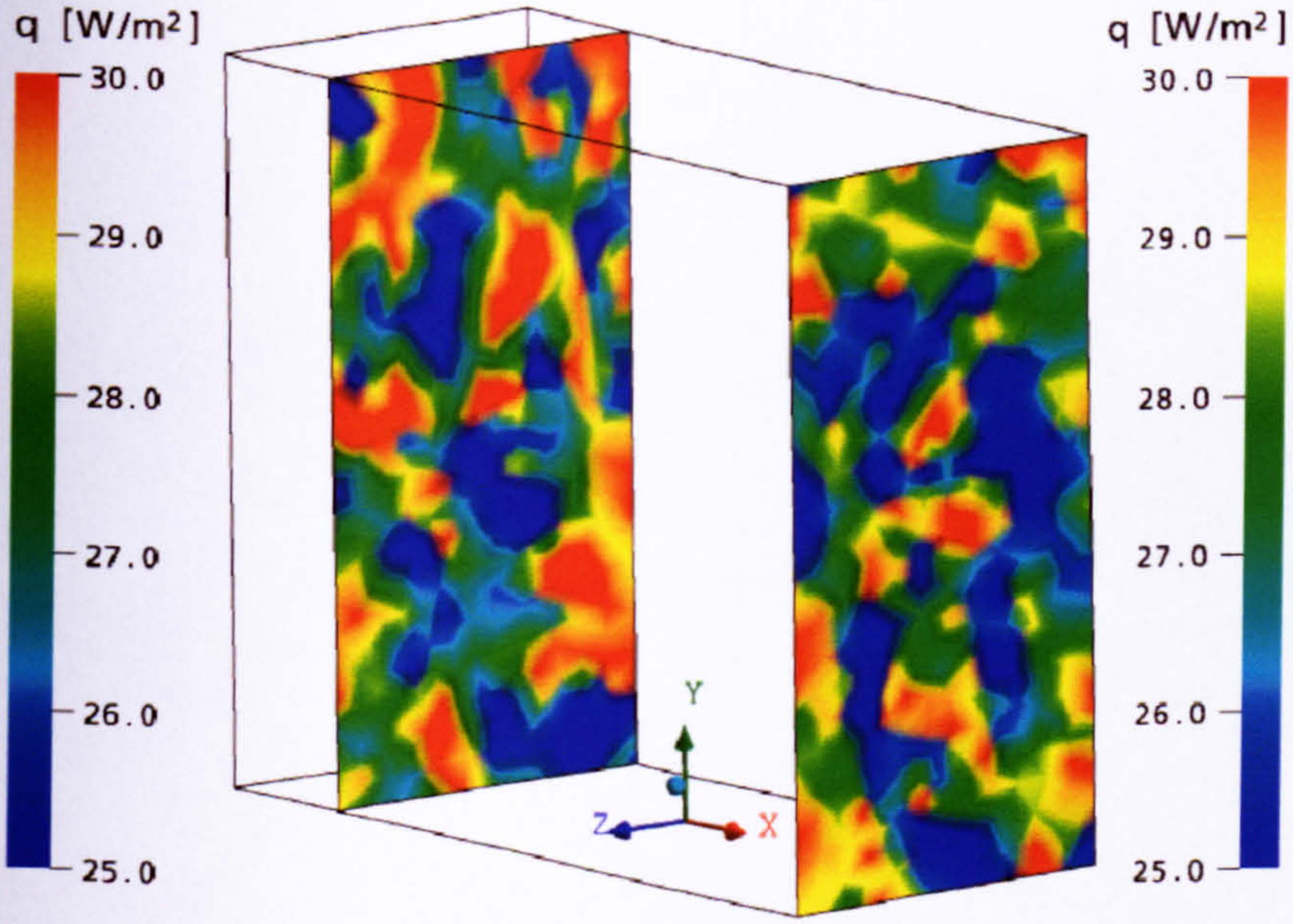

Figure B.26: Predicted wall radiative heat flux for surfaces 1 and 3 using the Monte Carlo model using 1,000,000 histories.

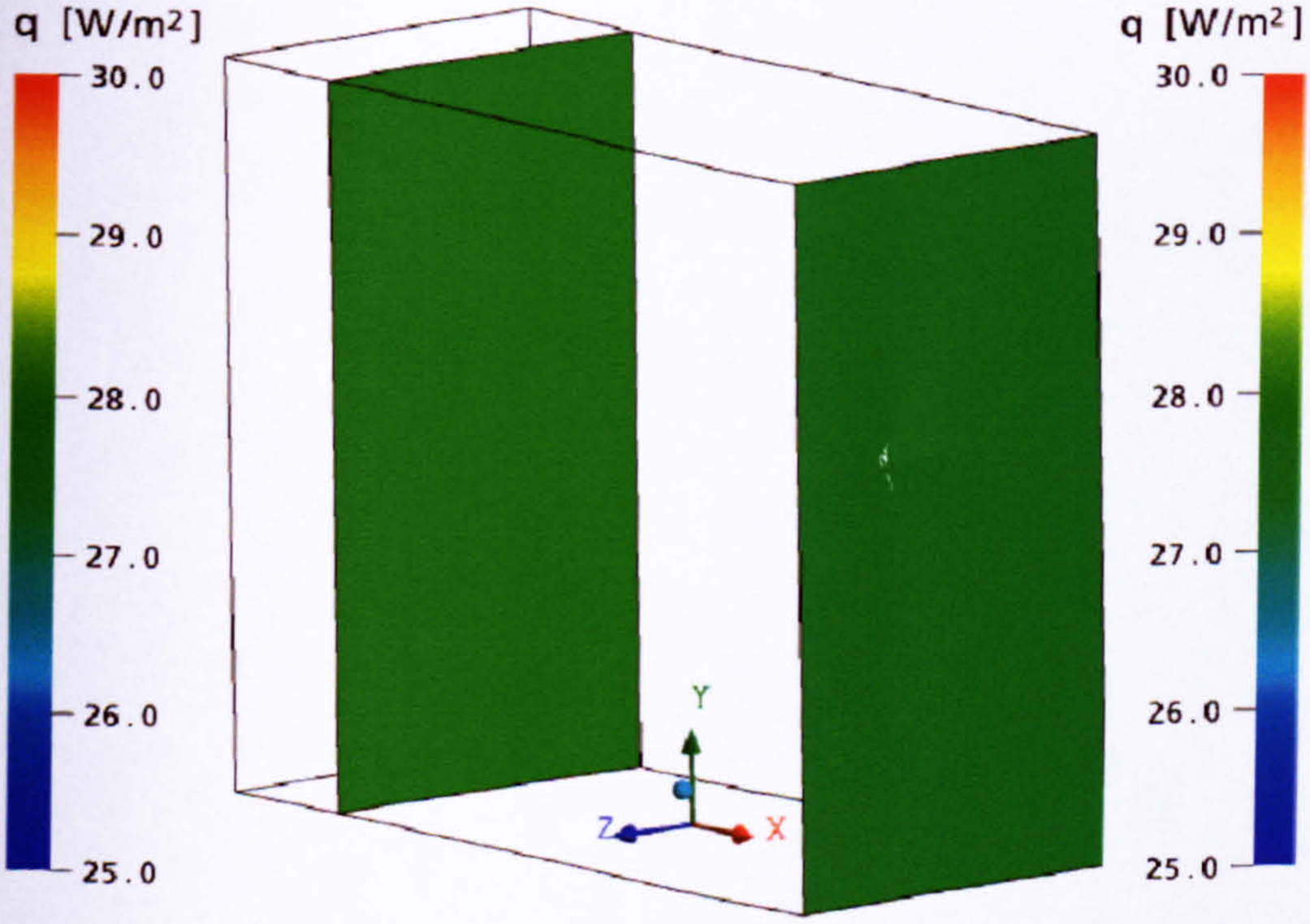

Figure B.27: Predicted wall radiative heat flux for surfaces 1 and 3 using the Discrete Transfer model using 8 rays.

An average temperature of 25.8°C is predicted for surface 1 after a simulation period of 2h. The analytically calculated radiative heat flux for surfaces 1 and 3 is 27.7W/m^2 using Eq. (3.19). The analytical solution compares well with the numerical predictions. However, the Discrete Transfer model shows better over-all results since the Monte Carlo model shows spatially unrealistic behaviour (compare Figures B.26 and B.27). Furthermore, the simulation using the Discrete Transfer model requires less than 1% of the CPU time required by the Monte Carlo model to achieve the same accuracy of the average radiative heat flux (see Table B.26) which suggests using the Discrete Transfer radiation model for modelling dynamic thermal behaviour of buildings.

B.3.2 Radiative heat transfer in an enclosure

Model Description

The model and boundary conditions of section 3.4.2 are adopted for this investigation.

Model implementation in CFX

The settings from section 3.4.2 are adopted (i.e. boundary and initial conditions, mesh discretisation, transient and advection scheme). Different model parameter settings for the Discrete Transfer model and the Monte Carlo model are used as shown in the following section.

Results and Discussion

A parameter variation study is carried out for the Discrete Transfer model investigating the influence of the spatial radiation discretisation (i.e. 8, 15, 30, 50 and 100 rays) on the radiative wall heat flux (see also a summary of results in Zitzmann et al. 2007d).

Table B.6 shows the predicted radiative wall heat fluxes for both radiation models after a simulation period of 2h. The solution is almost constant for ray numbers of 30 and more. However, the computational effort increases significantly for more rays. Small differences exist between the radiative heat flux predictions using less than 30 rays compared with simulations using 30 rays ($\Delta \dot{q}_{ave} \leq 0.8 \mathrm{W/m^2}$). Due to the smaller radiative heat transfer for 8 and 15 rays, the solid wall cools down slightly slower than

for 30 rays and the average temperature of surface 1 is slightly higher (ΔT=0.3K after 2h of simulation).

Table B.6: Predicted radiative surface heat transfer for surfaces 1 and 3 for the Discrete Transfer model using CFX (Enclosure model).

Number of rays	$\dot{q}_1$ [W/m²]			$\dot{q}_3$ [W/m²]			CPU Time [s]
	Min	Max	Ave	Min	Max	Ave	
8	0.1	22.2	20.4	-23.2	-6.3	-20.8	251
15	0.0	23.8	21.5	-24.3	-5.4	-20.6	415
30	0.1	22.4	20.7	-22.9	-6.4	-21.2	1169
50	0.1	22.4	20.8	-22.9	-6.5	-21.2	2389
100	0.1	22.4	20.8	-22.9	-6.5	-21.2	9110

An average temperature of 26.16°C is measured at surface 1 after a simulation period of 2h. Using the boundary conditions of surfaces 1 and 3 (T_1=299.31K and T_3=293.15K) and view factors of φ_{13}=0.42 and φ_{12}=0.29 (with $\varphi_{13}=\varphi_{31}=\varphi_{24}=\varphi_{42}$ and $\varphi_{12}=\varphi_{21}=\varphi_{14}=\varphi_{41}=\varphi_{34}=\varphi_{43}=\varphi_{32}=\varphi_{23}$) from diagrams of Wagner (1998), the equation Eq. (3.20) for B_i can be calculated analytically for each surface:

Surface 1: $B_1 - 0.29 \cdot B_2 - 0.042 \cdot B_3 - 0.29 \cdot B_4 = 172.0124$

Surface 2: $-0.029 \cdot B_1 + B_2 - 0.029 \cdot B_3 - 0.42 \cdot B_4 = 228.0612$

Surface 3: $-0.042 \cdot B_1 - 0.29 \cdot B_2 + B_3 - 0.29 \cdot B_4 = 158.2831$

Surface 4: $-0.029 \cdot B_1 - 0.42 \cdot B_2 - 0.029 \cdot B_3 + B_4 = 228.0612$

A calculation of the linear system gives B_1=443.4866, B_2=436.8988, B_3=430.3109 and B_4=436.8988. The radiative heat absorbed at surface 1 and 3 is calculated inserting the B_i values in Eq. (3.21):

$$\dot{q}_1 = 0.9 \cdot 443.4868 - 0.9 \cdot 5.67 \cdot 10^{-8} \cdot 293.15^4 = \underline{22.27 W/m^2}$$

$$\dot{q}_3 = 0.9 \cdot 430.3109 - 0.9 \cdot 5.67 \cdot 10^{-8} \cdot 299.31^4 = \underline{-22.27 W/m^2}$$

A comparison of numerical results for the Discrete Transfer model with analytical solutions is given in section 3.2.2. The average temperatures at surfaces 2 and 4 are analytically calculated inserting the relevant B_i values in Eq. (3.22):

$$T_{2/4} = \sqrt[4]{\frac{436.8988}{5.67 \cdot 10^{-8}}} = \underline{296.28K}$$

An insertion of B_2, B_4, T_2 and T_4 in Eq. (3.21) results in a heat flux of zero as expected from section 3.4.1 for adiabatic surfaces which cannot store energy.

The Monte Carlo model is investigated using a different number of histories (i.e. 2,000,000, 1,000,000 and 200,000 histories; results are presented here and are also summarised in Zitzmann et al. 2007b) to investigate if the problems which occurred for this model in section B.3.1 are also displayed here.

Table B.7 shows the predicted wall radiative heat fluxes after a simulation period of 2h. The range between minimum and maximum values is about 30W/m^2 for the Monte Carlo model using 2,000,000 histories and the average values obtained for surfaces 1 and 3 are 21.4W/m^2 and 20.9W/m^2, respectively. A reduced average heat transfer is observed for smaller numbers of histories. The average values are similar to those obtained for the Discrete Transfer model.

The differences in average values between surface 1 and 3 for the Monte Carlo as well as for the Discrete Transfer model might be the consequence of (i) numerical inaccuracies due to mesh discretisation and equation imbalances and (ii) heat conduction considered within the transient simulation. The latter case means that the adiabatic surfaces adapt the temperatures to the adjacent air which can lead to a change of the radiative surface heat transfer at the adiabatic surfaces and therefore to a change of the radiative heat transfer at the surfaces 1 and 3 compared with the case in which no thermal conduction is included.

Table B.7: Predicted radiative surface heat transfer for surfaces 1 and 3 for the Monte Carlo model using CFX (Enclosure model).

Number of histories	$\dot{q}_1$ [W/m^2]			$\dot{q}_3$ [W/m^2]			CPU Time [s]
	Min	Max	Ave	Min	Max	Ave	
2,000,000	0	31	20.9	-33.8	-6.0	-21.4	65205
1,000,000	0	35.6	20.5	-34.8	-2.7	-21.0	32736
200,000	-18.4	56.8	19.9	-46.2	10.9	-20.1	6996

Figure B.28 shows the distribution of the radiative heat flux at the surfaces 1 and 3 for the Monte Carlo model. A similar distribution is mapped for the Monte Carlo model as in section B.3.1 for two parallel plates (compare with Figure B.26). The solution shows again an unrealistic radiative heat transfer distribution at the surfaces which is thought to be caused by an insufficiently long tracking of particles.

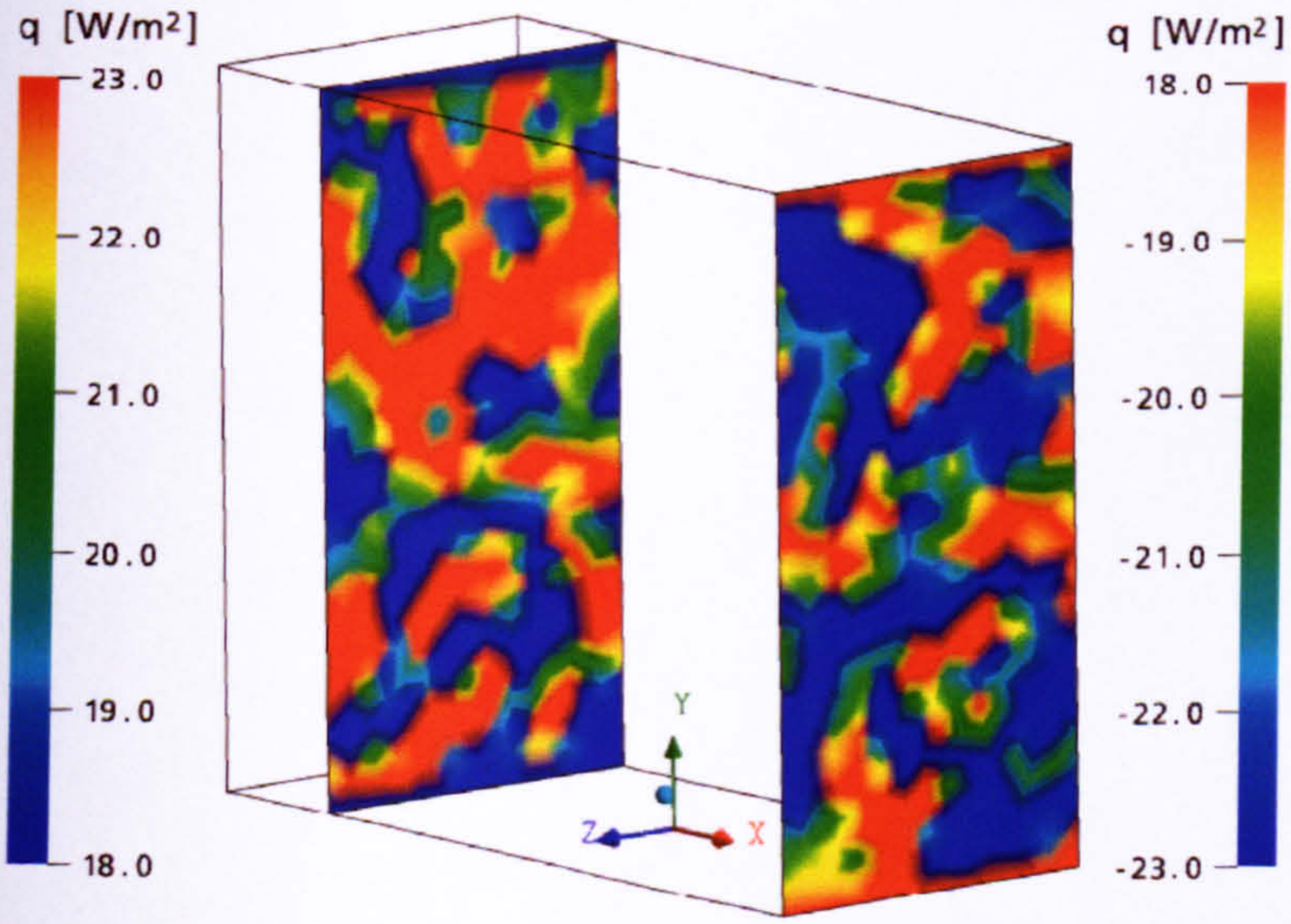

Figure B.28: Predicted wall radiative heat flux for surfaces 1 and 3 using the Monte Carlo model using 1,000,000 histories.

The predicted average surface temperatures obtained for the Monte Carlo model at surface 2 after a simulation period of 2h is 26.16°C. Using Eqs. (3.20) and (3.21) a wall radiative heat flux of 22.3W/m^2 is analytically calculated as shown above. Good

agreement between the Monte Carlo model and the analytical data is achieved using 2,000,000 histories (5% difference) when using the average radiation heat exchange between surfaces 1 and 3. Using a smaller number of histories this leads to higher deviations between predictions and the analytical solution.

However, since the radiative distribution on the surfaces for the Monte Carlo model is unrealistic and the simulations require high computational resources (see Table B.7), this suggests that the Monte Carlo model is unlikely to be suitable for dynamic thermal building simulations.

APPENDIX C

PRELIMINARY STUDIES USING THE FREEZE-FLOW METHOD

C Preliminary studies using the freeze-flow method

This section shows preliminary CFD results of modelling dynamic thermal room behaviour using the freeze-flow method. This includes a comparison of different freeze-flow methods and sensitivity studies of key parameter settings for the CFD methods.

C.1 Transient-transient and transient-steady method

Two basic principles of the freeze-flow method have been presented in Somarathne (2003), the transient-transient method for which the thermal and flow fields are updated in an unfrozen flow period using a transient calculation scheme and the transient-steady method using a steady-state scheme for the update instead. To test if both freeze-flow methods can be transferred to the CFD program CFX, the room model of benchmark 1 was used here.

The CFX pre-processor used for model definition setup contains an expert parameter section of Boolean parameters determining whether equations are calculated or frozen. The controlling Boolean for Eq. (A.13) and (A.14) is 'solve fluids', for Eq. (A.15) it is 'solve energy' and for Eq. (A.19) and (A.20) it is 'solve tke omega'. These Booleans are used in the model set up in order to apply the manually controlled freeze-flow procedure.

For investigation the model boundary conditions of case 3 (i.e. cooling of a massive wall in an enclosure by free convection) were used since a similar case was used by Somarathne (2003). The CFD code used by Somarathne contains an option for which the energy equations for solid and fluid domains can be frozen separately. This is necessary when the steady-state scheme is used for the flow update during unfrozen flow periods. Otherwise the simulation would proceed until equilibrium (i.e. a linear temperature distribution is obtained throughout the solid). However, an option for a separation in domains does not exist in CFX. An alternative was found using a physical time step for the solid domain for the steady-state scheme which is significantly (i.e.

1000 times) smaller than the time step used for the fluid domain. Since the thermal time constant of the building fabric is significantly larger than for air, the thermal distribution in the solid domain thus changes only marginally until a quasi steady-state condition is achieved in the fluid domain.

The periods of frozen and unfrozen flow were started manually using the previous solution as initial condition, as in Somarathne et al. (2002). In this research a time step size of 2s was used throughout the frozen flow periods in order to calculate the turbulence flow characteristics and to achieve convergence. For the transient-transient case the same time step size was used for the unfrozen flow period, while for the transient-steady method physical time steps of 1s and 10^{-3}s were used for the fluid and solid domain, respectively. A period of 1h was provided as preconditioning time for the air flow and temperature patterns to develop. Both freeze-flow methods were then compared with the base case (i.e. full dynamic CFD simulation) for a subsequent simulation period of 4h which contained one frozen and one unfrozen flow period. In the transient-transient case the frozen flow period remained for 3h50min and the following unfrozen flow period for 10min; in the transient-steady case a steady-state calculation followed a transient period of 4h. The output data was stored every 10min. The transient-transient and the transient-steady simulations were considered to have converged when a RMS normalised residual of 10^{-5} was achieved for the equations calculated (i.e. RANS equations and energy equation for the unfrozen and frozen flow periods, respectively).

The resulting velocities (vertical components) and temperatures at different monitor points (see Table 5.1) are shown in Figures C.1 and C.2. Figure C.1 displays constant vertical velocities at MP 7 and MP 8 during the frozen flow period which starts after the preconditioning period of 1h. The deviation to the base case increases gradually throughout the simulation. Afterwards a step in the velocity curves appears which approach the values of the base case. At the end of the frozen flow period at 0500 the velocity values agree well with the base case. A similar behaviour is shown for monitored temperatures in Figure C.2. At the end of the unfrozen flow period the temperature curves approach those of the base case. Figure C.3 shows the temperatures at MP5 in detail. Only the curve for the transient-steady method shows a slight under-

prediction of 0.25K at the end of the unfrozen flow period. The reason is thought to be the thermal lag of air which is neglected in steady-state solutions. Compared with the base case, the CPU time was reduced by 76% and 77% using the transient-transient and transient-steady method, respectively.

However, an unexpected thermal behaviour was observed for both manually controlled freeze-flow methods when the simulation was restarted in frozen mode. At the beginning of the simulation a temperature step is displayed at MP 3 and MP 5 in Figure C.2 which does not appear for the velocity curve shapes in Figure C.1. A parametrical study was carried out using different time steps for the frozen flow period. The temperature curves in Figure C.4 show that the result is independent of the time step size. In contrast, the temperature steps disappeared when the automated freeze-flow approach described in chapter 4 was applied after the preconditioning period of 1h (see Figure C.2). A small deviation of less than 0.05K compared with the base case exist at the end of the frozen flow period in Figure C.3 due to the over-predicted convective surface heat transfer from the frozen-flow condition and results agree again well with the base case at the end of the unfrozen flow period (see Figure C.3). The reason for the discrepancy for the manual approaches is thought to be the internal initial interpolation procedure of the CFD program at the beginning of the frozen flow periods.

The investigation has shown that the freeze-flow methods (i.e. transient-transient and transient-steady) can be applied to CFX whereby both methods have shown a similar performance. However, the transient-transient method has exhibited a slightly better performance since it does not neglect the thermal lag of air. An automated approach improves the accuracy of the results.

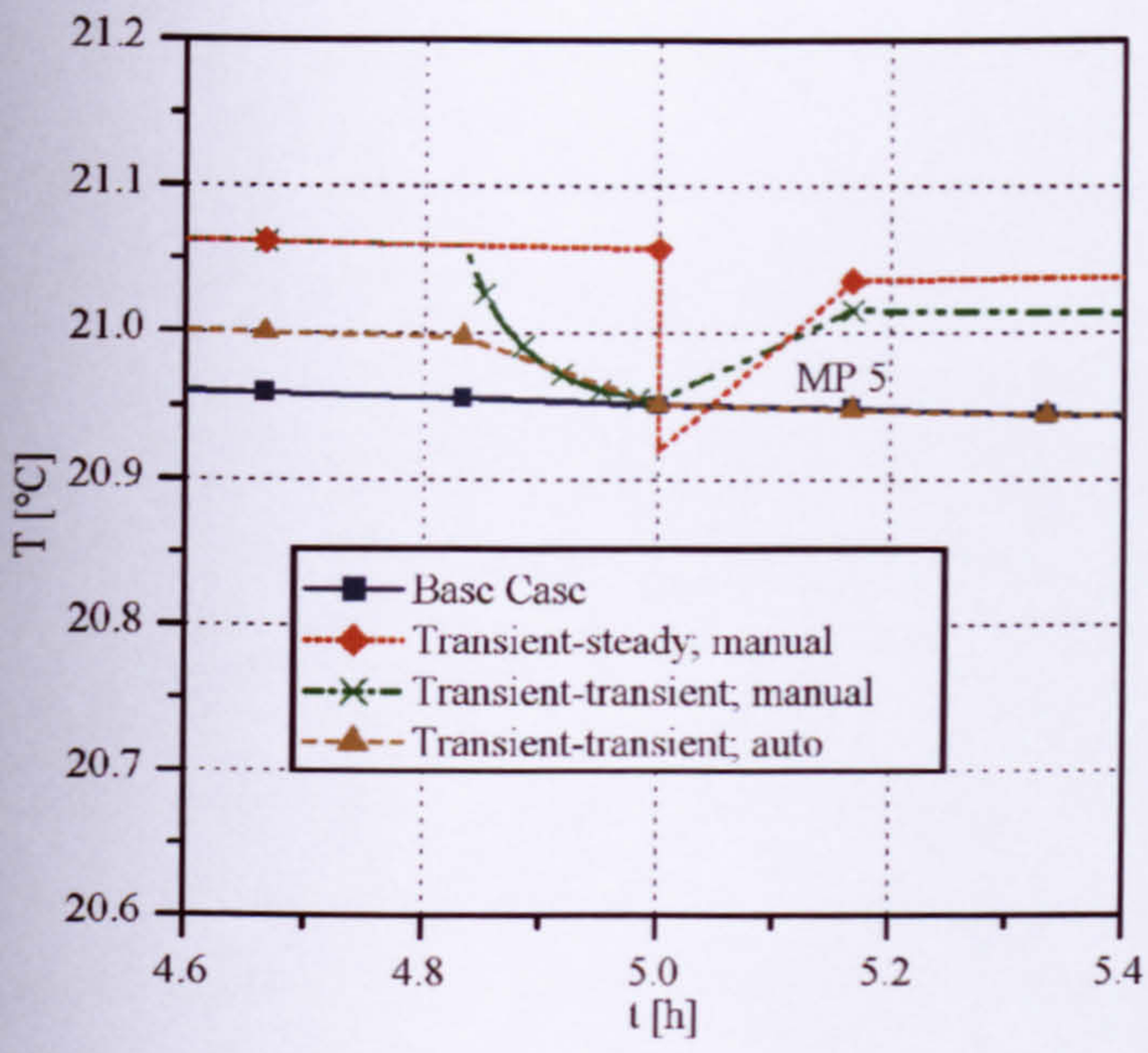

Figure C.3: Detailed plot of temperature predictions at monitor point MP 5 for the manual and automatic transient-transient and manual transient-steady freeze-flow method (Benchmark 1, Case 3).

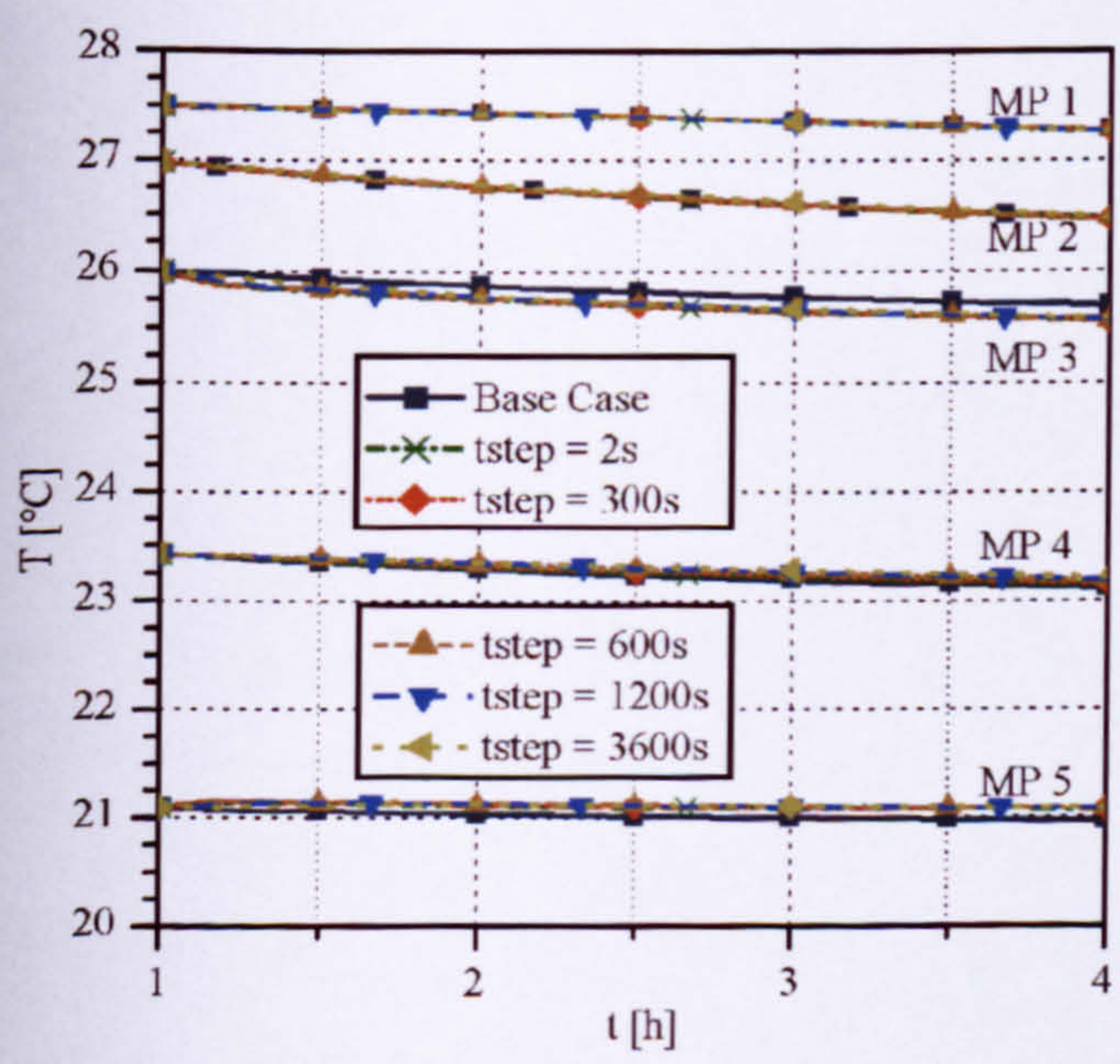

Figure C.4: Temperature predictions for the manual transient-transient freeze-flow method using different time step sizes for the frozen flow period (Benchmark 1, Case 3).

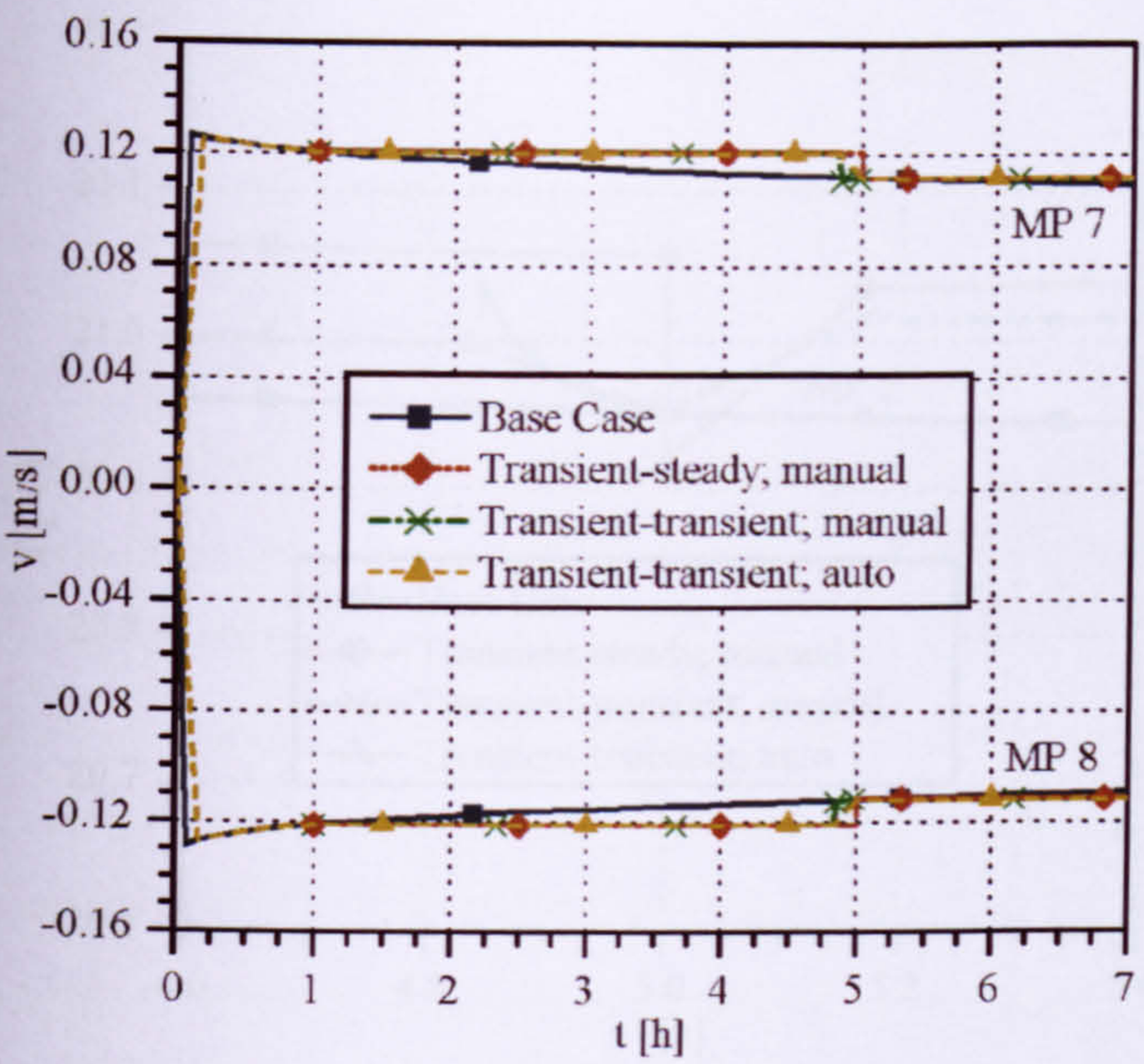

Figure C.1: Velocity predictions for the transient-steady and transient-transient freeze-flow method (Benchmark 1, Case 3).

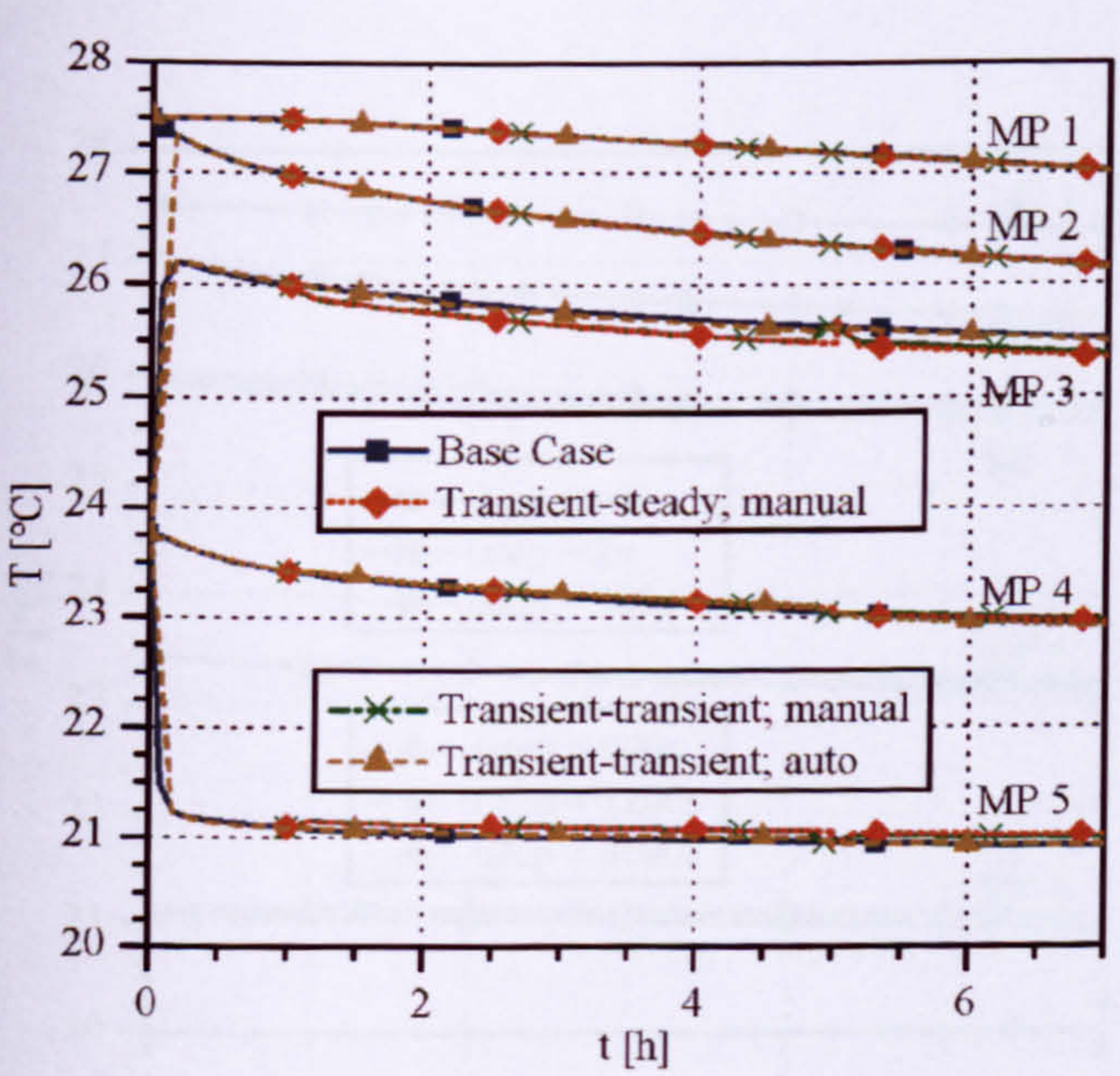

Figure C.2: Temperature predictions for the transient-steady and transient-transient freeze-flow method (Benchmark 1, Case 3).

C.2 Freeze-flow key control parameter settings

Investigations were carried out to determine key parameter values for both freeze-flow control methods to achieve a trade off between error and computation time. Benchmark 1 of section 5.2 for the cooling of a massive wall was used. The space for case 1 (natural ventilated space) is expected to contain large regions of unstable and weak flow regions since free convection due to temperature differences at a surface can only occur at the solid-fluid interface. Furthermore, the speed at the openings is thought to be too small to have a significant impact on the air flow patterns in the room. Thus convergence problems can occur and errors which might occur due the freeze-flow methods can remain for long time until they have declined. Hence, case 1 needs a more restrictive range of relevant freeze-flow parameter values compared with the other test cases. Investigations therefore focused on case 1.

A small time step of a few seconds is required to achieve convergence when all equations are solved. In periods in which only energy equations are solved, time step sizes can be increased without any loss in accuracy leading to a reduction in CPU time as shown by Somarathne (2003). However, in order to react sufficiently quickly to changes in boundary conditions, the period should be limited to a few minutes.

C.2.1 Invariable control method

For investigation, time step sizes of 1s and 300s were used for the unfrozen and frozen flow periods, respectively. Frozen flow periods of 30min and 60min were tested for the invariable control method and results were compared with a fully dynamic CFD simulation (base case). A length of 300s was considered for the unfrozen flow periods since the temperatures were already close to those of the base case after this time in section C.1. A preconditioning time of 1500s at the beginning of the simulations ensured a full development of the thermal and air flow patterns before the first frozen period started.

Smooth temperature curve shapes are displayed at the monitor points for simulations of 30min frozen flow intervals and results compare well with the base case (Figure C.5). Only for the monitor point at mid height of the air domain do the temperature shapes

show small deviations of less than 0.05K (and 0.15K at the beginning of the simulation) compared with the base case. In contrast, for simulations which use 60min frozen flow intervals the air flow field begins to oscillate in the room centre (maximum amplitudes of 0.2 K after a simulation time of 12h, see MP 4). The reason for the oscillation is thought to be due to the sudden change of the air flow rate at the bottom opening after the switch from frozen to unfrozen flow mode which causes a strong momentum impulse into the weak and unstable flow region. The unfrozen flow period is then shorter than the time the impulse would need for a full declination. The oscillation propagates to other room regions as for example shown in MP 5).

The investigation has shown that accurate results can be obtained for benchmark 1 case 1 using the invariable control method using unfrozen flow periods of 5min and frozen flow periods of 30min.

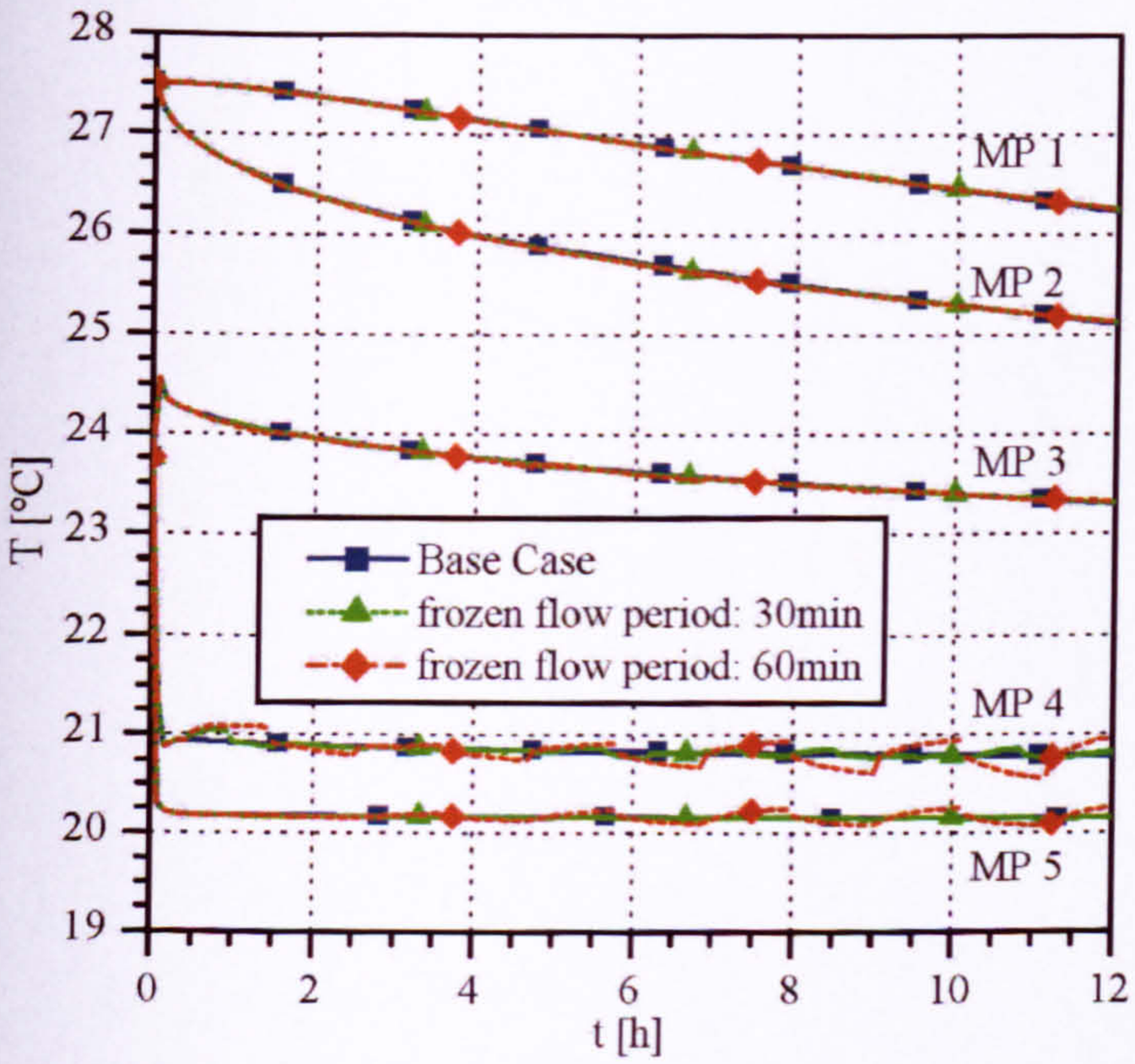

Figure C.5: Temperatures at monitor points for frozen flow periods of (a) 1800s and (b) 3600s using the invariable control method (Benchmark 1, Case 1).

C.2.2 Adaptive control method

For the base case and unfrozen flow periods a time step size of 1s was used as in section C.2.1. For the frozen flow period a time step size of 1min was used which is smaller than that used for the invariable control method in an attempt to react more precisely and quicker to changes in the thermal conditions and thus to ensure a switch to an unfrozen flow period at the appropriate time. This was not necessary for the invariable control since frozen and unfrozen flow periods were fixed. No temperature plots are shown for the following parametrical study since the number of parameter variations and curves was large.

The parameter 'EXTENSION' was varied in the range 5 - 900s. Simulations using a value of 300s and above showed good agreement with the base case. However, higher values resulted in a reduction of CPU performance without improving the solution significantly (for example, 600s gave 7% less time reduction than 300s). Values below 300s resulted in oscillations which propagated throughout the entire room (for example an oscillation with amplitudes of 0.1K at the bottom of the room for a value of 240s). Although a small local oscillation might be negligible for the dynamic thermal room behaviour, if it increases in strength and propagates throughout the domain, the method becomes ineffective because the frozen flow period is reduced or even eliminated.

For 'MAXLOOPS', values of 2 and 3 were investigated. While a value of 2 displayed good results, a value of 3 resulted in a slight propagation of oscillation to the entire room for 'EXTENSION' values of 300s. Although the oscillation for 'MAXLOOPS'=3 disappeared for higher 'EXTENSION' values, a 'MAXLOOPS' value of 2 is favourable in order to keep the unfrozen flow period as short as possible.

The key parameter 'MAXTEMP' was varied in the range 0.06–0.7K with 'MAXLOOPS'=2 and 'EXTENSION'=300s. Larger values resulted in additional CPU time reduction (e.g. 'MAXTEMP' values of 0.1K, 0.2K and 0.7K resulted in CPU times of 45%, 19% and 10% of the base case, respectively) since the lengths of the frozen flow periods were longer. However, larger 'MAXTEMP' values generate larger prediction errors during frozen flow periods resulting in a higher sensitivity to possible

oscillations. A value of 'MAXTEMP' = 0.2K was found to give an optimum trade off between prediction errors and CPU time reduction.

Simulations in which the 1st order backward Euler scheme was used for all equations indicated a slightly better performance compared to the 2nd second order scheme since over- and under-shoots were reduced which can lead to oscillation as stated by Oertel and Laurien (1995). See also 'numerical dispersion' effects in section A.7.

In conclusion, an optimum for case 1 was obtained for parameter values 'MAXLOOPS'=2, 'EXTENSION'=5min, 'MAXTEMP'=0.2K. The value for 'EVENT' had no influence in the case investigated since the user defined boundary conditions were constant.

Compared to the cases 1-3 the thermal conditions are changing faster in case 4 due to the rapid temperature boundary condition changes in Eq. (5.1). A maximum temperature change of about 0.5 K would occur during frozen flow periods of 30min for the invariable control method in this case. For comparison of the performances between the invariable and adaptive control method a value of 0.5K was initially adopted for the parameters 'MAXTEMP' and 'EVENT' of the adaptive control method. Due to the faster changing boundary conditions more iteration numbers are required in case 4. Therefore, 'MAXLOOPS' was increased from 2 to 3. In a test, it was possible to reduce the time period 'EXTENSION' from 300s to 180s without a significant influence on accuracy.

APPENDIX D

ADDITIONAL INFORMATION FOR BENCHMARK 2

D Additional information for Benchmark 2

This section comprises the calculation of the thermal conductivity of single glazed windows for equivalent U-values of double-glazed windows and mesh consistency studies for benchmark 2.

D.1 Thermal conductivity calculation for the window

A standard double glazed window (6/12/6 mm) with a thermal transmittance of $U=2.1 W/(m^2 \cdot K)$ is used in the VDI 6020-1 (2001). To obtain a single glazed window of the same thickness with an equivalent thermal transmittance, a new thermal conductivity was calculated as described in the following.

The thermal transmittance, U is calculated after DIN EN ISO 6946 (1996) as follows:

$$U = \frac{1}{R_e + R_i + \frac{s}{\lambda}} \qquad \text{Eq. (D.1)}$$

Solving Eq. (D.1) for the thermal conductivity, λ [W/(m·K)], and the thickness, s [m], this results in (DIN standard values for internal and external heat resistances: $R_i=0.13 m^2 \cdot K/W$ and $R_e=0.04 m^2 \cdot K/W$):

$$\lambda = \frac{s}{\frac{1}{U} - R_e - R_i} = \frac{0.024m}{\frac{1}{0.48\frac{m^2 \cdot K}{W}} - 0.13\frac{m^2 \cdot K}{W} - 0.04\frac{m^2 \cdot K}{W}}$$

$$\lambda = \underline{0.078\ W/(m \cdot K)}$$

D.2 Mesh consistency study

The following preliminary study was carried out to investigate the dependency of the mesh size on the thermal results for benchmark 2. The model of benchmark 2 was slightly different for the following tests: the glazed material of the window contained a thermal conductivity of λ=2.3W/(m^2·K) and the PVC floor layer was modelled such as stated in the VDI 6020-1 (2001). Benchmark 2.1 (radiative heat source) and benchmark 2.2 (convective heat source) were investigated using different mesh resolutions for the room model. Tables D.1-D.3 contain information about the test room type and the mesh properties (the starting point for prism inflation in Table D.2 is related to the normal distance of the node from the surface). The solid domains are discretised in direction to the surface normal in about 5 elements in all tests. When the model mesh was refined somewhere (e.g. wall boundary layer), it was coarsened elsewhere (e.g. domain core) due to the restriction of the computational capacity. Radiation was only updated at the beginning of each unfrozen flow period to reduce the calculation time. The convergence criterion was a RMS normalised residual of 10^{-4}.

Table D.1: Preliminary mesh consistency tests (Benchmark 2).

Test	Benchmark	Mesh
1	2.1	1
2	2.1	2
3	2.2	1
4	2.2	3
5	2.2	4

Table D.2: Variation of the near wall mesh resolution (Benchmark 2).

Mesh	Height of 1st prism [mm]	Height of 2nd prism [mm]	Prism inflation starts from [mm]	Prism inflation factor	Total number of prisms
1	0.1	0.4	1.0	2.0	9
2	0.1	0.4	0.5	1.2	17
3	0.2	0.8	1.0	2.6	5
4	0.2	0.8	1.0	2.3	6

Table D.3: Variation of global mesh scales for the fluid/solid domains (Benchmark 2).

Mesh	Air domain max surface mesh scale [m]	Air domain max core mesh scale [m]	Solid domain max mesh scale [m]	Total no. of elements x 10^3
1	0.4	0.4	0.7	67
2	0.25	0.25	0.7	152
3	0.2	0.2	0.25	211
4	0.2	0.7	0.25	159

The investigation was restricted to a simulation period ranging from 0600 – 0800 since significant computational time was required. The Figure D.1 shows predicted average air temperatures for tests 1-5 of Table D.1. A comparison of test 1 and 2 demonstrates that the room temperature prediction for benchmark 2.1 is consistent since a refinement of the near wall mesh resolution does not change the results. Test 3 uses the same mesh as in test 1 but refers to benchmark 2.2. Convergence problems occurred for tests 2 and 3 which are thought to result from the extreme stretching of the elements in the near wall region. The surface mesh was therefore refined and the mesh in the near wall region was coarsened (i.e. test 4). Convergence problems were not displayed and results agreed favourably with test 3. However, the simulation was manually stopped after a simulation period of 6.8h since some oscillation of flow patterns occurred in the fluid domain which slowed down the performance of the freeze-flow method. In test 5, the PVC layer was not modelled to reduce the number of total mesh elements and to reduce potential convergence problems due to the extreme stretching of the elements in the layer. The mesh in the core of the domain was coarsened to reduce the total number of elements. Results for test 5 are close to those of the former tests (max ΔT=0.2K) and the freeze-flow method performed well.

Although convergence and oscillation problems were displayed for some of the simulations, the simulation results compared favourably for the test cases. In order to obtain a full mesh consistency, further mesh variation studies and longer simulation periods might be required. This was not possible here due to the restriction of computer resources. The use of a less restricted convergence criterion might improve the robustness of the simulation without a reduction of accuracy.

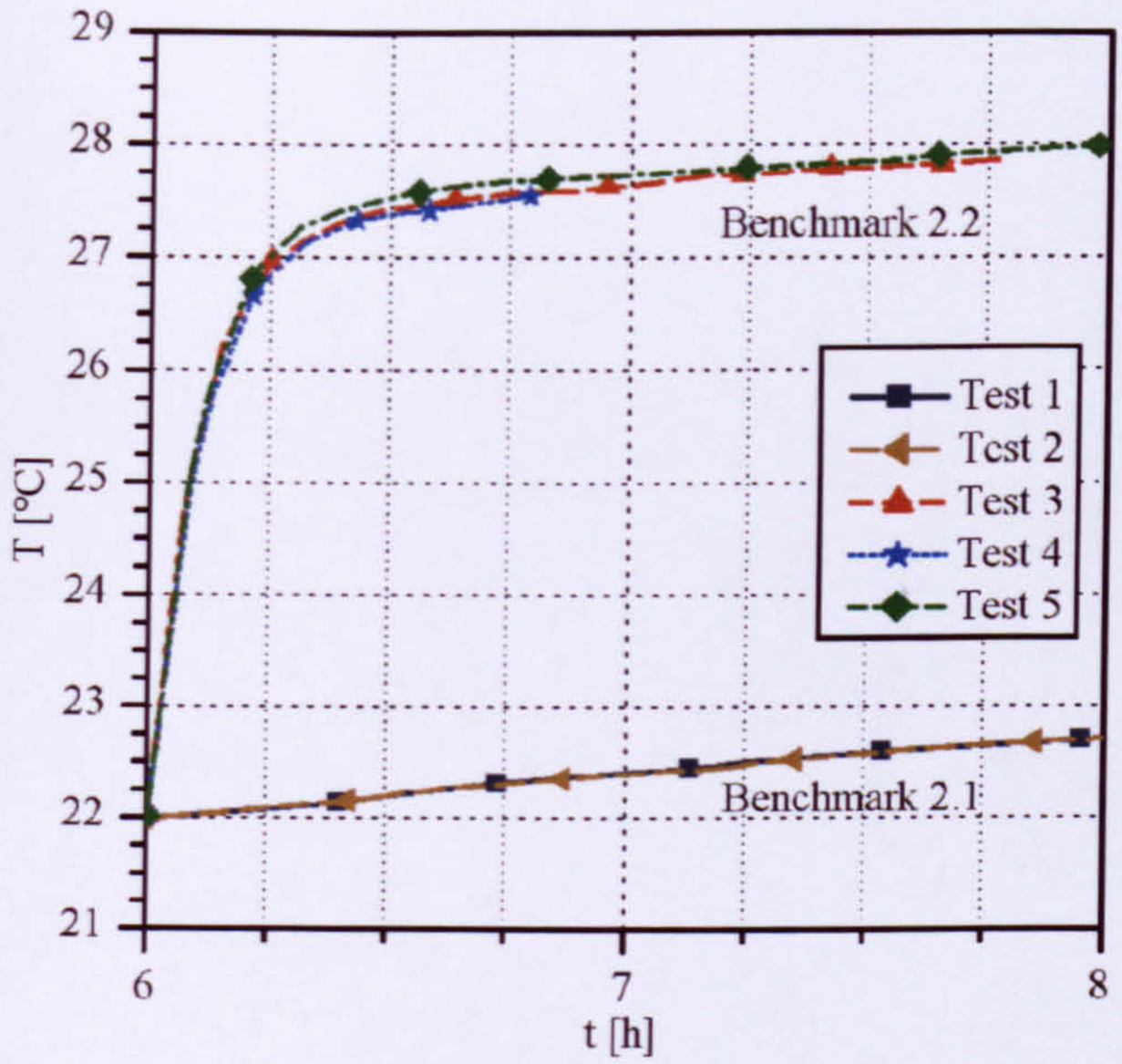

Figure D.1: Predicted average air temperatures for different mesh resolutions for benchmarks 2.1 and 2.2.

APPENDIX E

MESH CONSISTENCY STUDY FOR BENCHMARK 3

E Mesh consistency study for Benchmark 3

A mesh consistency study was conducted for benchmark 3 using CFX. The simulations were restricted to the first 36h of the preconditioning period due to the high computational resources required. A convergence criterion of residual RMS of 10^{-3} was used.

In meshes for which the region of prism layer heights exceeded 37mm, divergence problems existed at the beginning of the simulation which led to a solver crash. This is thought to be caused by flow for which the direction is different from the direction of the element stretching, in the worst case normal to the stretching direction. It was further found that a prism layer height of 0.1mm for the first element close to the wall surface is too small and also leads to a solver crash. It was also found that in the region near the openings the mesh resolution needs to be sufficiently fine to avoid convergence problems. Two meshes were therefore compared which showed convergence over a certain dynamic period.

Mesh 1 consists of a maximum mesh element edge length scale of 0.4m for the core of the fluid domain and a maximum length scale of 0.35m for the room surface discretisation. At the openings, the maximum element edge length is 0.025m with gradual mesh inflation (i.e. increase) of factor 2.3 into the air space. The solids contain a maximum mesh length scale of 0.30m (except for the ceiling where it is 0.4m) and are discretised in direction to the surface normal in about 5 elements using prism elements. Prism layers with a first prism layer height of 0.2mm followed by 3 additional layers with a prism inflation factor of 2.8 is used to refine the near wall region of the fluid domain.

Mesh 2 contains a maximum element edge length scale of 0.4m in the fluid domain and the solid domains. The mesh resolution at the openings is 0.025m using a mesh inflation into the air space of factor 2.8. Prism layers with a first prism layer height of 0.2mm and 7 additional layers using a prism inflation factor of 1.9 are used to refine the near wall region.

Figure E.1 shows the average surface temperatures for the ceiling and floor and average air temperature predictions for CFX for both mesh cases for the first 36 simulation hours. The surface temperatures agree well for meshes 1 and 2. For the air, the predicted diurnal temperature swing is slightly larger using mesh 2. During the day a maximum difference of 0.4K and during the night a maximum difference of 0.2K exist comparing simulations of meshes 1 and 2. This indicates a slightly better coupling between the air and the thermal mass of the building fabric for mesh 1.

The length of frozen flow periods were significantly reduced at the end of the simulation period using mesh 2 which is thought to result from the extreme stretching of the prism layers which therefore led to convergence problems. Thus, mesh 2 is not recommended for long dynamic thermal simulations. Although further detailed studies are required to find a full mesh consistency over the entire simulation period, this was not possible due to the restriction of computational resources.

Since a well converged solution was obtained for mesh 1 which led to a high efficiency for the adaptive freeze-flow method and since the errors were small compared with mesh 2, this mesh was recommended for further studies with this room model.

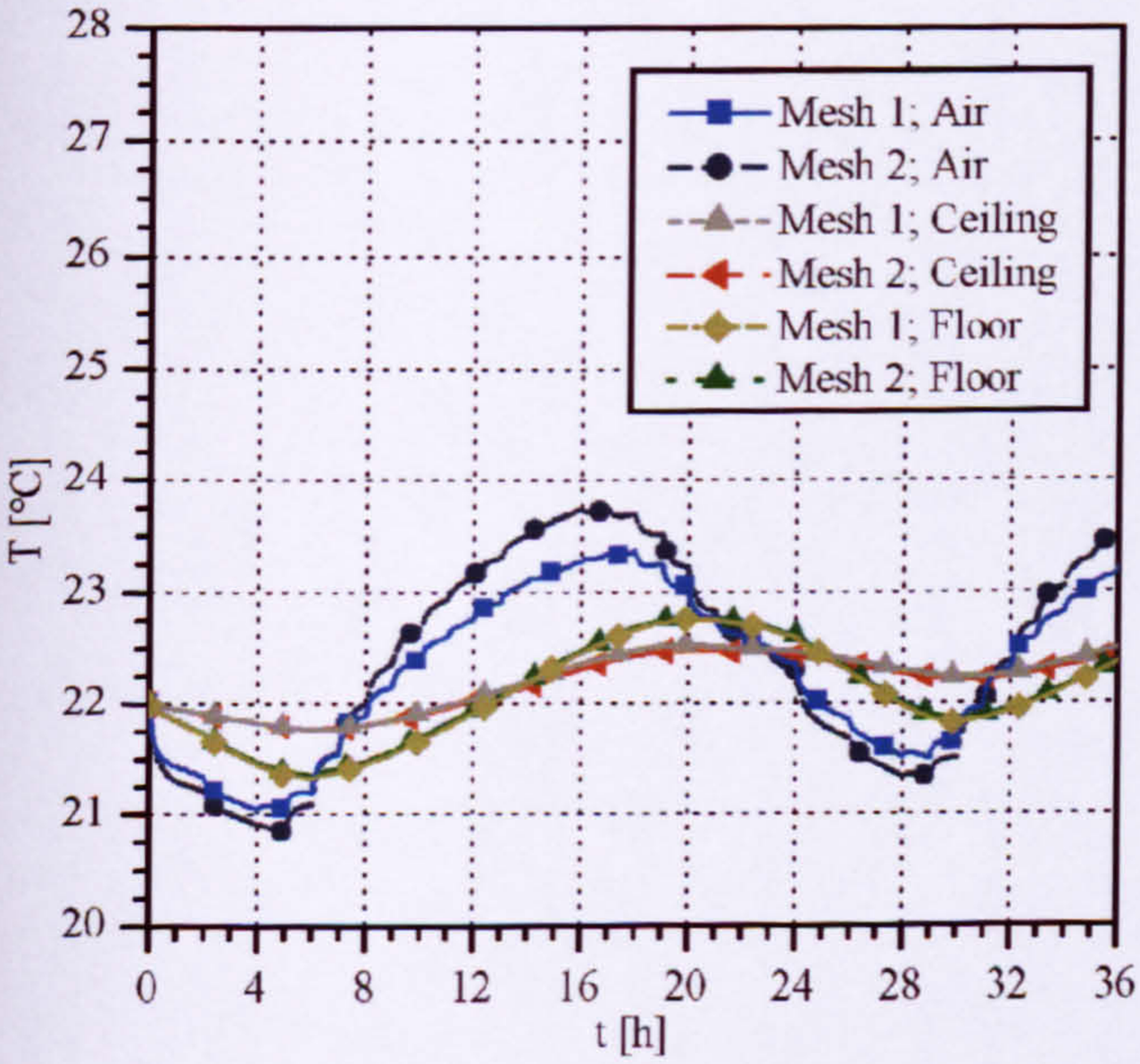

Figure E.1: Predicted average air temperature and surface temperatures for the ceiling and the floor using CFX for different mesh resolutions (Benchmark 3).

APPENDIX F

PUBLICATIONS

F Publications

This chapter comprises the journal and conference papers published or accepted for publication during the research.

PAGE NUMBERING AS ORIGINAL

Ninth International IBPSA Conference
Montréal, Canada
August 15-18, 2005

SIMULATION OF STEADY-STATE NATURAL CONVECTION USING CFD

Tobias Zitzmann[1], Malcolm Cook[2], Peter Pfrommer[1],
Simon Rees[2], Ljiljana Marjanovic[2]
[1]University of Applied Sciences Coburg, Germany, [2]Institute of Energy and Sustainable *Development, De Montfort University, Leicester, UK*
Email: zitzmann@fh-coburg.de, Tel: *+49 9561 317 302*
Email: mcook@dmu.ac.uk, Tel: +44 116 257 7969

ABSTRACT

This paper investigates the air flow and heat transfer over a heated vertical plate and in a differentially-heated cavity using Computer Fluid Dynamics (CFD).

Parametric studies have been carried out to investigate the influence of near wall mesh density on air flow and heat transfer for natural-convection. Benchmark models have been used for steady-state simulations of laminar and turbulent free-convection flow for different turbulence models. Results have been validated with experimental data (Tian et al, 2001) and analytical predictions (Ostrach, 1956).

Appropriate meshing parameters and turbulence models were found which gave results which agreed well with the experiment and analytical data.

Key words: CFD, free convection, buoyancy, turbulence, heat transfer, Nusselt number, cavity

INTRODUCTION

A large part of building energy consumption world wide results from air-conditioning, mechanical ventilation and mechanical cooling. To achieve a comfortable interior climate without high energy demanding cooling components the building fabric is often used. For example, in the night-time cooling concept the solar and internal heating loads absorbed into the fabric during the day are re-emitted to the room and exhausted out of the building during night-time ventilation. The simulation and evaluation of these strategies demands the correct prediction of heat transfer between the building structure and interior. The heat transfer depends on the velocity and temperature distribution in a room, especially in the wall boundary layer. Free convection is typically the main driving force of the flow. However, using CFD for modelling these flows in enclosures is difficult since the buoyancy forces produce a weak coupling between the enthalpy and v-momentum equations, and accurately predicting the heat transfer coefficient at the surface is highly dependent on the mesh size. Very little literature is available which offers guidance on how to model buoyancy-driven flows using unstructured meshes in CFD, since most authors used structured mesh in the past (e.g. Peng and Davidson, 1999 and 2001, Thompson, Wilkes and Jones, 1985).

This paper provides guidelines on how to use CFD with unstructured meshes to model buoyancy-driven flow in a cavity. Benchmark CFD results are compared with published analytical data of Ostrach (1956), hereafter refered to as Ostrach, experiment data of Tian and Karayiannis (2001), hereafter refered to as TK, and numerical solutions of Berghein, Penot, Mergui and Allard (1993).

The paper is devided into three sections: 'Simulation Models', which gives details of the CFD code used and definitions of the boundary conditions; 'Results and Discussion', in which the comparisons between the CFD predictions and the analytical/experimental data are analysed; 'Conclusions', which summarize the most accurate method for modelling these flows with the CFD code used.

SIMULATION MODELS

Introduction to the CFD Solver

The CFD code used in this work uses CFX-5 (Ansys CFX (2003)) and is based on a finite volume method which uses an unstructured mesh containing tetrahedral and prism elements. This has the advantage that local numerical diffusion is reduced and is therefore suitable for complex flows with e.g. flow reversal. The code is based on a coupled solver for solving the differential equations using the fully implicit discretisation method and treating the hydrodynamic equations as one single system. To reduce the number of iterations required for convergence, a false-time stepping method is imposed which guides the approximate solutions in a physically based manner to a steady-state solution. Buoyancy is modelled using the Boussinesq approximation in which the forces are modelled as source terms in the momentum equations.

Various models exist in CFX-5 code for modelling turbulent flow. Two-equation models based on the eddy-viscosity concept include the k-ε (Launder and Spalding, 1974), k-ω (Wilcox, 1998) and Shear Stress Transport (SST) k-ω based (Menter, 1994)

models. Compared to the commonly used k-ε turbulence model, the k-ω model implies a new formulation for the near wall treatment which provides an automatic switch from a wall-function to a low-Reynolds number formulation based on the near-wall grid spacing. This makes it more accurate and more robust. The turbulence viscosity is assumed to be linked to the turbulence kinetic energy (k-equation) and turbulent frequency (ω-equation) instead of the turbulence dissipation rate (ε-equation in the k-ε model). To overcome the sensitivity of the k-ω model to freestream conditions, the SST model was developed. It blends the k-ω model near the surface with the k-ε model in the outer region.

In contrast, Reynolds Stress Turbulence models such as the standard Launder-Reece-Rodi Isotropic Production (LRR-IP) model (Launder et al, 1975) and Second Moment Closure-ω (SMC-ω) model (Wilcox, 1998), do not use the eddy-viscosity hypothesis, but solve transport equations for all components of the Reynolds stresses. This makes Reynolds Stress models more suited to complex flows. However, practice shows that they are often not superior to two-equation models because convergence difficulties often occur. The LRR-IP model is based on the k-ε model, whereas the SMC-ω is based on the k-ω model with the advantages already explained.

Benchmark 1: Quasi-2D-model for laminar flow over a heated vertical plate

The numerical model contained a 33°C isothermal wall of 381mm height. An adjacent ambient flow domain of 76mm width and an additional adiabatic wall and part of the ambient region at the low end of the isothermal heated wall (Figure 1) were imposed to allow sufficient space to avoid the surrounding boundaries influencing the results. 'Opening' boundaries were placed at the top the bottom and the right vertical boundary to allow air to flow in both directions depending on the pressure field. An ambient temperature of 21°C and zero velocity vector field were imposed for initial domain conditions and the 'opening' inflow. For this model a Rayleigh number of $Ra=3.9x10^5$ was calculated which indicates a purely laminar flow. Since the flow is two-dimensional, a 'symmetry' boundary condition with a model thickness of 10mm was chosen for the front and back of the domain. The walls and the core consisted of tetrahedral and triangular finite elements (see Figure 1) with maximum element edge length of 10mm to achieve high resolution. At the interface region between the isothermal and adiabatic wall the mesh was refined to increase the resolulution where the wall boundary layer begins to develop. Based on the equation of Yang and LaValle (2002) a maximum thermal boundary layer thickness of 21mm was calculated for the top end of the heated vertical plate. A sufficient nodal resolution in the wall boundary layer region (at least 15 nodes with the first node within $y+\leq 2$, as recommended by the code developers) required the use of prisms.

The influence of mesh resolution on temperatures and velocities in the wall boundary layer and on heat transfer at the heated plate was investigated by varying three key parameters for prism layer sizing: first prism size (use of 0.1mm, 0.2mm, 0.4mm, 1.0mm and 2.0mm), core prism size (use of 1.33mm, 2mm, 3mm and 4mm) and prism inflation (use of 1.5, 2.0 and 2.5). For investigations of constant core prism scales (by setting the prism inflation factor to unity) and prism inflation, a first prism size of 0.1mm was used (see Figure 2). In the sensitivity study of first prism sizes a constant core prism scale of 2.0mm was chosen. The first prism size determines the prism edge length in conversed direction of the surface normal for the first prism layer adjacent to the wall. The core prism size determines the prism edge length for the other prism elements towards the edge of the wall boundary layer and the outer region. A high mesh quality with finite element scales similar to the neighbouring elements reduces the risk of convergence problems. Therefore, with prism inflation the prism layer size can be increased gradually towards the core such that the last prism layer size has a similar scale to the edges of the neighbouring tetrahedral elements.

Results for benchmark 1 at y=380mm are compared with analytical work of Ostrach who derived expressions for velocity and temperature laminar wall boundary layer profiles at any height of a heated vertical plate. Ostrach's work was validated using data obtained from experiments of Schmidt and Beckmann (1930).

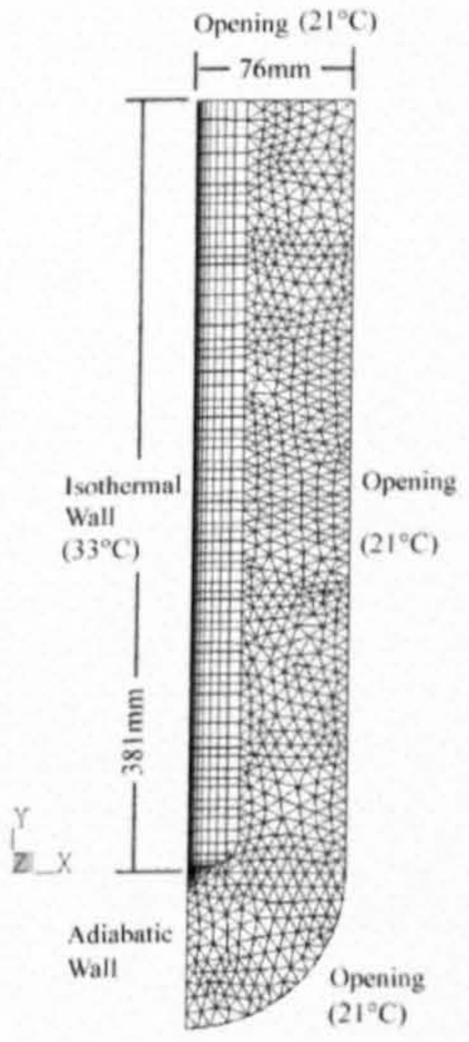

Figure 1: Numerical model for laminar flow at a heated vertical plate (benchmark 1).

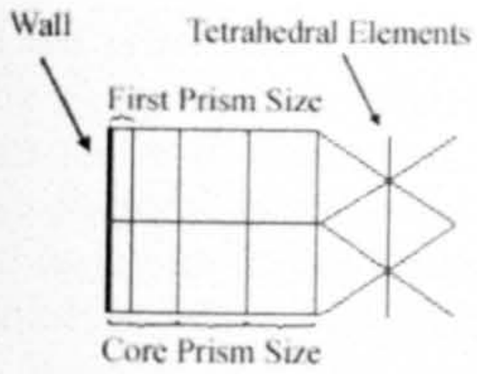

Figure 2: Near wall grid sizing

Benchmark 2: Quasi-2D-model for turbulent flow in a differentially heated cavity

This benchmark is based on experimental work carried out by TK. A cube with dimensions of X=750mm and Y=750mm and depth of Z=10mm was used for a quasi 2-D geometry. Constant temperatures of T_{Cold}=10°C and T_{Hot}=50°C were used at the isothermal vertical walls (Figure 3) for which a Rayleigh number of $Ra=1.56x10^9$ was calculated. Initial conditions of a zero velocity flow field and a homogeneous temperature of 30 °C were chosen for the fluid domain. In experiments adiabatic conditions are difficult to achieve. Therefore TK published the temperature profiles for the horizontal walls obtained in his experiments for adoption into numerical models which were used here for T_{Top} and T_{Bottom} (Figure 3). Since all wall boundary conditions have fixed temperature profiles and the absorption of radiation in the air was thought to be negligible, radiation effects were neglected. Hence no radiation model was used. Based on the results of benchmark 1, a mesh structure with a maximum surface and core mesh length scale of 10mm and 20mm, respectively, with mesh refinement in the corners was chosen. In the wall boundary layer (boundary layer thickness of 40mm at y/Y=0.5 based on Yang and LaValle) 13 prism layers with inflation factor 1.1 starting 1mm from the wall were positioned with two additional layers at 0.1mm and 0.5mm from the wall.

Using the geometry and boundary conditions described above, the four turbulence models k-ω, SST, LRR-IP and SMC-ω results were compared with experiments of TK.

Benchmark 3: 3D-model for turbulent flow in a differentially heated cavity

This was the same as benchmark 2, except the depth was extended to Z=375mm to analyse the influence of 3D effects on the results. The mesh was modified so that the elements were not refined at the corners. This was to keep the total number of elements within a practical limit for computing power. For the wall boundary layer 15 prism layers with an inflation factor of 1.2 starting at 0.5mm from the wall, with an additinal layer at 0.1mm from the wall, was used.

The most appropriate turbulence models for benchmark 2 were further used in benchmark 3 and results compared with experiments of TK.

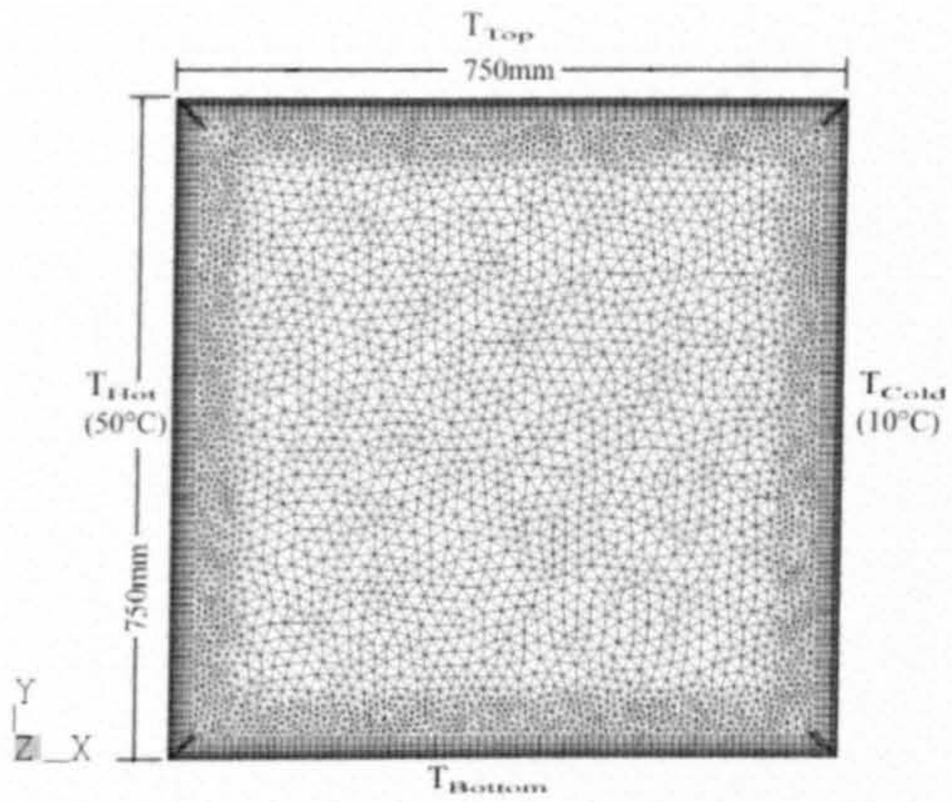

Figure 3: Numerical model for turbulent flow in a differentially heated cavity (benchmark 2).

RESULTS AND DISCUSSION

In the following figures the symbols on the interpolation are only for identification of the curves and do not represent nodes in the model. All data is plotted on the mid-depth line, z/Z=0.5 (V_0=1m/s is the buoyancy velocity). Solutions for benchmark 1 and 2 have converged to RMS (a root mean square residual) for the momentum equations of 10^{-7} and velocities remained constantly during the solution process at a certain monitoring point (except for the SMC-ω model). Each simulation required less than half a day for a Pentium 4, 2.55GHz machine. Simulations of benchmark 3 converged to RMS of 10^{-4} which is considered to have converged sufficiently as recommended by CFX. In contrast to the other benchmarks, steady-state values for benchmark 3 oscillated within a small range. Therefore, the results were statistically analysed and averaged over the oscillatory period. Each simulation required more than a week, which was clearly higher than for the quasi-2D models since 18 times more finite elements were used and more iterations were necessary for convergence.

BENCHMARK 1

Wall Boundary Layer

In Figure 4 the vertical velocity components and temperatures in the wall boundary layer at the top of the geometry at y=380mm close to the isothermal heated wall and average Nusselt numbers (Nu_{av}) are illustrated for different prism sizes. The vertical velocity components agreed well with the analytical solution of Ostrach for small 'core' prism sizes and deviated slightly with increased values at locations further away from the wall starting at about the velocity peak value (Figure 4a). For small 'first' prism sizes the velocities agreed well with the analytical solution and deviated only slightly between the wall and the location of the velocity

peak value as the prism size was increased (Figure 4b). Only the 2.0mm case showed significant deviations from the analytical solution. For various prism 'inflation factors' investigated the numerical solution agreed well with that of Ostrach between the wall and the location of the peak velocity value but deviated from there towards the core (Figure 4c). The deviation increased as the inflation factor was increased. The temperature profiles showed negligible deviation from the analytical solution for the prism scales investigated (compare Figures 4a-c).

Heat Transfer

Local heat transfer (indicated by local Nusselt numbers Nu_y) along the isothermal vertical plate was investigated. Nu_y deviated only marginally from the analytical solution for investigated prism scales and are hence not explicitly presented here in figures. Instead, the calculated average Nusselt numbers (Nu_{av}) for increased core prism sizes were compared with that of Ostrach for the isothermal surface (Figure 4d). For increased 'core' prism sizes a slight under-prediction of Nu_{av} existed. However, even for a prism size of 4.0mm the average Nusselt number only deviated from the analytical result by 2%. For a size of 2.0mm negligible deviation existed. The slightly higher average Nusselt number than that for the analytical results, for the potentially most accurate simulation (prism size of 1.33mm), may be caused by thermal effects from the adjacent adiabatic wall which are not present in the analytical model. An over-prediction was shown as the 'first' prism size was increased. For the tallest first prism size investigated (2.0mm) the average Nusselt number deviated from the analytical solution by 8%. Comparing average Nusselt numbers for core and first prism size variation the values were more sensitive to the first prism size, indicated by larger deviations. For prism 'inflation factors' investigated even the smallest factor investigated (1.5) over-predicted the average Nusselt Number by 2%.

Summary of Benchmark 1 Results

The parametric study showed that the temperature profile in the wall bounday layer might not change for a coarser wall boundary grid, although the air speeds and thus the heat transfer at the surface may be effected. Based on results for constant 'first' prism size of 0.1mm, core prism sizes of 2mm compared favourably well with the analytical solution. For constant 'core' prism sizes of 2mm, a first prism size of 0.2mm was found to be optimal for accurate predictions. However, results were more sensitive to the first prism size. In investigations with prism inflation, a small inflation factor gave best results. However, even the smallest factor investigated of 1.5 was too high to give results that agree exactly with experiment.

a)

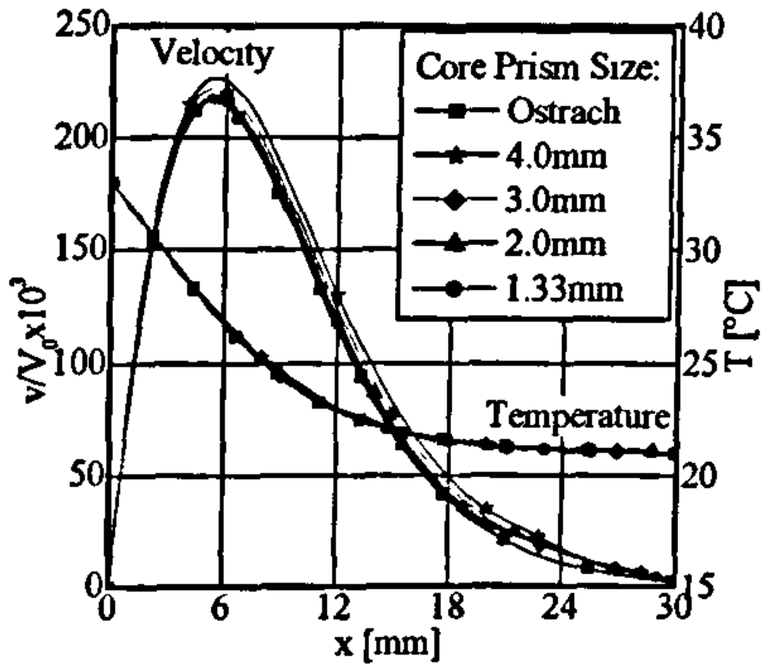

b)

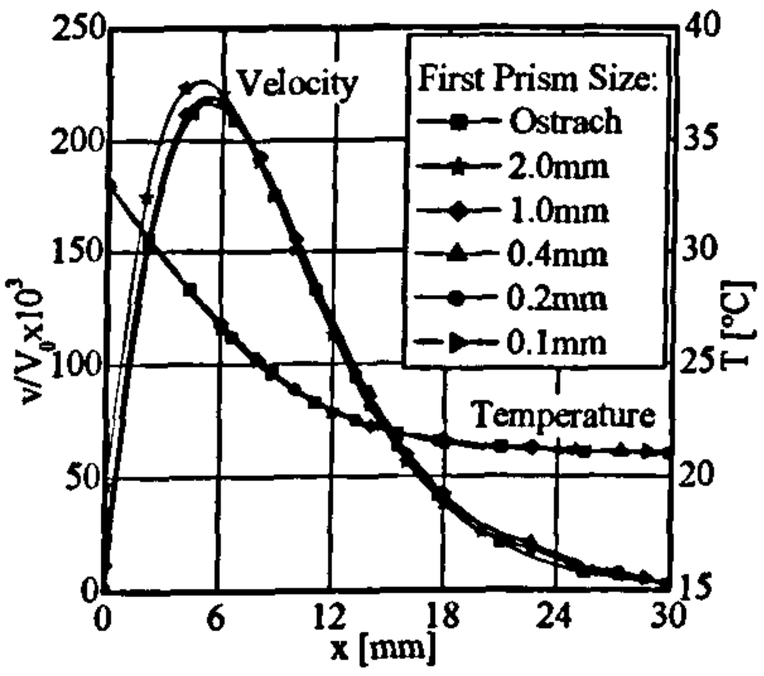

c)

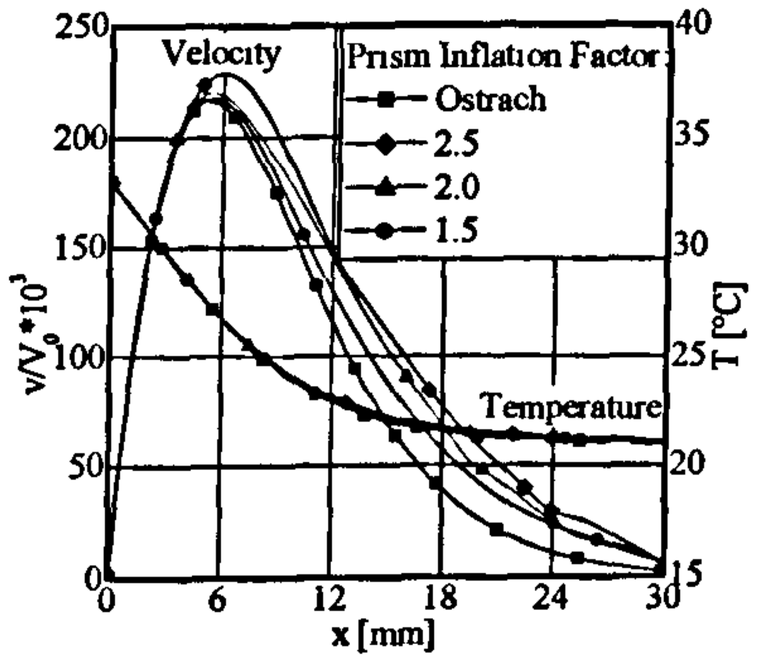

d)

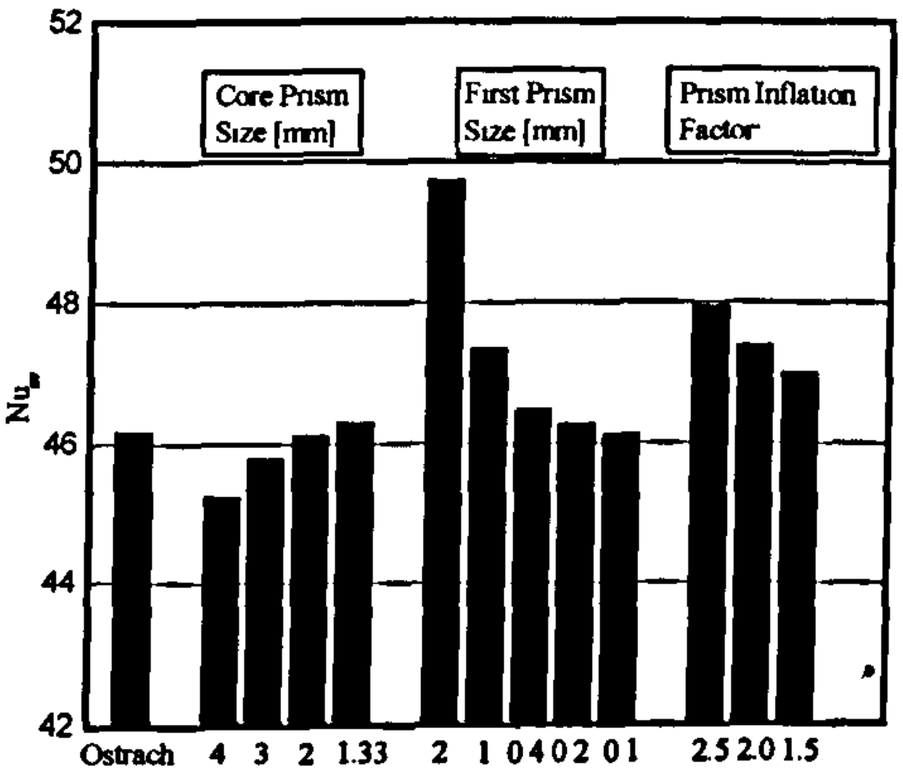

Figure 4: Comparison of predictions for various prism sizes with the analytical solution for y=380mm (benchmark1): a) Variation of prism sizes towards the core; b)Variation of wall adjacent prism sizes; c)Variation of prism inflation factors; d) average Nusselt numbers.

BENCHMARK 2

Wall Boundary Layer

Using the LRR-IP model the vertical velocity components and temperatures in the wall boundary layer at mid height of the space were significantly under-predicted (Figure 5a). When the SST model and SMC-ω were used the peak velocity was slightly over-predicted, temperatures were slightly under-predicted towards the cavity core. For the k-ω model, velocity and temperature profiles were in good agreement with experiments and deviated only for the peak velocity and temperatures further away from the wall.

Fluid properties at mid width

At mid width, deviation of differences between the temperature at mid height of the cavity and the peak temperature at the low end and high end, respectively, indicate a small horizontal displacement of the measured values (Figure 5b). For the numerical models no horizontal displacement of temperature existed and the point symmetry to the mid point of the space was well predicted. However, except for LRR-IP model which showed significant under-prediction, simulations slightly over-predicted the temperature peaks. Closest agreement with the measurements was shown for the k-ω model.

For horizontal velocity components at mid width of the enclosure, the numerical models slightly under-predicted the measured main flow peak values (Figure 5c), except the SST model which favourably agreed adjacent to the lower wall. The LRR-IP model gave largest discrepancies. A flow reversal at cavity mid width was only shown by using the SMC-ω and SST model, but velocities were significantly under-predicted (Figure 5c).

A typical velocity vector plot for the cavity mid plane (z/Z=0.5), however, showed small regions of weak flow reversal for the k-ω model further away from the mid width (Figure 6a), which therefore was not visible in figure 5c. The deviation of reversal regions were thought to be due to two flow disturbances in the bottom-right and top-left corners (Figure 6a), which were not visible in the experiments of TK (see Figure 6b). The reason for these disturbances was thought to be the use of a shallow geometry in benchmark 2 which prohibited 3D effects of turbulence being dissipated. Additional investigations with a higher numerical resolution (10mm core element edge scale) resulted in larger regions of flow reversal, however, under-prediction still existed. Since the higher resolution would exceed the practical limit for computer power and results are only marginally better for the prediction of the flow reversal, this was not investigated further.

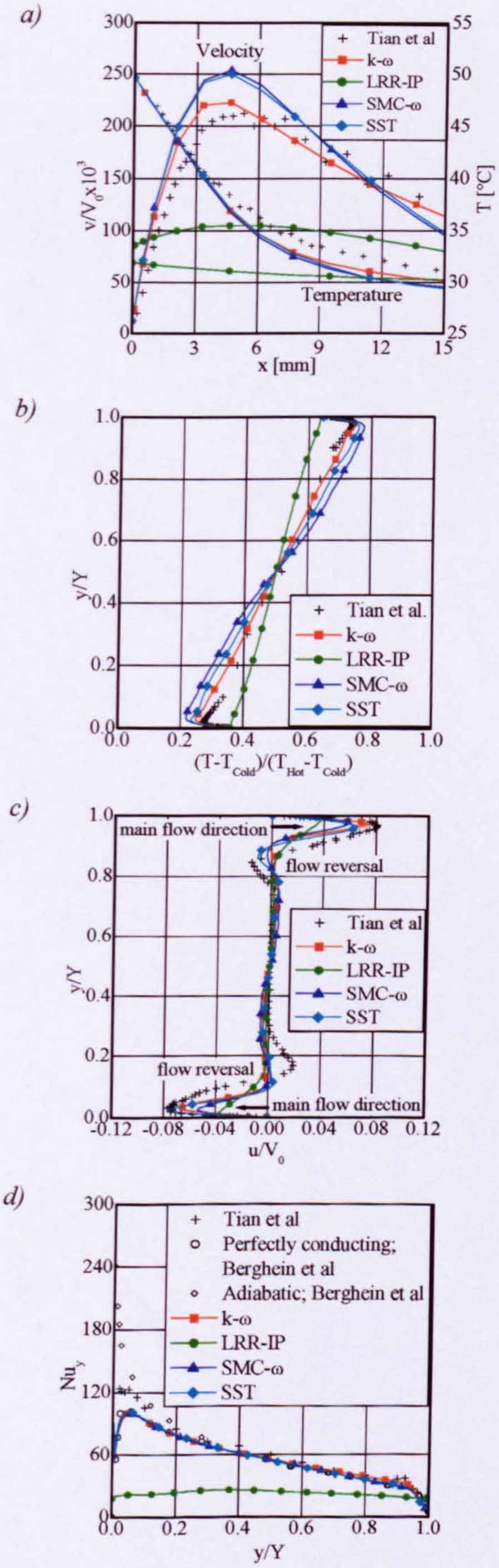

Figure 5: Comparison of predictions for various turbulence models with experiments (benchmark 2): a) Vertical velocity components and temperatures at y/Y=0.5; b) temperatures at x/X=0.5; c) horizontal velocity components at x/X=0.5; d) local Nusselt numbers at x/X=0.

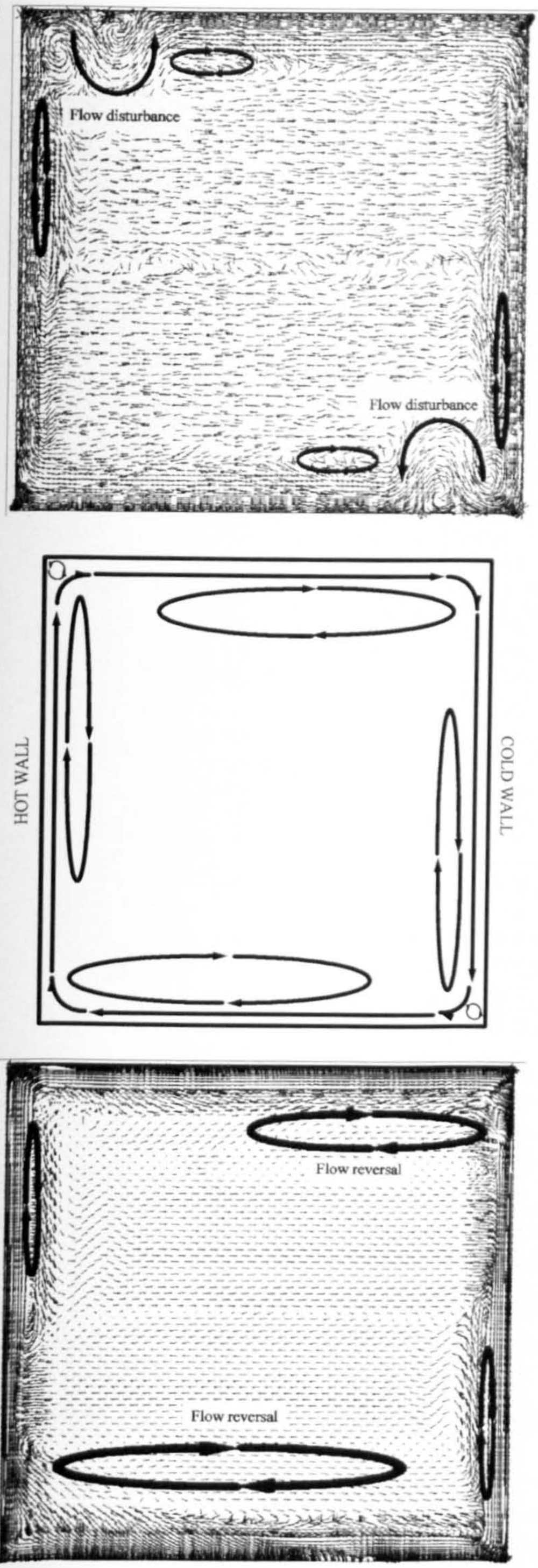

Figure 6: Flow fields: a) vector plot for benchmark 2 using the k-ω model; b) schematic of the flow field showing recirculation regions as observed by TK (2001); c) vector plot (for a selected iteration step) for benchmark 3 using the k-ω model.

Heat Transfer

The heat transfer from the hot vertical wall for different turbulence models are compared with experiments of TK and numerical solutions of Berghein et al (1993) for adiabatic and perfectly conducting horizontal wall boundary conditions (for $Ra=1.34x10^9$) in Figure 5d. The Nusselt numbers for the turbulence models investigated (except LRR-IP) followed the perfectly conducting curve shape of Bergein et al since the horizontal boundaries acted as perfectly conducting conditions because of the profiles carried over from TK. The numerical solutions were in good agreement with experiments between mid height and top of the enclosure. Towards the bottom experiments lay somewhere between the numerical solutions of Bergein et al.

Summary of Benchmark 2 Results

Numerical investigations with benchmark 2 agreed qualitatively with published experimental data for turbulent free-convection. The k-ω and SST turbulence model gave the most favourable agreement with experimental work. However, flow reversal near the horizontal walls which existed in the experiments was under-predicted using the CFD model. This was thought to be due to flow disturbances predicted in the corners of the geometry (Figure 6a) caused by the quasi two-dimensional geometry in which the close proximity of the symmetry planes prohibited airflow in all directions.

BENCHMARK 3

In benchmark 3 the k-ω and SST turbulence models were further investigated as they provided the most accurate results for benchmark 2.

Wall Boundary Layer

Both turbulence models over-predicted the peak velocity (Figure 7a); the k-ω model gave results closest to the experiment. The temperature profiles were slightly under-predicted towards the cavity core by both turbulence models.

Fluid properties at mid width

The numerical solution for temperatures at mid width of the cavity showed a well predicted point symmetry to the mid point of the space for both turbulence models (Figure 7b). Discrepancies existed in the temperature profile and the peak temperature values were slightly over-predicted. Although the temperature curve shapes of both turbulence models agreed quantitatively in the core, the peaks predicted with the k-ω model were closer to the experiments.

Flow reversal was shown by both turbulence models in the plot of horizontal velocity components at mid width of the enclosure (Figure 7c), although it was significantly under-predicted by both (except for the

k-ω model at the lower end, where it was well predicted). The k-ω model slightly underpredicted the peak velocities of the main flow, whereas the SST model agreed well with the experiments. In the core region the velocities were slightly higher for both turbulence models than in the experiments. Flow disturbances in the corners as predicted in benchmark 2 did not exist in benchmark 3 and the reversal flow regions shown in the velocity vector plots (e.g. the the k-ω model, Figure 6c) are comparable with those of TK (Figure 6b).

Heat Transfer

Results for local Nusselt numbers at the hot vertical wall agreed well with the experiments and the numerical results of Berghein et al towards the top of the cavity (Figure 7d). However, Nusselt numbers were under-predicted towards the bottom of the cavity for both turbulence models. In contrast to benchmark 2 no element refinement was used in the corners of benchmark 3. Based on the horizontal wall temperature profiles of TK the temperatures at both ends of the horizontal walls deviate slightly from the adjacent vertical wall temperatures. Thus a greater heat flux was caused at the interface than for benchmark 2 which is indicated by the Nusselt number peaks near the horizontal walls in Figure 7d. At mid height the local Nusselt numbers predicted using the k-ω model were closer to the measured data and solutions of Berghein et al than those using the SST model; at the low end the SST model showed better agreement.

Summary of Benchmark 3 Results

Numerical solutions of benchmark 3 results agreed qualitatively well with the experiments using the k-ω and SST model. The flow reversal was predicted for both cases. However, temperatures were slightly over-predicted for mid width and marginally under-predicted for the mid height of the cavity. The velocities were slightly over-predicted for mid height and under-predicted for the mid width of the space.

COMPARISON OF BENCHMARK 2 AND 3

For the fluid properties and heat transfer investigated, the results for velocity, temperature and Nusselt number were closer to the experiments using benchmark 2 than benchmark 3 for both turbulence models. However, using the k-ω model, the flow reversal regions were better predicted for benchmark 3 than benchmark 2. Furthermore, flow disturbances existed in the corners for benchmark 2 which did not appear in benchmark 3 which was thought to be caused by the close proximity of the symmetry planes. This suggested that the geometry depth of benchmark 3 was sufficient to allow flow at z/Z=0.5 to move in all directions without being influenced by the symmetry planes.

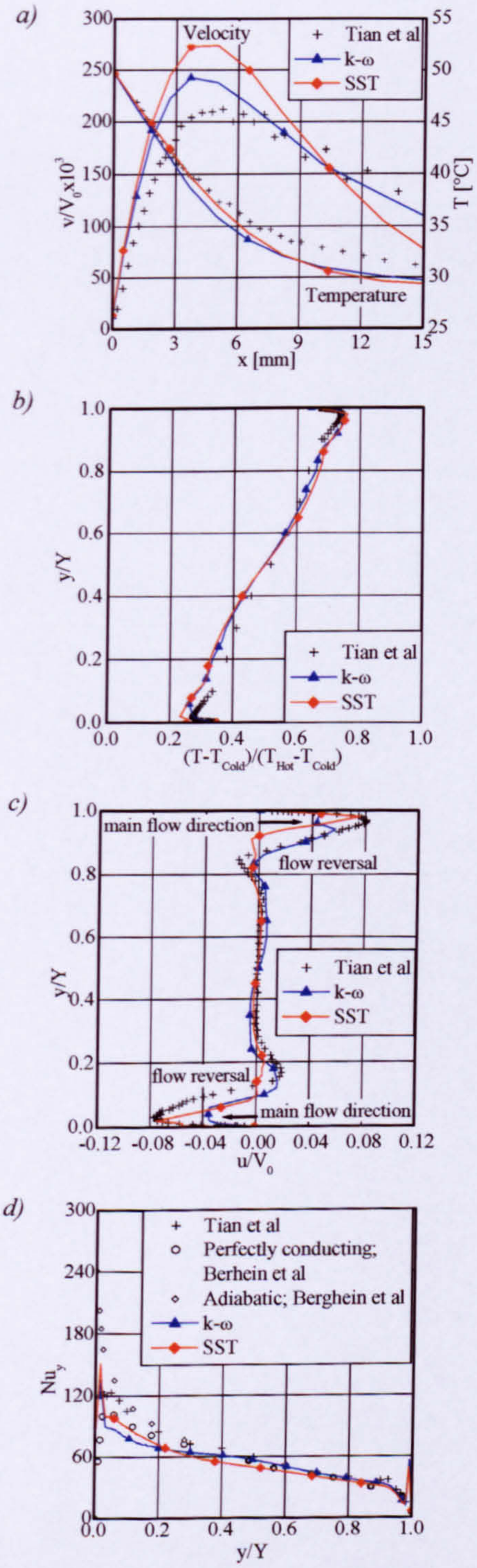

Figure 7: Comparison of predictions for selected turbulence models with experiments (benchmark 3): a) Vertical velocity components and temperatures at y/Y=0.5; b) temperatures at x/X=0.5; c) horizontal velocity components at x/X=0.5; d) local Nusselt numbers at x/X=0.

CONCLUSIONS

For the free convection flows studied in this work, it was found that prisms were required in the near wall region to accurately resolve the wall boundary layer. For the laminar case, the predicted numerical results for heat transfer, velocities and temperatures in the wall boundary layer agreed well with published analytical data. It was found that a maximum first prism size of 0.2mm and constant core prism sizes no larger than 2.0mm were required to obtain accurate results. Prism inflation might increase mesh quality and hence improve convergence. Initial investigations showed that the inflation factor should be at least lower than 1.5 for the cases considered.

For turbulent natural convection modelling, the mesh parameter settings were based on the results of benchmark 1. Results for different turbulence models to predict flow in a differentially heated cavity compared favourably with experiments using benchmark 2. Only the LRR-IP turbulence model deviated significantly from experiments; the SST and k-ω turbulence models predicted the most favourable results. However, velocity disturbances existed in the corners of the geometry where the flow impinged on the top or bottom of the space. A further investigation of the SST and k-ω models in 3D suggested that these deviations from measurements were caused by the close proximity of the symmetry planes which inhibited 3D dissipation of turbulence effects of the flow. Benchmark 2 (quasi-2D) compared well with the 3D case (benchmark 3) except for the flow disturbances which appeared in the cavity corners in the quasi-2D case. Both the k-ω and SST turbulence models gave favourable results for both benchmarks.

The investigations showed that CFX-5 has the capability to predict buoyancy-driven turbulent flow in a differentially-heated cavity.

NOMENCLATURE

α	thermal diffusivity [m^2/s]
β	thermal expansion coeff. [1/K]
ε	turbulence eddy dissipation [m^2/s^3]
g	gravity [m/s^2]
k	turbulence kinetic energy [m^2/s^2]
Nu_{av}	average Nusselt Number [-]
Nu_y	local Nusselt No. [-], $=0.386Ra^{0.25}y^{-0.25}$
Ra	Rayleigh No. [-], $=g\beta(T_{Hot}-T_{Cold})Y^3\alpha^{-1}\nu^{-1}$
T_{Top}, T_{Bottom}	temperature profiles at the top and bottom of the geometry [°C]
T_{Hot}, T_{Cold}	isothermal temperatures at the hot and cold vertical walls [°C]
u	horizontal velocity comp. [m/s]
u_τ	friction velocity [m/s]
v	vertical velocity comp. [m/s]
ν	kinematic viscosity [m^2/s]
V_0	buoyant velocity [m/s], $=(g\beta\Delta TY)^{-0.5}$
X, Y, Z	geometry dimensions [mm]
x, y, z	local dimensions for analysis [mm]
ω	turbulence frequency [1/s]
y+	normalised wall distance [-], $=\Delta y u_\tau/\nu$

REFERENCES

Ansys CFX, 2003: CFX-5 Solver Models and Theory User Manuals, Version 5.6.

Berghein C., Penot F., Mergui S., Allard F., 1993: Numerical and experimental evaluation of turbulent models for natural convection simulation in a thermally driven square cavity, Proc. ASME Conf., pp 1-12.

Launder B.E., Spalding D.B., 1974: The numerical computation of turbulent flows, Comp. Meth. in Applied Mech. Eng., Vol 3, pp 269-289.

Launder B., Reece G. and Rodi W., 1975: Progress in the development of a Reynolds-stress turbulence closure, J. Fluid Mech., Vol 68 (3), pp 537-566.

Menter, F.R., 1994: Two-equation eddy viscosity turbulence models for engineering applications, AIAA Journal, Vol 32 (8), pp. 1598-1605.

Ostrach S., 1953: An analysis of laminar free-convection flow and heat transfer about a flat plate parallel to the direction of the generating body force, NACA, Report 1111, Madison.

Peng S.-H., Davidson L., 1999: Computation of turbulent buoyant flows in enclosures with low-Reynolds-number k-ω models, Int J. Heat Fluid Flow, Vol 20, pp 172-184.

Peng S.-H., Davidson L., 2001: Large eddy simulation for turbulent buoyant flow in a confined cavity, Int. J Heat Fluid Flow, Vol 22, pp 323-331.

Schmidt E. and Beckmann W., 1930: Das Temperatur- und Geschwindigkeitsfeld vor einer Wärme abgebenden senkrechter Platte bei natürlicher Konvektion, Tech. Mech. Thermodyn., Bd 1 (10 u 11), Germany.

Thompson C.P., Wilkes N.S. and Jones I.P., 1987: Numerical studies of buoyancy-driven turbulent flows in a rectangular cavity, Int. J. Num. Meth. Eng., Vol 24, pp89-99.

Tian J., Karayiannis T.G., 2001: Low turbulence natural convection in an ait filled square cavity, Part 1: the thermal and fluid flow fields, J. Heat and Mass Transfer, Vol 43, pp 849-866.

Wilcox D.C., 1998: Turbulence modeling for CFD, 2nd edn., DCW Industries Inc., Canada.

Yang R., LaValle P., 2002: Heat transfer by natural convection, Course Script, Uni. of Michigan.

Tobias Zitzmann
Peter Pfrommer
Malcolm Cook

DOI: 10.1002/bapi.200610009

Simulation dynamisch-thermischen Langzeitverhaltens in Gebäuden mittels CFD

Die Planung komplexer Gebäude erfordert immer häufiger den Einsatz von Simulationsprogrammen. Die hierfür derzeit verwendeten dynamischen Gebäudesimulationsprogramme sind jedoch nicht in der Lage, die Luftströmungen und die Temperaturverteilung innerhalb eines Raumes zu erfassen. Eine Lösung der Problematik besteht in der Verlagerung der Gebäudesimulation auf eine CFD-Plattform, deren Berechnung derzeit allerdings noch mit extrem langen Rechenzeiten und großen Datenmengen verbunden ist. Um diese Rechenzeiten zu verringern, wurde für ANSYS CFX-5 eine neue Freeze-Flow-Methode entwickelt, die auf der periodischen Einfrierung der hydrodynamischen Gleichungen basiert und so dynamische Langzeitsimulationen erlaubt. Zudem wurden die CFD-Simulationen für die in Räumen vorherrschende freie Konvektion validiert. Im Ergebnis ergaben Freeze-Flow-Simulationen einfacher Testmodelle schließlich eine erhebliche Reduzierung der Simulationszeit ohne einhergehenden Verlust an Genauigkeit im Vergleich zur volldynamischen CFD-Simulation.

Dynamic CFD simulation of thermal long-term behaviour of buildings. *The design of complex buildings increasingly demands the usage of simulation programmes. Actual dynamic thermal simulation programmes in use are incapable to determine the air flow and the temperature distribution in a room. One solution is to displace building simulations to a CFD platform which involves extremely long calculation times and large amounts of data. To reduce the calculation time a new freeze-flow method was developed for ANSYS CFX-5. It is based on the periodic freezing of the hydrodynamic equations enabling long term simulations. The CFD simulations were validated for free convection which is the dominating driving force of flow in rooms. Freeze-flow simulations of simple test models confirmed a dramatic reduction in calculation time without any loss in accuracy compared to full dynamic CFD simulations.*

1 Einführung

In der Gebäudeplanung steht für die Lösung einfacher Problemstellungen mit z. B. stationären Randbedingungen oder eindimensionaler Wärmeleitung in Bauteilen eine Vielzahl analytischer Lösungen zur Verfügung. Werden die Probleme komplexer, wie zum Beispiel bei der dynamisch thermischen Rückkopplung des Raumes mit Massivbauteilen, sind für die effektive Abstimmung der einzelnen Komponenten im Gebäude andere Lösungswege erforderlich. Ein Beispiel aus der modernen energiesparenden Gebäudeplanung ist das Prinzip des bewußten Einsatzes der sommerlichen Nachtauskühlung zur Verbesserung des sommerlichen Wärmeschutzes von Gebäuden (z. B. in [1]). Hierbei werden die inneren und äußeren Kühllasten am Tag teils von den massiven Bauteilen, wie der Raumdecke, aufgenommen, nachts an den mit kühler Außenluft durchströmten Raum wieder abgegeben und mechanisch oder durch Fensterlüftung nach außen abgeführt. Um Aussagen über die Wirksamkeit derartiger Klimatisierungsmaßnahmen treffen zu können, waren früher zeitintensive Langzeitstudien an bereits existierenden Gebäuden oder teure experimentelle Untersuchungen in Klimakammern und Strömungskanälen erforderlich. Seit Zunahme der Rechnerleistung ersetzen Simulationsprogramme jedoch verstärkt solche aufwendigen Messungen. Die derzeit vorhandenen Simulationswerkzeuge finden aber aufgrund des niedrigen Detaillierungsgrads Grenzen in der Anwendung.

In einer gemeinsamen Forschungsarbeit zwischen dem Institute of Energy and Sustainable Development, Leicester, England, und der Fachhochschule Coburg wurde daher ein leistungsfähiges Werkzeug auf Basis der mit hohem Detaillierungsgrad arbeitenden Luftströmungs-Simulation (Computer Fluid Dynamics – CFD) entwickelt, das dynamische Langzeitsimulationen erlaubt. Mit der zugrunde liegenden Methodik entsteht so das Potential für eine Vielzahl neuer Anwendungsbereiche in der Gebäudesimulation.

2 Struktur und Grenzen der Simulationsprogrammgruppen

Für die Gebäudesimulation konnten sich drei Hauptprogrammgruppen herausbilden, welche durch ihre jeweils unterschiedliche Codestruktur verschieden nutzbar sind: Dynamic Thermal Simulation (DTS), Multi Zone und Computer Fluid Dynamic (CFD) Air Flow Models.

Die DTS-Programme, wie z. B. TRNSYS [2], haben sich seit vielen Jahren etabliert. Mit ihnen können Parameter- und Designstudien im Vergleich zu Messungen in relativ kurzer Zeit durchgeführt werden. Im Ergebnis können hier energetische Aussagen für Gebäude für mehrere simulierte Monate oder Jahre getroffen werden. Ein wesentlicher Nachteil dieser Programme besteht jedoch darin, daß sich die Wärmeströme durch das Bauteil nur vereinfacht eindimensional annähern lassen. Vor allem aber wird pro Raum bzw. thermischer Zone i. d. R. nur ein einziger Temperaturpunkt be-

TEXT BOUND INTO

THE SPINE

trachtet und damit lediglich eine räumlich gemittelte Raumlufttemperatur ermittelt. Somit fehlen Informationen über die örtlich schwankenden wandnahen Lufttemperaturen. Der Einfluß der mehrdimensionalen Luftströmungsfelder auf den konvektiven Wärmeaustausch zwischen der Konstruktion und der Raumluft wird daher nur näherungsweise über konvektive Wärmeübergangskoeffizienten erfaßt. Diese Koeffizienten beruhen jedoch entweder auf empirischen Algorithmen für ganz bestimmte Konfigurationen (z. B. in [3] beschrieben) oder müssen vom Anwender selbst vorgegeben werden. In geschlossenen Räumen, in denen der Wärmeaustausch über freie Konvektion vorherrscht, aber auch in größeren Räumen (z. B. in Atrien) mit teils ausgeprägter Temperaturschichtung, können so große Simulationsfehler auftreten.

Dynamische Gebäude-Simulationsprogramme, die mit (multi-)zonalen Luftströmungs-Programmen, wie z. B. COMIS [4], gekoppelt werden, sind in der Lage, den Luftaustausch zwischen Räumen infolge des vorhandenen Luftdruckunterschieds in die Simulationen einzubeziehen. Hierzu sind jedoch aufwendige Schnittstellen zwischen beiden Programmen notwendig. Ein weiterer Nachteil besteht darin, daß das Binnenklima, d. h. die Luftbewegung und die Temperaturverteilung innerhalb eines Raumes, nicht erfaßt werden kann.

Zur letzten vorzustellenden Programmgruppe gehören die dynamischen Luftströmungs-Simulationsprogramme (CFD), wie z. B. CFX [5] und FLUENT [6]. Sie basieren auf der Finiten Volumen-Methode. Durch das hier angewendete typisch feine Bilanzknotennetz sind sie potentiell in der Lage, in komplexen Raumgeometrien die Luftströmungen und die Turbulenzen genau zu erfassen. Auf diese Weise können die lokalen Zustände, wie Temperatur, Geschwindigkeit, Behaglichkeit, Wärmeströme usw., ermittelt werden. Solare Strahlungsprozesse können zwar derzeit noch nicht explizit simuliert werden, doch lassen sich diese Vorgänge z. B. durch unabhängige Simulationsmodelle aus der thermischen Simulation auslagern bzw. vorschalten. Die solare Einstrahlung wird dann innerhalb der CFD-Simulation durch Wärmequellen repräsentiert, die sich in Datensätzen bereitstellen lassen [7].

Durch den derzeit noch großen rechnerischen Mehraufwand sind mit CFD aber gegenwärtig meist nur stationäre Simulationen praktikabel; bei instationären Simulationen kann durch die sehr unterschiedlichen thermischen Zeitkonstanten der Luft und der Bauteile der Einfluß der thermischen Gebäudemasse bisher nur begrenzt mit in die Berechnungen einfließen. Dies wäre aber für eine ganzheitliche und akkurate Gebäudesimulation notwendig.

3 Erweiterung der Simulationsmöglichkeiten

Um die Nachteile der oben diskutierten Programmgruppen zu kompensieren, ist es heute Stand der Technik, DTS- und CFD-Programme miteinander zu koppeln [8]. Im einfachsten Fall werden Ergebnisse aus DTS oder CFD als reine Initialrandbedingungen an das andere Programm übertragen (Bild 1a), wobei kein Feedback an das erste Programm zurückgegeben wird (z. B. in [9]). Komplizierter ist die dynamische Koppelung, wie dies in [10] genauer dargestellt ist. Hierbei werden die berechneten Daten entweder nach jedem Zeitschritt (Ping-Pong-Prinzip, Bild 1b) oder bereits nach jedem Iterationsschritt (Onion-Prinzip, Bild 1c) zwischen beiden Programmen ausgetauscht. Die genannten Methoden stoßen an ihre Grenzen, wenn sich Randbedingungen dynamisch verändern (dies gilt für die Methode in Bild 1a) oder wenn hydrodynamische und energetische Gleichungen, wie z. B. bei freier Konvektion, stark miteinander korrelieren (dies gilt für die Methoden in den Bildern 1a und 1b); auch erfordert dies eine große Menge an Rechenleistung (insbesondere bei der Methode in Bild 1c).

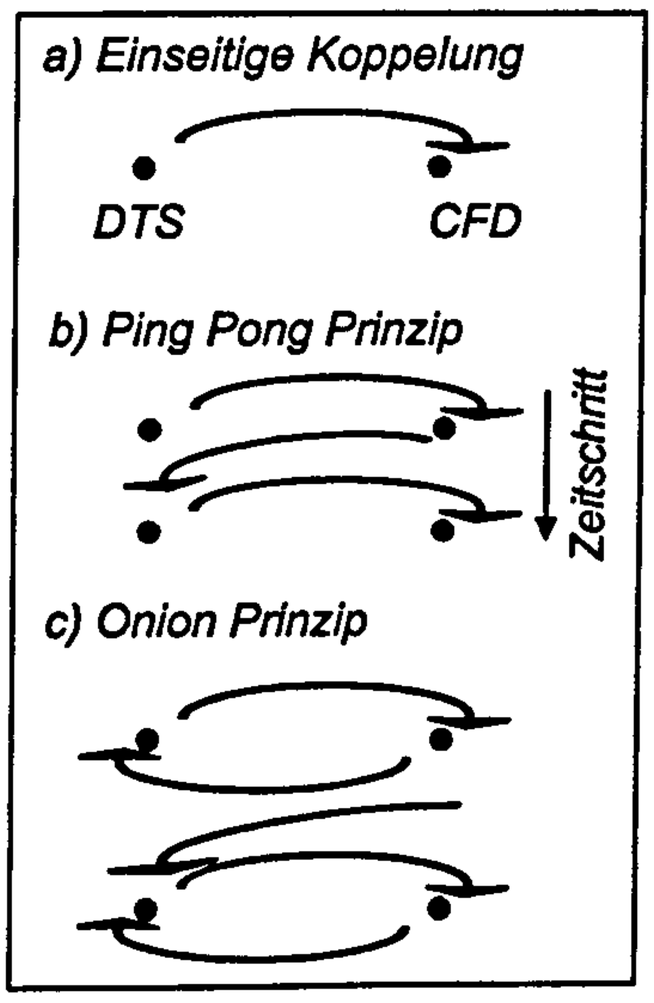

Bild 1. Unterschiedliche Prinzipien zur Koppelung von DTS und CFD
Fig. 1. Different principles for the coupling of DTS and CFD

Allgemeine Probleme beim ausschließlich energetischen Datentransfer zwischen CFD und DTS sind außerdem:

- Geeignete Schnittstellen und ein Zusatzmodul zum Datenaustausch *müssen vorhanden sein.*
- Wichtige Informationen, z. B. die Luftströmungsverteilung im Raum, gehen verloren.
- Schnittstellenprobleme und Datenverlust durch den unterschiedlichen geometrischen Detaillierungsgrad beider Programme treten auf.

CFD allein ist aber durch den *conjugate heat transfer* (d. h., die Energiegleichungen von Bauteil und Luft werden gekoppelt gelöst) [11] in der Lage, alle Aufgaben zu übernehmen, die mit DTS durchführbar sind. In [12] wurde dementsprechend versucht, ein einziges CFD-Programm zu verwenden und für die dynamisch-thermischen Gebäudesimulationen zu modifizieren. Die in [12] entwickelte Freeze-Flow-Methode baut auf der Grundidee auf, das Luftströmungsfeld (bestimmend sind die Impuls-, Kontinuitäts- und Turbulenz-Gleichungen) im Raum in Perioden mit relativ konstanten Randbedingungen zeitweise einzufrieren. In dieser Zeit werden nur die Energiegleichungen gelöst. Bei ausreichender Änderung der Randbedingungen für den Innenraum werden die eingefrorenen Gleichungen wieder hinzugeschaltet und den neuen Gegebenheiten angepaßt. Die Prozedur während der eingefrorenen Phase ähnelt der eines herkömmlichen DTS-Programms, allerdings wird hier der Wärmeaustausch mehrdimensional betrachtet.

Für den Zustand der Strömungsanpassung nach einer eingefrorenen Periode wurden in [12] zwei unterschiedliche Methoden eingeführt – die dynamisch-dynamische Methode 1 und die dynamisch-stationäre Methode 2. Beiden Methoden geht eine dynamische Simulation voraus, in der die Strömungsgleichungen eingefroren sind. Bei Methode 1 wird im An-

schluß in einer volldynamischen Simulation (alle Gleichungen werden gelöst) das Strömungsfeld innerhalb eines bestimmten Zeitraumes nachgeführt. Hingegen werden in Methode 2 die Außenbedingungen und das aktuelle Temperaturfeld im Bauteil fixiert und danach die Strömung in einer stationären Simulation den festen Randbedingungen angepaßt. Gegenüber einer normalen CFD-Simulation wird mit Methode 1 nach Angabe von [12] eine Reduzierung der Simulationszeit um 36 %, bei Methode 2 sogar eine Reduzierung um 90 % bei gleichbleibender Genauigkeit der Temperaturen und Geschwindigkeiten an den untersuchten Monitorpunkten erreicht. Methode 2 besitzt jedoch im Gegensatz zu Methode 1 den Nachteil, daß zwischen den eingefrorenen und uneingefrorenen Zuständen die Simulationen manuell gestoppt und wieder gestartet werden müssen. Zudem ist das Einfrieren der Außenbedingungen mit einem größeren Aufwand verbunden.

Es war zunächst Aufgabe innerhalb des beschriebenen Forschungsprojekts gewesen, die in [12] beschriebenen Methoden im kommerziellen CFD-Programm ANSYS CFX-5 [5] umzusetzen. Hierzu mußte das Programm vorab für die in Gebäuden überwiegend vorkommende freie Konvektion validiert werden.

4 Simulation freier Konvektion mit CFX

Die Hauptanwendung der CFD-Simulation beschränkt sich derzeit meist noch auf die stationären erzwungenen Strömungen. Streicht in diesem Fall die Luftströmung mit der Geschwindigkeit v_F [m/s] (grüner Pfeil, Bild 2) entlang einer Wand, so entsteht im wandnahen Bereich eine Wandgrenzschicht mit der hydrodynamischen Grenzschichtdicke δ [m], in der die Strömung durch Reibung mit der Wand beeinflußt wird. Das Geschwindigkeitsprofil innerhalb dieser Schicht beruht dabei teilweise auf logarithmischen Gesetzen. In CFX-5 existieren hierfür semi-empirische Wandfunktionen [5], wodurch eine rechenintensive numerische Auflösung der Grenzschicht mit feinem Berechnungsgitter überflüssig wird.

Dem entgegen tritt in gelüfteten Gebäuden mit geringen Luftwechselzahlen überwiegend eine freie Konvektion auf. Sie entsteht durch das Erwärmen der Luft an warmen Oberflächen, wie von z. B. Heizkörpern, Menschen, Bauteilen usw., mit der Temperatur T_{Hot} [°C] (roter Pfeil, Bild 3), die wiederum aufgrund der geringeren Dichte aufsteigt (grüner Pfeil, Bild 3). Wie bei der erzwungenen Konvektion entstehen auch hier Wandgrenzschichten, wobei die sich entwickelnde thermische Grenzschichtdicke δ_T [m] größer ist als die hydrodynamische Grenzschichtdicke δ. Die genannten Wandfunktionen würden hier ein falsches Grenzschichtprofil aufprägen und so zu einer sehr ungenauen Berechnung der Wärmeübertragung führen. Aus diesem Grund müssen die Wandgrenzschichten in Gebäuden weiterhin numerisch gelöst werden.

Da in der einschlägigen Literatur für CFX-5 kaum Informationen über geeignete Parametereinstellungen und Maschengrößen im wandnahen Bereich für die freie Konvektion existieren, galt es, diese zu ermitteln. Im folgenden wird eine kurze Übersicht über die verwendeten Modelle und deren Validierung gegeben. Eine vollständige Ausführung zu diesem Thema wurde 2005 in [13] veröffentlicht.

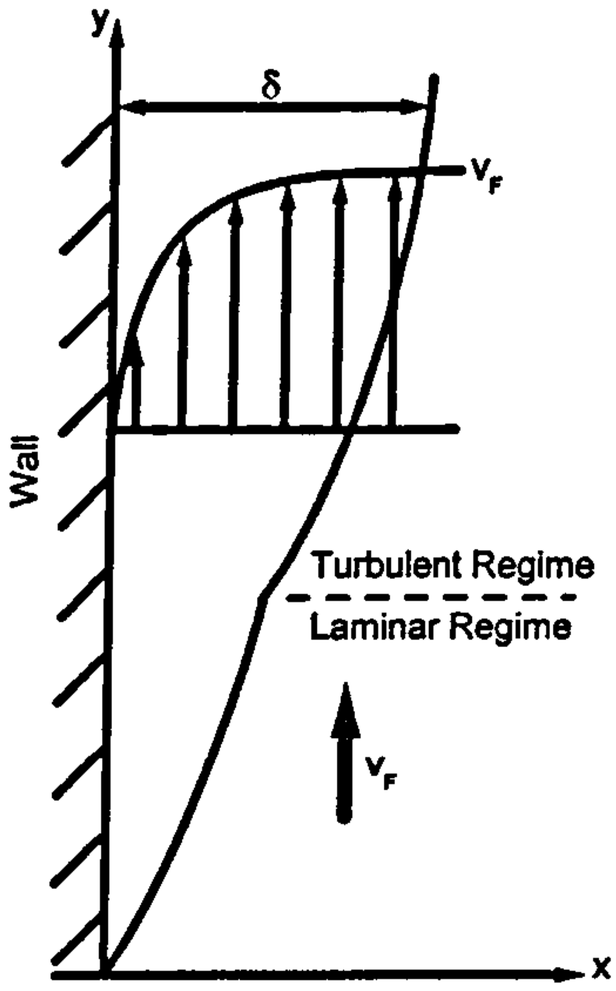

Bild 2. Schema des Grenzschichtprofils bei erzwungener Konvektion (grüner Pfeil: Luftströmung entlang einer Wand); x,y – lokale Koordinatenpunkte [m]; δ – hydrodynamische Wandgrenzschicht [m]; v_F – Strömungsgeschwindigkeit [m/s]
Fig. 2. Schematic of the wall boundary layer for forced convection (green arrow indicates air flow direction); x,y – local coordinates [m]; δ – hydrodynamic boundary layer [m]; v_F – fluid velocity [m/s]

Zur Validierung der laminaren freien Strömung wurden das Modell der beheizten senkrechten Platte von [14] verwendet und die Ergebnisse mit analytischen Algorithmen von [15] verglichen (Ergebnisse siehe [13]). Die Untersuchung der turbulenten freien Konvektion stützte sich auf die experimentellen Untersuchungen von [16] und die numerischen Referenzwerte aus [17]. Hierbei wurde ein quadratischer Raum mit zwei gegenüberliegenden senkrechten Wänden unterschiedlicher Temperaturen T_{Hot} und T_{Cold} betrachtet (Modell 1, Bild 4). In Verbindung mit diesem Modell wurde eine Vergleichsstudie der verschiedenen, in CFX optional vorhandenen Turbulenzmodelle durchgeführt. Die numerischen Resultate für das Launder-Reece-Rodi Isotropic Production, *k-ω-Modell, Shear-Stress-Transport*-Modell und das ω-basierende Second-

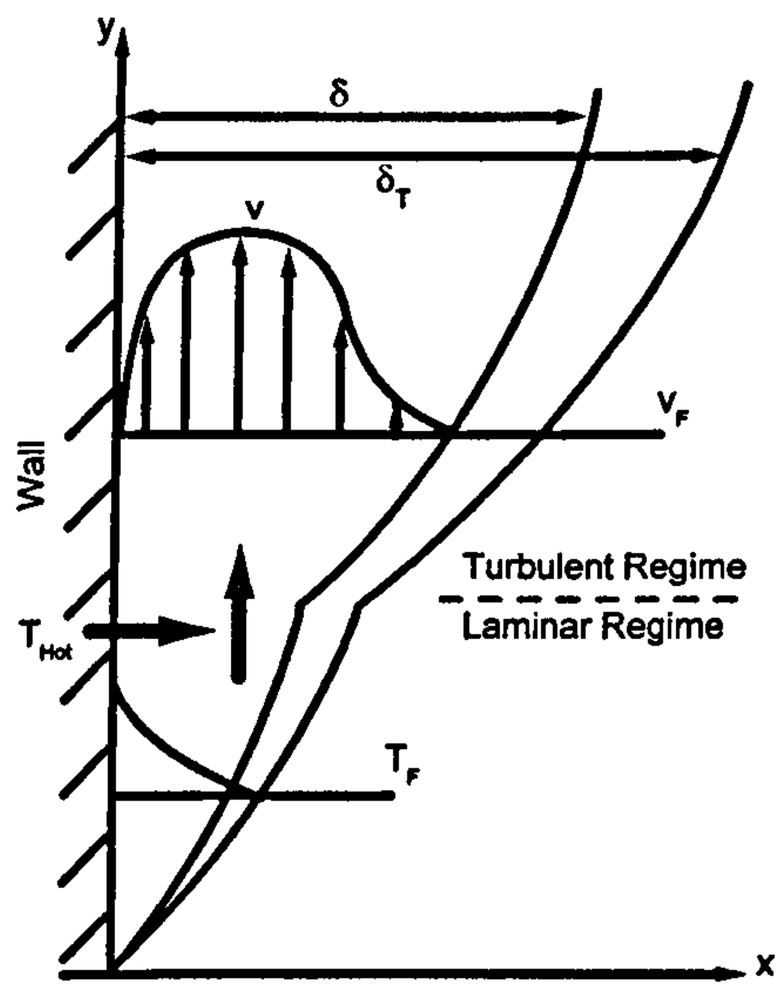

Bild 3. Schema des Grenzschichtprofils bei freier Konvektion. Bei Wärmeübertrag von der Wand zur angrenzenden Luft (roter Pfeil) steigt die Luft aufgrund der abnehmenden Dichte auf (grüner Pfeil); T_{Hot} – Temperaturrandbedingung linke Wandseite; δ_T – thermische Wandgrenzschicht [m]; v – vertikale Geschwindigkeitskomponente [m/s]; v_F – Geschwindigkeit der Hauptströmung; T_F – Fluidtemperatur [°C]
Fig. 3. Schematic of the wall boundary layer for free convection. Due to heat transfer from the wall to the adjacent air (red arrow) the air rises because of the reduced density (green arrow); T_{Hot} – surface temperature left wall side [°C]; δ_T – thermal boundary layer [m]; v – vertical velocity component [m/s]; vF – velocity of main fluid flow [m/]; T_F – fluid temperature [°C]

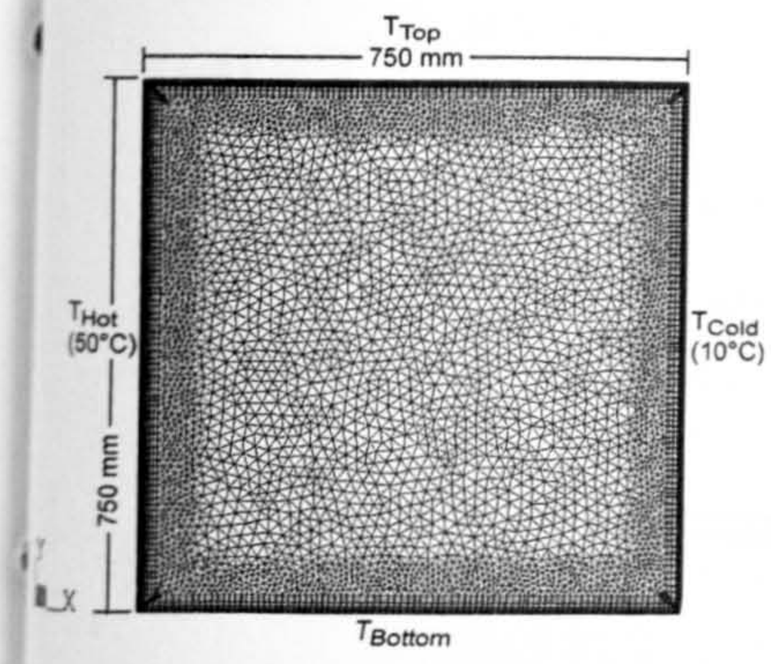

Bild 4. Numerisches Modell für die Untersuchung turbulenter Strömung (Modell 1)
Fig. 4. Numerical model for the investigation of turbulent air flow (Model 1)

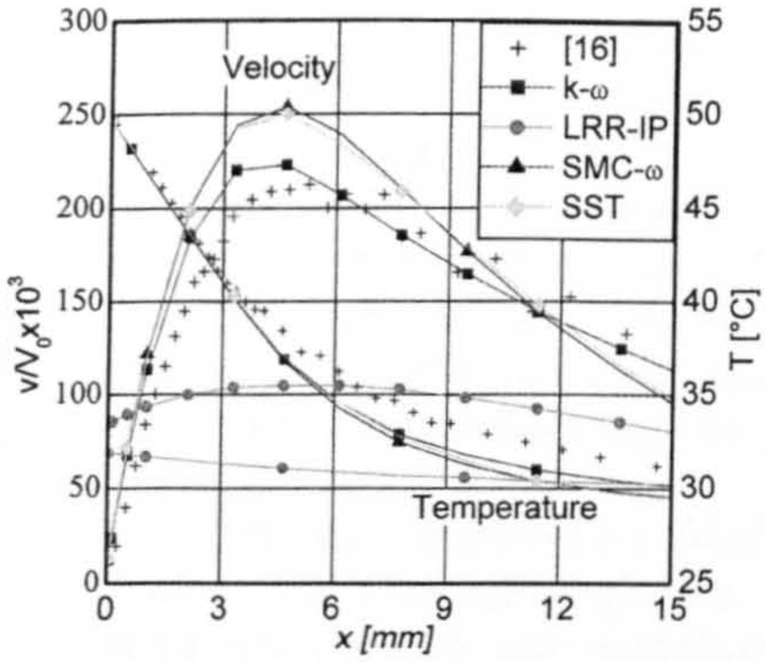

Bild 5. Vergleich numerisch und experimentell ermittelter Wandgrenzschichtprofile auf halber Raumhöhe (Modell 1); v – vertikale Geschwindigkeitskomponente [m/s]; V_0 – Referenzgeschwindigkeit, induziert durch Auftriebskraft [m/s], hier 1 m/s
Fig. 5. Comparison of numerical and experimental identified wall boundary layer profiles at mid height (Model 1); V_0 – reference fluid velocity, given by lifting force [m/s], 1 m/s in this case

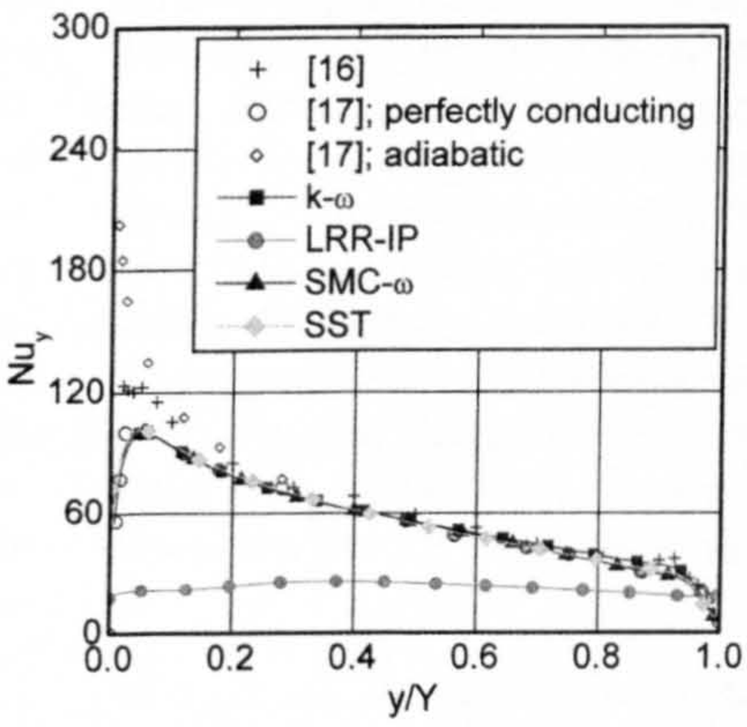

Bild 6. Vergleich numerischer und experimenteller lokaler Wärmeströme Nu_y an der Wandoberfläche (Modell 1); y – lokale Koordinate [m]; Y – Dimension des Modells [m]
Fig. 6. Comparison of numerical and experimental local heat flow Nu_y at the wall surface (Model 1); y – local coordinate [m]; Y – model dimension [m]; Nu_y – Nusselt n n [-] (reference temperature: 30 °C)

Moment-Closure-Turbulenz-Modell wurden analysiert (siehe [13]). Die zugehörigen Algorithmen sind in [5] näher erläutert. Von Interesse waren die Strömungs- und Temperaturverteilungen im Raum sowie die Wärmeströme an den Oberflächen. Um den räumlichen Einfluß der Geometrie auf die Strömung zu untersuchen, wurden die Ergebnisse eines quasi zweidimensionalen (Raumtiefe 10 mm) und eines dreidimensionalen Modells (Raumtiefe 375 mm) miteinander verglichen.

Das k-ω-Modell und das Shear-Stress-Transport-Modell erwiesen sich für die Simulationsaufgabe als am geeignetsten und zeigten sowohl im quasi-2D- als auch im 3D-Modell allgemein gute Übereinstimmung mit den experimentellen [16] und den numerischen [17] Referenzwerten. In Bild 5 sind beispielhaft die numerisch berechneten Grenzschichtprofile für das quasi-2D-Modell in halber Raumhöhe sowie die Referenzdaten dargestellt. Bild 6 zeigt den lokalen Wärmeübergang unmittelbar an der Wandoberfläche in Form der lokalen *Nusselt*-zahl Nu_y (Referenztemperatur hier: 30 °C). Trotz allgemein guter Ergebnisse existieren beim quasi-2D-Modell lokal kleine Störungen in der Luftströmung, die im 3D-Modell verschwinden. Diese Störungen haben aber nur einen vernachlässigbar kleinen Einfluß auf das Temperaturfeld im Raum und auf die Wärmeübertragung an den Oberflächen. Für die nachfolgenden Simulationen wurde deshalb aufgrund der geringeren Anzahl an Bilanzknotenpunkten und der damit stark reduzierten Rechenzeit anstelle des 3D-Modells das quasi-2D-Modell weiter verwendet.

5 Entwicklung von Methoden für CFX zur dynamisch thermischen Simulation

Bereits bei den zuvor beschriebenen stationären Simulationen zur Validierung der freien Konvektion ergeben sich aufgrund der Anzahl der benötigten Finiten Volumen-Elemente im quasi-2D-Modell zur Zeit noch lange Rechenzeiten und große Datenmengen. Dynamische Simulationen der freien Konvektion bei zeitveränderlichen Randbedingungen sind daher mit CFD kaum mehr praktikabel. Aus diesem Grund werden die vorher bereits beschriebenen Methoden aus [12] genutzt, um so in einer akzeptablen Zeit Langzeitsimulationen durchführen zu können. Hierzu mußten die Methoden auf eine andere kommerzielle CFD-Plattform (hier: ANSYS CFX-5) übertragen werden. In [12] erfolgte die Sequenz der Simulationsabschnitte (freeze/unfreeze flow) entweder *rein dynamisch (Methode 1)* oder durch den Wechsel einer instationären mit einer stationären Simulation (Methode 2). Obgleich auch die Methode 2 mit CFX nachvollzogen werden konnte, beschränken sich die folgenden Darstellungen auf die Methode 1, die sich bei sehr ähnlichen Rechenzeiten als programmtechnisch weniger aufwendig erwies.

Zuerst wurden die Simulationsabschnitte durch manuelles Stoppen und Starten des Rechenprogramms zum Einfrieren/Auftauen der hydrodynamischen und der Turbulenzgleichungen realisiert. Dies erwies sich jedoch als sehr umständlich. Im nächsten Schritt wurde daher ein Regelungsmodul programmiert, das als einfache Windows-Bibliothek bedienerfreundlich in die Simulation eingebunden werden kann und dort nach jedem Zeitschritt abgefragt wird. Durch dieses Modul ist es möglich, die Gleichungen zu beliebigen Zeitpunkten automatisch einzufrieren und wieder zuzuschalten, ohne die Simulation zwischendurch stoppen zu müssen. Die neue Programmethode wird im folgenden anhand zweier einfacher Simulationsmodelle veranschaulicht.

5.1 Fall 1: Abkühlung einer Wand über freie Konvektion

Als Testmodell (Modell 2) dient ein 1 m² großer Raum (quasi-2D-Modell mit 50 mm Raumtiefe) mit einer massiven Innenwand ($C_P = 835$ J/kgK, $\rho = 1920$ kg/m³, $\lambda = 0{,}72$ W/mK), siehe Bild 7. Die Außentemperatur Text wird zunächst auf konstante 20 °C (Fall 1) und das Initialluftströmungsfeld auf null gesetzt; die gegenüberliegende massive Innenwand und der Luftraum werden mit 27,5 bzw. 23,75 °C initialisiert; die horizontalen Flächen und die Rückseite der Innenwand bilden adiabatische Abschlüsse. Der Strahlungseinfluß wird zu ersten Test-

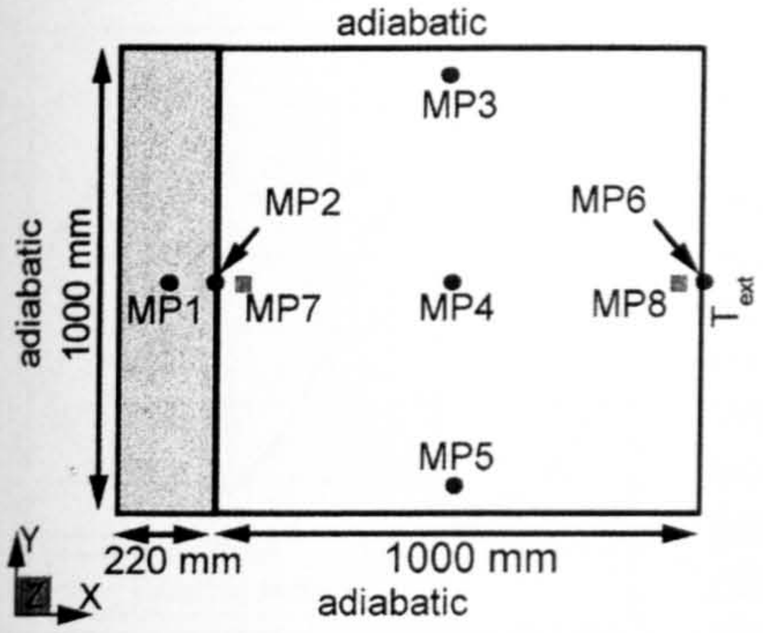

Bild 7. Modell mit massiver Innenwand und veränderlicher Außentemperatur T_{ext} (Modell 2) mit Position der Monitorpunkte für Luftgeschwindigkeiten (grüne Quadrate) und Temperaturen (rote Punkte); X, Y, Z – Dimension des Modells [m]
Fig. 7. Model with massive internal wall and variable external temperature T_{ext} (Model 2) with monitor positions for air velocity (green) and temperature (red); X, Y, Z – model dimensions [m]

zwecken vorläufig vernachlässigt. Als Referenz dient eine volldynamische Simulation (Basisfall) mit Zeitschrittweiten von 2 s. Zur Untersuchung der Freeze-Flow-Methode werden die relevanten Luftströmungsgleichungen knapp 4 Std. eingefroren und anschließend wieder für 10 Min. zugeschaltet; somit werden das Strömungs- und Temperaturfeld den aktuellen Randbedingungen angepaßt. Im Anschluß werden die Luftströmungsgleichungen wieder eingefroren usw.

Die Simulationsergebnisse der Freeze-Flow-Methode im Vergleich zum Basisfall sind anhand ausgewählter Monitorpunkte in den Bildern 8 und 9 dargestellt. Sie zeigen die zeitlichen Kurvenverläufe der vertikalen Geschwindigkeitskomponente bzw. der Temperaturen. Die Daten wurden während der Simulation alle 10 Min. gespeichert und ausgewertet; die Diagrammwerte zwischen diesen Punkten sind daher vom Grafikprogramm interpoliert.

Der Energieeintrag über die warme Innenwandoberfläche an den kühleren Innenraum bewirkt eine Erwärmung der wandnahen Umgebungsluft, die durch freie Konvektionsvorgänge nach oben steigt (positiver Wert der Luftgeschwindigkeit an MP 7) und die in der Wand gespeicherte Wärme langsam abführt. An der gegenüberliegenden kühleren Außenwand fällt die Luft wieder ab (negativer Wert der Luftgeschwindigkeit an MP 8) und bewirkt so eine sich langsam bewegende Luftwalze und eine Lufttemperaturschichtung im Raum (vgl. Temperaturpunkte MP 3 bis 5). Mit Abnahme der Innenwandtemperatur (siehe MP 1) und der verbundenen Oberflächentemperatur (siehe MP 2) reduzieren sich die Luftgeschwindigkeiten im Raum (siehe MP 7 und 8).

Bei der Freeze-Flow-Methode bleiben die Geschwindigkeiten während der Periode mit eingefrorener Luftströmung konstant, wobei sich deutliche Abweichungen zum Basisfall ergeben. Diese Abweichungen der Geschwindigkeiten wirken sich jedoch nur geringfügig auf die Temperaturen im Raum bzw. im Bauteil aus. Nach dem Zuschalten der Strömungsgleichungen passen sich Strömungs- und Temperaturfeld den neuen Randbedingungen wieder an und stimmen danach sehr gut mit denen des Basisfalls überein (Bilder 8 und 9). Insgesamt wird – bei gleicher Zeitschrittweite von 2 s – durch die Freeze-Flow-Methode eine Simulationszeiteinsparung von ca. 75 % im Vergleich zum Basisfall erreicht. Um den Zeitaufwand für die Simulationen weiter zu reduzieren, wurde die Zeitschrittweite in der eingefrorenen Phase stufenweise vergrößert. Für eine Zeitschrittweite von 5 ergibt sich, ohne eine einhergehende Abnahme der Genauigkeit, eine Reduzierung des Simulationsaufwandes um 93 % im Vergleich zum Basisfall.

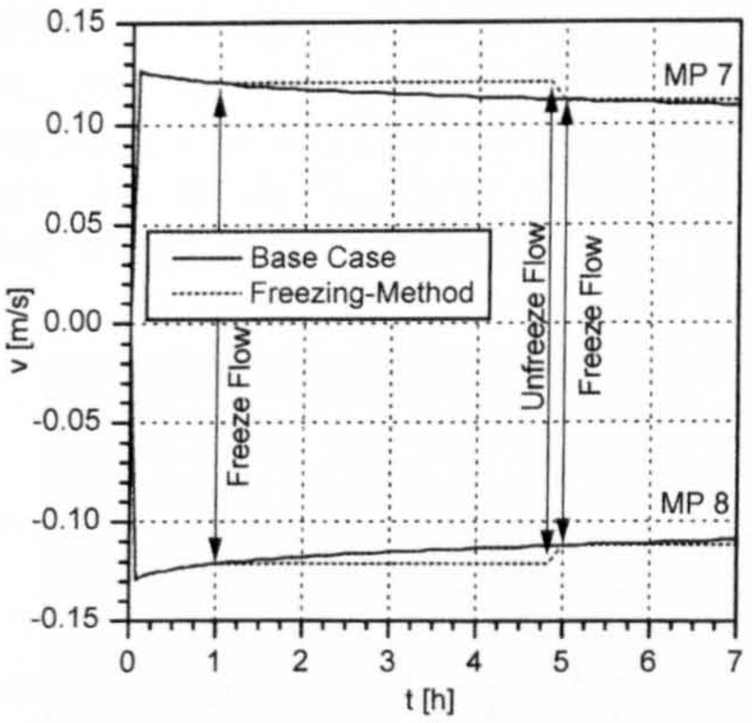

Bild 8. Vergleich der Geschwindigkeitskurvenverläufe an verschiedenen Monitorpunkten für konstante Temperaturrandbedingungen (Modell 2, Fall 1) ; v – vertikale Geschwindigkeitskomponente [m/s]; t – simulierte Zeit
Fig. 8. Comparison of velocity curve shapes at different monitor points for constant temperature boundary conditions (Model 2, Case 1); v – vertical velocity component [m/s]; t – simulated time

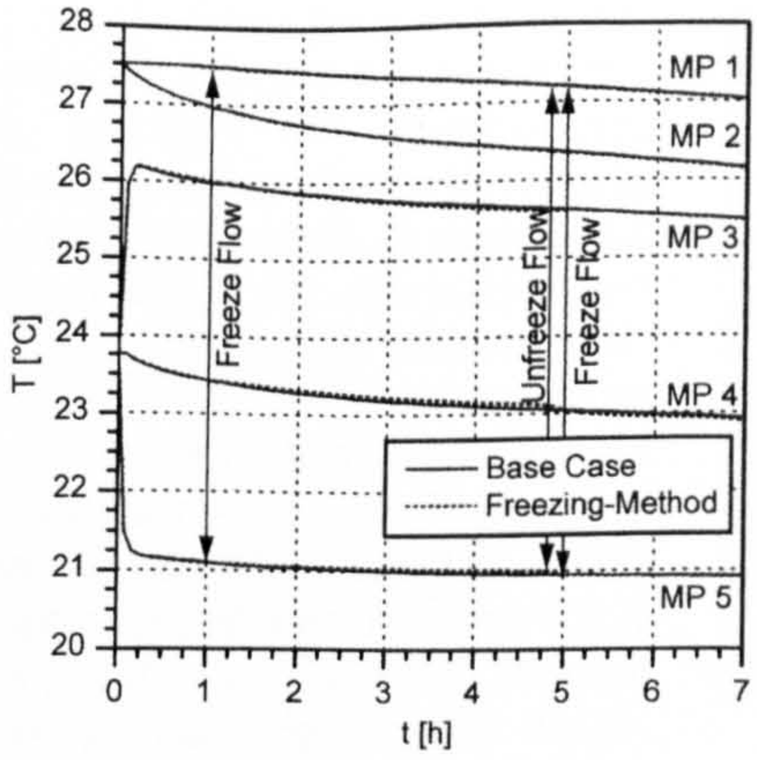

Bild 9. Vergleich der Temperaturkurvenverläufe an verschiedenen Monitorpunkten für konstante Temperaturrandbedingungen (Modell 2, Fall 1); t – simulierte Zeit
Fig. 9. Comparison of temperature curve shapes at different monitor points for constant temperature boundary conditions (Model 2, Case 1); t – simulated time

5.2 Fall 2: Sinusförmige Temperaturrandbedingungen

Dem Modell 2 (siehe Bild 7 und Abschnitt 5.1) wurde im Anschluß ein zeitveränderliches sinusförmiges Temperaturprofil auf die Außenwand aufgeprägt (Fall 2):

$$T_{ext} = 7{,}5 \sin(2\pi \cdot t/86400) + 20 \quad [°C] \qquad (1)$$

mit:
t simulierte Zeit [s].

Auf diese Weise sollen die täglichen Temperaturschwankungen des Außenklimas nachgebildet werden. Diese Annahme berücksichtigt die sommerliche Situation in modernen Bürogebäuden, die zunehmend große Glasfassaden besitzen und in denen externe Wärmelasten das Raumklima stark beeinflussen. Die thermisch nutzbaren Massen liegen dabei häufig an den Innenabschlüssen des Raumes. Auch für Fall 2 wurde die solare Strahlung innerhalb des Raumes nicht berücksichtigt.

Die Bilder 10 und 11 zeigen die berechneten Luftgeschwindigkeiten (MP 7 und 8) und die Temperaturverläufe (MP 1 bis 6) für den Basisfall und die automatisierte Freeze-Flow-Methode bei jeweils konstanter Zeitschrittweite von 1 s. Die dargestellte Periode beschränkt sich auf einen

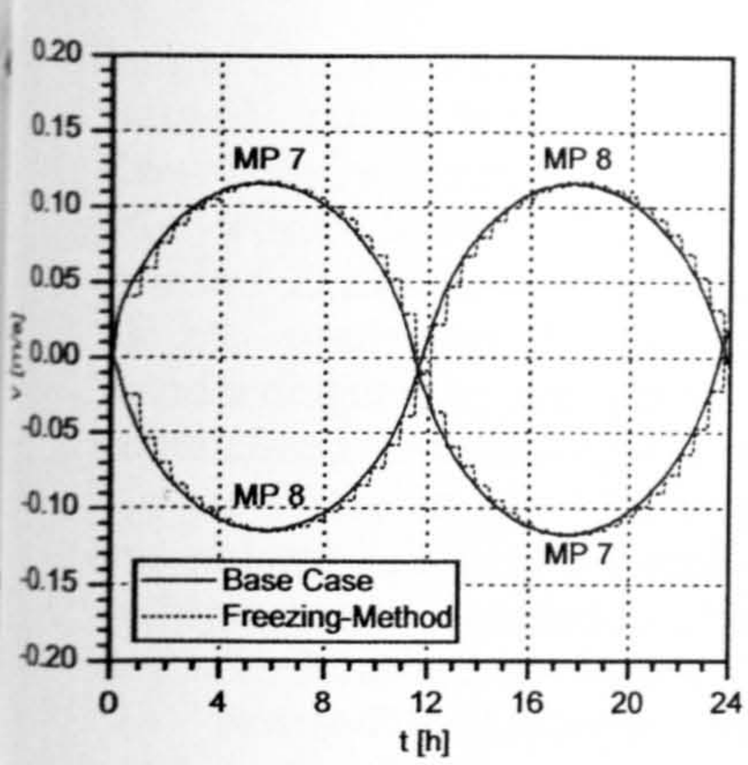

Bild 10. Vergleich der Geschwindigkeitskurvenverläufe an verschiedenen Monitorpunkten für sinusförmige zeitveränderliche Temperaturrandbedingungen (Modell 2, Fall 2); v – vertikale Geschwindigkeitskomponente [m/s]; t – simulierte Zeit
Fig. 10. Comparison of the velocity curve shapes at different monitor points for sinusoidal time varying temperature boundary conditions (Model 2 , Case 2); v – vertical velocity component [m/s]; t – simulated time

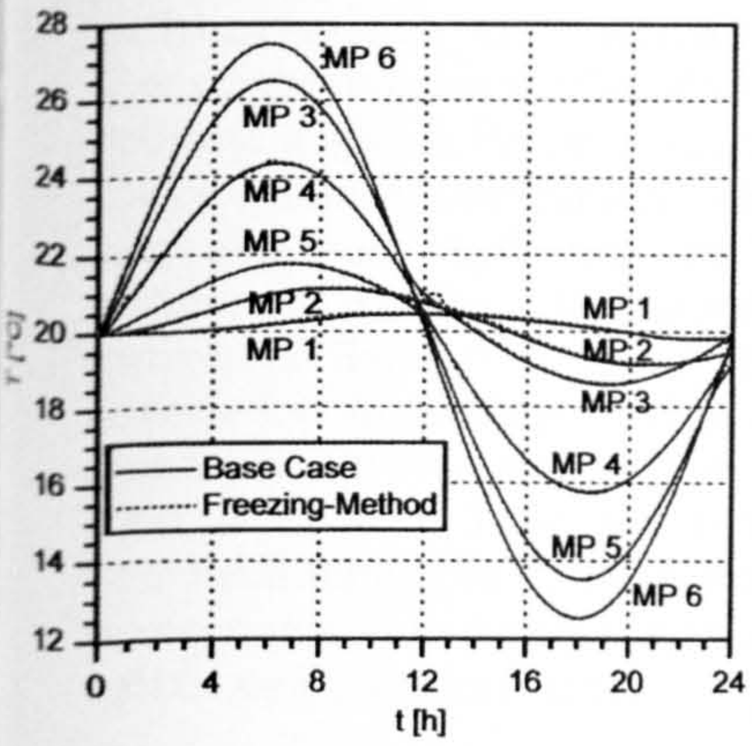

Bild 11. Vergleich der Temperaturkurvenverläufe an verschiedenen Monitorpunkten für sinusförmige zeitveränderliche Temperaturrandbedingungen (Modell 2, Fall 2); v – vertikale Geschwindigkeitskomponente [m/s]; t – simulierte Zeit
Fig. 11. Comparison of the temperature curve shapes at different monitor points for sinusoidal time varying temperature boundary conditions (Model 2, Case 2); v – vertical velocity component [m/s]; t – simulated time

Zeitraum von 24 Std. Eine Speicherung und Auswertung der Ergebnisse erfolgt nach jeweils 10 Min. für den Basisfall und nach jeweils 5 Min. für die angewendete Methode.

Zu Beginn besitzen die Innenwand und der Raum eine ausgeglichene Temperatur von 20 °C. An der Innenoberfläche der Außenwand steigt die Temperatur an und erwärmt aufgrund der freien Konvektion die Luft im Raum. Die Innenwand nimmt zeitverzögert zunächst die Wärmeenergie aus dem Raum auf (vgl. Temperaturen an MP 1 mit MP 6). Nachdem die externe Temperatur (MP 6) nach einer Weile wieder unterhalb der Innenwand-Oberflächentemperatur (MP 2) gefallen ist, drehen sich die Verhältnisse um und die Wärme wird von der Wand langsam wieder abgegeben. In diesem Zeitraum (etwa bei 11 Std. 35 Min.) findet auch eine Umkehr des Strömungsfeldes statt, was anhand der Vorzeichenumkehr der Geschwindigkeiten an MP 7 und MP 8 ersichtlich ist. Bild 12 stellt die Temperaturverhältnisse in der massiven Innenwand und im Raum im Zeitraum der Strömungsumkehrung dar. An der Innenwandoberfläche besteht zwischen dem Boden und der Decke ein vertikaler Temperaturgradient von ca. 1,2 K. Herkömmliche Simulationen mit dynamischen Gebäude-Simulationsprogrammen können diesen Effekt jedoch nicht nachbilden.

Bei der Freeze-Flow-Methode wurde das Strömungsfeld für 30 Min. eingefroren und danach wieder für 5 Min. angepaßt. Nach der jeweiligen Anpassungszeit stimmen sowohl die Luftgeschwindigkeiten als auch die Temperaturen mit denen des Basisfalls gut überein. Im Vergleich zum Basisfall ergeben sich durch die Freeze-Flow-Methode eine Simulationszeiteinsparung von 72 % und eine Reduzierung der Datengröße der Ausgabedatei um 65 %. Auch bei diesem Modell wurde versucht, den Zeitaufwand für die Simulation und die Datengrößen nochmals zu reduzieren, indem während der eingefrorenen Phase mit einem größeren Zeitschritt von 5 gerechnet wurde. In diesem Fall verringert sich die Simulationszeit (bzw. die Datengröße) allerdings lediglich von 72 % (65 %) auf insgesamt 80 % (76 %), was etwas enttäuschend ist. Außerdem zeigen die Temperaturen am Bauteil (MP 1 und MP 2) teils eine schwache Abweichung von 0,2 K im Vergleich zum Basisfall. Weitere Simulationsläufe ergaben, daß die Simulationsdauer und die produzierte Datenmenge primär nicht durch die Zeitschrittweite in den eingefrorenen Perioden, sondern maßgeblich durch die Dauer der uneingefrorenen Perioden bestimmt werden. Hierzu sind in Zukunft noch weitere Untersuchungen vorgesehen.

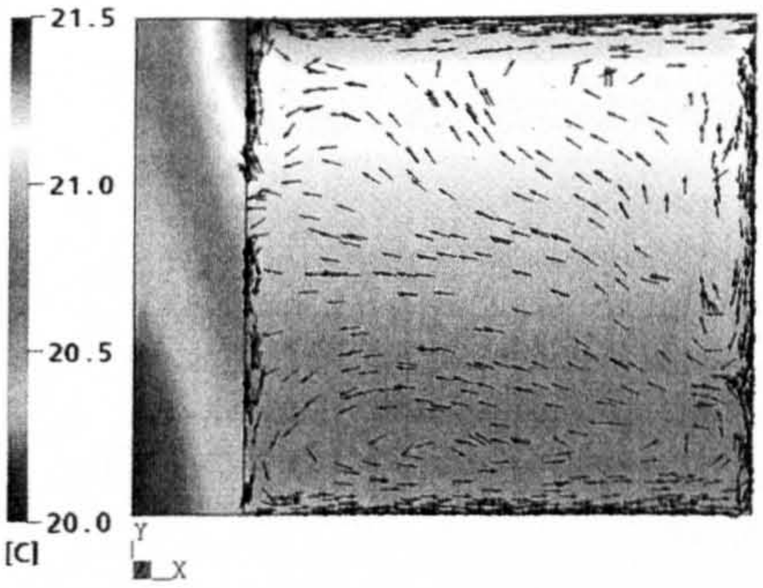

Bild 12. Temperatur- und Strömungsfeld im Modell 2, Fall 2 nach einer simulierten Zeit von etwa 11 h 35 min; X, Y, Z – Dimension des Modells [m]
Fig. 12. Temperature and flow fields for model 2, case 2 after a simulation time of about 11 hours 35 min; X, Y, Z – model dimensions [m]

6 Zusammenfassung

Wie zuvor dargestellt, sind herkömmliche dynamische Simulationsprogramme nicht in der Lage, die Luftströmungen und die Temperaturverteilung innerhalb eines Raumes zu erfassen. Die Kopplung dieser Programme mit detaillierteren Luftströmungs-Simulationsprogrammen (CFD) führt zu zahlreichen Simulations- und Schnittstellenproblemen. Eine Lösung besteht darin, die gesamte Simulationsaufgabe auf die CFD-Plattform zu verlagern, was heutzutage allerdings extrem lange Rechenzeiten zur Folge hat. Um diese Rechenzeiten zu verringern, wurde für ANSYS CFX-5 eine neue Freeze-Flow-Methode entwickelt, die auf der periodischen Einfrierung der hydrodynamischen Gleichungen basiert und dynamische Langzeitsimulationen erlaubt.

Besonders rechenintensiv ist noch die Simulation der in Gebäuden vorherrschenden freien Konvektion, da hierfür ein ausreichend feines Maschengitter in Wandnähe erforderlich ist. Außerdem müssen die Strömungsturbulenzen durch geeignete Turbulenzmodelle erfaßt werden. Die Validierung von CFX-5 zur Simulation der freien Konvektion zeigte dabei allgemein eine gute Übereinstimmung mit experimentellen, analytischen und numerischen Referenzen.

Die für CFX-5 entwickelte Freeze-Flow-Methode wurde zunächst anhand eines einfachen Modells für die

langsame Abkühlung eines massiven Bauteils durch Wärmeabgabe über Konvektion getestet. Das Strömungsfeld wurde hierbei über eine bestimmte Zeitspanne eingefroren und danach wieder an die veränderten Randbedingungen angepaßt. Nach ausreichender Anpassungszeit stimmten die Werte an den Monitorpunkten nahezu mit dem Basisfall (eine volldynamische Simulation ohne periodische Einfrierung) überein. Durch die Freeze-Flow-Methode konnte hierbei eine Zeiteinsparung von bis zu 93 % erzielt werden. Für ein zweites Modell mit einer sinusförmig zeitveränderlichen Temperaturrandbedingung konnte eine Simulationszeitreduzierung von 80 % bei sehr geringem Genauigkeitsverlust verzeichnet werden. Weitere Simulationsversuche zeigten, daß die Zeit- und Dateneinsparung i. w. von der Dauer der uneingefrorenen Zeitperiode abhängt.

Anhand der Simulationsergebnisse konnte aufgezeigt werden, daß mit CFD dynamisch thermische Langzeitsimulationen ohne wesentlichen Genauigkeitsverlust möglich sind. Dies eröffnet zugleich Potential für dynamische Simulationsaufgaben, bei denen eine feine Auflösung der Luftströmungs- und der Temperaturbedingungen im Raum wichtig ist (z. B. die Simulation des Kühlpotentials einer sommerlichen Nachtlüftung von Räumen oder einer Bauteilaktivierung). Mit herkömmlichen Gebäudesimulationsprogrammen war dies bisher nur relativ ungenau simulierbar.

7 Ausblick

Die bisher bei der Freeze-Flow-Methode in Anlehnung an [12] angewendeten Regelkriterien für den Wechsel zwischen eingefrorenen und uneingefrorenen Gleichungszuständen bestanden aus einem fest vorgegebenen Zeitraster. Die Prozedur reagiert somit nicht auf die dynamischen Änderungen der hydrodynamischen Vorgänge während der Simulation. Hier aufzuführen wären beispielsweise die Auswirkung verschiedener thermischer Zeitkonstanten zwischen dem Bauteil und dem Fluid, die schnellen Änderungen der natürlichen oder mechanischen Lüftung oder ein schnell wechselnder Wärmeeintrag bei Sonneneinstrahlung oder Raumbelegung. Darum ist es Ziel zukünftiger Untersuchungen, verbesserte Regelkriterien, die auf eine größere Zahl an Einflußvariablen automatisch und intelligent reagieren, zu finden und in das Modul einzubinden. Außerdem soll durch weitere Untersuchungen die Simulationszeit auf ein Minimum gesenkt werden.

Danksagung

Dieses Forschungsprojekt wird vom Bundesministerium für Bildung und Forschung innerhalb des aFuE-Programms „Aktive und passive Nutzung von Massivbauteilen zur Unterstützung der Raumkonditionierung“ unterstützt.

Literatur

[1] *Pfafferott J.*: Passive Kühlung mit Nachtlüftung. BINE Informationsdienst, Themeninfo 1/2003, Fachinformationszentrum Karlsruhe, S. 1–12.

[2] TRNSYS: Version 16, http://www.trnsys.com, 2005.

[3] *Beausoleil-Morrison, I.*: Modelling mixed convection heat transfer at internal building surfaces. Building Simulation, 1999.

[4] COMIS: Version 3.0, http://www-epb.lbl.gov/comis/, 2004.

[5] ANSYS CFX: CFX-5 Solver Models and Theory User Manuals, Version 5.7, 2004.

[6] FLUENT: Version 6.2, http://www.fluent.com/, 2005.

[7] *Pfrommer, P.*: Thermal Modelling of Highly Glazed Spaces. PhD thesis, De Montfort University, Leicester, England, 1995.

[8] *Negrao, C.*: Conflation of computational fluid dynamics and building thermal simulation, PhD thesis, University of Strathclyde, Glasgow, UK, 1995.

[9] *Kendrick, J.*: An overview of combined modelling of heat transport and air movement. Technical Note 40, Air Infiltration and Ventilation Centre, Coventry, England, 1993.

[10] *Zhai, Z., Chen, Q.*: Strategies for coupling energy simulation and computational fluid dynamics programs, 7. International IBPSA Conference, Brazil, pp 59–66, 2001.

[11] *Chen, Q., Peng, X., Van Paassen, A.*: Prediction of room thermal response by CFD technique with conjugate heat transfer and radiation models. ASHREA Transactions, 1998, pp 50–60.

[12] *Somarathne, S., Seymour, M., Kolokotroni, M.*: Transient solution methods for dynamic thermal modelling within CFD. International Journal of Ventilation, Vol. 1:2, 2002. Veetech Ltd., England, pp 141–156.

[13] *Zitzmann, T., Pfrommer, P., Cook, M., Rees, S., Marjanovic, L.*: Simulation of steady-state natural convection by using CFD. Proceedings of the 9th International Building Simulation Conference, Montreal, Canada, 2005.

[14] *Phillips, J., Naylor, D., Harrison, S. J., Oosthuizen, P. H.*: Free convection from a glazing with a venetian blind: Numerical model development. Transactions of the CSME, Vol. 23 (1999), No. 1B, pp 159–172.

[15] *Ostrach, S.*: An analysis of laminar free-convection flow and heat transfer about a flat plat parallel to the direction of the generating body force. NASA, 1953. Report 1111, Madison, pp 63–79.

[16] *Tian, J., Karayiannis, T. G.*: Low turbulence natural convection in an air-filled square cavity, Part 1: the thermal and fluid flow fields. Journal Heat and Mass Transfer, Vol. 43 (2001), pp 849–866.

[17] *Beghein, C., Penot, F., Mergui, S., Allard, F.*: Numerical and experimental evaluation of turbulent models for natural convection simulation in a thermally driven square cavity. Proceedings ASME Conference, 1993, pp 1–12.

Autoren dieses Beitrages:
Dipl.-Ing. (FH) Tobias Zitzmann,
Prof. Dr. Peter Pfrommer
beide: Fachhochschule Coburg, Studiengang Bauingenieurwesen, Studienrichtung Gebäudetechnik und Bauphysik, Friedrich-Streib-Str. 2, 96450 Coburg
Dr. Malcolm Cook, De Montfort University, Institute of Energy and Sustainable Development, Queens Building, The Gateway, Leicester LE1 9BH, England

IBPSA

Erste deutsch-österreichische IBPSA-Konferenz
Technische Universität München
R. Koenigsdorff, C. van Treeck (Hrsg.)

BauSIM 2006

DYNAMISCH THERMISCHES CFD VERFAHREN

Tobias Zitzmann[1], Peter Pfrommer[1], Malcolm Cook[2]
[1]Fachhochschule Coburg, Bauingenieurwesen, Germany
[1]Institue of Energy and Sustainable Development, De Montfort University, England
zitzmann@fh-coburg.de

KURZFASSUNG

Zur Reduktion des Zeitaufwands von dynamisch thermischen Langzeitsimulationen mit CFD Programmen wurde in kürzlich veröffentlichten Studien eine neuartige Freeze-Flow Methode vorgestellt. Diese basiert auf der periodischen Umschaltung zwischen der volldynamischen Lösung aller Gleichungen und der ausschließlichen Lösung der Entalphie-Gleichungen (eingefrorene Luftströmung).

Dieser Artikel beschreibt eine neue automatisierte Regelung für diese Umschaltung, wodurch eine zusätzliche Reduzierung der Simulationszeit erzielt wird. In Tests an Modellen für die mechanische und freie Lüftung sowie der freien Konvektion im geschlossenen Raum für feste und zeitveränderliche thermische Randbedingungen wurde im Vergleich zur ununterbrochenen volldynamischen Simulation eine Simulationszeiteinsparung von bis zu 93 % erreicht.

ABSTRACT

Previously published studies have presented a novel freeze-flow method for reducing CPU requirements of long-term dynamic thermal simulations using CFD programs. This works by intermittently switching between solution of the full dynamic equations and solution of the enthalpy equation only (frozen flow).

This paper describes a new automated control method for this switching strategy and shows an additional decrease in simulation time. In tests with models for mechanical and natural ventilation and for free convection in a sealed room with constant and time varying thermal boundary conditions, a simulation time reduction of up to 93 % was achieved when compared to a continuous fully dynamic simulation.

EINLEITUNG

Zur dynamischen Gebäudesimulation wurden in der Vergangenheit hauptsächlich zonale Computermodelle wie TRNSYS eingesetzt, die jedoch den Wärmetransport durch die Bauteilmasse nur eindimensional annähern und die - vor allem - keine Raumluftströmungen einbeziehen. Dies kann in bestimmten Fällen zu erheblichen Rechenungenauigkeiten führen. Aufgrund der Zunahme an Rechnerleistung und einer neu eingeführten zeitreduzierenden Freeze-Flow Technik lassen sich inzwischen auch CFD Programme mit ihrer viel höheren Detailgenauigkeit für dynamische Langzeitsimulationen einsetzen. Bei dieser Methode wird das Strömungsfeld zeitweise für feste Zeitspannen eingefroren, wodurch sich der Rechenaufwand nur auf die Lösung der Entalphie-Gleichungen reduzieren lässt. Außerdem sind größere Zeitschritte möglich, da in dieser Zeit Strömungsturbulenzen nicht berechnet werden müssen. Das Strömungsfeld wird zwischenzeitlich in bestimmten Abständen „aufgetaut" und den neuen Bedingungen angepasst.

Somarathne et al. (2005) ermittelten mit dieser Methode für die freie Konvektion in einem einfachen geschlossenen Raum Zeiteinsparungen von bis zu 90%, für die mechanische Lüftung in einem komplexeren Testraum mit wechselnden Wärmequellen immerhin eine Reduzierung um 20 %. Hierbei musste die Simulation für einen Wechsel zwischen uneingefrorener und eingefrorener Periode noch per Hand gestoppt und wieder neu gestartet werden.

In Untersuchungen von Zitzmann et al. (2006) konnte mit einer entsprechenden (jedoch automatisierten) Technik unter Verwendung der kommerziellen CFD Plattform CFX für ein ähnliches Raummodell vergleichbare Leistungen erzielt werden. CFX wurde im Rahmen der hier vorgestellten Forschungsarbeit bereits zuvor für die Simulation der freien Konvektion im Raum validiert (Zitzmann et al., 2005).

In der von Somarathne beschriebenen Freeze-Flow Technik wird der Wechsel zwischen eingefrorenem und uneingefrorenem Strömungszustand zeitlich starr vorgegeben. Dadurch ist die Regelung nicht in der Lage auf unvorhersehbare dynamische Änderungen der temporären und lokalen thermischen Bedingungen im Raum differenziert einzugehen, was größere Rechenfehler zur Folge haben kann. Daher wurde in weiterführenden Untersuchungen eine neue Regelung entwickelt, die auf diese thermischen

Bedingungen effizient und automatisch reagieren kann. Hierbei soll die Simulationsdauer uneingefrorener Luftströmung verkürzt und die Dauer eingefrorener Strömung möglichst verlängert werden.

REGELUNG

Wechsel von uneingefrorenem zu eingefrorenem Strömungszustand

Die Anzahl der notwendigen Iterationen innerhalb eines Zeitschritts zur Erreichung einer vorgegebenen Konvergenz reduziert sich während einer uneingefrorenen Strömungsperiode von einem großen Wert am Anfang (starke Strömungsänderung aufgrund der neuen Randbedingungen) allmählich auf eine niedrige konstante Zahl (geringe Strömungsänderung). Erst nach Erreichen dieses Zustandes ist es sinnvoll, in den eingefrorenen Strömungszustand zu wechseln. Als Hauptkriterium für das Umschalten zum eingefrorenen Zustand dient daher das Erreichen einer definierten maximalen Iterationsanzahl MAXLOOPS. Aufgrund der thermischen Trägheit der Luft sind die thermischen Fehler im Raum, die während der eingefrorenen Periode unterlaufenen sind, trotz Erreichen der vorgegebenen Iterationszahl häufig noch nicht vollständig kompensiert. Daher ist in der Regel eine zusätzliche Verlängerung EXTENSION der uneingefrorenen Zeitspanne notwendig.

Wechsel von eingefrorenem zu uneingefrorenem Strömungszustand

Während der Periode eingefrorener hydrodynamischer Gleichungen ändern sich nur die Entalphie-Gleichungen. In diesem Fall lässt sich das Simulationsproblem auf die lokalen Temperaturwerte reduzieren. Da das eingefrorene Strömungsfeld eine vorgegebene thermische Situation repräsentiert, führt während einer eingefrorenen Periode jede Änderung des Temperaturfeldes in der Strömung bzw. an den Raumoberflächen zu einem Berechnungsfehler. Um diesen Fehler zu minimieren, dürfen die Änderungen der Temperaturen nicht zu groß ausfallen. Als Kriterium zum Umschalten in den uneingefrorenen Zustand dient daher ein vordefiniertes Maximum MAXTEMP der lokalen Temperaturdifferenzen im Raum (d.h. in jedem finiten Volumenelement) zwischen Beginn und aktuellem Zeitpunkt während des eingefrorenen Zustandes.

Im untersuchten Fall der freien Konvektion liefern beispielsweise Werte von 3, 180 s und 0.5 K für die Parameter MAXLOOPS, EXTENSION bzw. MAXTEMP hinsichtlich Genauigkeit und Simulationszeit optimale Ergebnisse.

Zusätzlich erkennt die Regelung durch vorzeitiges Einlesen der vorgegebenen Randbedingungen aus Datensätzen oder Zeitfunktionen im Voraus, ob in nächster Zeit eine größere Änderung an den Randbedingungen stattfindet und unterbindet oder forciert, falls notwendig, einen Wechsel zwischen den Strömungszuständen.

SIMULATIONSMODELL

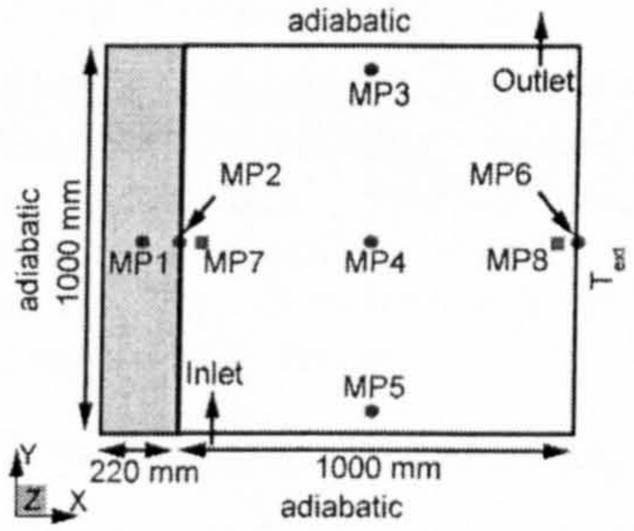

Abbildung 1: Skizze des Simulationsmodells

Die Effizienz der neuen Regelung wurde anhand eines einfachen Modells (Abbildung 1) für die typischen Strömungsfälle der mechanischen, der freien Lüftung sowie für die reine freie Konvektion im geschlossenen Raum überprüft. Als Testmodell diente ein 1 m^2 quasi zwei-dimensionaler Raum (Tiefe = max. Kantenlänge der finiten Volumenelemente), mit einer angrenzenden massiven Mauerziegelwand der Dicke 220mm. Die markierten, durchnummerierten (roten) Kreise und (grünen) Quadrate geben die Positionen der bei der Analyse verwendeten Monitorpunkte für die Temperaturen bzw. Geschwindigkeiten an.

ERGEBNISSE UND DISKUSSION

Konstante Randbedingungen

Aus Platzgründen wird hier nur der Fall für die freie Konvektion nach einem Temperatursprung dargestellt. In diesem Fall wurden alle Lüftungsöffnungen geschlossen und das gesamte Raummodell mit 27,5°C (Mauerwerk) bzw. 23,75 °C (Raumluft) initialisiert. Zu Beginn der Simulation wurde die Außentemperatur an T_{ext} sprunghaft auf 20°C reduziert, was einen Abkühlvorgang des Raumes bzw. des Mauerwerks bewirkt.

Abbildungen 2a aund 2b zeigen eine hohe Übereinstimmung (Unterschiede kleiner 0.1 K bzw. 0.006 m/s) der Temperaturwerte und Geschwindigkeiten an den untersuchten Monitorpunkten für die neue Freeze-Flow Methode mit dem Basisfall (klassische Simulation ohne Strömungseinfrierung). In diesem Fall wurde gegenüber dem Basisfall eine Reduktion der CPU Zeit von 93 % und der Datenmenge von 78 % ermittelt.

a)

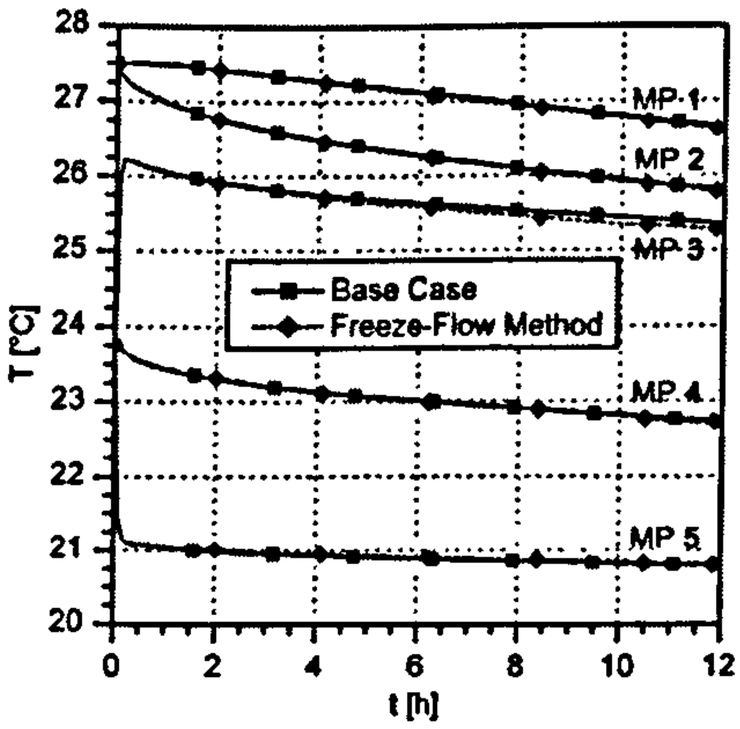

b)

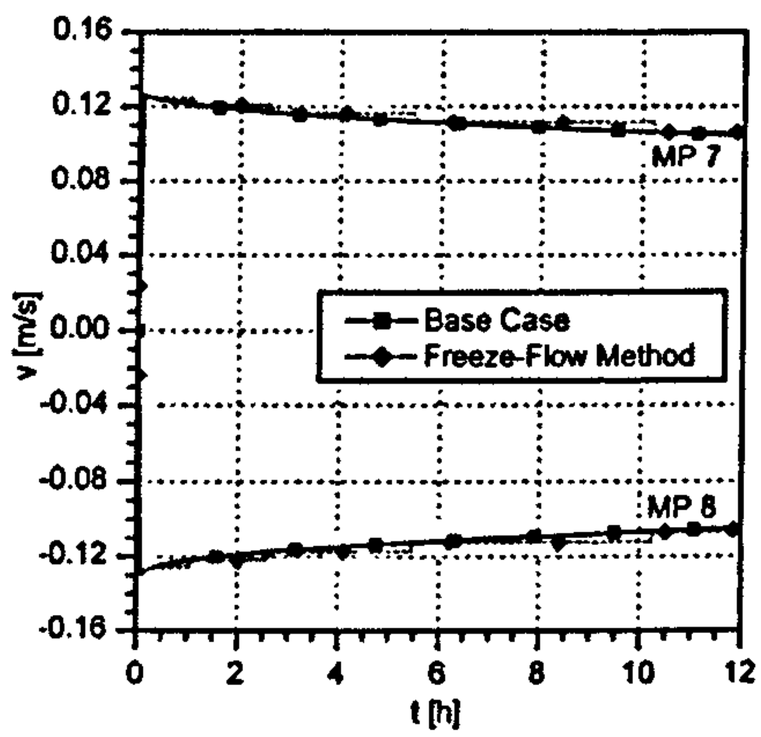

c)

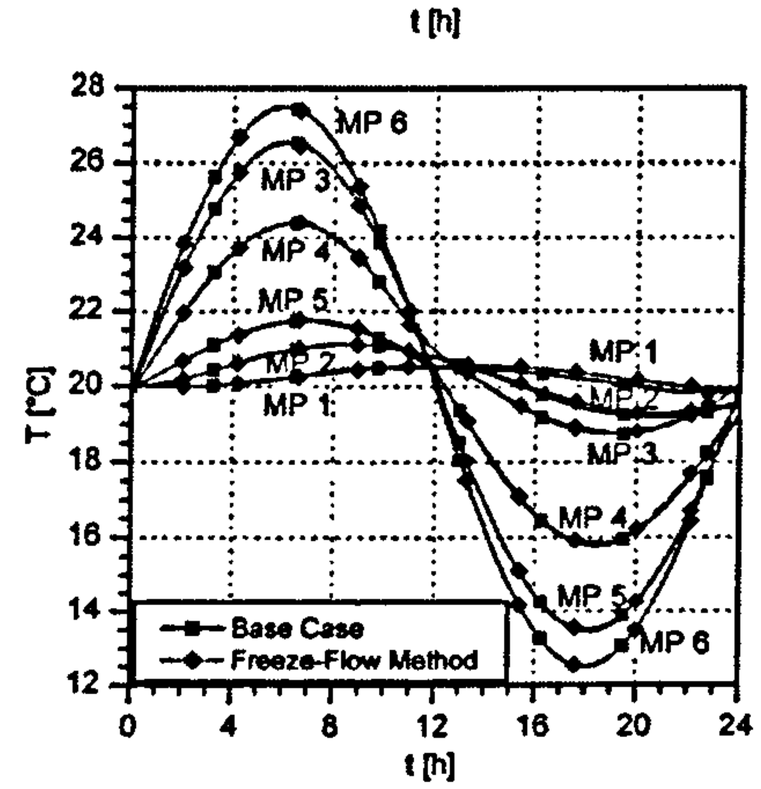

d)

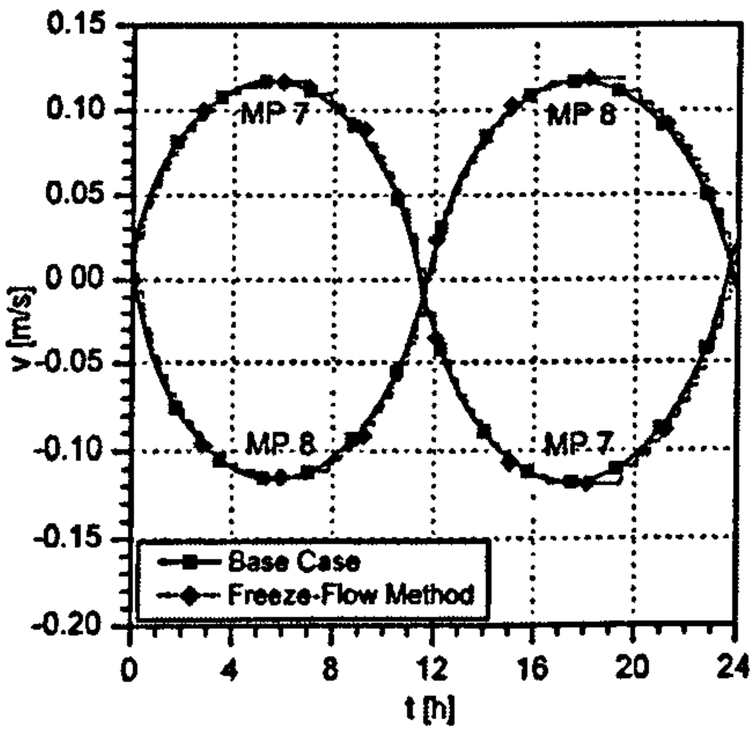

Abbildung 2: (a) Temperatur- und (b) Geschwindigkeitsverläufe für konst. Randbed.; (c) Temperatur- und (d) Geschwindigkeitsverläufe für zeitvar. Randbed. an verschiedenen Monitorpunkten

Sinusförmige Randbedingungen

Um die Regelmethode bei wechselnden Randbedingungen zu testen, wird dem Modell von Abbildung 1 ein sinusförmiges Temperaturprofil T_{ext} an der Außenwand aufgeprägt:

$$T_{ext} = 7{,}5 \cdot \sin(2 \cdot \pi \cdot t / 86400) + 20 \qquad [°C]$$

Aus Abbildungen 2c und 2d ist zu erkennen, dass auch in diesem Fall die Werte für die neu entwickelte Regelung mit dem Basisfall ähnlich gut übereinstimmen. Hierbei wurde eine CPU Zeiteinsparung von 74 % und eine Reduktion der Datenmenge von 78 % erzielt.

Vergleich zur Regelung mit festen Zeitperioden

Die neue angepasste und die bisherige starre Regelung der ein- bzw. uneingefrorenen Zeitperioden führten für alle untersuchten Fälle zu vergleichbaren Ergebnissen, die mit dem Basisfall weitgehend übereinstimmen. Die neue Regelung erwies sich jedoch insbesondere in Zeiten mit schnell wechselnden Umgebungsbedingungen als genauer. Außerdem konnte mit dieser Regelung die Effizienz der Freeze-Flow-Methode bei fast allen Tests nochmals gesteigert werden. Im Beispiel der freien Konvektion im geschlossenen Raum und konstanter Randbedingungen wurde mit der starren Regelung eine Reduktion der Simulationszeit und Datenmenge von 78 % bzw. 68 % erreicht. Die neue Regelung verbesserte die Werte auf 93% bzw. 78%. Für den Fall mit zeitveränderlichen Randbedingungen ergab sich für beide Regelungen eine nahezu identische Effizienz.

DANKSAGUNG

Das diesem Bericht zugrunde liegende Vorhaben wurde mit Mitteln des Bundesministeriums für Bildung und Forschung unter dem Kennzeichen 1749B04 gefördert. Die Verantwortung für den Inhalt dieser Veröffentlichung liegt beim Autor.

LITERATUR

Somarathne S, Seymour M., Koloktroni M., 2005: Dynamic thermal CFD simulation of a typical office by efficient transient solution methods, Building and Environment 40, S. 887-896.

Zitzmann T., Cook M., Pfrommer P., Rees S., Marjanovic L., 2005: Simulation of steady-state natural convection by using CFD, Proc. of the 9th Int. Building Simulation Conf., Montreal, Kanada, S. 1448-1456.

Zitzmann T., Pfrommer P., Cook. M., 2006: Simulation dynamisch thermischen Langzeitverhaltens in Gebäuden mittels CFD, BAUPHYSIK 28, S. 96-102.

Tobias Zitzmann
Peter Pfrommer
Malcolm Cook

DOI: 10.1002/bapi.200710004

Dynamisch-thermisches CFD-Verfahren mit angepaßter Regelungsmethode

Zur Reduktion des Zeitaufwands von dynamisch-thermischen Langzeitsimulationen mit CFD-Programmen wurde in kürzlich veröffentlichten Studien eine neuartige Freeze-Flow Methode vorgestellt. Diese basiert auf der periodischen Umschaltung zwischen der volldynamischen Lösung aller Gleichungen und der ausschließlichen Lösung der Enthalpie-Gleichungen (eingefrorene Luftströmung). Dieser Artikel beschreibt eine neue, angepaßte Regelung für diese Umschaltung, wodurch eine zusätzliche Reduzierung der Simulationszeit erzielt wird. In Tests an Modellen für die mechanische und freie Lüftung sowie der freien Konvektion im geschlossenen Raum für feste und zeitveränderliche thermische Randbedingungen wurde im Vergleich zur ununterbrochenen volldynamischen Simulation eine Simulationszeiteinsparung von bis zu 93 % erreicht.

Dynamic thermal CFD approach using an adaptive control method.
Previously published studies have presented a novel freeze-flow method for reducing CPU requirements of long-term dynamic thermal simulations using CFD programs. This works by intermittently switching between solution of the full dynamic equations and solution of the enthalpy equation only (frozen flow). This paper describes a new automated control method for this switching strategy and shows an additional decrease in simulation time. In tests with models for mechanical and natural ventilation and for free convection in a sealed room with constant and time varying thermal boundary conditions, a simulation time reduction of up to 93 % was achieved when compared to a continuous fully dynamic simulation.

1 Einführung

Zur dynamischen Gebäudesimulation wurden in der Vergangenheit hauptsächlich zonale Computermodelle wie TRNSYS eingesetzt, die jedoch den Wärmetransport durch die Bauteilmasse nur eindimensional annähern und die – vor allem – keine Raumluftströmungen einbeziehen. Dies kann in bestimmten Fällen zu erheblichen Rechenungenauigkeiten führen. Aufgrund der Zunahme an Rechnerleistung und einer neu eingeführten zeitreduzierenden Freeze-Flow Technik lassen sich inzwischen auch CFD Programme mit ihrer viel höheren Detailgenauigkeit für dynamische Langzeitsimulationen einsetzen. Bei dieser Methode wird das Strömungsfeld zeitweise für feste Zeitspannen eingefroren, wodurch sich der Rechenaufwand auf die Lösung der Enthalpie-Gleichungen reduzieren läßt. Außerdem sind größere Zeitschritte möglich, da die zeitliche Dynamik des Strömungsfeldes in dieser Zeit nicht betrachtet wird. Das Strömungsfeld wird zwischenzeitlich in bestimmten Abständen „aufgetaut" und den neuen Bedingungen angepaßt.

In Simulationen von [1] wurden mit dieser Methode für die freie Konvektion in einem einfachen geschlossenen Raum Zeiteinsparungen von bis zu 90 %, für die mechanische Lüftung in einem komplexeren Testraum mit wechselnden Wärmequellen immerhin eine Reduzierung um 20 % ermittelt. Hierbei mußte die Simulation für einen Wechsel zwischen uneingefrorener und eingefrorener Periode noch per Hand gestoppt und wieder neu gestartet werden.

In Untersuchungen von [2] konnte mit einer entsprechenden (jedoch automatisierten) Technik unter Verwendung der kommerziellen CFD-Plattform CFX für ein ähnliches Raummodell vergleichbare Leistungen erzielt werden. CFX wurde im Rahmen der hier vorgestellten Forschungsarbeit bereits zuvor für die Simulation der freien Konvektion im Raum validiert [3]. Dem impliziten Rechenverfahren von CFX liegen die *Reynolds*-gemittelten *Navier-Stokes*-Gleichungen (RANS) zugrunde [4]. Während der Perioden eingefrorener Strömung werden die hydrodynamischen Gleichungen, d. h. die Massenerhaltungs- und die Impulserhaltungs-Gleichungen, sowie die Gleichungen des in dieser Untersuchung verwendeten k-ω-Turbulenzmodells nicht erneut berechnet, sondern es wird das am Ende der vorherigen uneingefrorenen Periode vorliegende Strömungsfeld beibehalten. Während der eingefrorenen Periode sind die RANS-Gleichungen daher weiterhin gekoppelt und die Stabilität des Verfahrens ist gewährleistet. Eine grundlegende Einführung der Freeze-Flow-Methode für CFD-Anwendungen wurde kürzlich bereits an anderer Stelle im Detail beschrieben (siehe [2]). Dieser Artikel beschreibt im Wesentlichen eine Weiterentwicklung dieser Freeze-Flow-Methode.

In der von [1] beschriebenen Freeze-Flow-Technik wird der Wechsel zwischen eingefrorenem und uneingefrorenem Strömungszustand zeitlich starr vorgegeben. Dadurch ist die Regelung nicht in der Lage auf unvorhersehbare dynamische Änderungen der temporären und lokalen thermischen Bedingungen im Raum differenziert einzugehen, was größere Rechenfehler zur Folge haben kann. Daher wurde in weiterführenden Untersuchungen eine neue Regelung entwickelt, die auf diese thermischen Bedingungen effizient und automatisch reagieren kann. Hierbei soll die Simulationsdauer uneingefrorener Luftströmung verkürzt und die Dauer eingefrorener Strömung möglichst verlängert werden.

2 Angepaßte Regelung

Der folgende Abschnitt stellt eine neue Regelung vor, die die Länge der Zeitperioden uneingefrorener und eingefrorener Strömung den Randbedingungen anpaßt. Dabei werden die Hauptregelkriterien beschrieben.

2.1 Kontrollkriterien zum Wechsel von uneingefrorenem zu eingefrorenem Strömungszustand

Die Anzahl der notwendigen Iterationen innerhalb eines Zeitschritts zur Erreichung einer vorgegebenen Konvergenz reduziert sich während einer uneingefrorenen Strömungsperiode von einem großen Wert am Anfang (starke Strömungsänderung aufgrund der neuen Randbedingungen) allmählich auf eine niedrige konstante Zahl (geringe Strömungsänderung). Erst nach Erreichen dieses Zustandes ist es sinnvoll, in den eingefrorenen Strömungszustand zu wechseln. Als Hauptkriterium für das Umschalten zum eingefrorenen Zustand dient daher das Erreichen einer definierten maximalen Iterationsanzahl MAXLOOPS.

Um sicher zu gehen, daß die Lösung quasi-stationär ist, muß über einen längeren Zeitraum kontrolliert werden ob die minimal erreichbare Iterationsanzahl konstant eingehalten wird. Dieser Zeitraum wird vom Nutzer über den Wert EXTENSION vorgegeben. Überschreitet während des EXTENSION-Zeitraums die Anzahl der benötigten Iterationen zwischenzeitlich MAXLOOPS, verlängert sich die uneingefrorene Periode jeweils um den Zeitraum EXTENSION. In der Praxis hat es sich bezüglich der Berechnungsdauer und Berechnungsgenauigkeit als sinnvoll erwiesen, den Wert von MAXLOOPS über den Minimalwert leicht zu erhöhen und stattdessen die Zeitspanne EXTENSION zu verlängern. Zur Veranschaulichung ist die Abfrage-Reihenfolge der Regelkriterien im Flussdiagramm, Bild 1, dargestellt.

2.2 Kontrollkriterium zum Wechsel von eingefrorenem zu uneingefrorenem Strömungszustand

Während der Periode eingefrorener hydro-dynamischer Gleichungen ändern sich nur die Enthalpie-Gleichungen. In diesem Fall läßt sich das Simulationsproblem auf die lokalen Temperaturwerte reduzieren. Da das eingefrorene Strömungsfeld eine vorgegebene thermische Situation repräsentiert, führt während einer eingefrorenen Periode jede Änderung des Temperaturfeldes in der Strömung bzw. an den Raumoberflächen zu einem Berechnungsfehler. Um diesen Fehler zu minimieren, dürfen die Änderungen der Temperaturen nicht zu groß ausfallen. Als Kriterium zum Umschalten in den uneingefrorenen Zustand dient daher ein vordefiniertes Maximum MAXTEMP der lokalen Temperaturdifferenzen im Raum (d. h. in jedem finiten Volumenelement) zwischen Beginn und aktuellem Zeitpunkt während des eingefrorenen Zustandes. Siehe hierzu Bild 1.

2.3 Kontrollkriterium zur Reaktion auf bevorstehende Veränderungen der Randbedingungen

Während der Simulation können deutliche Fehler entstehen, wenn bei eingefrorener Strömung signifikante Änderungen in den Randbedingungen auftreten. Ein Beispiel hierfür ist das Auftreten einer zusätzlichen inneren Last

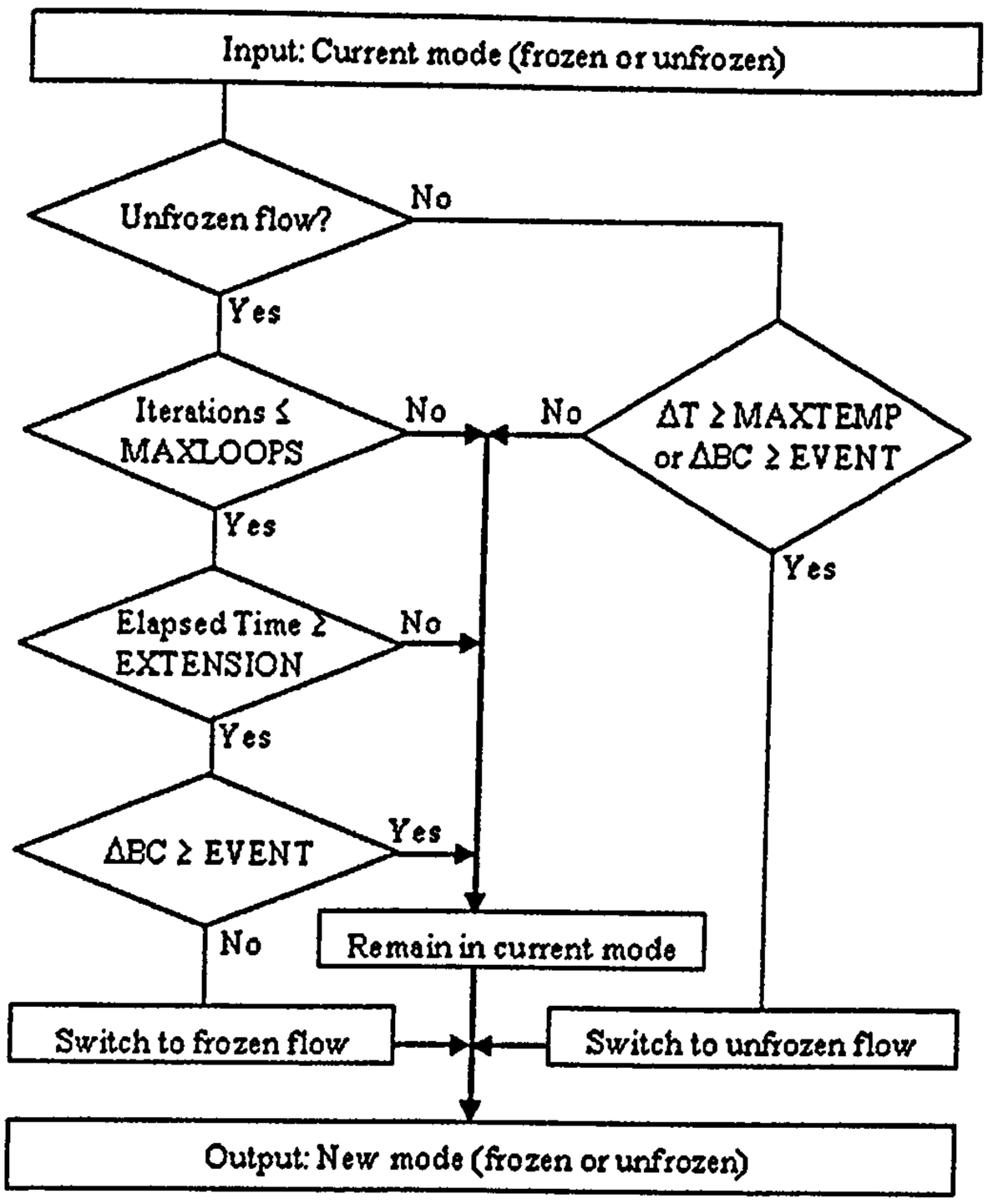

Bild 1. Flußdiagramm zur Darstellung der Regelungsstruktur für die angepaßte Regelungsmethode; Kontrollkriterien: MAXLOOPS = Anzahl der Iterationen, EXTENSION = Verstrichene Zeit, MAXTEMP = Lokale Temperaturänderung, EVENT = Randbedingungsänderung
Fig. 1. Flow chart for the illustration of the control structure of the adaptive control method. Control criteria: MAXLOOPS = Number of iterations, EXTENSION = Elapsed time, MAXTEMP = Locale temperature change, EVENT = boundary condition change

durch Personen und deren Computer in einem Büroraum. Die Regelung überprüft daher die Randbedingungen aus Datensätzen oder Zeitfunktionen im Voraus dahingehend, ob in nächster Zeit eine größere Änderung – das bedeutet größer als ein zuvor definiertes Maß EVENT – in den Randbedingungen stattfindet. Ist dies der Fall, dann erzwingt sie kurz vor dem Ereignis einen Wechsel in den uneingefrorenen Zustand bzw. unterbindet den Wechsel in den eingefrorenen Zustand so lange bis das Ereignis statt gefunden hat.

2.4 Parameterwerteinstellungen für die angepaßte Regelung

Optimale Einstellungen der Werte für die Regelparameter MAXLOOPS, EXTENSION, MAXTEMP sind abhängig von den jeweiligen Eigenschaften der Raumströmung. Bei Eingabe ungünstiger Werte können Konvergenzprobleme bzw. Oszillationen auftreten. Ein instabiles Strömungsfeld, wie z. B. bei freier Konvektion bei geringen räumlichen Temperaturunterschieden, bedarf eine feinere Wahl der Werte (z. B. MAXTEMP und MAXLOOPS relativ klein), während stabile Strömungsfelder wie bei erzwungener Konvektion in dieser Beziehung weniger kritisch sind. Für die untersuchten Beispiele der freien Konvektion im geschlossenen Raum liefern beispielsweise Werte von 3, 180 s und 0,5 K für die Parameter MAXLOOPS, EXTEN-

SION bzw. MAXTEMP hinsichtlich Genauigkeit und Simulationszeit optimale Ergebnisse.

3 Simulationsmodell

Die Effizienz der neuen Regelung wurde anhand eines einfachen Modells (Bild 2) für die typischen Strömungsfälle der mechanischen, der freien Lüftung sowie für die reine freie Konvektion im geschlossenen Raum überprüft. Als Testmodell diente ein 1 m^2 quasi zweidimensionaler Raum (Tiefe = max. Kantenlänge der finiten Volumenelemente) mit einer angrenzenden massiven Mauerziegelwand der Dicke 220 mm. In Bild 2 geben die markierten, durchnummerierten (roten) Kreise und (grünen) Quadrate die Positionen der bei der Analyse verwendeten Monitorpunkte für die Temperaturen bzw. Geschwindigkeiten an.

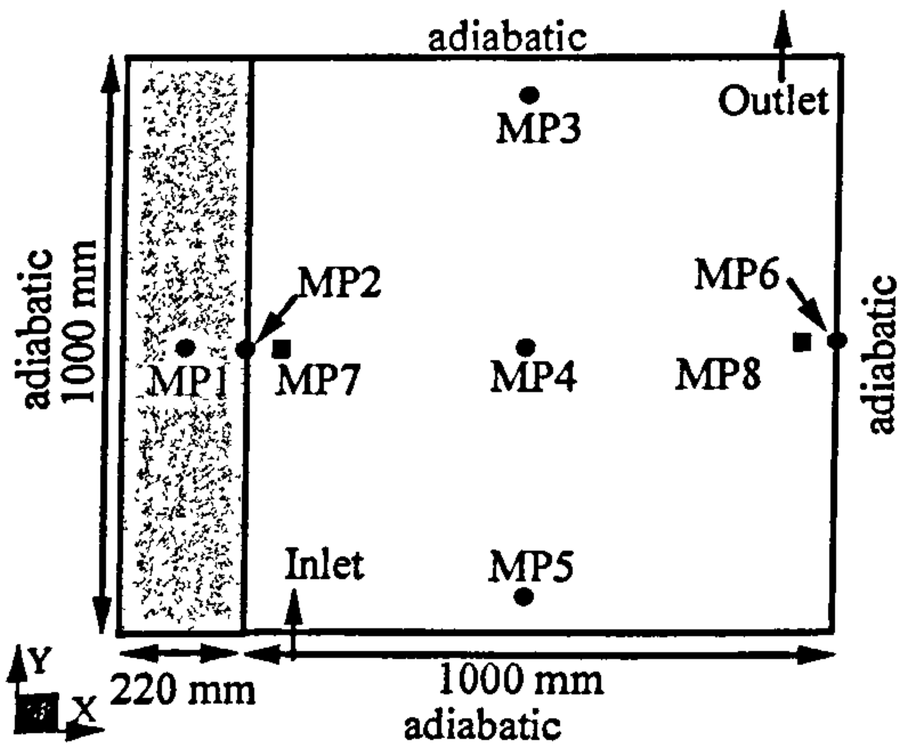

Bild 2. Skizze des Simulationsmodells eines Luftraums mit angrenzender Ziegelwand; Stellen der Monitorpunkte MP für Temperatur und Geschwindigkeiten sind mit Kreisen bzw. mit Rechtecken gekennzeichnet; x, y, z sind die Koordinatenpunkte [m]
Fig. 2. Sketch of the simulation model of an air domain and an adjacent brick wall; Locations of monitor points MP for temperature and velocity are assigned with circles and squares, respectively; x, y, z – coordinates [m]

4 Ergebnisse und Diskussion

Die neue Regelung wurde mit Ansys CFX [4] für die mechanische und freie Lüftung sowie für die freie Konvektion im geschlossenen Raum getestet. In diesem Artikel wird aus Platzgründen nur der Fall für die freie Konvektion im geschlossenen Raum dargestellt bzw. diskutiert und das grundlegende Prinzip der Freeze-Flow Regelung nachvollzogen. Zu diesem Zweck wurde der Regelprozeß aus Abschnitt 3 auf Basis der Programmiersprache Fortran programmiert und als User Junction Box (Implementierungsdetails finden sich in [4]) in CFX eingebunden. In den nachfolgenden Simulationen wurden Zeitschrittweiten von 1 s bzw. 60 s für die uneingefrorenen und eingefrorenen Strömungsperioden verwendet.

4.1 Auskühlung einer Wand an den Raum nach Temperatursprung

Für die freie Konvektion nach einem Temperatursprung wurden alle Lüftungsöffnungen geschlossen und das gesamte Raummodell mit 27,5 °C (Mauerwerk) bzw. 23,75 °C (Raumluft) initialisiert. Zu Beginn der Simulation wurde die Außentemperatur an T_{ext} sprunghaft auf 20 °C reduziert, was einen Abkühlvorgang des Raumes bzw. des Mauerwerks bewirkt.

Die Bilder 3a und 3b zeigen eine hohe Übereinstimmung der Temperaturwerte und Geschwindigkeiten (Unterschiede kleiner 0,1 K bzw. 0,006 m/s) an den untersuchten Monitorpunkten für die neue Freeze-Flow-Methode (adaptive F-F) mit dem Basisfall (klassische Simulation ohne Strömungseinfrierung). In diesem Fall wurde gegenüber dem Basisfall eine Reduktion der CPU-Zeit von 93 % und der Datenmenge von 78 % ermittelt.

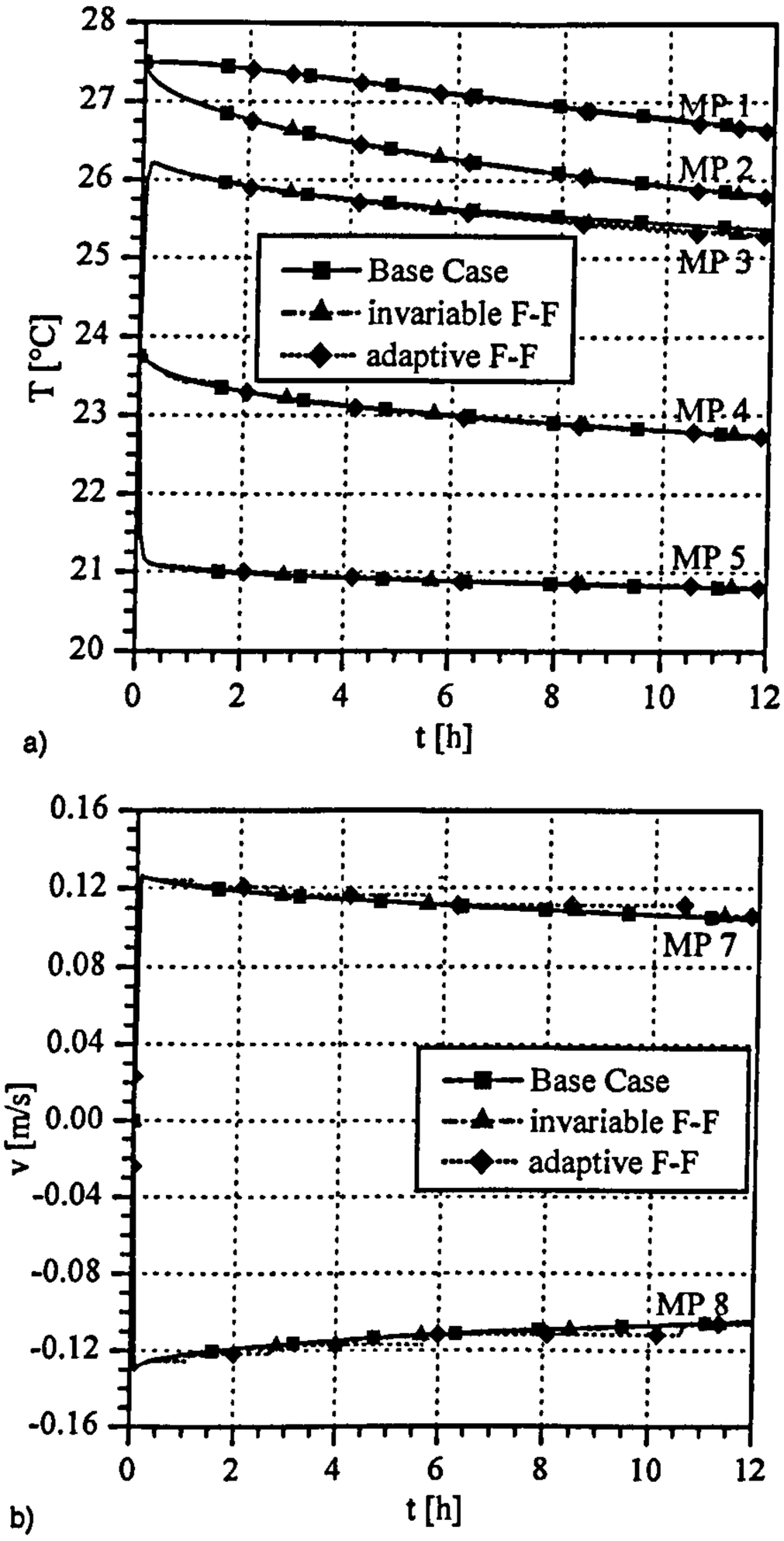

Bild 3. (a) Temperatur- und (b) Geschwindigkeitsverläufe an verschiedenen Monitorpunkten für unterschiedliche Freeze-Flow (F-F)-Regelungsmethoden für den Fall eines Temperatursprungs; T ist die Temperatur [°C] und v die vertikale Geschwindigkeitskomponente [m/s] für den bezeichnenden Monitorpunkt MP
Fig. 3. (a) Temperature and (b) velocity changes at various monitor points for different freeze-flow (F-F) control methods for the case of free convection after a temperature jump; T is the temperature [°C] and v is the vertical velocity component [m/s] at the designated monitor point MP

4.2 Sinusförmige Außentemperaturen

Um die Regelmethode bei wechselnden Randbedingungen zu testen, wurde dem Modell von Bild 2 ein sinusförmiges Temperaturprofil T_{ext} an der Außenwand aufgeprägt:

$$T_{ext} = 7{,}5 \cdot \sin(2 \cdot \pi \cdot t/86400) + 20 \quad [°C]$$

mit:
t simulierte Zeit [s]
T_{ext} externe Temperatur [°C]

Aus den Bildern 4a und 4b ist zu erkennen, daß auch in diesem Fall die Werte für die neu entwickelte Regelung mit dem Basisfall ähnlich gut übereinstimmen. Hierbei wurde eine CPU Zeiteinsparung von 74 % und eine Reduktion der Datenmenge von 78 % erzielt.

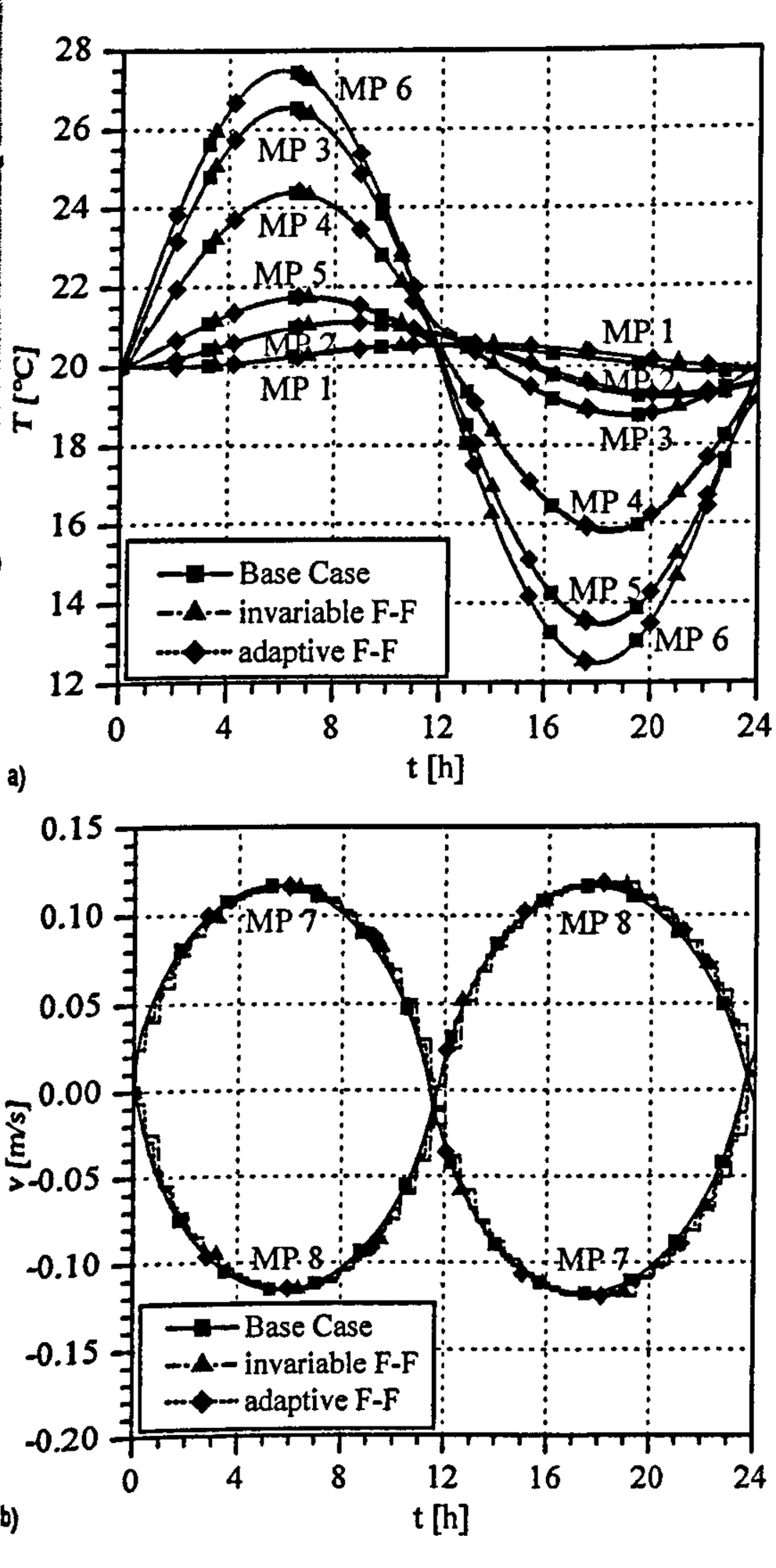

Bild 4. (a) Temperatur- und (b) Geschwindigkeitsverläufe an verschiedenen Monitorpunkten für unterschiedliche Freeze-Flow (F-F) Regelungsmethoden für den Fall der freien Konvektion bei zeitvariierenden sinusförmigen Randbedingungen; T ist die Temperatur [°C] und v die vertikale Geschwindigkeitskomponente [m/s] für den bezeichnenden Monitorpunkt MP
Fig. 4. (a) Temperature and (b) velocity changes at various monitor points for different freeze-flow (F-F) control methods for the case of free convection at time varying sinusoidal boundary conditions, T is the temperature [°C] and v is the vertical velocity component [m/s] at the designated monitor point MP

4.3 Vergleich zwischen angepaßter und starrer Regelung

Die o. g. Testfälle wurden auch für die starre Regelung (invariable F-F) mit festen eingefrorenen bzw. uneingefrorenen Zeitperioden simuliert. Hierbei betrugen die Zeitperioden 300 s bei einer Zeitschrittweite von 1 s für uneingefrorene Perioden, 1800 s bzw. 300 s für eingefrorene Perioden. Die Simulationsergebnisse wurden bereits zuvor in [3] für ähnliche Parameterwerte näher erläutert und sind dort grafisch dargestellt. Im folgenden werden die Berechnungsergebnisse der neuen angepaßten Regelung mit denen der starren Regelung verglichen.

Grundsätzlich zeigt sich, daß sowohl die neue angepaßte als auch die bisherige starre Regelung für alle untersuchten Fälle zu vergleichbaren Ergebnissen führt, die mit dem volldynamisch simulierten Basisfall weitgehend übereinstimmen. Die neue Regelung erweist sich jedoch insbesondere in Zeiten mit schnell wechselnden Umgebungsbedingungen als genauer. So ergeben sich z. B. bei sinusförmigen Randbedingungen um ca. 12 Uhr bei der starren Regelung für die untersuchten Monitorpunkte Abweichungen in der berechneten Lufttemperatur von bis zu 0,3 K.

Außerdem konnte mit der angepaßten Regelung gegenüber der starren Regelung die Effizienz der Freeze-Flow Methode bei fast allen Tests nochmals gesteigert werden. Im Beispiel der freien Konvektion im geschlossenen Raum nach einmaligem Temperatursprung wurde mit der starren Regelung eine Reduktion der Simulationszeit und der Datenmenge von 78 % bzw. 66 % (verglichen mit der volldynamischen Simulation) erreicht. Die neue Regelung verbesserte die Werte auf 93 % bzw. 78 %. Für den Fall mit zeitveränderlichen Randbedingungen ergab sich für beide Regelungen zunächst eine nahezu identische Zeit- und Datenmengeneinsparung. Um mit der starren Regelung jedoch die Genauigkeit der angepaßten Regelung zu erreichen, muß die Länge der eingefrorenen Periode gegenüber den zunächst angesetzten 1800 s deutlich verringert werden, so daß auch hier eine angepaßte Regelung effizienter erscheint.

5 Zusammenfassung und Ausblick

Kürzlich wurde eine neue Methode vorgestellt, mit welcher die Simulationszeit dynamisch thermischer Simulationen unter Verwendung von CFD erheblich reduziert werden kann. Bei dieser so genannten Freeze-Flow Methode werden die Strömungsgleichungen zeitweise eingefroren. Bisher wurde eine starre Regelung mit festen Zeitperiodenlängen verwendet, die jedoch an ihre Grenzen stößt, wenn die Umgebungsbedingungen zeitlich stark variieren.

Eine neu entwickelte Regelung passt die Zeitperioden eingefrorener und uneingefrorener Strömung den aktuellen und bevorstehenden Bedingungen so an, daß die eingefrorenen Perioden so lange wie möglich und die uneingefrorenen Perioden so kurz wie notwenig ausfallen. Diese angepaßte Regelung wurde an einem einfachen Raummodell

mit massiver Innenwand getestet. Durch die neue Regelung wurde im Vergleich mit der starren Regelung eine Senkung der Simulationszeit erreicht. Außerdem erhöhte sich die Genauigkeit der Ergebnisse.

Derzeitige und künftige Untersuchungen konzentrieren sich auf die Anwendung der Freeze-Flow Methode mit angepaßter Regelung zur Simulation praxisrelevanter Bedingungen in Büroräumen. Hierbei werden typische Randbedingungen der Lüftung und der inneren bzw. äußeren Lasten berücksichtigt. Außerdem wird der Einfluss der thermischen IR-Strahlung einbezogen. Ein typischer Anwendungsfall ist die transiente Untersuchung der Nachtlüftungseffektivität in Büroräumen durch Ausnutzung der thermischen Masse der Bausubstanz.

Danksagung

Das diesem Bericht zugrunde liegende Vorhaben wurde mit Mitteln des Bundesministeriums für Bildung und Forschung (BMBF) unter dem Kennzeichen 1749B04 gefördert. Die Verantwortung für den Inhalt dieser Veröffentlichung liegt beim Autor.

Literatur

[1] *Somarathne, S., Seymour, M., Koloktroni, M.:* Dynamic thermal CFD simulation of a typical office by efficient transient solution methods. Building and Environment 40 (2005), S. 887–896.

[2] *Zitzmann T., Cook M., Pfrommer, P., Rees, S., Marjanovic, L.:* Simulation of steady-state natural convection by using CFD. Building Simulation Konferenz (2005), Montreal, Kanada, S. 1448–1456.

[3] *Zitzmann, T., Pfrommer, P., Cook, M.:* Simulation dynamisch thermischen Langzeitverhaltens in Gebäuden mittels CFD. BAUPHYSIK 28 (2006), S. 96–102.

[4] ANSYS: CFX Benutzerhandbuch, Version 10.0, 2005.

Autoren dieses Beitrages:

Dipl.-Ing. (FH) Tobias Zitzmann, Fachhochschule Coburg, Studiengang Bauingenieurwesen, Studienrichtung Gebäudetechnik und Bauphysik, Friedrich-Streib Str. 2, 96450 Coburg

Prof. Dr. Peter Pfrommer, Fachhochschule Coburg, Studiengang Bauingenieurwesen, Studienrichtung Gebäudetechnik und Bauphysik, Friedrich-Streib Str. 2, 96450 Coburg

Dr. Malcolm Cook, De Montfort University, Institute of Energy and Sustainable Development, Queens Building, The Gateway, Leicester LE1 9BH, England.

Aktuell

„IBP18599" – das Tool von Profis für Profis ist da!

Die Entwicklungsarbeiten für das erste Rechenprogramm zur professionellen Praxisanwendung der DIN V 18599 und EnEV 2007 sind abgeschlossen.

Im Bereich des Nicht-Wohnungsbaus wurde durch die von der EU-Richtlinie vorgegebene Einbeziehung des Energiebedarfs für Klimatisierung und Beleuchtung eine Revision der relevanten Rechenmethoden zur Energieeinsparverordnung (EnEV) erforderlich.

Die neue technische Regel DIN V 18599 erfüllt diese Anforderungen.

Mit den in diesem Regelwerk standardisierten Algorithmen für die Bewertung der energetischen Qualität der Gebäude inklusive der installierten Raumkonditionierungssysteme wird im großen Umfang Neuland betreten. Entsprechendes gilt für die Verrechenbarkeit der Anlagenverluste über die internen Wärmelasten und bezüglich der umfangreichen Berechnungsrahmenbedingungen aufgrund vielfältig unterschiedlicher Nutzungsprofile bei derartigen Gebäuden.

Aufgrund der größeren anlagentechnischen Komplexität können die in DIN V 18599 dokumentierten Algorithmen und Kennwerte nur noch unter großem Zeitaufwand von Hand in Energiebilanzrechnungen angewendet werden. Zur praktischen Durchführung von Nachweis-, Wirtschaftlichkeits- und Optimierungsrechnungen sind deshalb geeignete Rechentools erforderlich. Mit dem excelbasierten Berechnungsprogramm zur Energieeffizienz von Gebäuden „EnEff Tool 18599" wurde ein erster Schritt zur rechentechnischen Unterstützung für das Normenwerk DIN V 18599 unternommen. Dieses Werkzeug bildet die Norm jedoch nur eingeschränkt ab und bietet nicht die üblichen Bedienfunktionen, die für eine effiziente Projektarbeit im Planungs- und Beratungsalltag erforderlich sind.

Das Fraunhofer-Institut für Bauphysik war zusammen mit einem Kooperationsverbund maßgeblich an der Entwicklung der professionellen Softwarelösung „IBP18599" zu DIN V 18599 für Endanwender wie Planer und Berater beteiligt. Weitere Kooperationspartner sind Saint-Gobain Isover G+H AG, 5S AG und Ingenieurbüro Prof. Hauser.

Bei der Software handelt es sich um eine vollständige Neuentwicklung, die gezielt auf die algorithmischen Anforderungen des Verfahrens nach DIN V 18599 abgestimmt ist. Die Berechnungen werden mit dem Rechenkern *ibp18599kernel* durchgeführt. Zeitgemäße Bedienoberflächen erlauben die übersichtliche sowie zeit- und kosteneffiziente Projektbearbeitung. Auf Grundlage des zurzeit diskutierten Referentenentwurfs der Energieeinsparverordnung (EnEV) können mit der Software bereits ab der ersten Version Energieausweise erstellt werden. Die Software ermöglicht den Nachweis der Förderbedingungen des neu aufgelegten KfW – Kommunalkreditprogramms zur energetischen Gebäudesanierung.

Dieses nutzt DIN V 18599 bereits ab dem 01. 01. 2007 als Berechnungsgrundlage.

Die Vermarktung von „IBP18599" erfolgt über 5SAG und Saint-Gobain Isover G+H AG. Das Fraunhofer-Institut für Bauphysik wird im Schulungsprogramm zur DIN V 18599 künftig mit „IBP18599" arbeiten.

Weitere Informationen:
Fraunhofer-Institut für Bauphysik
Nobelstraße 12 , 70569 Stuttgart
Tel. 0711/9703301
Fax 0711/9703395
www.ibp.fraunhofer.de/wt
www.ibp18599.de

Published in the Proceedings of Roomvent 2007

Modelling Thermal Mass and Night-Time Ventilation using Dynamic CFD

Tobias Zitzmann[1], Peter Pfrommer[1] and Malcolm Cook[2]

[1]University of Applied Sciences Coburg, Germany

[2]Institute of Energy and Sustainable Development, De Montfort University, UK

Corresponding email: zitzmann@fh-coburg.de

SUMMARY

Due to the requirement of high computational resources it is currently impractical to use Computational Fluid Dynamics (CFD) for full dynamic thermal building simulation. This has been overcome by an *adaptive freeze-flow* method recently developed by the authors. This paper documents the work that has been carried out investigating night-time ventilation in a typical office room of medium thermal mass which is exposed to time varying internal and external heat sources using dynamic CFD.

An inter-model comparison of CFD with predictions from a zonal simulation program has shown a good agreement. Small differences which occurred were thought to be caused mainly by differences in the convective surface heat transfer coefficient values used for the zonal model. The comparison of a single-sided and a cross ventilation night-time cooling strategy using CFD demonstrated that the inlets and outlets were a sufficient distance apart to prevent short-circuiting effects.

INTRODUCTION

Overall energy consumption for heating, cooling, lighting and other electrical equipment in buildings represents approximately 40% of Europe's energy budget, [1]. Modern office buildings are sealed, have facades with a high proportion of glazing and increasing quantities of electrical equipment. This leads to a significant increase of the room heat gains and to high energy consumptions for cooling of the offices in the summer. HVAC systems were popular in the past to maintain the required thermal comfort. However, they consume large amounts of energy. Since the Kyoto protocol [2], which has the aim to reduce the CO_2-emissions to the value of 1990 until 2010, actual German building regulations demand the use of energy-efficient room conditioning strategies. One strategy which is increasingly used in moderate climates is night-time cooling which exploits the effect of the heat absorption capacity of the thermal mass of the building. However, an optimisation of such a strategy for high efficient cooling is difficult since the heat storage of the building depends on various dynamic effects which are difficult to calculate.

Building regulations and guidelines such as [3] and [4] advocate the use of simulation programs. Zonal programs are common for the investigation of dynamic behaviour such as night ventilation due to their simplicity. However, these can bear significant prediction errors since they only predict spatially average zone conditions. Computational Fluid Dynamics (CFD) programs are potentially more accurate since they are based on the Finite Volume Method and can therefore predict the spatial air flow and temperature distribution in the room,

[5]. However, the use of CFD for dynamic thermal building simulations is impractical since it requires large amounts of computational resources. A so called *adaptive freeze-flow* method was recently developed by Zitzmann et al [6] which overcomes the limitation of using purely CFD for dynamic thermal building simulations. The air flow quantities are 'frozen' over variable time periods in CFD which results in significant savings of computer resources (savings of up to about 93% were achieved). Other authors have also successfully worked with a similar idea (see [7] and [8]).

This paper documents the results of CFD simulations for two different night-time ventilation strategies and their influence on the dynamic thermal behaviour of a typical medium thermal mass office room. Reliable experimental data for verification of the numerical results for rooms containing high and medium thermal mass is rare since most data is based on field measurements from existing buildings or chambers exposed to real weather conditions which thus contain many uncertainties (e.g. [9], [10] and [11]). This makes an accurate comparison of measurements with CFD predictions cumbersome. Since inter-model comparisons are often used to verify the plausibility of zonal simulation programs (see for example [12]) the same method was used here to gain information about the dynamic CFD procedure. The comparison of CFD with zonal programs does not of course validate one of the codes, but it may show the plausibility and common fundamental differences of the calculation procedures. The commercial state-of-the-art CFD platform ANSYS CFX [13] and the zonal program TRNSYS [14] were used for the investigations. The CFD program and zonal program are NOT coupled for the investigations shown in this paper and are used for comparison only.

MODELLING METHODS

A new benchmark has been defined which is used to compare CFD predictions with zonal model predictions. The room geometry of the benchmark contains inner dimensions of 3.5m x 3m x 5m (XxZxY) and is based on the VDI guide [15] (see Figure 1). The benchmark is described in the following and contains some modifications of the geometry of [15].

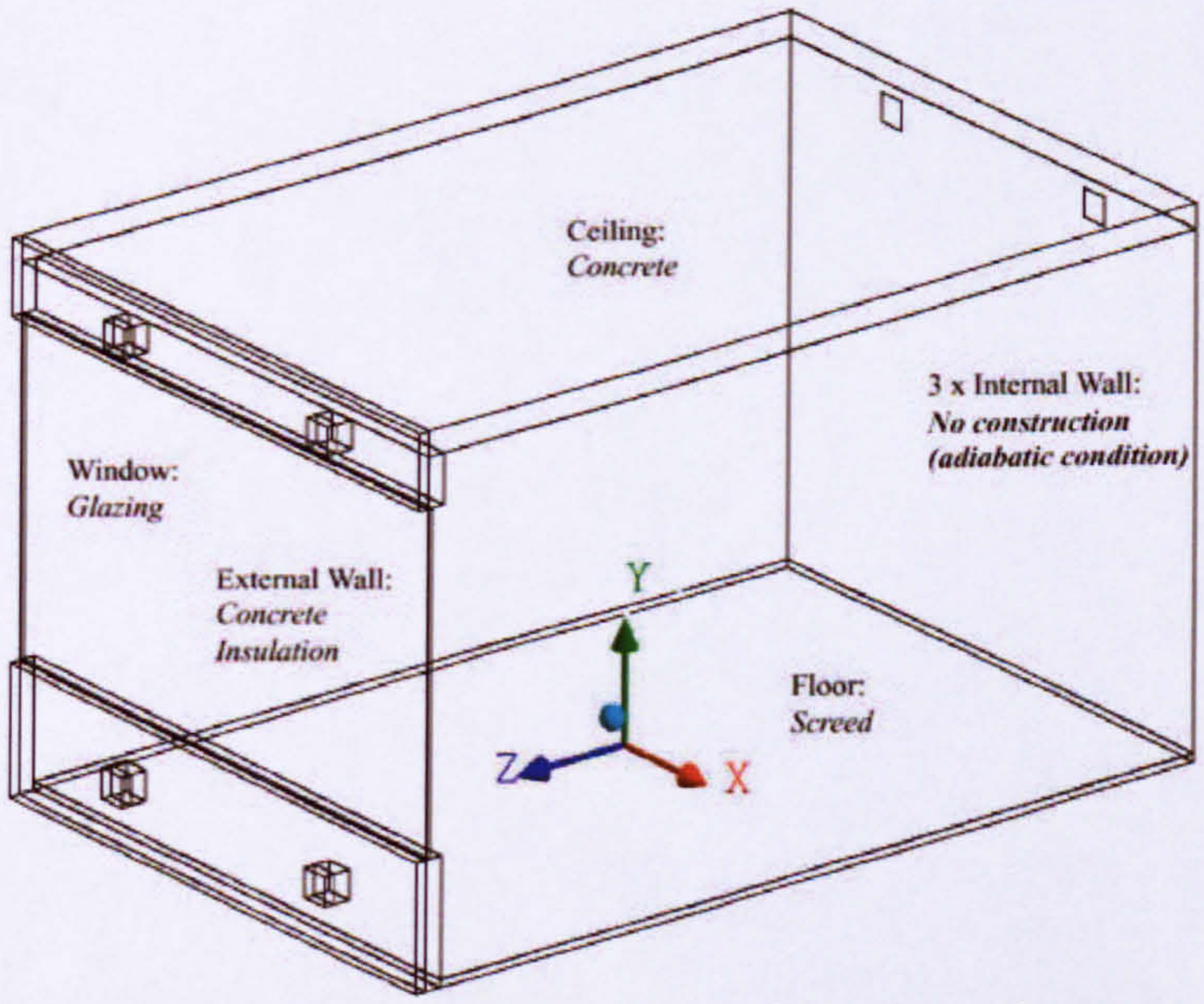

Figure 1: Benchmark room model which contains a medium thermal mass and openings for ventilation at the exterior and rear wall.

Conditions of the neighbouring rooms are the same as for the room investigated. The internal walls in [15] are light-weight structured and hence have only negligible dynamic thermal effect on the thermal room conditions as demonstrated in Engert et al [16]. Thus, the internal wall structure is not modelled in the benchmark. Adiabatic conditions are considered instead at these room surfaces. The layers of the building elements above the concrete ceiling and below the floating screed at the floor are almost fully thermally decoupled from the room investigated as shown by [16] which leads to a heat flux approaching zero at their interface. Thus, adiabatic boundary conditions are considered there. The window is located at the opening of the external concrete wall component at the outer dimension and is considered as an opaque material without thermal mass. Details of the properties of the building components are listed in Table 1. The calculated ratio between the effective heat capacity and the net ground area for room is C_{eff}/A_{net}=111Wh/m^2·K, which assigns it to the 'medium-weight' building category containing medium thermal mass ([17]).

Table 1: Building fabric properties for the benchmark room model.

Component	Construction	d [m]	λ [W/(m·K)]	ρ [kg/m^3]	c [J/(kg·K)]
Floor	Screed	0.047	1.4	2200	1050
Ceiling	Concrete	0.15	2.035	2400	1050
External wall	Concrete	0.10	2.035	2100	920
	Insulation	0.062	0.047	75	840
Window	Glazing	0.024	0.078	-	-

The model boundary conditions are based on a verification procedure described in [12]. Various realistic boundary conditions are applied to the benchmark model using a shading device and hourly values of external temperature, solar radiation and internal heat gains (see Tables 2 and 3). The simulation time scheme considers a preconditioning period of 3 days without internal heat gains and solar radiation followed by a period of 3 hot and sunny days in which the conditions of Table 2 apply. The diffusive solar radiation is distributed evenly on all internal room surfaces and the direct solar radiation is distributed evenly on the floor area. Internal convective and radiative heat gains are distributed evenly in the air space and on all room surfaces, respectively. The outer surfaces of the external wall contains a convective heat transfer coefficient, h_c, of 20W/m^2·K. Where the convective heat transfer at the inner surfaces is not automatically calculated by the simulation program, the convective heat transfer coefficients are adopted from [12], i.e. 2.7W/m^2·K for the horizontal heat flow and 1.67W/m^2·K for the vertical heat flow. A radiation emissivity of ε=0.9 is assumed at the room surfaces. The air, solid and surface temperatures in the entire room model are initially 22°C which leads to air flow patterns of zero velocity at the beginning of the simulation.

Table 2: Boundary conditions for the benchmark room adopted from [12].

Boundary conditions	Value
External temperature	see Table 3
Solar radiation	see Table 3
Maximum global radiation limit for closing the shading device	100W/m^2
Shading-factor	0.15
Machines, convective	200W
Machine operation time	0800-1700
People, convective	80W
People, radiative	80W
Occupation time	0800-1700

Table 3: External temperature and solar radiation measured behind the window, [12].

t [h]	T [°C]	$\dot{q}_{rad,global}$ [W/m^2]	$\dot{q}_{rad,diff}$ [W/m^2]	t [h]	T [°C]	$\dot{q}_{rad,global}$ [W/m^2]	$\dot{q}_{rad,diff}$ [W/m^2]
1	17.3	0	0	13	30.0	359	125
2	16.9	0	0	14	30.7	287	115
3	16.1	0	0	15	31.6	186	99
4	16.1	0	0	16	31.0	98	80
5	16.8	17	17	17	30.5	59	59
6	18.7	38	38	18	29.6	38	38
7	21.8	59	59	19	28.1	17	17
8	23.8	98	80	20	25.9	0	0
9	25.8	186	99	21	23.5	0	0
10	27.5	287	115	22	22.3	0	0
11	28.6	359	125	23	21.4	0	0
12	29.4	385	129	24	20.3	0	0

To simulate the room ventilation, two square openings are considered at low level of the external wall. Another two openings of the same size are placed at high level of the external wall for the investigation of single-sided ventilation and two openings are placed at the back wall at the same height for the investigation of cross-ventilation (see Figure 1). For the single-sided ventilation strategy, the openings at high level at the opposite side rear wall are closed and treated as adiabatic walls; for cross ventilation, the openings at high level at the exterior wall are closed. Since the calculation of the air flow rate for natural ventilation might lead to discrepancies between the simulation codes and hence lead to different boundary conditions, a specified air flow rate is therefore considered for the benchmark model using fans at the high level openings to exhaust the contaminated room air. Subsequently the air which enters the room through the low level openings is at ambient temperature. A typical air change rate of 0.7ach^{-1} is considered during the daytime. Each opening has an area size of 17cm x 17cm which leads to an inlet air speed of 0.18m/s. For night-time ventilation, a rate of 0.7ach^{-1} is used during the preconditioning period and a higher ventilation rate of 3ach^{-1} operational from 2000-0600 is considered for the following 3 days.

A total number of 59,000 volume elements were used to discretise the room model using CFX. Prism elements were used near the wall to accurately represent the existing high pressure, velocity and temperature gradients in this region. In further distance apart tetra-elements were used. The mesh resolution near the wall showed a small effect on the predicted convective heat transfer and surface temperatures compared with a finer resolution. CFX solves the Reynolds Averaged Navier Stokes (RANS) equations. The approximation models used for simulating the benchmarks were the k-ω turbulence model, the Discrete Transfer radiation model and the buoyancy Boussinesq approximation (see [13]). A first order backward Euler transient scheme was applied to all equations. The simulation was considered to have converged if the solution reached a residual root mean square (RMS) of 10^{-3} for the RANS, radiation and the turbulence equations. A preliminary study indicated only marginal deviations between the indoor air temperatures for a similar room model compared with a simulation where a residual of 10^{-4} was obtained ([18]). The time step sizes for the unfrozen and frozen flow periods due to the *adaptive freeze-flow* method were 2s and 60s, respectively. In TRNSYS, a time step size of 60 mins was used. In CFX, the convective surface heat transfer coefficient is determined directly from the numerical simulation based on the flow patterns and thermal conditions close to the wall using a refined mesh in the near wall region. The TRNSYS program does not calculate the convective heat transfer directly. Therefore, the internal h_c values stated in [12] are used.

RESULTS

All CFX simulations achieved the convergence criterion of 10^{-3} for all residuals. A comparison of CFX results for the single-sided and cross ventilation strategy for the hot, sunny day period exhibits only marginal differences in the thermal room conditions (comparing the spatially averaged temperatures of the air and ceiling and floor surface) and negligible differences for the spatially averaged wall heat fluxes at the ceiling and the floor (Figure 2). The single-sided ventilation strategy showed only occasional higher peak air temperatures of less than 0.1K during the daytime.

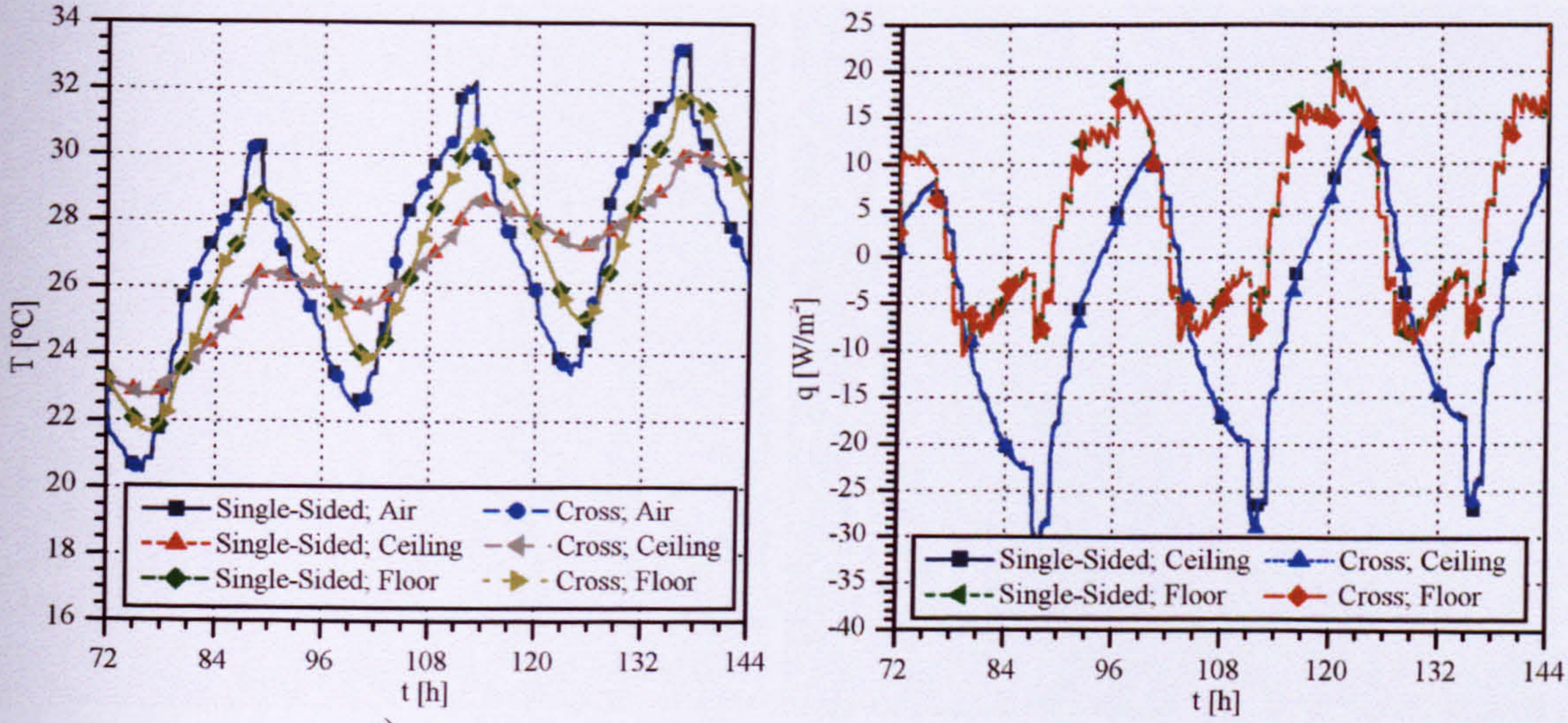

a) b)

Figure 2: CFX predictions for single-sided and cross ventilation showing (a) internal temperatures and (b) wall heat fluxes.

Only the single-sided case is further considered from here, as the results are very similar to those of the cross ventilation.

The temperature efficiency, T_{eff}, defined by Hagström et al [19] can be used for assessing the efficiency of the night time ventilation strategy and is given by:

$$T_{eff} = \frac{T_{out} - T_{in}}{T_{room} - T_{in}} \qquad (1)$$

where T_{out} is the temperature at the outlets, T_{in} is the temperature at the inlets and T_{room} is the average room temperature. The temperature efficiency is an indicator of the efficiency of a ventilation system to exhaust the contaminated warm air to the outside, [19]. If a short-circuit effect exists, the outlet temperature is close to the inlet temperature and the efficiency approaches zero. In the case of perfectly mixed conditions in the room, the outlet temperature is close to the room temperature and the temperature efficiency approaches one. For ventilation strategies similar to displacement ventilation, the outlet temperature is higher than the average room and inlet temperature and the temperature efficiency is higher than one. Figure 3a shows the temperature efficiency for the single-sided ventilation night-time cooling strategy at the last day of the simulation using Eq. (1). The temperature efficiency increases from 1 to 1.3 when the external temperature falls below the room temperature and the

ventilation rate is increased (compare with Figure 2a). During the daytime using a reduced air-change rate of 0.7ach^{-1}, the temperature efficiency falls below 1.

In Figure 3b the temperatures at different heights in the centre of the room are shown for the last day at 0400 and 1600 as representatives for the thermal distribution in the room as predicted by CFX. A temperature difference of about 5K is exhibited between bottom and top of the air domain during the night. During the day the air temperature is smaller close to the surfaces than in the room centre.

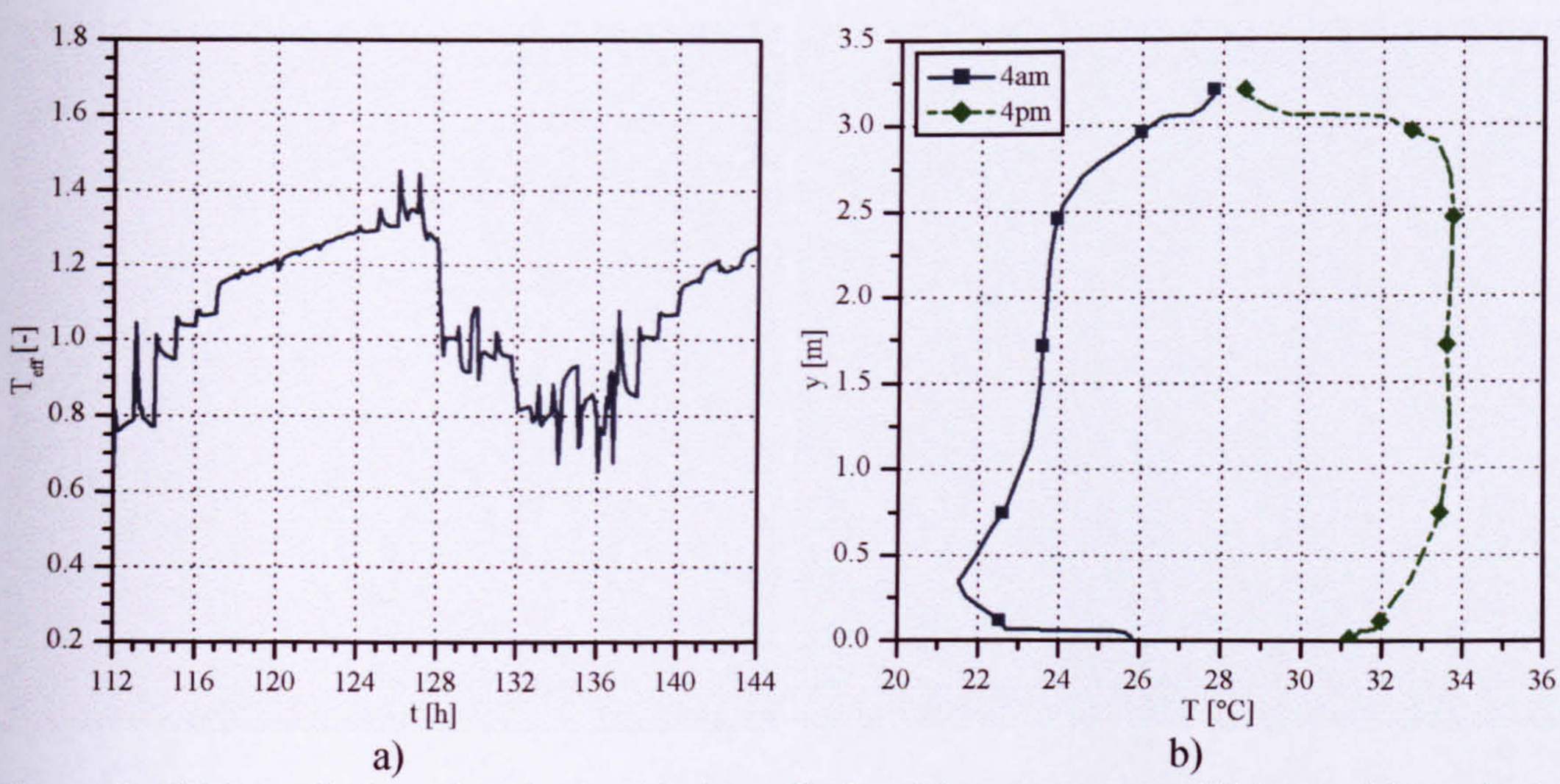

Figure 3: CFX predictions for single-sided ventilation (a) temperature efficiency (b) vertical temperature distribution in the centre of the room.

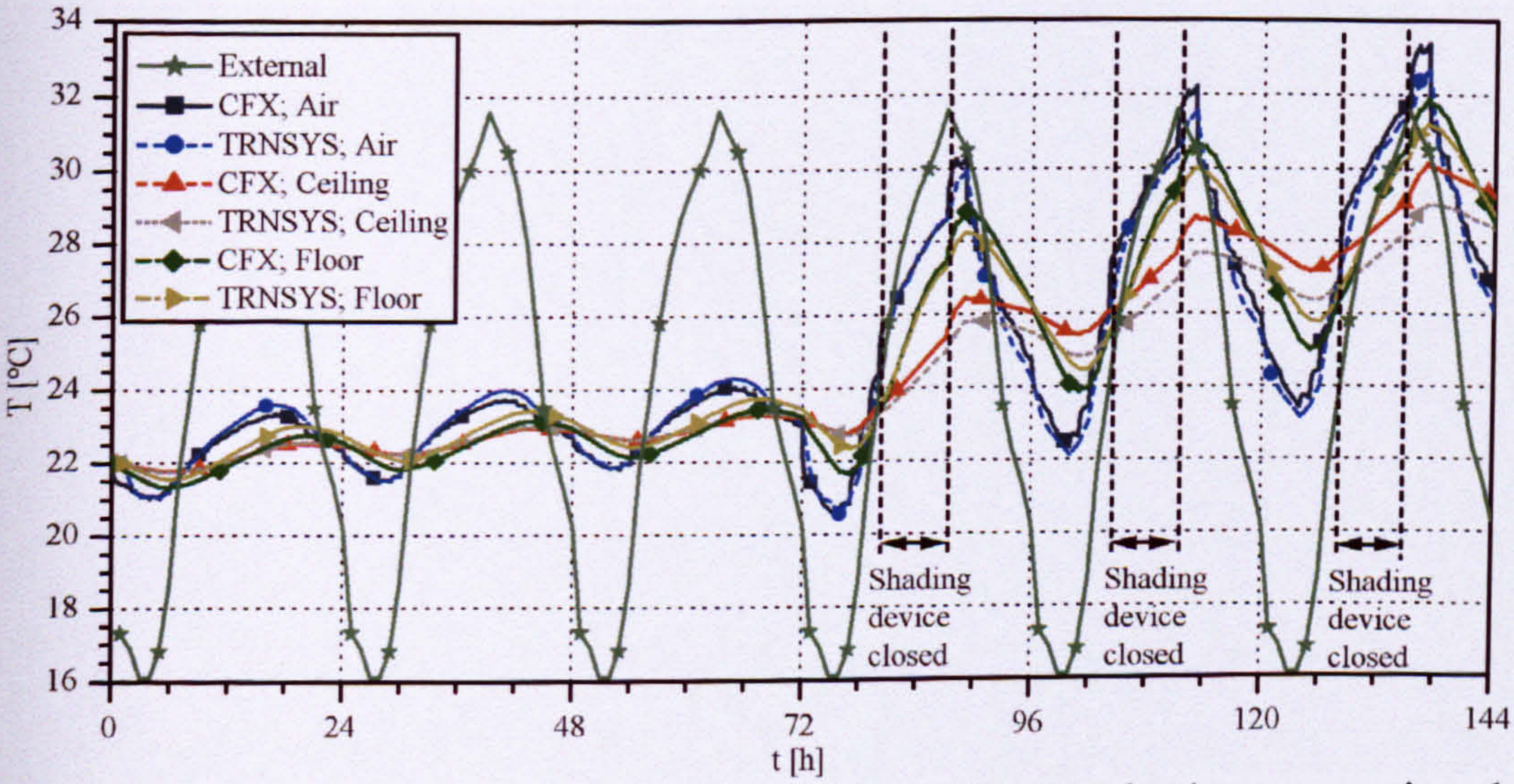

Figure 4: Comparison between predictions for CFX and TRNSYS for the average air and average surface temperature of the ceiling and the floor.

CFX predictions were compared with those of TRNSYS for a period of 6 days, including the preconditioning time. For TRNSYS, the data output interval was 1h and for CFX it was approximately every 5mins. The average temperatures for the air and the surfaces of the

ceiling and the floor are shown in Figure 4. The diurnal amplitudes of the internal temperature curves are relatively small during the preconditioning time and greater during the period of additional heat gains and increased ventilation. Furthermore, a gradual increase of the room temperature condition is observed throughout the simulation. The average surface heat flux at the ceiling and the floor during the simulation period are shown in Figure 5.

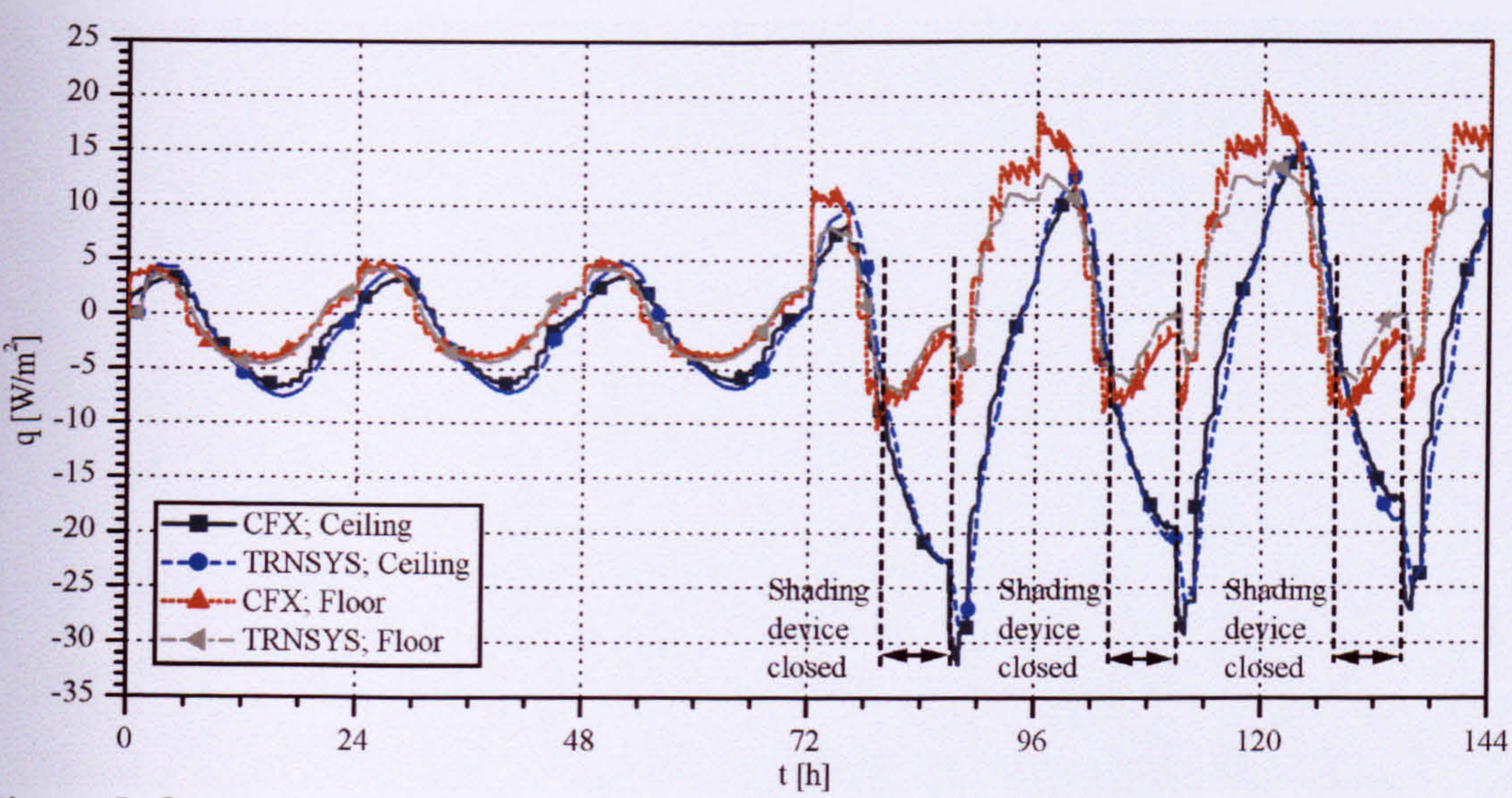

Figure 5: Comparison between predictions of CFX and TRNSYS for the average surface heat flux at the ceiling and the floor.

The curve shapes in figures 4 and 5 for CFX and TRNSYS compare favourably. The maximum differences between CFX and TRNSYS predictions are summarized in Table 4. The differences are higher for the hot sunny day period compared with the preconditioning period.

Table 4: Maximum differences of average internal temperatures and wall heat fluxes.

Time	ΔT [K]			$\Delta \dot{q}$ [W/m^2]	
	Air	Ceiling	Floor	Ceiling	Floor
Preconditioning period	0.2 at 65h	0.1 at 70h	0.25 at 54h	1.0 at 52h	0.5 at 50h
Hot and sunny day period	0.7 at 136h	1.1 at 137h	0.7 at 137h	4.0 at 135h	7.0 at 121h

No thermal lag is observed between the predictions of TRNSYS and CFX. The amplitudes of the surface temperatures tend to be slightly smaller for TRNSYS than for CFX. Less cooling of the floor during the nights and a generally slower warming of the ceiling during the hot and sunny day period is evident in the TRNSYS predictions relative to the CFX predictions, particularly when the shading device is removed from the window. This is also reflected by the differences in the surface wall heat flux between the TRNSYS and CFX predictions shown in Figure 5. Separating the surface heat fluxes into their radiative and convective components for the CFD calculation (TRNSYS can not separate radiation and convection) shows that the downward convective heat flow is small relative to the upward heat flow while the radiative heat transfer is generally significant (Figure 6). Particularly at night, the ceiling is cooled (almost) entirely by radiation.

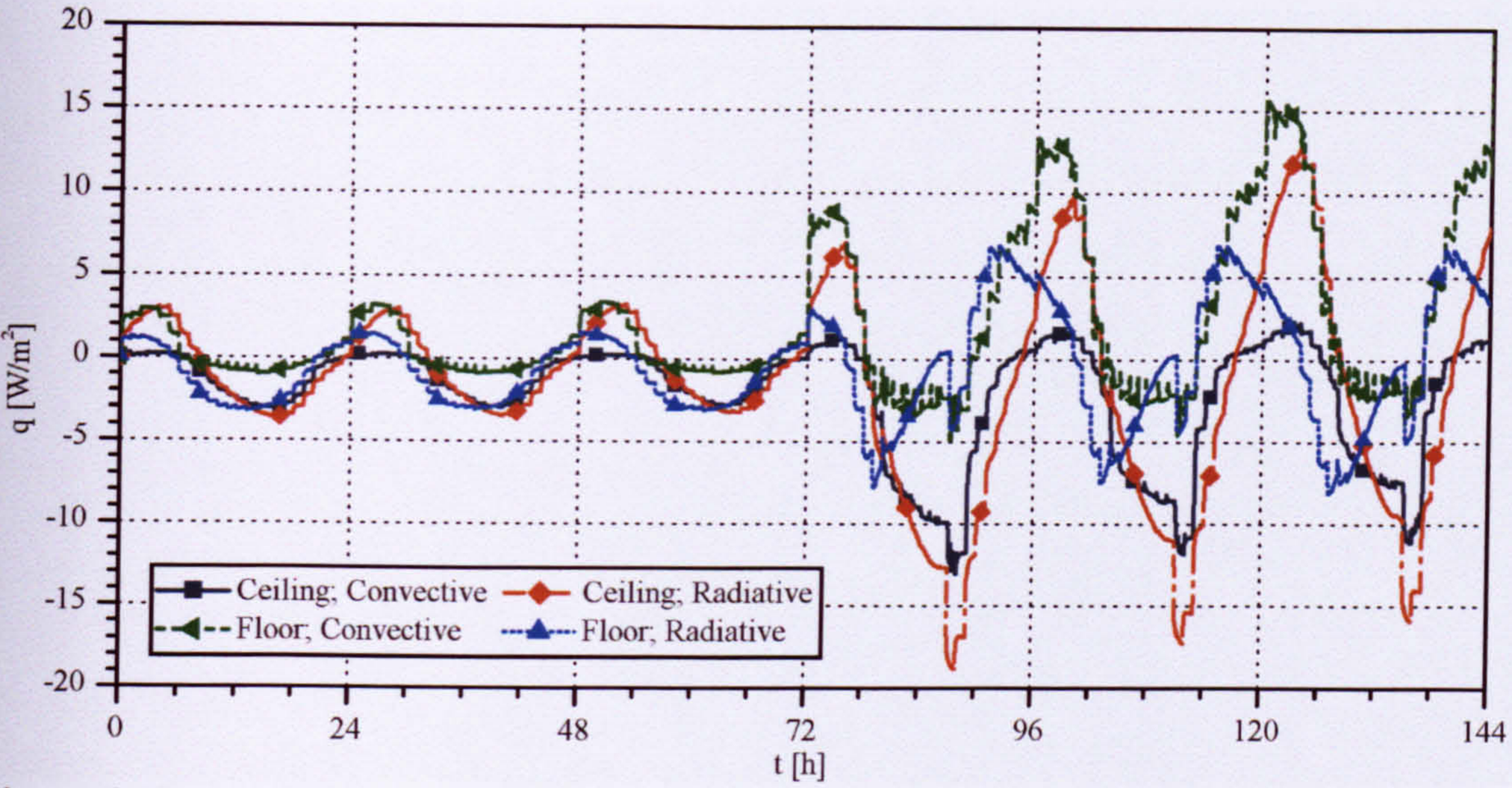

Figure 6: Comparison of average surface heat flux predictions at the ceiling and the floor separated in radiative and convective components using CFX.

DISUSSION

The gradual increase of the daily room air temperatures, which exceed the outdoor air temperature within the simulated period (see Figures 2a and 4), demonstrates that the use of the night-ventilation strategy alone was insufficient in maintaining the daily room air temperatures at a constant level of thermal comfort. However, the investigation was based on a period of extreme hot and sunny summer days. It is possible that the night-time ventilation might work well for moderate climate periods.

The good agreement of results for both the single-sided and cross ventilation strategies indicate that the distance between the inlet and outlet is sufficiently large to avoid short circuiting most of the time (i.e. a flow directly from the inlet to the outlet) and that the air flow distribution is similar in both cases. The temperature efficiency falls slightly below 1 during the day for the single-sided ventilation case (see Figure 3a) which exhibits a small short-circuit effect. However, this short-circuit effect is negligible and only marginally influences the thermal conditions in the room as demonstrated in Figure 2a. The temperature efficiency greater than 1, predicted during the night by CFX, demonstrates a high night-time ventilation efficiency which is similar to that of displacement ventilation, which is also confirmed by the vertical temperature gradient at night shown in Figure 3b. Such an assessment for different ventilation strategies would not be possible for a zonal simulation program which assumes a perfectly mixed room air condition and hence always predicts a temperature efficiency of 1. This leads to a slight under-prediction of the night-time ventilation efficiency for the benchmark model using TRNSYS.

Although the agreement between the CFX and TRNSYS results is good in Figures 4-6, there are small differences in the surface heat transfer which can be explained as follows.

TRNSYS uses fixed h_c values for the floor and ceiling as stated in [12], whereas CFX calculates the convective heat transfer due to the time-varying flow and thermal conditions in the room. For example, a vertical temperature gradient develops in the air space for CFX during the night which can not be predicted by TRNSYS (see Figure 3b). The gradient occurs

due to the development of a cool air layer at low level initiated at the inlet and the existence of a warm air layer at the top due to a warming of the air at the warmer ceiling. This is also reflected by the differences of convective surface heat transfer for upward and downward flow observed for CFX (see Figure 6). It is expected that the upward heat flow is higher than the downward heat flow which is also reflected by the h_c values in [20] in which $5 W/m^2 \cdot K$ is suggested for upward and $0.7 W/m^2 \cdot K$ for downward heat flow. It is therefore expected that the use of direction dependent h_c values would lead to a better agreement of TRNSYS and CFX predictions for the internal thermal room conditions and surface heat transfer.

The convective surface heat transfer does not only depend on the direction of heat flow, but also on the instantaneous temperature difference between the solid and the air. Many investigations have shown that the correlation between the temperature difference and the convective surface heat transfer is non-linear and depends strongly on the spatial flow patterns, [1]. This might also explain the smaller cooling rates at night at the floor when the air change rate is increased using TRNSYS in comparison with CFX. Furthermore, spatial effects exist which is indicated by a temperature gradient along the building element surfaces calculated by CFX (not shown here), which cannot be reflected by the one-dimensional heat transfer calculation using TRNSYS.

The representation of the room geometry is different between the models of TRNSYS and CFX. This leads to a simplified one-dimensional approximation of heat transfer in the building fabric using TRNSYS, which means the thermal mass at the joints of two building fabric components is neglected. This thermal mass can significantly influence the dynamic thermal behaviour of the room as shown in a preliminary study for a high thermal mass room ([21]). Since the additional thermal mass is relatively small for the benchmark considered, this effect is thought to be negligible.

The close agreement between CFX and TRNSYS might only be valid for simple room geometries without obstructions such as furniture, with forced ventilation rates and favourable opening positions to prevent short-circuiting of the air flow. Due to the simplicity and relatively small computational effort of the zonal program, this might be the preferred solution. However, the convective surface heat transfer coefficients should be selected carefully. For other cases in which the spatial air flow distribution is more complex, it is recommended to use a CFD program to reduce the simulation error and to provide information on local conditions such as the thermal comfort in the occupied zone. Further research has begun in which dynamic CFD simulations are being used to investigate the influence of obstructions (e.g. acoustic panels at the ceiling and furniture) on surface heat transfer in rooms. Design studies will be carried out to optimise the locations of the openings for natural and mechanical ventilation to improve the night-time cooling efficiency.

ACKNOWLEDGEMENT

This publication is based on research funded by the German Ministry of Education and Research (funding No: 1749B04). The content of this paper is the responsibility of the authors, not the funding body.

NOMENCLATURE

A_{net}	net area of floor [m^2]	T	temperature [°C]
c	heat capacity [$kJ \cdot kg^{-1} \cdot K^{-1}$]	T_{eff}	temperature efficiency [-]

d	thickness [m]	T_{in}	temperature at the inlets [°C]
C_{eff}	effective heat capacity [Wh·K^{-1}]	T_{out}	temperature at the outlets [°C]
$\dot{q}$	wall heat flux [W·m^{-2}]	T_{room}	average room temperature [°C]
$\dot{q}_{rad,global}$	global solar radiative heat flux [W·m^{-2}]	x,y,z	room width, height and length [m]
$\dot{q}_{rad,diff}$	diffuse solar radiative heat flux [W·m^{-2}]	λ	heat conductivity [W·m^{-1}·K^{-1}]
t	time [h]	ρ	density [kg·m^{-3}]

REFERENCES

1. Santamouris M. Argiriou A. Dascalaki E. Balaras C. Gaglia A. 1994. "Energy characteristics and savings potential in office buildings", Solar Energy 52, pp 59-66.
2. UNFCCC. 2005. Kyoto protocol. http://unfccc.int/kyoto_protocol/items/2830.php
3. DIN standard 4108-2. 2003. Thermal protection and energy economy in buildings - Minimum requirements to thermal insulation. Beuth Verlag. Germany.
4. CIBSE Guide A. 1999. Environmental design. UK.
5. Versteeg, H, Malalasekera, W. 1995. An introduction to Computational Fluid Dynamics. The Finite Volume Method. Pearson Education Limited. UK.
6. Zitzmann, T, Pfrommer, P, Cook, M. 2007. „Dynmaisch-thermisches CFD-Verfahren mit angepasster Regelungsmethode". Bauphysik 29 (1). Ernst & Sohn. pp. 12-16. Germany.
7. Onishi, J, Koga, S, Mizuno, M, et al. 1998. "Computer effort saving methods in unsteady calculations of room airflows and thermal environments", Proceedings of the Roomvent 98 conference. Vol 1. AIVC. Stockholm. Sweden. pp. 117-124.
8. Somarathne, S, Seymour, M, Kolokotroni, M. 2002. "Transient solution methods for dynamic thermal modelling within CFD.",International Journal of Ventilation 1 (2). pp 141-156.
9. Kusuda, T, Bean, J. 1981. "Comparison of calculated hourly cooling load and indoor temperature with measured data for a high mass building tested in an environmental chamber", ASHRAE Transactions 87 (1). pp. 1232-1240.
10. Flourentzou, F, Van der Mass, J, Roulet, C. 1998. "Natural ventilation for passive cooling: measurement of discharge coefficients", Energy and Buildings 27 (1998). pp. 283-292.
11. Alloca, C, Chen, Q, Glicksman, L. 2003. "Design analysis of single-sided natural ventilation", Energy and Buildings 35. pp. 785-795.
12. VDI Guide 6020-1. 2001. Requirements on methods of calculation to thermal and energy simulation of buildings and plants. Springer-VDI-Verlag. Germany.
13. ANSYS CFX. 2005. Version 10.0. User manual.
14. Transsolar. 2006. TRNSYS. Version 15. User Manual.
15. VDI Guide 2078. 1996. Cooling load calculation of air-conditioned rooms. Beuth Verlag. Germany.
16. Engert, G, Pfrommer, P, Zitzmann, T, 2007. Dynamische Simulation des sommerlichen Waermeschutzes gemaeß DIN 4108-2 und der Nachtkuehlung mit TRNSYS. Diploma thesis. University of Applied Sciences Coburg. Germany.
17. DIN standard 4108-6. 2003. Ventilation and Air conditioning – Ventilation for residential buildings. Requirements, performance, acceptance. Beuth Verlag. Germany.
18. Schulz, M, Pfrommer, P, Zitzmann, T. 2007. Dynamische Simulation der Nachtkühlung mit CFD. Diploma thesis. University of Applied Sciences Coburg. Germany.
19. Hagström K. Sandberg E. Koskela H. Hautalampi T. 2000. "Classification for the room air condition strategies", Energy and Buildings 35 (8). pp. 699-707.
20. DIN standard EN ISO 6946. 1996. Building components and building elements – thermal resistance and thermal transmittance – Calculation method. Beuth Verlag. Germany.
21. Zitzmann T. 2007. Simulation of the dynamic thermal performance of buildings using Computational Fluid Dynamics. PhD thesis. Current version (state 03/2007). De Montfort University. UK.

Accepted for publication at Building Simulation 2007 conference

DYNAMIC THERMAL BUILDING ANALYSIS WITH CFD – MODELLING RADIATION

Zitzmann T.[1], Pfrommer P.[1], Cook M.J.[2]

[1]University of Applies Sciences Coburg, Germany
[2]Institute of Energy and Sustainable Development, De Montfort University, UK

ABSTRACT

In an attempt to reduce the high computational efforts for dynamic thermal simulations using Computational Fluid Dynamics (CFD) the authors have recently developed an *adaptive freeze-flow method* (i.e. freezing of flow equations over variable time periods). This paper documents the work that has been carried out to predict the radiative surface heat transfer in dynamic thermal building processes using CFD.

The Monte Carlo and Discrete Transfer radiation models were investigated and results compared with analytical solutions. The Discrete Transfer model has shown good performance whereas an unrealistic radiation distribution on the surfaces was observed for the Monte Carlo model. A further investigation of the Discrete Transfer model for the cooling of a solid wall has shown that the adaptive freeze-flow method is an efficient and accurate way to carry out dynamic thermal CFD simulations which involve radiation.

KEYWORDS

Radiation modelling; dynamic CFD; conjugate heat transfer; freeze–flow method.

INTRODUCTION

Zonal programs are commonly used for predicting the dynamic thermal performance of buildings. However, due to their assumption of perfectly mixed thermal conditions and one-dimensional heat conduction in the building fabric, this can lead to significant prediction errors. Although CFD programs potentially lead to greater accuracy as they are based on the Finite Volume Method (Versteeg and Malalasekera 1995), they are often restricted to steady-state problems or to only few minutes of simulation due to the high requirement of computational resources (e.g. see Groleau 1997, Haupt 2001 and Farvarolo et al 2005).

In an attempt to overcome this limitation, an invariable freeze-flow method was developed by Somarathne et al (2002) The 'freezing' of the flow equations for fixed time periods enabled dynamic CFD simulations to be completed in about 80% of the time required for a full dynamic CFD simulation in which all equations were calculated continuously at every time step. Prediction errors were small. An enhanced, *adaptive freeze-flow method* was developed by Zitzmann et al (2007a) which 'freezes' the flow equations for variable time periods. This method further reduced the computational effort compared with a fully dynamic CFD simulation. However, the method was verified for conjugate heat transfer processes in which radiative heat transfer was not considered. Radiative surface heat transfer often dominates the convective surface heat transfer in buildings (e.g. Ghatti and Autif 2002 and Sharma et al 2007). It is thus still unknown how the method behaves if radiation is considered.

CFD is mainly used to predict the air flow patterns using steady-state schemes (e.g. Cook et al 2003 and Farvarolo et al 2005). Since the thermal mass of the enclosure is often not modelled and fixed thermal boundary conditions are assigned to the surfaces to reduce the compuational effort, radiation modelling is often neglected. Thus, little information has been published which provides reccomendations on the use of radiation models and appropriate parameter settings for dynamic building simulations using CFD. This paper documents the work that has been carried out to investigate the influence of radiation models in CFD for the application to dynamic thermal simulation. Predictions were verified by comparing the results with analytical solutions for two simple test models. Radiative heat transfer was then implemented in a room model of conjugate heat transfer for dynamic CFD simulations to verify the adaptive freeze-flow method. Simulation results have been compared with a fully transient CFD simulation.

In this work the CFD program ANSYS CFX (ANSYS 2005) has been used.

ANALYTICAL METHODS

The radiative heat flux, E, emitted from a grey body is derived from the law of Stefan-Boltzmann and is calculated as follows:

$$E = \varepsilon \cdot \sigma \cdot T^4 \qquad (1)$$

where ε is the radiative emissivity, σ is the Stefan-Boltzmann constant and T the surface temperature of the body.

The radiative heat exchange between surfaces can be analytically derived for certain simple cases (see

Wagner 1998). Two analytical cases which have been used for comparison with numerical solutions in this work are described as follows. The analytical solutions are based on the assumption that the surfaces are grey and diffuse reflective.

Parallel plates (Infinite surfaces)

For two parallel infinite large surfaces, with rays reflected multiple times between the surfaces before the reflected radiation intensity approaches zero, e.g. for $\varepsilon \ll 1$, Eq. (2) is used for calculating the radiative heat exchange (Wagner 1998):

$$\dot{q}_{ik} = \frac{\sigma}{\frac{1}{\varepsilon_i} + \frac{1}{\varepsilon_i}} \cdot (T_i^4 - T_k^4) \qquad (2)$$

Enclosure (Finite surfaces)

For the case of finite surfaces in a realistic room, the total incident radiation, B_i, at a surface is the sum of the emitted and reflected radiation from n participating surfaces (Sharma et al 2007):

$$B_i = \sum_n (\varphi_{ki} \cdot \sigma \cdot \varepsilon_k \cdot T_k^4 + \varphi_{ki} \cdot (1 - \varepsilon_k) \cdot B_k) \qquad (3)$$

where φ_{ik} is the view factor between two surface-elements which may be divided into sub-elements to increase accuracy. For simple geometries, typical view factors are known, which accurately consider the spatial distribution of the geometrical conditions (see for example Wagner 1998). Eq. (3) leads to an equation-system which couples all surfaces. An implicit solution of the system in a matrix becomes difficult due to the non-linearity of the temperature terms. If the surface temperatures are known, the system becomes linear and can be solved with standard matrix solution techniques giving the total incident radiation, B_i, at each surface. Due to the law of Kirchhoff ($\varepsilon=\alpha$) the radiative heat absorbed at each surface is given by the difference between the incident and emitted radiation using Eq. (4):

$$\dot{q}_{ik} = \varepsilon_i \cdot B_i - \varepsilon_i \cdot \sigma \cdot T_i^4 \qquad (4)$$

No heat can be stored at adiabatic wall conditions and Eq. (4) becomes zero. The equation simplifies to Eq. (5):

$$\sigma \cdot T_i^4 = B_i \qquad (5)$$

Inserting Eq. (5) into Eq. (3) the emissivities and temperatures disappear in the equations for the adiabatic surfaces. For the calculation of radiative heat transfer only the temperatures of the other, non-adiabatic surfaces need to be known which simplifies the solution of the matrix. The resulting surface temperatures for the adiabatic walls are then determined by inserting the relevant B_i in Eq. (5).

RADIATION MODELS IN CFX

In CFX, radiation is represented by particles which are tracked through the air domain using a ray-tracing method. The spectral radiative transport equation used in CFX (ANSYS 2005) is:

$$\frac{dI_\nu(\vec{r},\vec{s})}{ds} = -(K_{a\nu} + K_{s\nu}) \cdot I_\nu(\vec{r},\vec{s}) + K_{a\nu} \cdot I_b(\nu,T) + \frac{K_{s\nu}}{4\pi} \int_{4\pi} dI\nu(\vec{r},\vec{s}') \cdot \Phi \cdot (\vec{s} \bullet \vec{s}') \cdot d\Omega' + S \qquad (6)$$

I_b	blackbody emission intensity [W/m^2]
I_ν	spectral emission intensity [W/m^2]
$\vec{r}$	position vector [m]
$\vec{s}$	direction vector [m]
s	path length [m]
K_a	absorption coefficient [-]
K_s	scattering coefficient [-]
V	frequency [s^{-1}]
T	local absolute temperature [T]
Φ	in-scattering phase function
Ω	solid angle [rad]
S	a source term [W/m^2]

The formal solution of the radiative transfer equation is very time consuming and achieved in CFX by using approximate models for the directional and spectral dependencies.

The spectral approximation used in this work is that the medium which takes part at radiation heat transfer is non-scattering and grey (i.e. independent of the wavelength). Opening boundary conditions are considered as fully transparent to radiation. Walls are treated as diffuse emitting and reflecting opaque boundaries whereas symmetry planes are treated as diffusely emitting and specular reflecting boundaries in CFX.

Two directional radiation models are recommended for optically thin media (i.e. transparent to radiation at wavelengths in which the majority of the heat transfer occurs) in ANSYS (2005). One is the Monte Carlo (MC) and the other is the Discrete Transfer (DT) radiation model. Non-linearities in the systems due to scattering, diffuse reflection, or temperature dependency of radiation quantities are overcome by an iterative solution technique.

Monte Carlo (MC) model

The MC model treats the radiation field as a photon gas. A photon is selected from a photon source and stochastically tracked through the system until its weight falls below some minimum at which point it 'dies.' Each time the photon experiences an event, for example a surface intersection, scattering or absorption, the physical quantity of the radiation intensity is updated along the ray. Using this method, a complete 'history' of that photon in the system is generated. Many photon histories need to be generated to achieve good estimates of the physical

quantity. This value can be specified by the user. The main computational overhead for CFX in generating a history is in tracking the photons across the domain.

Discrete Transfer (DT) model

The DT assumes that the spatial radiation gradients are relatively small and the radiation is emitted isotropically from the surfaces. The user defined parameter 'number of rays' in CFX determines the degree of spatial discretisation of the hemisphere above each finite surface element for radiation emission. Higher values mean a better representation of the reality and a higher accuracy, but at the same time will result in a significant increase in computational effort. The paths of rays are calculated only once, at the beginning of the simulation, and are then stored and re-used which leads to significant savings of computer resources.

Due to the high computational resources required for the calculation of the radiation field for the MC and DT radiation models, it is essential to find a trade-off between accuracy and computational effort. This is obtained using a coarser mesh for the radiation field than for the flow field assuming that the radiation field changes at a slower rate than any other transport variables (ANSYS 2005).

MODEL DETAILS

The quasi-2D model used for verification of radiation modelling using CFX contains a square cavity of X=1000mm and Y=1000mm which interacts thermally with an adjacent internal wall of X=220mm thickness (see Figure 1). The high and low end z-planes form symmetry boundaries. The other surfaces are opaque to radiation.

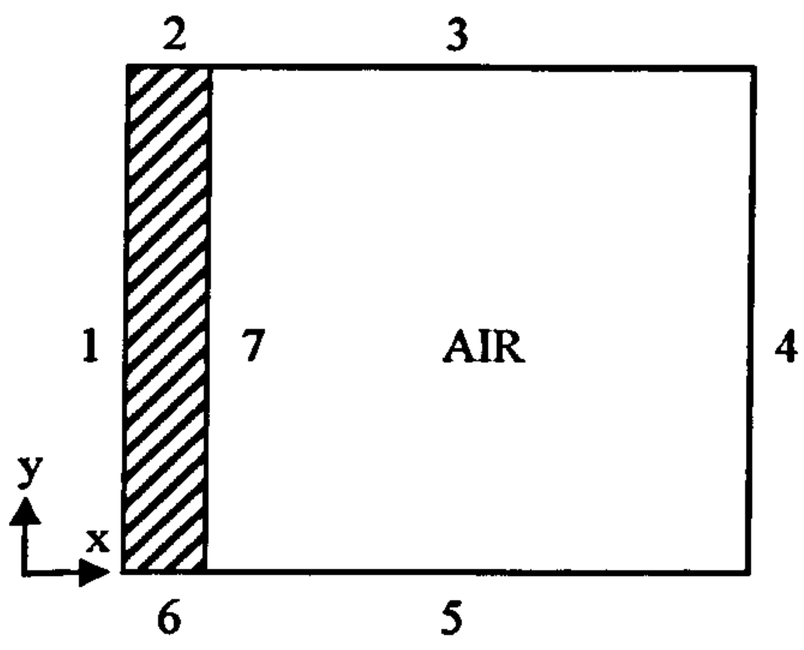

Figure 1: Room model of conjugate heat transfer. The surface numbers assign the boundary conditions specific to the cases investigated to the surfaces.

Verification has been carried out in three steps using test cases 1, 2 and 3.

Case 1

The model in case 1 represents two parallel infinite surfaces of different temperature. The surface numbers 3 and 5 shown in Figure 1 contain symmetry conditions. The surfaces 1, 2 and 6 are adiabatic and surface 4 contains an isothermal temperature of 20°C. The thermal condition at the interface surface 7 adjusts to the conditions of the solid wall (c=880 J/(kg·K), ρ=2300kg/m^3, λ=1.4W/(m·K)) and the adjacent air. The solid has an initial temperature of 27.5°C and the fluid has an initial temperature of 20°C throughout the domain. Radiative emission coefficients of ε=0.9 are considered at the enclosure surfaces. Convective heat transfer is neglected in this model (i.e. mass and momentum equations are not calculated) and only conduction and radiation heat transfer is considered.

Case 2

This model represents a room cavity enclosed by finite walls. The model boundary conditions of case 1 are modified for case 2 replacing the symmetry boundary conditions of surfaces 3 and 5 by adiabatic boundary conditions which contain a radiative emissivity of ε=0.01. Heat transfer due to radiation and conduction is considered as for case 1.

Case 3

The room model for case 3 contains all aspects of heat transfer (i.e. conduction, convection and radiation). Case 2 was modified using radiation emissivity values of ε=0.9 for surfaces 3 and 5 and common brick material for the solid wall (c=835J/(kg·K), ρ=1920kg/m^3, λ= 0.72W/(m·K)). The fluid domain contains an initial temperature of 23.75°C.

Numerical results of CFX for radiative heat exchange were verified for cases 1 and 2 using analytical solutions for two parallel plates of infinite size and for a cavity enclosed by finite surfaces, respectively. The radiative surface heat transfer for surfaces 4 and 7 was evaluated for the thermal conditions after a dynamic CFX simulation of 2h. Although verification could have been carried out using a steady-state solution scheme for cases 1 and 2, the transient scheme was used in order to investigate the potential application of the radiation models to future research of transient problems in terms of computational effort. To consider the conjugate heat transfer between the solid wall and the air, heat conduction was also calculated. The radiation and energy equations were calculated every time step in CFX using a time step size of 60s. The room model depth used in CFX for cases 1 and 2 was Z=500mm. The mesh surface and core elements contained maximum edge length scales of 50 mm and 100mm, respectively. The mesh was refined close to the surfaces using prism inflation

(first prism layer height 0.1 mm, total number of prisms 4).

Dynamic predictions for CFX using the *adaptive freeze-flow method* (Zitzmann et al 2007a) were verified using the room model of case 3. Thus, the radiation and energy equations were calculated every time step while the flow equations were frozen for variable time periods and later updated. The time step sizes for the unfrozen and frozen flow periods were 1s and 60s respectievely, adopting the parameter settings for the lengths of unfrozen and frozen periods from Zitzmann et al 2007a. The maximum edge length scale of the mesh in the core of the air space was reduced to a value of 50mm to predict the air flow patterns more accurately in case 3. To resolve the wall boundary layer for an accurate prediction of convective surface heat transfer, the near wall region was further refined using more prism elements (16 prisms) than in case 2. The model depth was reduced to Z=50mm to reduce the additional computational effort. The dynamic temperature distribution in the room was compared with that of a traditional CFD simulation in which all equations are solved without interruption for each time step (1s). Temperatures were evaluated for different monitoring points (i.e. at x/X=0.5 at 10%, 50% and 90% of the cavity height and at y/Y=0.5 in the core and the surface of the solid domain, see Zitzmann et al 2007a for a period of 12h. The k-ω turbulence model was applied (ANSYS 2005).

CFD simulations were considered to have converged if a residual root mean square value of 10^{-4} for all equations solved was achieved.

RESULTS AND DISCUSSION

The data output interval for simulations was 5min. All CFD simulations reached convergence as defined by the criterion above.

Case 1

Simulations were carried out using the MC model using 1,000,000 and 200,000 number of histories, and simulations were carried out using the DT model using 8 rays. The predicted maximum, minimum and average wall radiative heat fluxes after a simulation period of 2h are summarised in Table 1. For the DT model an average value of 27.7W/m^2 is predicted without spatial variation. For the MC model similar average values (27.8W/m^2 for 1,000,000 and 27.6W/m2 for 200,000 histories, respectively) are predicted. However, the surface radiative heat transfer range spatially considerably for the MC model shown by the minima and maxima in Table 1. This unrealistic behaviour is thought to be caused due to an insufficient long tracking of radiation particles. Figure 2 shows the distribution of radiative heat flux for the MC and the DT model which reflect the observations for Table 1.

An average temperature of 25.8°C is predicted for surface 7 after two simulation hours. The analytically calculated radiative heat flux for surface 7 for these conditions is 27.7W/m^2 using Eq. (2). The analytical solution compares well with the numerically predicted average values. However, the DT model is the preferable model since the MC Model showed spatially unrealistic behaviour (compare Figures 2a and 2b). Furthermore, the simulation using the DT model required less than 1% of the CPU time required by the MC model for the prediction of the same average values.

a)

b)

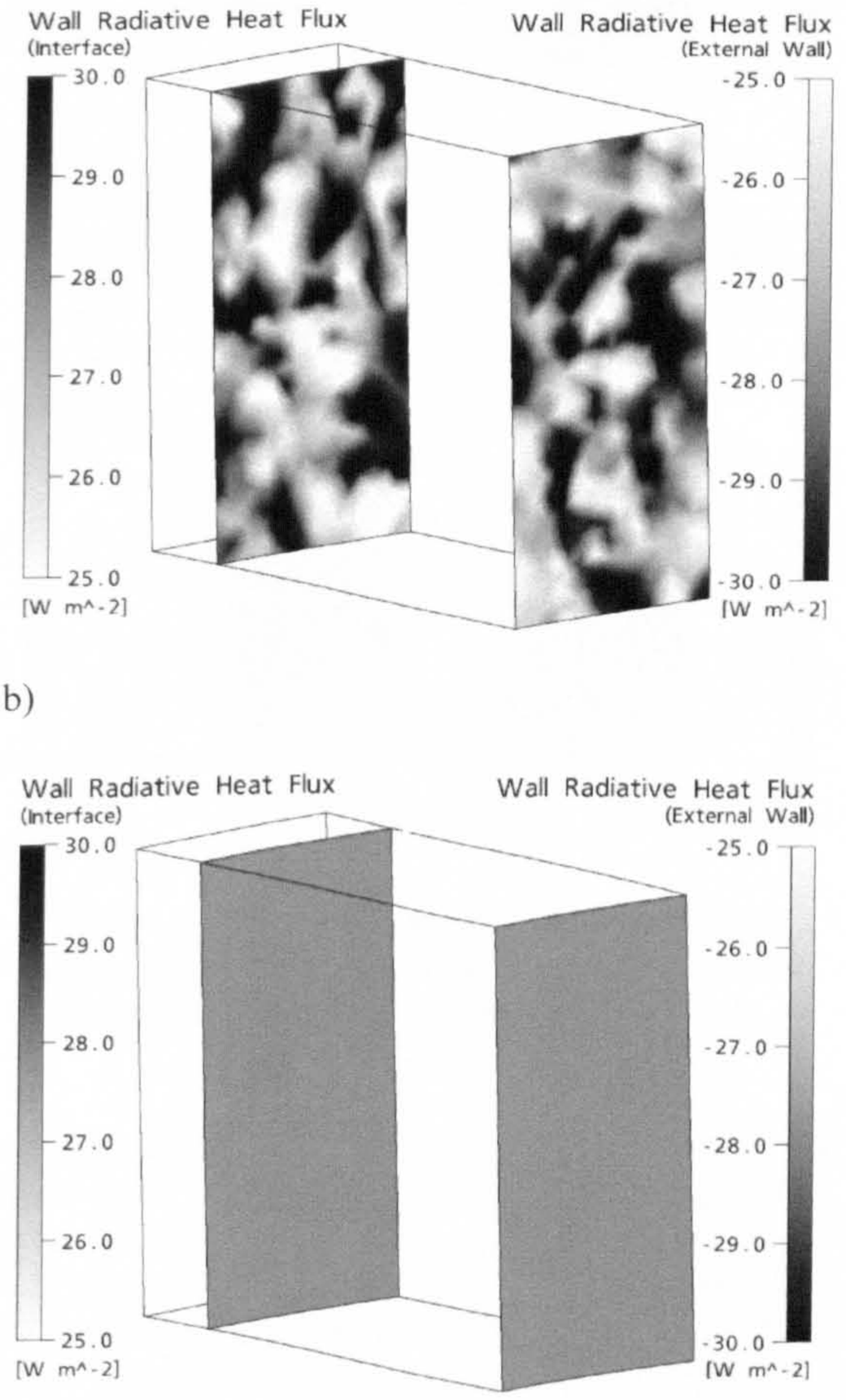

Figure 2: Case 1: Predicted wall radiative heat flux for surfaces 4 and 7 using (a) the Monte Carlo model using 1,000,000 histories and (b) the Discrete Transfer model using 8 rays.

Case 2

Predictions of the wall radiative heat flux are compared for the MC model (2,000,000, 1,000,000 and 200,000 histories) and the DT model (8, 15, 30, 50 and 100 rays). Table 2 shows the predicted wall

radiative heat fluxes after a simulation period of 2h. The range of values for the MC model using 2,000,000 histories was about 30W/m^2 and the average values obtained for surfaces 4 and 7 are 21.4W/m^2 and 20.9W/m^2, respectively. Reduced average heat transfer rates are observed for smaller numbers of histories. Similar ranges of radiative heat flux are obtained for the DT model. However, the maximum wall radiative flux is about 23 W/m^2 for the DT model using 30 rays and is smaller than for the MC model. Average values predicted for surfaces 4 and 7 are 21.2 W/m^2 and 20.7W/m^2 using 30 rays. Small differences exist between the average radiative heat flux predictions of DT model simulations using less than 30 rays compared with simulations using 30 rays ($\Delta\ \dot{q} \leq 0.8$W/m^2). The differences in average values between the emitted and absorbed radiation for the MC and DT models might be the consequence of (i) numerical inaccuracies due to mesh discretisation and equation imbalances and (ii) heat conduction considered within the transient simulation. The latter case means that the adiabatic surfaces adapt the temperatures to the adjacent air which can lead to a change of the radiative surface heat transfer at the adiabatic surfaces and therefore to a change of the radiative heat transfer at the surfaces 4 and 7 compared with the case in which no thermal conduction is included.

Figure 3 shows the distribution of the radiative heat flux at the surfaces 4 and 7. A similar distribution is mapped for the MC model as for case 1 (Figure 3a). The solution showed again an unrealistic radiative heat transfer distribution at the surfaces which is thought to be caused by an insufficiently long tracking of particles as indicated above for case 1. However, a tendency towards smaller wall radiative heat fluxes is observed near the top and bottom where the surfaces approach the horizontal adiabatic surfaces. This behaviour is also clearly shown for the DT model (Figure 3b). Such distribution was expected since the elements close to the boundary of the surface 'see' the opposite wall with a smaller view factor than the elements in the core of the surface. Due to the higher radiative heat transfer at the core regions (see Figure 3b), the solid wall (surface 7) cools down faster than in the regions close to the horizontal adiabatic surfaces. Temperature differences of about 0.1K are observed along surface 7 for a simulation using 30 rays.

The predicted average surface temperatures obtained for the MC and the DT model at surface 7 after two hours of simulation is 26.16°C. Using Eqs. (3) and (4) a wall radiative heat flux of 22.3W/m^2 is analytically calculated. For the analytical model, the surfaces are not discretised. However, the average view factors used from Wagner (1998) consider implicitly the spatial distibution of the local view factors.

a)

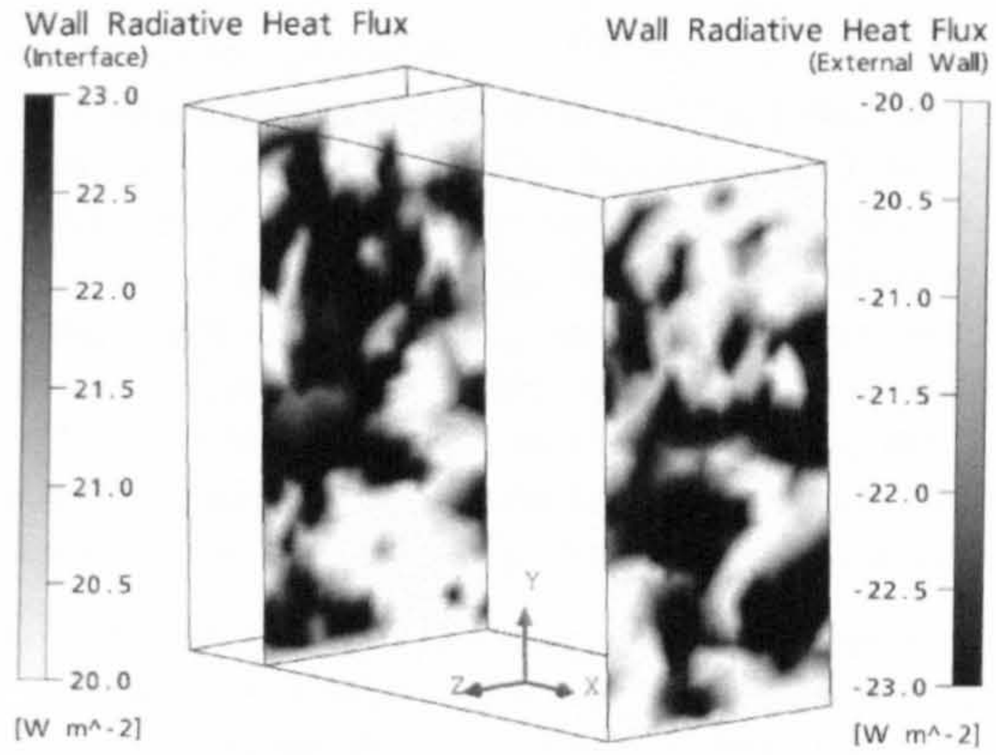

b)

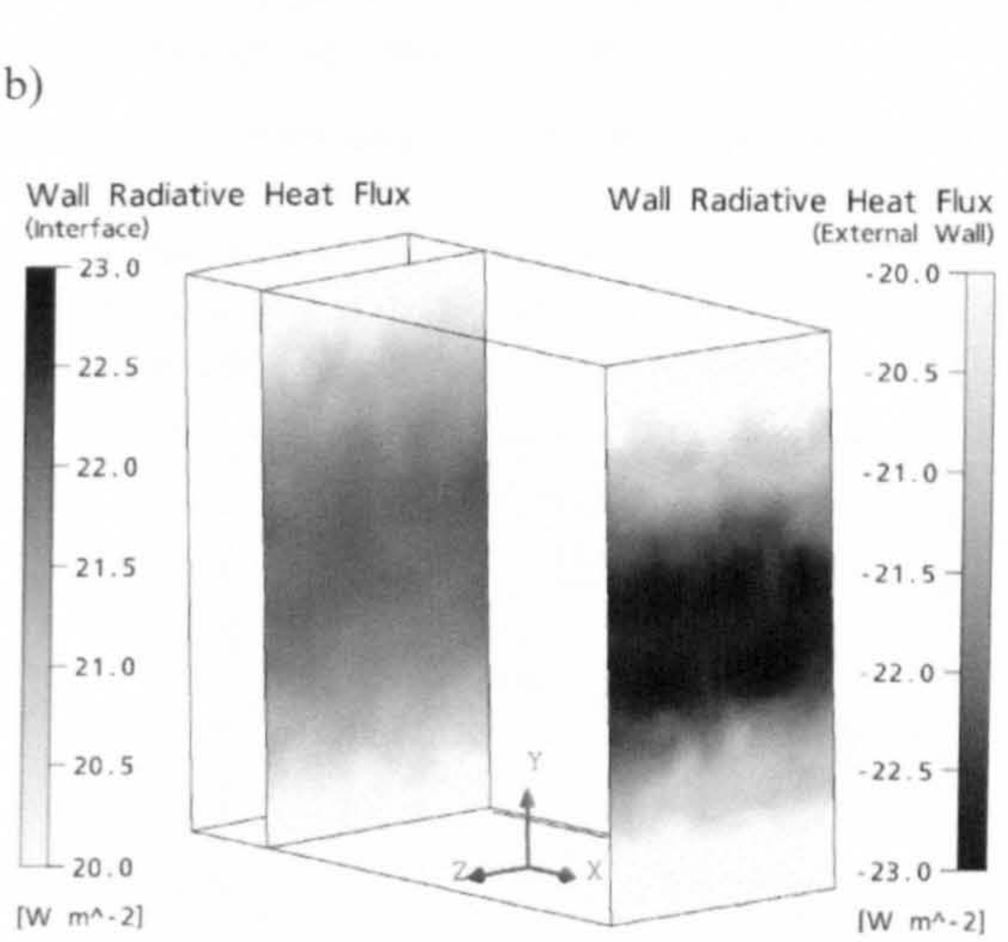

Figure 3: Predicted wall radiative heat flux for surfaces 4 and 7 using (a) the Monte Carlo model using 1,000,000 histories and (b) the Discrete Transfer model using 8 rays.

Good agreement between the MC model and the analytical data was achieved using 2,000,000 histories when comparing the average radiation heat exchange between surfaces 4 and 7 (5% difference). Simulations using a smaller number of histories led to higher deviations. The average radiative heat transfer predictions for the Discrete Transfer model also compare favourably with the analytical solution (6% difference for ray numbers of 30 and more).

The small differences between the analytical solution and the numerical predictions of the MC and DT models are thought to be caused by the following:

- Inaccuracies of view factor values used for the analytical solution which were obtained from view-factor diagrams from the literature.

- The simplified use of average surface temperatures for the analytical solution. A change of the temperature difference of 0.15K at the investigated temperature level for example leads to a change of 0.7W/m^2 of the radiative wall heat exchange for the analytical calculation (3% deviation from the solution obtained above). This demonstrates the sensitivity of radiation heat exchange on the boundary temperatures for the analytical solution.

Taking into consideration the possible reasons considered above, the numerical predictions were considered to be satisfactory compared with the analytical solution. However, since the radiative distribution on the surfaces for the MC model is unrealistic and the simulations required high computational resources (see Table 2), this leads to the conclusion that the MC model might not be suitable for dynamic thermal building simulations. The DT model predicts the radiative distribution well and the simulation time required for the dynamic simulation is significantly reduced (2% of CPU time for the DT model using 30 rays compared with the MC model using 2,000,000 histories). However, an increase of the number of rays leads to a significant increase of computational time for the DT model thus suggesting careful use of this parameter for time-efficient simulations.

Additional simulations using an emissivity of ε=0.9 instead of ε=0.01 for the adiabatic surfaces 3 and 5 led only to marginal changes in the numerical predictions. This corresponds with the theory that the emission coefficient at the adiabatic boundaries is irrelevant in the analytical solution. In contrast, a variation of the emmissivity at surfaces 4 and 7 led to significant changes.

Case 3

Cases 1 and 2 have demonstrated that the DT model is capable of predicting the surface heat transfer accurately and was therefore considered to be the prefered radiation model for use in this work. This model was further investigated using case 3. Since the following inter-model comparison was conducted with the same CFD code a number of 8 rays was used instead of 30 rays to reduce the computational effort.

Figure 4a compares the predicted temperatures at different monitor points for a simulation period of 12h using the *adaptive freeze-flow method* and a simulation for which the flow patterns are updated every time step (base case). The observed temperature decrease at all monitor points indicates a gradual cooling of the solid wall. The temperature predictions agree well using the *adaptive freeze-flow method* with those of the base case. A marginal maximum temperature difference at the end of the simulation period of less than 0.03K is observed (see MP 1 at the end of a simulation period of 12h). Compared with the base case, a CPU time reduction of 84% was possible using the freeze-flow method.

Figure 4b shows the temperature predictions obtained for the same room model without radiative surface heat transfer, published in Zitzmann et al (2007a). The temperatures in Figure 4a show a faster cooling than in Figure 4b which indicates a noticeable influence of radiation on the overall surface heat transfer. Furthermore, the increasing temperature under-prediction observed using the *adaptive freeze-flow method* when radiation was not modelled (ΔT_{max}=0.15K at MP3) is reduced by 80% when the radiation heat transfer is included. Two reasons are thought to be responsible for the reduction in error:

- The reduction of influence of convection surface heat transfer on the thermal room behaviour due to the domination of radiative heat transfer as shown by Zitzmann et al 2007b.
- The compensation of the over-predicted cooling from convection due to a coherent decrease of radiative heat transfer (Sharma et al 2007) which subsequently occurred due to the smaller temperature difference between surfaces 4 and 7.

a)

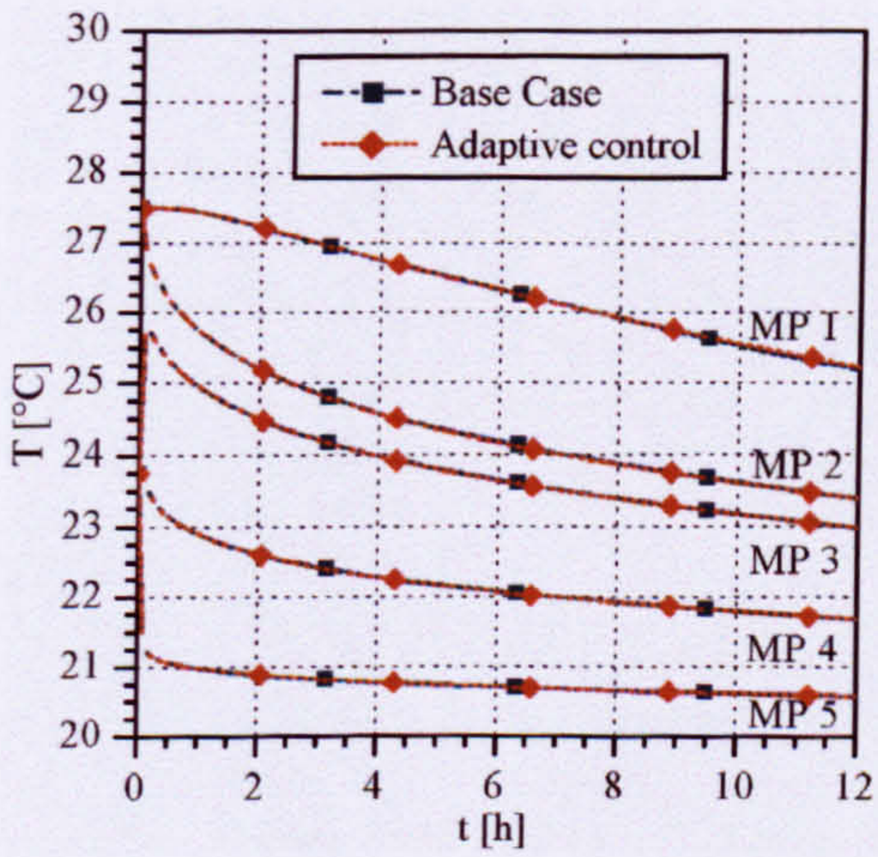

b)

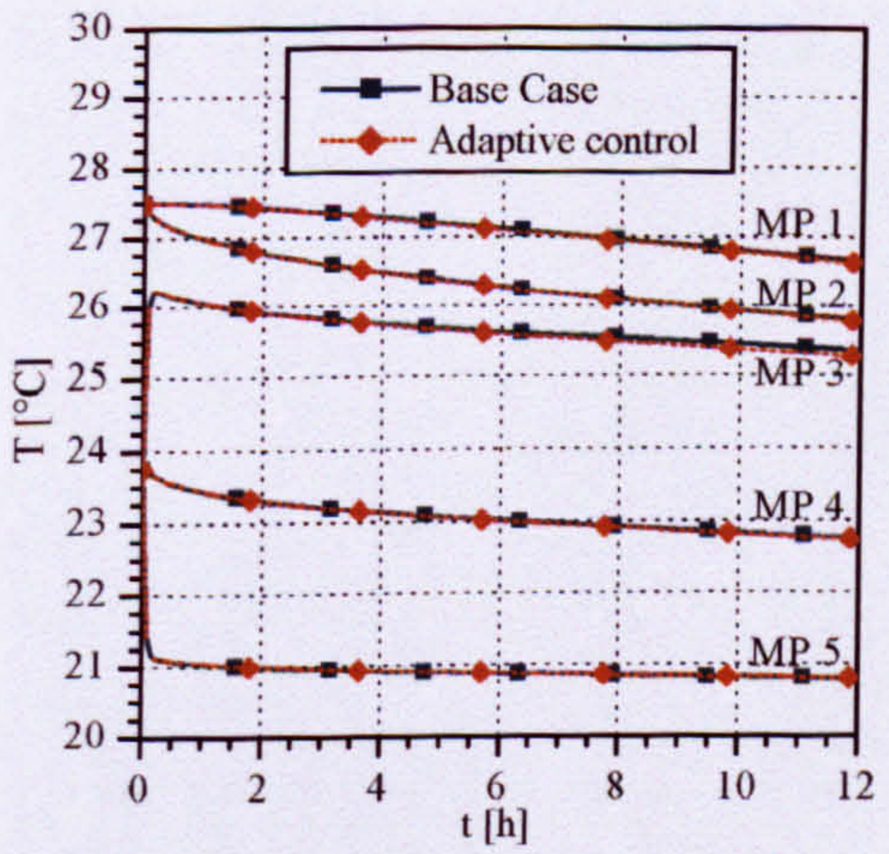

Figure 4 Temperature predictions applying the

adaptive freeze-flow control method to case 3 in which radiation modelling is (a) included and (b) excluded.

Further investigations were carried out to investigate whether the radiation equation can be 'frozen' for certain time periods to reduce the CPU time. However, for some of the room models investigated significant discrepancies were observed which led to the conclusion that the radiation equation should be calculated almost every time step.

CONCLUSIONS

Radiation modelling in spaces with high thermal mass was verified for two simple test cases using CFD. The predicted surface radiative heat transfer was compared with analytical solutions. In case 1, the radiative heat exchange occurred between two parallel surfaces of infinite size. Case 2 contained a room enclosure with two walls of different temperature. The Monte Carlo and the DT radiation model implemented in CFX were used. The Monte Carlo model showed an unrealistic radiation distribution in all cases. The reason was thought to be the result of an insufficient number of histories used to track the reflected radiation particles through the domain. However, an increase of the number of histories led to a significant increase in computational effort. The unrealistic representation of radiative surface heat transfer and the high computational resources required led to the conclusion that the Monte Carlo model might not be suitable for dynamic thermal building simulations. The Discrete Transfer model was computational cost efficient and predictions for radiative surface heat transfer showed good agreement with analytical solutions. As a result from this study, the Discrete Transfer model is suggested as the prefered model for dynamic thermal building simulations.

In case 3 the dynamic cooling of a solid wall was investigated using the Discrete Transfer model. CFX predictions using the adaptive freeze-flow control method have been compared with a full dynamic CFX simulation in which all equations were solved at every time-step. The predicted temperatures at different monitoring points compared well with the base case. The small prediction errors which existed for investigations of Zitzmann et al (2007a) using the adaptive freeze-flow method in which radiation was neglected were reduced by 80% when radiation was considered. The CPU time was reduced by 84% using the adaptive freeze-flow control method compared with the base case.

The investigation has demonstrated that radiation heat transfer in buildings can be predicted well using the Discrete Transfer model in CFX. Furthermore, an efficient method was demonstrated for modelling dynamic thermal building simulations in which all mechanisms of heat transfer are considered using CFD by applying the *adaptive freeze-flow method.*

ACKNOWLEDGEMENT

This report is based on a research project which was funded by the German Ministry of Education and Research (funding NO: 1749B04). The responsibility for the content lies with the lead author of this publication.

NOMENCLATURE

B	incident radiation [W/m^2]
E	emitted radiation [W/m^2]
I	radiation intensity [W/m^2]
K	coefficient [-]
$\dot{q}$	exchanged radiative heat flux [W/m^2]
$\vec{r}$	position vector [m]
$\vec{s}$	distance vector [m]
s	path length [m]
S	radiative source [W/m^2]
T	temperature [K]
β	angle between surface element normals [rad]
Ω	solid angle [rad]
ε	emissivity [-]
φ	view factor [-]
ϕ	in-scattering phase function
ν	frequency [s^{-1}]
σ	Stefan–Boltzmann constant ($5.67 \cdot 10^{-8}$ W/(m^{2}K^4))

INDICES

a	absorption
b	black body
i,k,n	surface number
s	specular
v	frequency [s^{-1}]

REFERENCES

ANSYS 2005. CFX manual. Theory. Version 10.0.

Cook M. Ji Y. and Hunt G. 2003. "CFD modelling of natural ventilation: combined wind and buoyancy forces." International Journal of Ventilation 1 (3), pp. 169-179.

Farvarolo P. Manz H. 2005. "Temperature-driven single-sided ventilation through large rectangular opening", Building and Environment 40, pp 689-699.

Ghatti V. Autif S. 2002. "Study of convective heat transfer in a radiatively cooled building using computational fluid dynamics", Reno: Solar 2002, Nevada, 6 pages.

Groleau D. Marenne C. Raymond F. 1997. "Simulation of the night cooling effect of the night time natural ventilation: a 3D numerical application to the <Maison Ronde> of Botta", Athens: 18th AIVC Conference Ventilation and Cooling (1), Greece.

Haupt W. 2001. Zur Simulation von auftriebsinduzierten Innenraumströmungen. Doctor thesis. Universität Gesamthochschule Kassel.

Sharma A. Velusamy K. et al. 2007. "Conjugate turbulent natural convection with surface radiation in air filled rectangular enclosures", International Journal of Heat and Mass Transfer 50, pp 625-639.

Somarathne S. Seymour M. Kolokotroni M. 2002. "Transient solution methods for dynamic thermal modelling within CFD", International Journal of Ventilation 1 (2), pp. 141-156.

Versteeg H. Malalasekera W. 1995. Computational Fluid Dynamics. The Finite Volume Method. Essex: Pearson Prentice Hall. UK.

Wagner W. 1998. Wärmeuebertragung. Würzburg: Vogel. Germany.

Zitzmann T. Pfrommer P. and Cook M. 2007a. "Dynamisch thermsiches CFD-Verfahren mit angepasster Regelungsmethode", Bauphysik 29 (1), pp 12-16.

Zitzmann T. Pfrommer P. and Cook M. 2007b. "Thermal Mass and Night-Time Ventilation using Dynamic CFD", Helsinki: Roomvent 2007, submitted.

Table 1: Predicted radiative surface heat transfer in W/m² for surfaces 4 and 7 using CFX (MC=Monte Carlo, DT=Discrete Transfer) (Case 1).

RADIATION MODEL	NUMBER OF HISTORIES/RAYS	$\dot{q}$ SURFACE 4			$\dot{q}$ SURFACE 7			CPU TIME
		MIN	MAX	AVE	MIN	MAX	AVE	
MC	1,000,000	-40.6	-19.9	-27.8	20.3	38.4	27.8	33926
MC	200,000	-58.9	24.5	-27.7	-100.1	60.3	27.5	7171
DT	8	-27.7	-27.7	-27.7	27.4	27.8	27.7	280

Table 2: Predicted radiative surface heat transfer in W/m² for surfaces 4 and 7 using CFX (MC=Monte Carlo, DT=Discrete Transfer) (Case 2).

RADIATION MODEL	NUMBER OF HISTORIES/RAYS	$\dot{q}$ SURFACE 4			$\dot{q}$ SURFACE 7			CPU TIME
		MIN	MAX	AVE	MIN	MAX	AVE	
MC	2,000,000	-33.8	-6.0	-21.4	0	31	20.9	65205
MC	1,000,000	-34.8	-2.7	-21.0	0	35.6	20.5	32736
MC	200,000	-46.2	10.9	-20.1	-18.4	56.8	19.9	6996
DT	8	-23.2	-6.3	-20.8	0.1	22.2	20.4	251
DT	15	-24.3	-5.4	-20.6	0.0	23.8	21.5	415
DT	30	-22.9	-6.4	-21.2	0.1	22.4	20.7	1169
DT	50	-22.9	-6.5	-21.2	0.1	22.4	20.8	2389
DT	100	-22.9	-6.5	-21.2	0.1	22.4	20.8	9110

Accepted for publication in the International Journal of Ventilation

Dynamic CFD modelling of thermal mass and air movement

T. Zitzmann[1], M. J. Cook[1], P. Pfrommer[2]
[1]Institute of Energy and Sustainable Development, De Montfort University, Queens Building, The Gateway, Leicester LE1 9BH, UK.
[2]University of Applied Sciences Coburg, Friedrich-Streib Str. 2, 96450 Coburg, Germany.

Abstract

Recent work has begun to consider the potential for using freeze flow techniques in Computational Fluid Dynamics programs for carrying out long term simulations of time dependent flows. This paper describes and tests a new, **adaptive control method** which automatically adjusts the lengths of the frozen and unfrozen flow periods in the solution procedure based on current and imminent conditions. The adaptive control method demonstrates improved performance compared with an invariable control method. Tests using the new method for different flow scenarios have shown good agreement with the results obtained using a traditional fully transient CFD simulation in which all equations are solved without interruption. Simulation CPU time and data storage requirements were reduced by up to 88% and 70% respectively when compared with a fully transient CFD simulation.
Key words: dynamic CFD simulation; adaptive control; freeze-flow; ventilation; thermal mass

1. Introduction

For simple thermal problems such as steady-state boundary conditions or one-dimensional heat conduction through building structures, many analytical models exist for use at the building design stage. More complex cases such as the dynamic thermal interaction of the room air with a massive building structure require more detailed mathematical models. A typical application is the intentional night time cooling of buildings in summer. Experiments or field studies have often been used in the past to investigate and optimise such strategies (e.g. Givoni 1993, Geros et al 1999 and Blondeau et al 1997). However, measurements are time consuming due to the thermal lag in the system caused by the thermal mass. In contrast, state-of-the-art simulation programs enable rapid parametric studies. For example, Kolokotroni et al (1999) investigated, numerically, the night-time cooling efficiency of a typical office building for several parameter variations. The resulting energy consumption of the office room over a year for each variation was obtained relatively quickly, whereas this would have taken much longer using measurement techniques.

Two groups of simulation programs have been established for building air flow and thermal analysis: zonal dynamic thermal simulation (DTS) programs (often coupled with multi-zone network air flow programs) and computational fluid dynamics (CFD) models. Each group is suited to specific types of application (the different capabilities of several DTS programs are discussed in Crawley et al 2005). Using zonal DTS programs, parametric and design studies can be examined relatively quickly to predict the energy performance of a building for several months or years. This is possible by accepting that only spatially averaged temperatures (i.e. assuming that the room air is perfectly mixed) and one-dimensional heat fluxes are evaluated, since only one 'node' is used to represent each thermal zone. Thus the effect of air flow patterns and temperature distribution throughout a space cannot be investigated. In high spaces such as atria where temperature stratification often occurs, this can lead to large simulation errors for the predicted heat transfer between the air and the surroundings if spatial variations are not modelled. By combining DTS with network air flow models, the effect of air flow can be approximated. Here the mean air change rate and infiltration between zones and between the interior and exterior is considered by taking into account pressure differences generated by wind and buoyancy. However, the limitation of failing to predict local spatial variations in

environmental conditions still remains. In contrast to zonal DTS programs, CFD programs are potentially capable of predicting the spatial flow and energy distribution in complex geometries. Integrated conjugate heat transfer enables calculation of the temperature distribution within solid and fluid domains simultaneously. However, CFD requires significant computational resources due to the high resolution of the solution domain. This makes it currently impractical for full dynamic thermal analyses of buildings.

To overcome the limitations of each technique, CFD and DTS programs are sometimes coupled for example as described in Negrao 1995. In the simplest case, the results from one program type are passed to the other as initial conditions (see for example Kendrick 1993). More complex is a dynamic coupling approach using the 'ping-pong' or 'onion' principles where data is dynamically exchanged between both programs (Zhai et al 2001). However, there are drawbacks to these coupling techniques. For example, results can become inaccurate because information is lost during the data transfer due to different levels of detail between the two program types. For example, when Zhai et al (2005) predicted the natural convection in a room containing a radiator, the coupled building simulation predicted the response of the room air to the changes of heat gain from the radiator faster than experimental tests. Also, the position of the radiator can not be determined by the zonal program which leads to erroneous predictions of heat distribution during the simulation periods. An improvement in accuracy was demonstrated by Chen et al (1988) for air flow and temperature distributions using a coupled cooling load and air flow program despite the use of a coarse grid. However, this model still needed the data input from a coupled external CFD program for updating the environmental patterns after certain time intervals which leads to additional simulation effort. Moreover, the heat transfer within the solid was still one-dimensional and the predicted heat transfer coefficients were based on traditional wall functions for forced flow. This can potentially lead to simulation errors in room airflows dominated by natural convection. Nevertheless, the principle idea of updating the flow patterns only at certain time intervals was shown to be valuable in terms of balancing efficiency and accuracy in dynamic building energy calculations.

Since it is easier to use only one program and CFD is potentially more accurate than DTS, research is beginning to focus on finding solution methods using CFD alone for dynamic thermal simulation (Onishi et al 1998, Marenne et al 1998, Rincon et al 2001 and Somarathne et al 2002). Some researchers have successfully started to use freeze-flow techniques (e.g. Onishi et al 1998 and Somarathne et al 2002) for dealing with the incompatibility of time constants between convection and solid heat transfer. These techniques use intermittent periods of frozen and unfrozen flow, i.e. simulation periods when only the energy equation is solved (frozen flow) and periods when all equations are solved (unfrozen flow). This approach is similar to the technique described above for the code coupling procedure, but considers 3D effects in both the fluid and solid domain within one program only. For free convection modelling in a sealed small-scale room, the CPU time required for the dynamic simulation was 36% less than the time required by a fully transient simulation with no frozen periods (hereafter referred to as the base case) (Somarathne et al 2002). The monitored temperatures agreed well with the base case at the end of each unfrozen flow period. However, frozen and unfrozen flow periods had to be instigated manually by stopping and restarting each period by hand, which makes the handling of the method cumbersome and time consuming for the user. Although another freeze-flow method was developed which further reduced the CPU time required (Somarathne et al 2005), this method neglected the thermal lag of air because the unfrozen flow period was calculated using a steady-state calculation scheme. Errors were, for example, produced in an office room simulation after mechanical ventilation was switched off and free convection became the only driving force.

Preliminary studies for the cooling of a solid wall in a room (Zitzmann et al 2006a) have shown that the freeze-flow method can successfully be employed and automated within ANSYS CFX

(2006). ANSYS CFX (ANSYS 2006) is one of the leading commercial CFD platforms worldwide and has been shown to generate good results for the prediction of free convection (Zitzmann et al 2005), which is an important driving force in buildings.

The freeze-flow control strategy used in Somarathne et al 2002 and Zitzmann et al 2006a is based on fixed user defined time periods of frozen and unfrozen flow, hereafter referred to as the **'invariable control method'**. The response of the room to significant changes at the boundary conditions can only be predicted correctly if these occur within unfrozen flow periods and at the beginning of a time step. Another drawback of the fixed period method compared with a method which adapts to the environmental conditions, is that in some situations the length of the frozen flow period is shorter or the length of the unfrozen flow period is longer than necessary. This could significantly increase simulation times and thus reduce the potential efficiency of the method. This paper presents the results of the development of a freeze-flow method in CFX using the automated control method of fixed periods and tests a new control method, hereafter referred to as the **'adaptive control method'**, which overcomes the major drawbacks of the invariable control method. An initial test of the new control method has shown good performance and agreement when compared with the base case for free convection in an enclosure with constant and time-varying external temperature conditions (Zitzmann et al 2006b). The further application to mechanically and naturally ventilated spaces is presented in this paper.

Section 2 provides information about the equations solved in CFX which are relevant in the freeze-flow method. Details of the new adaptive control method are given in section 3. Both control methods have been verified using a test model which is described in section 4. The parameter settings for both control methods and the results for the application to mechanical and natural ventilation are presented and discussed in section 5. Conclusions are given in section 6.

2. Governing equations in CFX

The work reported in this paper uses the commercial CFD program ANSYS CFX (ANSYS, 2006). This is a general purpose CFD program based on the finite volume method which uses an unstructured hybrid mesh containing tetrahedral elements in the core of the room and prism layers near surfaces to achieve a high resolution of nodes for accurately predicting the surface heat transfer (see also Zitzmann et al 2005). The equations solved in each computational cell in the building model are the Navier Stokes equations as follows:

Continuity equation

$$\partial\rho/\partial t + \nabla\bullet(\rho\mathbf{U}) = 0 \qquad (1)$$

Conservation of momentum equation

$$\partial(\rho\mathbf{U})/\partial t + \nabla\bullet(\rho\mathbf{U}\otimes\mathbf{U}) = \nabla p + \nabla\bullet\tau + S_m \qquad (2)$$

Conservation of thermal energy equation

$$\partial(\rho h)/\partial t - \partial p/\partial t + \nabla\bullet(\rho\mathbf{U}h) = \nabla\bullet(\lambda\nabla T)) + \mathbf{U}\bullet\nabla p + S_e \qquad (3)$$

S_m and S_e are additional momentum and energy sources which can apply in certain situations.

Turbulence is accounted for by time-averaging these equations to produce the so-called Reynolds Averaged Navier Stokes (RANS) equations and using a turbulence model to solve for the additional terms that this process generates. It has been shown in Zitzmann et al 2005 that accurate results for turbulent flow driven by free convection can be obtained using the k-ω turbulence model developed by Wilcox (1998). This model uses additional equations for the turbulence kinetic energy (Eq. 4) and the turbulence frequency (Eq. 5):

k-equation

$$\partial(\rho k)/\partial t + \nabla\bullet(\rho U k) = \nabla\bullet[(\mu + \mu_t/C_1)\nabla k)] + S_k - C_2\rho k\omega \quad (4)$$

ω-equation

$$\partial(\rho\omega)/\partial t + \nabla\bullet(\rho U\omega) = \nabla\bullet[(\mu + \mu_t/C_3)\nabla\omega)] + C_4 S_k\omega/k - C_5\rho\omega^2 \quad (5)$$

C_1, C_2, C_3 C_4, and C_5 are empirical constants. Values used in CFX are: C_1=2, C_2=0.09, C_3=2, C_4=5/9 and C_5=0.075. The quantities k and ω are related through the turbulence viscosity by Eq. (6):

$$\mu_t = \rho k/\omega \quad (6)$$

In buildings, buoyancy is an important driving force of air flow. Therefore, the impact of buoyancy needs to be taken into account in the calculation. This is modelled in CFX by including the buoyancy source term, Eq. (7), in the momentum Eq. (2).

$$S_m = (\rho - \rho_{ref})g \quad (7)$$

Since the density differences are usually small, the Boussinesq approximation can be applied whereby:

$$\rho - \rho_{ref} = \rho_{ref}\beta(T - T_{ref}) \quad (8)$$

The source S_k in Eqs. (4) and (5) is the turbulence production due to viscous and buoyancy forces and is given by:

$$S_k = \mu_t \nabla U\bullet(\nabla U + \nabla U^T) - 2/3\nabla\bullet U(3\mu_t\nabla\bullet U + \rho k) - (\mu_t/C_6)\beta g\bullet\nabla T \quad (9)$$

where C_6=0.9 is an empirical constant.

3. Development of the adaptive control method

A new and automated control method, referred to as the **adaptive control method**, has been developed whereby the lengths of the frozen and unfrozen periods are automatically adjusted by the program based on prevailing and imminent conditions. The routine is called automatically at the end of each time step and determines whether the next time step should belong to the frozen or unfrozen flow mode. During an unfrozen time period, Eqs. (1) - (5) are solved within each time step. During a frozen flow period Eqs. (1), (2), (4) and (5) are frozen by the freeze-flow method, i.e. these equations are not solved during that period and the values at the last time step of the previous unfrozen period are used. Eq. (3) is solved throughout the simulation process. A flow chart illustrating the adaptive control procedure is shown in Figure 1 to aid the understanding of the underlying control procedure. The following paragraphs describe the function of the new adaptive control method in more detail.

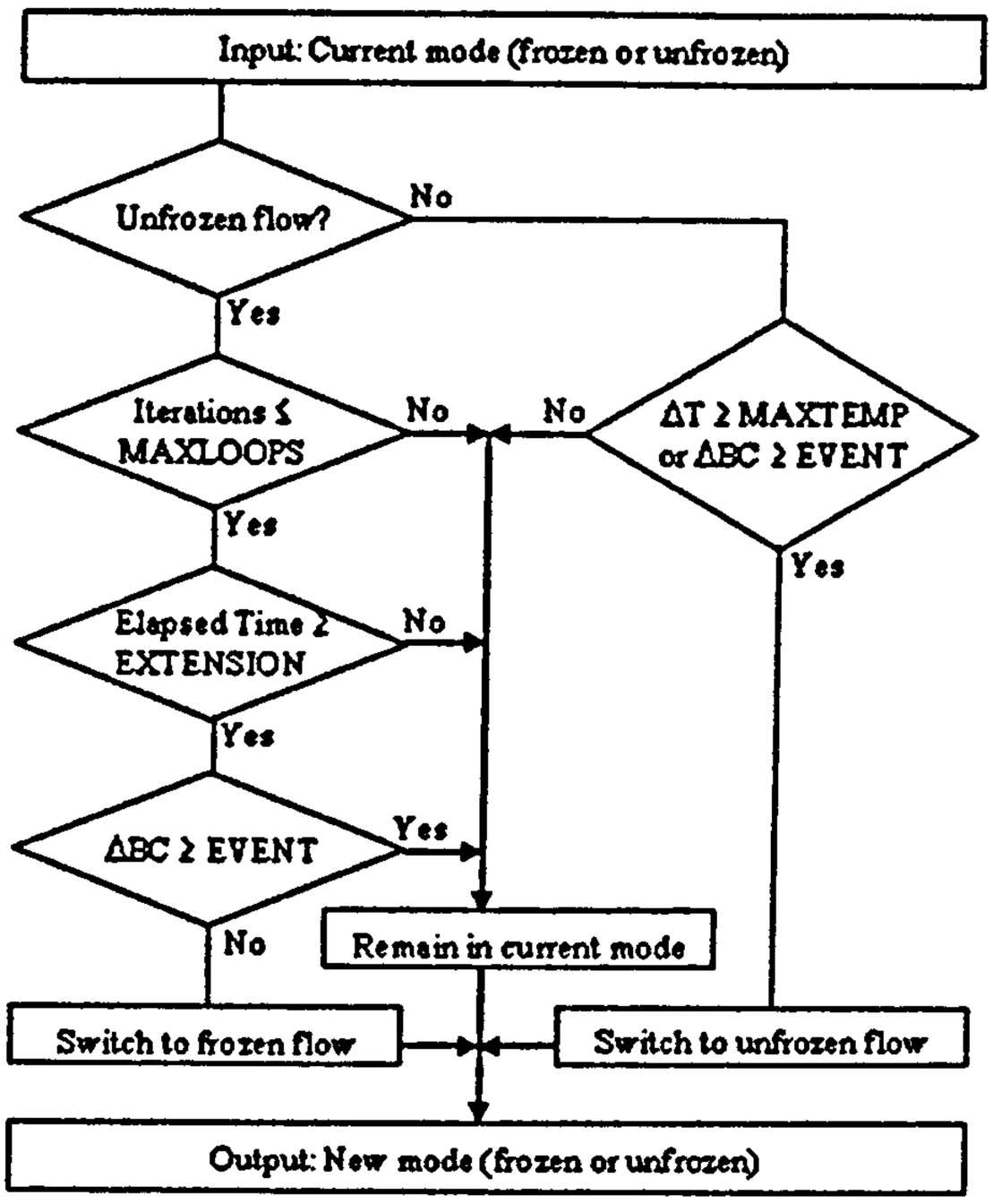

Figure 1: Flow chart for the adaptive freeze-flow control method (MAXLOOPS is a maximum number of iterations required for a switch, EXTENSION is the minimum time extension of the unfrozen time period, ΔT is a change in the local temperature, MAXTEMP is the maximum allowed temperature difference, ΔBC is a change in the boundary conditions and EVENT is the maximum change permitted in a boundary condition).

3.1 Control criteria for switching from unfrozen to frozen flow mode

The transient solution scheme in CFX uses coefficient iteration loops to achieve convergence for each time step. Convergence is achieved when a specified Root Mean Square (RMS) residual of the momentum and mass equations is reached, which is usually of the order of 10^{-5}. The solver then proceeds to the next time step.
Discrepancies between the flow field and the temperature field can be large at the start of a simulation (if the initial values for environmental variables are poor) or at the end of a frozen flow period. If so, then the number of iterations per time step required for convergence during the early stages of the subsequent unfrozen flow period will be large. As the unfrozen flow period progresses, then the number of iterations required gradually reduces as the agreement between the temperature and airflow fields improves. The possible minimum number of iterations depends on the case being investigated and thus on the physical characteristics of the air flow and the quality of the mesh. To achieve the maximum benefit from the unfrozen flow period, a switch to a frozen flow period should occur after a quasi-stationary solution (i.e. unchanging flow and temperature patterns between the former and the next time step) has been reached. The solution is considered to be quasi-stationary if the minimum number of iterations has been achieved and remains constant in time. To ensure this state has been achieved, the minimum iteration number achieved should hold over some time period which is specified by the parameter, EXTENSION. Each time the number of iterations required exceeds the minimum iteration number during the EXTENSION period, the unfrozen flow period is increased again by a further period, EXTENSION. Due to the turbulent nature of the flow, the required number

of iterations can sometimes increase, although the quasi-steady state still remains. This would reduce the performance of the freeze-flow control method due to an unnecessarily extended unfrozen flow period. In practice it was found that by adopting a strategy in which the period EXTENSION was increased and a less restrictive user defined value, MAXLOOPS, was used as a switching criterion rather than the minimum number of iterations, acceptable calculation times and accuracy could be achieved. MAXLOOPS is the maximum number of iterations permitted within the time period EXTENSION after which the solver will switch from the unfrozen to a frozen flow period.

3.2 Control criteria for switching from frozen to unfrozen flow mode

During periods of frozen flow, when all hydrodynamic and turbulence equations are frozen, only values for enthalpy and temperature can change. Since moisture is not considered in this simulation model, the numerical problem can therefore be reduced to the task of predicting the local temperature values in each finite volume. Since the frozen air flow distribution represents a certain thermal situation, each change in the temperature field leads to increasing calculation errors in the frozen air flow field and in the heat transfer at room surfaces. To minimize these errors, the changes in thermal conditions of the air should be less than a certain value, 'MAXTEMP'. Therefore, the new criterion for switching from frozen to unfrozen flow is defined as the point at which the maximum local temperature difference in the air domain between the last time step of the previous unfrozen flow period and the current time step in the frozen flow period reaches or exceeds 'MAXTEMP' (see Figure 1).

3.3 Control criterion for responding to imminent changes in boundary conditions

When significant changes are likely to occur due to imminent changes in the user-defined boundary conditions, an additional, and overriding control is required which prohibits a switch from unfrozen to frozen flow or forces a switch from frozen to unfrozen flow periods, despite all other criteria being met. For example, if computers are turned on in an office at 8am and turned off at 6pm, the solver needs to force an unfrozen flow mode at that time in order to respond accurately to these changes. A controlling subroutine automatically checks for changes in the boundary conditions within the subsequent period (equivalent to the duration of a frozen time step). This information is typically stored in a model definition setup file (often in the form of time dependent functions). If a change in boundary condition reaches or exceeds the value of a specified criterion 'EVENT', the controlling subroutine responds as described above (see Figure 1). A different value for 'EVENT' can be set for each variable.
The parameters 'MAXLOOPS', 'EXTENSION', 'MAXTEMP' and 'EVENT' need to be specified by the user before the simulation starts, and depend mainly on the physical characteristics of the flow. If the flow field is continuously unstable and weak in most parts of the air domain, 'EXTENSION' needs to be large and all other values small to minimise errors in the air flow and temperature fields. If the flow field is predominantly stable, 'EXTENSION' can be smaller and other parameters larger, which increases the performance of the freeze-flow method by reducing computation time. Parameter values used in this paper are given in section 5.

4. Details of the Test Model

The invariable and adaptive freeze-flow control methods were tested using the geometry in Figure 2 (a coupled solid and fluid domain) with various driving forces for the flow. To minimize the computation for the parametric studies, a quasi 2D geometry was used whereby only one element was used to define the model depth. Case 1 is a naturally ventilated space and case 2 is a mechanically ventilated space.

The solid domain consists of a 220mm thick massive internal brick wall ($C_P = 835J/kg{\cdot}K$, $\rho = 1920kg/m^3$, $\lambda = 0.72W/m{\cdot}K$), and the adjacent air domain forms a quasi-2D square cavity of 1000mm x 1000mm x 50mm. The xy-planes at the low- and high- z faces have symmetry conditions and all other wall surfaces are adiabatic (except the common interface of the solid and the air). The wall temperatures result from the heat balances with the air. Since radiation is not considered here, the temperatures at the adiabatic walls adopt the temperature of the adjacent air. Openings measuring 10mm × 50mm in the top and bottom of the cavity are located 100mm from the external and internal walls, respectively. In case 1 the temperature at the openings is 20°C and the pressure (relative to some reference determined by the solver) is zero. For case 2, the opening at the bottom is defined as an inlet with an air velocity of 1m/s and a temperature of 20°C. The top opening is defined as an outlet with a zero relative pressure. Selected monitor points (MPs) are placed throughout the domain to gain an overview of the thermal and air flow patterns in the model. These monitor points are used to discuss results and the performance of the new, and automated control methods. Figure 2 shows the locations of measured temperatures (circles) and vertical velocity components (squares).

In previous work by the authors (Zitzmann et al 2005) CFX simulations have demonstrated that it is sufficient to use a quasi 2D geometry for time-averaged two-dimensional flows. Furthermore, the sizes of the near-wall prism elements were investigated in detail to achieve accurate surface heat transfer. A discretisation of the wall boundary layer using 16 prism elements gave accurate results. The authors have also investigated different nodal grid resolutions at the surfaces and in the core of the room and have found that tetrahedral surface and volume elements with an edge length scale of up to 50mm were possible without influencing the surface heat transfer predictions provided the mesh in the wall boundary layer was sufficiently refined. The mesh used in the test model is based on the results of these investigations.

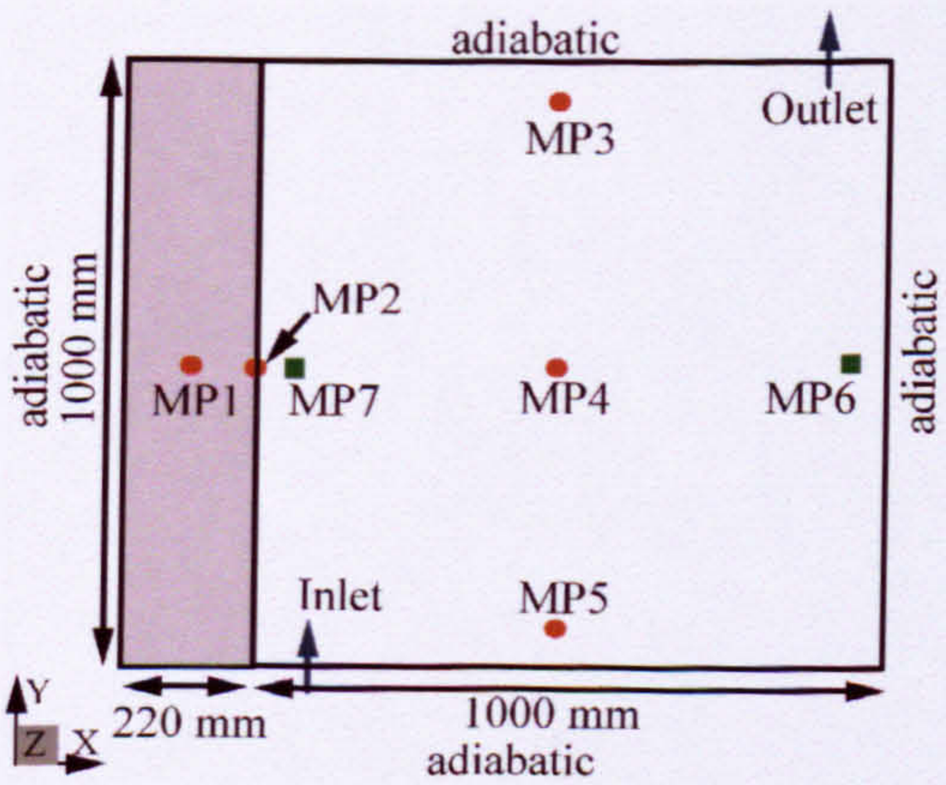

Figure 2: Test model containing a massive internal wall (shaded). For temperature evaluation, monitor points are positioned in the solid and fluid centres, at their common interface and at 10% and 90% of the fluid domain height (filled circles); monitor points for measuring the vertical velocities are positioned within the wall boundary layer at the domain mid height 6mm away from the vertical surfaces (filled squares).

5. Results and Discussion

To assess the performance of the freeze-flow methods, all results are compared with a base case where all equations, i.e. hydrodynamic, turbulence and energy equations (see section 2), are solved without interruption using a fully transient simulation with a constant time step size of 1s. The small time step was necessary in order to achieve convergence when all equations are solved (see Zitzmann et al 2006a). In the test cases, a fully transient preconditioning time of 1500s was used to ensure fully developed air flow and temperature fields before the first frozen period was permitted to start. This preconditioning time is generally not necessary for the adaptive control method since the control does not switch to unfrozen flow before the flow patterns have fully developed. However, to provide accurate comparison with the invariable control method the same preconditioning time was used. For evaluation, simulation results for the base cases and both control methods are stored every 5 minutes. For the adaptive control, the output data is also stored immediately before the program switches between frozen and unfrozen periods since these periods are invariable and a constant time grid for data output storage would not sufficiently accurately represent the results. The symbols in Figures 3b, 3c, 4b and 4c are only for designation of the curves to the legend and do not represent the time grid for data output.

5.1. Control parameter settings for the invariable and adaptive control methods

Since the air flow in case 1 (natural ventilation) is weak and therefore less stable compared with case 2 (mechanical ventilation), the ranges of the relevant freeze-flow method parameters for case 1 need to be more restrictive to prevent non-convergence. The values optimised for case 1 are also used for case 2 to facilitate better comparison of the performances of the control methods for both ventilation cases.

A time step size of 1s was adopted from the base case for the unfrozen flow period. In periods where only the energy equation is solved, time step sizes can be increased without any loss of accuracy leading to a reduction in CPU time (Somarathne et al 2002 and Zitzmann et al 2006a). However, in order to react sufficiently quickly to changes in boundary conditions, the time step should be limited to about 1 - 5mins. For the invariable control method a time step size of 5mins is therefore used for the frozen flow period; for the adaptive control method a time step of 1min is used in an attempt to react more precisely and quicker to changes in the thermal conditions and thus to ensure a switch to an unfrozen flow period at the appropriate time.

The length of unfrozen and frozen time periods, 5mins and 30mins respectively, is adopted for the invariable control method based on the work in Zitzmann et al 2006a. Optimal parameter values found for the adaptive control method are 'MAXLOOPS' = 2, 'EXTENSION' = 5mins and 'MAXTEMP' = 0.2K. Higher values for 'MAXLOOPS' and 'MAXTEMP' tended to produce oscillatory results and an increase of 'EXTENSION' did not significantly improve the results but increased simulation time for the adaptive freeze-flow control method. The value of 'EVENT' has no influence on the results in these cases as the model boundary conditions do not change with time.

5.2 Natural ventilation (Case 1)

The invariable and the adaptive freeze-flow methods have been tested for the case of natural ventilation and the effect of this on the interaction with the building structure. The boundary and initial condition settings for case 1 are described in section 4. Results in Figure 3 comprise the air flow and temperature conditions at certain monitor points (MPs) for the base case and both freeze-flow control methods for a simulation period of 12h.

In the base case, air enters the room at low level through the opening driven by the temperature difference at the opening (see Figure 3a). The cool air is warmed by the wall, rises along the

wall and leaves the air domain through the opening at high level. The flow field elsewhere is weak and temperature stratification occurs (see Figures 3b and c, showing different velocity magnitudes at MPs 6 and 7 and different temperature values at MPs 3 - 5). Since the temperature difference between the wall and the adjacent air is greater at low level, a higher heat transfer occurs relative to high level which subsequently leads to a faster cooling of the solid at low level (see the temperature distribution in the solid wall in Figure 3a). The descending curves for MPs 1 and 2 in Figure 3b indicate a gradual cooling of the solid wall.

a)

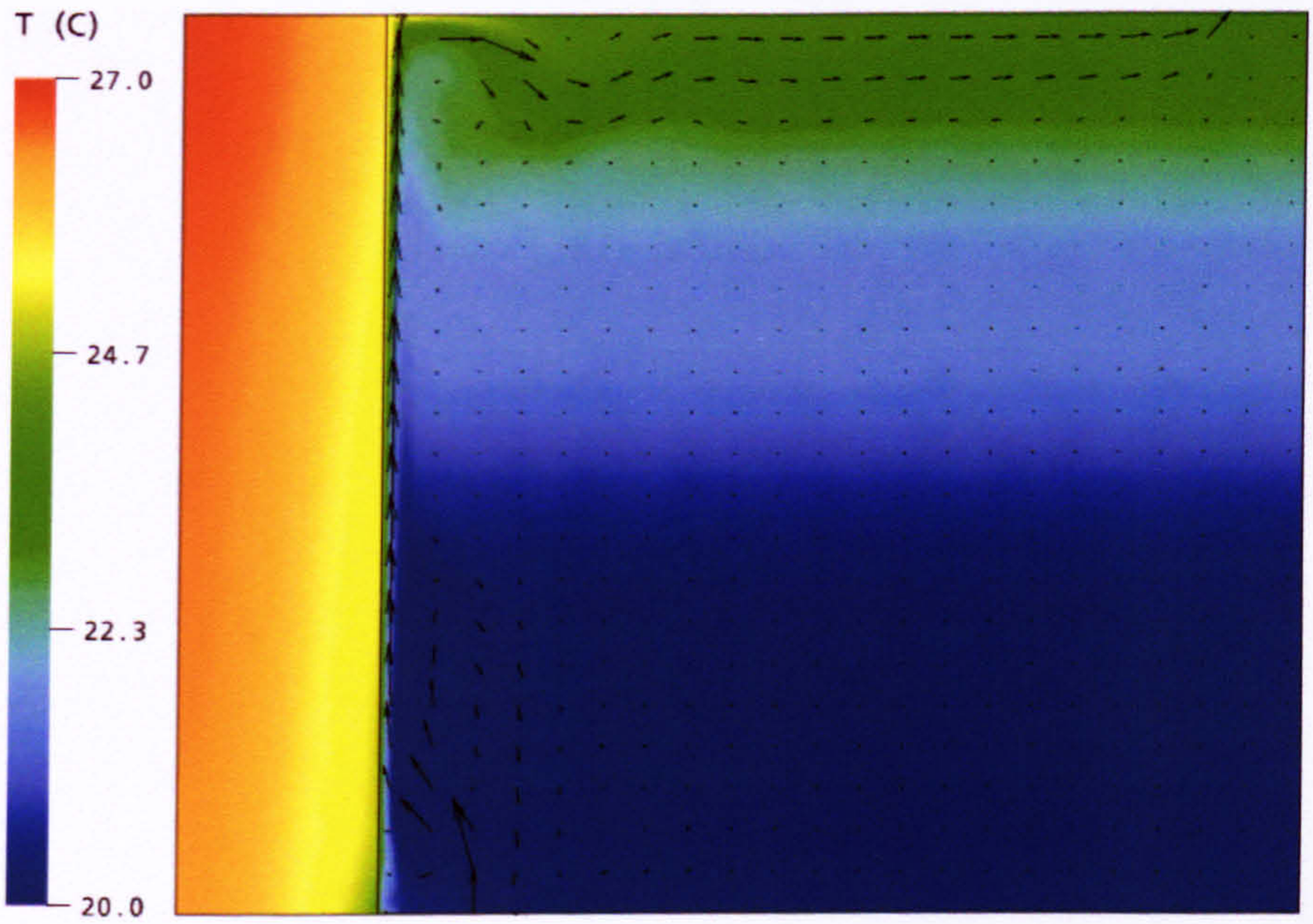

b)

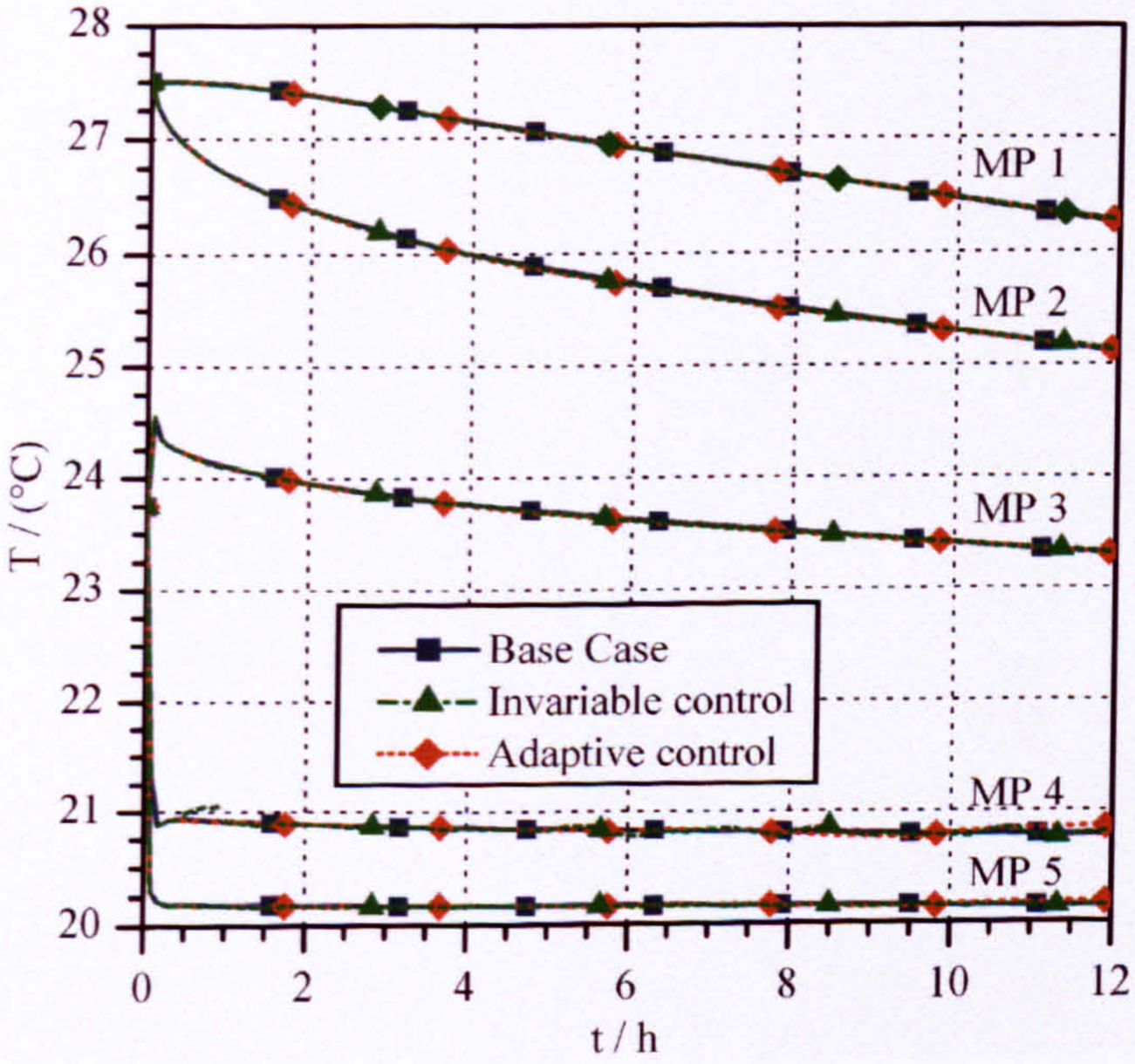

c)

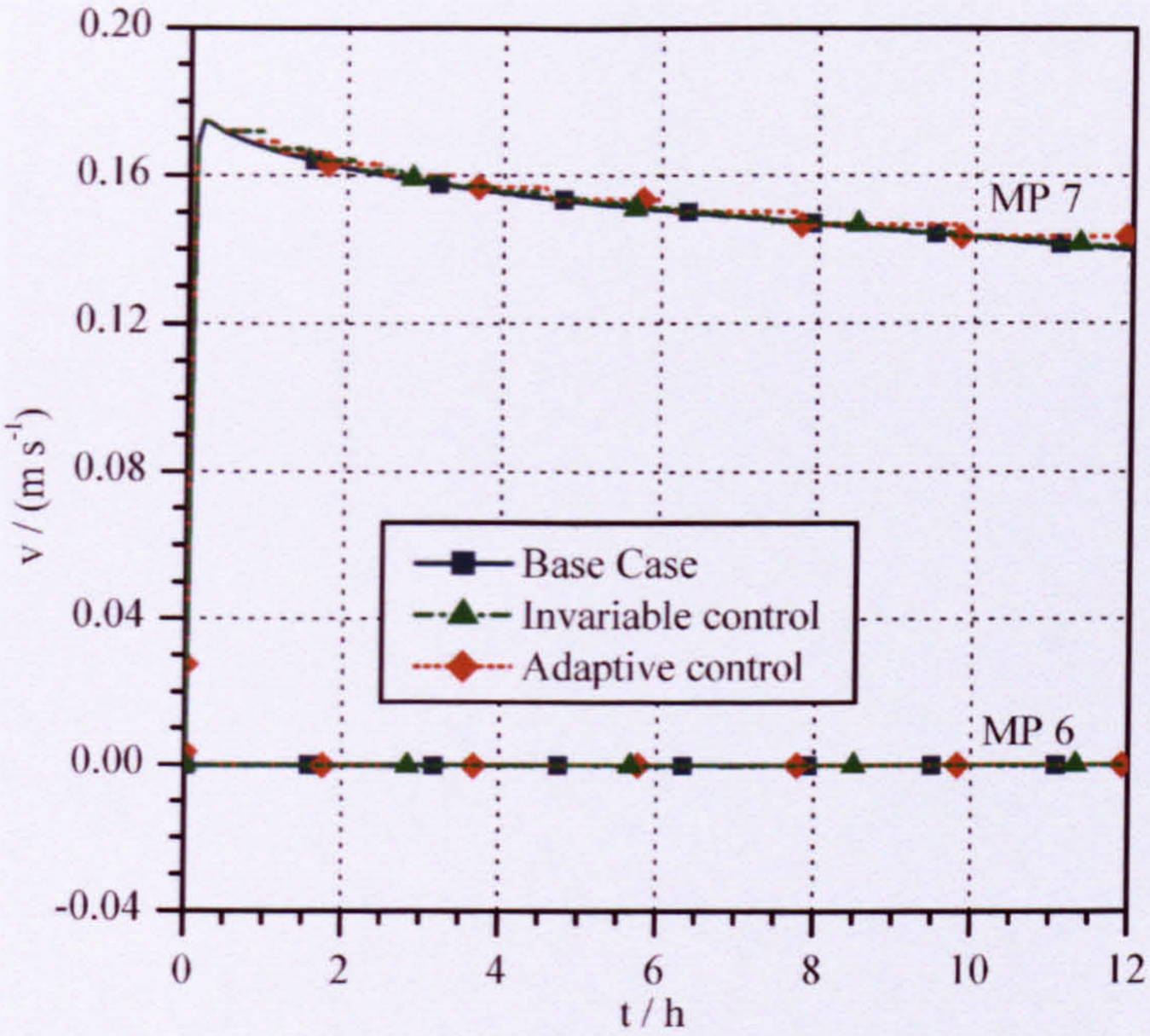

Figure 3: Simulation results for a naturally ventilated space with constant ambient temperature condition (Case 1); (a) temperature and air flow field for the base case after a simulation time of 12h; (b) temperature predictions and (c) velocity predictions.

5.3 Mechanical ventilation (Case 2)

In the base case, air enters the room at low level through the inlet and warms as it rises along the hot surface (see Figure 4a). The warm air leaves the room at high level through the outlet as observed in case 1. Elsewhere in the room a circulating air flow develops creating a homogeneous air temperature as illustrated in Figure 4a and indicated by equal values for MPs 3-5 in Figure 4b. The descending curves for MPs 1 and 2 show a gradual cooling of the solid wall. In the mechanical ventilation case the cooling of the solid material occurs quicker than case 1 (natural ventilation) since the air entering the room has a higher flow-rate (compare Figures 3 and 4 for MPs 1 and 2) which leads to a higher heat transfer at the wall surfaces. The curve shapes in Figures 4b and 4c show similar results for the invariable and adaptive freeze-flow control methods and the base case. However, the control methods predict a greater cooling rate for the solid wall than the base case (see MPs 1-2). A temperature difference of about 0.2K exists at the end of the 12h simulation. Analysis of temperatures throughout the solid domain at different heights at x=0.11m and from the inner to the outer wall surface at y=0.5m shows only a marginally higher temperature difference of 0.25K at the top of the massive wall for the freeze-flow method compared with the base case. Elsewhere, the temperature difference between the two methods did not exceed 0.2K. This greater cooling rate prediction is thought to be caused by an over-predicted surface heat transfer rate due to the frozen flow periods which contain velocity values from the last unfrozen flow period. Since the temperature difference between the solid and the external wall gradually decreases, the momentum of the flow field would decrease and lead to reduced convection, if the flow was not 'frozen'. The velocities are higher for case 2 compared with case 1. Thus the effect of the over-predicted convective surface heat transfer due to the frozen flow condition is more significant within the solid in case 2.

The resultant CPU time and output data file size using the invariable control method showed 79% and 62% reductions respectively compared with those of the base case. Better performance

(84% and 66% respectively) was achieved using the adaptive control method. The reason for this improvement is the gradual increase of frozen flow periods with accumulated time for the adaptive control, resulting in a frozen time period of up to 1h 31mins compared to the fixed periods of 30mins in the invariable control simulation.

a)

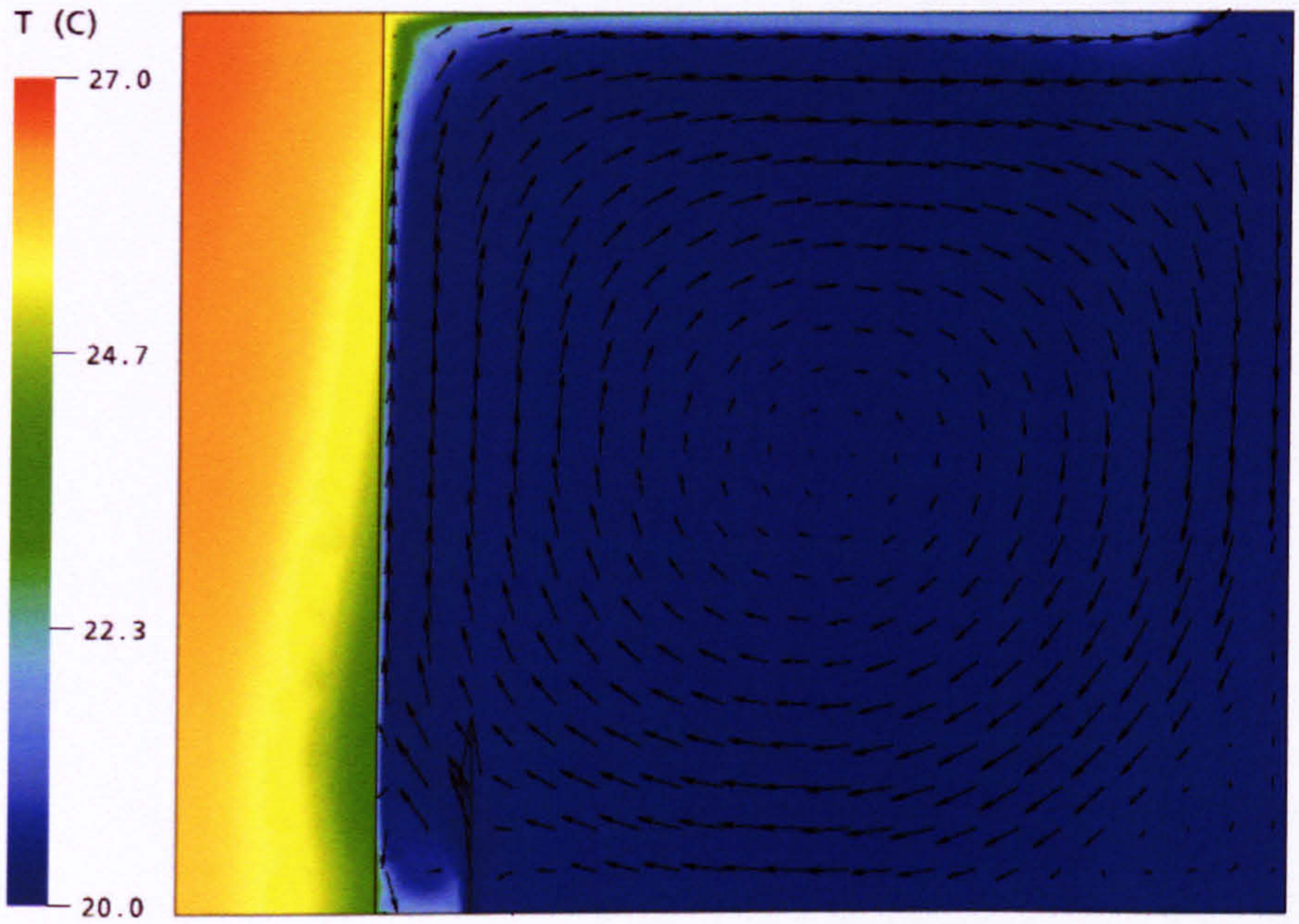

b)

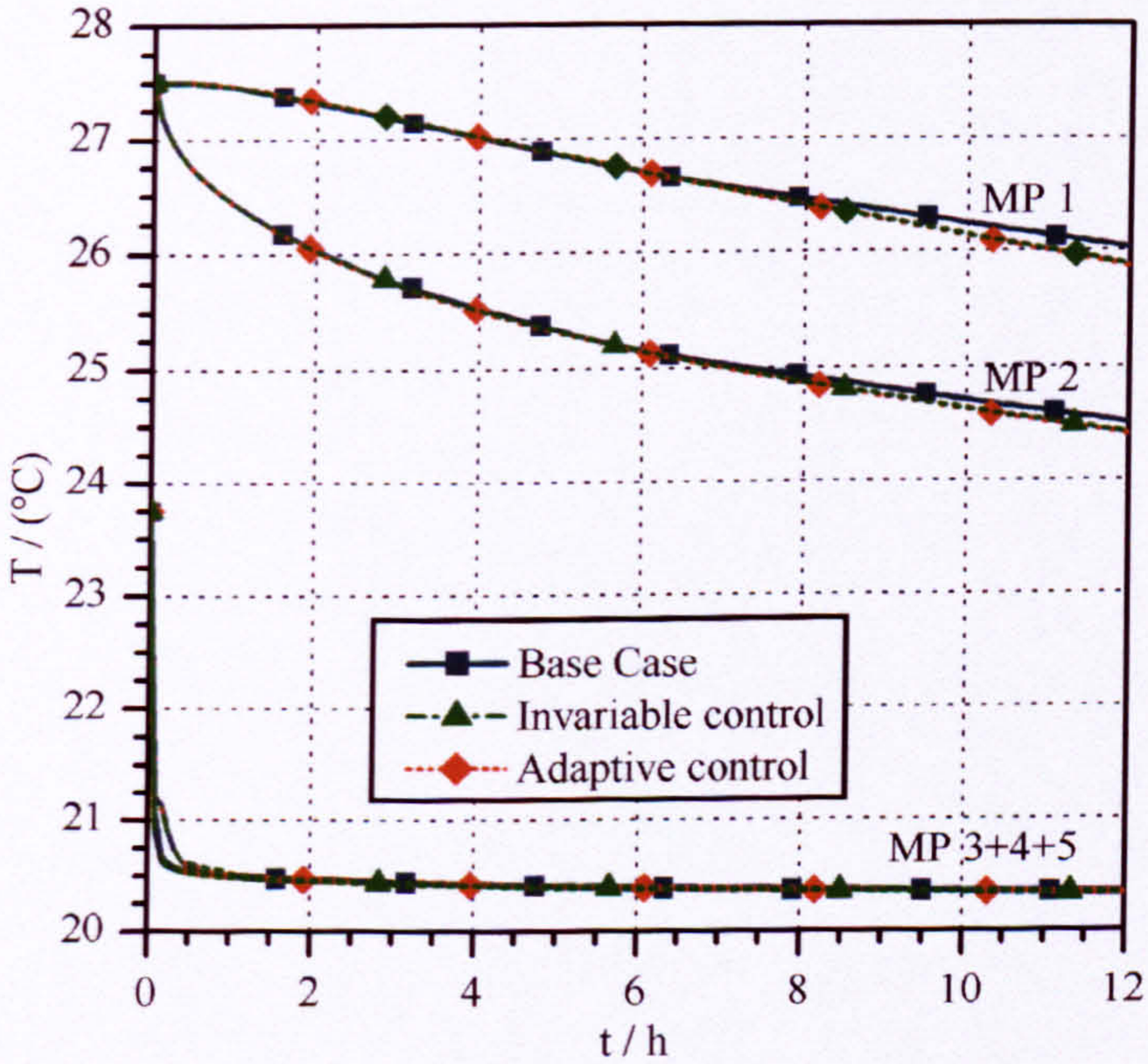

c)

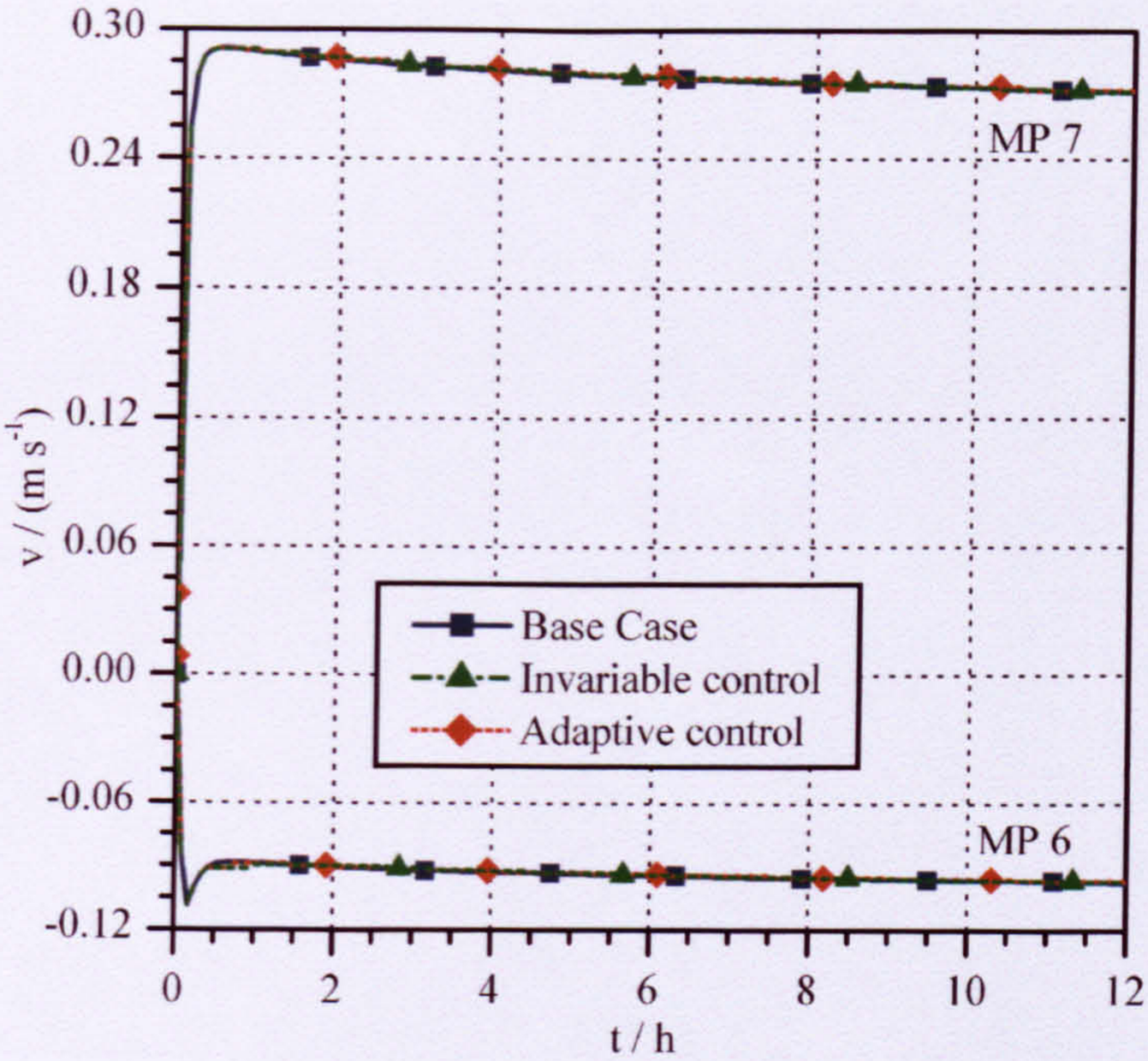

Figure 4: Simulation results for a mechanically ventilated space with fixed inlet condition (Case 2); (a) temperature and air flow field for the base case after a total simulation time of 12h; (b) temperature predictions and (c) velocity predictions.

6. Conclusions

Dynamic thermal simulations have been conducted previously using CFD alone by applying a freeze-flow method which operates by periodically freezing and unfreezing the hydrodynamic and turbulence equations (Somarathne et al 2002 and Zitzmann et al 2006a). A new adaptive control method has been developed in this work which adjusts the period lengths of frozen and unfrozen flow based on prevailing and imminent flow conditions. Compared to the previous invariable control method of fixed periods, the new method has the advantage that the solver remains in the frozen flow mode for longer when flow conditions are stable or changing only slowly, thus improving the efficiency of the simulation.

Both control strategies were tested using natural and mechanical ventilation to cool a massive wall. Both predicted similar results and agreed well with the base case at the end of each unfrozen flow period in which all equations were solved transiently without interruption. However, the better performance was achieved with the adaptive control method. Compared with the base case, the invariable control method typically showed a 75% and 63% reduction in CPU time and data storage, respectively, whereas the adaptive control method demonstrated an 88% and 70% reduction, respectively. Thus for the cases investigated it was possible to reduce the simulation time again by about half by using the adaptive control method rather than an invariable control method.

This approach offers new opportunity for dynamic simulation work where detailed resolution of air flow and temperature conditions in buildings is important. The next stage of this work is to use the new adaptive freeze flow control method to incorporate radiation. It is then planned to apply the method to a typical office space with a range of scenarios, including varying internal heat loads, varying ventilation rates and passive night-time cooling.

Acknowledgement

This publication is based on research funded by the German Ministry of Education and Research (funding No: 1749B04). The content of this paper is the responsibility of the authors, not the funding body.

Nomenclature

g	gravity vector (m s^{-2})	Greek Symbols	
C	constant (-)	β	thermal expansivity (K^{-1})
C_p	specific heat capacity (J kg^{-1} K^{-1})	ρ	density (kg m^{-3})
h	static enthalpy (kg m^2 s^{-2})	λ	thermal conductivity (W m^{-1} K^{-1})
k	turbulence kinetic energy (m^2 s^{-2})	μ	viscosity (kg m^{-1} K^{-1})
p	pressure (kg m^{-1} s^{-2})	τ	stress tensor (kg m^{-1} K^{-2})
S	source term		
t	simulation time (s)	**ω**	**turbulence frequency (m^2 s^{-2})**
T	temperature (K)	Subscripts	
U	velocity vector (m s^{-1})	e	energy
v	vertical velocity component (m s^{-1})	k	turbulence kinetic energy
x, y, z	coordinates (m)	m	momentum
Superscripts		ref	reference
		t	turbulence
T	**transposed**		

References

ANSYS, CFX, Version 10.0, http://ww.ansys.com/products/cfx.asp, accessed 08.06.2006.

Blondeau P, Sperandio M, Allard F. "Night ventilation for building cooling in summer", Solar Energy 1997 **61(5)** pp327-335.

Chen Q, Kooi J van der. "ACCURACY – a computer program for combined problems of energy analysis, indoor airflow and quality", ASHRAE Transactions 1988 **94(2)** pp196.214.

Crawley D, Hand J, Kummert M, Griffith B. "Contrasting the capabilities of building energy performance simulation programs", Proceedings of Building Simulation 2005, Montreal, Canada, pp231-238.

Geros V, Santamouris M, Tsangrasoulis A., Guarracino G. "Experimental evaluation of night ventilation phenomena", Energy and Buildings 1999 **29(2)** pp141-154.

Givoni B. "Effectiveness of mass and night ventilation in lowering the indoor daytime temperatures. Part I: 1993 experimental methods", Energy and Buildings 1993 **28(1)** pp25-32.

Kendrick JF. "An overview of combined modelling of heat transport and air movement", Technical Note 1993 **40**, AIVC, Coventry, England.

Kolokotroni M, Aronis A. "Cooling-energy reduction in air conditioned offices by using night ventilation", Applied Energy 1999 **63(4)** pp241-253.

Marenne C, Groleau D, Raymond F. "Simulation of the cooling effect of the night time natural ventilation: a 3D numerical application to the "Maison Ronde" of Mario Botta", Environmentally Friendly Cities 1998, Procedings of PLEA '98, Lisbon, Portugal, pp495-498.

Negrao C. "Conflation of computational fluid dynamics and building thermal simulation", PhD thesis 1995, University of Strathclyde, Glasgow, England.

Onishi J,Koga S, Mizuno M, Takeya N, Kitagawa K. "Computer effort saving methods in unsteady calculations of room airflows and thermal environments", Proceedings of Roomvent'98, pp117-124.

Rincon J, Almao N, Gonzalez E. "Experimental and numerical evaluation of a solar passive cooling system under hot and humid climatic conditions", Solar Energy 2001 **71(1)** pp71-80.

Somarathne S, Seymour M, Kolokotroni M. "Transient solution methods for dynamic thermal modelling within CFD", International Journal of Ventilation 2002 **1(2)** pp141-156.

Somarathne S, Seymour M, Koloktroni M. "Dynamic thermal CFD simulation of a typical office by efficient transient solution methods", Building and Environment 2005 **40** pp887-896.

Wilcox D. "Turbulence modeling for CFD", second edition, 1998 DCW Industries Inc.

Zhai Z, Chen Q. "Strategies for coupling energy simulation and computational fluid dynamics programs", Proceedings of Building Simulation 2001, Rio de Janeiro, Brazil, pp59-66.

Zhai Z, Chen Q. "Performance of coupled building energy and CFD simulations", Energy and Buildings 2005 **37** pp333-344

Zitzmann T, Pfrommer P, Cook M, Rees S, Marjanovic L. "Simulation of steady-state natural convection by using CFD", Proceedings of Building Simulation 2005, Montreal, Canada, pp1448-1456.

Zitzmann T, Pfrommer P, Cook M. "Simulation dynamisch thermischen Langzeitverhaltens in Gebäuden mittels CFD", Bauphysik 2006a **28** pp96-102.

Zitzmann T, Pfrommer P, Cook M. "Dynamisch Thermisches CFX Verfahren", Proceedings of BauSIM2006, Munich, Germany, 2006b pp217-219.